predictive mineral discovery
COOPERATIVE RESEARCH CENTRE

pmd*CRC

Final Report

Total Systems Analysis of the Mt Isa Eastern Succesession

Project I2

April 2002 - March 2005

Tom Blenkinsop (editor)

CSIRO
AMIRA INTERNATIONAL
Australian Government
Geoscience Australia
MONASH University
THE UNIVERSITY OF MELBOURNE
JCU James Cook University
THE UNIVERSITY OF WESTERN AUSTRALIA

predictive mineral discovery
COOPERATIVE RESEARCH CENTRE

Total Systems Analysis of the Mt Isa Eastern Succession

Project I2+3

Final Report

APRIL 2002 – MARCH 2005

Tom Blenkinsop (editor)

Table of Contents

SECTION 3: ARCHITECTURE

SECTION 4: FLUIDS AND METALS: DRIVERS, SOURCES, PATHWAYS, SINKS

DIGITAL APPENDICES
(See attached DVD for Digital Files)

Reports
- Worms and Prospectivity: reports on Mt Isa and Osborne: *F. C. Murphy*
- Potential Field Modelling: *M. Barlow*
- Melt inclusions and gold at Timbara: *R. Mustard*
- Magmatic evolution of Timbara. *R. Mustard*
- I2 Quarterly and Annual Reports

PhD Theses
- Brecciation within the Mary Kathleen Group of the Eastern Succession, Mt Isa Block, Australia: implications of district-scale structural and metasomatic processes for Fe-oxide-Cu-Au mineralisation: *L. Marshal*
- Numerical Modelling of Deformation and Fluid Flow in Hydrothermal Systems: *J. McLellan*
- N-S shortening during orogenesis in the Mt Isa Inlier: The preservation of W-E structures and their tectonic and metamorphic significance: *M. Sayab*

Honours Theses
- Breccias and mineralization at Ernest Henry Mine: *T. Laneyrie*
- A classification scheme for brecciation in the Fullerton River Gorge concerning the evolution of the Eastern Succession of the Mt Isa Inlier: *J. Josey*
- Structural and metamorphic evolution along the Cloncurry fault: *R. Hingst*

Databases
- Mt Isa Eastern Fold belt mapping database
- Mafic Geochemistry Database
- Petrophysical database
- FracSYS data base: geology, geochemistry, geophysics

Maps, Cross-sections and 3D model
- 3D model of part of the Eastern Succession
- Reprocessed Mt Isa seismic line
- Geological and geophysical cross sections of the Squirrel Hills and Wimberu granites
- Prospectivity layers and Maps
- New Geological map of the Eastern Succession, with crustal scale cross-sections
- Metamorphic Map (A3)
- Eastern Fold Belt Mapping Database
- Time-Space plot for Mount Isa Inlier (A3)

Presentations and Posters
- Annual Project Review December 2002
- Annual Project Review November 2003
- Barossa Valley Conference June 2004
- Final Project Review: Mt Isa March 2005

SUMMARY

Tom Blenkinsop[1], James Austin[1], Tim Baker[1], Kris Butera[1], Mark Edmiston[1], Arianne Ford[1], Damien Foster[1],Cameron Huddlestone-Holmes[1], Piter Lepong[1], Geordie Mark[2], John McLellan[1], Barry Murphy[3], Roger Mustard[1], Nick Oliver[1], Mike Rubenach[1], Mohammed Sayab[1], Michelle Stark[1], Pat Williams[1]

[1]School of Earth Sciences, James Cook University, Townsville, Qld

[2]School of Geoscience, Monash University, Melbourne, Vic

[3]School of Earth Sciences, The University of Melbourne, Vic

EXECUTIVE SUMMARY

The lower crustal basement of the Eastern Succession of the Mt Isa inlier is divided into a western block and an eastern block, the latter with a distinctly younger crustal residence age. The overlying metasedimentary and meta-volcanic rocks were deposited in extensional basins and comprise two major Cover Sequences (CS2 and CS3). CS2, consisting of mafic and felsic volcanic rocks overlain by carbonates, was deposited from *ca* 1780 to 1690 Ma diachronously from west to east, possibly in a back-arc environment. CS3 (quartzites, pelites, carbonates and volcanic rocks), was deposited from *ca* 1655 to 1600 Ma, with important lateral facies changes from west to east. Major thickness changes in both sequences are localised over NS trending structures, which were presumably basin margins. Low pressure metamorphism and albitisation occurred at the time of EW extensional basin formation.

The Isan Orogeny from *ca* 1600 Ma to 1500 Ma was dominated by EW compression that lasted at least episodically until *ca* 1500 Ma. From *ca* 1550 to 1500 Ma, voluminous mafic and felsic potassic magmatism was emplaced at mid-crustal levels. Despite having A-type geochemical signatures, the granites are syn-tectonic. P-T-t paths were complex, showing an initial anticlockwise segment, followed by a clockwise segment and then heating events corresponding to granite intrusion. Metamorphism was caused by advective heating in the lower-middle crust, due to melt migration, and conductive heating in the upper crust. The major crustal structures produced during the orogeny were km scale upright folds and steep faults. The coincidence of these major structures with thickness changes in the cover sequences suggests that positive inversion was a dominant process during the orogeny. A preliminary 3D geological model has been constructed which identifies some key relationships of the basement and cover sequences, and provides important pointers for further research in resolving the architecture of the region.

Iron Oxide Copper Gold (IOCG) deposits in the Eastern Succession have strong spatial associations with the tectonic CS2/CS3 contact, with faults and fault bends and with mafic intrusions. The role of mafic rocks in IOCG genesis appears to be important in many cases: metals may have been transported and deposited from magmatic-hydrothermal fluids on crystallisation of the mafic rocks, or from metamorphic fluids that subsequently leached them. In the largest IOCG deposit, Ernst Henry, fluids from highly fractionated Williams Batholith rocks may have mixed with primitive mantle or gabbro-derived fluids. In all cases strong structural controls in the form of NS and NE-SW faults, bends and

intersections are apparent. The importance of structural controls on fluid pathways is demonstrated by numerical modelling, which predicts known deposits and corresponds closely with prospectivity results. The prospectivity studies highlight a number of targets under cover, based on geophysical data.

The base metal endowment of the Eastern Succession can be seen as a product of several geological processes in a volume of crust that has experienced high fluid fluxes and prolonged deformation and thermal anomalism. Reactivation of structures and lithological diversity are also ingredients of a highly distinctive geological history that has lead to extensive mid-Proterozoic mineralization.

1. INTRODUCTION

The pmd CRC I2+3 project started on 1 April 2002 and lasted for three years. The major inputs came from James Cook University, Monash University, Melbourne University and Geoscience Australia. Twenty-three people contributed substantively to the project.

The visionary goal of the project is:

> *By linking conventional exploration databases with a) numerical potential field (wavelet) analysis ("worms"), b) advanced microanalytical metal path tracers and c) a fully fused geochemical, tectonothermal, and tectonostratigraphic model, the project will generate a comprehensive prospectivity analysis for Iron Oxide Copper Gold and related deposit styles.*

Contributions to the CRC objectives are encapsulated in the following statement:

The I2+3 project (Total systems analysis of the Eastern Succession, Mt Isa), will contribute to a fundamental shift in discovery by:

- *Utilisation of major new data sets (from wavelet analysis of geophysical data) to understand the three dimensional architecture of the Eastern succession of the Mt Isa Inlier*
- *A ground-breaking analysis by fractal geometry of the spatial distribution of known mineralization*
- *The first comprehensive prospectivity analysis of the whole of the Eastern Succession, based on the first two methods with new knowledge about fluid flow and alteration*
- *Specific predictions about the possibility of blind mineral deposits under cover adjacent to the exposed Inlier*

The major deliverables were revised half way through the project, when they became:

1. An advanced structural synthesis and a **3D model** of the crustal architecture
2. Evaluation of the **critical ingredients for IOCG** deposits
3. Understanding controls on the Isa district **mineralising fluids**
4. An understanding of the **P-T-t evolution**
5. A **thermal model**
6. A revised **time-space model**; comparisons with the Georgetown Block.
7. Reactor/titration-style, **chemical numerical models**
8. A full **prospectivity analysis** of the eastern half of the terrain

The project was organised into six modules, which are presented in this report in three sections based on the Five Questions (Table 1).

Table 1. Project Modules and report Sections

Project Modules	Report Sections
	1. Summary
Tectonothermal evolution	2. Geodynamic Setting
Structural framework	3. Architecture
Tectonostratigraphic framework	
Key ingredients for IOCGS	4. Fluids and Metals: Drivers, Sources, Pathways and Sinks:
Numerical modelling	
Prospectivity Analysis	

The study area for the project is shown in Fig. 1.

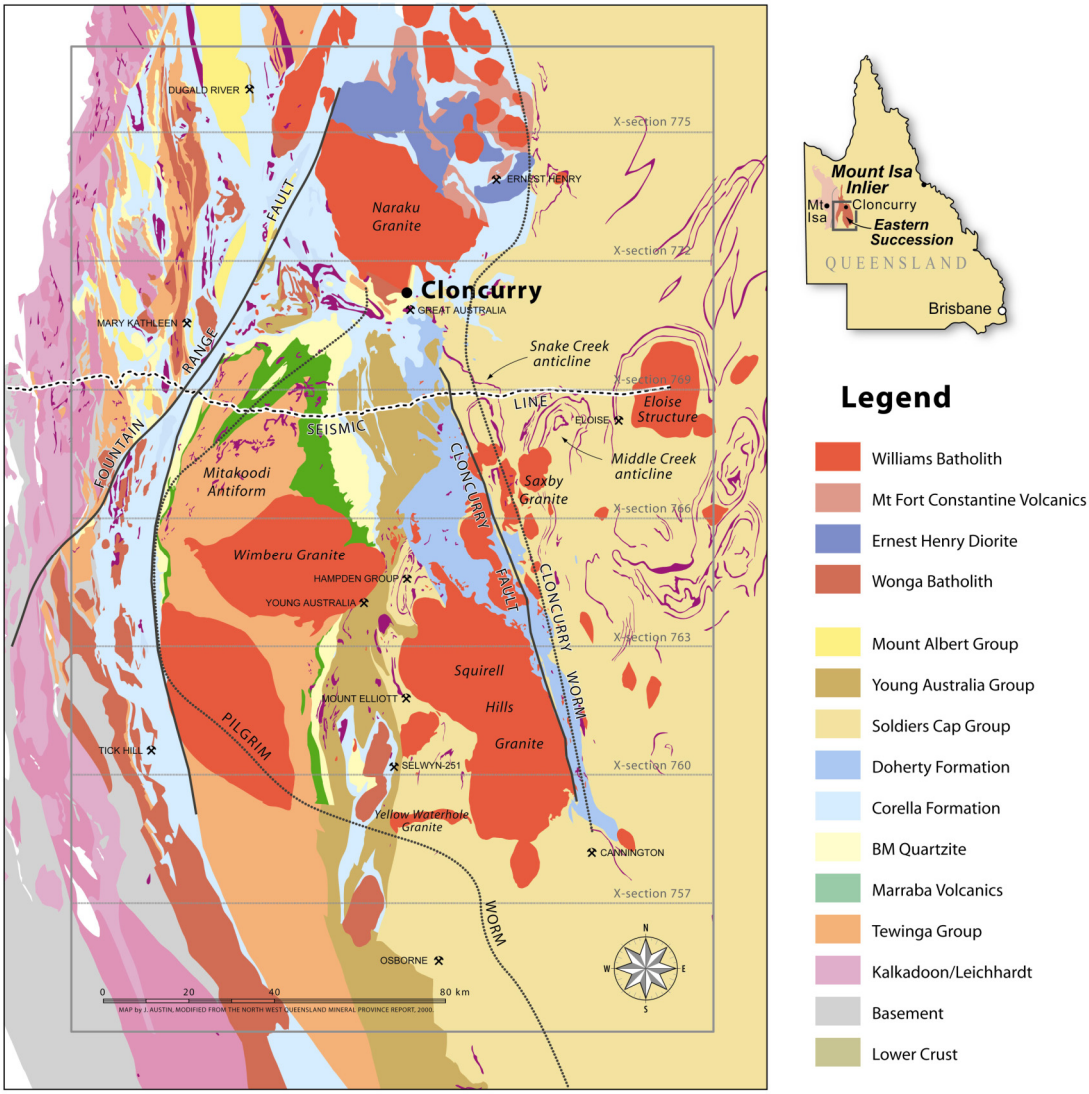

Fig. 1. Locality Map. Geology shown here is modified from the NWQMPR. The Cloncurry and Pilgrim Worms are shown as dotted lines. Grey lines show cross-sections used for the 3D model.

From the inception of the project, student participation has been an important aspiration. 9 PhD students have started under the project, of which 3 are complete, and three honours project have been completed (Appendix 1). The student research comprises a significant part of the results presented here.

The aim of this summary is to present the key findings and their relevance to exploration for IOCG deposits. The rest of the final report consists of the detailed reports, on which this summary is based.

2. GEODYNAMIC SETTING

Most of the rocks of the Eastern Succession of the Mt Isa inlier described in this report were formed between 1760 and 1500 Ma, post-dating the Archaean and early Palaeoproterozoic history recorded in other parts of the inlier (Etheridge et al. 1987; McDonald et al. 1997). Sedimentary and volcanic rocks are described in terms of two "Cover Sequences" (CS2 and CS3) deposited at 1780-1690 and 1655-1600 Ma respectively (Blake, 1987; Foster and Austin, 2005) and deformed episodically from *ca* 1650 – 1500 Ma. The geodynamic settings of both the depositional and orogenic parts of this history have been extensively debated in the past and are still unresolved at present. However, progress has been made in this report through an examination of the isotopic signatures of crustal blocks comprising the basement to the cover sequences, by analysing the geodynamic implications of mafic rocks and the voluminous late-orogenic felsic magmatism, and by a more detailed examination of the tectonothermal evolution

2.1 Basement blocks and crustal isotopic signatures

The protracted Isan Orogeny (*ca* 1.60-1.50 Ga) coincided with the emplacement of a diverse range of intrusions (Mark et al. 2005a, b). The whole-rock geochemistry of these intrusions fingerprint different parts of the crust during the formation of the various magmas and may bear some relationship to mantle activity during that time. Sr isotopic compositions of both peak metamorphic pegmatites (*ca* 1.59 Ga) and their host rocks (deposited *ca* 1.67-1.65 Ga) are highly radiogenic and largely characterised by $^{87}Sr/^{86}Sr_i$ of 0.7075-0.7185 and 0.7059-0.7161 respectively (Fig. 2).

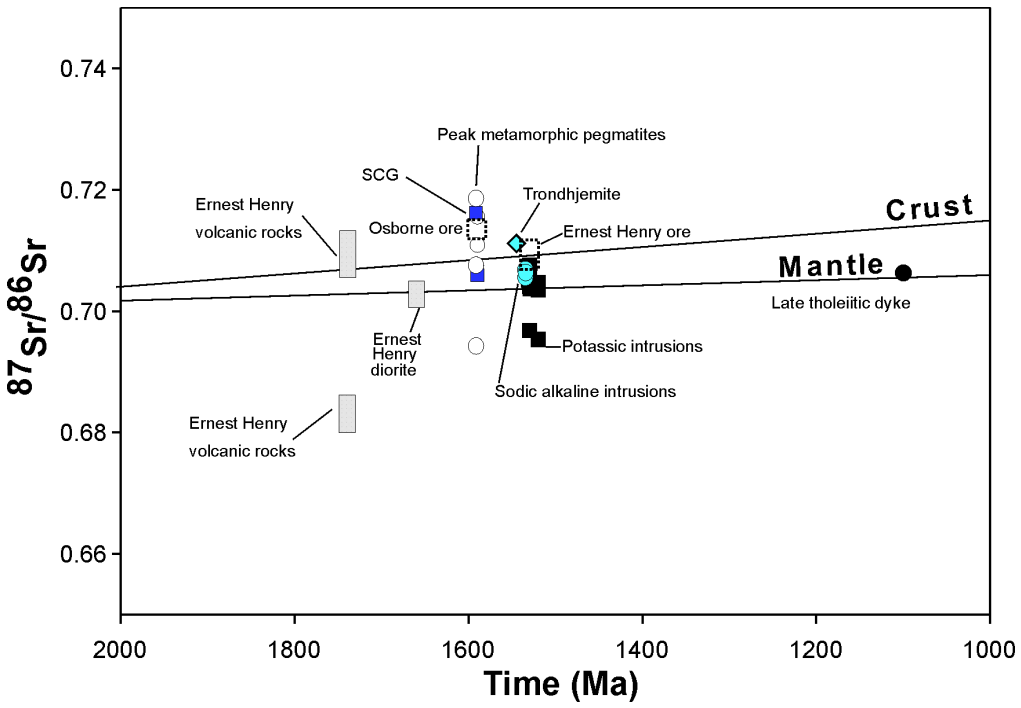

Fig. 2. Initial $^{87}Sr/^{86}Sr$ of magmatic and sedimentary rocks, and selected ore samples from the Ernest Henry and Osborne Cu-Au deposits in the Eastern Succession.

Depleted mantle T_{DM} ages (See Fig. 3 for a summary) for the pegmatites and host rocks are also comparable, ranging between 2.45-2.51 Ga and 2.53-2.57 Ga respectively, and most closely resemble the *ca* 1.89-1.85 Ga felsic basement rocks (T_{DM} 2.45-2.58 Ga). The younger *ca* 1.55-1.50 Ga intrusions largely have mixed crust-mantle $^{87}Sr/^{86}Sr_i$ (0.6968-0.7112) and εNd (-1.0 to –3.8), and exhibit a range in T_{DM} between 2.08 and 2.30 Ga. The *ca* 1.55 Ga trondhjemite has higher $^{87}Sr/^{86}Sr_i$ (0.7112) than the younger sodic, alkali granites and the potassic 'A-type' intrusions, which mainly range from 0.7067 to 0.7085, and 0.6968 to 0.7065 respectively.

The magnetite-, pyrite- and chalcopyrite-rich ores at Osborne (*ca* 1.59 Ga) and Ernest Henry (*ca* 1.525 Ga) have $^{87}Sr/^{86}Sr_i$ of 0.7135 and 0.7084-0.7100 respectively that closely reflect their host rocks, and indicate that Sr in the ores is probably locally derived. The Nd isotope composition of one sample at Osborne (εND –4.5; T_{DM} 2.40 Ga) also supports local derivation of REE.

Broad-scale Nd isotope patterns constrained by 1.74-1.50 Ga magmatic rocks show that to the east of the line marked as the "Pilgrim Worm" on Fig. 1, the mid- to lower-crust is isotopically distinct, and generally has younger average crustal residence ages (T_{DM} *ca* 2.25 Ga) than *ca* 1.74 intrusions west of this inferred fault (T_{DM} >2.45 Ga). This distinction is highlighted by the *ca* 1.74 Ga Ernest Henry meta-andesite to the east of the Pilgrim Worm that has consistently younger T_{DM} ages (2.18-2.23 Ga) than coeval intrusions to the west (e.g., Burstall Granite and Levian Granite, T_{DM} 2.38-2.55 Ga). Outcrop of the younger generations of I- and A-type 1.67 Ga and 1.55-1.50 Ga intrusions (with T_{DM} between 2.08 and 2.30 Ga) is restricted to the east of the Pilgrim Worm. This east-west contrast in T_{DM} ages, somewhere in the vicinity of the Pilgrim Worm, is interpreted to represent the margin of an ancient, broadly north-south oriented, terrane boundary. We suggest that the eastern block represents an allochthonous block that was probably accreted to the inlier between the Barramundi Orogeny (*ca* 1.89 Ga) and the cessation of magmatism in the Kalkadoon-Leichhardt Belt (*ca* 1.84 Ga). Nd isotope data for the overlying, 1.74-1.62 Ga sedimentary rocks (e.g. calc-silicates and psammo-pelitic sediment rocks) show that they were derived from a hinterland that was dominated by late Archaean to early Paleoproterozoic components (2.45-2.57 Ga) that are much older than the basement rocks sampled by the intrusions to the east of the Pilgrim Worm, and are most compatible with the basement rocks in the Kalkadoon-Leichhardt Belt (KLB). However, the paucity of 1.89-1.84 Ga zircons in the younger sedimentary rocks probably indicates that the KLB rocks were not the predominant sediment source. The additional source components may have had a similar provenance to the sedimentary rocks in the Georgetown, Coen, Yambo and Dargalong inliers, which exhibit similarities in both T_{DM} ages and ages of detrital and inherited zircons to the Eastern Succession rocks.

Fig. 3. (next page). Geological correlation diagram showing the temporal correlations between the average crustal residence ages (T_{DM}) (opaque circles) and depositional ages (grey circles) for magmatic-stratigraphic rocks in the Eastern Succession (simplified after Foster and Austin, 2005), as well as associated detrital and inherited ages (open circles). Also shown are selected hornblende Ar-Ar ages (half-filled circles) from magmatic rocks in the succession. Tie lines joining two data points (full line for Sm-Nd isotope data, and dashed line for U-Pb data) represent populations with multiple data points. Data sources: 1. Spikings et al. (2001); 2. Page and Sun (1998), 3. Davis et al. (2001); 4. Geoscience Australia (Unpublished data), 5. Pollard and McNaughton (1997); 6. Mark (2001); 7. Pollard et al. (1998); 8. Gauthier et al. (2001); 9. Giles and Nutman (2003); 10. Giles and Nutman (2002); 11. Page (1983); 12. Maas et al. (1988); 13. McDonald et al. (1997); 14. Bierlein and Betts (2004).

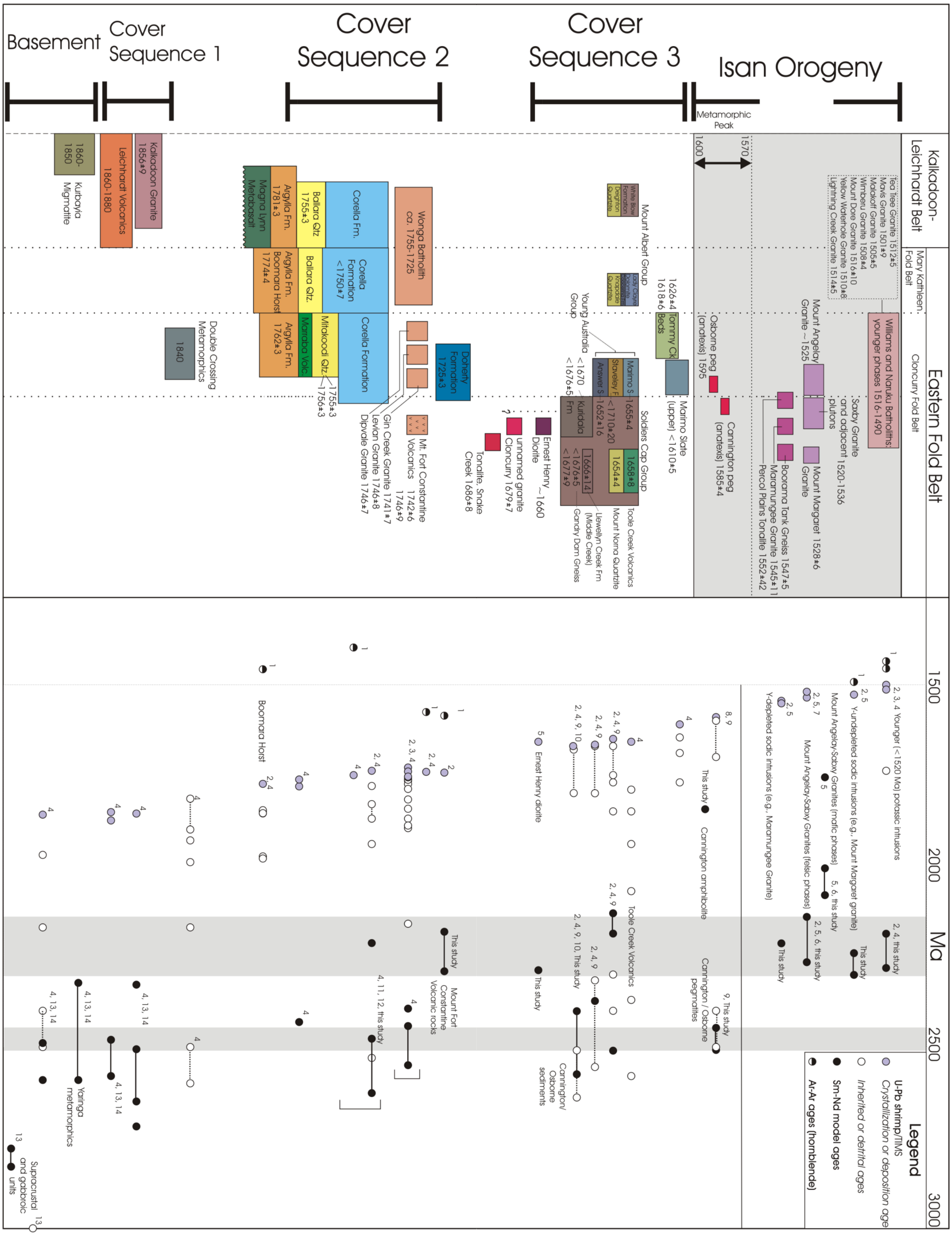
Basement
Cover Sequence 1
Cover Sequence 2
Cover Sequence 3
Isan Orogeny
Metamorphic Peak

2.2 Felsic magmatism: Intrusive phases of the Williams-Naraku batholith

The later phases of the Williams-Naraku batholith are potassic and were emplaced episodically over a 30 Ma period between 1.53 and 1.50 Ga. These apparent anorogenic intrusions were emplaced during three phases of magmatism that are largely confined to discrete spatial domains in the Eastern Succession, namely: 1. 1.53-1.52 Ga (centre), 2. 1.52-1.51 Ga (west and south), 3. 1.51-1.50 Ga (north). On an outcrop-scale, igneous complexes representing each of the phases of magmatism exhibit geological relationships supporting the coincident emplacement of mafic and felsic intrusions early in magma genesis, and the subsequent fractionation of the felsic intrusions during sub-horizontal EW compressional deformation. A syn-tectonic timing of these intrusions contradicts their apparent anorogenic character defined using their geochemistry, and implies that intrusions of this composition are not restricted to 'strictly' anorogenic environments.

The recognition of distinct phases of geochemically similar, LILE (large-ion-lithophile-element) enriched, potassic intrusions across the succession implies that they were derived from previously unmelted crustal material of tonalitic composition. The prolonged duration over which steep NS tectonic fabrics were produced throughout the Eastern Succession suggests that subhorizontal EW compression was dominant during that time, and that the higher apparent strain around the intrusions was associated with localized thermal weakening linked to heat advection from the crystallizing intrusions. Repeated, short-lived, slab rollback (Fig. 4) from a distal eastern arc is invoked for the initiation of periodic mantle emplacement into the crust, the subsequent generation of felsic magmas and the syn-compressional regime during emplacement of the mid-crustal intrusions.

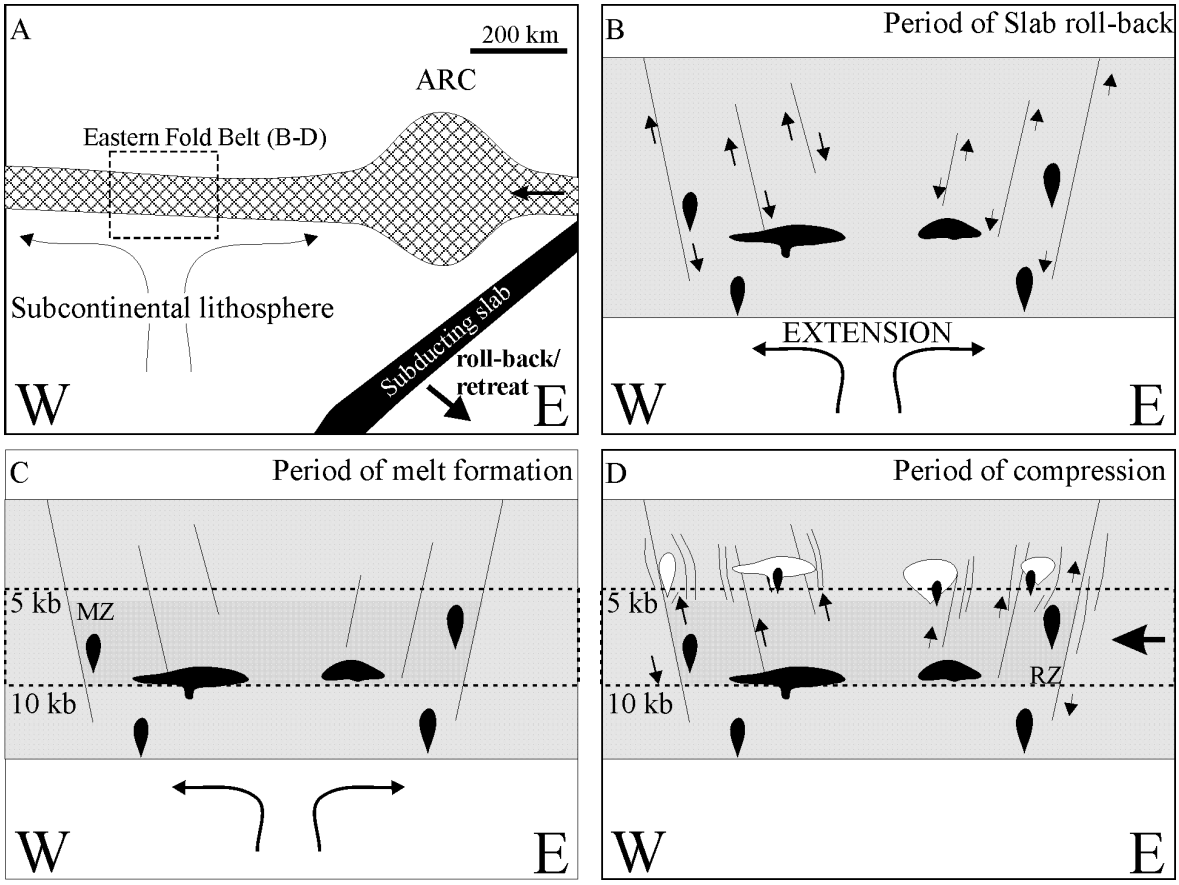

Fig. 4. A series of schematic diagrams showing a mechanism for the relations between post-peak metamorphic batholith emplacement in the Eastern Fold Belt and a hypothesized destructive margin and arc to the east (A) (cf. Giles et al., 2002). The batholith is interpreted to have formed during a sequence of events including: the episodic emplacement of mantle-derived mafic material (opaque intrusions) during extension at the base of the crust (B); mid-crustal melt formation (C); and, syn-compressional felsic (white intrusions) ± mafic (opaque intrusions) magma emplacement (D) associated with episodes of slab roll-back/ retreat (cf. Giles et al., 2002). The sequence from B to D is interpreted to have occurred during three periods between *ca* 1530 Ma to *ca* 1500 Ma (*ca* 1530-1520 Ma; 1520-1510 Ma; 1510-1500 Ma). Abbreviations: MZ, melting zone; RZ, residual zone.

2.3 Mafic geochemistry

Mafic rocks of the Soldiers Cap Group (Fig. 3) most likely developed in a back-arc basin. Irrespective of the age of the mafic rocks within and emplaced into the Soldiers Cap Group, their chemistry is remarkably similar, indicating that they were all derived via similar processes from parental magmas of a common composition (Butera et al., 2005). A back-arc basin basalt chemistry is inferred on the basis of spider-gram patterns that indicate a mix between an enriched MORB source that has undergone high degrees of partial melting (flat REE pattern) and a steeper slope for lighter elements reflecting a subducted slab component (Fig. 5). A distinctive feature of the chemistry of the mafic rocks is a consistently high Pb content (25-30ppm). This is interpreted as a consequence of a chlorine flux during partial melting of a contaminated subducted slab.

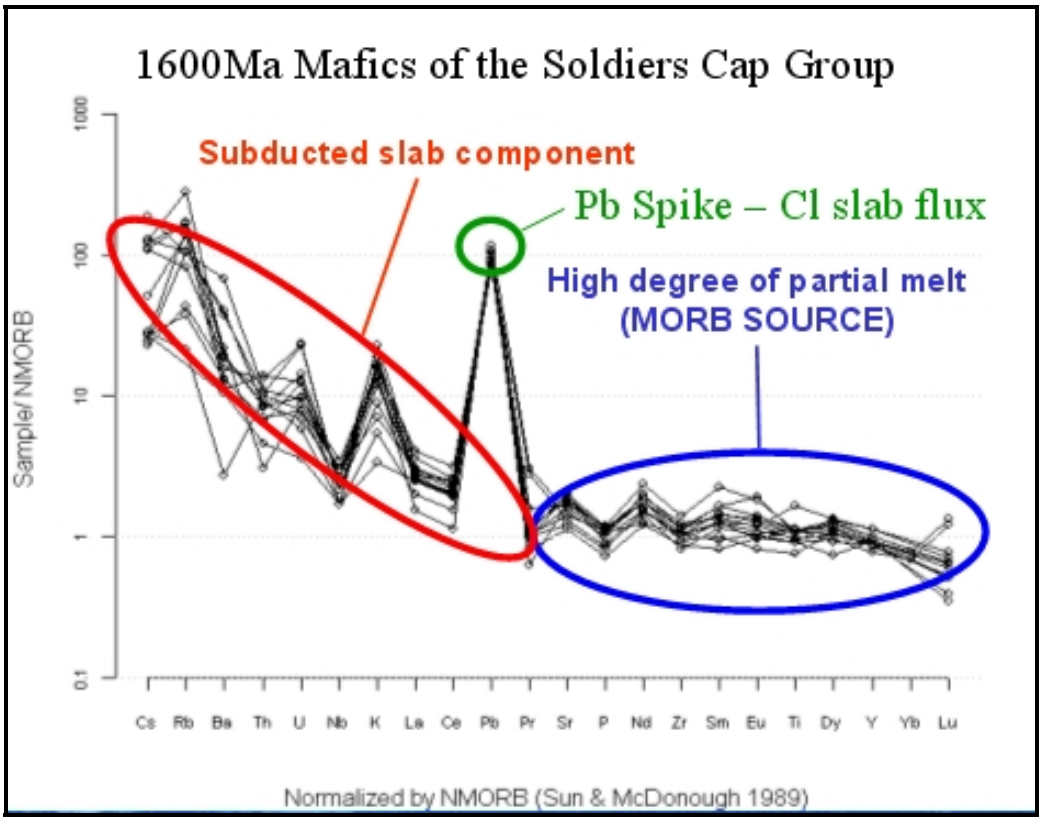

Fig. 5. Typical spider diagram (multi-element plot) of 1600Ma mafic rocks from the Eastern Succession, normalised to NMORB (after Sun & McDonough, 1989). Highlighted are the flat REE patterns, indicating high degrees of partial melting of an EMORB source, high Pb spike typical of magmas that have had a significant Cl contribution from subducted slabs, and the variability of the more mobile LILE and HFSE also typical of back-arc basalts. Mafic rocks at 1686 and 1530 Ma show similar trends.

Ce/Y ratios were used to determine the depth at which the mafics fractionated, based on the technique of Collins (in prep). For the 1686 Ma mafics, a pressure of *ca* 2.2 kb was determined, corresponding to a source depth as shallow as 8 km. This may reflect fractionation in the mid to upper crust, or, more likely, that the crust was very thin, and the magmas fractionated just below the Moho. Given a typical modern day oceanic crust thickness of 5 km, this implies that the magmas were generated in a highly attenuated rifted continental environment that almost resulted in generation of oceanic crust.

Thermodynamic modelling using pMelts software indicates that the geochemistry of these mafic rocks is consistent with their derivation via the fractionation (to 58%) of a high Fe-picrite parental magma, with an initial liquidus temperature of 1377^{o}C at 2.2 kb, and an initial H_2O content of 0.5wt%.

The Ce/Y ratios of 1660, 1600 and 1530 Ma mafic rocks indicate they formed at pressures greater than 2.2 kb, reflecting intermittent crustal thickening, and hence deeper mafic source regions, during the post-1686 Ma orogenic events. Modifying the pressure appropriately in the pMelts models yields similar results to the 1686 Ma model regarding Fe-rich picritic parental magmas and a high % fractionation. All the models require a contribution of H_2O in the source region in order to converge upon the real compositions. True continental rift basalts would be completely anhydrous, thus supporting the hypothesis of a hydrous (and Cl-bearing) subducted slab component to the magma.

2.4 Tectonothermal evolution

A significant output of this project has been the compilation of a metamorphic map of the Mt Isa inlier (Rubenach, 2005a; Fig. 6). This is a composite map in which the timing of metamorphism is not represented.

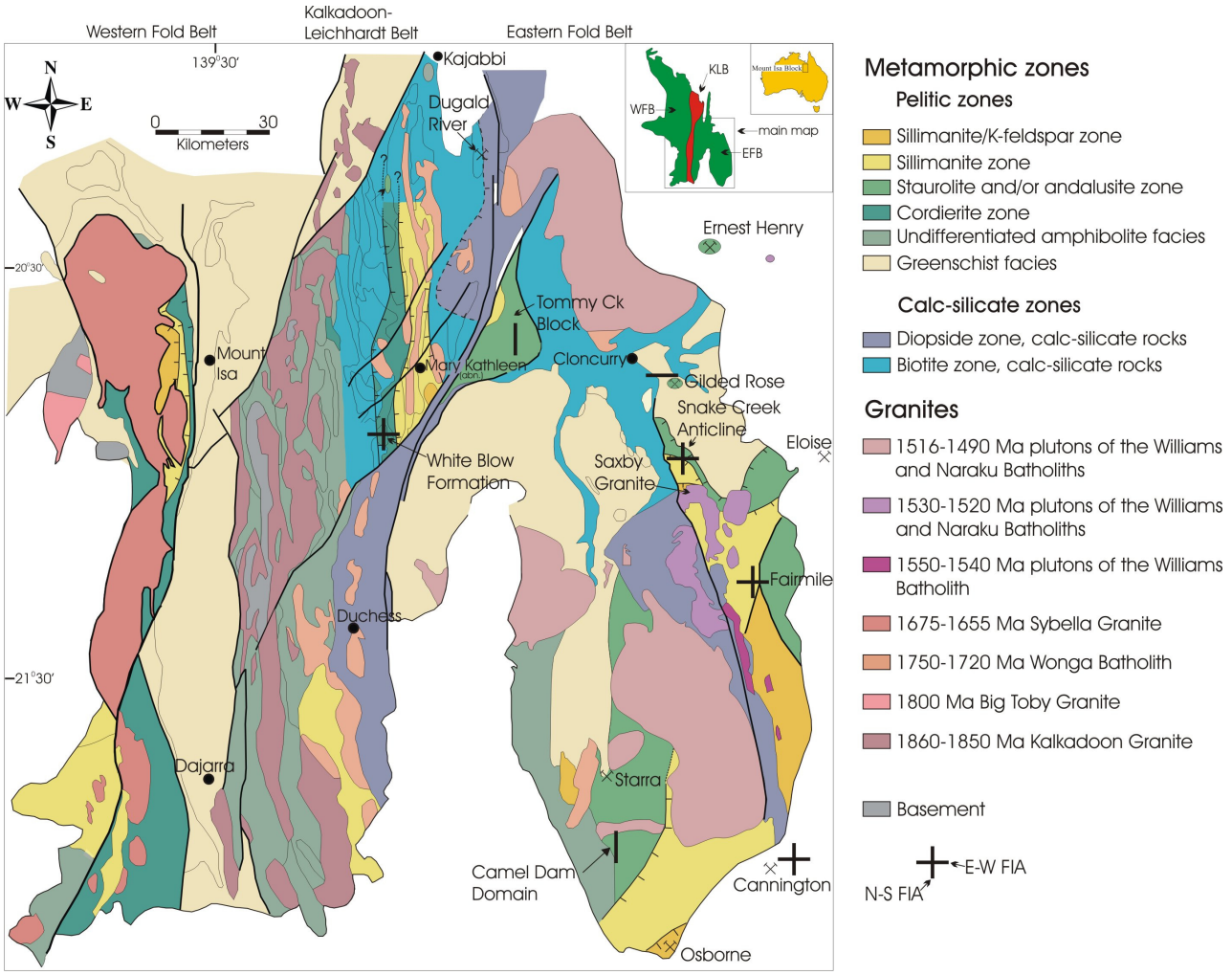

Fig. 6. Isograd Map of the Mt Isa Inlier, modified from Foster (2003, Appendix 1). Major mines and key areas in the Eastern Fold Belt are designated. Also shown are summary FIAs from Sayab (2005), summarized as either EW orientations (due to NS compression in D_1), or NS FIAs (due to EW compression in D_2), the latter representing orientations from NNW to NNE. Note the two NS zones of amphibolite facies in the Eastern Fold Belt, the Cloncurry-Osborne zone and the Mary Kathleen-Duchess zone

The overall isograd pattern is a series of amphibolite facies tongues elongate north-south, and alternating with greenschist facies belts. As a generalization, metamorphic grade decreases northwards, with the largest areas of sillimanite and sillimanite/K-feldspar rocks in the southeast of the Mt Isa Inlier. In the Eastern Fold Belt the higher-grade rocks are concentrated in two NS zones, one though Duchess and Mary Kathleen and the other from Osborne to Cloncurry (Fig. 6). There are no obvious relationships between metamorphic grade and stratigraphy. Grade changes across major faults such as the Cloncurry and Pilgrim Faults. Granites are absent from such greenschist facies areas as the Marimo Basin and the Duck Creek Anticline. A zone of granites (e.g. the Wonga Batholith) corresponds to the narrow high grade Wonga Belt extending through the Mary Kathleen-Duchess zone

(Fig. 6). There appears to be a broad spatial relationship between amphibolite facies metamorphic rocks and the Williams Batholith in the SE of the Inlier (Fig. 6).

A summary of the deformation and metamorphism sequence in the Eastern Succession is given in Table 2, omitting the first event D_w, which is the Wonga event of Pearson et al. (1992) and the "Big" event of Southgate et al. (2000) in the Eastern Fold Belt. Ages in the range 1735-1750 Ma are associated with this event This affected the Corella Formation and correlatives (Doherty Formation, Corella Beds) and the Double Crossing Metamorphics, but not the Soldiers Cap Group as this was not deposited at this time (Fig. 3). Greenschist to amphibolite facies, with the number of discrete events unknown.

Microstructures suggest that there are probably more events in D_1, D_2, and D_3 than those listed in the table, but these extra events rarely have a significant affect on the meso- and macroscopic structures.

Table 2. Summary of deformation events and Metamorphism in the Eastern Succession

Event	**D_{Ab}**	**D_1**	**D_{2a}**	**D_{2b}**	**$D_{3a,b}$**
Timing	1660-1630	Pre1595	1595		1527
Kinematics	Extensional Basin in CS3 times	EW folding	NS upright folding	Vertical shortening	N to NE upright folding
Fabrics		EW Axial planar foliation	NS Axial planar upright cleavage	Gently dipping crenulations	Crenulations, Reactivation of S2
Distribution		Local	Pervasive, dominant	Very localised	
Cordierite					
Garnet					
Staurolite		?			
Andalusite					
Kyanite					
Sillimanite			?		
Albite		?		?	
Chlorine		?		?	
Gedrite		?		?	
K Feldspar					
Brecciation					
Chlorite			?	?	

The most significant new aspect of this work has been the recognition of a very early albitizing event, labelled D_{ab}. This has been dated at 1660 – 1630 Ma from monazites in albitised samples from Snake Creek and Osborne mine. The coincidence of these ages with the depositional ages of the Mt Norna Quartzite and the Llewellyn Creek Formations is the basis for relating this event to extensional basin formation.

A composite P-T-t path for the Snake Creek area is presented in Fig. 7, with details given in Rubenach (2005a). Of critical importance is the abundant evidence of early cordierite replaced by andalusite (and staurolite, kyanite and sillimanite), andalusite to staurolite to andalusite reactions, and andalusite to sillimanite. Note that the paths only work because of

the metastable persistence of minerals that would have reacted out if strict equilibrium was maintained along the path. This in turn implies a type of "metamorphic fractionation" equivalent to igneous fractionation, so that strictly the bulk rock composition should be continually modified along the path. The restriction of kyanite to the north and northwest of the Snake Creek Anticline implies a field gradient such that maximum pressure decreased from the NW to the SE.

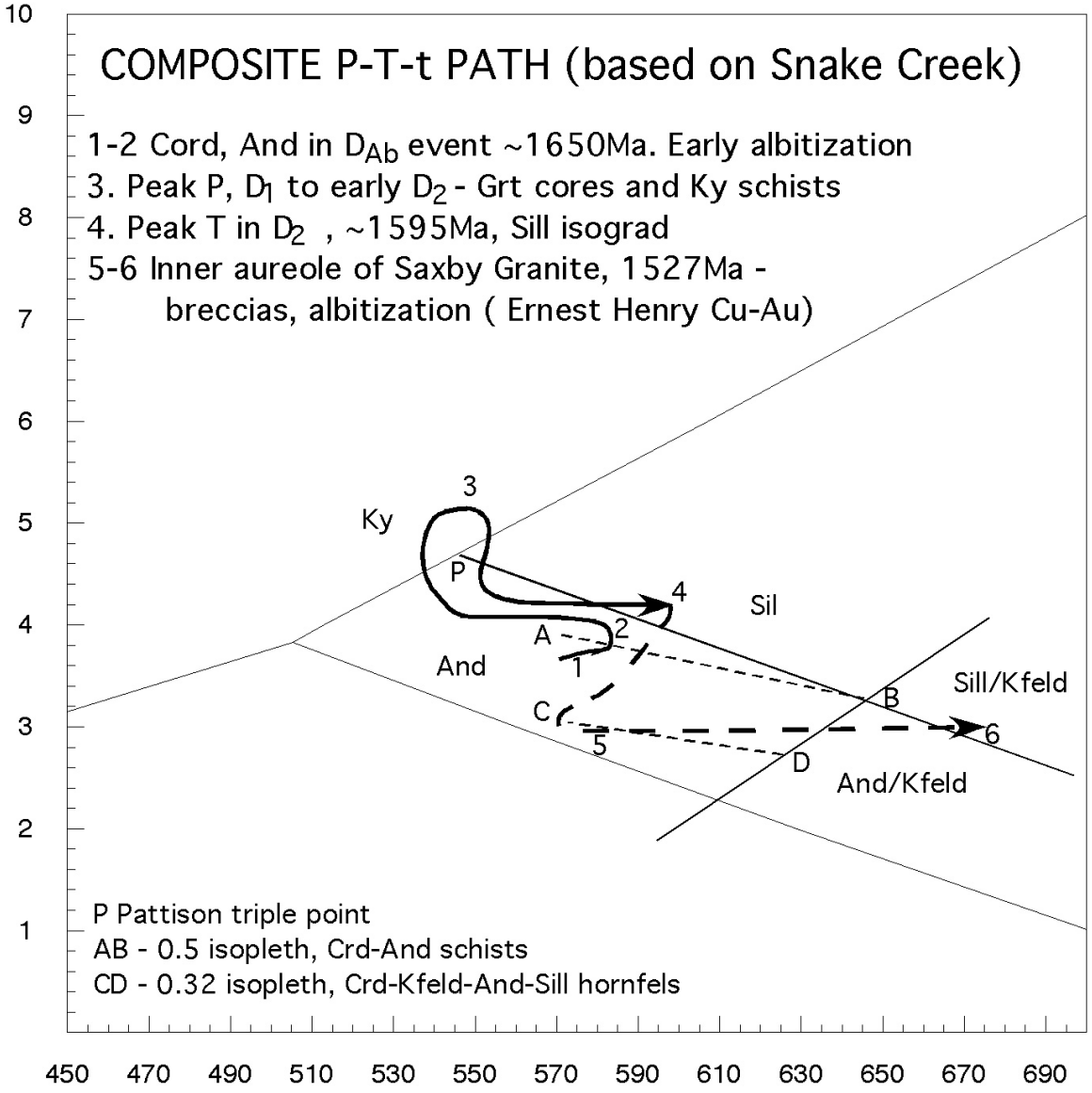

Fig. 7. Composite PT path for Snake Creek.

An important point about this complex P-T-t path is that it cannot be characterised simply as anticlockwise or clockwise, because there are several portions in both directions. Nevertheless, it is interesting that the maximum pressures are reached on a clockwise part of the trajectory, which apparently followed an earlier anticlockwise loop. The latter parts of the path, with isobaric heating events, correspond to granite intrusions. This path appears to apply to most of the Eastern Succession, but to differ from the Wonga Belt, which may have had a simpler anticlockwise P-T-t path.

The cooling history of the Eastern Succession consists of temperature reduction from 700ºC (in the south, Osborne mine) or 600ºC (Snake Creek) through to 300ºC at 1550 Ma (Osborne) or 1525 Ma (Snake Creek) with the exception of later heating events probably

due to granites of the Williams-Naraku suite that cause Ar-Ar cooling ages less than 1500 Ma in the eastern part of the Eastern Succession. Pressure constraints imply that the Eastern Fold belt was not significantly unroofed until after 1510 Ma, with perhaps only 3.5 km removed by 80 Ma after the metamorphic peak.

2.5 Summary

Crustal isotopic signatures suggest that there is a profound difference between the lower crust to the east and west of the Pilgrim Worm (Fig. 1), which may have been created by juxtaposition of crustal blocks in the early Proterozoic. These contrasting blocks were the basement to the two major depositional sequences, Cover Sequences 2 and 3. The geochemistry of the mafic rocks in the Marraba Volcanics suggests an arc environment for that group and possibly the whole of CS2. At 1686 Ma, before deposition of CS3 rocks, the crust may have been as thin as 8 km. Extensional basin formation, deepening to the east, is suggested for the thick CS3 rocks, with a thicker crust at this time, and a metamorphic event that reached 580ºC and *ca* 4 kb, involving albitisation. Although these are useful constraints, the specific geodynamic environment is unclear: for example whether a proximal back-arc or a distal intracontinental setting is appropriate. Some current evidence favours the latter (Scott et al. 2000; Giles et al., 2002). However, true continental rift basalts would be completely anhydrous, thus supporting the hypothesis of a hydrous (and Cl-bearing) subducted slab component to the magma.

The Isan Orogeny has no generally accepted geodynamic setting, with both intracontinental orogeny and continental collisional tectonics advocated. The earliest Isan contractional deformation was NS shortening, followed by the major deformation involving EW shortening at around 1595 Ma. Episodic magma emplacement in the latter stages of the Isan orogeny (1550-1500 Ma) may relate to periods of extension due to slab roll-back in a distal arc to the east, alternating with EW contraction. A-type granites may have been emplaced in this environment, thus demonstrating that granites classified geochemically as anorogenic can be emplaced syntectonically.

P-T-t paths in the Eastern Succession cannot be characterised simply as clockwise or anticlockwise. Early medium pressures and temperatures during the first metamorphic event were followed by a clockwise excursion into the kyanite field, then reduced P and T, before intrusion of dominantly felsic magmas associated with increased T from 1550 - 1500 Ma. This complex pattern is not diagnostic for any geodynamic setting, and it requires a heat source or sources for multiple metamorphic/intrusive events over the period from 1660 to 1500 Ma.

The central geodynamic problem of the Eastern Succession is how to achieve medium temperature metamorphic conditions episodically over this 150 Ma period, including a peak of metamorphism during a contractional orogenic event at *ca* 1600 Ma. Possible sources of heat include self-heating, due to relatively high contents of heat-producing radioactive isotopes in the metasedimentary rocks or adjacent granites, extensional tectonics, involving major crustal thinning and mantle upwelling, possibly accompanied by mafic igneous activity, or mantle delamination. There are time and space problems with all these hypotheses. The most likely direct cause of metamorphism was heat advection into the lower crust by melt migration above mafic intrusions, and into the upper crust by conduction. However, the ultimate source of such long-lived, episodic thermal anomalies is unclear.

3. ARCHITECTURE

3.1 3D geological model

Seven east-west geological cross-sections of the Eastern Succession of the Mt Isa Inlier have been completed from 7570000mN to 7750000mN at 30km spacing (Fig. 1). These sections show the crustal architecture from the top of the transition zone to the current land surface, and were the basis of a preliminary 3D geological model. .Revised chronostratigraphy (Foster and Austin, 2005), gravity, magnetics, worms (multiscale wavelet edges of potential field data) (Murphy, 2005) and seismic data (Lepong and Blenkinsop, 2005) were also used for the model (Blenkinsop et al., 2005a).

3.2 Revised chronostratigraphy

A revision of the Eastern Succession chronostratigraphy was essential as a prelude for constructing the 3D model. The standard chronostratigraphy is based on Blake (1987), but an abundance of new depositional, magmatic, and metamorphic age constraints have been produced since, including during this project.. The major changes to Blake (1987) have been:

- Including the Kuridala Formation with the Soldiers Cap Group;
- Moving the Llewellyn Creek Formation out of and below the Soldiers Cap Group;
- Moving the Soldiers Cap Group from Cover Sequence 2 equivalence (or older) to an unequivocally young, cover Sequence 3 age (most deposited *ca* 1675-1650 Ma).
- Grouping the siliciclastic rocks of the Mary Kathleen Group (Answer Slate, Marimo Slate, Stavely Formation) together as the informal Young Australia Group
- Grouping the Ballara and Mitakoodi Quartzites as age equivalents

Other changes that have affected the production of a new 1: 500 000 map are also described by Foster and Austin (2005).

The most significant change has been the definition of the Young Australia Group. This has allowed great simplification for section construction, since the Mt Albert Group, the Young Australia Group and the Soldiers Cap Group are regraded as lateral equivalents. (Fig. 8). This exercise also reveals that CS2 appears to be transgressive from west to east.

A yet more important result from the chronostratigraphic review is the identification of marked thickness changes across major structural boundaries, as shown in Fig. 9, and explained in more detail below.

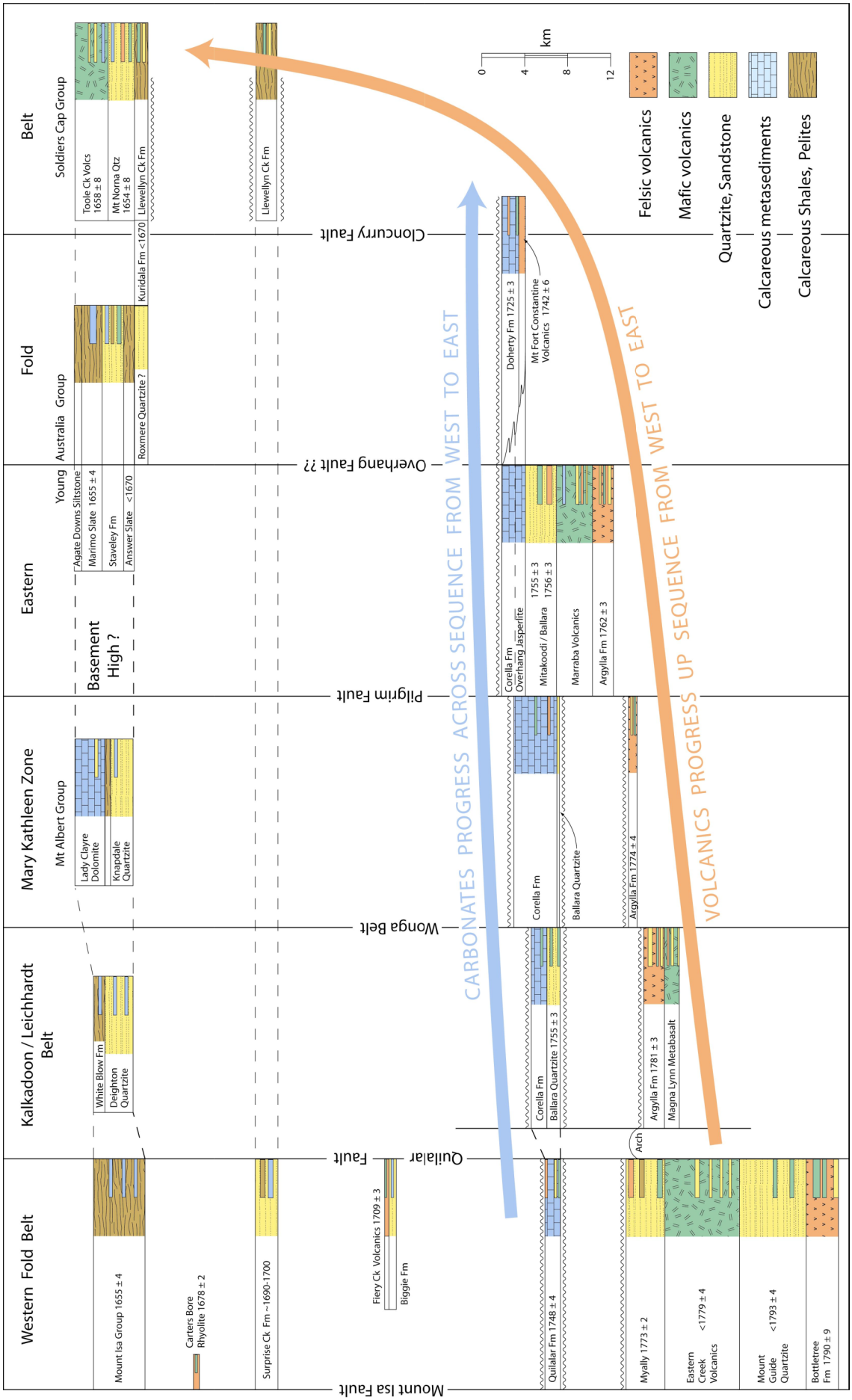

Fig. 8. Time –Space plot for the Mt Isa inlier, showing the lateral facies of Cover Sequence 3, and the transgressive nature of Cover Sequence 2

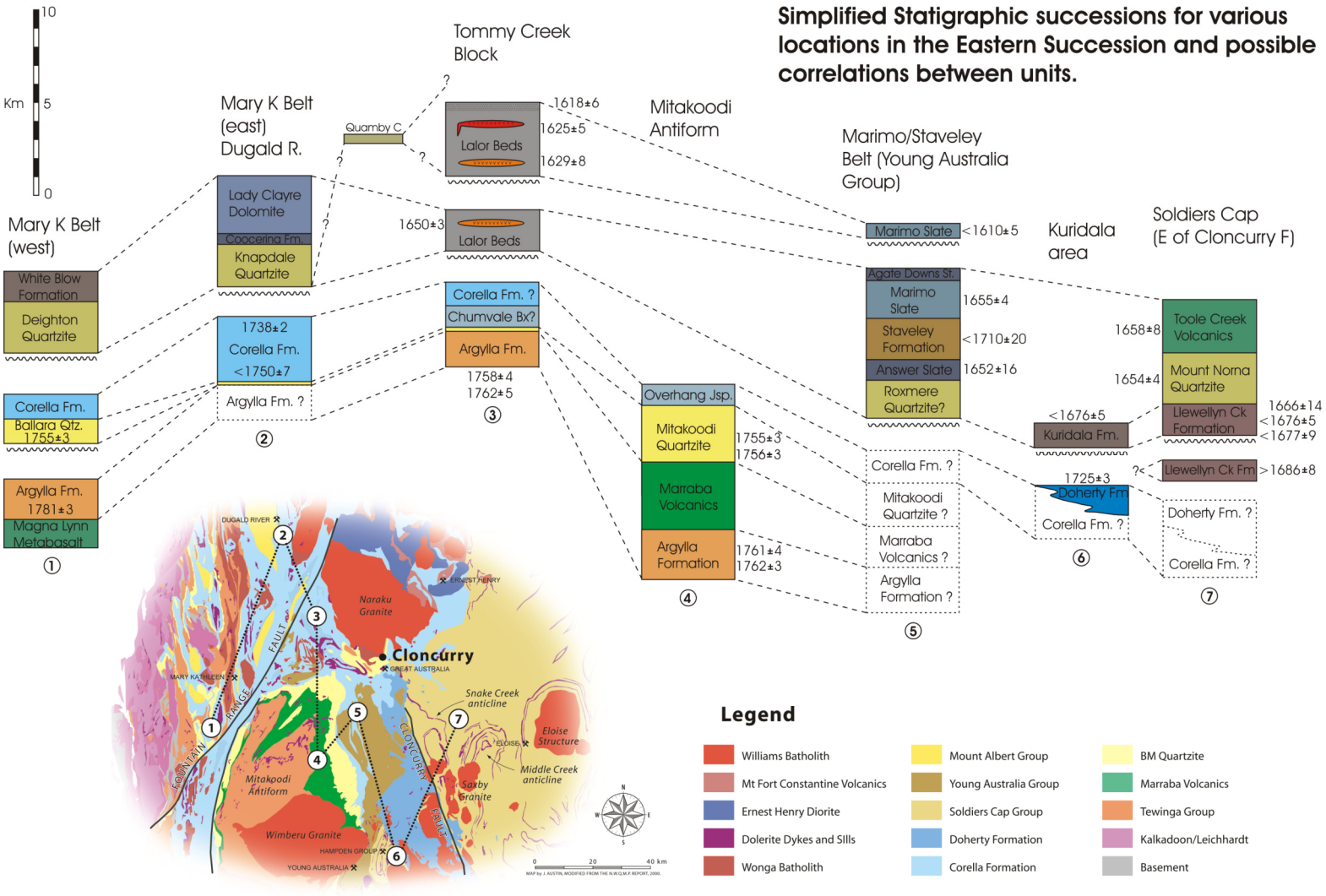

Fig. 9. Suggested correlations between simplified stratigraphic columns in the Eastern Succession.

3.3 Basement architecture

Basement architecture has been interpreted on the basis of the long-wavelength gravity features and the gravity worms. There are three major gravity worms referred to as the Kalkadoon-Leichhardt, (KL), Pilgrim and Cloncurry worms (Fig. 10), all trending generally NS.

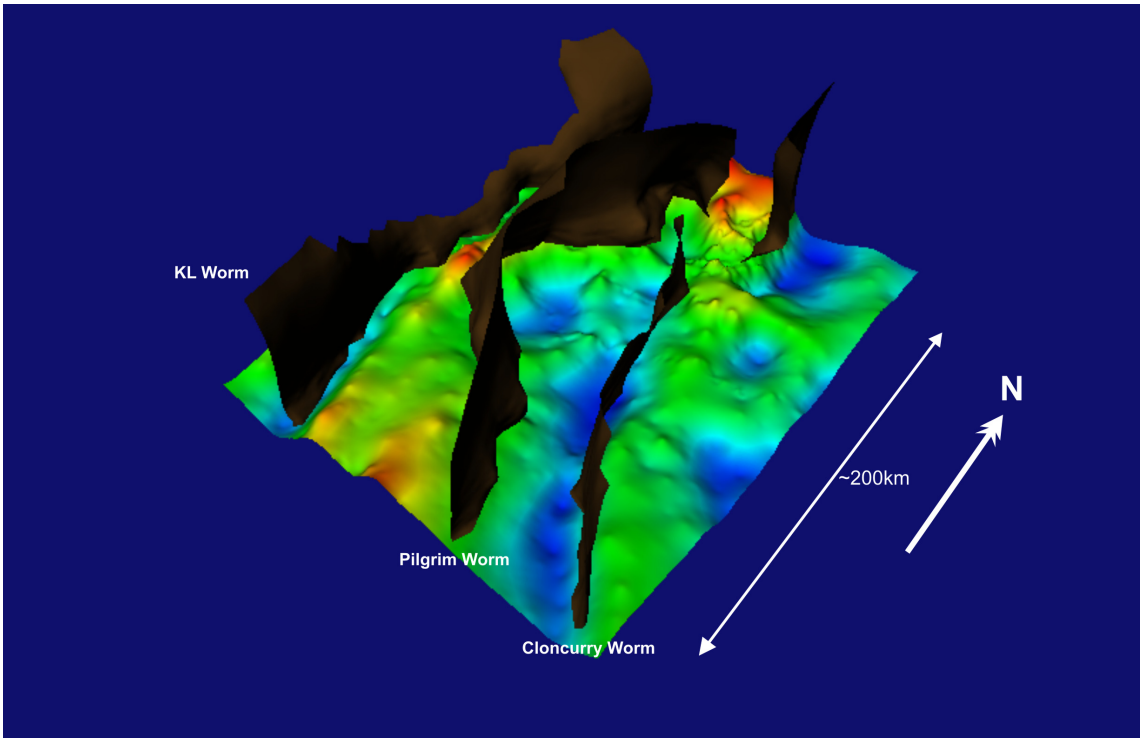

Fig. 10. Bouguer gravity anomaly as a 3D surface overlain by surfaces corresponding to the three major gravity worms.

The KL worm is a steep surface that intersects the ground at the western edge of the outcrop of Eastern Succession rocks. The Pilgrim worm is readily defined at high levels of upward continuation, but is less readily defined as a discrete structure near the surface, and there is no unique surface structure that corresponds to the Pilgrim worm, although it is nearly coincident with the Pilgrim fault in its central section. It dips generally to the west (indicating an east dipping density contrast). In the southern part of the model area, the NW-trending section of the Pilgrim worm (Figs. 1, 10) is likely to be due to the merging at high levels of upward continuation between the worm to the north, and separate, N- to NNW-trending worms through Selwyn and Osborne. The Cloncurry gravity worm dips steeply either to the west or east. It does not persist to the highest levels of upward continuation south of about 7700000mN. The Cloncurry gravity worm differs from the KL and Pilgrim worms in that it has a coincident magnetic gradient.

The major gravity worms are interpreted in the 3D model as steps in the lower crust because they separate long-wavelength anomalies of different magnitudes. Elevated gravity anomalies suggest a basement high. An alternate hypothesis would be that these gravity highs are caused purely by the intrusion of a large volume of mafic rocks in the regions that are now gravity highs. This is considered unlikely for several reasons. Firstly, the area of mafic outcrop is not high enough to significantly increase the average density at

the surface; secondly, the seismic refraction study suggests the density of the crust down to 18-20 km is "granitic" (i.e. metasediments, felsic volcanics, granite) in terms of its silica content (Goncharov et al. 1997); finally, if a large volume of mafic rocks was intruded into crust with a "granitic" composition, melting should occur producing granites with an S-type geochemical signature for which there is no evidence.

At the latitude of Cloncurry a subtle but consistent change in strike occurs in the gravity and magnetic anomalies, which are deflected to more easterly strikes over a zone approximately 20 km wide striking NE which is referred to here as the Cloncurry Flexure (Fig. 11). The distribution of gravity highs and lows changes across this structure, with a broad central high to the north and the two ridges to the south. The lack of a direct surface expression of this flexure, combined with the above observations suggest that it is a deep and fundamental crustal structure. It may have been a transfer zone during basin formation that has been active from early stages of basin formation through orogenesis.

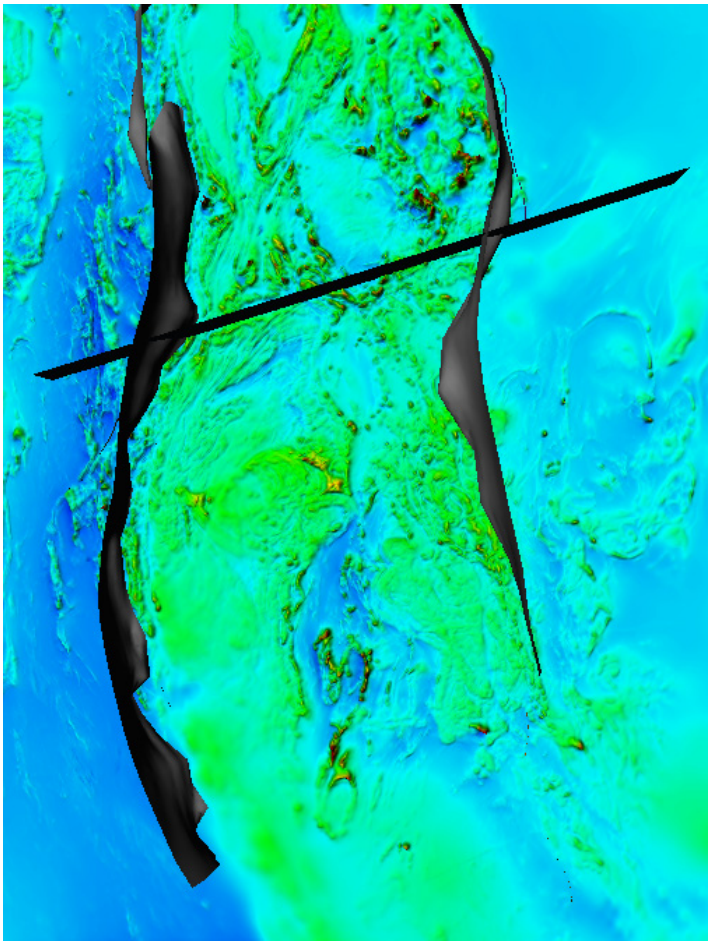

Figure 11. TMI Aeromagnetic image superimposed with surfaces representing the major magnetic worms showing a change in strike of major features at Cloncurry, represented by the ENE trending vertical surface: the Cloncurry Flexure

3.4 Depositional basin architecture and stratigraphy

The Eastern Succession rocks are interpreted to represent the western margin of a sedimentary basin that had a depocentre to the east of where Proterozoic rocks now crop out. This basin formed as the result of E-W extension and the Pilgrim and Cloncurry Worms and Cloncurry Flexure, are interpreted as formed by basement–cutting structures that were active during basin formation. CS1 rocks were deposited early during basin formation and outcrop only on its western margin. The lateral extent of CS1 and CS2 to the east is unknown. As basin formation progressed in CS2, the depocentre migrated to the east.

3.5 Upper crustal structure

Major new insights into upper crustal structure have come from reprocessing the Mt Isa seismic section and from building the 3D model, in particular from the use of aeromagnetic worms to constrain dips of contacts.

The newly processed seismic section (Lepong and Blenkinsop, 2005) suggests that a correlation of one reflector could be made with the base of CS2 on the west limb of the Mitakoodi anticlinorium, and this was used to constrain the shape of the fold: a similar reflector on the East limb was interpreted as the other limb. An important result from the reprocessed section is that a sub-horizontal surface, previously interpreted as a detachment (MacCready et al., 1998), could not be seen across the whole section (Fig. 12).

The major upper crustal folds on the crustal-scale cross-sections are the Mitakoodi Anticlinorium, the Snake Creek Anticline, the Weatherly Creek Syncline, the Middle Creek Anticline and a structure to the east of Eloise referred to as the Eloise structure (Fig. 1). Significant faults include the Fountain Range Fault, the Pilgrim Fault, the Overhang Shear, the Cloncurry Fault and a number of N-S faults inferred to be under cover in the eastern part of the area.

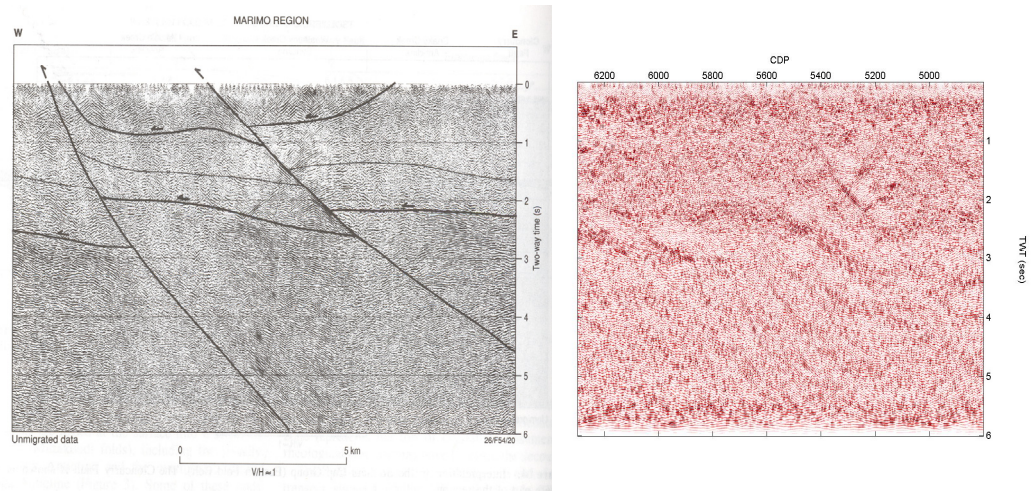

Fig. 12. Seismic sections showing previous interpretation by MacCready et al. (1998) (left) compared to reprocessed section by Lepong & Blenkinsop (2005) (right). The reprocessed section does not show the sub-horizontal reflector previously interpreted as a decollement by MacCready et al. (1998).

All the major folds have upright to steeply east dipping, approximately NS axial surfaces (Fig. 1). The Mitakoodi Anticlinorium, which is the largest fold, plunges gently N to NE and becomes the Wakeful Syncline and the Bulonga and Duck Creek Anticlines to the north. The Pilgrim worm at surface follows approximately the axial surface of the Mitakoodi Anticlinorium in the northern part. The Snake Creek Anticline is markedly different from the Mitakoodi Anticlinorium in that its fold hinge plunges subvertically in the northern part of the structure, and overturned beds are common. The Cloncurry worm structure underlies part of the Snake Creek Anticline, which is separated by the tight angular Weatherly Creek Syncline from the Middle Creek Anticline; the latter appears to have a similar geometry to the Snake Creek Anticline.

The Eloise structure is delineated on the aeromagnetic interpretation by almost continuous high susceptibility thin units, commonly in a pair, which are readily interpreted as mafic

sills by analogy with their signature around the Snake Creek and Middle Creek structures. The structure has been modelled as a doubly plunging synform on the basis of dips suggested by aeromagnetic worms over the mafic sills in the limbs.

The Mitakoodi, Snake Creek, Middle Creek and Eloise structures are all intruded by plutons of the Williams-Naraku batholith (respectively the Wimberu granite, the Saxby granite and the unnamed granite in the Eloise structure (Fig. 1).

All the major faults are subvertical at surface on the basis of dips given by corresponding worms, and strike approximately NS. Their depth can be inferred to some extent by the levels of upward continuation in worms corresponding to the faults. NE trending faults of generally shorter strike length appear to offset the Cloncurry Fault and worm dextrally in places.

A major regional structure is defined on the eastern edge of the Mt Isa inlier by both gravity and aeromagnetic worms, extending from Cannington in the south to north of the Ernest Henry mine, a distance of over 200 km (Fig. 1). These worms trends NNW and generally dip steeply to the east but also to the west in places. Because the worms are seen in high levels of upward continuation, their depth extent is inferred to be greater than 20 km. The surface trace of the magnetic worms is referred to as the Cloncurry Lineament, and was studied in detail (Austin, 2005) in order to understand the geological significance of major worms.

The worms that generate the Cloncurry Lineament, like other major worms, are continuous and relatively straight at high levels of upward continuation, but have a complex geometry at low levels. The gravity contrast across the worm shows that it marks an elevation of basement to the east. The Cloncurry Lineament does not have a unique or diagnostic expression in the surface geology, but it is a zone of highly folded metasediments, breccias, mylonites, and numerous granitic to mafic intrusions. The Cloncurry Lineament corresponds to three geological features: 1) the boundary between the Doherty Formation and the Soldiers Cap Group, 2) contacts of intermediate plutons of the Saxby Granite and Maramungee Granite and 3) NE-trending faults with dextral separations. Variations in the orientation and occurrence of these features are reflected in the complex geometry of the worm at low levels of upward continuation; at higher levels, they are simplified by the smoothing effect of upward continuation. Gravity data suggest that the Cloncurry Lineament cuts and displaces basement with an east side up sense, and it also coincides with part of the Snake Creek Anticline. Because of the crustal scale of the worms, the Cloncurry Lineament is interpreted as the surface trace of a major crustal fault.

The Cloncurry Lineament and the Cloncurry Fault are coincident around latitude 21.7 º S but diverge to the north so that the Cloncurry Fault is 10 km west of the lineament at 21º S. The Cloncurry Fault does not have a clear expression on the seismic line; the most likely orientation is sub-vertical, as judged by terminations of reflectors. An important aspect of the Cloncurry Fault discovered in this project is that there has been a component of post-Jurassic displacement on the fault. Jurassic sediments have a normal separation of 50 – 100 m to prominent beds of sandstone.

3.6 Intrusions

The largest intrusions are all bodies of the Williams-Naraku batholith (including the Squirrel Hills, Wimberu, Mt Angelay, Naraku, Saxby and Yellow Water Hole granites, and the unnamed interpreted granites south of the Wimberu granite and under the Eloise structure). Results from geophysical modelling of shallow crustal cross sections indicate that the edges of these granites generally dip steeply, but that the granites are no more than a few km thick. They have been shown as tabular bodies in the 3D model. Both radiometrics and aeromagnetic patterns show clearly that the larger bodies such as the Wimberu and Squirrel Hills granites are composite, containing several discrete intrusions which may have approximately concentric internal zones, and they contain a wide range of compositions.

3.7 Inversion in the Eastern Succession – A working hypothesis

A striking feature on the largest scale brought to light by the 3D model is the relationship between the structures corresponding to the major gravity worms and the major fold structures. The Mitakoodi anticlinorium overlies the structure corresponding to the Pilgrim worm and the Snake Creek anticline overlies the structure corresponding to the Cloncurry worm. Cross-sections 763 (Fig. 13), 766 and 769 show this relationship clearly. Stratigraphic evidence shows that the Pilgrim worm structure served as a major locus of thickening to the east from CS2 to CS3 times. This structure is likely to have been of fundamental significance since before the Isan orogeny, because it marks a contrast in lower crustal isotopic signatures (Mark et al. 2005a). The worm corresponds to a structure with a normal separation of basement. These observations are strong evidence that the Pilgrim worm structure represents a basement fault that controlled the architecture of the depositional basins in CS2 and CS3, with thickening to the east in its hanging wall if its dip direction has not changed. The Pilgrim worm structure also coincides with the axial trace of the largest fold in the model, the Mitakoodi anticlinorium. This suggests the hypothesis that the fault has been inverted, and that the Mitakoodi anticlinorium may have developed in response to reverse movement on a fault corresponding to the Pilgrim worm. In places the surface expression of the Pilgrim worm appears to be the Pilgrim fault itself.

Inversion is compatible with some features of the fault inferred to mark the Cloncurry worm, which may have played a role in the thickening of CS3 to the east. The location of the Snake Creek anticline on top of the Cloncurry worm structure (Fig. 13) may be due to the localizing effect of this structure, which may owe its steep and changeable dip direction to reorientation during positive inversion. Other structures inferred in the basement between the Cloncurry and Pilgrim worms may have played a role in the facies changes observed in CS2 and CS3 (i.e. the change from Corella to Doherty Formation in CS2 and from Young Australia to Soldiers Cap Group in CS 3), and the thickening of CS3 to the east.

In summary, the relationship between major basement structures, stratigraphy and contractional structures supports the hypothesis that positive inversion is a key process in the evolution of the inlier. The dominant role of NS structures was established at least as early as CS2 and continued throughout the crustal evolution.

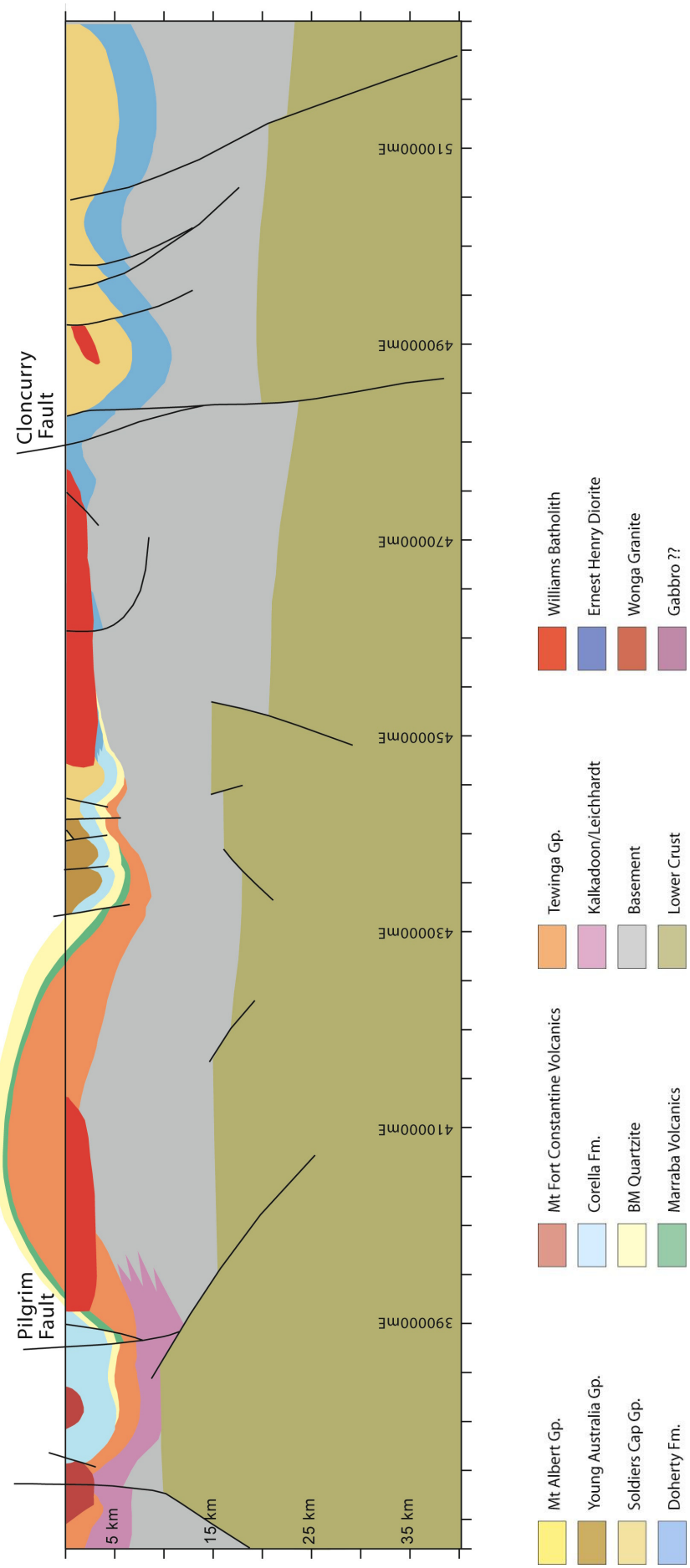

Fig. 13. Crustal scale cross section along line 763, showing how the Mitakoodi anticlinorium overlies the basement normal fault interpreted to cause the Pilgrim Worm. A similar relation exists between the Snake Creek Anticline and the structure corresponding to the Cloncurry worm.

3.8 Implications of positive inversion for crustal structure and basement-cover relations in the Eastern Succession

The alignment between stratigraphic changes, extensional, and contractional structures has an important implication for the relationship between the basement and cover in the Eastern Succession over the Pilgrim worm structure. This alignment would not be preserved if large-scale nappe structures or decollement had occurred either in extension or shortening. The cover appears to be broadly autochthonous relative to the Pilgrim worm. Decoupling on the order of a maximum of 10 km may have occurred.

This conclusion is not necessarily so surprising for D2 EW shortening, which is generally manifest in the form of upright folding. However, it is a significant constraint on any earlier deformation, for example NS shortening in D1.

The parautochthonous relationship of the cover to the basement implies that shortening must also have occurred in the basement. A simple line length balance over the Mitakoodi anticlinorium as drawn in cross-section 768 indicates a stretch of 0.44 (or 56% shortening), which must also have occurred in the basement. The present thickness of the crust is approximately 40 km, but evidence from the Ce/Y ratios indicates that it was only 8 km at 1686 Ma, giving a thickening factor of 5. Underplating, thrust stacking (possibly on reactivated normal faults) and penetrative deformation are all ways in which the crust may have thickened, and thickening may have occurred in more than one event.

4. FLUIDS AND METALS: DRIVERS, SOURCES, PATHWAYS, SINKS

4.1 Spatial data modelling

Spatial Data Modelling has been an important data source for evaluating key questions about fluids and metals involved in IOCG mineralization. Results from three different scales of study area are summarised in Mustard et al. (2005a). The following summarises the largest study only which occupies an area of 82,733 km^2 located between 325,000mE to 525,000mE and 7,955,000mN to 7,535,000mN (Fig. 14).

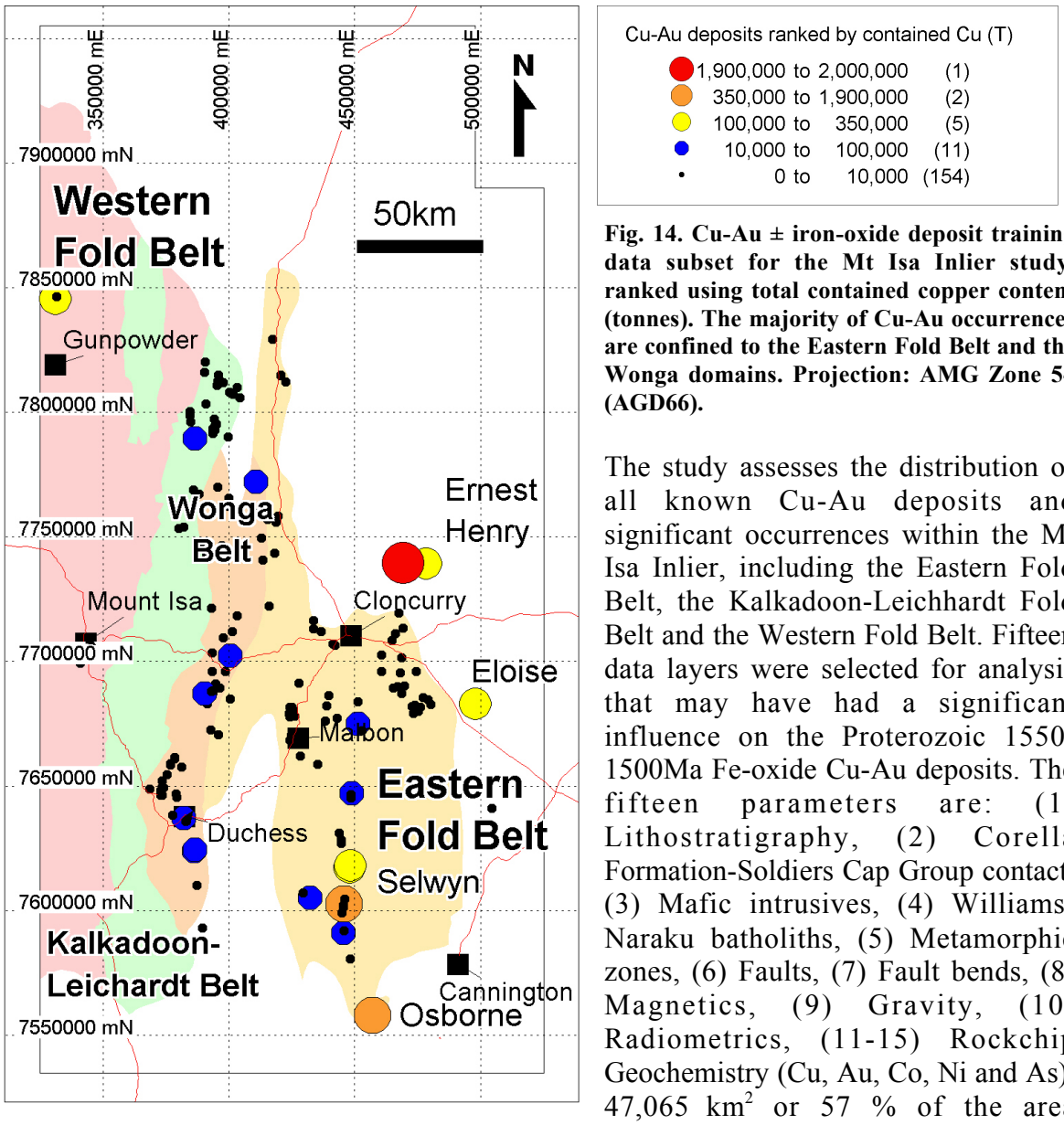

Fig. 14. Cu-Au ± iron-oxide deposit training data subset for the Mt Isa Inlier study, ranked using total contained copper content (tonnes). The majority of Cu-Au occurrences are confined to the Eastern Fold Belt and the Wonga domains. Projection: AMG Zone 54 (AGD66).

The study assesses the distribution of all known Cu-Au deposits and significant occurrences within the Mt Isa Inlier, including the Eastern Fold Belt, the Kalkadoon-Leichhardt Fold Belt and the Western Fold Belt. Fifteen data layers were selected for analysis that may have had a significant influence on the Proterozoic 1550-1500Ma Fe-oxide Cu-Au deposits. The fifteen parameters are: (1) Lithostratigraphy, (2) Corella Formation-Soldiers Cap Group contact, (3) Mafic intrusives, (4) Williams-Naraku batholiths, (5) Metamorphic zones, (6) Faults, (7) Fault bends, (8) Magnetics, (9) Gravity, (10) Radiometrics, (11-15) Rockchip Geochemistry (Cu, Au, Co, Ni and As). 47,065 km^2 or 57 % of the area comprises post-mineralisation cover belonging to Phanerozoic basins. For a large portion of this (16,162 km^2) or 20 % of the study area, the cover is <100m deep, with much of the potential of the region located in these zones.

A total of 567 Cu-Au occurrences are recorded in the Mineral Occurrence 2002 database within the study area. A subset of 181 occurrences were selected as the training data set based on the presence of both commodities (Cu and Au), and either recorded historical production or the existence of a cited geological resource (Fig. 14). Some of the main occurrences include Ernest Henry (167 Mt @ 1.1% Cu; 0.54 g/t Au), Eloise (3.2 Mt @5.8% Cu; 1.5g/t Au; 19g.t Ag), Osborne (11.2 Mt @ 3.51% Cu; 1.49 g/t Au), Mt Elliot (3.3 Mt @ 3.6% Cu; 1.8 g/t Au), Starra (6.9 Mt @ 1.65% Cu; 4.8 g/t Au) and Mt Dore (26 Mt @ 1.1% Cu; 5.5 g/t Au; Williams and Skirrow, 2000).

The training sites selected are a critical factor in determining the meaning of a model. The shared characteristics of the Cu-Au ± iron-oxide deposits in the Mt Isa Inlier provide a sound basis for treating the deposits as a single related group or training data set with common genetic features, despite the wide range in geological styles. The subset of 181 Cu-Au ± iron-oxide occurrences was chosen because the targeting was aimed at the larger, more significant examples. Spatial correlations were calculated using the Weights of Evidence technique using the Spatial Data Modeller extension developed for MapInfo software. A unit area of 0.25 km^2 was used in these calculations assuming the known deposits have a 0.25 km^2 area of influence.

Geological data such as lithological and structural information was derived from the Northwest Queensland Mineral Province Report (Queensland Department of Mines and Energy, 2000). The report provides a solid geology map of Proterozoic basement and structural framework based on an integrated interpretation of outcropping geology combined with aero-magnetics and gravity. As a result, this data potentially enables us to look under cover. The high resolution regional aero-magnetic and radiometric data was obtained from Xstrata. Regional gravity data was provided by Geoscience Australia. Surface rock chip geochemistry was obtained from the Geological Survey of Queensland geochemical database (Queensland Department of Natural Resources and Mines, 2003) and the Rockchem Database from Geoscience Australia.

4.1.1 Results

Table 3 ranks the parameters analysed from one to twelve in terms of their spatial association with the Cu-Au deposits. The higher the contrast (C), the better the spatial association. As a rule of thumb, Contrast values above 0.5 are considered reasonable and Confidence values above 1.5 considered better than random.

Ranking	Key Ingredient	Contrast	Confidence
1	Copper in rockchips (>249 ppm Cu)	2.50	36.31
2	Gold in rockchips (>0.11ppm Au)	2.38	26.45
3	Corella-Soldiers Cap Contact (750m buffer)	1.87	13.98
4	Aeromagnetics (magnetic highs)	1.82	14.36
5	N-S and ENE faults (650m buffer)	1.45	17.20
6	Mafic Intrusives (750m buffer)	1.25	7.47
7	Lithologies (dominantly Cycle 3)	1.21	5.09
8	Gravity (Gradients)	1.03	15.91
9	Bends on N-S and ENE faults	1.03	2.33
10	Metamorphic Grade (Amphibolite Facies)	0.98	7.85
11	Radiometrics (U/Th)	0.83	4.46
12	Williams and Naruku batholiths (4km buffer)	0.64	3.36

Table 3. Ranking of critical ingredients for the Mt Isa Cu-Au study based on Contrast values.

Rockchip geochemistry is clearly the best parameter for Cu-Au occurrences. Cu and Au in rockchip geochemistry are the only two parameters that produced C values above 2, returning 2.5 and 2.38 respectively. Note however that geochemistry is restricted to areas of outcrop.

Corella + Doherty Formation / Soldiers Cap Group contact. A significant proportion of the Cu-Au mineral occurrences were located less than 750m from the contact between the Corella + Doherty Formation (CS2) and Soldiers Cap Group (CS3). The Corella + Doherty Formation consists of calc-silicate rocks, marbles and minor pelitic and volcanic rocks, whereas the Soldiers Cap Group consists of siliciclastic metasedimentary rocks and mafic metavolcanics. The juxtaposing of these different rock types may provide: (1) a physical barrier to upward directed fluid flow from the more permeable into less permeable rocks (2) favourable sites for fluid mixing or fluid-wallrock reaction, (3) regions of significant chemical and/ rheological contrast.

Aeromagnetic highs, which may reflect areas of magnetite ± pyrrhotite precipitation, also have a strong correlation with Cu-Au occurrences. However, the spatial relationship between Cu-Au deposits and iron oxides (reflected by magnetic highs) is not simple. Despite these problems, the high contrast values generated in the weights of evidence study indicates that aeromagnetics is a very effective exploration tool for targeting Cu-Au mineralisation in the Mt Isa inlier. It provides targets that are potentially mineralised and significantly reduces the area that requires exploration.

Structure. The ENE and NS orientated fault sets have a strong to moderate association with Cu-Au occurrences. All significant Cu-Au deposits in the study area are associated with at least one of these two orientations. The spatial association of Cu-Au occurrences with fault bends indicates a moderate to strong association with fault bends on ENE faults (Ernest Henry), SSE and N-S faults. The spatial association of Cu-Au occurrences with fault intersections indicates intersections with ENE faults were best, followed by SSE, NNE and N-S faults (Table 3). Continued east-west directed shortening during D_2 and D_3 has been accommodated by movement along pre-existing fault zones.

Mafic Intrusions. The Cu-Au deposits within the Mt Isa study area have a strong spatial association with mafic intrusions with a significant proportion located < 650 m from or within these rock types. Distance to mafic intrusions (650 m buffer) has a much higher contrast C values than does distance to Williams and Naraku intrusives (4 km buffer). The suggested roles of mafic intrusions in IOCG deposits include: (1) A potential source of

sulphur ± metals (leached during hydrothermal activity or contributing directly), and (2) Rheological and chemical contrast (reduced).

Gravity. Weights of evidence indicated that gravity highs and steep gradients adjacent to gravity highs or gravity lows have a strong spatial association with the Cu-Au occurrences. The gravity highs are considered to reflect large volumes of mafic rock within the middle to upper crust. The gravity gradients are interpreted to reflect a combination of crustal scale basement architecture as well as the margins of large felsic intrusions.

Felsic Intrusions. Although O, C, H and S isotope studies suggest that magmatic fluids provide a dominant component to IOCG deposits, the interpreted source have a moderate spatial association with coeval granites. If granitic fluids are responsible then they must have travelled several km's from their source, whist retaining their isotopic signature.

4.2 Metal and fluid sources

4.2.1 Mafic intrusions as a metal and fluid source

The 1686 Ma (and similarly the 1660-1650 Ma Toole Creek Volcanics) mafic rocks of the Soldiers Cap Group were derived via strong fractionation of an Fe-picrite parental magma (Butera et al., 2005). The systematic decrease in the S and metal concentrations of these magmas with increasing Fe content shown in Fig. 15 can not be explained by

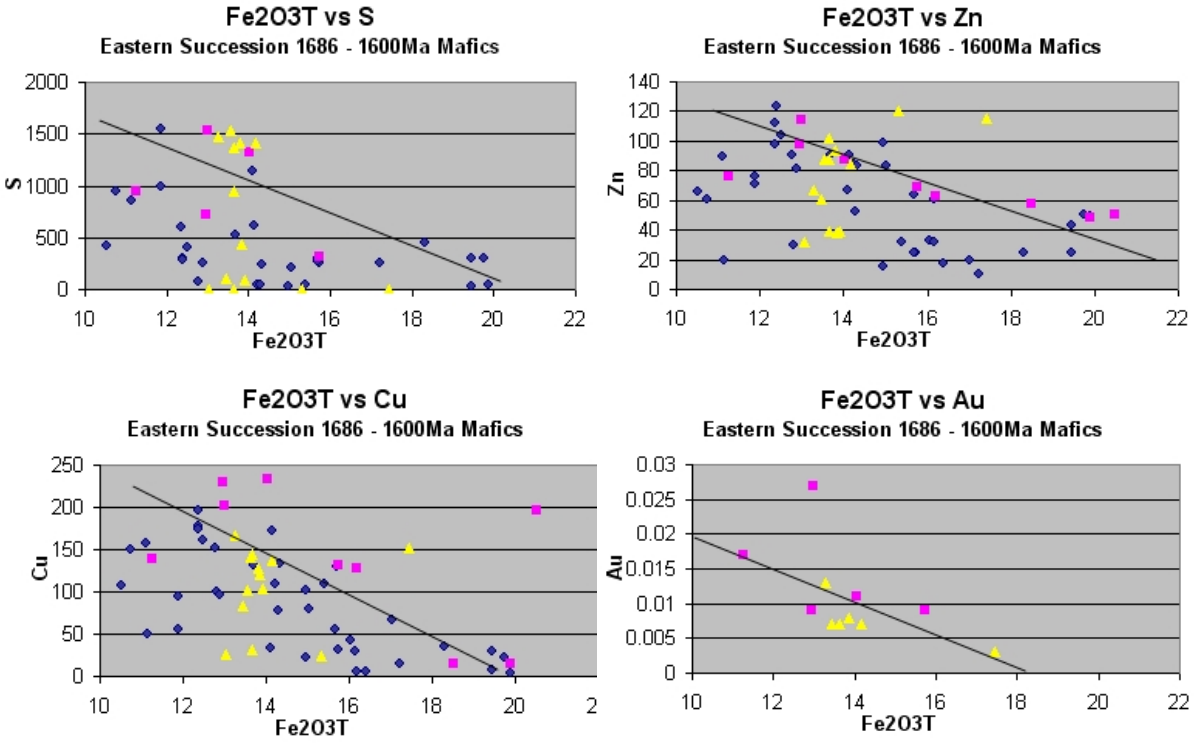

orthomagmatic sulphide

Fig. 15 a-d. Fe2O3T vs S, Cu, Au, Zn displaying consistent decreases in S and metals with increasing Fe content (fractionation). The slope of the line on each graph (position estimated from least altered samples) illustrates the S, Cu, Au, and Zn trends with increasing differentiation of the magma. The majority of the points below the lines are interprted as representing elemental losses during metamorphism, while points above the lines are likely to represent enrichment associated with hydrothermal alteration. Data from KB 1686MA (pink), KB 1600Ma (yellow) and Ozchem Database *ca* 1686-1650Ma (blue).

sulphide precipitation, because these melts lie well below the sulphide saturation values at 2.2 kb. The decrease in S and metal concentrations with increasing fractionation reflects the increasing ability of an exsolved aqueous fluid to transport these elements out of the magmatic system. Some of the Fe-oxides and Au-bearing iron and iron-copper sulphides present in the mafic rocks as interstitial minerals to late stage magmatic silicates were most likely precipitated from this exsolving fluid.

The minimum amount of S, Cu and Au that has been exsolved from the mafics and potentially contributed to the overall IOCG budget, can be estimated by taking into account that the mafic rocks intimately associated with IOCG mineralisation average around 15.6wt% Fe_2O_3 (total). The highest concentrations of S, Cu, Au and Zn appear to correlate with a melt containing *ca* 11 wt% Fe_2O_3 (initial Fe content of pre-fractionated magma). A melt containing 15.6wt% Fe_2O_3 (total) would contain *ca* 1.22 wt% H_2O available to leave the system along with *ca* 350ppm S, *ca* 10 ppb Au, and *ca* 55 ppm Cu. For the measured volume of *ca* $2x10^{11}$ m^3 down to 2000m depth for mapped *ca* 1686-1650 Ma mafic rocks of the Angelay-Selwyn area, this corresponds to *ca* $2.1x10^8$ t S, *ca* $3x10^7$ t Cu and *ca* 6000 t Au, or an IOCG deposit @ 1% Cu and 0.5 g/t Au of *ca* 3 Bt. This is *ca* 10 times more mineralisation than has been thus far discovered in the area (334 Mt). Conservatively then, the observed surface outcrop of mapped mafic rocks of this age, extrapolated to 200m depth, can account for the total Cu budget of the district, if Cu was extracted and deposited at 100% efficiency at the time of final crystallisation of the mafic magmas. Even if transport and deposition processes were inefficient, the calculated maximum amounts of metals and sulphur that could have been derived in this manner are extraordinarily high compared to the known deposits.

4.2.2 Metamorphic fluids and leaching of mafic rocks as a metal source

The main phase of the Isan Orogeny liberated metamorphic CO_2 from the Corella Fm and equivalents, and H_2O from the Soldiers Cap Group, as well as significant quantities of salt probably from scapolite breakdown (Butera et al., 2005). However, stable isotope data from carbonate veins hosted in the Soldiers Cap Group require a mixed CO_2-source, from both Corella Fm carbonates (by dissolution or devolatilisation), but also from a magmatic or mantle source. As felsic magmas were absent at this time except for pegmatites at Osborne, mafic rocks or the mantle are clearly implicated in the metamorphic fluid budget. The key characteristic of fluids at this time (metamorphic-magmatic-mantle) was their reduced nature, unlike at least some fluids exsolved off the later Williams Batholith.

Geochemical investigations of mafic rocks that have undergone varying degrees of metamorphism reveals that S and certain metals are scavenged from the rocks, proportional to the degree of metamorphic recrystallisation (or amphibolitisation) (Butera et al., 2005). Figure 16 shows an isocon plot comparing igneous-textured dolerites retaining clinopyroxene and magnetite, compared with hydrothermally altered and/or amphibolitized and variably foliated equivalents. Clearly outlined is the significant loss of S, Cu, Au, Ni, Zn and Cr, while additions to the rocks via metamorphic fluids include Ba, U, Sn, and Sb.

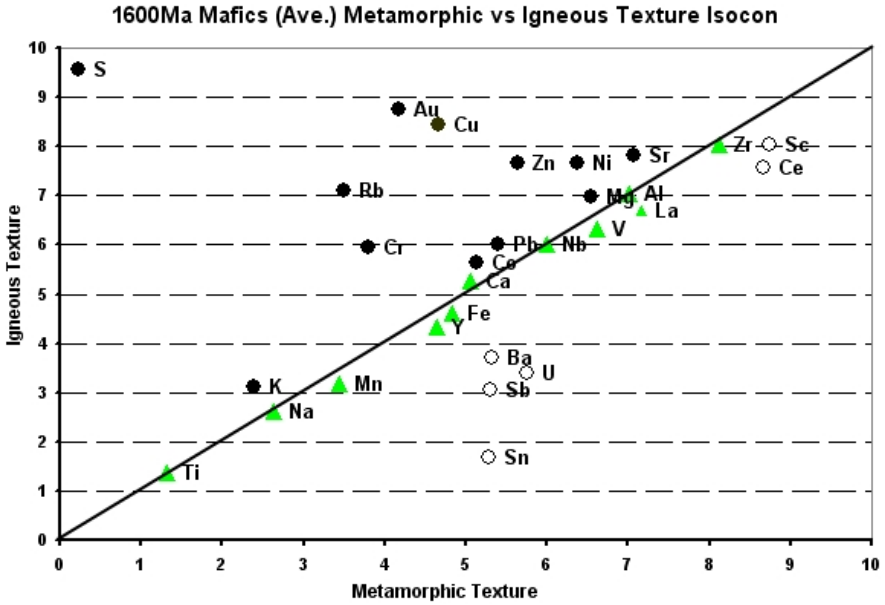

Fig. 16. Isocon plot (with individual elements multiplied by factors which distribute them from 0 to 10) of average geochemical analysis for elements of igneous textured vs metamorphic textured dolerites from the Snake Creek Anticline. Significant loss of S, Au and Cu during metamorphism (black dots) have potentially contributed important amounts to the IOCG metal and sulphur budget. Green triangles are inferred immobile elements, including Fe; open circles are gains.

A semi-quantitative analysis of the S and metal loss via metamorphic leaching processes highlights the potential for mass contribution to the IOCG budget. For the volumetrically significant 1686-1650 Ma mafic rocks, the rock compositions indicate leaching of 747ppm S, 53 ppm Cu and 6 ppb Au, or 66%, 26% and 37.5% respectively. For an assumed 2000 m depth for mafic rocks over the Selwyn Angelay study area, and 70% amphibolitisation of all 1686-1650 Ma mafic rock (Foster, 2003), a minimum addition to the IOCG sulphur and metal budget via this process would be *ca* 300 Mt S, 21 Mt Cu and 2470 t of Au. On a 2 to 1 py:cpy ratio, and an average grade of 1% Cu, 0.5g/t Au, this addition could be capable of directly forming a minimum *ca* 2 Bt of IOCG ore, quite comparable to the amounts of these elements released by the aforementioned syn-magmatic volatile release.

4.2.3. The Williams–Naraku intrusions as a fluid and metal source

Many of the district's IOCG deposits have Ar-Ar and some U-Pb ages synchronous with the 1530-1500Ma Williams-Naraku Batholith of felsic to intermediate intrusions (e.g. Williams, 1998; Oliver et al., 2004), leading to hypotheses of a direct magmatic-hydrothermal connection between these granitoids and the IOCG deposits (e.g. Perring et al., 2000; Pollard, 2001). A connection between 1530 Ma magmas and IOCG deposits was made by Williams (1998) and Oliver et al. (2004) who demonstrated that some of the ingredients found in the deposits may have been leached from various country rocks by the passage of magmatic-hydrothermal oxidised brines. Fluid inclusions at Lightning Creek are distinctive for their highly elevated Fe, Ba and Cu contents, implying at least one of the fluids present was sulphur-deficient (Perring et al., 2000). The apparent absence of sulphur in these granite-proximal fluid systems, but the presence of sulphur with distinctive mantle- or magmatic _^{34}S values in the deposits, requires derivation of deposit sulphur from sources other than the *ca* 1530-1500Ma Williams Batholith.

The Williams Batholith released large volumes of oxidised, sulphur-poor fluids that locally carried copper and iron, and released some of this fluid via violent brecciation processes. This fluid may have oxidised earlier reduced iron oxide ± sulphide assemblages at Osborne and Starra. Without adding significant copper, such oxidised fluids may simply have remobilized earlier IOCGs and produced hematite-ore associations that reworked or possibly concentrated earlier copper produced during or before peak-metamorphism

Recent studies have demonstrated that the most effective mechanism by which Cu and Fe may partition into a granite-derived hydrothermal fluid is via magma mixing with mafic magmas (Kress, 1997; Edmonds et al, 2001; Hattori & Keith, 2001). Magma mixing and mingling is evident throughout the Williams-Naraku Batholith, with a large proportion of the batholiths comprised of dioritic and monzodioritic to granodioritic intrusions. Further evidence for magma mixing potential is provided by magnetic highs at the base of the felsic plutons that we interpret to be large, underlying mafic bodies. The addition of this Cu and Fe into the IOCG district, along with remobilisation of pre-existing ores, may have resulted in partial or complete destruction of recognisable pre-1530Ma ore characteristics and the possible accumulation of new ores.

4.2.4 Reduced, mantle-derived fluids

Another important fluid source at 1550-1500 Ma was probably derived by mantle degassing (Rubenach and Oliver, 2005) (the "carbonatite connection"), as inferred from the association of calcite-actinolite-clinopyroxene-apatite with minor titanite-pyrrhotite-chalcopyrite at Knobby Quarry (MKFB) and similar high temperature calcite pods in the Eastern Succession. These fluids contained reduced sulphur, abundant CO_2, and Ca- and Na-chlorides (Fu et al., 2003). Although the surrounding albitic alteration was previously inferred to be related to salt dissolution or a felsic magmatic component in this fluid (e.g. Oliver et al., 1993), partial melting of seafloor-altered oceanic crust can carry alkalis into the crust during subduction. Given that there are no Williams-age felsic intrusions in the MKFB, then speculation of a mantle source to these fluids is warranted. Trace element geochemistry of apatite and carbonates should be used to determine the extent to which such fluids were directly mantle-derived.

4.2.5 Fluid pathways and drivers

The pre-eminent role of NS faults as fluid pathways is clear from the prospectivity analysis in which this group of faults has the closest spatial association to Cu-Au deposits. This is a logical consequence of their early formation and long-lived history of reactivation. NE faults are also very important. Fault intersections (which can allow pipe-like fluid flow) between the NS and other faults, and fault bends are also associated with deposits.

Some of the diversity in the range of IOCG deposit types and models may be due to the importance of fluid transport and mixing in their genesis. A common mineralizing process could generate deposits in a variety of host rocks depending on the fluid pathways. The dominance of the fluid pathways means that fluid sources cannot be clearly recognized from spatial associations of the deposits alone, and mineralizing fluids may be complex and heterogeneous in view of their possible interactions with a variety of wall rocks. A detailed understanding of fluid pathways and structures at all scales is the most important direction for future research. Mechanical modelling directed at understanding fluid flow in

the Mt Isa Eastern Succession based on this structural knowledge will also be an important tool.

Numerical modelling based on discrete element analysis has generated some important insights into fluid pathways and drivers (McLellan & Oliver, 2005). Sites of lower mean stress, lower least principal stress, lower values of pore fluid pressure required for failure, and higher differential stress and fluid flow rates can be taken to indicate fluid pathways and possible mineralization. The modelling compared pre-1550 and 1530 Ma states to evaluate the effect of granite intrusion on fluid flow. The best results, as evaluated by comparing sites at yield with known deposits, were achieved for the 1530 Ma model. Stress and failure-influenced fluid flow on pre-existing faults appears to have been an important influence on fluid pathways. Furthermore, the intrusion of granites would have had a significant effect on creating more heterogenous fluid flow and conditions favourable to the creation of more potential sites of mineralization

4.3 Genesis of IOCG deposits

Spatial, temporal and geochemical evidence now supports a much more important role for mafic magmas and rocks in IOCG deposit genesis than previously recognised. Mafic rocks of similar composition were intruded over 150 Ma from 1680 to 1500 Ma, and could have provided a source of both metals and sulphur, either in magmatic-hydrothermal metal-rich volatile fluids during crystallisation or by subsequent leaching during metamorphism. Hydrothermal, albitisation and metamorphic events at 1640 Ma, 1600-1580 Ma and 1530-1500 Ma were all capable of remobilising pre-existing sulphide concentrations, from deposits, proto-ores or disseminated country rock metal accumulations, at scales of less than 1 km. Oxidised hydrothermal brines and albitic fluids associated with the 1530 Ma felsic-mafic mixed Williams-Naraku Batholith may have leached further metals, and potentially added more copper to the system directly, but probably did not directly contribute sulphur.

Fluids for metal transport may have originated in one of four ways:

1. As direct magmatic-hydrothermal fluids from the crystallising mafic magmas
2. As metamorphic fluids
3. As magmatic-hydrothermal fluids from crystallising felsic intrusion of the Williams batholith.
4. A direct or indirect mantle source, as implicated in the genesis of the Ernest Henry deposit (Cleverley & Oliver, (in revision); Oliver & Cleverley, 2004; this report).

Fluids from, or passing through, mafic rocks deposited metals by mixing or wall-rock interaction in the vicinity of the mafic rocks, within N or NE faults, particularly on bends and at the Corella + Doherty Formation contact with CS 3 hosts.

A summary diagram of the processes leading to IOCG ore deposition is given in Fig. 17.

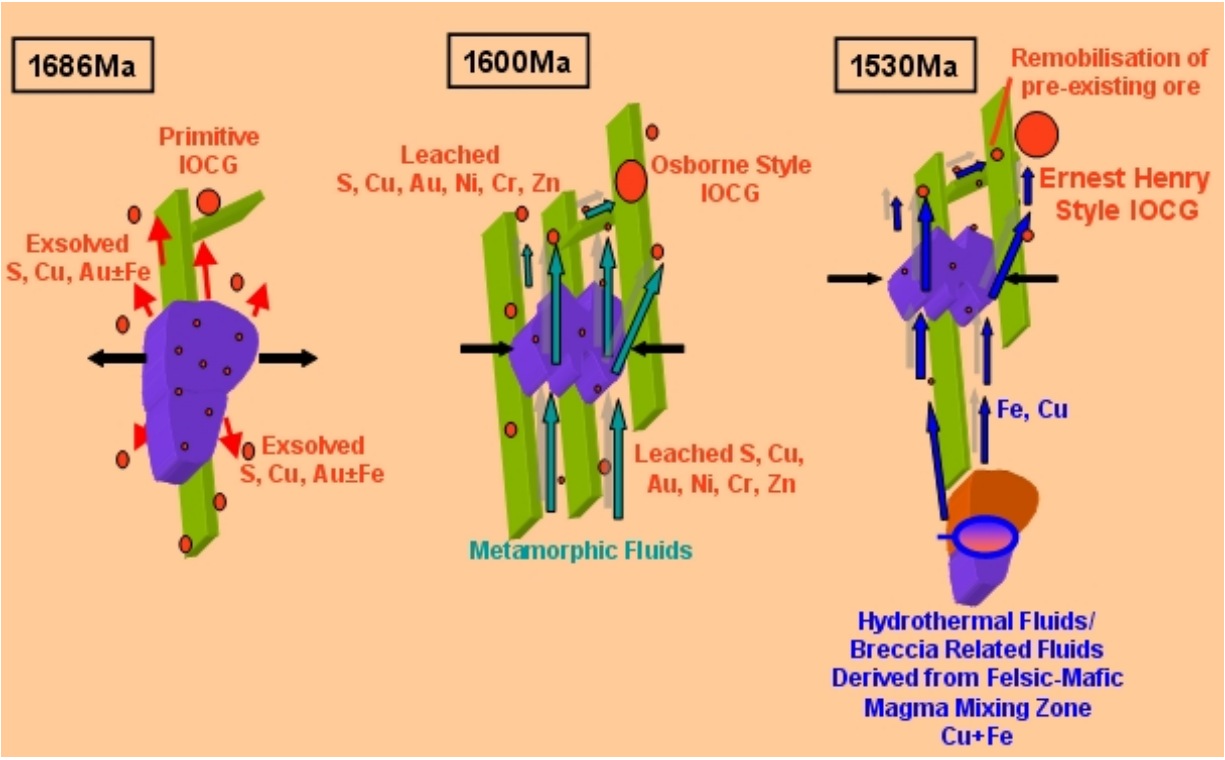

Fig. 17. Evolutionary model of the contribution of S and metals via direct exsolution from mafic magmas at 1686Ma, metamorphic leaching at 1600Ma, and hydrothermal remobilisation with addition of Cu and Fe from mixed felsic-mafic magmatic fluids at 1530Ma.

A more speculative model, which includes a hypothetical direct mantle CO_2 fluid, has the following steps and is illustrated in Fig. 18.

1. Prior to 1550 Ma, significant concentrations of IOCGs had already occurred, by release of fluids directly off the top of crystallising mafic intrusions, potentially even by exhalation in mixed sedimentary-mafic rock packages, and probably by leaching and reprecipitation during regional metamorphism (Butera et al., 2005).
2. At *ca* 1550 Ma, a phase of extension or possibly volatile fluxes from deep in the mantle lithosphere triggered renewed generation of basaltic melt just below the Moho, and triggered anatexis of lower crustal felsic melts with a distinctive mantle radiogenic isotope signature (Mark et al., 2005a).
3. Some felsic intrusions, e.g. Lightning Creek, may have been contaminated with voluminous mafic melts at a relatively early stage of crystallisation, leading to widespread mingling, mixing, and transfer of metals in the melts. The net result may have been dispersion of metals throughout the mafic/felsic complex, retention of sulphur in the mafic rocks, rapid saturation of iron oxides in the mingled zones, and precipitation of magmatic-hydrothermal magnetite bodies.
4. Other felsic intrusions evolved to a much greater extent by protracted crystallisation (e.g. Mt Angelay, Mt Margaret), such that the remaining felsic liquid was near saturated with large volumes of oxidized, hematite-stable brine. Emplacement of CO_2-and possibly Cu-bearing mafic magmas into these rocks may have triggered release of Cu and CO_2 during quenching of the mafic rocks, which in turn forced exsolution of the brine from the granitoids. Consequently, explosive release of mixed volatiles at the granitoid carapaces produced violent breccia pipes which carried Fe, Mn, K, Na, Ca and possibly Cu to sites above the intrusions, potentially to make orebodies. The same fluid, where it interacted with pre-existing ironstones and/or IOCGs, oxidized these

rocks and either redistributed or added copper as sulphide via redox reactions (e.g. Starra, Osborne western domain).

5. Direct release of reduced CO_2- and S-bearing fluids from crystallising mantle melts (or gabbros emplaced at higher levels) produced carbonate-dominated vein systems in rocks away from the Williams Batholith. Because these fluids did not "collide" with crystallising felsic magmas (e.g. MKFB), they did not cross-fertilize with the alkali-laden and potentially Cu-carrying source.
6. Where the primitive mantle- or gabbro-derived HCOS fluids met with the brine-laden fluids evolved off highly fractionated Williams Batholith, Ernest Henry may have formed. Alternately, the S was derived from remobilised sources proximal to Ernest Henry. It is possible that orebodies such as Starra formed where oxidised Williams-derived fluids interacted with pre-existing sulphides until a point where the fluid became sufficiently reduced that sulphide saturation was imminent, with final ore precipitation occurring due to pressure changes and phase separation. However, this "single fluid" model does not explain the fluid inclusion complexity at Starra nor the presence of barite (see also Williams et al., 2001).

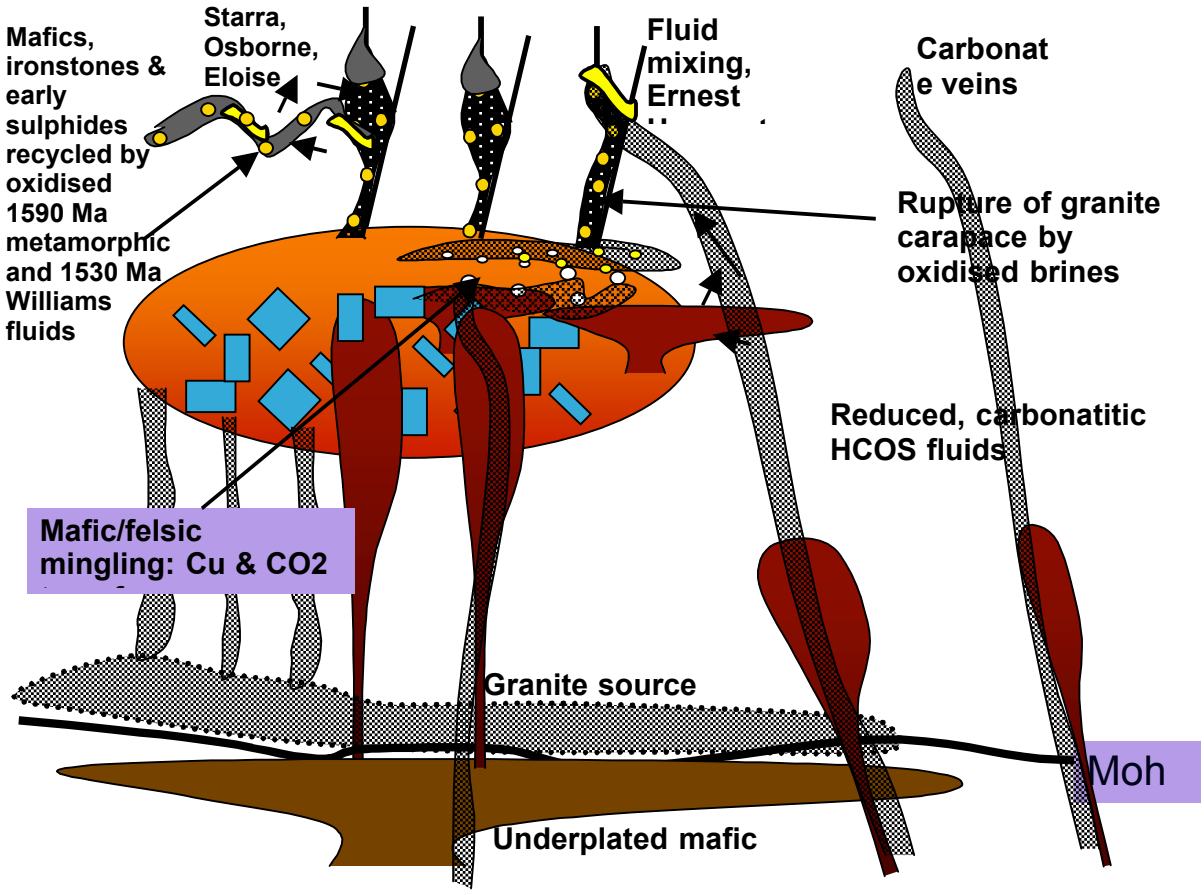

Fig. 18. Cartoon showing the inferred relationships between mantle fluids and melts, granite crystallisation, fluid sources, and recycling of early sulphides at the time of emplacement of the Williams Batholith. In some domains, sulphides were overprinted and reworked by Williams age oxidised fluids, leading to dissolution, remobilisation and reprecipitation (e.g. Starra); but in other domains the early reduced signal survived (Osborne eastern domain, Eloise). Release of oxidised brines at the top of the Williams/Naraku batholiths may have been triggered by mafic-felsic mingling and consequent CO_2 contributions; mixing of this fluid with primitive, potentially carbonatitic HCOS fluids can explain fluid mixing attributes of Ernest Henry. In all cases, mantle derived CO2 and sulphur was added to the orebodies, by contamination of granites, release of fluid from mid crustal mafic rocks, recycling of earlier sulphides and carbonates by metamorphic and magmatic fluids, and direct mantle degassing.

4.4 Mineralising systems in the Mt Isa Inlier

Although the above aspects of melt and fluid sources and pathways have been considered for the Eastern Succession in relation to IOCG deposits, they may have relevance for the whole inlier. An important question is the extent to which other types of deposit may have been formed by any of the processes described above. New evidence on this is provided by fractal analysis of different mineralising systems over the whole inlier (Ford, 2005). This shows (Table 4) that there are significant difference between the degree of clustering, measured by the fractal dimension, between Cu only and IOCG mineral occurrences (the least clustered with D = 1.4) and gold (highly clustered with D = 0.7). A simple interpretation of these results is that the different mineral occurrences were formed by different mineralising systems (Ford, 2005).

Table 4: Results of Fractal Dimension Calculations for Mt Isa Inlier with correlation coefficient R and standard error E

Mineral	Number	Fractal Dimension	R	E
Cu	1869	1.4	0.988	0.032
Au	416	0.7	0.981	0.022
CuAu	416	1.4	0.980	0.063
IOCG	198	1.3	0.989	0.038
U-REE	144	0.9	0.993	0.016

5. EXPLORATION IMPLICATIONS: THE IOCG COOKBOOK

5.1 Potential for IOCG deposits

We estimate that the total possible contribution of sulphur and metals from mafic rocks over the Selwyn-Angelay study area is grossly in excess of known ores, potentially being capable of forming a minimum 7 Bt of IOCG ore (Butera et al., 2005). The inferred relative addition of new components during the evolution of the accumulated metal history was moderate to strong via direct exsolution of mafic magmas at 1686 Ma, moderate via metamorphic leaching at 1600 Ma and potentially moderate via hydrothermal fluids from the Williams-Naraku Batholith. The amount of IOCG and Cu mineralisation that has thus far been discovered is around 334 Mt (based on all mineralisation in the GA Minocc database, with a cut off of 500t contained Cu). Taking into account the present erosion level, and current exploration and mining capabilities down to a depth of *ca* 1 km, there is the potential for >1.5 Bt of IOCG ore yet to be discovered in the area, especially for non-ironstone hosted Cu-Au, assuming *ca* 75% transport and deposition efficiency of metals and sulphur.

5.2 Ingredients for formation of IOCG deposits

The most important ingredients from spatial data modelling appear to be:

- The Corella + Doherty Formation contact, particularly with Soldiers Cap Group
- N-S (350-15°) and NE (40-75°) faults
- Bends in faults
- Mafic intrusions
- Cover Sequence 3/top of CS 2 hosts

- Proximity to gravity gradients (basement architecture) and gravity highs (mafics in crust).

Ernest Henry contains about a third of all of the currently mineable or mined Cu ore yet discovered in the Eastern Succession, implying that this event was potentially the most important of all, at least in a targeting sense. Special consideration needs to be given to targeting similar deposits because Ernest Henry appears to be distinct in a number of respects from other IOCG deposits in the Eastern Succession. If the sulphur in that deposit was truly primitive and juvenile, an understanding of how oxidised brines and reduced mantle-derived fluids could meet to make orebodies by fluid mixing will require close analysis of the 3D model and consideration of how mantle fluid pathways and oxidised Williams corridors could meet. Several clear strategies are apparent to advance this further:

1. Define zones of abundant hematite alteration that can be temporally linked with the Williams Batholith;

2. Attempt to identify which regional carbonate vein systems contain pyrrhotite ± pyrite in preference to magnetite;

3. Determine where these two types of chemical indicators intersect with the favoured locations in the prospectivity analysis, and the geomechanical analysis; and

4. Determine to what extent the presence of dense mafic bodies could reflect a source of either sulphur (by leaching) or a juvenile HCOS fluid, by comparing the gravity data with the magnetics and results of petrographic studies that identify the fate of mafic-sourced sulphide.

5.3 Exploration targets

General recommendations for exploration targets, based on genetic concepts, are:

- Within 750 m of mafic intrusives (but not in mafic rocks themselves)
- N and NE trending faults
- Fault bends/rough faults (Blenkinsop et al., 2005b)
- On gravity gradients, proximal to gravity highs
- Systematic exploration of the entire CS2/3 contact
- Zones of hematite alteration related to the Williams batholith
- Specific targets under cover are given in the prospectivity maps

Detailed recommendations are given by the posterior probability maps from the weights of evidence analysis. The first posterior probability Cu-Au map consists of 9 weighted map patterns including favourable lithostratigraphy, proximity to the Corella Formation - Soldiers Cap Group contact, proximity to mafic intrusives, proximity to the Williams-Naraku batholith, metamorphic zones, fault orientations, fault bends, magnetics and gravity (Fig. 19). The 9 layer model excluded surface geochemistry and radiometrics so as to look through the cover to some degree.

Several observations can be made about the 9 layer model:

- The Ernest Henry deposit which is the largest known Cu-Au deposit in the Mt Isa Inlier with a resource of 167 Mt @ 1.1% Cu and 0.54 ppm Au (Ryan, 1998),

produced the largest single anomalous region within the study area. There are some analogous Ernest Henry type targets to the north and west.

- The Selwyn group defined the single largest anomalous linear trend extending for 40km strike length, of which the southernmost *ca* 10 km is located under cover. Interesting areas in this same region include: NW of Labour victory, north of Answer and north of Hampden.
- The Eloise deposit is also highlighted, and several Eloise type targets are located NNE to NNW of Ernest Henry.
- The Osborne deposit is not strongly highlighted and is considered to reflect the lack of detailed geology in the interpretation as a result of cover.
- Mt Elliot, Mt Dore and Victoria-Stewart deposits are highlighted.
- Trekelano and SE Duchess and areas NW of Lady Ethleen are highlighted in the Wonga belt.
- Numerous other areas are highlighted particularly around Cloncurry township and to the west.

The second posterior probability Cu-Au map consists of 12 weighted map patterns including those present within the 9-layer model as well as outcrop based data for Cu and Au rockchip geochemistry, and radiometrics (Fig. 20). The effect of addition of the extra 3 layers was to further highlight areas of anomalous geochemistry around the Cloncurry Fold Belt and Wonga belt, without significantly reducing areas previously highlighted in the 9 layer model.

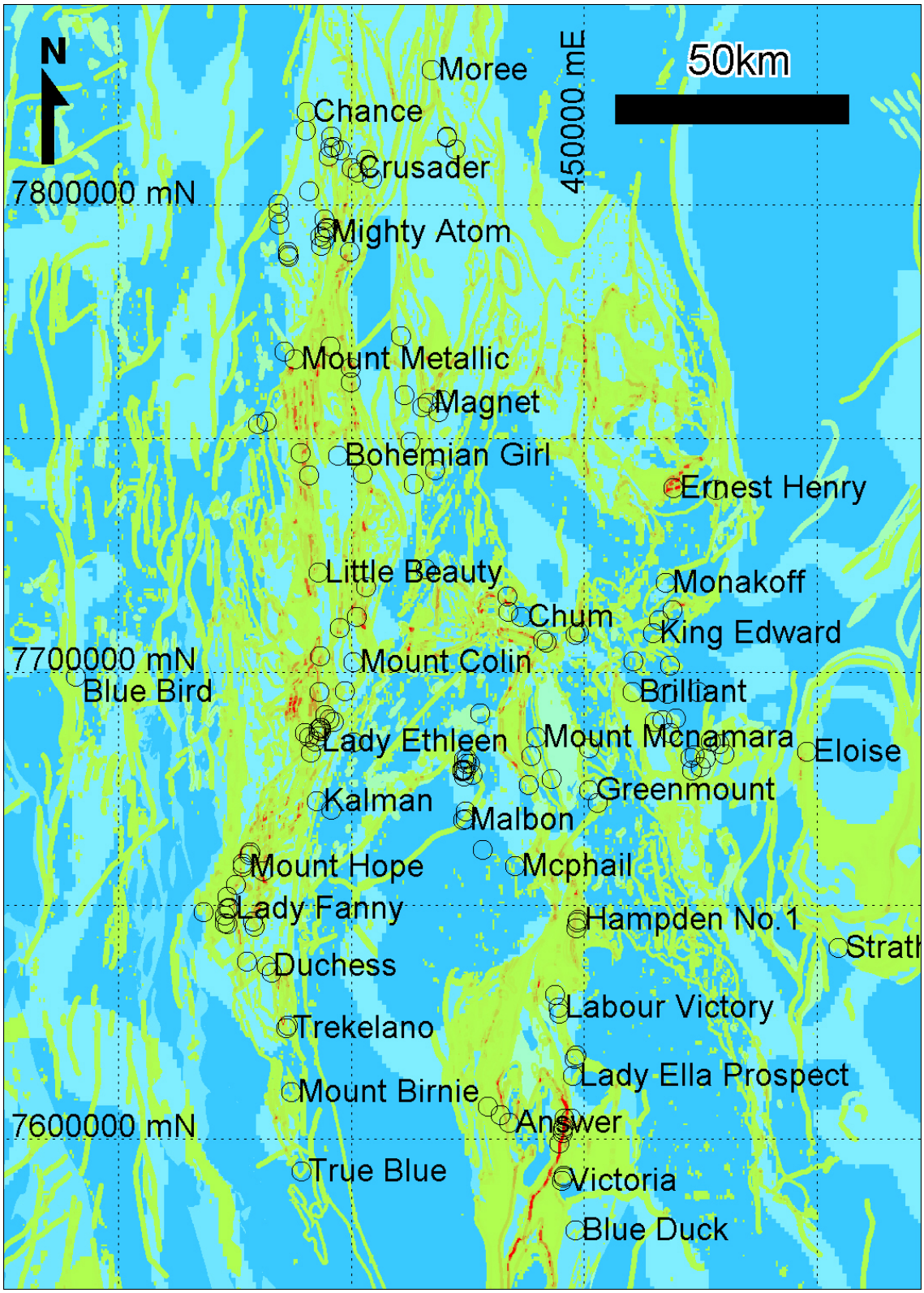

Fig. 19. The 9 Layer Cu-Au posterior probability map for the Mt Isa Inlier, NW Queensland. Projection: AMG Zone 54 (AGD66).

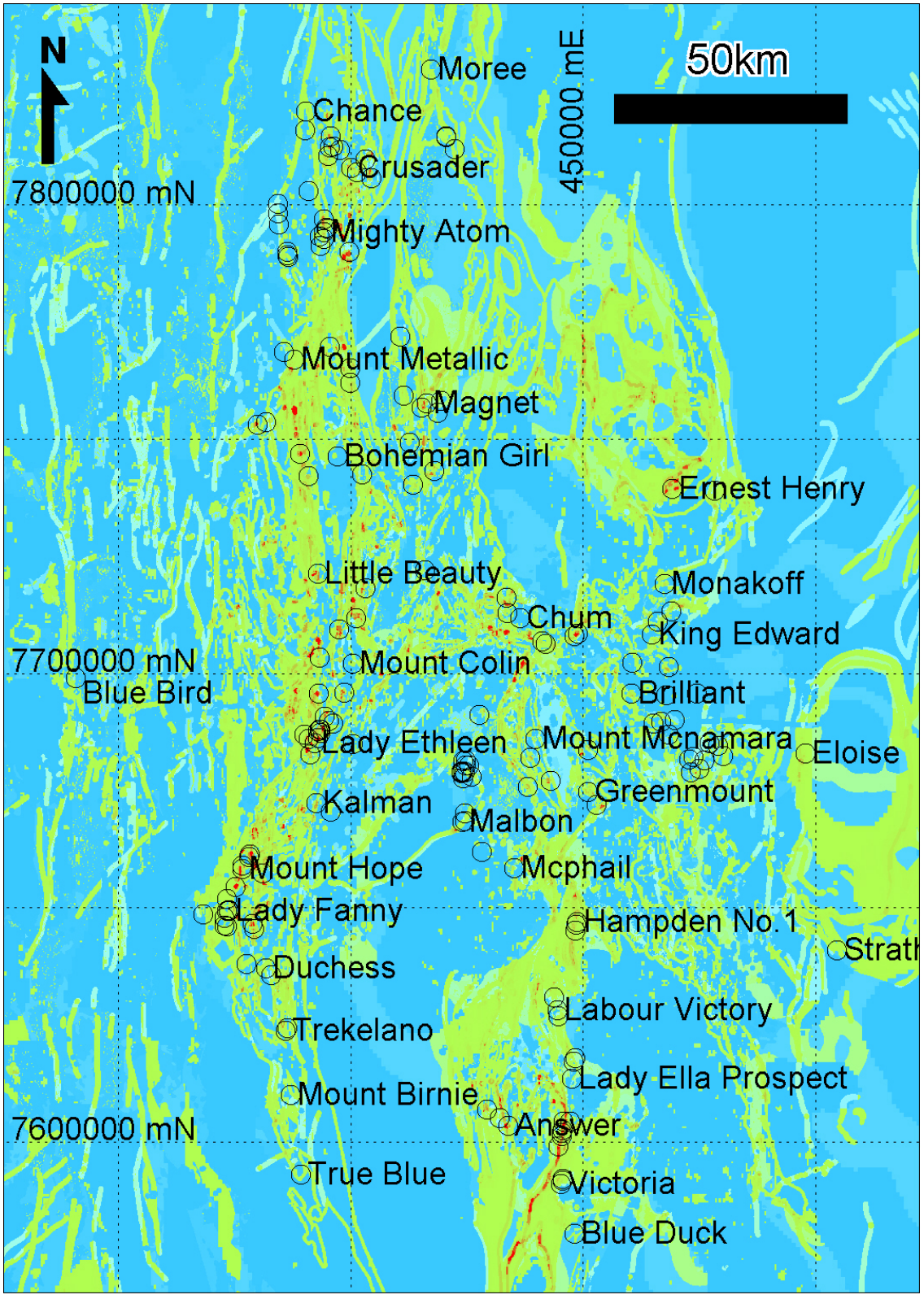

Fig. 20. The 12 Layer Cu-Au posterior probability map for the Mt Isa Inlier, NW Queensland. Projection: AMG Zone 54 (AGD66).

Additional potential targets are revealed by the results of the numerical modelling (McLellan & Oliver, 2005). Many sites correspond to either known deposits or targets generated by the prospectivity analysis. In the best model, 80% of the numerical results coincide with prospectivity targets (Fig. 21)

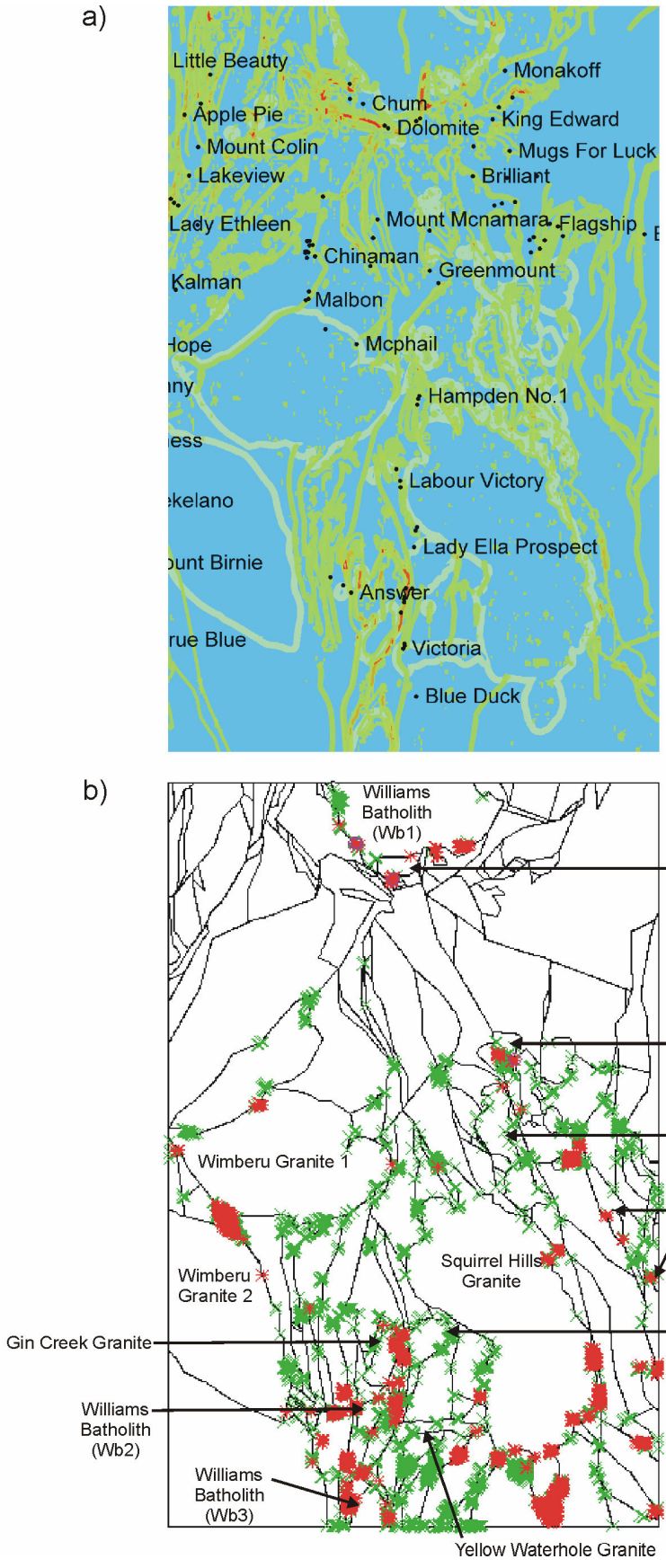

Fig. 21. Comparison of prospectivity analysis by Mustard et al. (2005a) and plasticity indicators for Model. a) prospectivity analysis, blue colours indicating no prospectivity and yellow to red indicating lower to higher prospectivity, with deposits and prospects indicated b) plasticity indicator for Model. Note: red indicates areas at yield, green indicates previously at yield but now not in contact with the failure envelope, and purple indicates areas in yield in tension.

5.4 New techniques for IOCG exploration with emphasis on exploration under cover

This study suggests that the following exploration techniques should be thoroughly investigated in the search for new IOCG deposits under cover:

- Airborne gravity for non-magnetic mafic rocks
- Fluid outflow modelling
- Mechanical modelling
- Oxidised vs reduced pathways: mapping
- Worms/lineaments
- Fault roughness
- Distance-size relationship for gravity highs (=mafic rocks)?
- A technique with regional coverage that can effectively determine the distribution of extensive sodic-calcic alteration and more proximal potassic alteration would be a useful additional layer for the model (remote sensing such as ASTER derived mineral maps may potentially be a useful technique for mapping alteration patterns).

It is clear that advances in geophysical exploration techniques will require a more extensive petrophysical database (Edmiston, 2005).

6. RECOMMENDATIONS

The most important insights in this report are a new view of IOCG genesis and of the large-scale architecture of the Eastern Succession. Both insights have the status of hypotheses that need testing. Several aspects of the tectonostratigraphy also require follow up work.

6.1 IOCG genesis

The role of mafic rocks in IOCG genesis needs to be investigated in detail by ore deposit studies including detailed geochemical, petrological, fluid and isotopic research designed to test the hypothesis that mafic rocks are a critical ingredient in IOCG genesis.

6.2 Architecture

The most important further work on architecture is the completion of the 3D model by creation of volumes for all rock units, and by incorporation of infill cross-sections between the existing skeleton. Geophysical forward modelling and inversion of the resultant model are urgent tasks to verify the basement architecture.

As a result of building the 3D model it has become apparent that several major structures need detailed field-based, modern structural investigation in the Eastern Succession. These have important implications for one or more aspects of the new model for IOCG deposits.

1. The major crustal-scale structure of the Eastern Succession is the Pilgrim worm structure. A field program with detailed mapping at carefully chosen localities is needed to contrast the tectonic history across the Pilgrim fault where it coincides with the Pilgrim worm with places where it does not coincide. This investigation needs to be paralleled by mapping of the Mitakoodi anticline, which is localised on the gravity worm.
2. The significance of the Cloncurry Flexure needs to be understood. In this area the Cover Sequence (CS) 2/3 contact appears to be gently dipping and may preserve some of its least reactivated character, with attendant implications for localisation of Cu-Au occurrences along this contact
3. The magnetic worm on the margin of the Wonga belt requires a geological explanation that can be established by several detailed cross-sections.
4. Mapping around and to the northwest of Ernest Henry, using Xstrata drilling data, needs to be incorporated into the 3D model.
5. The Starra-Selwyn corridor is a NS shear zone, which partly corresponds to an important gravity worm. A deformation chronology, linked to mineralization, is needed for this zone.

All the above structures are in NS or NE orientations that also correspond to the dominant orientations of faults associated with mineralization. They have the potential to be fluid pathways.

6.3 Tectonostratigraphy

The creation of the model also emphasised the need for a better stratigraphic understanding of the Eastern Succession based on high calibre new geochronological work. Our review of the tectonostratigraphy of the Eastern Succession, raised several critical issues:

1. The age and significance of the Double Crossing Metamorphics. This is very important to the 3D model and understanding the deeper architecture of the Eastern Succession. The Double Crossing Metamorphics are the only possible candidate for a basement to the cover sequences. If they are indeed such a basement, that places a major constraint on the model.
2. Diachroneity of the Corella/Doherty Formation. Meagre radiometric evidence suggests that the Doherty formation may be 20 Ma younger than the Corella Formation.
3. Facies changes in CS3. There appear to be major facies changes from E to W in Cover Sequence 3. This has been recognised in the 3D model by the definition of a new group (the Young Australia Group), that encompasses Cover Sequence 3 rocks in the region of the Young Australia mine. A clear definition and date for these rocks needs establishing. Furthermore the possibility that the Mt Albert Group is a western facies of CS 3 has been raised by the 3D model and needs further testing.

Both the above points are important because of the recognition that the CS2/3 contact is a major factor in localising Cu-Au mineralization. However, the stratigraphic and the tectonic investigations are important in a broader sense – it will not be possible to choose between several viable alternatives for the basic architecture of the Eastern Succession unless the stratigraphy is better understood. Map patterns cannot be correctly interpreted at present, even on a 1: 500 000 scale, because of the fundamental uncertainties in the stratigraphic relations of the major cover sequences.

7. REFERENCES

Austin, J., 2005. The Cloncurry Lineament: Interpretation of a major crustal worm. J. Austin. I2+3 Final Report, pmdCRC.

Blake, D.H., 1987. Geology of the Mt Isa Inlier and environs. Queensland and Northern Territory. Bureau of Mineral Resources, Journal of Australian Geology and Geophysics Bulletin, v. 225, 83 pp.

Blenkinsop, T. G., Huddlestone-Holmes, C., Foster, D., Mark, G., Austin, J., Edmiston, M., Lepong, P., Ford, A., and Murphy, F.C. 2005a. 3-D model and crustal architecture of the Mt Isa Eastern Succession. I2+3 Final Report, pmdCRC.

Blenkinsop, T., Mustard, R., and Bierlein, F. 2005b. Fractal dimensions of faults and mineralization: I2+3 Final Report, pmdCRC

Butera' K., Oliver, N., Rubenach, M., Collins, W., and Cleverley' J., 2005. Multiple generations of metal and sulphur contribution from mafic rocks to the IOCG budget of the Mt Isa Eastern Succession. I2+3 Final Report, pmdCRC.

Cleverley, J.S., Oliver, N.H.S. (in revision) Equilibrium dynamic modelling of fluid-rock interaction concepts using HCh: Examples from K-alteration in Fe-oxide Cu-Au systems

Davis, B.K., Pollard, P.J., Lally, J.H., McNaughton, N.J., Blake, K. and Williams, P.J., 2001. Deformation history of the Naraku Batholith, Mt Isa Inlier, Australia: implication for pluton ages and geometries from structural study of the Dipvale Granodiorite and Levian Granite. Australian Journal of Earth Sciences, 48, 113-129.

Edmiston, M. 2005. The role of geophysics in exploration for iron oxide copper-gold deposits. I2+3 Final Report, pmdCRC

Edmonds, M., Pyle, D., and Oppenheimer, C., 2001. A model for degassing at Soufriere Hills Volcano, Monsterrat, West Indies, based on geochemical data. Earth and Planetary Science Letters, 186, 159-173

Etheridge, M. A., Rutland, R. W. R. and Wyborn, L. A. I. (1987). "Orogenesis and tectonic processes in the Early to Middle Proterozoic of northern Australia." Am. Geophys. Union, Geodyn. Ser. 17: 131-147.

Ford, A. 2005. Fractal distribution of mineral deposits for exploration. I2+3 Final Report, pmdCRC.

Foster, D.R.W, 2003. Proterozoic low-pressure metamorphism in the Mt Isa Inlier, northwest Queensland, Australia, with particular emphasis on the use of calcic amphibole chemistry as temperature-pressure indicators. Unpubl. PhD thesis, James Cook University.

Foster, D., and Austin, J. 2005. Revised chronostratigraphy for the Mt Isa Inlier with emphasis on the Eastern Succession. I2+3 Final Report, pmdCRC.

Fu, B., Williams, P. J., Oliver, N. H. S., Dong, G., Pollard, P. J. and Mark, G. (2003). "Fluid mixing versus unmixing as an ore-forming process in the Cloncurry Fe-oxide-Cu-Au District, NW Queensland, Australia: evidence from fluid inclusions." J. Geochem. Expl. 78-79: 617-622.

Gauthier, L., Hall, G., Stein, H. and Schaltegger, U., 2001. The Osborne deposit, Cloncurry district: a 1595 Ma Cu-Au skarn deposit. In: Williams, P.J. (ed.), 2001: a hydrothermal odyssey, new developments in metalliferous hydrothermal systems research, extended conference abstracts. EGRU contribution, v. 59, pp. 58-59.

Giles, D., Betts, P. and Lister, G., 2002. Far-field continental backarc setting for the 1.80-1.67 Ga basins of northeastern Australia. Geology, 30, 823-826.

Giles, D. and Nutman, A.P., 2002. SHRIMP U-Pb monazite dating of 1600-1580 Ma amphibolite facies metamorphism in the southeastern Mt Isa Block, Australia. Australian Journal of Earth Sciences, 49, 455-465.

Giles, D. and Nutman, A.P., 2003. SHRIMP U-Pb zircon dating of the host rocks of the Cannington Ag-Pb-Zn deposit, southeastern Mt Isa Block, Australia: Australian Journal of Earth Sciences, v. 50, p. 295-309.

Goncharov, A., Sun, S-s. and Wyborn, L., 1997. Balanced petrology of the crust in the Mount Isa region. Australian Geological Survey Organisation, Research Newsletter, 26: 13-16.

Hattori, H.H., and Keith, J.D., 2001. Contribution from mafic melt to porphyry copper mineralisation: evidence from Mt Pinatubo, Philippines, and Bingham Canyon, Utah, USA. Mineralium Deposita, 36, 799-806

Kress, V., 1997. Magma mixing as a source for Pinatubo sulphur. Nature, 389, 591-593

Maas, R., McCulloch, M. T. and Campbell, I. H. (1988). "Sm-Nd isotope systematics in uranium rare-earth element mineralization at Mary Kathleen uranium mine, Queensland." Econ. Geol. 82: 1805-1826.

MacCready, T., Goleby, B.R., Goncharov, A. and Drummond, B.J., 1998. A framework of overprinting orogens based on interpretation of the Mt Isa Deep Seismic Transect. Economic Geology, 93, 1422-1434.

Mark, G., Foster, D., Mustard, R., and Pollard, P. 2005a. Sr-Nd isotopic constraints on the crustal architecture and evolution of the Eastern Succession, Mt Isa Block, Australia. I2+3 Final Report, pmdCRC.

Mark, G., Pollard, P., Foster, D., McNaughton, N. and Mustard, R., 2005b. Episodic syn-tectonic magmatism in the Cloncurry district, NW Queensland, Australia: Implications for the origin, derivation and tectonic setting of "A-type" magmas. I2+3 Final Report, pmdCRC.

Mark, G., 2001, Nd isotope and petrogenetic constraints for the origin of the Mt Angelay igneous complex: Implications for granitoid formation in the Cloncurry district, Australia. Precambrian Research, 105, 17-35.

McDonald, G.D., Collerson, K.D., Kinny, P.D. 1997. Late Archean and early Proterozoic crustal evolution of the Mt Isa block, northwest Queensland, Australia, Geology 25, 1095– 1098.

McLellan & Oliver, N.H.S., 2005. Discrete element modelling of stress partitioning and fluid flow in the Eastern Succession of the Mt Isa Block. I2+3 Final Report, pmdCRC.

Murphy, F.C. 2005. Composition of multi-scale wavelets (worms) in the potential field of the Mt Isa region. I2+3 Final Report, pmdCRC.

Mustard, R., Blenkinsop, T., Foster, D., Mark, G., McKeagney, C., Huddlestone-Holmes, C., Partington, G., and Higham, M. 2005. Critical ingredients in Cu-Au ± iron oxide deposits, NW Queensland: an evaluation of our current understanding using GIS spatial data modelling. I2+3 Final Report, pmdCRC.

Mustard, R., Mark, G., Ulrich, T., Gillen, D., and Foster, D., 2005. Geochemistry of magmatic fluids from intrusions of the Williams-Naraku Batholith, Cloncurry District, Northwest Queensland: preliminary results from laser ablation ICP-MS analysis. I2+3 Final Report, pmdCRC.

Oliver, N.H.S., and Cleverley, J.J., 2004. The role of sodic alteration in the genesis of iron-oxide copper gold deposits, eastern Mt Isa Block, Australia. Econ. Geol. 99, 1145-1176

Oliver, N. H. S., Cartwright, I., Wall, V. J. and Golding, S. D. (1993). "The stable isotopic signature of large-scale fracture-hosted metamorphic fluid pathways, Mary Kathleen, Australia." J. Metamorphic Geol. 11: 705-720.

Oliver, N.H.S., Cleverley, J.S., Mark, G., Pollard, P.J., Fu, B., Marshall, L.J., Rubenach, M.J., Williams, P.J. and Baker, T., 2004. The role of sodic alteration in the genesis of iron oxide-copper-gold deposits, eastern Mt Isa Block, Australia. Economic Geology, 99, 1145-1176.

Oliver, N.H.S. Butera, K., Cleverley, J. S., Marshall, L., Rubenach, M. J., Collins, W. J., Fu, B., Mustard, R., & Baker T. 2005. From source to sink: evolution of fluid systems in the Eastern Succession of the Mt Isa Block. I2+3 Final Report, pmdCRC.

Page, R. W. and Sun, S-S. 1998. Aspects of geochronology and crustal evolution in the Eastern Fold Belt, Mt Isa Inlier. Australian Journal of Earth Sciences 45: 343-361.

Page, R. W. (1983a). "Chronology of magmatism, skarn formation and uranium mineralisation, Mary Kathleen, Queensland, Australia." Econ. Geol. 78: 838-853.

Pearson, P.J., Holcombe, R.J. and Page R.W., 1992. Synkinematic emplacement of the Middle Proterozoic Wonga Batholith into a mid-crustal extensional shear zone, Mt Isa Inlier, Queensland, Australia. In: Stewart, A.J. and Blake, D.H., (eds.), Detailed studies of the Mt Isa Inlier. Australian Geological Survey Organization,

Perring, C. S., Pollard, P. J., Dong, G., Nunn, A.J. & Blake, K.L. 2000. The Lightning Creek sill complex, Cloncurry District, Northwest Queensland; a source of fluids for Fe oxide Cu-Au mineralization and sodic-calcic alteration, Economic Geology, 95, 1067-1089

Pollard, P.J., 2001. Sodic (-calcic) alteration associated with Fe-oxide-Cu-Au deposits: an origin via unmixing of magmatic-derived H_2O-CO_2-salt fluids. Mineralium Deposita, 36, 93-100.

Pollard, P.J., Mark, G. and Mitchell, L.C., 1998. Geochemistry of post-1540 granites spatially associated within regional sodic-calcic alteration and Cu-Au-Co mineralisation, Cloncurry district, northwest Queensland. Economic Geology, 93, 1330-1344.

Pollard, P.J. and McNaughton, N., 1997. U-Pb geochronology and Sm/Nd isotope characteristics of Proterozoic intrusive rocks in the Cloncurry district, Mt Isa Inlier, Australia. AMIRA P438 Final Report: Cloncurry Base Metals and Gold, 4: 19.

Queensland Department of Mines and Energy, Taylor Wall & Associates, SRK Consulting Pty Ltd & ESRI Australia, 2000. North-west Queensland Mineral Province Report, Queensland department of mines and energy, Brisbane.

Rubenach, M. 2005. Tectonothermal Evolution of the Eastern Fold Belt, Mt Isa Inlier. I2+3 Final Report, pmdCRC.

Rubenach, M.J. and Oliver, N.H.S. 2005. Geochemistry of albitites and related metasomatic rocks, Eastern Succession of the Mount Isa Block. I2+3 Final Report, pmdCRC

Ryan A (1998) Ernest Henry copper-gold deposit. In (eds.) Berkman DA, Mackenzie DH. Geology of Australian and Papua New Guinean Mineral Deposits. Australasian Inst Mining Metall 22: 759-768.

Sayab, M., 2005. N-S shortening during orogenesis in the Mt Isa Inlier: the preservation of W-E structures and their tectonic and metamorphic significance. Unpubl. PhD thesis, James Cook University. Pmd-CRC report

Scott, D.L., Rawlings, D.J., Page, R.W., Tarlowski, C.Z., Idnurm, M., Jackson, M.J and Southgate, P.N., 2000. Basement framework and geodynamic evolution of the Palaeoproterozoic superbasins of north-central Australia: an integrated review of geochemical, geochronological and geophysical data. Australian Journal of Earth Sciences, 47: 341-380.

Southgate, P.N, Bradshaw, B.E., Domagala, J., Jackson, M.J., Idnurm, M., Krassay, A.A., Page, R.W., Sami, T.T., Scott, D.L., Lindsay, J.F., McConachie, B.A. and Tarlowski, C., 2000. Chronostratigraphic basin framework for Palaeoproterozoic rocks (1730-1575 Ma) in northern Australia and implications for base metal mineralization. Australian J. Earth Sciences 47, 461-483.

Spikings, R.A., Foster, D.A., Kohn, B.P. and Lister, G.S., 2001. Post-orogenic (<1500 Ma) thermal history of the Proterozoic Eastern Fold Belt, Mount Isa Inlier, Queensland. Precambrian Research, 109, 103-144.

Sun, S.S. and McDonough, W.F., 1989. Chemical and isotopic systematics of oceanic basalts: implications for mantle composition and processes. In: A.D. Saunders and M.J. Norry (eds), Magmatism in the Ocean Basins. Geological Society Special Publication, v. 42, pp. 313-345.

Williams, P.J., 1998. An introduction to the Metallogeny of the McArthur River-Mt Isa-Cloncurry Minerals Province. Economic Geology 93, 1120-1131

Williams, P. J., Dong, G., Ryan, C. G., Pollard, P. J., Rotherham, J. F., Mernagh, T. P. and Chapman, L. C. (2001). Geochemistry of hypersaline fluid inclusions from the Starra (Fe-oxide)-Au-Cu deposit, Cloncurry District, Queensland. Econ. Geol. 96: 875-884.

Williams, P.J. and Skirrow, R.G., 2000. Overview of Iron Oxide-Copper-Gold deposits in the Curnamona Province and Cloncurry district (Eastern Mt Isa Block), Australia. In: Porter, T.M. (ed.), Hydrothermal Iron Oxide Copper-Gold and Related Deposits: A Global Perspective, AMF, pp. 105-122.

Appendix 1: Student participation in I2+3

PhD projects

Student	Project Title	Supervisor	Dates
Lucas Marshal	Brecciation within the Mary Kathleen Group of the Eastern Succession, Mt Isa Block, Australia: implications of district-scale structural and metasomatic processes for Fe-oxide-Cu-Au mineralisation.	Nick Oliver	00-03
John McLellan	Numerical Modelling of Deformation and Fluid Flow in Hydrothermal Systems	Nick Oliver	02-05
Mohammed Sayab	N-S shortening during orogenesis in the Mt Isa Inlier: The preservation of W-E structures and their tectonic and metamorphic significance	Mike Rubenach	02-05
Kris Butera	Mafic Geochemistry of the Mt. Isa Eastern Succession	Mike Rubenach	03-06
Piter Lepong	Crustal Architecture of the Mt. Isa Eastern Succession as revealed by geophysical interpretation and inversion	Tom Blenkinsop	03-06
James Austin	Geological and Geophysical significance of the Cloncurry Worm	Tom Blenkinsop	03-06
Arianne Ford	Application of Fractal Geometry to Mineral Deposit Distributions with Special Reference Mt Isa Inlier to the Mt Isa Eastern Succession	Tom Blenkinsop	04-07
Mark Edmiston	New Exploration techniques for IOCG deposits under Cover in the Eastern Succession of Mt isa	Tom Blenkinsop	04-07
Michelle Stark	Deformation zone architecture, reactivation and mineralization processes in the Eastern Succession of the Mt Isa Inlier	Tom Blenkinsop	04-07

Honours Projects

Tim Laneyrie	Breccias and mineralization at Ernest Henry Mine	Nick Oliver	2004
Janine Josey	A classification scheme for brecciation in the Fullerton River Gorge concerning the Evolution of the Eastern Succession of the Mt Isa Inlier	Tom Blenkinsop	2004
Richard Hingst	Structural and metamorphic evolution along the Cloncurry fault	Mike Rubenach	2003

Shaded cells are completed projects.

Section 2

Geodynamic Setting

Detailed Reports

Episodic syn-tectonic magmatism in the Eastern Succession, Mount Isa Block, Australia: implications for the origin, derivation and tectonic setting of 'A-type' magmas

Geordie Mark[1], Peter Pollard[2], Damien Foster[2], Neal McNaughton[3], and Roger Mustard[2]

[1]School of Geosciences, Monash University, PO Box 28E, Victoria, 3800, Australia
[2]School of Earth Sciences, James Cook University, Townsville QLD 4811, Australia
[3]Department of Geology and Geophysics, University of Western Australia, Perth, W.A. 6009, Australia

ABSTRACT

SHRIMP U-Pb zircon dating of intrusive phases of the Williams-Naraku Batholiths in the Eastern Succession, Mount Isa Block, Australia shows that potassic magmatism was emplaced episodically over a thirty million year period between 1.53 and 1.50 Ga. These apparent anorogenic intrusions were emplaced during three phases of magmatism that are largely confined to discreet spatial domains in the Eastern Succession, namely: 1. 1.53-1.52 Ga (centre), 2. 1.52-1.51 Ga (west and south), 3. 1.51-1.50 Ga (north). On an outcrop-scale, igneous complexes representing each of the phases of magmatism exhibit geological relationships supporting the coincident emplacement of mafic and felsic intrusions early in magma genesis, and the subsequent fractionation of the felsic intrusions during sub-horizontal east-west compressional deformation. A syn-tectonic timing of these intrusions contradicts their apparent anorogenic character defined using their geochemistry, and implies that intrusions of this composition are not restricted to 'strictly' anorogenic environments.

The recognition of distinct phases of geochemically similar, LILE (large-ion-lithophile-element) enriched, potassic intrusions across the succession implies that they were derived from previously unmelted crustal material of tonalitic composition. The prolonged duration over which steep north-south tectonic fabrics were produced throughout the Eastern Succession is used to argue that subhorizontal east-west compression was dominant during that time, and that the higher apparent strain around the intrusions was associated with localized thermal weakening linked to heat advection from the crystallizing intrusions. Repeated, short-lived, slab rollback from a distal eastern arc is invoked for the initiation of periodic mantle emplacement into the crust, the subsequent generation of felsic magmas, and the syn-compressional regime during emplacement of the mid-crustal intrusions.

Keywords: Mesoproterozoic intrusions, Mount Isa Inlier, mantle, diorite, tectonism

1. INTRODUCTION

Potassic igneous rocks with 'A-type' geochemical affinities represent a globally significant type of magmatism that largely was produced during Precambrian times (Anderson, 1983; Anderson and Bender, 1989; Creaser and White, 1991; Ramo and Haapala, 1995; Pollard et al., 1998; Persson, 1999; Lenharo et al., 2003). These magmas formed large-scale felsic extrusive rock sequences and batholith-scale intrusive complexes with extensive evidence for coeval mafic and felsic magmatism. The majority of rapakivi-textured intrusions (or intrusion complexes) fall into this category and are commonly spatially and/or temporally associated with hybridisation of mafic and felsic magmas. The mafic magmas typically have a juvenile mantle parentage, variably contaminated by the incorporation of crustal material and or granitic melt, whereas the felsic components are largely considered to have been derived from crustal sources of Paleoproterozoic age or older. Models for the generation of the felsic rocks, particularly for the relatively oxidized variants, primarily invoke the emplacement of mantle-derived material into the crust and subsequent melting of pristine tonalitic crust (Anderson, 1983; Wyborn et al., 1988; Creaser et al., 1991; Pollard et al., 1998; Dall'Agnol, 2005). Alternately, other models suggest that the relatively reduced and Fe-rich felsic intrusions are the direct fractionates from mantle-derived melts (cf. Frost and Frost, 1997).

Mechanisms for the generation of the 'A-type' melts are well documented, however their precise relationship to orogenesis is not well constrained. The tectonic setting of these rocks has been a contentious issue since attempts to differentiate their tectonic environment using geochemical data (cf. Whalen, 1987; Creaser, 1991; Collins et al., 1992; Eby, 1992). Many studies, particularly those concerned with alkaline-subalkaline, potassic Precambrian magmas, have shown that intrusions with geochemical characteristics synonymous with 'A-type' magmas (enriched in LILE and high-field strength elements (HFSE), and depleted in Ni, Co and Cr) were not artefacts of truly anorogenic environments, but rather were emplaced during periods of orogenesis involving crustal shortening (cf. Nyman, 1994). This dichotomy indicates that the chemistry of the intrusions is not inherently related to the tectonic environment. The predominance of these types of magmas in the Precambrian indicates that conditions for their formation appear to have been more favourable then, and in particular may have related to higher mantle activity and perhaps kinetic effects associated with the apparently more rapid rate of plate margin processes. Determining the interplay between mantle- and tectonic-related processes that drive magmatism will therefore help resolve how this globally significant style of magmatism was generated, how it relates to other types of magmatism, and to tectono-thermal processes in the crust generally.

The Cloncurry district, Mount Isa Inlier (Fig. 1), is a key area for studying the origin and formation mechanisms of apparent intracratonic, episodic magmatism as it is dominated by ca 1530-1500 Ma K-rich granitoids with classic 'A-type' geochemical characteristics. These intrusions were emplaced during crustal compression, and exhibit an intimate spatial and temporal relationship with the incursion of mantle-derived mafic intrusions. This paper discusses the significance of episodic magmatism and its relationship to mantle activity, tectonism and crustal composition.

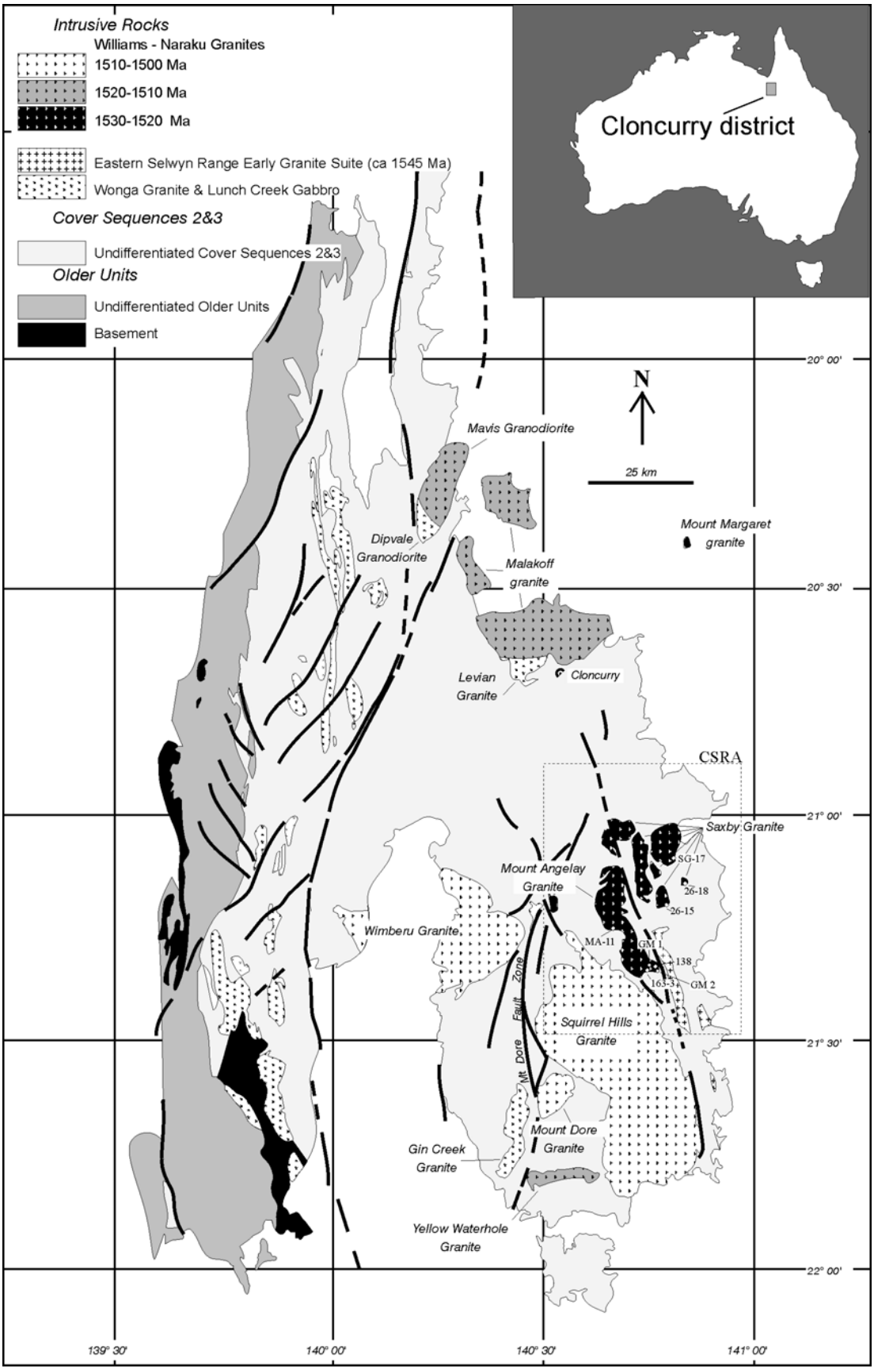

Fig. 1. Simplified geological map of the eastern Mount Isa Block showing the location of U-Pb zircon and titanite age dates discussed in this study (modified after Williams, 1998). CSRA refers to the generalized Central Selwyn Range Area.

2. CLONCURRY DISTRICT

The Cloncurry district comprises the eastern exposed margin of the Mount Isa Inlier, and contains Fe oxide-Cu-Au deposits hosted within Paleoproterozoic (ca. 1760-1660 Ma; cf. Page and Sun, 1998) carbonate-evaporite and siliciclastic metasedimentary and metavolcanic rocks (Fig. 1). The district is largely composed of mixed sedimentary-volcanic cover sequences (ca. 1760-1720 Ma and 1670-1610 Ma) deposited during periods of intracrustal rifting (Blake, 1987; O'Dea et al., 1997). The cover sequences underwent a protracted deformation and metamorphism during the Isan Orogeny (1600-1500 Ma), within which at least three ductile tectonic fabrics are typically identified (cf. Davis et al., 2001; Rubenach and Lewthwaite, 2002), although a significantly greater number of tectonic events have been recorded locally, indicating a more complicated orogenic evolution (Adshead-Bell, 1998; Mares, 1998; Rubenach and Barker, 1998; Rubenach and Lewthwaite, 2002). Regional greenschist to upper amphibolite facies metamorphism peaked early in the Isan Orogeny during a period of east-west compression (Rubenach and Barker, 1998). The timing of metamorphism is poorly constrained and is complicated by locally significant thermal pulses associated with the emplacement of the Williams and Naraku Batholith (cf. Foster and Rubenach, 2005), although the published age constraints largely indicate a regional metamorphic peak ca. 1600-1570 Ma across most of the Cloncurry district (Page and Sun, 1998; Giles and Nutman, 2002; Hand and Rubatto, 2002, Table 1). A regional association between localized N-S post-peak metamorphic corridors of intense deformation and Cu-Au mineralisation has been recognised by many workers in the Cloncurry district (Rotherham, 1997; Adshead, 1998; Baker and Laing, 1998; Mark et al., 2000). However, the age and relative timing of the syn-ore fabrics with respect to the local structural evolution is variable (cf. Davis et al., 2001; Rubenach et al., 2001).

The district's Paleoproterozoic cover sequence rocks were intruded by a series of syn- to post-peak metamorphic intrusions of the Williams and Naraku Batholiths (1550-1500 Ma: Page and Sun, 1998; Davis et al., 2001; Perring et al., 2001). These intrusions have an outcrop exposure >2100 km^2, and are predominantly potassic. These phases are largely composed of metaluminous, alkaline to subalkaline, magnetite-bearing granitoids (Wyborn et al., 1988; Pollard et al., 1998) that mainly plot within 'A-type' fields on geochemically-based tectonic discrimination diagrams (cf. Whalen et al., 1985). However, field relationships indicate a syn- to post-tectonic timing for the majority of the intrusions (Mark and de Jong, 1996), which range from diorite to syenogranite to pegmatite, and are typically more oxidized than older counterparts west of Mount Isa (Wyborn, 1998).

The formation of regional-scale hydrothermal Na-Ca alteration systems was synchronous with this period of magma emplacement, and locally overlapped with high-grade metamorphism (Mark et al., 2004a,b; Oliver et al., 2004). The hydrothermal systems were focussed along large active fault systems that locally host structurally-controlled Cu-Au mineralisation (cf. Williams and Pollard, 2003). The precise relationship between magmatism, metamorphism, tectonism and mineralisation has not been fully constrained (cf. Adshead et al., 1998; Rotherham et al., 1998; Baker et al., 2001; Mark et al., 2000).

3. CENTRAL SELWYN RANGE AREA

The magmatic phases in the Central Selwyn Range Area (Fig. 1) largely comprise potassic intrusions of the Saxby and Mount Angelay igneous complexes that crop out to the east and west of the Cloncurry Fault respectively (Wyborn, 1998). Rare deformed trondhjemitic-tonalitic intrusions and undeformed sodic alkali-granitoids are also present

(Darvall, 1998; Mark and Foster, 2000; Mark, 2001). Both sets of intrusions were emplaced into metamorphosed Paleoproterozoic siliciclastic and calc-silicate-rich metasedimentary rocks (Mitchell, 1993; Mark, 1999) that were affected by multiple generations of tectonism preserved as variously oriented tectonic fabrics and hand- to outcrop-scale folds. The two main tectonic fabrics (locally termed D_2 and D_3) are associated with east-west sub-horizontal compression, exhibit a north-south orientation, and steep to sub-vertical dips. D_2 fabrics represent the most significant phase of deformation, and indicate an apparent syn-peak metamorphic timing (Mark et al., 1998; Rubenach and Lewthwaite, 2002). Multiple phases of Na, Na-Ca, K and Si-rich hydrothermal veining and alteration display a range of paragenetic timing relationships where pre- to syn-magmatic breccia-hosted Na and Na-Ca alteration pre-dates fracture-controlled K- and Si-rich epithermal-style veining and alteration (Mark et al., 2004a,b).

3.1 Intrusions:

The intrusions that comprise the Saxby and Mount Angelay igneous complexes are the oldest examples of post-peak metamorphic potassic magmatism in the Cloncurry district that exhibit geochemical characteristics definitive of 'A-type' granites. The Mount Margaret Granite (ca. 1530 Ma, Fig. 1) to the north of Cloncurry was also emplaced during this period, but is composed largely of K-poor, sodic intrusions. Although the intrusions of the Mount Angelay and Saxby igneous complexes exhibit many mineralogical similarities, they are geochemically distinct and represent components of the Eureka and Cloncurry Supersuites respectively (Pollard et al., 1998). Detailed mapping of the Mount Angelay (Dare, 1995; Mark, 1998; Tolman, 1998; Richmond, 2000) and Saxby igneous complexes (Mitchell, 1993; Pollard et al., 1998) shows that each exhibits significant compositional diversity mainly associated with magma hybridization via mingling and mixing. This diversity is common to most large intrusive bodies in the district (e.g., Knight, 1995; Wyborn, 1998; Richmond, 2000; Perring *et al.*, 2001).

3.2 SAXBY IGNEOUS COMPLEX

The Saxby igneous complex occurs as a number of intrusive masses that crop out on the eastern side of the Cloncurry Fault approximately 50 km southeast of Cloncurry (Figs 1, 2). The intrusions are hosted within siliciclastic metasedimentary rocks and minor amphibolite of the Soldiers Cap Group. Biotite granite predominates in the northern part of the complex, but the southeastern outcrops (Wiley igneous complex; Mitchell, 1993) contain extensive evidence for mixing and mingling between mafic and felsic magmas and between hornblende-biotite granite and biotite-hornblende granite (Mitchell, 1993; Pollard et al., 1998). Hybrid rocks were formed at the margins of mafic bodies by blending of mafic and felsic magmas (Pollard et al., 1998; Fig. 2). Medium-grained syenogranite cuts the earlier intrusions as dyke-like bodies (Mitchell, 1993). The easternmost outcrop of the Saxby igneous complex is composed of two-mica granite whose strongly peraluminous character suggests a significant component of aluminous metasedimentary rock was incorporated into the magma. Xenocrystic zircons from the two-mica granite have ages (1666 ±24 Ma) similar to the age of the host Soldiers Cap Group.

Intrusion Name	Age: Ma	Method	Reference
Peak metamorphic pegmatite (M_1)			
Osborne Cu-Au	1595±5	TIMS: Ttn	Rubenach et al., 2001
Cannington Ag-Pb-Zn	1585±5	SHRIMP: Mon	Giles and Nutman, 2002
Metamorphic Zircon (M_1)	1584±17	SHRIMP	Page and Sun, 1998
Boorama Tank Gneiss (D_3)	1547±5	SHRIMP	Page and Sun, 1998
Maramungee Granite (Trondhjemite) (M_2)	1545±11	SHRIMP	Page and Sun, 1998
Mount Angelay Trondhjemite (M_2)	1552±42	SHRIMP	Pollard and McNaughton 1997
MOUNT ANGELAY GRANITE:			
Hornblende monzogranite-pre-D_3	1524±4	SHRIMP	
Hornblende monzogranite- post-D_3	1529±4	SHRIMP	
Hornblende quartz monzogranite- pre- D_3	1523±4	SHRIMP	
SAXBY GRANITE:			
Hornblende-biotite granite- deformed (D_3)	1520±8	SHRIMP	
Hornblende-biotite granite- undeformed	1536±12	SHRIMP	
Two-mica granite- igneous zircon	1536±20	SHRIMP	
- xenocrystic zircon	1666±24	SHRIMP	
Mount Margaret Granite	1528±6	SHRIMP	Page and Sun, 1998
	1530±8	SHRIMP	
Squirrel Hills Granite- monzodiorite	1514±5	SHRIMP	Perring et al., 2000; Perring et al., 2001
- monzogranite	1511±9	SHRIMP	
Wimberu Granite	1508±4	SHRIMP	Page and Sun, 1998
Mavis Granodiorite- deformed (D_3)	1505±7	SHRIMP	Davis et al., 2001
Malakoff Granite	1505±5	SHRIMP	Page and Sun, 1998
Mount Elliott Cu-Au deposit (Syn-ore monzodiorite)	1510±3	Ar-Ar:Bio	Wang and Williams, 2001
Yellow Waterhole Granite	1493±8	SHRIMP	Page and Sun, 1998
	1510±8	SHRIMP	Pollard and McNaughton 1997
Na AND Na-Ca ALTERATION			
Osborne Cu-Au deposit	1595±5	TIMS: Ttn	Rubenach et al., 2001
Mount Angelay area: stage 1- pre-D_3	1517±17	SHRIMP: Ttn	Mark 1998
Mount Angelay area: stage 2- post-D_3	1515±32	SHRIMP: Ttn	Mark 1998
Central Selwyn Range Area	1523±16	TIMS: Ttn	Oliver et al. (2004)
Gilded Rose Breccia: albitization	1488±11	K-Ar: Musc	Perkins and Wyborn (1998)

Table 1. Summary of age constraints for post-1600 Ma magmatism and Na and Na-Ca alteration in the Cloncurry district. Abbreviations: M_1, regionally extensive metamorphic peak; M_2, local to regional metamorphic event; D_3, locally significant third ductile tectonic fabric; Ttn, titanite; Bio, biotite; Musc, muscovite; Mon, monazite; TIMS, Thermal Ion Mass Spectrometry; SHRIMP, Sensitive High Resolution Ion Microprobe, zircon analysis unless otherwise stated.

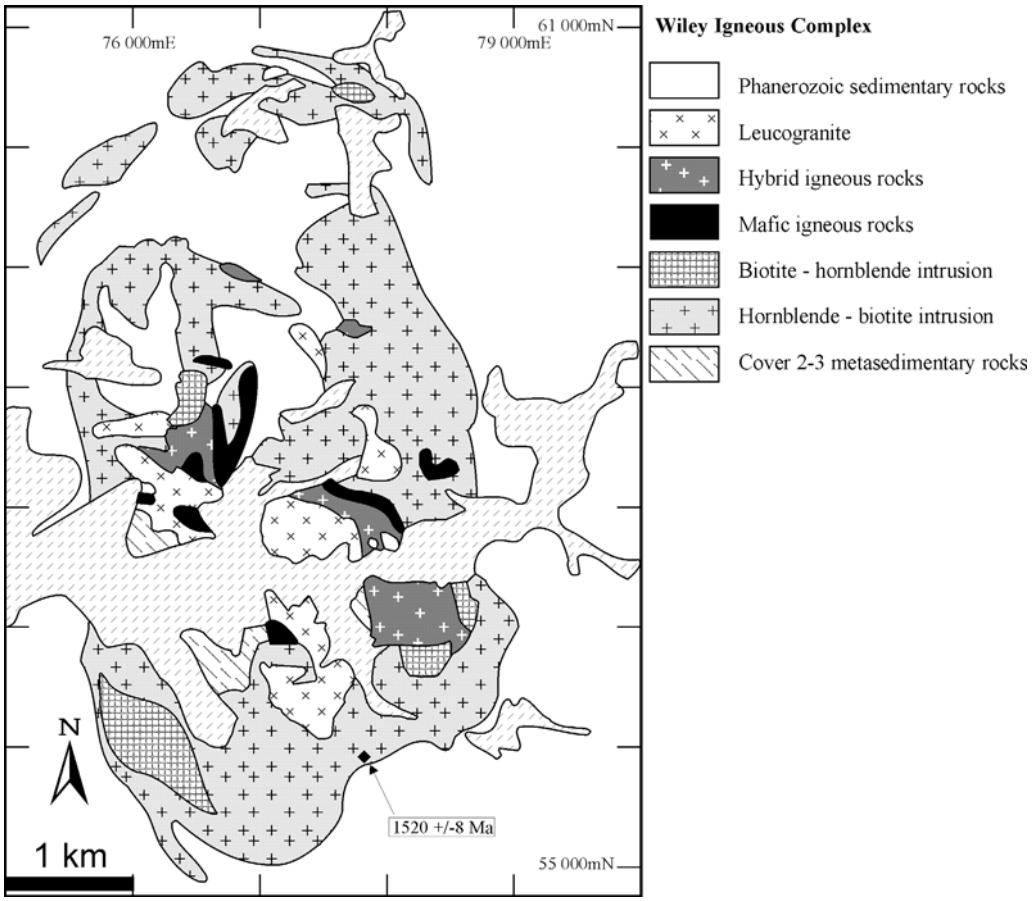

Fig. 2. Simplified geology of the Wiley igneous complex within the Saxby igneous complex showing the location of a SHRIMP U-Pb zircon age date (modified after Mitchell, 1993; Pollard et al., 1998).

3.3 MOUNT ANGELAY IGNEOUS COMPLEX

The Mount Angelay igneous complex (Fig. 3) lies approximately 80 km south of Cloncurry and crops out to the west of the Cloncurry Fault. The complex consists of multiple phases of igneous intrusions that were emplaced into poly-deformed amphibolite facies calc-silicate, metadolerite, quartz-rich psammitic and pelitic rocks, and affected by multiple stages of syn- to post-intrusive Na and/or Na-Ca alteration. Mapping has revealed three cycles of granitoid emplacement and alteration, where each igneous intrusion was emplaced, solidified and then altered by hydrothermal fluids prior to the emplacement of a younger intrusion. These three periods of igneous emplacement and alteration are documented in more detail below, and record an alteration paragenesis from early Na alteration followed by Na-Ca alteration at 1517 ± 17 Ma and 1515 ± 32 Ma.

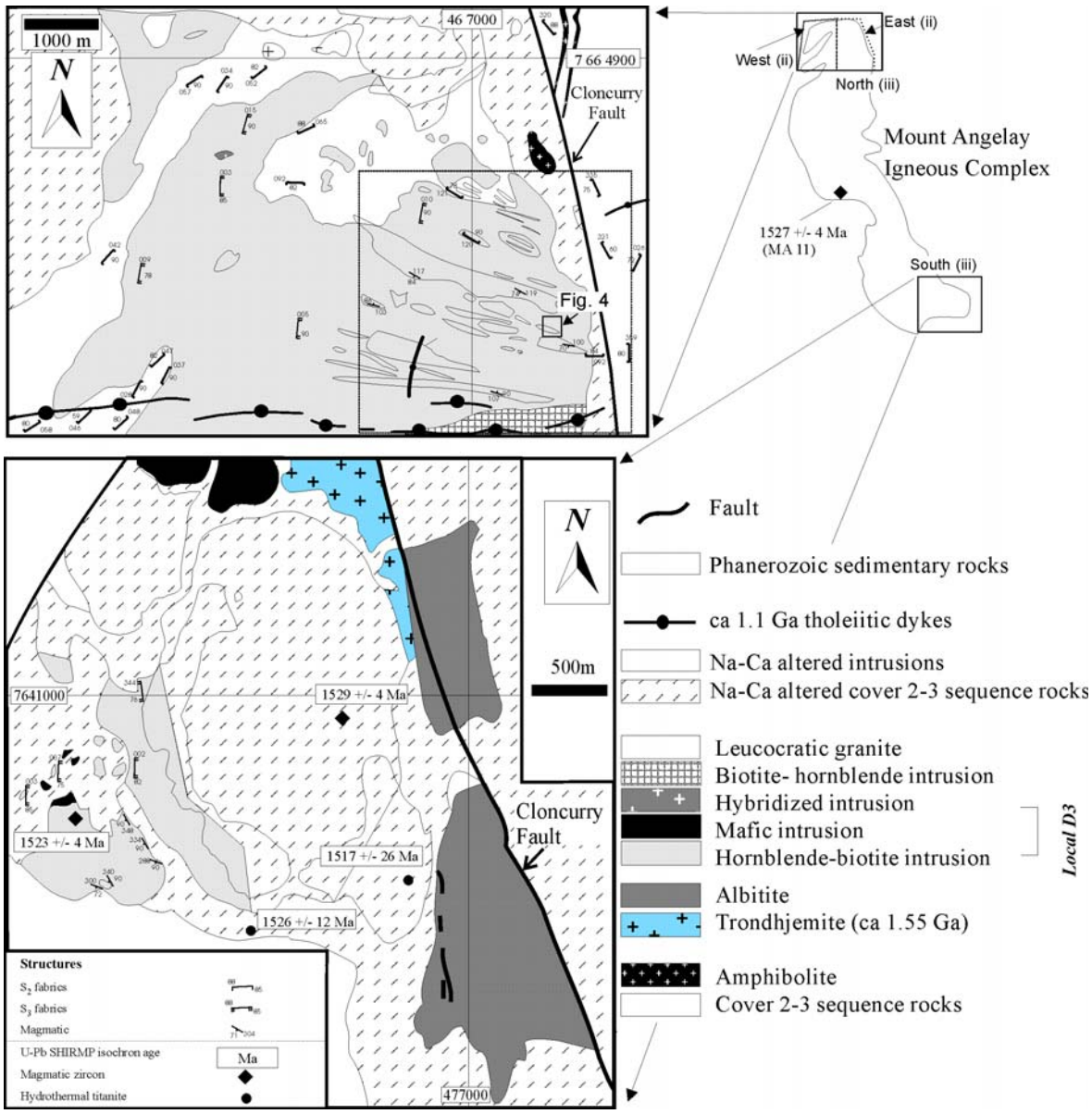

Fig. 3 (above). Local solid geology of the Mount Angelay igneous complex (modified from Mark, 2001) with the location of SHRIMP U-Pb zircon dates, and including the location of fig. 4 that shows the detailed lit-par-lit magma-metasediment intrusive relationships. Also shown are the S2 tectonic fabrics in the metasedimentary rocks around the northern margin of the complex, as well as the orientation of magmatic flow fabrics, and S3 fabrics within the earlier, least evolved intrusions in both the southern and northern margins of the complex.

(i) an insert of the simplified geology of the northern Mount Angelay igneous complex showing the fan-like distribution of late leucocratic granite dykes interpreted to be associated with dilation during sinistral movement along the Cloncurry fault;

(ii) Equal area stereonet projections of S2 tectonic fabrics in the eastern and western parts of the northern Mount Angelay igneous complex. Note that the S2 fabrics in the metasedimentary rocks define the closure of an open D3 fold, showing that the earliest magmatic rocks of the intrusive complex sit within the fold hinge.

(iii) an equal area stereonet projection showing the orientation of D3 tectonic fabrics within hornblende-biotite intrusions in both the southern and northern margins of the complex.

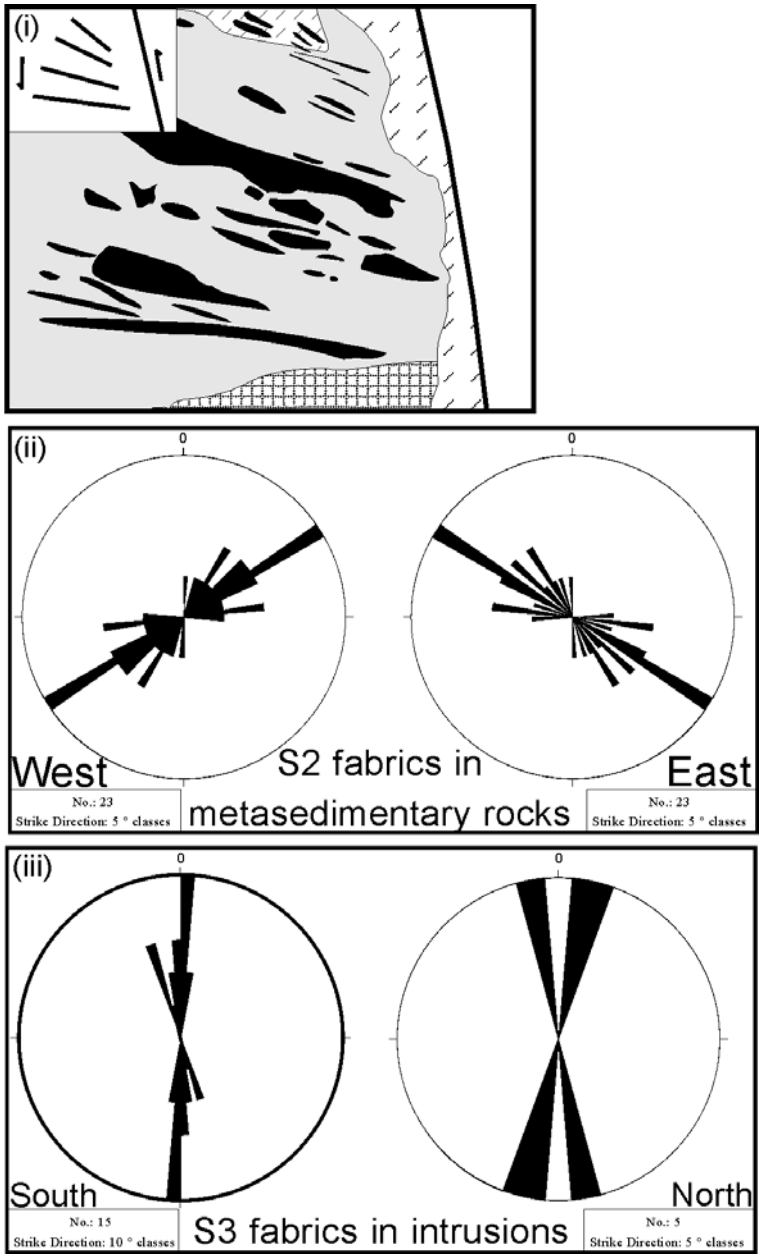

The Mount Angelay igneous complex is composed of deformed quartz monzodiorite and quartz monzogranite intrusions cut by undeformed monzogranite, syenogranite and pegmatite. The steep, commonly sub-vertical, N-S orientation of ductile tectonic fabrics preserved within the older phases suggests the igneous complex was emplaced during a period of sub-horizontal east-west compression. Two main features support a syn-tectonic timing for the emplacement of the complex: 1. the apparent emplacement of the northern mass of the complex into the hinge of an open D3 fold in which the older components locally preserve weak north-south oriented S3 fabrics, whereas the younger, genetically-related and more evolved intrusions are undeformed; and, 2. the fan-like distribution of kilometre long late quartz syenogranite dykes, where rotation in their orientation is interpreted to have formed in response to sinistral movement along the Cloncurry fault during east-west shortening (cf. Fig. 3). Additional support of this hypothesis is supported by biotite forming a weak north-south trending (S3 foliation) overprinting earlier-formed peak metamorphic fabrics in the metamorphic rocks west of the Cloncury fault. U-Pb SHRIMP ages of zircon from deformed quartz monzogranite (1523 ± 4 Ma) and

undeformed syenogranite (1529 ± 4 Ma) from the Mount Angelay igneous complex intrusions are within error, and given these field relationships, constrain the timing of deformation to ca. 1526 Ma. Similarly oriented tectonic fabrics are also observed within and at the margin of intrusions in the Saxby igneous complex (Mitchell, 1993).

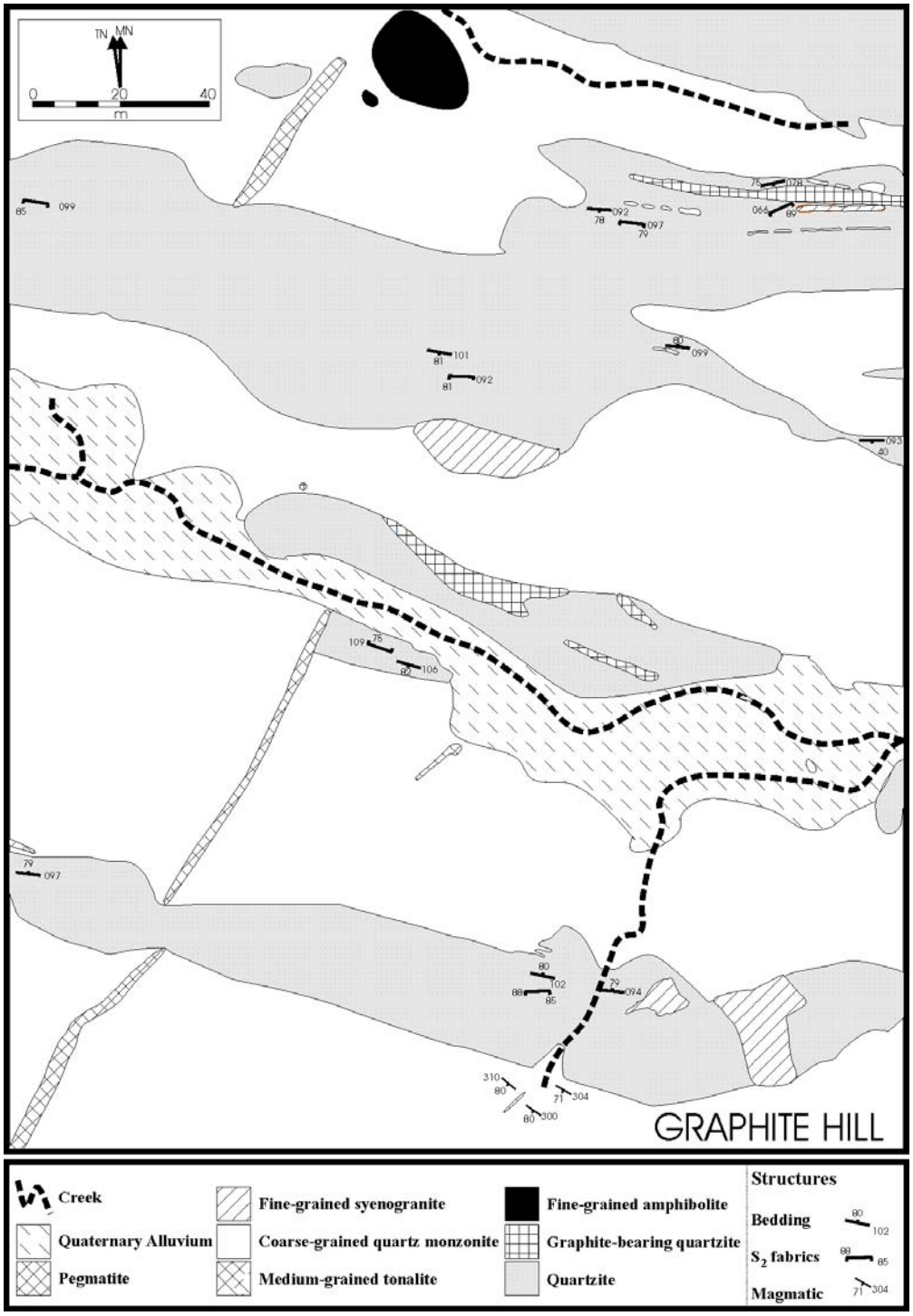

Fig. 4 (above). Detailed solid geology of a segment of the eastern margin of the Mount Angelay Igneous complex showing the lit-par-lit-style of magma emplacement, where the orientation of the felsic intrusions and their corresponding flow fabrics are broadly parallel to that of the dominant S2 tectonic fabric formed during the earlier metamorphic peak.

4 DISCUSSION

4.1 Regional context

The granitoid geochemistry and U-Pb crystallization ages of the Williams and Naraku Batholiths indicate that they include elements of two geochemically and geochronologically distinct periods of magmatism. The older phases (ca. 1550 Ma) represent tonalite-trondhjemite-granodiorite series intrusions, whereas the younger Y-depleted phases were emplaced between 1530 Ma and 1500 Ma. The younger granites form the main body of the batholiths, and include the Squirrel Hills, Wimberu, Mount Angelay, Mt Dore, Yellow Waterhole, Mt Cobalt, and Saxby Granites (cf. Wyborn, 1998).

Pollard *et al.* (1998) used geochemical criteria to differentiate the post-1540 Ma granites into the Cloncurry and Eureka Supersuites. The Cloncurry Supersuite ranges from dominantly monzogranite to syenogranite in composition (59 - 74 wt% SiO_2) and is interpreted to be the product of partial melting of a dioritic to tonalitic source. In contrast, the Eureka Supersuite varies in composition from diorite to syenogranite (50 - 76 wt% SiO_2) and is interpreted to be the product of partial melting of a variably incompatible-element-enriched gabbroic source that probably included some mantle-derived material (Mark, 2001). The composition of the Eureka Supersuite, in particular the more mafic to intermediate phases, is similar to some intrusions associated with Cu-Au mineralisation in other terranes (Pollard *et al.*, 1998). Geochemical variation in both supersuites is consistent with the fractionation of minerals observed within the granites together with the effects of locallized magma mixing and mingling.

The recognition of contemporaneous bimodal magmatism throughout the Proterozoic has raised many questions about the petrogenesis of these igneous systems (Ramo and Haapala, 1995; Richmond, 2000; Mark, 2001). The felsic components to these systems are typically dominant and are considered to have a crustal origin (Creaser, 1996; Pollard *et al.*, 1998; Wyborn, 1998), whereas the mafic rocks are interpreted largely as derivatives of a direct mantle source (Ramo and Haapala, 1995). Granitic rocks with compositions intermediate to the felsic and mafic varieties are typically less abundant and commonly exhibit a spatial association with the contacts between the two primary intrusive rock types. Granitoids of intermediate composition are variously interpreted as: 1. fractionation products of mafic magma (Wiebe, 1980); 2. intermediate magmas from which mafic and felsic rocks were derived as cumulates and residual liquid respectively (Creaser, 1996); and, 3. Hybridized bodies of the mafic and felsic magmas (Anderson and Cullers, 1978).

Contemporaneous mafic and felsic magmatism is commonly inferred for mixed igneous suites in the Mount Isa Block, and occurred where dolerite dykes and gabbroic bodies of mantle origin intruded both molten and crystalline felsic granitoids (Blake, 1981; Mitchell, 1993; Mark, 2001). Recent work in the block has revealed that mixing and mingling between mafic (quartz monzodiorite) and felsic (granite) magmas were significant processes in the formation of some of the K-rich granitoids (Richmond, 2000). This field evidence and geochemical data indicates that many of the rocks of granodiorite composition in the district are probably the hybrid products of magma mixing.

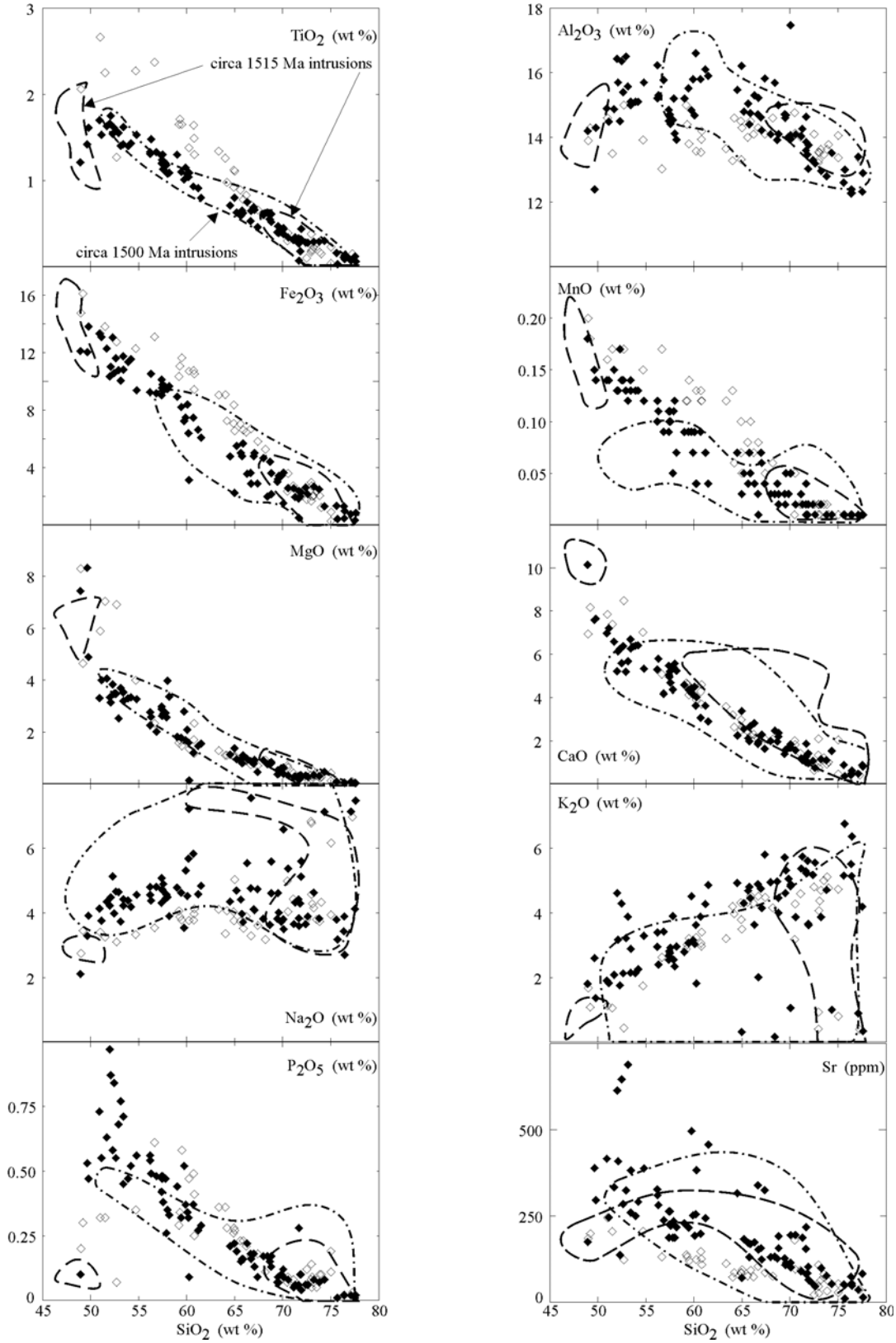

Fig. 5. Harker diagrams of selected major and trace elements of K-rich post 1530 Ma intrusions in the Cloncurry district. Closed diamonds and open diamonds represent individual analyses for the Mount Angelay and Saxby igneous complexes respectively, whereas representative fields have been drawn for the composition of ca 1515 and 1500 intrusions (data from Mitchell, 1993; Pollard and Mark, 1996; Mark, 1998; Pollard et al., 1998; Tolman, 1998; Richmond, 2000).

The coeval emplacement of mafic and felsic magmas also has significant implications for the origin of 'A-type' Proterozoic magmatism and its relationship to mantle activity (Ramo and Haapala, 1995; Creaser, 1996; Pollard *et al.*, 1998; Mark, 2001). K-rich intrusions in the Cloncurry district have broadly similar Sm-Nd isotope ratios that indicate they were largely derived from crustal sources with an average residence age of ca. 2200 Ma (cf. Mark et al., 2005a, and references therein). However, the pattern of decreasing _Nd with increasing SiO_2, is interpreted as suggesting that a significant mantle-derived component is present in the mafic intrusions and that this component decreases in intrusions of intermediate composition. This isotopic trend, together with the occurrence of bimodal magmatism, and magma mingling and hybridization, indicates that mantle activity was intimately associated with felsic magmatism and that the injection of mantle-derived mafic material into the crust probably instigated felsic magma generation.

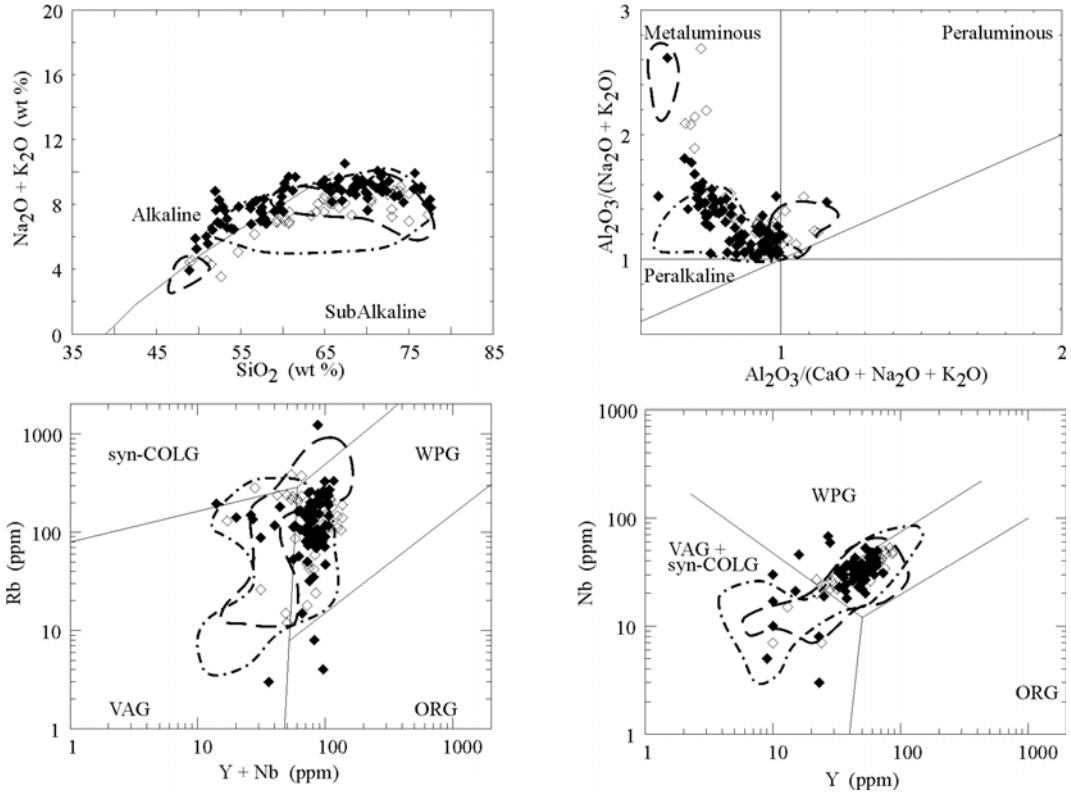

Fig. 6. Selected bi-plots of K-rich post 1530 Ma intrusions in the Cloncurry district (data from Mitchell, 1993; Pollard and Mark, 1996; Mark, 1998; Pollard et al., 1998; Tolman, 1998; Richmond, 2000). Symbols and fields as in Fig. 5.

(i) SiO_2 vs ($Na_2O + K_2O$) (Irvine and Barager, 1971; Fig. 3).

(ii) Al_2O_3/($CaO + Na_2O + K_2O$) vs Al_2O_3/(Na_2O) + K_2O). (Maniar and Piccoli, 1989; Fig. 2).

(iii) (Y + Nb) vs Rb. (Pearce et al., 1982; Fig. 4)

(iv) Y vs Nb geochemical discrimination plot (Pearce et al., 1982; Fig. 3).

Abbreviations: WPG- Within-plate granite; ORG- Orogenic Granite; VAG- Volcanic Arc Granite; syn-COLG- syn-Collisional Granite.

4.2 Age and intrusive relationships of post-peak metamorphic intrusions

As indicated, the Mount Angelay and Saxby igneous complexes (emplaced at ca. 1530-1520 Ma) are the oldest examples of post-peak metamorphic potassic magmatism within the Williams and Naraku Batholiths. However, the generalized sequence of granite emplacement and petrogenesis that characterize these rock suites is typical of all the younger intrusive complexes in the district. Early coeval mafic and felsic intrusions (and local hybridization) are invariably followed by younger, more fractionated, felsic

intrusions, with late mafic dykes rarely observed (cf. Pollard et al., 1998; Richmond, 2000; Mark, 2001; Perring et al., 2001). Collectively, these intrusions exhibit a range in U-Pb zircon crystallization ages between 1530 Ma and 1500 Ma (Table 1), that can be arranged into three broad temporal categories (i.e. 1530-1520 Ma, 1520-1510 Ma, and 1510-1500 Ma) that also form demonstrable spatial associations. Each temporal phase of magmatism largely exhibits a similar range in composition (Figs 5-7), intrusive type, and mineralogy.

The emplacement of the Mount Angelay intrusive complex synchronously with an east-west compressional deformation event (producing a steep subvertical to vertical N-S foliation) restricts the timing of the local deformation to ca. 1526 Ma (Table 1). Similar tectonic fabrics are also observed in younger intrusions (and adjacent metasedimentary rocks) within the Cloncurry district, e.g. the Mavis Granodiorite emplaced ca. 1505 Ma (Davis et al., 2001). There is, therefore, an apparent diachroneity in the formation of similarly-oriented tectonic fabrics, which highlights the need for caution when correlating between generations of tectonic fabrics in the absence of adequate age constraints.

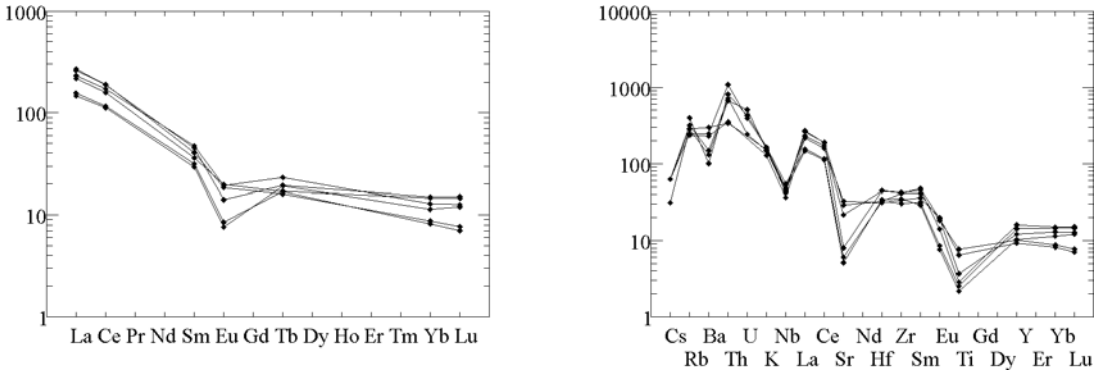

Fig. 7. Primitive mantle normalised diagrams of intrusions from the Mount Angelay and Saxby igneous complexes (data from Mitchell, 1993; Mark, 1998; Pollard et al., 1998; Tolman, 1998; Richmond, 2000). Primitive mantle after Sun and McDonough (1989).

(i) Mount Angelay and Saxby igneous complex intrusions / Primitive mantle normalised diagram. Note the intrusions with relatively flat REE trends and the smallest –ve Eu represent mafic intrusions, whereas those samples that exhibit a pronounced –ve Eu anomaly represent intrusions of granitic composition (cf. Fig. 7ii).

(ii) Mount Angelay and Saxby igneous complex intrusions / Primitive mantle normalised diagram.

4.3 Origin and nature of Potassic Magmatism

The combined field relationships, and geochemical and geochronological data most likely indicate that the same melt-forming reactions and processes occurred episodically between 1530 Ma and 1500 Ma. Given the range in composition and the enrichment in incompatible elements of intrusions emplaced during each period of magmatism, the protolith to each of these batches of magma was not melted previously (cf. Creaser and White, 1991). The evolution of each granitoid suite is consistent with the interpreted sequence of Huppert and Sparks (1988), who invoked the initiation of crustal melting through the emplacement of hot, mantle-derived magma. The production of crustal melts as a consequence of mantle-derived magma emplacement is a commonly invoked mechanism for the formation of both Proterozoic and Paleozoic potassic intrusions with 'A-type' geochemical characteristics (Wyborn et al., 1988; Hildreth et al., 1991; Ramo and Haapala, 1995; Creaser, 1996). The predicted and experimentally-derived high temperatures of these melt types (Clemens et al., 1987; Huppert and Sparks, 1988) broadly conform to temperature estimates for mafic and least-evolved felsic intrusions in the

Cloncurry district (Wyborn, 1998; Mark, 1999), and with compositionally similar intrusions elsewhere (e.g., ca 1.88 Ga Jamon Granite, Brazil; Dall'Agnol et al., 2005). The high solidus temperature, combined with the short residence period of ponded mafic magmas in the crust (10^2 - 10^3 Y; Huppert and Sparks, 1988) is consistent with the production of post-peak-metamorphic crustal melts as a response to the episodic emplacement of hot, mafic, mantle-derived material into the crust.

The Y-undepleted and Sr-depleted signature of the Williams and Naraku Batholiths was highlighted by Wyborn et al. (1992), who suggested that these geochemical associations imply that the intrusions were formed by melting of garnet-absent, plagioclase-bearing crustal material. The source material probably contained a mixture of tonalitic and amphibolitic material (cf. Creaser et al., 1991; Creaser, 1995; Wyborn, 1995; Pollard et al., 1998; Mark, 2001) that was melted at high temperatures (>900^{o}C: Clemens et al., 1987; Singh and Johannes, 1996 a, b; Mark, 2001). Therefore, amphibole dehydration reactions must have occurred at pressures <0.8-1.0 GPa for the residuum to remain garnet-free and plagioclase-stable (cf. Wolf and Wyllie, 1995). These limitations on melting for the post-1530 Ma potassic intrusions indicate that hot mantle-derived material must have ponded at depths of <30 km during each stage of partial melting and granite emplacement.

The emplacement of magma in the crust can be controlled by the density of the magma, mechanical properties of the crust, and ambient stress regime (Ryan, 1987). As a consequence, the mafic intrusions may have been localized along the transition zone between crustal horizons with significant density or thermal contrasts, or along crustally-significant structures. The results of deep seismic analysis across the Mount Isa Inlier show the presence of a tabular, high velocity refractor at a depth (present day = ca. 20 km) that has been suggested as a potential heat source for melting and the production of the Williams and Naraku Batholiths (MacCready et al., 1998; Pollard et al., 1998; Mark, 2001). However, layers of similar character are not recorded at geologically appropriate depths beneath older Y-undepleted and Sr-depleted intrusions to the west, and therefore the high velocity layer may bear no genetic relationship to K-rich magmatism in the Cloncurry district (cf. MacCready et al., 1998).

Models for the origin of potassic granites with 'A-type' geochemical characteristics (e.g. enriched in K, U, Th and HFSE, and depleted in Cr, Ni and Co) generally involve partial melting of tonalitic crust (cf. Creaser and White, 1991; Singh and Johannes, 1996 a, b) with various contributions of more mafic, amphibole-rich crustal or juvenile mantle components (Pollard et al., 1998; Mark, 2001). The degrees of partial melting (10-50%) generally required for the formation of 'A-type' magmas from source rocks of this type indicates a source volume on the order of 20000 km^3 was required to produce the Williams and Naraku Batholiths (assuming an average thickness of 2 km for the 2100 km^2 of exposure). The broadly similar compositions of the least evolved felsic intrusions formed during each period of magmatism (cf. Figs 5-7) suggests that either the fertile source region exhibited minor variation in bulk composition, and/or broad-scale homogenization at each source region. Variation in the composition of more evolved felsic differentiates is likely to have been produced via differences in fractional crystallization processes (e.g. Δ^o of fractionation, ΔP, Δmineralogy) during intracrustal ponding and/or on transfer to the site of emplacement

The synchronicity of K-rich magmatism and east-west compression may have resulted from far-field stresses related to plate boundary processes (cf. Nyman et al., 1994), and/or

local thermal weakening of the crust associated with the emplacement of the intrusions. The recognition of similarly oriented N-S structures formed at least 20 million years apart, but with the same relative timing to the regionally-dominant tectonic fabric (Davis et al., 2001), implies that there was an ambient horizontal east-west compressional stress regime between 1530 and 1500 Ma. The spatial association of most intrusions of the Williams Batholith to the Selwyn Shear Zone (Adshead-Bell, 1998) or the Cloncurry Fault (ductile-brittle shear zone during that time; de Jong and Williams, 1995) suggests that both structures were the major controlling conduits for melt migration. The episodic emplacement of magmas during this time implies that these structures acted as aquifers for newly generated mid-crustal melts.

The emplacement of intrusions during tectonism associated with orogenic processes at a distal plate margin is better understood for Phanerozoic magmatic systems, and for Precambrian systems associated with trondhjemitic-tonalitic magmatism. The formation of Precambrian, K-rich, intrusions with 'A-type' geochemical affinities typically have been ascribed to anorogenic environments (Whalen et al., 1985; Ramo and Haapala, 1995). However, a growing body of evidence indicates that many intrusions with 'A-type' geochemical affinities exhibit syn-tectonic emplacement relationships (Eby, 1992; Nyman et al., 1994). This apparent contradiction is perhaps best explained if the magma composition is not intrinsically related to the tectonic environment, but rather to the composition of the source region and the conditions of melt formation. Where these parameters are met, K-rich intrusions with 'A-type' geochemical affinities can be formed. The prevalence of these rock types during the Proterozoic rather than the Phanerozoic probably reflects four main geological characteristics of the Proterozoic: (1) higher crust and mantle temperatures; (2) greater relative volume of trondhjemite-rich material in the crust; (3) lower volume of mature sedimentary rocks; and, (4) thinner crust.

4.4 Mechanism for episodic magmatism

The results of this work suggests that the bulk of the Williams and Naraku Batholiths were emplaced during at least three periods of synchronous mafic and felsic magmatism during subhorizontal, east-west compression. The episodic timing of magmatism involving both mafic and felsic intrusions can be used to appeal to an intimate link between mantle processes, heating in the mid-crust, and felsic magmatism (cf. Stüwe et al., 1993; Scott et al., 2000). However, the main driving mechanism(s) linking these processes and the formation of potassic 'A-type' magmas during the Proterozoic is unconstrained. We believe that the advection of heat into the mid-crust via the emplacement of mantle-derived mafic material on an episodic basis is the likely mechanism for the instigation and formation of the post-peak metamorphic, potassic magmas discussed here. However, the mechanism for the generation and egress of the mafic rocks into the crust and the apparent syn-compressional emplacement of these magmas into the crust remains unconstrained.

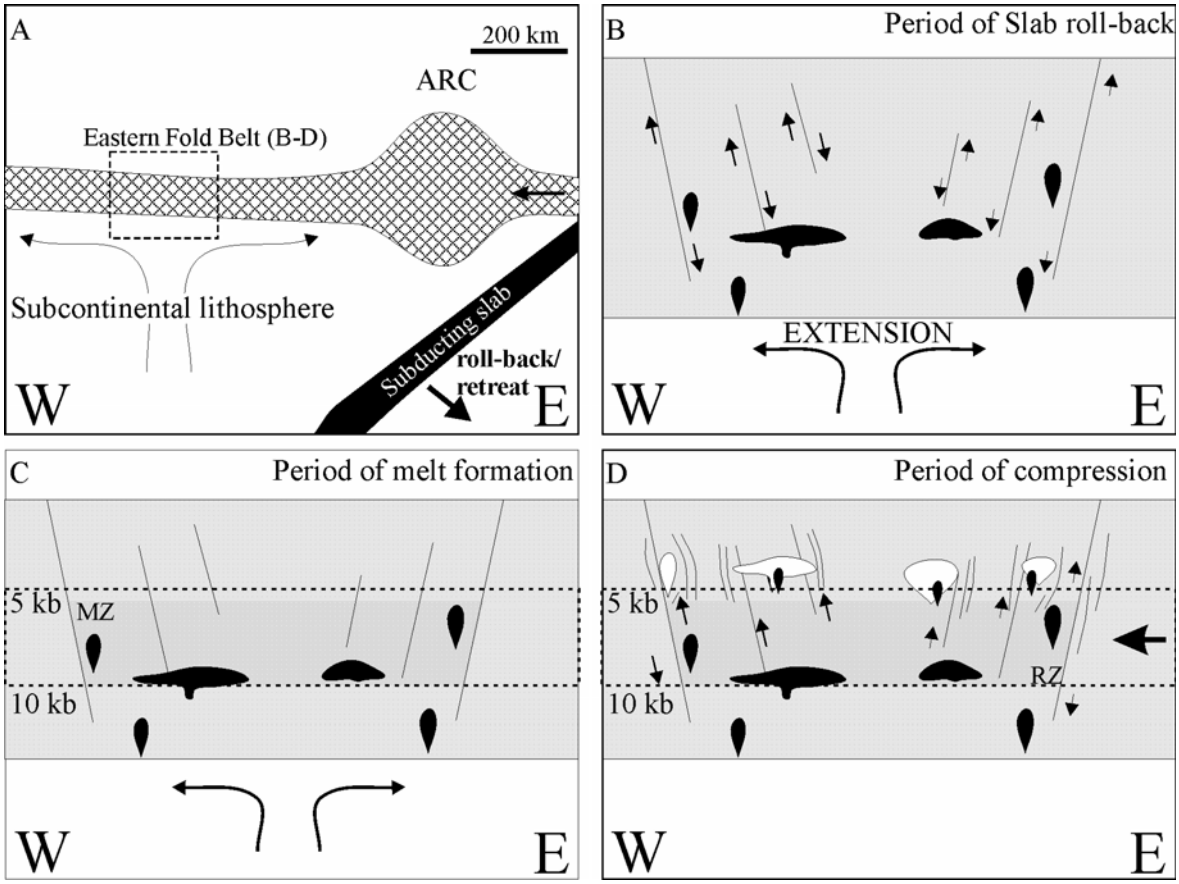

Fig. 8. A series of schematic diagrams showing a mechanism for the relations between post-peak metamorphic batholith emplacement in the Eastern Fold Belt and a hypothesized destructive margin and arc to the east (A) (cf. Giles et al., 2002). The batholith is interpreted to have formed during a sequence of events including: the episodic emplacement of mantle-derived mafic material (opaque intrusions) during extension at the base of the crust (B); mid-crustal melt formation (C); and, syn-compressional felsic (white intrusions) ± mafic (opaque intrusions) magma emplacement (D) associated with episodes of slab roll-back/ retreat (cf. Giles et al., 2002). The sequence from B to D is interpreted to have occurred during three periods between ca 1530 Ma to ca 1500 Ma (ca 1530-1520 Ma; 1520-1510 Ma; 1510-1500 Ma). Abbreviations: MZ, melting zone; RZ, residual zone.

Episodic magmatism is well known in Phanerozoic arc environments in which multiple generations of magmatism are commonly affiliated with changes in the structural dynamics at plate boundary margins (e.g. slab-roll back/retreat). A similar mechanism involving short-lived, episodic slab rollback can be invoked here, where periods of slab rollback instigate renewed mantle convection; and coincident thinning at the base of the crust leading to the egress of mantle material into the crust (cf. Fig. 8). Repeated short-lived activity over a 30 million year period is plausible given evidence from modern-day plate motion analogues (cf. Shellart et al., 2000, 2002; and references therein). Cessation of these periods of rollback would also lead to the resumption of east-west horizontal compression within the crust, which is consistent with the syn-compressional timing of potassic magmatism and the orientation of the tectonic fabrics (cf. Fig. 3ii). Clear evidence for such margins during the Proterozoic is difficult to establish (cf. Blewett and Black, 1998; Scott et al., 2000). However, a recent interpretation of the Paleo- to Mesoproterozoic tectonic environment for blocks within the Australian continent, including the Mount Isa Block, suggests the presence of a broadly north-south trending, westward dipping, destructive margin outboard, and to the east of the Mount Isa Block and the Georgetown, Yambo and Coen inliers during the time of the Isan Orogeny and the emplacement of

potassic magmatism discussed here (cf. Betts et al., 2002; Giles et al., 2002, 2004). This scenario is consistent with the timing of ca 1550-1530 Ma I- and S-type magmatism in the Georgetown inlier, and the kinematics of synchronous tectonic fabrics (cf. Blewett et al., 1998; Boger and Hanson, 2004). A similar tectonic framework is also invoked for synchronous mafic and felsic magmatism between 1820 and 1670 Ma in the western Mount Isa Block (cf. Scott et al., 2000), where transpressional fault systems are invoked as the conduits for intrusions. Structural data from along the Cloncurry Fault supports such an association with the 1530 Ma potassic intrusions in the Eastern Succession emplaced adjacent to, and along the fault during transpression.

5. Conclusions

- The Mount Angelay and Saxby igneous complexes were emplaced during 1530-1520 Ma, and represent the oldest recorded post-peak metamorphic potassium-rich intrusions of the Williams and Naraku Batholiths.
- Potassic magmatism in the Cloncurry district was emplaced during three periods: 1. 1530-1520 Ma, 2. 1520-1510 Ma, and 3. 1510-1500 Ma, where magmatic complexes from each period exhibit the same magmatic evolutionary steps from early bi-modal mafic and felsic magmatism and hybridization, to late emplacement of more evolved, but genetically related, felsic intrusions.
- Field and geochronological constraints indicate that the district experienced an ambient horizontal east-west compressional stress field related to far-field processes at a distal plate margin between 1530 and 1500 Ma, and that local intensification of N-S trending, post-peak metamorphic tectonic fabrics around or within granites of that age was associated with thermally-induced crustal weakening produced by heat transfer from the crystallising intrusions.
- The intrusions were emplaced during a period of east-west compressive deformation, and along and adjacent to transpressional fault zones (e.g., Cloncurry Fault).
- Episodic magmatism between 1530 Ma and 1500 Ma occurred in response to repeated slab rollback at a distal plate margin to the east. Rollback instigated renewed mantle convection and the advection of heat into the mid-crust via the emplacement of mantle-derived mafic material.

Acknowledgements

This work was partly funded through the pmd*CRC. SHRIMP and TIMS analysis of magmatic and hydrothermal phases was funded via a JCU ARC small grant and the AMIRA P728 Cloncurry district: gold and base metals project. GM is a Logan Fellow funded by Monash University. The authors would like to thank Mike Rubenach, Patrick Williams, Julie Richmond, Justin Tolman, Michael Darvall, Eamon Dare, Tom Blenkinsop and Nick Oliver for their assistance in the field and during the first phase of the pmd*CRC. Peter Betts, David Giles and Steve Boger are also gratefully acknowledged for fruitful discussions relating to the tectono-magmatic evolution of the Mount Isa Inlier and neighbouring Precambrian blocks. Andy Barnicoat is also thanked for reviewing an earlier version of this manuscript.

6. REFERENCES

Adshead, N.D., Voulgaris, P. and Muscio, V.N., 1998. Osborne copper-gold deposit. In: Berkman, D.A. and Mackenzie, D.H. (eds), Geology of Australian and Papua New Guinean mineral deposits. Australasian Institute of Mining and Metallogeny, v. 22, pp. 793-799.

Adshead-Bell, N.S., 1998. Evolution of the Starra and Selwyn high strain zones, Eastern Fold Belt, Mount Isa Inlier: Implications for Au-Cu mineralization. Economic Geology, 93, 1450-1462.

Anderson, J.L., 1983. Proterozoic anorogenic granite plutonism of North America. Geological Society of America Bulletin, v. 161, pp. 133-154.

Anderson, J.L. and Bender, E.E., 1989. Nature and origin of Proterozoic A-type granitic magmatism in the southwestern United States of America. Lithos, 23, 19-52.

Anderson, J.L. and Cullers, R.L., 1978. Geochemistry and evolution of the Wolf River batholith, a late Precambrian rapakivi massif in north Wisconsin, USA. Precambrian Research, 7, 287-324.

Baker, T. and Laing, W.P., 1998. Eloise Cu-Au deposit, east Mt Isa Block: structural environment and structural controls on ore. Australian Journal of Earth Sciences, 45, 429-444.

Baker, T., Perkins, C., Blake, K.L. and Williams, P.J., 2001. Radiogenic and stable isotope constraints on the genesis of the Eloise Cu-Au deposit, Cloncurry district, NW Queensland. Economic Geology, 96, 723-742.

Blake, D.H., 1981. Intrusive net-veined complexes in north Queensland. Bureau of Mineral Resources Journal of Australian Geology and Geophysics Bulletin, v. 6, 95-99.

Blake, D.H., 1987. Geology of the Mount Isa Inlier and environs. Queensland and Northern Territory. Bureau of Mineral Resources, Journal of Australian Geology and Geophysics Bulletin, v. 225, 83 pp.

Blewett, R.S. Black, L.P., Sun, S-S., Knutson, J., Hutton, L.J. and Bain, J.H.C., 1998. U-Pb zircon and Sm-Nd geochronology of the Mesoproterozoic of North Queensland: implications for a Rodinian connection with the Belt supergroup of North America. Precambrian Research, 89, 101-127.

Boger, S.D. and Hanson, D., 2004. Metamorphic evolution of the Georgetown Inlier, northeast Queensland, Australia; evidence for an accreted Palaeoproterozoic terrane? Journal of Metamorphic Petrology, 22, 511-527.

Bons, P.D., Dougherty, J. and Elburg, M.A., 2001. Stepwise assumulation and ascent of magmas. Journal of Metamorphic Geology, 19, 627-633.

Clemens, J.D., Holloway, J.R. and White, A.J.R., 1986. Origin of an A-type granite: experimental constraints. American Mineralogist, 71, 317-324.

Collins, W.J., Beams, S.D., White, A.J.R. and Chappell, B.W., 1982. Nature and origin of A-type granites with particular reference to southeastern Australia. Contributions to Mineralogy and Petrology, 80, 189-200.

Creaser, R.A., 1995. Neodymium isotopic constraints for the origin of Mesoproterozoic felsic magmatism, Gawlor Craton, South Australia. Canadian Journal of Earth Sciences, 32, 460-471.

Creaser, R.A., 1996. Petrogenesis of a Mesoproterozoic quartz latite-granitoid suite from the Roxby Downs area, South Australia. Precambrian Research, 79, 371-394.

Creaser, R.A., Price, R.C. and Wormald, R.J., 1991. A-types revisited: assessment of a residual-source model. Geology, 19, 163-166.

Creaser, R.A. and White, A.J.R., 1991. Yardea Dacite- large volume, high-temperature felsic volcanism from the middle Proterozoic of South Australia. Geology, 19, 48-51.

Dall'Agnol, R., Teixeira, N.P., Rämö, T., Moura, C.A.V., Macambira, M.J.B. and de Oliveira, D.C. 2005. Petrogenesis of the Paleoproterozoic rapakivi A-type granites for the Archean Carajás metallogenic province, Brazil. Lithos, 80, 101-129.

Dare, E.M., 1995. The textural and geochemical variation of the central Mt Angelay igneous complex, Cloncurry, Northwest Queensland, Australia. Unpublished BSc (Honours) thesis, James Cook University Townsville, Australia, 109 p.

Darvall, M., 1998. Sodic-calcic alteration in the Roxmere igneous complex of the Cloncurry district. Unpublished BSc (Honours) thesis. James Cook University.

Davis, B.K., Pollard, P.J., Lally, J.H., McNaughton, N.J., Blake, K. and Williams, P.J., 2001. Deformation history of the Naraku Batholith, Mt Isa Inlier, Australia: implication for pluton ages and geometries from structural study of the Dipvale Granodiorite and Levian Granite. Australian Journal of Earth Sciences, 48, 113-129.

de Jong, G. and Williams, P.J., 1995. Giant metasomatic system formed during exhumation of mid-crustal Proterozoic rocks in the vicinity of the Cloncurry Fault, northwest Queensland. Australian Journal of Earth Sciences, 42, 281-290.

Drabsch, B., 1998. The relationship between mafic skarn development, microdiorite intrusion and alteration and mineralisation in the Corbould Zone of the Proterozoic Mount Elliott Cu-Au deposit, Eastern Fold Belt, northwest Queensland. Unpublished BSc (Honours) thesis. James Cook University.

Eby, 1992. Chemical subdivision of A-type granitoids: petrogenetic and tectonic implications. Geology, 20, 641-644.

Emslie, R. and Taylor, B., 1992. Rapakivi and related granitoids of central Labrador in 29th IGC, Kyoto, Japan. abstracts, v. 2 of 3, pp. 562.

Foster, D. and Rubenach, M.J., 2000. Comment: High radiogenic heat-producing granites and metamorphism – An example from the western Mount Isa inlier, Australia. Geology, 28, 671.

Foster, D. and Rubenach, M.J., 2005. Isograd pattern and regional low-P, high-T metamorphism of pelitic, mafic and calc-silicate rocks along an east-west section through the Mount Isa inlier. Australian Journal of Earth Sciences, 52 (in press).

Frost, C.D. and Frost, B.R., 1997. Reduced rapakivi-type granites: the tholeiite connection. Geology, 25, 647-650.

Gauthier, L., Hall, G., Stein, H. and Schaltegger, U., 2001. The Osborne deposit, Cloncurry district: a 1595 Ma Cu-Au skarn deposit. In: Williams, P.J. (ed.), 2001: a hydrothermal odyssey, new developments in metalliferous hydrothermal systems research, extended conference abstracts. EGRU contribution, v. 59, pp. 58-59.

Giles, D., Betts, P. and Lister, G., 2002. Far-field continental backarc setting for the 1.80-1.67 Ga basins of northeastern Australia. Geology, 30, 823-826.

Giles, D. and Nutman, A.P., 2002. SHRIMP U-Pb monazite dating of 1600-1580 Ma amphibolite facies metamorphism in the southeastern Mt Isa Block, Australia. Australian Journal of Earth Sciences, 49, 455-465.

Giles, D. and Nutman, A.P., 2003. SHRIMP U-Pb zircon dating of the host rocks of the Cannington Ag-Pb-Zn deposit, southeastern Mt Isa Block, Australia: Australian Journal of Earth Sciences, v. 50, p. 295-309.

Hand, M. and Rubatto, D., 2002. The scale of the thermal problem in the Mount Isa Inlier. In: Preiss, V.P., (ed.), Geoscience 2002: expanding horizons, Geological Society of Australia, v. 67, pp. 475.

Hildreth, W., 1981. Gradients in silicic magma chambers: implications for lithospheric magmatism. Journal of Geophysical Research, 86, 10153-10192.

Hodgson, W.T., 1997. Timing of albitisation in Mallee Gap, Eastern Selwyn Range Area, Cloncurry, NW Queensland. Unpublished BSc (Honours) thesis. James Cook University.

Huppert, H.E. and Sparks, R.S.J., 1988. The generation of granitic magmas by intrusion of basalt into continental crust. Journal of Petrology, 29, 599-624.

Irvine, T.N. and Barager, W.R.A., 1971. A guide to the chemical classification of the common volcanic rocks. Canadian Journal of Earth Sciences, 8, 523-548.

Knight, F.C. 1995. Petrology of the Mount Margaret Granitoids, Cloncurry iron oxide Cu-Au district, Northwest Queensland. Unpublished MSc thesis. University of Exeter.

Lenharo, S.L.R., Pollard, P.J. and Born, H., 2003. Petrology and textural evolution of granites associated with tin and rare-metals mineralization at the Pitinga mine, Amazonas, Brazil. Lithos, 66, 37-61.

Little, G.A., 1997. Structural evolution and paragenesis of alteration and mineralization at Mount Elliot Cu-Au mine, Northwest Queensland. BSc (Honours) thesis. James Cook University.

MacCready, T., Goleby, B.R., Goncahrov, A. and Drummond, B.J., 1998. A framework of overprinting orogens based on interpretation of the Mount Isa Deep Seismic Transect. Economic Geology, 93, 1422-1434.

Maniar, P.D. and Piccoli, P.M., 1989. Tectonic discrimination of granitoids. Geological Society of America Bulletin, v. 101, pp. 635-643.

Mark, G., 1999. Petrogenesis of Mesoproterozoic K-rich granitoids, Southern Mount Angelay igneous complex, Cloncurry District, Northwest Queensland, Australia. Australian Journal of Earth Sciences, 45, 933-949.

Mark, G., 2001, Nd isotope and petrogenetic constraints for the origin of the Mount Angelay igneous complex: Implications for granitoid formation in the Cloncurry district, Australia. Precambrian Research, 105, 17-35.

Mark, G. and Foster, D.R.W., 2000, Magmatic albite-actinolite-apatite-rich rocks from the Cloncurry district, Northwest Queensland, Australia. Lithos, 51, 223-245.

Mark, G., Foster, D.R.W., Pollard, P.J., Williams, P.J., Tolman, J., Darvall, M. and Blake, K.L., 2004b, Magmatic fluid input during large-scale Na-Ca alteration in the Cloncurry Fe oxide-Cu-Au district, NW Queensland, Australia. Terra Nova, 16, 54-61.

Mark, G., Oliver, N.H.S., Williams, P.J., Valenta, R.K. and Crookes, R.A., 2000, The evolution of the Ernest Henry hydrothermal system, *in* Porter, T.M., ed., Hydrothermal Iron Oxide Copper-Gold and Related Deposits. A Global Perspective: Australian Minerals Foundation, pp. 123-136.

Mark, G., Williams, P.J. and Boyce, A.J., 2004a. Low-latitude meteoric fluid flow along the Cloncurry Fault, Cloncurry district, NW Queensland, Australia: geodynamic and metallogenic implications. Chemical Geology, 207, 117-132.

Mark, G., Phillips, G.N. and Pollard, P.J., 1998. Highly selective partial melting of pelitic gneiss at Cannington, Cloncurry District. Australian Journal of Earth Sciences, 45, 169-176.

Mitchell, L.C., 1993. Geology and Geochemistry of the Wiley Igneous Complex, Eastern Fold Belt, Mt Isa Inlier. Unpublished BSc (Honours) thesis. James Cook University.

Nyman, M.W., Karlstrom, K.E., Kirby, E. and Graubard, C.M., 1994. Mesoproterozoic contractional orogeny in western North America: evidence from ca. 1.4 Ga plutons. Geology, 22, 901-904.

Oliver, N.H.S., Cleverley, J.S., Mark, G., Pollard, P.J., Fu, B., Marshall, L.J., Rubenach, M.J., Williams, P.J. and Baker, T., 2004. The role of sodic alteration in the genesis of iron oxide-copper-gold deposits, eastern Mt Isa Block, Australia. Economic Geology, 99, 1145-1176.

Page, R.W. and Sun, S-S., 1998. Aspects of geochronology and crustal evolution in the Eastern Fold Belt, Mount Isa Inlier. Australian Journal of Earth Sciences, 45, 343-362.

Pearce, J.A. and Cann, J.R., 1973. Tectonic setting of basic volcanic rocks determined using trace element analyses. Earth and Planetary Sciences Letters, 19, 290-300.

Pearce, J.A., Harris, N.B.W. and Tindle, A.G., 1984. Trace element diagrams for the tectonic interpretation of granitic rocks. Journal of Petrology, 25, 956-983.

Perkins, C. and Wyborn, L., 1998. Age of Cu-Au mineralisation, Cloncurry district, Mount Isa Inlier, as determined by $^{40}Ar/^{39}Ar$ dating. Australian Journal of Earth Sciences, 45, 233-246.

Perring, C.S., Pollard, P.J., Dong, G., Nunn, A.J. and Blake, K.L., 2000. The Lightning Creek sill complex, Cloncurry district, northwest Queensland: A source of fluids for Fe-oxide Cu-Au mineralisation and sodic-calcic alteration. Economic Geology, 95, 1067-1089.

Perring, C.S., Pollard, P.J. and Nunn, A.J., 2001. Petrogenesis of the Squirrel Hills granite and associated magnetite-rich sill and vein complex: Lightning creek prospect, Cloncurry district, Northwest Queensland. Precambrian Research, 106, 213-238.

Persson, A.I., 1999. Absolute (U-Pb) and relative age determinations of intrusive rocks in the Ragunda rapakivi complex, central Sweden. Precambrian Research, 95, 109-127.

Pollard, P.J., 2001. Sodic(-calcic) alteration associated with Fe-oxide-Cu-Au deposits: an origin via unmixing of magmatic-derived H_2O-CO_2-salt fluids. Mineralium Deposita, 36, 93-100.

Pollard, P.J., Mark, G. and Mitchell, L.C., 1998. Geochemistry of post-1540 granites spatially associated within regional sodic-calcic alteration and Cu-Au-Co mineralisation, Cloncurry district, northwest Queensland. Economic Geology, 93, 1330-1344.

Pollard, P.J. and McNaughton, N., 1997. U-Pb geochronology and Sm/Nd isotope characteristics of Proterozoic intrusive rocks in the Cloncurry district, Mount Isa Inlier, Australia. AMIRA P438 Final Report: Cloncurry Base Metals and Gold, 4: 19.

Ramo, O.T. and Haapala, I., 1995. One hundred years of Rapakivi Granite. Mineral. Petrol. 52, 129-185.

Richmond, J.M., 2000. Mapping intrusions using gamma-ray spectrometry: a case study in the Cloncurry district, Northwest Queensland. Unpublished PhD thesis. James Cook University.

Rotherham, J.F., 1997. A metasomatic origin for the iron-oxide Au-Cu Starra Orebodies, Eastern foldbelt, Mount Isa Inlier. Mineralium Deposita, 32, 205-218.

Rotherham, J.F., Blake, K.L., Cartwright, I. and Williams, P.J., 1998. Stable isotope evidence for the origin of the Starra Au-Cu deposit, Cloncurry district. Economic Geology, 93, 1435-1449.

Rubenach, M.J., Adshead, N.D., Oliver, N.H.S., Tullemans, F., Esser, D. and Stein H., 2001. The Osborne Cu-Au deposit: geochronology, and genesis of mineralization in relation to host albitites and ironstones. In Williams, P.J. (ed.) 2001: a hydrothermal odyssey, new developments in metalliferous hydrothermal systems research, extended conference abstracts. EGRU contribution 59: 172-173.

Rubenach, M.J. and Barker, A.J., 1998. Metamorphic and metasomatic evolution of the Snake Creek Anticline, Eastern Succession, Mount Isa Inlier. Australian Journal of Earth Sciences, 45, 363-372.

Rubenach, M.J. and Lewthwaite, K.A., 2002. Metasomatic albitites and related biotite-rich schists from a low-pressure polymetamorphic terrane, Snake Creek Anticline, Mount Isa Inlier, north-eastern Australia: microstructures and P-T-d paths. Journal of Metamorphic Geology,

20, 191-202.

Ryan, M.P., 1987. Neutral buoyancy and the mechanical evolution of magmatic systems. In: Mysen, B.O. (ed.), Magmatic Processes: Physicochemical Principles. Special Publication v. 1 Geochemical Society, pp. 259-288.

Scott, D.L, Rawlings, D.J., Page, R.W, Tarlowski, C.Z., Idnurm, M., Jackson, M.J. and Southgate, P.N., 2000. Basement framework and geodynamic evolution of the Palaeoproterozoic superbasins of north-central Australia: an integrated review of geochemical, geochronological and geophysical data. Australian Journal of Earth Sciences, 47, 341-380.

Singh, J. and Johannes, W., 1996a. Dehydration melting of tonalites. Part I. Beginning of melting. Contributions to Mineralogy and Petrology, 125, 16-25.

Singh, J. and Johannes, W., 1996b. Dehydration melting of tonalites. Part II. Composition of melts and solids. Contributions to Mineralogy and Petrology, 125, 26-44.

Stüwe, K. Sandiford, M. and Powell, R., 1993. Episodic metamorphism and deformation in low-pressure, high-temperature terranes. Geology, 21, 829-832.

Sun, S.S. and McDonough, W.F., 1989. Chemical and isotopic systematics of oceanic basalts: implications for mantle composition and processes. In: A.D. Saunders and M.J. Norry (eds), Magmatism in the Ocean Basins. Geological Society Special Publication, v. 42, pp. 313-345.

Tolman, J.L., 1998. Origin and formation of complexly textured albite-, actinolite-, apatite-rich rocks within the Central Mount Angelay igneous complex, Cloncurry district, Northwest Queensland. Unpublished BSc (Honours) thesis. James Cook University.

Wang, S. and Williams, P.J., 2001. Geochemistry and origin of Proterozoic skarns at the Mount Elliott Cu-Au (-Co-Ni) deposit, Cloncurry district, NW Queensland. Mineralium Deposita, 36, 109-124.

Whalen, J.B., Currie, K.L. and Chappell, B.W., 1985. A-type granites: geochemical characteristics, discrimination and petrogenesis. Contributions to Mineralogy and Petrology, 95, 407-419.

Wiebe, R.A., 1980. Comingling of contrasted magmas in the plutonic environment: examples from the Nain anorthositic complex. Journal of Geology, 88, 197-209.

Williams P.J., 1998. Metalliferous economic geology of the Mount Isa Eastern Succession, Queensland. Australian Journal of Earth Sciences, 45, 329-342.

Williams, P.J. and Skirrow, R.G., 2000. Overview of Iron Oxide-Copper-Gold deposits in the Curnamona Province and Cloncurry district (Eastern Mount Isa Block), Australia. In: Porter, T.M. (ed.), Hydrothermal Iron Oxide Copper-Gold and Related Deposits: A Global Perspective, AMF, pp. 105-122.

Wolf, M.B. and Wyllie, P.J., 1994. Dehydration-melting of amphibolite at 10 kbar: the effects of temperature and time. Contributions to Mineralogy and Petrology, 115, 369-383.

Wyborn, L.A.I., 1998. The younger ~1500 Ma granites of the Williams and Naraku Batholiths, Cloncurry district, eastern Mount Isa Inlier: geochemistry, origin, metallogenic significance and exploration indicators. Australian Journal of Earth Sciences, 45, 397-412.

Wyborn, L.A.I., Page, R.W. and McCulloch, M.T., 1988. Petrology, geochronology and isotope geochemistry of the post-1820 Ma granites of the Mount Isa Inlier: mechanisms for the generation of Proterozoic anorogenic granites. Precambrian Research, 40/41, 509-541.

Wyborn, L.A.I., Wyborn, D., Warren, R.G. and Drummond, B.J., 1992. Proterozoic granite types in Australia: implications for lower crust composition, structure and evolution. Transactions of the Royal Society of Edinburgh, Earth Sciences, 83, 201-209.

Sr-Nd isotopic constraints on the crustal architecture and evolution of the Eastern Succession, Mount Isa Block, Australia

Geordie Mark[1], Damien Foster[2], Roger Mustard[2] and Peter Pollard[2]
[1]School of Geosciences, Monash University, PO Box 28E, Victoria, 3800, Australia
[2]School of Earth Sciences, James Cook University, Townsville QLD 4811, Australia

ABSTRACT

The Eastern Succession of the Mount Isa Inlier, Australia was affected by a protracted period of orogenesis (Isan Orogeny: ca. 1.60-1.50 Ga) that coincided with the emplacement of a diverse range of intrusions. The whole-rock geochemistry of these intrusions fingerprint different parts of the crust during the formation of the various magmas and may bear some relationship to mantle activity during that time. Sr isotopic compositions of both peak metamorphic pegmatites (ca. 1.59 Ga and their host rocks (deposited ca. 1.67-1.65 Ga) are highly radiogenic and largely characterised by $^{87}Sr/^{86}Sr_i$ of 0.7075-0.7185 and 0.7059-0.7161 respectively. Depleted mantle T_{DM} ages for the pegmatites and host rocks are also comparable, range between 2.45-2.51 Ga and 2.53-2.57 Ga respectively, and most closely resemble the ca. 1.89-1.85 Ga felsic basement rocks (T_{DM} 2.45-2.58 Ga). The younger ca. 1.55-1.50 Ga intrusions largely have mixed crust-mantle $^{87}Sr/^{86}Sr_i$ (0.6968-0.7112) and εNd (-1.0 to –3.8), and exhibit a range in T_{DM} between 2.08 and 2.30 Ga. The ca.1.55 Ga trondhjemite has higher $^{87}Sr/^{86}Sr_i$ (0.7112) than the younger sodic, alkali granites and the potassic 'A-type' intrusions, which mainly range from 0.7067 to 0.7085, and 0.6968 to 0.7065 respectively. In contrast to the 'A-type' intrusions, the only known two-mica intrusion in the succession (ca.1.53 Ga) contains highly radiogenic $^{87}Sr/^{86}Sr_i$ (0.8062) as well as numerous zircon xenocrysts of similar age (ca.1.66 Ga) to the psammo-pelitic country rocks, compatible with a derivation from this source.

The magnetite-, pyrite- and chalcopyrite-rich ore at Osborne (ca. 1.59 Ga) and Ernest Henry (ca. 1.525 Ga) have $^{87}Sr/^{86}Sr_i$ of 0.7135 and 0.7084-0.7100 respectively that closely reflect their host rocks, and indicate that Sr in the ores is probably locally derived. The Nd isotope composition of one sample at Osborne (εNd –4.5; T_{DM} 2.40 Ga) also supports local derivation of REE.

Broad-scale Nd isotope patterns constrained by 1.74-1.50 Ga magmatic rocks show that to the east of the Pilgrim Worm the mid- to lower-crust is isotopically distinct, and generally has younger average crustal residence ages (T_{DM} ca. 2.20-2.25 Ga) than ca. 1.74 intrusions west of the worm (T_{DM} >2.45 Ga). This distinction is highlighted by the ca. 1.74 Ga Ernest Henry meta-andesite to the east of the Pilgrim Worm that has consistently younger T_{DM} ages (2.18-2.23 Ga) than coeval intrusions to the west (e.g., Burstall Granite, T_{DM} 2.38-

2.55 Ga). Outcrop of the younger generations of I- and A-type 1.67 Ga and 1.55-1.50 Ga intrusions (with T_{DM} between 2.08 and 2.30 Ga is restricted to the east of the Pilgrim Worm. This east-west contrast in T_{DM} ages, somewhere near the Pilgrim Worm, is interpreted to represent the margin of an ancient, broadly north-south oriented, terrane boundary. We suggest that the eastern block represents an allochthonous block that was probably accreted to the inlier sometime between 2.20 Ga and the cessation of magmatism in the Kalkadoon-Leichhardt Belt (ca. 1.84 Ga). Nd isotope data for the overlying 1.74-1.62 Ga sedimentary rocks (e.g. calc-silicates and psammo-pelitic sedimentary rocks) show that they were derived from a hinterland that was dominated by late Archean to early Paleoproterozoic components (2.45-2.57 Ga) that are much older than the basement rocks sampled by the intrusions to the east of the Pilgrim Worm, and are most compatible with the basement rocks in the Kalkadoon-Leichhardt Belt (KLB). However, the paucity of 1.89-1.84 Ga zircons in the younger sedimentary rocks probably indicates that the KLB rocks were not the predominant sediment source. The additional source components may have had a similar provenance to the sedimentary rocks in the Georgetown, Coen, Yambo and Daralong inliers, which implies a close spatial association between all of these inliers at and after 1.67 Ga.

Keywords: Crustal architecture, magmatism, terrane boundary, Archean, Paleoproterozoic

1. INTRODUCTION

The Mount Isa Inlier is one of the world's premier Proterozoic base metal terranes, containing numerous economically significant Cu-(Au) (e.g., Mount Isa, Ernest Henry and Osborne) and Pb-Zn-Ag (e.g., Mount Isa, Century, Cannington) resources formed late in the inlier's geological evolution (cf. Williams, 1998 a,b). The Mount Isa inlier records a protracted geological history that probably began with initial nucleation on a late Archaean-early Paleoproterozoic crustal protolith (cf. McDonald et al., 1997). This protolith is argued to have subsequently grown via a range of crustal accretion mechanisms (e.g., mafic underplating and/or mantle upwelling; cf. Etheridge et al., 1987; Wyborn, 1988; Williams, 1998c; Giles et al., 2002, and lateral accretion associated with continental-margin arc magmatism; McDonald et al., 1997; Condie, 2002). Scott et al. (2000) argue for a long-lived thermal anomaly and largely compressional setting (rather than a rift-sag or plume model) for the evolution of north-central Australia between ca. 1800 to 1575 Ma. They suggest that basin formation processes were far-field responses to an active southern margin. Formation of the Mount Isa Inlier took place between ca. 1.88 and 1.59 Ga (cf. Wyborn and Page, 1983; Page and Bell, 1986; McCulloch, 1987; Wyborn, 1988; Wyborn et al., 1988; McDonald et al., 1997; O'Dea et al., 1997; Page and Sun, 1998; Pollard et al., 1998; Betts et al., 2002; Giles et al., 2002; Giles and Nutman, 2002, 2003). Late 1.55-1.50 Ga potassic magmatism in the Eastern Succession (cf. Fig. 1a) supplemented earlier crustal accretion (cf. Pollard et al., 1998; Wyborn, 1998; Mark et al., 2005b) during the Isan Orogeny (ca. 1.60-1.50 Ga).

The crustal architecture and composition, as well as geodynamic setting of terranes are increasingly acknowledged as being intimately connected with their metallogenic character and metal endowment. These associations are better constrained for intrusion-related Cu-Au-Mo systems (porphyry and intrusion-related Au deposits), carbonate and shale hosted Pb-Zn-Ag systems (e.g., MVT and Irish type deposits); and orogenic lode gold systems than for epigenetic Cu-Au systems in the Fe oxide Cu-Au family of deposits (cf. Hitzman 2000; Williams and Pollard 2003; Williams et al., in press). This lack of understanding is

probably the result of the relatively recent categorization of this deposit type (cf. Hitzman et al., 1992), as well as the comparatively diverse spectrum of deposits included within this classification. This problem is particularly acute in the Mount Isa Inlier, which is characterized by two fold belts with broadly different metallogenic characteristics where the Western Fold Belt (WFB) is dominated by sediment-hosted Pb-Zn-Ag mineral deposits, and the Eastern Fold Belt (EFB) is dominated by epigenetic Cu-Au mineral deposits (cf. Fig. 1a). Although still controversial (cf. Williams, 1998c), the timing of Pb-Zn-Ag and Cu-Au mineralization in the inlier is largely accepted to have occurred during two periods: around 1.67-1.60 Ga for the former; and 1.60-1.50 Ga for the latter (cf. Boden, 1998; Large, 1998; Perkins and Wyborn, 1998; Baker et al., 2001; Wang and Williams, 2001; Davidson et al., 2002; Betts et al., 2003; Chapman, 2004; Davis, 2004; Mark et al., 2005a). One significant difference between the two is the predominance of siliciclastic rocks in the younger sequences in the east compared to siltstones and dolomitic shales in the west, and voluminous ca 1.55-1.50 Ga potassic magmatism in the east. A fundamental difference in the basement architecture was first highlighted by Page and Sun (1998), who noted that the Mesoproterozoic igneous rocks in the east have significantly lower Nd T_{DM} ages than geochemically comparable rocks in the west. Page and Sun (1998) suggested that this difference might signify that the eastern terrain was either: 1) an allochthonous block amalgamated early in the inlier's history, or, 2) part of a single, contiguous block that experienced greater mafic underplating in the east. That the crust below the eastern succession represents a compositionally distinct, allochthonous block is consistent with the interpretation by McDonald et al. (1997). These authors interpreted the ca.1.88-1.84 Ga igneous rocks of the Kalkadoon-Leichhardt Belt (KLB, Fig. 1a) as of calc-alkaline affinity and that they formed at the eastern edge of a continent-margin arc. However, these interpretations are at odds with earlier works by Etheridge et al. (1987) and Wyborn (1988) who both suggest that the KLB rocks were formed in an intracontinental setting. In order to address these questions we present Sr and Nd isotopic data on selected 1.74-1.50 Ga igneous and sedimentary rocks in the Eastern Succession and compare these data to igneous and sedimentary rocks west of the Pilgrim Worm and Fault (cf. Fig. 1b). This work will constrain the succession's evolutionary history and its consequent influence on the inlier's diverse magmatic and metallogenic character. The results presented here also address the broader issues concerning the timing and character of northern Australia cratonization via the amalgamation of the Mount Isa inlier with the eastern inliers (e.g., Georgetown and Coen).

2. EASTERN SUCCESSION

The Eastern Succession comprises the eastern exposed margin of the Mount Isa Inlier, and is endowed with numerous epigenetic Cu-Au deposits hosted within Paleoproterozoic carbonate-evaporite and siliciclastic metasedimentary rock sequences and metavolcanic rocks that were deposited during periods of intracrustal rifting (1.79-1.72 Ga and 1.67-1.61 Ga; Blake, 1987; Foster and Austin, 2005). Comparable successions in the west overlie older granite, schist, gneiss and metamorphosed felsic volcanic rocks dating to the Barramundi Orogeny. In the Eastern Succession, the Cover Sequence two rocks are comprised of lower bi-modal volcanic rock packages (e.g., Argylla Formation and Marraba Volcanics) interleaved with minor, psammo-pelitic (locally calcareous) sedimentary units. The basal volcanic units are overlain (possibly unconformably) by quartz- and feldspathic- sandstone and quartzite (locally calcareous) and minor volcanics of the Ballara Quartzite and Mitakoodi Quartzite (deposited ca. 1755 Ma). The upper part of the sequence is comprised of thick, well-bedded calc-silicate rocks of the apparently

diachronously deposited Corella (ca. 1750-1740 Ma) and Doherty Formations (ca. 1725 Ma). The Corella Formation is cut by intrusive phases of the Wonga Batholith and the Mount Fort Constantine Volcanics (ca. 1740 Ma, Page and Sun, 1998).

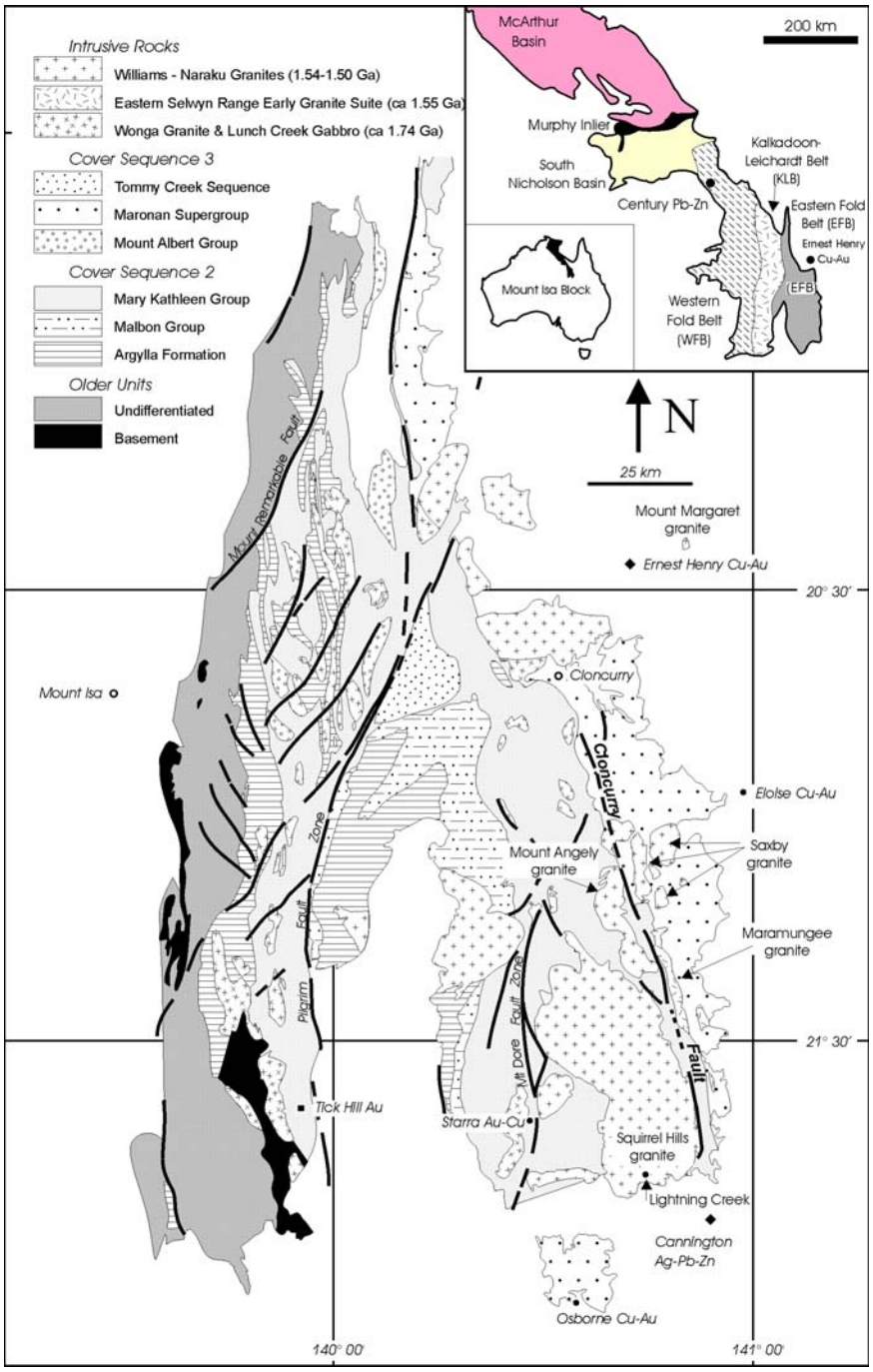

Fig. 1a (above). Geology of the Mount Isa Inlier (modified after Williams, 1998a).

Fig. 1b (below). Bouguer gravity anomaly as a 3D surface overlain by surfaces corresponding to the three major gravity worms (Blenkinsop et al. 2005).

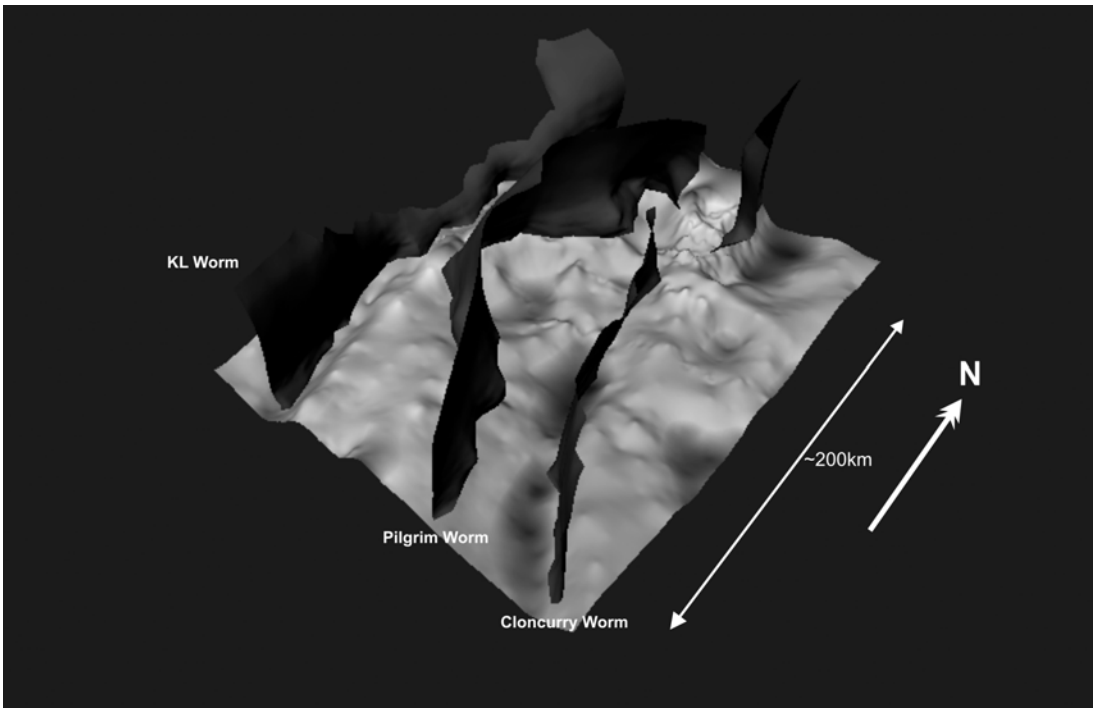

The cover sequence three rocks of the Eastern Succession preserve a shorter period of accumulation (ca. 1.68-1.60 Ga) than their counterparts to the west (1.71-1.59 Ga), although the basal Llewellyn Creek Formation may correlate with the older cover sequence 3 rocks in the west (Foster and Austin, 2005) The Eastern Succession rocks are dominated by psammo-pelitic rock packages (e.g., Soldiers Cap Group) interleaved with mafic volcanic rocks, and variably carbonaceous and calcareous (and locally sulphidic) shales. During the earlier stages of sediment accumulation, magmatic intrusions of intermediate-felsic composition (e.g., Ernest Henry diorite: ca. 1.66 Ga) were emplaced into the cover sequence two rocks and possibly the basal units of cover sequence three. However, igneous activity between 1.67 to 1.60 Ga was dominated by widespread and voluminous Fe-rich tholeiitic magmatism, manifested as lavas (Toole Creek Volcanics) and sills and dykes emplaced into the psammo-pelitic rocks of the Soldiers Cap Group (Williams, 1998c; Giles and Nutman, 2003).

These two cover sequences underwent a protracted period of compressional deformation and metamorphism during the Isan Orogeny (ca. 1.60-1.50 Ga; O'Dea et al., 1997; Page and Sun, 1998) within which three main fabrics are typically identified, although more complicated tectonothermal histories have been recorded near hydrothermal ore deposits and Isan-age igneous intrusive rocks (cf. Rubenach, 2005). Regional metamorphism ranges in grade from greenschist to upper amphibolite facies, although the timing of this thermal peak remains poorly constrained in rocks preserving different metamorphic facies, and is complicated by evidence for multiple thermal episodes, especially in the vicinity of the Williams and Naraku Batholiths (Rubenach and Barker, 1998; Rubenach and Lewthwaite, 2002). Nevertheless, published age constraints indicate that the metamorphic peak occurred ca. 1.60-1.58 Ga across much of the district (Page and Sun, 1998; Hand and Rubatto, 2000; Giles and Nutman, 2002).

The Paleoproterozoic cover sequence rocks in the Eastern Succession are intruded by a series of syn- to post-peak metamorphic intrusions that are predominantly comprised of four chemically distinctive suites of igneous rocks: 1. Anatectic pegmatites (ca. 1590 Ma);

2. Y-depleted, Sr-undepleted (TTG series) intrusions (ca. 1550 Ma); 3. Sodic, Y-undepleted, alkaline intrusions (ca. 1540-1500 Ma); and, 4. K-rich, Y-undepleted intrusive complexes (ca. 1540-1500 Ma) (cf. Table 1). The earliest magmatism during the Isan Orogeny is represented by volumetrically minor, peak metamorphic pegmatites (ca. 1.59 Ga) that are commonly garnet- or muscovite-bearing, and hosted in upper amphibolite facies siliciclastic metasedimentary rocks. These anatectic pegmatites are the products of fluid-present melting at the minimum melt curve, or by higher temperature, fluid-absent, muscovite dehydration reactions and consequent partial melting of the host siliciclastic sedimentary rocks (cf. Mark et al., 1998). These pegmatites are found only in upper amphibolite facies metasedimentary rocks. However, most intrusions were emplaced later in the Isan orogeny between ca. 1.55 and 1.50 Ga, and are comprised of ca. 1.55 Ga TTG (tonalite-trondhjemite-granodiorite) intrusions, ca. 1.53 Ga sodic, alkali granites, and ca. 1.53-1.50 Ga potassic 'A-type' intrusions (Table 1). The TTG intrusions range in composition from granodiorite to trondhjemite, and form a suite of plutonic bodies emplaced along the southeastern margin of the Cloncurry fault (cf. Fig. 1a). These intrusions have low Y and HREE, as well as moderate to elevated Al, Fe/Mg and Sr, a common characteristic of both Archaean and Phanerozoic TTG, but not adakitic intrusions. The mass of the batholith is comprised of ca. 1.53-1.50 Ga intrusions (>2100 km^2; Wyborn et al., 1988), which are predominantly potassic, although rare sodic varieties of comparable age are also present. The potassic phases of the batholiths are largely composed of metaluminous, alkaline to subalkaline, magnetite-bearing granitoids that largely plot within 'A-type' fields on geochemical discrimination diagrams (cf. Figs. 3 and 4), although field relationships suggest a syn to post-tectonic timing for the majority of the intrusions (Pollard et al., 1998; Mark et al., 2005b). Potassic intrusions range from diorite to syenogranite to pegmatite, and are typically more oxidized than older counterparts in the western half of the Mount Isa Inlier. Hybridized magmas of intermediate composition are common, and are spatially associated with zones of magma mixing and mingling between coeval mafic and felsic intrusions (cf. Fig. 3). Al-in-hornblende geobarometry indicates emplacement depths between 160 and 550 MPa (cf. Pollard et al., 1998; Mark, 2001; Perring et al., 2001).

The potassic and sodic intrusions exhibit a temporal, and less commonly observed spatial relationship to Na-Ca alteration and Cu-Au mineralization (cf. Mark et al., 2004a). The close relationship between magmatism, regional alteration and mineralisation (1590-1500 Ma) has engendered a range of highly contentious arguments as to whether intrusions played a passive role (e.g. source of thermal input to drive fluid convection), or active role (e.g. direct input of saline fluids, metals or sulphur) in the generation of the hydrothermal systems, and the formation of localized base metal mineralization (Williams and Pollard 2003; Mark et al., 2005a). Stable isotope, fluid inclusion and geochemical data from a range of deposits and regional hydrothermal systems provide evidence for a substantial role for magmatic fluids in the formation of these systems (Williams and Pollard, 2003; Mark et al., 2004a; Oliver et al., 2004).

3. THE PRE-1.8 Ga HISTORY: A REVIEW

The pre-1.80 Ga basement and cover sequence one rocks in the Mount Isa Inlier (e.g., Leichhardt Volcanics: ca. 1.87-1.86 Ga and Kalkadoon Granite: ca. 1.86-1.85 Ga) mainly crop out in the Kalkadoon-Leichhardt Belt (KLB), which forms the western margin to the Eastern Succession (Fig. 1). These crystalline rocks have the oldest Nd T_{DM} ages (2.80-2.30 Ga) as well as a spread in inherited zircon U-Pb ages between late Archaean and early

Paleoproterozoic (cf. Fig. 4; McDonald et al., 1997; Page and Sun, 1998; Bierlein and Betts, 2004). Collectively, these isotopic data indicate the rocks in the KLB igneous rocks were sourced from material that had in large part separated from the mantle and probably formed the nucleus of the Mount Isa Block during the late Archaean (cf. Wyborn et al., 1988; McDonald et al., 1997). The Eastern Succession is devoid of exposed pre-1.80 Ga rock packages (cf. Fig. 2), which prevents direct analysis of the succession's basement. However, detrital and inherited zircon U-Pb and whole-rock Sm-Nd isotopic data from various sedimentary and igneous rocks in the succession afford some insight into the evolutionary history of the mid- to lower crust. Archaean and Paleoproterozoic detrital and inherited zircons are commonly found in many of the 1.78-1.61 Ga sedimentary and igneous rocks, although apart from the rocks in the Boorama Horst – forming part of the basal section of cover sequence two (Fig. 2)- zircons of equivalent age to the KLB rocks (ca. 1.87-1.85 Ga) are rarely found. Archaean zircons are found in many of the cover sequence rocks as well as some of the younger igneous intrusions, although the main populations of Archaean zircons identified to date occur in the 1.67-1.61 Ga psammo-pelitic rocks of the Soldiers Cap Group and their associated anatectic pegmatites (cf. Page and Sun, 1998; Giles et al., 2002, 2003). This in part probably reflects the difficulty of identifying tuffaceous units in the higher metamorphic grade rocks of the Soldiers Cap Group (i.e. a potentially wider range of detrital zircon ages are being accessed in non-tuffaceous sediments). The ca. 1.78-1.60 Ga sedimentary and igneous rocks also record a number of inherited or detrital Paleoproterozoic zircon U-Pb ages that range between 1.65 and 2.50 Ga, although there is a dearth of zircons with U-Pb ages between 1.87 and 1.85 Ga (Barramundi basement and Kalkadoon-Leichhardt interval) and 2.20 and 2.30 Ga (cf. Fig. 4).

Nd T_{DM} ages for all rocks in the Eastern Succession are invariably older than their formation age. Most 1.78-1.65 Ga sedimentary and igneous rocks have T_{DM} ages that are typically 600-900 million years greater than their emplacement and depositional ages, and mainly range between 2.70 and 2.10 Ga (cf. Fig. 4). Most of the sedimentary rocks deposited between 1.78 and 1.65 Ga typically have late Archaean and early Paleoproterozoic Nd T_{DM} ages, whereas the contemporaneous igneous rocks typically have younger Nd T_{DM} ages between 2.10 and 2.30 Ga reflecting a greater juvenile component. Collectively, these data from the 1.78-1.61 Ga igneous and sedimentary rocks show that the underlying crust is mainly comprised of a late Archaean to early Paleoproterozoic nucleus that was largely accreted by the time of the Barramundi orogeny (cf. McCulloch, 1987; Wyborn, 1988; Page and Williams, 1988; McDonald et al., 1997; Page and Sun, 1998; Mark, 2001).

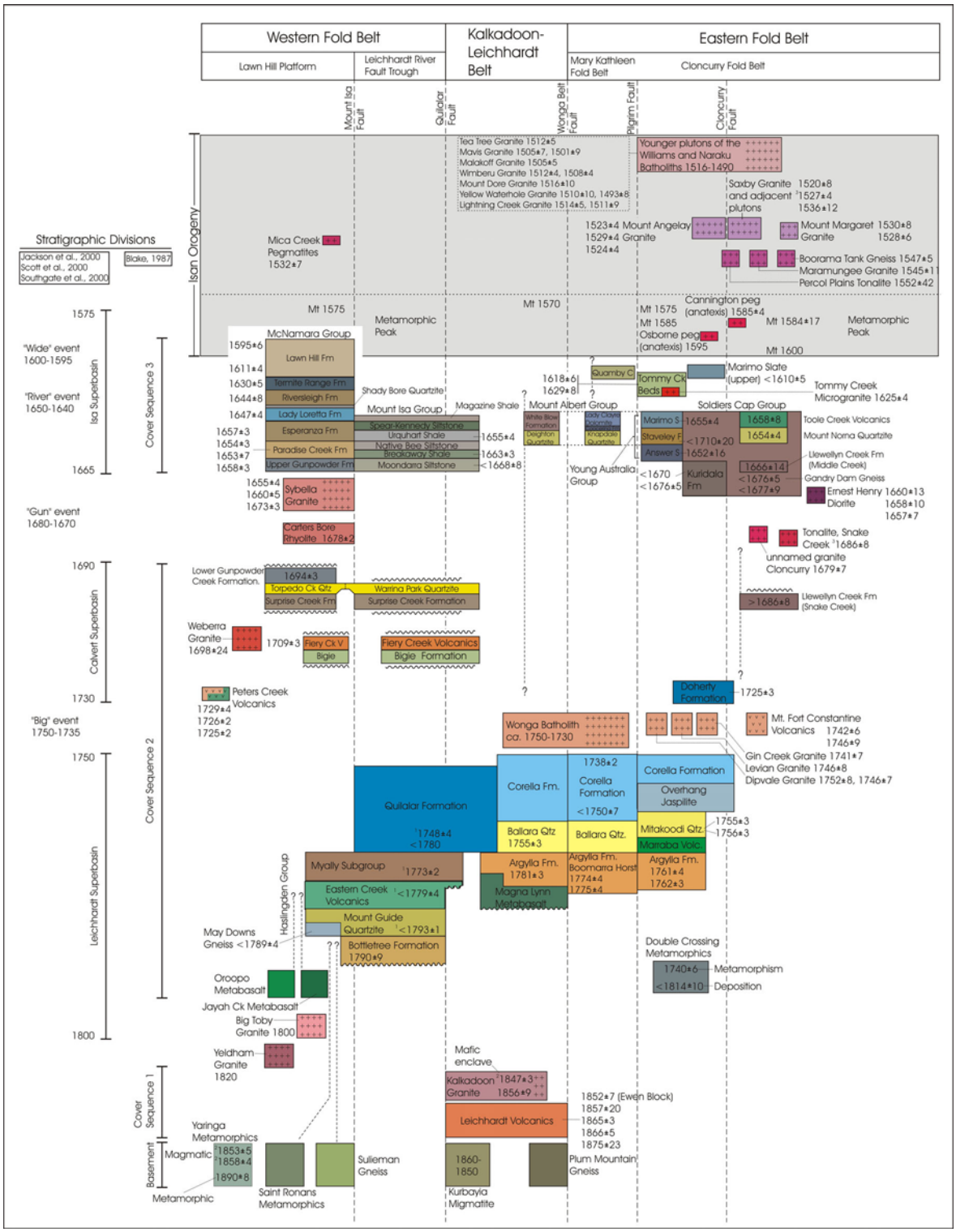

Figure 2. Simplified stratigraphic section of the Mount Isa Inlier (from Foster and Austin, 2005)

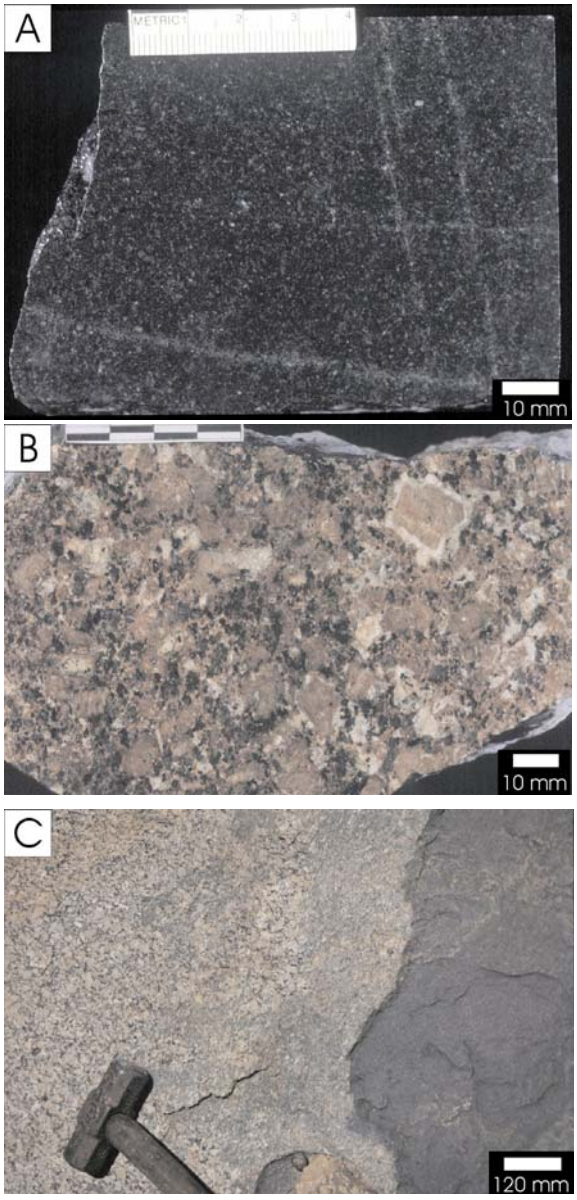

Figure 3 (left). Photographs of representative potassic 'A-type' granitoids from the Williams Batholith.

A. Fine-grained equigranular quartz diorite dominated by hornblende, plagioclase, clinopyroxene and magnetite (Mount Angelay igneous complex, ca. 1525 Ma).

B. Coarse-grained rapakivi textured biotite-hornblende monzogranite (Mount Angelay igneous complex, ca. 1525 Ma).

C. Mingling-mixing zone showing hybridization between diorite and monzogranite (Mount Angelay igneous complex, ca. 1525 Ma).

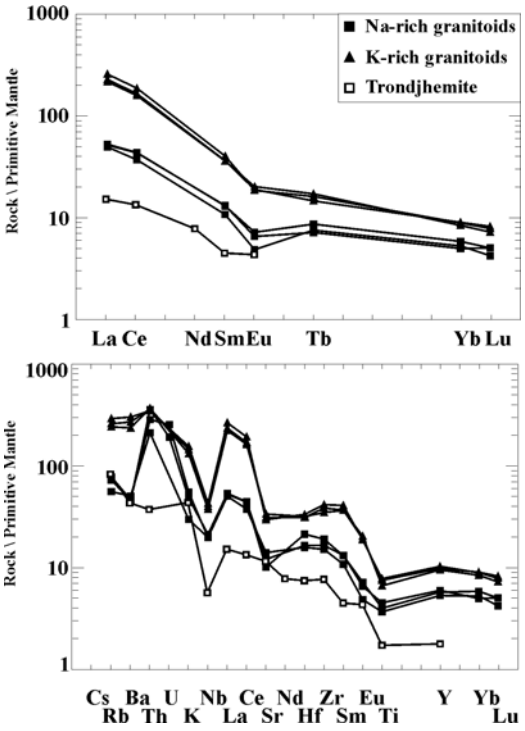

Figure 4 (right). Primitive mantle normalized diagrams comparing the whole-rock geochemistry of selected ca. 1.55 Ga trondhjemite and 1.54-1.50 Ga Na- and K-rich granitoids of the Williams and Naraku Batholiths. Primitive mantle after Sun and McDonough (1989).

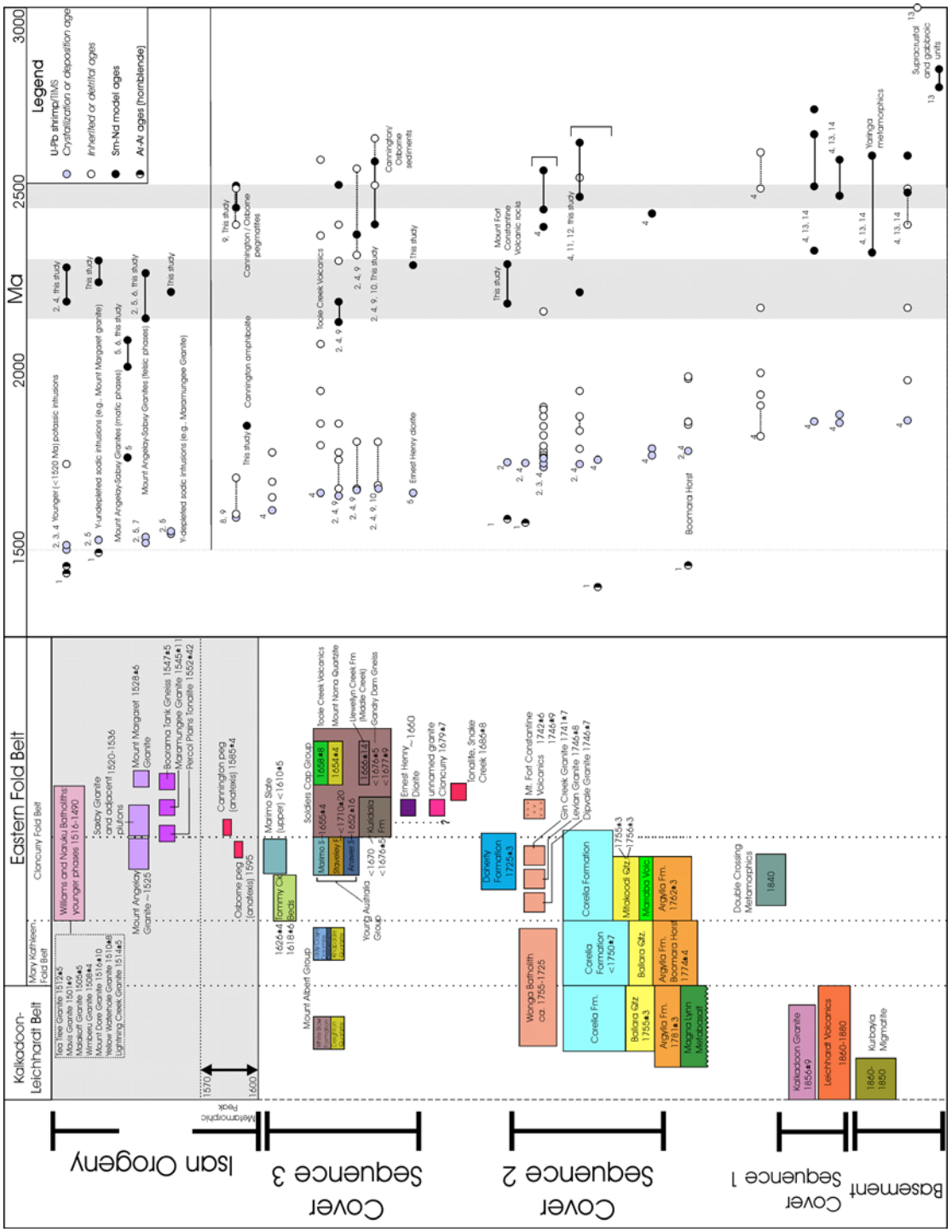

Fig. 5. Geological correlation diagram showing the temporal relations between the average crustal residence ages (T_{DM}) (opaque circles) and depositional or emplacement ages (grey circles) of magmatic and sedimentary units in the Eastern Succession, as well as associated detrital and inherited ages (open circles) in the same rock packages (stratigraphy after Foster and Austin, 2005). Also shown are selected hornblende Ar-Ar ages (half-filled circles) of magmatic rocks in the succession showing metamorphic and post-crystallization cooling ages. Note that tie lines joining data points (full line for Sm-Nd isotopic data, and dashed line for U-Pb data) represent populations containing multiple data points. Data sources: 1. Spikings et al. (2001); 2. Page and Sun (1998); 3. Davis et al. (2001); 4. Geoscience Australia (Unpublished data), 5. Pollard and McNaughton (1997); 6. Mark (2001); 7. Pollard et al. (1998); 8. Gauthier et al. (2001); 9. Giles and Nutman (2003); 10. Giles and Nutman (2002); 11. Page (1985); 12. Maas et al. (1988); 13. McDonald et al. (1997); and, 14. Bierlein and Betts (2004).

4. Sm-Nd AND Rb-Sr RESULTS

4.1 Overview

This paper presents new whole-rock Sm-Nd and Rb-Sr isotopic data for a range of 1.74 to 1.53 Ga igneous and sedimentary rocks (Table 2). The new data set includes: 1.74 Ga Ernest Henry meta-andesite (3 Nd) and Corella Formation calc-silicate (1 Nd); ca. 1.66 Ga Ernest Henry diorite (1 Nd) and psammo-pelitic rocks (2 Nd, 2 Sr) of the Soldiers Cap Group; ca. 1.59 Ga anatectic pegmatites at Osborne and Cannington (3 Nd, 5 Sr); ca. 1.55 Ga trondhjemite (1 Sr); ca.1.54-1.52 potassic, 'A-type' intrusions (8 Nd, 15 Sr); and ca. 1.53 sodic, alkaline intrusions (3 Nd, 3 Sr). A few ore samples from the Osborne and Ernest Henry deposits (1 Nd, 3 Sr) were also selected for comparison with the igneous and sedimentary rocks.

4.1.1. Anatectic pegmatites and host metasedimentary rocks

The ca. 1590 Ma pegmatites and their psammo-pelitic metasedimentary host rocks of the Soldiers Cap Group (ca. 1670 Ma) collected from around the Cannington Ag-Pb-Zn and Osborne Cu-Au mines have similar, highly radiogenic $^{87}Sr/^{86}Sr_i$ (initial) of 0.7075-0.7185 and 0.6942-0.7161 respectively, and yield depleted mantle model ages (T_{DM}) of 2.45-2.57 Ga and 2.53-2.57 Ga respectively (Figs. 6a,b, 7; Table 2).

4.1.2 Williams and Naraku Batholiths

Representative samples of Y-depleted, Sr-undepleted trondhjemite (ca. 1550 Ma) and Y-undepleted sodic and K-rich intrusions (1530-1520 Ma) have mixed crust-mantle initial $^{87}Sr/^{86}Sr$ (0.6953-7112) and εNd (-1.0 to –3.4), and exhibit a range in T_{DM} between 2081 and 2301 Ma (Figs. 6a,b, 7; Table 2). In detail trondhjemite has higher $^{87}Sr/^{86}Sr_i$ (0.7112) than both the Y-undepleted sodic and K-rich intrusions (Fig. 7) that mainly range from 0.7067 to 0.7085, and 0.6953 to 0.7065 respectively, although one two-mica granite (Wallaby Granite) contains highly radiogenic $^{87}Sr/^{86}Sr_i$ (0.8062) with a T_{DM} of 2246 Ma (Table 2). Compared to the supracrustal cover sequence rocks, and most of the ca.1.76-1.74 Ga igneous rocks in the Eastern Succession, these 1.55-1.50 Ga intrusions contain a REE component that was removed from the mantle at a much later time (average crustal residence age of ca. 2200 Ma), and apart from minor xenocrystic zircons show very little evidence for significant interaction with older material.

4.1.3. 1.74-1.66 Ga igneous and calc-silicate rocks

The ca.1.74 Ga meta-andesite and scapolitic calc-silicate around the Ernest Henry Cu-Au deposit have similar Nd T_{DM} ages of 2181-2291 Ma, and 2237 Ma respectively (Figs. 6a,b, 7; Table 2). These ages overlap with the T_{DM} ages of the ca. 1.55-1.50 Ga intrusions of the Williams and Naraku Batholith, and are significantly younger than those for the ca.1.76-1.74 Ga intrusions (e.g., Burstall Granite, T_{DM} 2382-2550 Ma) and calc-silicate rocks (e.g., Mary Kathleen area, T_{DM} 2459-2627 Ma) elsewhere in the Eastern Succession (Table 2). Sm-Nd isotopic data for the Ernest Henry diorite (ca. 1.66 Ga, Pollard and McNaughton, 1997) return an Nd T_{DM} age of 2243 Ma, virtually identical to the 1.74 Ga meta-andesite and scapolitic calc-silicate rocks around Ernest Henry (cf. Fig. 6a,b).

Collectively, these Sm-Nd data indicate that the 1.74-1.67 Ga igneous rocks studied here were derived predominantly from a crustal source with an average REE isotopic component separated from the mantle during the Paleoproterozoic.

4.14 Ore samples from the Osborne and Ernest Henry Cu-Au deposits

Magnetite-, pyrite- and chalcopyrite-rich ore from the Osborne deposit has highly radiogenic Sr ($^{87}Sr/^{86}Sr_i$: 0.7135; Table 2) and a relatively old Sm-Nd isotopic composition that returns a Nd T_{DM} of 2401 Ma (Table 2), and as such is compositionally similar to the host rocks ($^{87}Sr/^{86}Sr_i$: 0.7161; T_{DM}: 2535 Ma) and the coeval anatectic pegmatites ($^{87}Sr/^{86}Sr_i$: 0.6943-0.7185; T_{DM}: 2508 Ma). The magnetite-, pyrite- and chalcopyrite-rich ore from Ernest Henry has a dominant crustal character (cf. Table 2), preserving a moderately radiogenic $^{87}Sr/^{86}Sr_i$ signature (0.7085-0.7100). Both deposits appear to indicate that Sr and REE were dominantly crustal in origin, and potentially sourced locally (Figs. 6a,b, 7).

5. DISCUSSION

5.1 Crustal architecture and composition

The whole-rock Nd and Sr isotopic and geochemical data of the 1.74-1.50 Ga igneous rocks in the Eastern Succession together with the geochronology of their inherited zircons provides the best means to constrain the composition and broad-scale accretionary evolution of the basement crust underlying the cover sequence rocks in the succession. The results of the isotopic component of this study show that the underlying basement is predominately composed of heterogeneous crustal material with two distinct REE reservoirs (cf. Fig. 6a) with Nd T_{DM} ages between 2400-2600 Ma and 2200-2250 Ma (cf. McCulloch, 1987; Wyborn, et al., 1987; Wyborn, 1998; McDonald et al., 1997; Page and Sun, 1998; Bierlein and Betts, 2004). The ca.1.76-1.74 Ga igneous rocks in the succession appear to best preserve this older REE signature (e.g., Burstall Granite), although some coeval magmatic rocks in the east record T_{DM} ages similar to the younger REE reservoir (e.g. the Ernest Henry volcanic rocks). The basement rocks and the 1.88-1.85 Ga igneous rocks of the Leichhardt volcanics and Kalkadoon Batholith in the KLB (T_{DM} 2700-2400 Ma) share a similar Nd T_{DM} as the 1.76-1.74 Ga intrusions in the Eastern Succession (cf. McDonald et al., 1997; Bierlein and Betts, 2004).

Broad-scale Nd isotope patterns constrained by the 1.74-1.50 Ga magmatic rocks in the Eastern Succession show that to the east of the Pilgrim Worm the mid- to lower-crust is isotopically distinct, and generally has younger average crustal residence ages (T_{DM} ~2.20-2.25 Ga) than ca.1.74 intrusions (T_{DM} >2.45 Ga) west of the worm. This distinction is highlighted by the ca.1.74 Ga Ernest Henry meta-andesite to the east of the Pilgrim Worm that has consistently younger T_{DM} ages (2.18-2.23 Ga) than coeval intrusions to the west (e.g., Burstall Granite, T_{DM} 2.38-2.55 Ga). Outcrop of the younger generations of I- and A-type 1.67 Ga and 1.55-1.50 Ga intrusions (with T_{DM} between 2.08 and 2.30 Ga) is almost entirely confined to the east of the Pilgrim Worm. The apparent 'younging' in Nd T_{DM} of the source material was first observed by Page and Sun (1998), who suggested that this difference might indicate that the lower crust in the east was: 1. an allochthonous block (which coincidentally showed a number of isotopic similarities with the Georgetown inlier); or, 2. part of the same continental nucleus as the counterparts to the west, but which

experienced significantly greater mafic underplating giving rise to its much younger 'average' REE age. These two hypotheses have significantly different implications for the geodynamic and accretionary evolution of the inlier, and have radical flow-on implications for the inlier's relations to the Proterozoic blocks to the east (e.g. Georgetown, Coen etc), as well as the succession's distinct metallogenic character.

Fig. 6 (below) A. Time (Ma) versus _Nd diagram of whole-rock Sm-Nd data for magmatic and sedimentary rocks, and syn-ore samples from the Osborne Cu-Au deposit in the Eastern Succession. Also shown are the compositional windows for the ca. 1590 Ma Hiltaba granites, South Australia (Roxby Granite; Creaser, 1995), the Leichhardt Volcanics and Kalkadoon granite (McDonald et al., 1997), and Corella calc-silicate rocks (Page, 1983; Maas et al., 1987). Note that most of the igneous rocks in the Eastern Succession (particularly those east of the Pilgrim Fault) exhibit higher _Nd values than the 1880-1740 Ma igneous rocks (e.g., Kalkadoon granite). Symbols: Potassic 'A-type' intrusions (black squares); ca.1530 Ma sodic, alkaline intrusions (pale blue squares); ca. 1550 Ma TTG intrusions (blue and grey diamonds); Osborne ore (red square); Soldiers Cap group psammo-peltic rocks (blue squares); Corella calc-silicate rocks (green rectangle and green triangle); Ernest Henry volcanic rocks (grey rectangle); Ernest Henry diorite (red circles); Kalkadoon granite (black triangle); Cannington core amphibolite (large black circle); and, late tholeiitic dyke (small black circle).

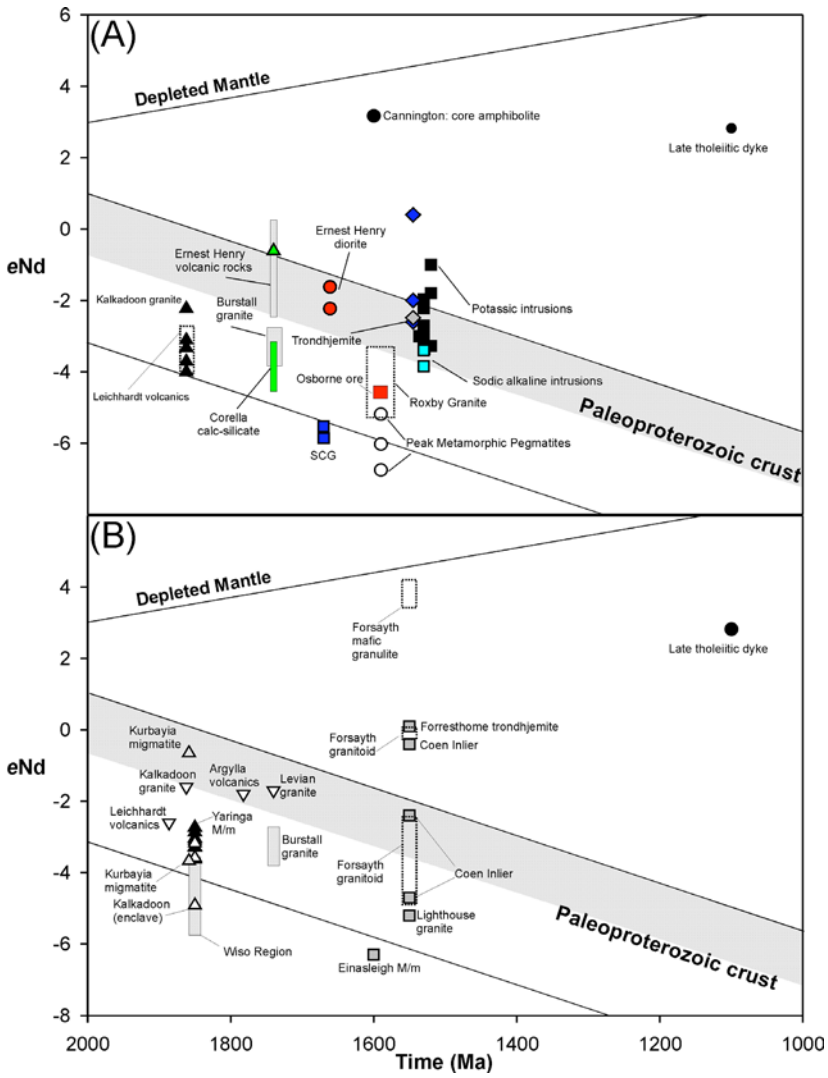

Fig. 6B. (above). Time (Ma) versus _Nd diagram of whole-rock Sm-Nd data for magmatic and sedimentary rocks in the Mount Isa Inlier (Mark 2001; Bierlein and Betts 2004; Geoscience Australia, unpublished data), and Georgetown, Coen, Yambo and Daralong inliers (Blewett et al., 1998; Geoscience Australia, unpublished data). Also shown are the Geoscience Australia data for various ca. 1860-1740 Ma intrusions (open inverted triangles); Kalkadoon enclave (open triangles, Bierlein and

Betts, 2004); Yaringa metamorphics (black triangles, Bierlein and Betts, 2004); and late ca. 1100 Ma tholeiitic dyke (black circle).

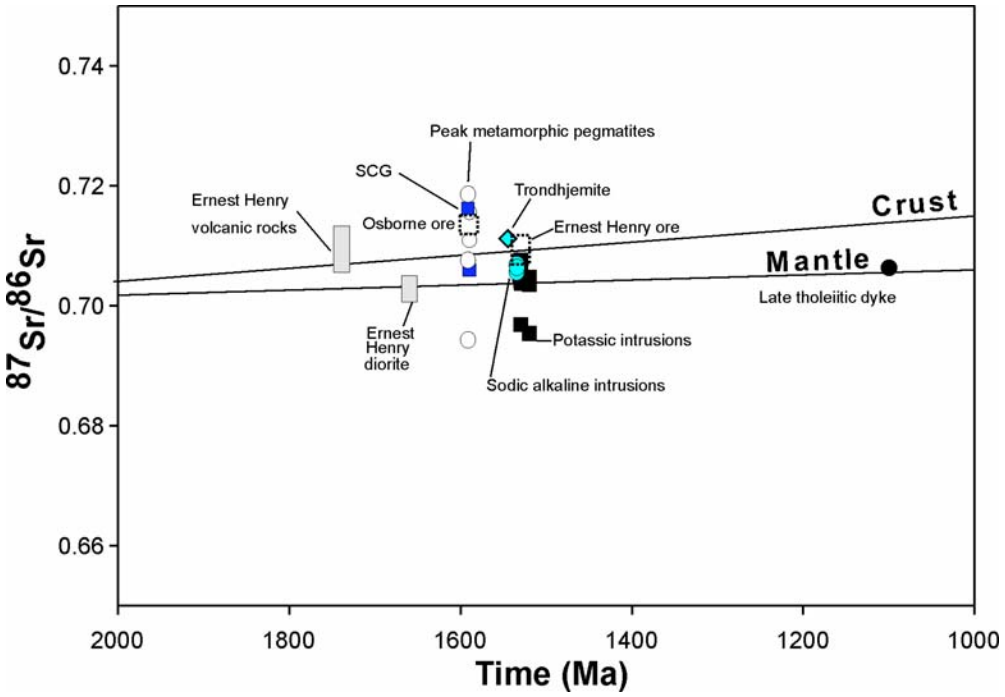

Fig. 7. Initial $^{87}Sr/^{86}Sr$ of magmatic and sedimentary rocks and selected ore samples from the Ernest Henry and Osborne Cu-Au deposits in the Eastern Succession. Note that the highly radiogenic composition of the Soldiers Cap Group psammo-pelitic sediments are also reflected in the peak metamorphic pegmatites at the Osborne and Cannington deposits, as well as the ore at Osborne. A strong crustal component is also exhibited by the Ernest Henry volcanic rocks, as well as the Ernest Henry ore, and ca. 1550 Ma TTG intrusions (trondhjemite). The 1530 to 1500 Ma potassic and sodic intrusions exhibit mixed crust-mantle values that reflect the Sm-Nd isotopic data, as well as the field relations showing mingling and mixing between coeval felsic and mafic intrusions. The low initial $^{87}Sr/^{86}Sr$ of some of the peak metamorphic pegmatites and potassic, 'A-type' intrusions relate to post-crystallization disturbance and/or alteration not reflected in the Sm-Nd isotopic data. The lower Sr isotopic values of the Ernest Henry diorite are inconsistent with the Sm-Nd isotopic data, and may reflect some post-depositional disturbance in the Sr isotope systematics.

Fig. 8 (below). Calculated Nd two-stage depleted mantle-model (T_{DM}) age against whole-rock SiO_2 for selected potassic 'A-type' intrusions of the Williams and Naraku Batholiths (diamonds (Mount Angelay Granite), circles (Saxby Granite); Table 2 data, squares; other potassic 1.54-1.50 Ga Williams and Naraku intrusions, data from Page and Sun (1998). The asymptotic character of these data points appears to show that the REE reservoir for the felsic intrusive rocks was probably removed from the mantle around 2200-2250 Ma. The trend to low SiO_2 (<67 wt %) formed by in situ magma hydridization processes (cf. Fig. 2c) within a single igneous rock suite (diamonds) shows mixing between an older REE reservoir separated from the mantle ca.2200-2250 Ma and a juvenile component present in the coeval mafic intrusions. This trend also supports the interpretation that younging in Nd T_{DM} ages directly correlate with an increase in the contribution of mafic magma in the hybridized intrusions, and that the felsic intrusions were crustally derived.

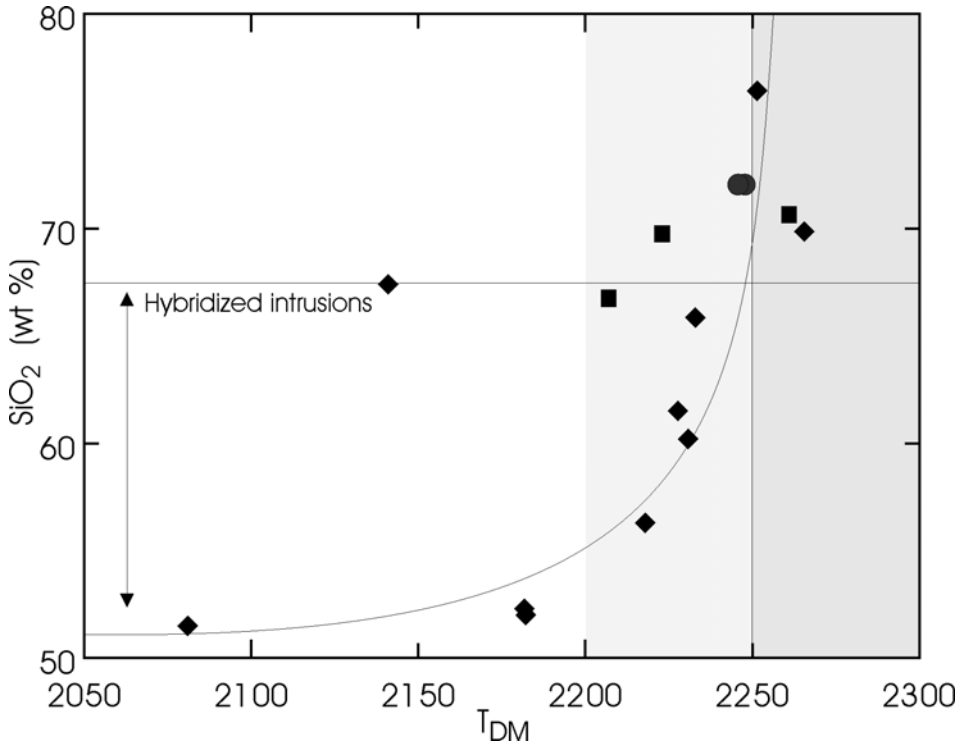

The younger 2200-2250 Ma REE reservoir is preserved only in igneous rocks east of the Pilgrim Worm, and is mainly characterised by intrusions of the Williams and Naraku Batholith. The ca.1.55-1.50 Ga intrusions of the Williams and Naraku Batholiths have Nd T_{DM} ages between 2081 and 2301 Ma, and included within this suite are potassic intrusions melted from tonalitic-gabbroic material at <1 GPa and >850^{o}C, and TTG intrusions melted from garnet-bearing, amphibolitic material at >1 GPa and >750^{o}C (cf. Wyborn, 1998; Pollard et al., 1998; Mark 2001). Apart from the potential effects of post-depositional alteration noted within some TTG intrusions (cf. Page and Sun, 1998), the potassic intrusions show the greatest range in Nd T_{DM} ages associated with primary magmatic processes, where T_{DM} and whole-rock SiO_2 show systematic, and asymptotic mixing relations (Fig. 8). This relationship indicates that the felsic, crustally-derived intrusions (>67 wt% SiO_2) were derived from crustal material of tonalitic-gabbroic composition that on-average separated from the depleted mantle ca. 2200 Ma. The remaining intrusions represent hybridized magmas formed by para-*in situ* mingling and mixing between coeval mantle-derived mafic melt and crustally-derived felsic melt, which (as a sub-suite) preserve a systematic increase in T_{DM} with progressive incorporation of more felsic melt (cf. Fig. 8). A ca.2200 Ma REE reservoir is also recorded by the ca.1.53 Ga alkaline sodic intrusions (e.g., Mount Margaret Granite, Table 2).

However, the Nd T_{DM} age of ca. 2200 Ma could represent an 'average' REE crustal residence age composed of an older 2600-2400 Ma source (identical to that preserved in the basement rocks in the KLB, cf. McDonald et al., 1997), mixed with juvenile components accreted after 2200 Ma (Page and Sun, 1998) Indeed, voluminous vertical accretion of mafic magmas occurred episodically during postulated rift-sag basin development at 1.78-1.72 Ga and 1.67-1.60 Ga and during compressional deformation 1.54-1.50 Ga (cf. Blake, 1981, 1987; Williams, 1998c; Giles and Nutman, 2003). This magmatism would have progressively reduced the bulk Nd isotopic age of the crust. Nevertheless, this magmatism was probably not evenly distributed and in all likelihood was in large-part underplated to the base of the crust or emplaced into the overlying cover

sequences, producing a geochemically and isotopically heterogeneous crustal profile. These different geochemical and isotopic components would be difficult to homogenise during subsequent post-1.74 Ga melting. Additionally, given the widespread nature of these episodes of mafic magmatism, the crustal rocks to the west of the Pilgrim Worm are likely to have witnessed the same degree of vertical accretion, or potentially greater given their apparent higher gravity signature (cf. Bierlein and Betts, 2004). Moreover, these mantle-derived mafic intrusions probably had little capacity to moderate the isotopic character of the melt given their naturally low REE contents (cf. Sun and McDonough, 1989) compared to the felsic source material involved in the generation of the 1.54-1.50 Williams and Naraku Batholiths (cf. Creaser and White, 1991; Pollard et al., 1998; Mark, 2001). Furthermore, Nd isotopic data of pristine TTG intrusions (cf. Table 2), which probably formed by partial melting of deep crustal amphibolitic material, have Nd T_{DM} ages ca. 2200 Ma, showing that a mafic component in the lower crust was also removed from the mantle well before the aforementioned periods of mafic magmatism. Consequently, we consider that the crust to the east of the Pilgrim Worm in all likelihood has a distinct 'average' Nd isotopic composition that is manifest by both mafic and felsic source rocks which give rise to a Nd T_{DM} ~2200-2250 Ma. In broader terms, the presence of rare Archaean inherited zircons within intrusions east of the Pilgrim Worm (cf. Page and Sun, 1998), together with the older Nd T_{DM} ages of the 1.74 Ga two-mica Gin Creek Granite (ca. 2.4 Ga) and Levian Granite (2.4 Ga) indicates that the crust had a protracted history of accretion that extended into the late Archaean, but which was dominated by a major period of crustal growth and reworking ca. 2200-2250 Ma.

The broad boundary for this isotopic change potentially corresponds to a postulated N-S oriented terrane boundary formed in association with the generation of the 1.88-1.84 Ga Leichhardt volcanics and the co-genetic intrusions of the Kalkadoon Granite in the KLB (cf. McDonald et al., 1997). In McDonald's model, lateral accretion and terrane amalgamation was associated with continental-margin arc magmatism during the ultimate closure of an eastern seaboard. However, this model contrasts with that proposed by Wyborn (1988) who suggested the 1.88-1.84 Ga igneous rocks formed as the products of broad-scale intracontinental magmatism associated with the waning stages of compressional deformation and high-T, low-P metamorphism during the Barramundi Orogeny. Whatever the geodynamic setting for the KLB magmatism, we favour the scenario where the crust east of the Pilgrim Fault-Worm represents an allochthonous block accreted to the remainder of the Mount Isa inlier sometime between 2.20 Ga and 1.84 Ga.

Source of Soldiers Cap Group sediments: a Georgetown connection?

The isotopic composition of the pegmatites at Cannington and Osborne is consistent with formation by partial melting of the host sedimentary package during upper amphibolite facies metamorphism (>670^{o}C; 300-500 MPa) at 1600-1580 Ma (cf. Mark et al., 1998; Giles and Nutman, 2002). The late Archaean to early Proterozoic T_{DM} ages of the pegmatites and their sedimentary hosts most closely resemble the felsic basement rocks (e.g., Kalkadoon Granite, T_{DM} 2.49-2.65 Ga; Leichhardt Volcanics, T_{DM} 2.51 Ga; Yaringa Metamorphics, T_{DM} 2.49 Ga). They overlap with the T_{DM} ages of the ca.1740 Ma calc-silicates (e.g., Mary Kathleen calc-silicates 2.46-2.63 Ga), and the Wonga-age intrusions (ca.1740 Ma) that crop out west of the Pilgrim Worm (e.g., Burstall and Levian Granites, 2.38-2.55 Ga). The similarly aged units of the Mount Norna Quartzite (T_{DM} 2.13-2.51 Ga) show some overlap in isotopic composition, but exhibit a greater range in T_{DM} that typically extends to compositions that are more juvenile. Given these considerations, the results most likely show that these Soldiers Cap Group metasedimentary rocks in the host

rocks to the Osborne and Cannington deposits are largely sourced from basement material that formed a topographic high ca. 1.67 Ga (cf. O'Dea et al., 1997). The basement rocks in the Kalkadoon-Leichhardt Belt are isotopically compatible with being the source to the psammo-pelitic sedimentary rocks of the Soldiers Cap Group. However, the distinct lack of ca.1.89-1.84 Ga detrital zircons in the sediments and anatectic pegmatites (cf. Giles and Nutman 2002, 2003) may indicate that the crystalline rocks in the KLB were not the sole provenance for the sediments at this time, and perhaps points toward a local contribution from younger overlying rock packages (e.g., ca.1.78 Ga Argylla Formation). The Precambrian rocks in the Georgetown, Coen, Yambo and Dargalong inliers exhibit remarkable similarity in both their range in Nd isotopic composition and age distribution of detrital-inherited zircons (some of these sequences have younger depositional ages than the Eastern Succession rocks) compared to the Soldiers Cap Group sediments (cf. Blewett et al., 1998; Page and Sun, 1998, Giles and Nutman, 2002, 2003). Consequently, this may indicate that SCG sediments were also partially sourced from a hinterland to the east of the Mount Isa Inlier. Such a provenance may indicate that the Georgetown and neighbouring inliers were proximal to the Mount Isa Inlier at, or prior to 1.67 Ga. However, this conclusion is inconsistent with a ca. 1.60 Ga timing for docking between the two inliers inferred by Boger and Hanson (2004), and highlights the need for further detailed stratigraphic correlation between these Proterozoic neighbours.

5.2. District metallogenesis and the origin of isotopic components: early results

As shown in many previous studies and summarized in Williams (1998b) and Williams and Pollard (2003), the Eastern Succession is dominated largely by syn-tectonic Cu-(Au) deposits formed during localized reverse faulting and shearing after the metamorphic peak that occurred at ca. 1600 Ma (in contrast to the ore systems in the west) These Cu-Au deposits largely preserve stable isotope and fluid inclusion data supporting a significant magmatic component to the ore-forming fluids with the exception of some smaller occurrences that preserve a greater host rock input (cf. Davidson and Davidson, 1992; Davidson, 1998). Given this data, and the results of earlier Ar-Ar dating of ore related gangue minerals showing a contemporary relationship between Cu-Au mineralization and the Williams and Naraku Batholith (cf. Tyweroud, 1997; Page and Sun, 1998; Perkins and Wyborn, 1998; Pollard et al., 1998; Baker et al., 2001), the 1.55-1.50 Ga magmatism was considered to have an intimate genetic relationship with the ore-forming processes. However, new Re-Os molybdenite age data for Osborne indicates that Cu-Au mineralization occurred at ca. 1595 Ma, well before the emplacement of the 'A-type' intrusions of the Williams and Naraku Batholith. Although a contemporary relationship between magmatism (anatectic pegmatites in the case of Osborne) and Cu-Au mineralization still holds, the protracted period over which mineralization occurred (1595-1500 Ma) negates a unique relationship between intrusion geochemistry and age, and the succession's metallogenic history. This apparent diversity in intrusive rock composition over time may play some part in the diversity in the composition and nature of mineralized ore systems in the district.

The results of preliminary Sr and Nd isotope work at Ernest Henry and Osborne support the need for amagmatic contributions to the ore systems as they have similar Sr isotopic characteristics to their host rocks. This indicates that Sr was probably 'buffered' locally during fluid-rock exchange reactions in these alkaline, high-T, hydrothermal systems (cf. Williams et al., 1994; Oliver et al., 2004). A single Nd isotope result for the Osborne ore may also support the Sr isotope data, and indicate that the REE were predominantly sourced locally. However, given the relatively small dataset included in this work

significantly more data is needed to validate this interpretation. Given the contrasting signatures preserved in the stable isotope, radiogenic isotope and fluid inclusion data, a single unifying model for the metallogenesis of the Cu-Au systems in the succession is not readily defined. This issue is complicated by the effects of fluid-rock interaction involving geochemical and isotopic exchange, as well as the involvement of multiple fluid sources. Nevertheless, the significant endowment of Cu-Au deposits in the succession compared to Pb-Zn-Ag deposits may correlate directly with the presence of large volumes of high-T, saline fluids circulating after the metamorphic peak. Fluids of this type enabled the transfer of a diverse suite of metals in solution (cf. Williams et al., 2001; Mark et al., 2005a), but largely facilitated the deposition of the less soluble metals in zones of dilation, cooling, fluid mixing and fluid:rock interaction (e.g. Cu, Au, Fe).

Acknowledgments

This work was funded through the pmd*CRC. GM is a Logan Fellow funded by Monash University. The authors would like to thank Mike Rubenach, Tom Blenkinsop and Nick Oliver for their assistance and advice. Graeme Luther and Chris Gray at Latrobe University are also thanked for undertaking isotope analysis.

REFERENCES

Blake, D.H., 1981. Intrusive net-veined complexes in north Queensland. Bureau of Mineral Resources Journal of Australian Geology and Geophysics Bulletin, v. 6, 95-99.

Blake, D.H., 1987. Geology of the Mount Isa Inlier and environs. Queensland and Northern Territory. Bureau of Mineral Resources, Journal of Australian Geology and Geophysics Bulletin, v. 225, 83 pp.

Baker, T., Perkins C., Blake, K.L., and Williams, P.J., 2001. Radiogenic and stable isotope constraints on the genesis of the Eloise Cu-Au deposit, Cloncurry district, NW Queensland. Economic Geology, 96, 723-742.

Blake, K., Pollard, P.J., and Xu, G., 1997. Alteration and mineralisation in the Mount Fort Constantine volcanics, Cloncurry district, northwest Queensland. In: Pollard PJ (Compiler), Cloncurry base metals and gold. AMIRA P438 Final Report 11: 53 p.

Betts, P.G., Giles, G., and Lister, G.S., 2003. Tectonic environment of shale-hosted massive sulfide Pb-Zn-Ag deposits of Proterozoic northeastern Australia. Economic Geology, 98, 557-576.

Blenkinsop, T. G., Huddlestone-Holmes, C., Foster, D., Mark, G., Austin, J., Edmiston, M., Lepong, P., Ford, A., Murphy, F.C. 2005. 3-D model and crustal architecture of the Mt Isa Eastern Succession. I2+3 Final Report, pmdCRC.

Blewett, R.S. Black, L.P., Sun, S-S., Knutson, J., Hutton, L.J. and Bain, J.H.C., 1998. U-Pb zircon and Sm-Nd geochronology of the Mesoproterozoic of North Queensland: implications for a Rodinian connection with the Belt supergroup of North America. Precambrian Research, 89, 101-127.

Bodon, S.B., 1998. Paragenetic relationships and their implications for ore genesis at the Cannington Ag-Pb-Zn deposit, Mount Isa Inlier, Queensland, Australia. Economic Geology, 93, 1463-1488.

Boger, S.D. and Hanson, D., 2004. Metamorphic evolution of the Georgetown Inlier, northeast Queensland, Australia; evidence for an accreted Palaeoproterozoic terrane? Journal of Metamorphic Petrology, 22, 511-527.

Chapman, L.H., 2004. Geology and mineralization styles of the George Fisher Zn-Pb-Ag deposit, Mount Isa, Australia. Economic Geology, 99, 233-255.

Condie, K.C., 2002. Continental growth during a 1.9-Ga superplume event. Journal of Geodynamics, 34, 249-264.

Creaser, R.A., 1995. Neodymium isotopic constraints for the origin of Mesoproterozoic felsic magmatism, Gawlor Craton, South Australia. Canadian Journal of Earth Sciences, 32, 460-471.

Creaser, R.A. and White, A.J.R., 1991. Yardea Dacite- large volume, high-temperature felsic volcanism from the middle Proterozoic of South Australia. Geology, 19, 48-51.

Davidson, G.J., 1998. Variation in copper-gold styles through time in the Proterozoic Cloncurry Goldfield, Mt Isa Inlier; a reconnaissance view. Australian Journal of Earth Sciences, 45, 445-462.

Davidson, G.J., Davis, B.K. and Garner, A., 2002. Structural and geochemical constraints on the emplacement of the Monakoff oxide Cu-Au (-Co-U-REE-Ag-Zn-Pb) deposit, Mt Isa Inlier. In: Potter TM (ed) Hydrothermal Iron oxide copper-gold and related deposits: a global perspective 2, pp. 49-76.

Davidson, G.J. and Dixon, G.H., 1992. Two sulphur isotope provinces deduced from ores in the Mount Isa eastern succession, Australia. Mineralium Deposita, 27, 30-41.

Davis, T.P., 2004. Mine-scale structural controls on the Mount Isa Zn-Pb-Ag and Cu orebodies. Economic Geology, 99, 543-559.

Davis, B.K., Pollard, P.J., Lally, J.H., McNaughton, N.J., Blake, K. and Williams, P.J., 2001. Deformation history of the Naraku Batholith, Mt Isa Inlier, Australia: implication for pluton ages and geometries from structural study of the Dipvale Granodiorite and Levian Granite. Australian Journal of Earth Sciences, 48, 113-129.

Etheridge, M..A., Rutland, R.W.R., and Wyborn, L.A.I, 1987. Orogenesis and tectonic process in the Easth to Middle Proterozoic of Northern Australia. In: Kroner, A. (ed), Proterozoic lithospheric evolution, v. 17, 131-148.

Ferris, G.M, Schwarz, M.P. and Heithersay, P., 2002. The Geological Framework, Distribution and Controls of Fe-Oxide Cu-Au Mineralisation in the Gawler Craton, South Australia. Part I - Geological and Tectonic Framework, *in* Porter, T.M. (Ed), 2002 - Hydrothermal Iron Oxide Copper-Gold & Related Deposits: A Global Perspective, volume 2; *PGC Publishing, Adelaide,* pp 9-31.

Foster, D. and Rubenach, M.J., 2005. Isograd pattern and regional low-P, high-T metamorphism of pelitic, mafic and calc-silicate rocks along an east-west section through the Mount Isa inlier. Australian Journal of Earth Sciences, 52 (in press).

Foster, D., and Austin, J., 2005. Revised chronostratigraphy for the Mount Isa Inlier with emphasis on the Eastern Succession. I2+3 Final Report, pmdCRC.

Gaál G., 1990. Tectonic styles of early Proterozoic ore deposition in the Fennoscandian Shield. Precambrian Research, 46, 83-114.

Gauthier, L., Hall, G., Stein, H. and Schaltegger, U., 2001. The Osborne deposit, Cloncurry district: a 1595 Ma Cu-Au skarn deposit. In: Williams, P.J. (ed.), 2001: a hydrothermal odyssey, new developments in metalliferous hydrothermal systems research, extended conference abstracts. EGRU contribution, v. 59, pp. 58-59.

Giles, D., Betts, P. and Lister, G., 2002. Far-field continental backarc setting for the 1.80-1.67 Ga basins of northeastern Australia. Geology, 30, 823-826.

Giles, D. and Nutman, A.P., 2002. SHRIMP U-Pb monazite dating of 1600-1580 Ma amphibolite facies metamorphism in the southeastern Mt Isa Block, Australia. Australian Journal of Earth Sciences, 49, 455-465.

Giles, D. and Nutman, A.P., 2003. SHRIMP U-Pb zircon dating of the host rocks of the Cannington Ag-Pb-Zn deposit, southeastern Mt Isa Block, Australia. Australian Journal of Earth Sciences, v. 50, p. 295-309.

Hand, M. and Rubatto, D., 2002. The scale of the thermal problem in the Mount Isa Inlier. In: Preiss, V.P., (ed.), Geoscience 2002: expanding horizons, Geological Society of Australia, v. 67, pp. 475.

Hitzman, M.W., 2000. Iron oxide-Cu-Au deposits. What, where, when and Why. In: Porter TM (ed) Hydrothermal Iron Oxide Copper-Gold and Related Deposits: A Global Perspective. AMF, Adelaide, pp 9-26.

Large, Ross R., Bull, Stuart W., Cooke, D.R. and McGoldrick, P.J. 1998. A genetic model for the H.Y.C. Deposit, Australia; based on regional sedimentology, geochemistry, and sulfide-sediment relationships. Economic Geology, 93, 1345-1368.

Maas, R., McCulloch, M.T., Campbell, I.H., and Page, R.W., 1987. Sm-Nd isotope systematics in uranium rare-earth element mineralization at the Mary Kathleen uranium mine, Queensland. Economic Geology, 82, 1805-1826.

MacCready, T., Goleby, B.R., Goncahrov, A. and Drummond, B.J., 1998. A framework of overprinting orogens based on interpretation of the Mount Isa Deep Seismic Transect. Economic Geology, 93, 1422-1434.

Mark, G., 1999. Petrogenesis of Mesoproterozoic K-rich granitoids, Southern Mount Angelay igneous complex, Cloncurry District, Northwest Queensland, Australia. Australian Journal of Earth Sciences, 45, 933-949.

Mark, G., 2001, Nd isotope and petrogenetic constraints for the origin of the Mount Angelay igneous complex: Implications for granitoid formation in the Cloncurry district, Australia. Precambrian Research, 105, 17-35.

Mark, G., Phillips, G.N. and Pollard, P.J., 1998. Highly selective partial melting of pelitic gneiss at Cannington, Cloncurry District. Australian Journal of Earth Sciences, 45, 169-176.

Mark, G., Williams, P.J. and Boyce, A.J., 2004a. Low-latitude meteoric fluid flow along the Cloncurry Fault, Cloncurry district, NW Queensland, Australia: geodynamic and metallogenic implications. Chemical Geology, 207, 117-132.

Mark, G., Wilde, A., Oliver, N.H.S. and Williams, P.J., 2005a. Geochemical modelling of outflow from the Ernest Henry Fe oxide Cu-Au deposit: implication for ore genesis and exploration. Journal of Geochemical Exploration, 85, 31-46.

Mark, G., Pollard, P., Mustard, R., Foster, D., McNaughton, N., 2005b. Episodic syn-tectonic magmatism in the Cloncurry district, NW Queensland, Australia: Implications for the origin, derivation and tectonic setting of "A-type" magmas. I2+3 Final Report, pmdCRC

McCulloch, M.T., 1987. Sm-Nd isotopic constraints on the evolution of Precambrian crust in the Australian continent. In: Kroner, A. (ed), Proterozoic lithospheric evolution, v. 17, 115-130.

Nyman, M.W., Karlstrom, K.E., Kirby, E. and Graubard, C.M., 1994. Mesoproterozoic contractional orogeny in western North America: evidence from ca. 1.4 Ga plutons. Geology, 22, 901-904.

O'Dea, M.G., Lister, G., MacCready, T., Betts, P. G., Oliver, N. H. S., Pound, H.S., Huang, W., and Valenta, R. K., 1997. Geodynamic evolution of the Proterozoic Mount Isa terrain. In: Burg, J.P., Ford, M., (Editor), Orogeny through time. Geol. Soc. Lon. Spec. Pub. No.121, pp. 99-122.

Oliver, N.H.S., Cleverley, J.S., Mark, G., Pollard, P.J., Fu, B., Marshall, L.J., Rubenach, M.J., Williams, P.J. and Baker, T., 2004. The role of sodic alteration in the genesis of iron oxide-copper-gold deposits, eastern Mt Isa Block, Australia. Economic Geology, 99, 1145-1176.

Page, R.W., 1983. Chronology of magmatism, skarn formation, and uranium mineralization, Mary Kathleen, Queensland, Australia. Economic Geology, 78, 838-853.

Page, R.W. and Bell, T.H., 1986. Isotopic and structural responses of granite to successive deformation and metamorphism. Journal of Geology, 94: 365-379.

Page, R.W. and Sun, S-S., 1998. Aspects of geochronology and crustal evolution in the Eastern Fold Belt, Mount Isa Inlier. Australian Journal of Earth Sciences, 45, 343-362.

Page, R.W. and Williams, I.S., 1998. Age of the barramundi orogeny in northern Australia by means of ion microprobe and conventional U-Pb zircon studies Precambrian Research, 40/41, 21-36.

Perkins, C. and Wyborn, L., 1998. Age of Cu-Au mineralisation, Cloncurry district, Mount Isa Inlier, as determined by $^{40}Ar/^{39}Ar$ dating. Australian Journal of Earth Sciences, 45, 233-246.

Perring, C.S., Pollard, P.J. and Nunn, A.J., 2001. Petrogenesis of the Squirrel Hills granite and associated magnetite-rich sill and vein complex: Lightning creek prospect, Cloncurry district, Northwest Queensland. Precambrian Research, 106, 213-238.

Pollard, P.J., Mark, G. and Mitchell, L.C., 1998. Geochemistry of post-1540 granites spatially associated within regional sodic-calcic alteration and Cu-Au-Co mineralisation, Cloncurry district, northwest Queensland. Economic Geology, 93, 1330-1344.

Pollard, P.J. and McNaughton, N., 1997. U-Pb geochronology and Sm/Nd isotope characteristics of Proterozoic intrusive rocks in the Cloncurry district, Mount Isa Inlier, Australia. AMIRA P438 Final Report: Cloncurry Base Metals and Gold, 4: 19.

Rubenach, M.J., Adshead, N.D., Oliver, N.H.S., Tullemans, F., Esser, D. and Stein H., 2001. The Osborne Cu-Au deposit: geochronology, and genesis of mineralization in relation to host albitites and ironstones. In Williams, P.J. (ed.) 2001: a hydrothermal odyssey, new developments in metalliferous hydrothermal systems research, extended conference abstracts. EGRU contribution 59: 172-173.

Rubenach, M.J. and Barker, A.J., 1998. Metamorphic and metasomatic evolution of the Snake Creek Anticline, Eastern Succession, Mount Isa Inlier. Australian Journal of Earth Sciences, 45, 363-372.

Rubenach, M.J. and Lewthwaite, K.A., 2002. Metasomatic albitites and related biotite-rich schists from a low-pressure polymetamorphic terrane, Snake Creek Anticline, Mount Isa Inlier, north-eastern Australia: microstructures and P-T-d paths. Journal of Metamorphic Geology, 20, 191-202.

Scott, D.L, Rawlings, D.J., Page, R.W, Tarlowski, C.Z., Idnurm, M., Jackson, M.J. and Southgate, P.N., 2000. Basement framework and geodynamic evolution of the Palaeoproterozoic superbasins of north-central Australia: an integrated review of geochemical, geochronological and geophysical data. Australian Journal of Earth Sciences, 47, 341-380.

Spikings, R.A., Foster, D.A., Kohn, B.P., and Lister, G.S., 2001. Post-orogenic (<1500 Ma) thermal history of the Proterozoic Eastern Fold Belt, Mount Isa Inlier, Australia. Precambrian Research, 109, 103-144.

Sun, S.S. and McDonough, W.F., 1989. Chemical and isotopic systematics of oceanic basalts: implications for mantle composition and processes. In: A.D. Saunders and M.J. Norry (eds), Magmatism in the Ocean Basins. Geological Society Special Publication, v. 42, pp. 313-345.

Twyerould, S.C., 1997. The geology and genesis of the Ernest Henry Fe-Cu-Au deposit, northwest Queensland, Australia. PhD thesis, unpublished. University of Oregon.

Wang, S. and Williams, P.J., 2001. Geochemistry and origin of Proterozoic skarns at the Mount Elliott Cu-Au (-Co-Ni) deposit, Cloncurry district, NW Queensland. Mineralium Deposita, 36, 109-124.

Williams P.J., 1994. Iron mobility during synmetamorphic alteration in the Selwyn Range area, NW Queensland: Implications for the origin of ironstone-hosted Au-Cu deposits. Mineralium Deposita, 29, 250-260.

Williams P.J., 1998a. Metalliferous economic geology of the Mount Isa Eastern Succession, Queensland. Australian Journal of Earth Sciences, 45, 329-342.

Williams, P.J., 1998b. An introduction to the metallogeny of the McArthur River Mount Isa Cloncurry Minerals Province. Economic Geology, 93, 1120-1131.

Williams, P.J., 1998c. Magmatic iron enrichment in high-iron metatholeiites associated with 'Broken Hill-type' Pb-Zn-Ag deposits, Mt Isa Eastern Succession. Australian Journal of Earth Sciences, 45, 389-396.

Williams, P.J., Barton, M.D., Fontboté, L., de Haller, A., Johnson, D.A., Mark, G., Marschik, R. and Oliver, N.H.S., 2005. Iron Oxide-Copper-Gold Deposits: Geology, Space-Time Distribution, and Genetic Constraints from Geochemical-Mineralogical Zoning and Theoretical Modelling. Economic Geology 100th Anniversary Volume, in press.

Williams, P.J., Dong, G., Ryan, C.G., Pollard, P.J., Rotherham, J., Mernagh, T.P. and Chapman, L.H., 2001, Geochemistry of hypersaline fluid inclusions from the Starra (Fe oxide)-Cu-Au deposit, Cloncurry district, Queensland. Economic Geology, 96, 875-884.

Williams, P.J. and Pollard, P.J., 2003. Australian Proterozoic iron oxide-Cu-Au deposits: an overview with new metallogenic and exploration data from the Cloncurry district, northwest Queensland. Exploration and Mining Geology, 10, 191-213.

Wyborn, L.A.I., 1988. Petrology, geochemistry and origin of a major Australia 1880-1840 Ma Felsic volcano-plutonic suite: a model for intracontinental felsic magma generation. Precambrian Research, 40/41, 37-60.

Wyborn, L.A.I., 1998. The younger ~1500 Ma granites of the Williams and Naraku Batholiths, Cloncurry district, eastern Mount Isa Inlier: geochemistry, origin, metallogenic significance and exploration indicators. Australian Journal of Earth Sciences, 45, 397-412.

Wyborn, L.A.I. and Page, R.W., 1983. The Proterozoic Kalkadoon and Ewen batholiths, Mount Isa Inlier, Queensland; source, chemistry, age, and metamorphism. BMR Journal of Australian Geology and Geophysics, 8, 53-69.

Wyborn, L.A.I., Page, R.W. and McCulloch, M.T., 1988. Petrology, geochronology and isotope geochemistry of the post-1820 Ma granites of the Mount Isa Inlier: mechanisms for the generation of Proterozoic anorogenic granites. Precambrian Research, 40/41, 509-541.

Wyborn, L.A.I., Wyborn, D., Warren, R.G. and Drummond, B.J., 1992. Proterozoic granite types in Australia: implications for lower crust composition, structure and evolution. Transactions of the Royal Society of Edinburgh, Earth Sciences, 83, 201-209.

APPENDIX 1-WHOLE ROCK GEOCHEMISTRY (below)

Rock Type	Diorite	Anatectic pegmatites			TTG	Sodic alkaline intrusions								Potassic, A-type intrusions								
Location	Ernest Henry	Osborne	Cannington	Cannington	MAIC	RIC	Mt Margaret	Mt Margaret	Saxby Granite			RIC		Mount Angelay Igneous Complex								
Age (Ma)	1650	1600	1600	1600	1550		1528	1528	1530	1530	1536		1525	1525	1525	1525	1525	1525	1525	1525	1525	1525
Sample No.	A8	62471	37777	37788	42712	42766	Ma	Me	26.04	26.15	26.18	42768	163-1	163-3	95019	95053	95067	95080	JTGC03	JTGC04	JTGC09	JTGC014
Rock Type	Diorite	Alkali feldspar Pegmatite	K-feldspar-rich Pegmatite	Albite altered Pegmatite	Granite	Alkali Granite	Granite	Granite	Diorite	Quartz Monzogranite	Two-mica Granite	Quartz diorite	Quartz Monzonite	Quartz Monzogranite	Syenogranite	Dolerite	Quartz Monzogranite	Quartz Monzonite	Quartz Monzogranite	Aplite	Quartz Monzogranite	Quartz diorite
Source	1	2	2	3	4	5	6	6	7	7	7	8	9	9	9	10	10	10	11	11	11	11
(wt %)																						
SiO_2	54.67	73.00	75.40	64.31	70.18	72.32	62.60	55.30	51.50	67.40	72.50	58.20	52.01	65.87	76.42	48.93	66.66	61.51	56.30	77.60	60.20	52.30
TiO_2	2.20	0.10	0.03	bd	0.18	0.32	0.65	1.84	2.25	0.66	0.10	0.86	1.66	0.62	0.13	1.21	0.53	0.80	1.48	0.06	1.04	1.54
Al_2O_3	14.37	15.20	12.46	20.17	15.62	13.97	17.50	14.10	13.50	14.10	14.10	15.30	16.43	14.75	12.39	14.20	14.71	15.90	15.30	12.90	16.60	14.50
Fe_2O_3*	12.11	0.72	0.52	0.11	1.42	2.20	4.64	12.72	13.80	5.82	1.77	7.95	10.34	5.69	0.47	12.10	3.63	6.09	10.52	0.85	6.39	13.06
MnO	0.20	0.00	0.03	0.03	0.02	0.02	0.06	0.33	0.17	0.05	0.02	0.08	0.13	0.05	0.01	0.18	0.03	0.04	0.11	0.01	0.04	0.17
MgO	3.21	0.34	0.01	0.19	0.76	0.26	0.72	1.82	7.03	0.71	0.20	3.43	3.35	1.11	0.05	7.44	0.88	1.56	2.59	0.03	1.60	3.83
CaO	5.11	0.69	0.62	1.68	1.40	0.84	2.20	4.15	7.38	2.07	0.63	4.85	5.20	2.68	0.49	10.13	1.85	2.90	5.78	0.80	3.63	6.24
Na_2O	6.26	7.40	0.99	10.86	6.95	4.19	9.36	6.03	3.25	3.61	3.81	5.91	4.22	3.71	3.89	2.11	4.76	4.84	4.38	7.47	5.68	5.13
K_2O	1.35	0.96	9.25	0.61	1.30	5.43	0.92	2.38	1.06	4.48	4.80	1.44	4.61	4.45	5.14	1.81	4.88	4.86	2.40	0.34	3.62	1.76
P_2O_5	0.31	0.23	0.32	0.40	0.05	0.01	0.36	0.58	0.32	0.18	0.12	0.12	0.97	0.16	0.02	0.10	0.18	0.29	0.49	0.02	0.32	0.58
S	na	bd	na	na	na	0.01	0.01	0.02	na	na	na	0.02	0.2	0.03	0.03	0.02	0.01	0.01	bd	bd	bd	0.02
F	bd	na	na	na	na	0.04	0.02	0.04	na	na	na	0.06	0.42	0.06	na	na	0.04	0.13	na	na	na	na
LOI	na	0.59	na	na	0.94	0.46	0.51	0.46	0.12	0.47	0.89	1.32	0.95	0.72	0.35	1.85	0.56	0.59	0.73	0.73	0.86	1.01
Total	99.80	99.23	99.63	98.36	98.82	100.07	99.55	99.77	100.38	99.55	98.94	99.54	100.49	99.90	99.39	100.08	98.72	99.52	100.08	100.81	99.98	100.14
(ppm)																						
Cr	9	20	6	8	21	62	13	13	386	34	39	66	bd	12	6	224	11	13	8	11	2	38
Ni	24	3	bd	bd	4	8	8	12	168	8	3	30	11	9	bd	99	5	8	29	bd	12	41
Co	26	60	bd	bd	3	22	8	22	41	8	bd	33	24	11	bd	49	bd	11	29	4	13	31
Sc	30	bd	2	2	6	3	12	30	25	9	5	17	15	10	2	37	5	10	18	2	14	21
V	211	13	9	7	27	15	22	67	186	35	11	162	172	52	11	302	42	74	163	22	64	246
Cu	40	6	bd	bd	16	6	71	77	67	12	12	28	74	30	11	179	15	15	38	63	40	74
Pb	11	6	2566	38	4	23	6	3	6	13	27	11	11	13	6	5	15	14	bd	16	bd	11
Zn	71	bd	61	22	13	13	14	31	117	31	11	34	67	32	3	87	12	22	64	5	20	59
Sn	bd	bd	bd	bd	5	bd	bd	15	bd	bd	bd	bd	4	9	bd	2	15	13	8	12	5	17
W	bd	bd	bd	bd	bd	bd	5	bd	bd	bd	bd	bd	bd	bd	bd	bd	bd	bd	bd	3	bd	4
Mo	bd	bd	bd	bd	bd	bd	bd	na	bd	bd	bd	bd	bd	bd	bd	bd	bd	bd	bd	8	bd	bd
As	7	12	54	1	bd	bd	2	7	1	3	2	bd	2	4	1	1	5	5	bd	bd	bd	bd
Rb	42	24	281	28	52	189	23	59	47	237	385	46	182	203	136	88	153	155	76	3	103	50
Cs	bd	bd	bd	bd	bd	bd	bd	bd	1	3	3	bd	2	2	bd	bd	1	2	bd	bd	bd	bd
Ba	300	270	751	28	299	743	295	880	236	751	190	316	2078	1039	274	322	1332	1728	804	40	1548	297
Sr	103	41	95	56	241	98	90	102	205	86	22	212	614	169	55	175	339	457	282	14	255	137
Ga	26	12	30	24	20	18	31	28	24	27	23	23	23	23	17	19	23	24	22	26	23	23
Ta	bd	bd	na	bd	2	3	3	3	4	4	5	2	3	bd	bd	bd	bd	bd	bd	bd	bd	bd
Nb	20	3	na	2	4	34	17	13	30	35	24	15	30	31	17	8	35	34	27	21	33	22
Hf	7	bd	na	bd	2	11	12	7	6	12	3	7	10	14	1	2	11	14	13	5	14	6
Zr	346	11	na	18	85	317	426	242	236	415	93	212	458	471	33	85	319	467	259	103	354	260
Y	54	23	na	9	8	34	36	50	42	55	30	26	46	73	10	23	45	55	53	15	45	50
Th	20	na	na	na	3	95	22	10	6	29	27	30	29	61	21	2	62	92	31	25	18	15
U	5.5	na	na	na	bd	20.0	3.0	bd	bd	5.8	15.9	4.0	bd	5.1	6.3	bd	bd	8.3	2.9	9.7	4.1	bd
La	41.5	na	na	na	10.3	158.0	47.4	54.4	26.0	78.0	28.0	37.0	179.0	185.0	29.0	10.0	46.0	159.0	76.2	2.7	81.0	67.6
Ce	97.1	na	na	na	23.5	334.0	103.0	117.0	57.0	162.0	57.0	78.0	336.0	332.0	58.0	22.0	139.0	304.0	172.0	9.8	173.0	147.0
Sm	9.8	na	na	na	2.0	15.5	8.5	12.7	9.0	15.0	5.0	5.8	18.0	20.0	2.0	3.0	12.0	21.0	13.9	0.7	12.7	11.4
Eu	1.7	na	na	na	0.7	1.3	2.2	2.9	2.2	1.5	-0.5	1.2	3.1	2.4	bd	0.8	1.7	3.2	1.9	-0.5	3.0	2.0
Tb	1.6	na	na	na	bd	1.7	1.2	1.7	1.5	1.9	-0.5	0.9	1.7	2.1	bd	bd	1.4	2.5	1.9	-0.5	1.7	1.5
Yb	5.1	na	na	na	bd	5.6	3.8	4.9	3.4	4.8	3.1	2.9	4.3	7.4	1.1	2.2	3.8	6.4	5.0	1.7	4.4	4.2
Lu	0.7	na	na	na	bd	0.8	0.6	0.7	0.4	0.6	0.4	0.4	0.6	1.1	bd	0.3	0.5	0.9	0.7	0.3	0.6	0.6
Cl	908	na	na	na	bd	352	351	340	963	1185	215	319	871	710	222	268	355	692	354	1431	282	594

Table 1. Representative whole-rock geochemistry of selected igneous rocks, Eastern Succession. Data compiled from Mark (1993), Mitchell (1993); Knight (1995); Pollard et al. (1998), and Kennedy (2001).

Sample No.	Rock Type	Age (Ma)	$^{87}Rb/^{86}Sr$	$^{87}Sr/^{86}Sr$	$^{87}Sr/^{86}Sr(t)$	$^{147}Sm/^{144}Nd$	$^{143}Nd/^{144}Ndo$	eNdo	$^{143}Nd/^{144}Ndt$	eNdt	$^{143}/^{144}CHURt$	T2 Model Age (Ma)
Ernest Henry meta-andesite												
A34L	Alb. Meta-andesite	1740				0.1669	0.5123	-17.3	0.5104	0.2	0.5104	2182
A27L	Meta-andesite	1740				0.1021	0.5115	-21.3	0.5104	-0.2	0.5104	2209
A41	Seriate meta-andesite	1740				0.1413	0.5119	-17.3	0.5103	-1.3	0.5104	2291
Mary Kathleen Calc-silicate rocks												
A11	Scapolitic calc-silicate	1740				0.0705	0.5112	-28.8	0.5104	-0.6	0.5104	2237
Mount Fort Constantine												
A8	Diorite	1660				0.1360	0.5119	-14.5	0.5104	-1.6	0.5105	2243
Cannington												
22	Amphibolite	1600	1.026	0.7243	0.7007	0.1873	0.5127	1.2	0.5107	3.2	0.5106	1844
61	Soldiers Cap sediments	1670	5.105	0.8225	0.7000	0.0965	0.5112	-27.3	0.5102	-5.9	0.5105	2565
27B	K-rich pegmatite	1590	8.646	0.9083	0.7109	0.1481	0.5119	-15.0	0.5103	-5.2	0.5106	2447
44A	Albitised, K-rich pegmatite	1590	1.244	0.7440	0.7156	0.2113	0.5124	-3.7	0.5102	-6.7	0.5106	2565
Williams and Naraku Batholith												
Trondjhemite												
103	Trondjhemite	1550	0.269	0.7170	0.7112	0.1192	0.5117	-17.8	0.5105	-2.5	0.5106	2214
Potassic intrusions												
MAIC												
163-1	Quartz monzodiorite	1530	0.838	0.7236	0.7052	0.0827	0.5114	-24.6	0.5105	-2.2	0.5107	2182
JTGC14	Quartz diorite	1530	1.079	0.7297	0.7060	0.1071	0.5116	-19.8	0.5105	-2.2	0.5107	2182
JTGC03	Megacrystic quartz monzogranite	1530	1.509	0.7373	0.7042	0.0916	0.5114	-23.3	0.5105	-2.7	0.5107	2218
JTGC09	Megacrystic quartz monzogranite	1530	0.979	0.7280	0.7065	0.1082	0.5116	-20.2	0.5105	-2.9	0.5107	2231
95080	Quartz monzonite	1530	0.961	0.7266	0.7055	0.0959	0.5115	-22.6	0.5105	-2.8	0.5107	2228
163-3	Quartz monzonite	1530	3.501	0.7845	0.7076	0.0983	0.5115	-22.2	0.5105	-2.9	0.5107	2233
JTGC07	Quartz monzonite	1530	6.342	0.8361	0.6968							
95067	Quartz monzonite	1530	1.301	0.7341	0.7056							
138	Quartz monzonite	1530	6.989	0.8572	0.7037	0.1059	0.5116	-21.1	0.5105	-3.4	0.5107	2266
95019	Alkali-rich syenogranite	1530	7.064	0.8505	0.6954	0.0803	0.5113	-25.9	0.5105	-3.3	0.5107	2251
JTGC04	Balloon-textured aplite	1530	0.764	0.7231	0.7063	0.1123	0.5117	-18.5	0.5106	-2.0	0.5107	2164
SIC												
LM26.04	Diorite	1520	0.648	0.7188	0.7047	0.1440	0.5121			-1.0		2081
LM26.15	Quartz monzogranite	1520	8.409	0.8870	0.7035	0.1260	0.5118			-1.8		2141
LM26.18	Two-mica granite	1536	49.260	1.8924	0.8062	0.1304	0.5118			-3.0		2246
Roxmere quartz diorite												
42766	Syenogranite	1530	6.418	0.8401	0.6992	0.0879	0.5114	-24.4	0.5105	-3.1	0.5107	2248

Table 2. Sm-Nd-Sr whole-rock isotopic data for selected magmatic and sedimentary rocks, and ore samples from the Osborne and Ernest Henry Cu-Au deposits in the Eastern Succession. $^{87}Sr/^{86}Sr_i$ data for rocks affected by amphibolite facies metamorphism have been recalculated at 1.59 Ga, whereas Nd isotope data for the same samples were calculated using their emplacement or depositional age.

Tectonothermal evolution of the Eastern Fold Belt, Mount Isa Inlier

Dr Mike Rubenach
School of Earth Sciences, James Cook University, Townsville, Queensland 4811
Email Michael.Rubenach@jcu.edu.au

ABSTRACT

In the eastern Cloncurry/Osborne zone of the Eastern Fold Belt, regional metamorphism of the Soldiers Cap Group involved multiple episodes in the period 1659-1500 Ma. The first event, DAb, overlapped with basin formation and may have been extensional; it involved growth of cordierite and andalusite and regional-scale albitization and associated biotite alteration. Deformation and metamorphism in the Isan Orogeny (~1610-1500 Ma) can be placed in several groups, each incorporating a number of separate events: the D1 group involved NS compression and growth of andalusite, garnet and staurolite, with kyanite in the north of the Snake Creek Anticline; the D2 and D3 groups involved ENE to ESE compression, with mainly andalusite, sillimanite, staurolite, garnet and minor localized kyanite. The age of the D2 group is around 1590 Ma, while D3b, during which there was some andalusite, staurolite and cordierite growth, was synchronous with the emplacement of Saxby Granite at 1527 Ma. The P-T-t path for the Cloncurry/Osborne zone is quite complex but exhibits an overall clockwise pattern but which also incorporated isobaric heating or cooling episodes. The maximum pressure of 5-6 kbar occurred during D1 to early D2, and was followed by a pressure and temperature drop. Temperature then rose to a peak during D2b at 4 kbar/590°C for the sillimanite isograd and up to 710°C in the sillimanite/K-feldspar zone at the Osborne Mine. Abundant plutons of granite and gabbro, comprising the Maramungie group and the Williams and Naraku Batholiths, intruded the Cloncurry/Osborne zone of the Eastern Fold Belt in the period 1500-1550 Ma. The pressure was around 3 kbar during the intrusion of the Saxby Granites (1527) and the Yellow Waterhole Granite (1510 Ma).

Although it also involved multiple growth episodes, Isan Orogeny metamorphism in the Mary Kathleen-Duchess zone, in contrast to that in the Cloncurry/Osborne zone, appears to have followed a simple anticlockwise path.

Proposed models for the thermal perturbations leading to regional metamorphism in the Mount Isa Inlier include mantle delamination, high values of heat-producing elements in adjacent older granites, crustal extension and mantle upwelling, and pluton emplacement synchronous with metamorphic episodes. Mantle delamination fails to explain the episodic metamorphic events that occurred over a considerable time-span. Older granites and metasedimentary rocks with high values of heat-producing elements are present in some of the high-grade belts. Although the D_{Ab} event may have been extensional, metamorphism during the Isan Orogeny (D_1 to D_3) occurred essentially in a compressional setting, with extension occurring in D_{2b}. Synchronous plutonism overlaps with only later metamorphic episodes in the Cloncurry-Osborne zone, and is absent from the Mary Kathleen-Duchess zone. Voluminous mafic igneous rocks were emplaced throughout the sedimentary and metamorphic history, but around the time of the metamorphic peak are manifested only as

local dykes. However, migmatization and widespread injection of pegmatites occurred in the sillimanite/K-feldspar zones. It is proposed that ponding of mafic magmas in the lower crust was concentrated along the higher-grade zones and occurred throughout the metamorphic history. Over the period of the metamorphic peak this led to widespread partial melting and transfer of heat via advection by intrusion of abundant small bodies of crustal melts to the level of the sillimanite zone. Lower grade zones formed by transfer of heat from the underlying sillimanite zone via conduction.

Keywords: Cloncurry, Eastern Fold Belt, regional metamorphism, Snake Creek Anticline, Soldiers Cap Group, P-T-t path

1. DELIVERABLES

Proposed deliverables at the commencement of the pmd-CRC were as follows:

1. Low risk deliverables

(a) Metamorphic isograd maps, incorporating metasomatism and mineralization occurrences, for all post-sedimentary deformation events
(b) Age determinations for metamorphic growth events, significant metasomatism, and intrusive events at critical localities
(c) P-T-t-d paths for critical localities
(d) Thermal modelling: influence on the thermal evolution of such factors as intrusives, high heat flow units, thermal blanketing, crustal thickening, and fluid advection.
(e) Preliminary model for sedimentary architecture will be used to ascertain how basin construction influenced subsequent thermal and metallogenic evolution
(f) Comparisons with the tectonothermal evolution of the Mount Isa area of the WFB, incorporating the newly-discovered syn-Sybella shear zone
(g) Comparisons with the tectonothermal evolution of the Georgetown Block

2. High Risk deliverables - potential for step change

Mineral deposits may be related to thermal factors such as sharp temperature gradients, and may have formed on cooling rather than heating P-T paths.
Mineral deposits may be directly related to intrusive events
Comparisons with the thermal evolution of the Georgetown Block may indicate why the EFB is so well endowed with deposits.

Deliverables 1(a)-(c) are included in this report.
There was insufficient time for detailed thermal modelling (1d) to be achieved, but instead this has been rolled over into Inew, where thermal modelling of the whole inlier will be undertaken. Likely causes for the thermal perturbations and complex P-T-t paths in the Eastern Fold Belt are, however, discussed in this report.

Comparisons with the Western Fold Belt are briefly discussed, as they will be considered in detail in Inew.

CRC meetings decided not to go ahead with detailed comparisons with the Georgetown Block.
Relationships between mineralization, thermal evolution and igneous activity are dealt with briefly in this report, but in far more depth in Oliver et al. (2005).

2. STRATIGRAPHIC/TECTONOTHERMAL SIGNIFICANCE OF NEW AGE DETERMINATION

A U-Pb SHRIMP age of 1686±8 Ma was determined (by Mark Fanning, ANU) for a tonalite specimen from the Snake Creek Anticline (Fig. 1). Tonalite sheets, lenses and small bodies are abundant within the mafic-tonalite complex, a sill-like body that intruded near the top of the Llewellyn Creek Formation. The tonalites generally preserve igneous textures, whereas the mafic rocks, which include gabbro, layered gabbro and dolerite, have been largely converted to hornblende-plagioclase amphibolites, locally preserving igneous textures but more commonly foliated. Mingling/mixing relationships between tonalite and gabbro indicate coeval emplacement, so that the above age is also the age of intrusion of the mafic rocks.

2.1 Significance of tonalite date

SHRIMP zircon ages of 1658±8 and 1654±4 have been determined for the Toole Creek Volcanics and Mt Norna Quartzite respectively (Page & Sun, 1998). Both these units overly the Llewellyn Creek Formation, implying that there is a significant depositional hiatus between them. Significantly the typical turbidite sedimentary structures in the Llewellyn Creek Formation are not seen in the overlying units. Mafic igneous activity extended for at least 30 Ma, given the volcanic rocks in the Toole Creek Volcanics and dolerite sills within the Mount Norna Quartzite north of the Snake Creek Anticline. Note also the age of the Ernest Henry Diorite (ca. 1660 Ma), and an albitized granite near Cloncurry (1679±7; Pollard & McNaughton, 1997), all indicating significant igneous activity during deposition of the Soldiers Cap Formation.

3 ISOGRAD MAP (deliverable 1a)

The enclosed isograd map (Fig. 2) is modified from one originally prepared for the pmd-CRC, and the one presented in Foster (2003). Note that the zones are composite, and are not related to any specific metamorphic event, even though the peak of metamorphism in the Isan Orogeny is dominant. Pelitic isograds were given preference, but otherwise calcsilicate zones were used. The biotite zone in calcsilicate rocks extends from greenschist facies to lower amphibolite facies, whereas the diopside isograd corresponds approximately to the sillimanite isograd in the Mount Isa Inlier. Note that regional “rock buffered” calcsilicate zones were plotted, not fluid buffered diopside related to granite intrusions and/or hydrothermal activity.

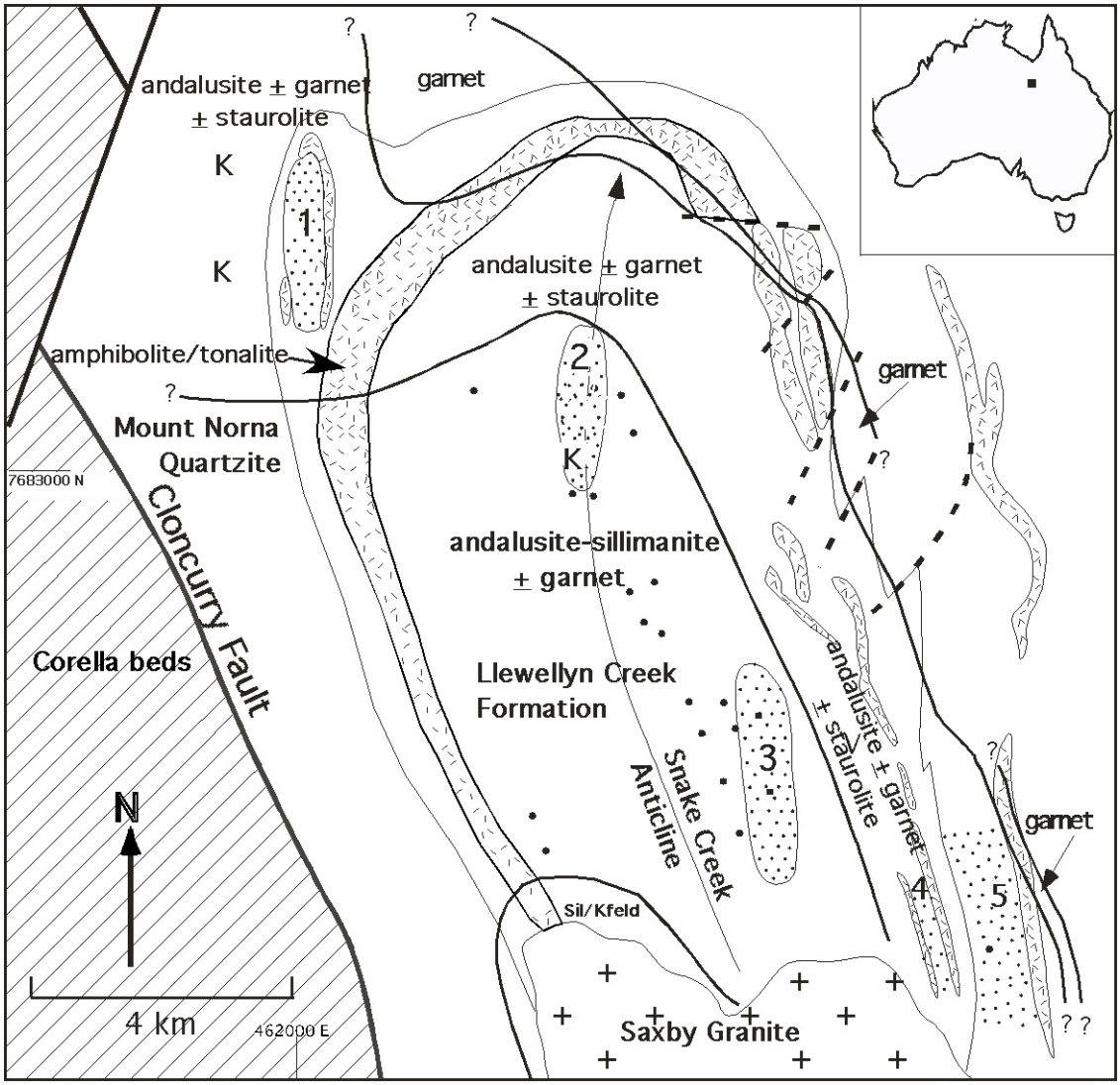

Fig. 1. Isograd map of the Snake Creek Anticline, modified from Rubenach & Lewthwaite (2002). The isograds are composite in that they refer to growth in both D_1 and D_2. Also shown are major albitite metasomatism areas 1-5, and kyanite locations (K). Cordierite is abundant in albitite areas 2 and 3, and other cordierite locations (commonly associated with albite) are shown as dots.

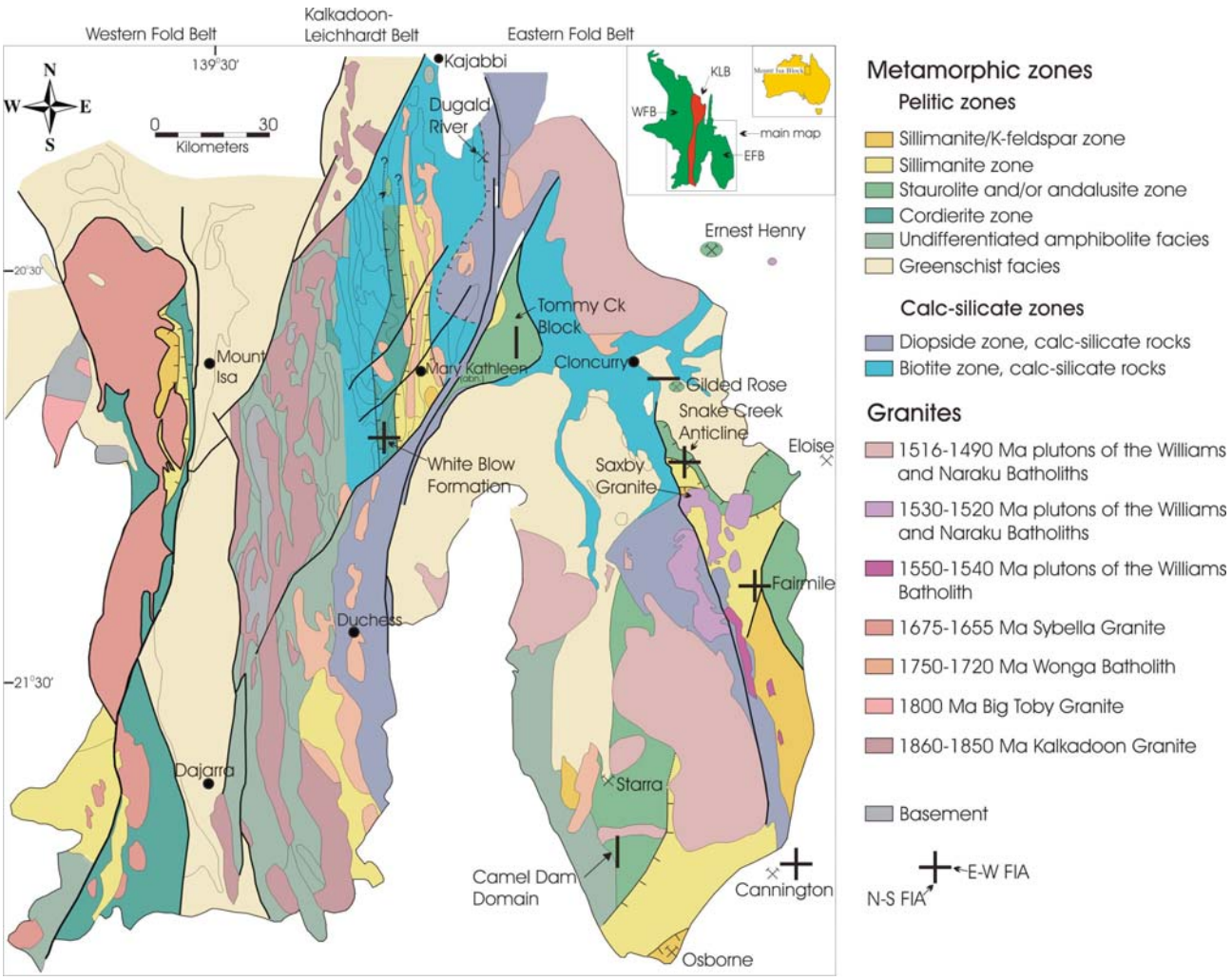

Fig. 2. Isograd Map of the Mount Isa Inlier, modified from Foster (2003, Appendix 1). Major mines and key areas in the Eastern Fold Belt are designated. Also shown are summary FIAs from Sayab,(2005), summarized as either EW orientations (due to NS compression in D_1), or NS FIAs (due to EW compression in D_2), the latter representing orientations from NNW to NNE. Note the two NS zones of amphibolite facies in the Eastern Fold Belt, the Cloncurry-Osborne zone and the Mary Kathleen-Duchess zone

Significant points concerning isograd patterns are as follows:

1.The overall isograd pattern is a series of amphibolite facies tongues elongate north-south, and alternating with greenschist facies belts. As a generalization, metamorphic grade decreases northwards, with the largest areas of sillimanite and sillimanite/K-feldspar rocks in the southeast of the Mount Isa Inlier. In the Eastern Fold Belt the higher-grade rocks are concentrated in two NS zones, one though Duchess and Mary Kathleen and the other from Osborne to Cloncurry (Fig. 2)

2. There are no obvious relationships between metamorphic grade and stratigraphy. For example, lower units of cover sequence 2 rocks in the Duck Creek Anticline are greenschist facies, while the cover sequence 3 Soldiers Cap Group is amphibolite facies throughout the SE of the Inlier. More locally, isograds are roughly parallel to the stratigraphy from the Middle Creek Anticline across to the eastern part of the Snake Creek Anticline, but sharply transect the stratigraphy on the northern and western sides of the Snake creek Anticline.

3. Grade changes occur across major faults such as the Cloncurry and Pilgrim Faults. The easterly-dipping Cloncurry Fault is almost certainly an old structure that was probably repeatedly reactivated. In the Snake Creek area, the juxtaposition of sillimanite zone Soldiers Cap Formation against greenschist facies Corella Beds to the west implies reactivation of the Cloncurry Fault as a post-metamorphism reverse fault. However, late-stage sinistral movement on the fault is another possibility that requires investigation.

4. There is a curious relationship between the presence of large granite bodies and amphibolite facies metamorphism, with no large bodies of granite (as opposed to migmatites and pegmatites – see Section 8) emplaced during the metamorphic peak, Thus granites are absent from such greenschist facies areas as the Marimo Basin and the Duck creek Anticline. A zone of granites (e.g. the Wonga Batholith) corresponds to the narrow high grade Wonga Belt extending through the Mary Kathleen-Duchess zone (Fig. 2). These granites intruded ca. 1730-1750 Ma, with accompanying deformation and amphibolite facies metamorphism (Oliver et al., 1991), but amphibolite facies metamorphism also occurred along the belt in the Isan Orogeny. This could be in part explained by the presence of elevated values of heat-forming elements in the granites, as suggested by MaClaren et al. (1999) for the Sybella Granite at Mount Isa, but the peak of metamorphism in the Isan Orogeny occurred ca. 150 Ma after the Wonga Batholith and ca. 100 Ma after the emplacement of the Sybella Granite (see Section 8).

There appears to be a broad spatial relationship between amphibolite facies metamorphic rocks and the Williams Batholith in the SE of the Inlier (Fig.2). If the Maramungee granites are included, the plutons were emplaced in the period 1500-1550 Ma, ca. 40-50 Ma after the metamorphic peak but synchronous with weaker ductile deformation events. However, there are no obvious relationships between amphibolite facies with the Wimberu and Naraku granites, almost all of which are younger than 1520 Ma. (See discussion in Section 8).

4. DEFORMATION HISTORY

Models for the tectonothermal evolution of the Eastern Fold Belt are based on the regional mapping and age determinations of geologists from the Bureau of Mineral Resources, now Geoscience Australia (e.g., Blake & Stewart, 1992; Jaques et al, 1982; Ryburn et al, 1988; Page & Sun, 1998; and references therein). Most university-based researchers agree that during the Isan Orogeny, NS to NNW-SSE compression (D_1 events) was followed by EW compression (D_2 and most subsequent events) (e.g., Loosveld & Scheurs, 1987; Loosveld 1989; O'Dea et al, 1997; Betts et al, 1997; Adshead-Bell, 2000; Mares, 1998; Lewthwaite, 2001; Rubenach & Lewthwaite, 2002; Sayab, 2005). However, significant differences between JCU workers and others concerns their use of FIAs (foliation intersection axes) within porphyroblasts, predicated on the arguments that porphyroblasts commonly do not rotate during ductile deformation (Mares, 1998; Sayab, 2005). In contrast, researchers from Monash University (e.g., O'Dea et al, 1997) emphasize thin-skinned tectonics and nappe formation during D_2. Details of the various structural models are summarized in Sayab (2005).

Arguments are presented in Rubenach & Barker (1998) and Rubenach & Lewthwaite (2002) that porphyroblasts, especially the relatively large staurolite and andalusite prisms (up to 40 cm in length) did not rotate but instead many show multiple growth events with inclusion trails in younger growth stages, and matrix foliations, clearly truncating trails in earlier stages (e.g., Rubenach & Barker, 1998, Fig. 8; Rubenach & Lewthwaite, 2002, Fig. 6a). This is supported by the consistency of FIAs across the Eastern Fold belt (Sayab, 2005).

Given the above, the proposed deformation history affecting the Corella beds and Soldiers Cap Group (i.e., amphibolite facies rocks of cover sequences 2 and 3 in the eastern Fold Belt) is as follows:

D_w – Wonga event, Pearson et al. (1992). Correlated with the "Big" event of Southgate et al. (2000) in the Eastern Fold Belt. Ages in the range 1735-1750 Ma. This affected the Corella Formation and correlatives (Doherty Formation, Corella beds) and the Double Crossing Metamorphics, but not the Soldiers Cap Group as this was not deposited at this time. Greenschist to amphibolite facies, with the number of discrete events unknown.

D_{Ab}. This is a previously unrecognised event, and is proposed as an outcome of dating of monazites using the JCU superprobe (see below). Previous work in the Snake Creek Anticline recognized the spatial association of cordierite and albite, and albite inclusions in cordierite (Rubenach & Lewthwaite, 2002; Rubenach, 2005). Inclusions in such cordierite show mainly weak to apparently non-existent preferred orientations, although good shallowly-dipping trails occur in some samples from Lewthwaite (2001) (Fig. 3). Age determinations of Ab+Crd±And schists from the Llewellyn Creek Formation and a gneiss with sillimanite after andalusite from Osborne yielded 1640-1660 Ma ages, suggesting this is a separate event to those listed below. These ages overlap with depositional ages of 1654 and 1658 Ma from the Mt Norna Quartzite and Toole Creek Volcanics respectively (Page & Sun, 1998), so may relate to an extensional basin-forming event.

D_1. The existence throughout the Eastern Fold Belt of recumbent F_1 folds, with axes plunging roughly EW, has been suggested by many workers (e.g., Loosveld, 1989; O'Dea et al., 1997; Betts et al., 1997; Holmes, 1992; New, 1993; Lewthwaite, 2001; Sayab, 2005, e.g. Section A, Fig. 4). An axial plane foliation, S_{1a}, subparallel to bedding is preserved in

many localities (Fig. 4). Early shallowly-dipping inclusion trails within porphyroblasts are also attributed to this event (e.g. Mares, 1998; Rubenach & Lewthwaite, 2002; Adshead-Bell, 2000; Sayab, 2005). However, it is clear that a number of deformation events preceded the regional D_2 in the Eastern Fold Belt (Giles & MacCready, 1997; Mares, 1998; Lewthwaite, 2001). Rubenach & Lewthwaite (2002) recognized a steep EW foliation in the Snake Creek area that succeeded S_1. Sayab (2005) attributes three FIAs to this early event, FIA-0, FIA-1 and FIA-2, which he attributes to NNW-SSE to NNE-SSW-directed shortening. In this report I refer to D_{1a} andD_{1b}, which respectively produced shallow and steeply dipping foliations (equivalent to S_1 and S_2 respectively of Rubenach & Lewthwaite, 2002) as the two major D_1 events. The Overhang Shear of Betts et al. (1997) probably belongs to D_1.

D_2. The predominantly NS-oriented steeply dipping penetrative foliation in the Eastern Fold Belt is generally referred to as S_2, although Rubenach & Lewthwaite (2002) called it S_3. In this report I refer to the steep foliation as S_{2a}, which was followed by folds and crenulations that formed in D_{2b}, which produced shallowly-dipping axial planar structures (Figs. 4, 5). Folds and crenulations related to D_{2b} are sporadic in the eastern Fold Belt, but quite abundant in the Sandy Creek area north of Osborne (Sayab, 2005, Section A, Figs 6, 7). The Snake Creek Anticline is interpreted as an F_1 structure by Loosveld (1989) and Giles & MacCready (1997), but given their very detailed structural mapping I concur with Holmes (1992), New (1993) and Lewthwaite (2001) that it is essentially an F_{2a} structure, with overturned sections the result of F_{1a} and F_{2b} interference. S_{2a} and S_{2b} are referred to as S_3 and S_4 by Rubenach & Lethwaite (2002), while in the literature S_{2a} is generally called S_2.

D_3. Folds and crenulations with steep roughly NNW- to NNE-oriented axial planes are commonly related to D_3, although the number of deformations that followed D_2 is uncertain. Dealing with multiple foliations is complicated by the process of reactivation of earlier foliations in younger events (Bell, 1986; Bell et al., 2003). For example, in many localities S_{2a} has been reactivated during D_3, so that the dominant foliation is really a composite of S_{2a} and S_3, and D_{2b} crenulations in the matrix have been commonly destroyed by decrenulation processes during reactivation, being preserved only in porphyroblasts and in strain shadows around porphyroblasts (Lally, 1997; Adshead-Bell, 2000; Lewthwaite, 2001; Sayab, 2005). In this report S_{3a} refers to a steep NNW to N-oriented foliation, while S_{3b} relates to late NE orientations, corresponding to FIA-5 of Sayab (2005, section C). As is discussed below, S_{3b} was probably synchronous with the Saxby Granite (Fig. 1), which intruded at 1527 Ma. For outcrops where later crenulations are absent, S_{2a} has commonly been reactivated during D_{3a} and/or D_{3b}, so is therefore a composite foliation, making timing of porphyroblast growth difficult unless there are good inclusion trails and multiple oriented thin sections are examined.

Detailed work on oriented samples suggests that there are probably more events in D_1, D_2, and D_3 than those listed above. It is emphasized that these extra events rarely have a significant affect on the meso- and macroscopic structures. Thus the geometry of the Snake Creek Anticline is mainly the result of D_{2a}, with the affects of D_1 and D_3 events being of local significance. However given multiple porphyroblast growth and the complexity of P-T-t paths (Section 6) the identity of any particular foliation or crenulation is critical in the timing of porphyroblasts and in determining the tectonothermal evolution.

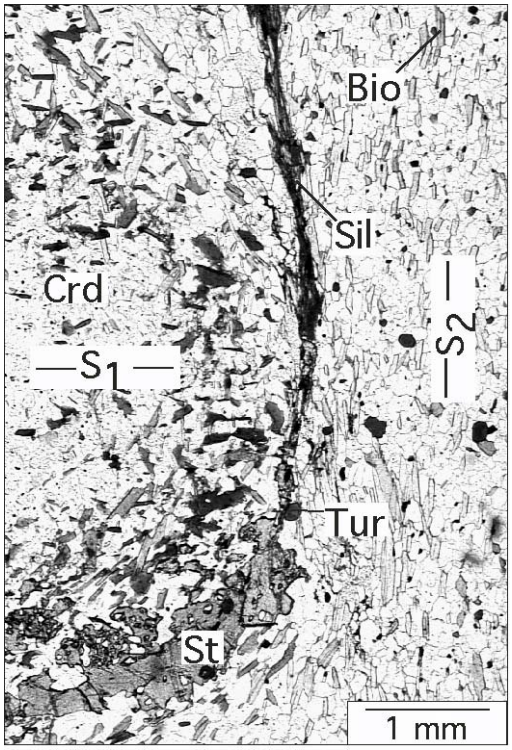

Fig. 3. Biotite inclusions in cordierite show a subhorizontal ? S_{1a} foliation, whereas the matrix shows an S_{2a} foliation. Staurolite and sillimanite are aligned in S_{2a}. Specimen 61476 of Lewthwaite (2001), modified from Rubenach & Lewthywaite (2002, Fig. 6a). Length of photo 5.6 mm. Tur is tourmaline.

Fig. 4. A rare F_{1a} isoclinal recumbent fold, east-central part of the Snake Creek Anticline. The rocks are interlayered metapsammites and andalusite schists of the Llewellyn Creek Formation. Note the axial planar S_{1a} foliation. The fold plunges to the east. The hinge of an overprinting F_{2a} antiform occurs to the right of the photo.

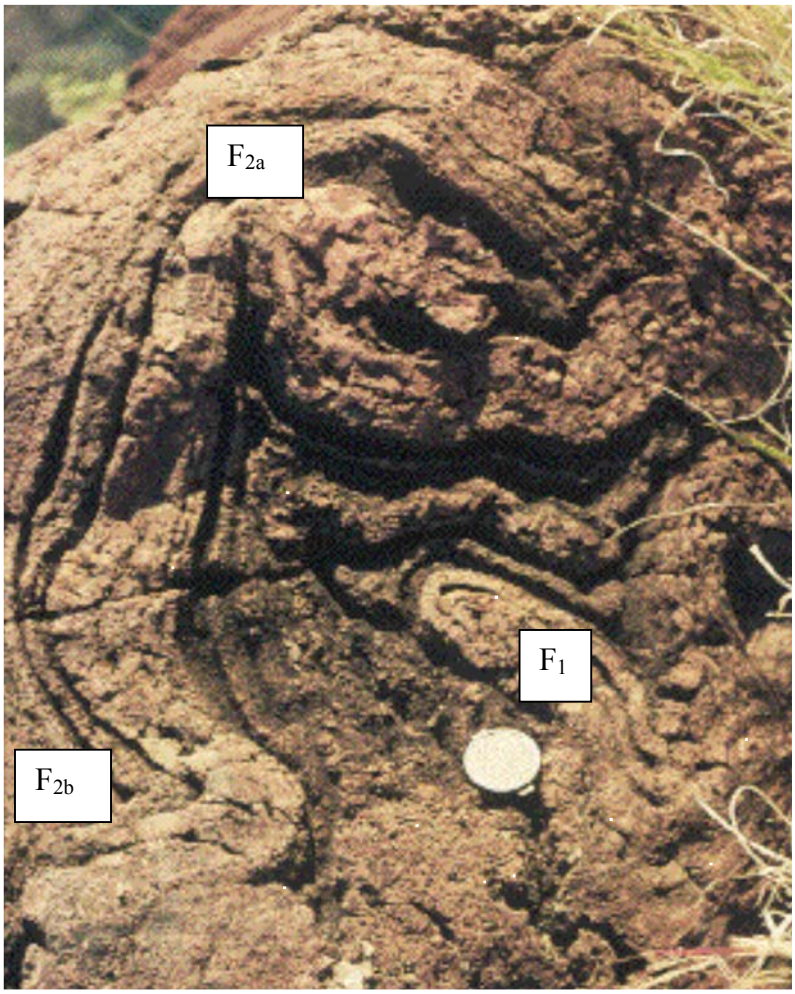

Fig. 5. Outcrop of folded calcsilicate rocks, Corella beds, Snake Creek Anticline. Camera lens cap for scale. Interpreted deformation history is shown.

5. TIMING OF METAMORPHISM

5.1 Snake Creek Anticline

As a result of good exposure, abundant porphyroblasts and its structural significance, the Snake Creek Anticline has been the subject of considerable metamorphic research (Ryburn et al., 1988; Loosveld, 1989; Holmes, 1992; New, 1993; Rubenach & Barker, 1998; Lewthwaite, 2001; Rubenach & Lewthwaite, 2002; Hingst, 2002; Rubenach, 2005; Sayab, 2005). Over 1200 samples, the majority of them oriented, have been sectioned by myself and JCU students, with between one and twelve sections from each, Over 100 samples have been analysed using the microprobe.

Figure 6 summarizes the timing of growth of porphyroblasts and significant metasomatic events in the Soldiers Cap Group in the Snake Creek Anticline. This is based on earlier work, especially Lewthwaite (2001) and Rubenach & Lewthwaite (2002). It is important to emphasize ambiguities in timing porphyroblasts from inclusion trails. For example, a porphyroblast that preserves a strong foliation (e.g., S_{2a}) may have grown late in that event or, more likely, early in a subsequent event (Bell & Hayward, 1991). Further ambiguities result from reactivation of foliations and problems in identifying foliations in unoriented samples. Even for samples where three orthogonal thin sections were cut, it clear that multiple oriented thin sections are required for key samples (Bell et al., 1998; Sayab, 2005). Taking these complications into account, research work within the pmd-CRC has lead to revision of the timing chart. Some of the evidence for timing is presented in Figs. 3, 7-16, 18 and 20-28. Summaries for minerals are as follows:

Cordierite. This commonly occurs as inclusions or pseudomorphs within early andalusite (Figs. 7, 10). Inclusion trails generally show no orientation, or are shallowly dipping (Fig.3). Where biotite has replaced cordierite it is randomly oriented (Fig. 10) or defines a shallowly-dipping foliation (Fig. 9). Cordierite is typically associated with metasomatic albite in the axial zone of the Snake Creek Anticline (Figs.1) (see also Section 7). Microprobe dating of monazites from albitites and schists with cordierite or pseudomorphed cordierite yielded ages between 1631 and 1652 Ma (see Section 6), providing additional evidence for the D_{Ab} event. The interpretation of Sayab (2005) that most cordierite is late is rejected in my report. However, late cordierite does occur in a few samples, particularly ones collected from aureoles of the Saxby Granite and related small intrusions along the Cloncurry Fault (see Section 7).

Andalusite. There is abundant evidence that andalusite grew in multiple events (Figs. 11-13; also see Lewthwaite, 2001). In many samples, the main andalusite growth event was relatively early, but the porphyroblasts contain inclusion trails that appear unoriented or define a weak shallowly-dipping foliation which could be S_{Ab} S_{1a}, or S_{2b} (Figs. 7, 12, 13). FIA determinations are quite difficult to determine for andalusite, but Sayab (2005, Section C) found one sample (SC103) with an EW FIA, and four others with NS FIAs. Late andalusite that has overgrown S_{2a}, S_{2b}, S_{3a} or S_{3b} generally forms only narrow rims on large older grains (Figs. 11-13). Note that in many staurolite or sillimanite-rich samples early andalusite has been replaced by coarse-grained muscovite so that its timing is uncertain.

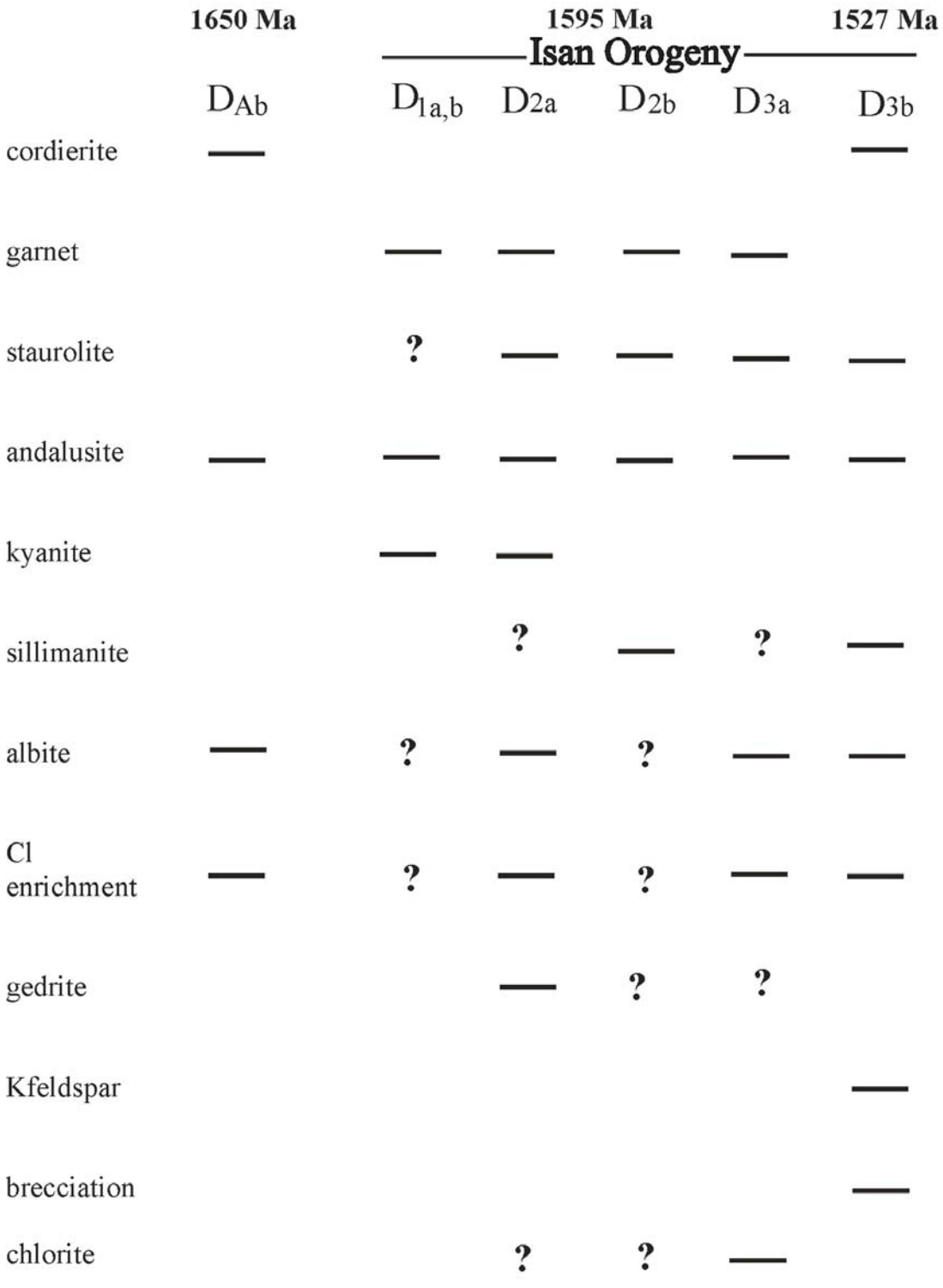

Fig. 6. Timing chart for the Snake Creek Anticline.

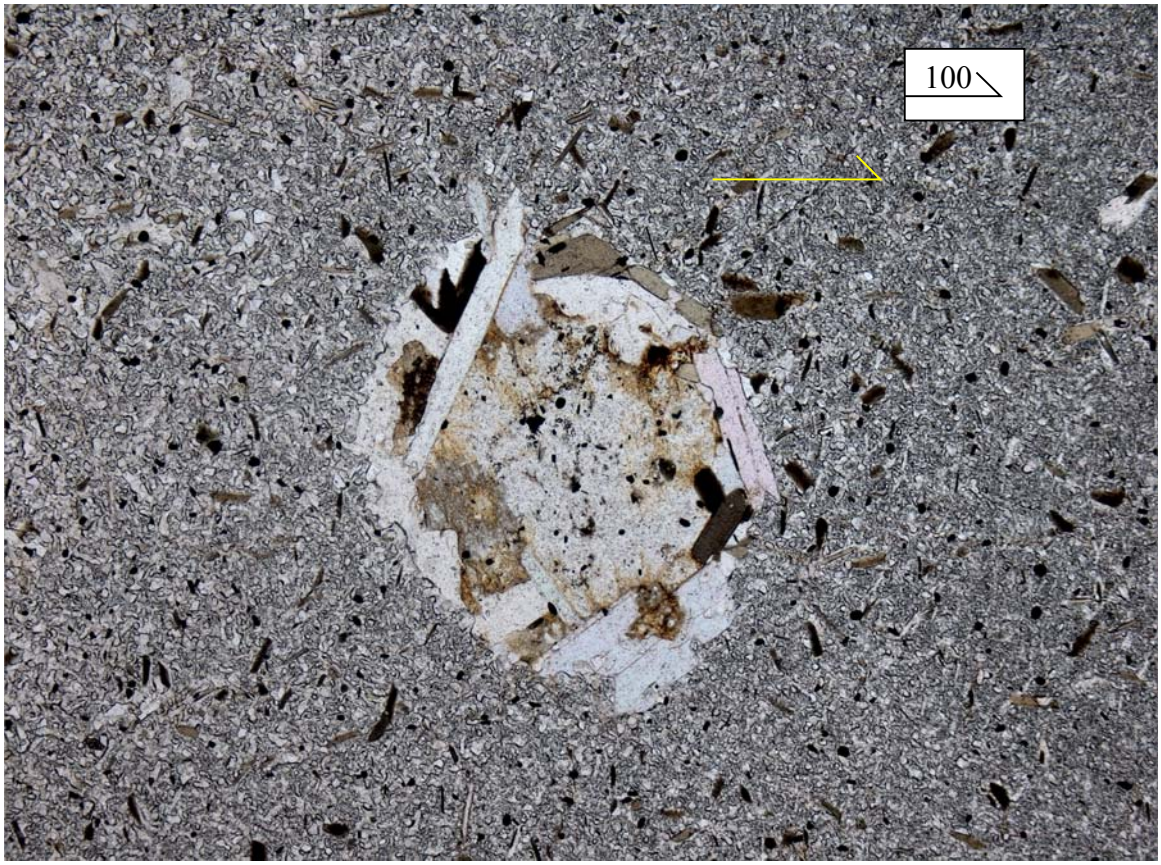

Fig. 7. Relict cordierite, partly replaced by muscovite and biotite, inside an early-growth andalusite porphyroblast that preserves biotite inclusions showing two foliations. Sample 814.2, photo length 5.6 mm.

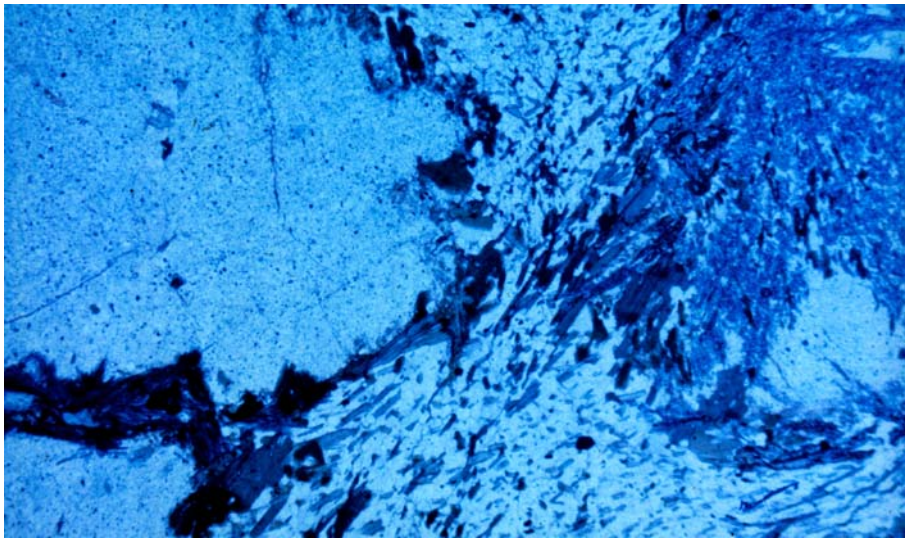

Fig. 8. Early-growth cordierite porphyroblasts in a matrix of albite and biotite that preserves an S_{2a} foliation. The cordierites on the left are rimmed by biotite, with the one on the right largely replaced by andalusite and small grains of staurolite. Sillimanite, aligned in S_{2a} also occurs in the rock. Poorly aligned very small ilmenite grains occur in cordierite. Sample 490. Length of photo 5.6 mm.

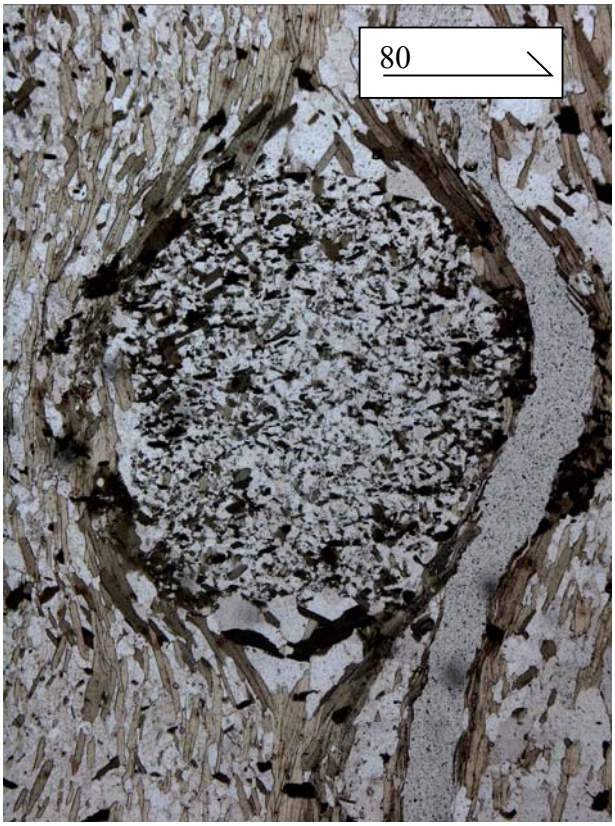

Fig. 9. Early cordierite replaced by quartz, albite and biotite showing a horizontal foliation, wrapped by a biotite-rich foliation, probably S_{3a}. Most of the cordierite grains in this rock have been replaced by andalusite, staurolite, biotite and sillimanite. A crack in the thin section occurs to the right of the Crd. Sample 519.3. Length 5.6 mm.

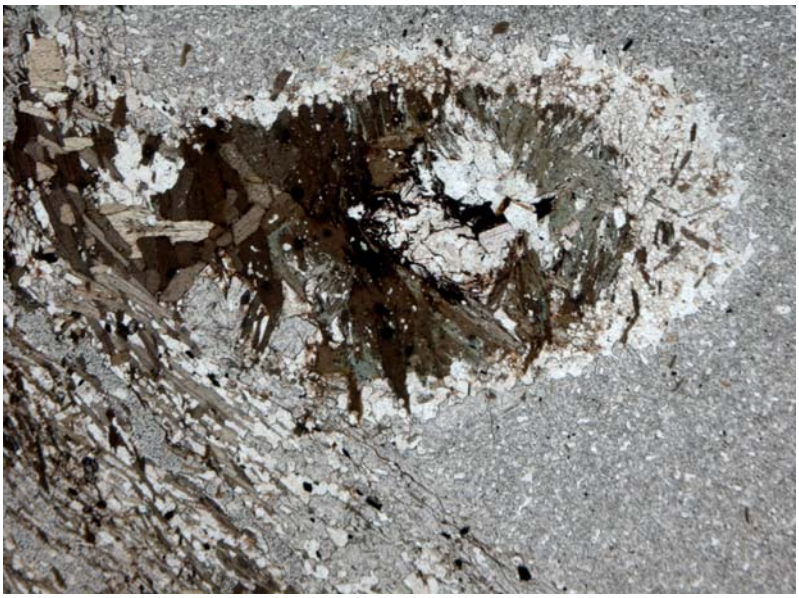

Fig. 10. Cordierite replaced by biotite and albite preserved in an early-growth andalusite, truncated by a rim of andalusite that has overgrown S_2 (also see Fig. 11). Length 5.6 mm.

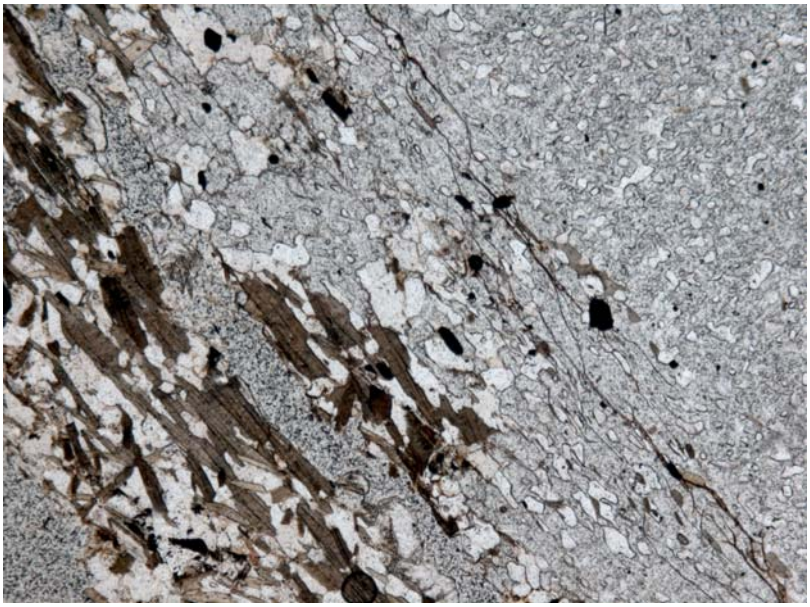

Fig. 11. Same sample as Fig. 10, but showing the truncation of the foliation in the early andalusite by the second growth stage that preserves S_2. Length 2.8mm.

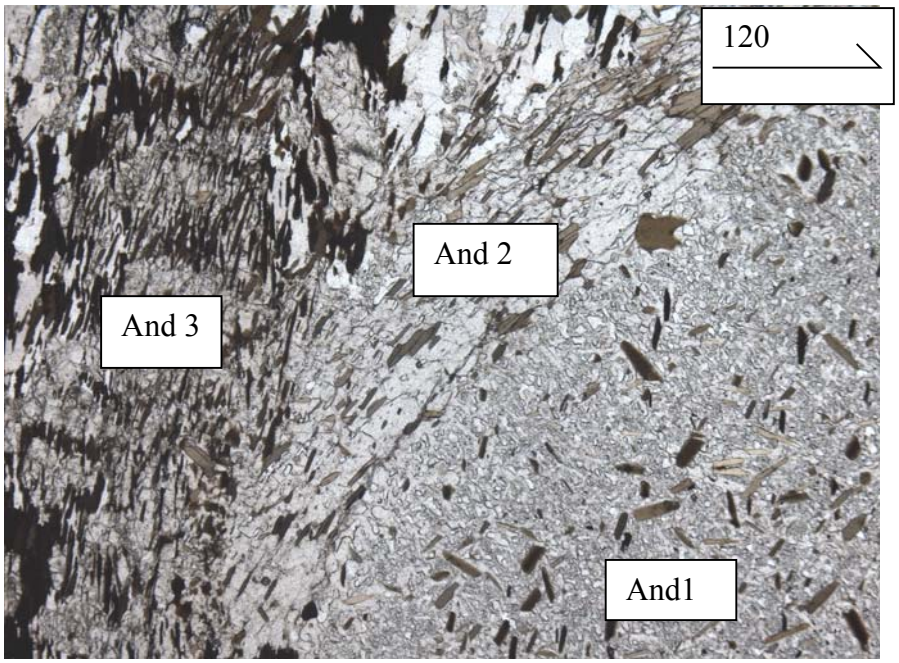

Fig. 12. Andalusite 1 has overgrown two weaker foliations, and elsewhere in the sample preserves early-growth andalusite. Andalusite 2 has overgrown a strong shallow foliation (shown in the strain shadow to the right of the photo), probably S_{2b}, that has been truncated by the S_3 foliation preserved in andalusite 3 and the matrix. Sample 838.2. Length 5.6 mm.

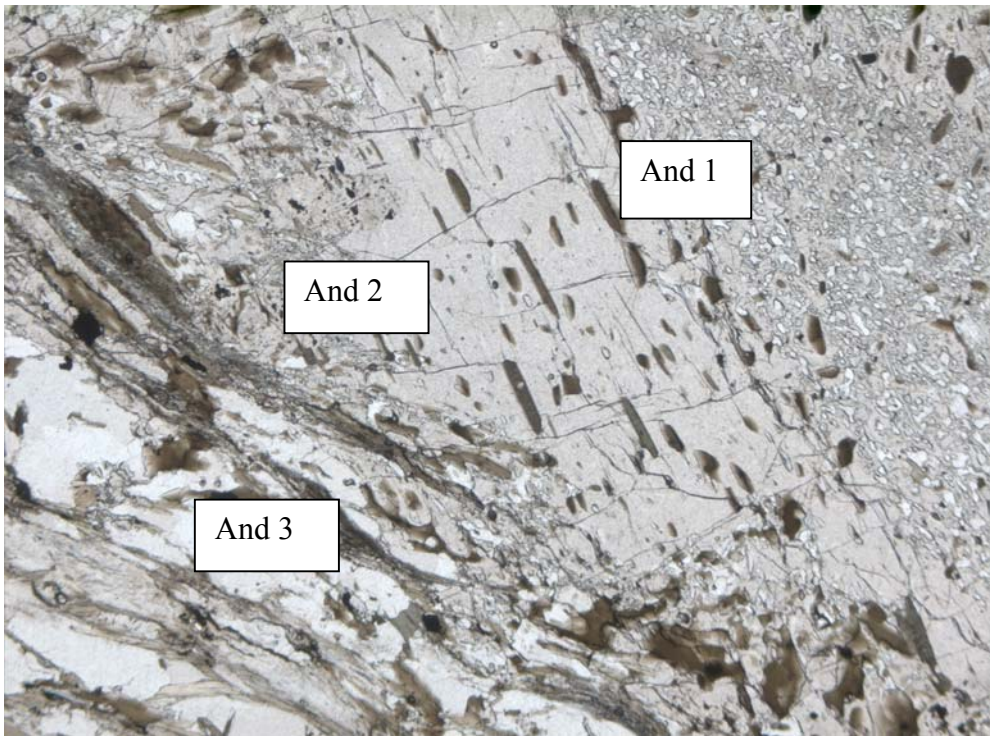

Fig. 13. Large andalusite showing 3 growth stages. The sample () was collected from the NE contact of the Saxby Granite (Fig. 1). Andalusite 3 contains intergrown sillimanite, the latter forming only within two metres of the contact at this locality and is clearly aureole-related. The matrix foliation and that preserved in And 3 is S_{3b}. Length 5.6 mm.

Sillimanite. This mineral is important in that it best defines the metamorphic peak. However, because it does not contain inclusion trails it is difficult to time. As it commonly occurs as fibrolite that is aligned in S_{2a}, the peak of metamorphism either corresponded to this event or to the subsequent D_{2b} event, as the growth of fibrolite could have been mimetically controlled by syn-D_{2a} micas. In a few rocks sillimanite shows two stages of growth in a crenulation cleavage (Fig. 14). It also occurs as prisms oriented parallel to the C-axes of andalusite grains – this crystallographically-controlled growth is referred to as paramorphic replacement, but its precise timing in the Snake Creek Anticline is difficult to determine microstructurally. Some sillimanite is related to the intrusion of the body of Saxby Granite (Fig. 1), occurring in the sillimanite/K-feldspar zone around the NW corner of the granite, and in a 2 metre zone at the NE contact (Fig. 13).

Staurolite. Staurolite commonly has inclusions of quartz, generally with well-defined trails. There is no clear evidence that it grew in D_{Ab} but it did grow in a number of subsequent events (Fig.15). Sayab (2005) found and EW FIA in one sample, and NS to 55° in four others.

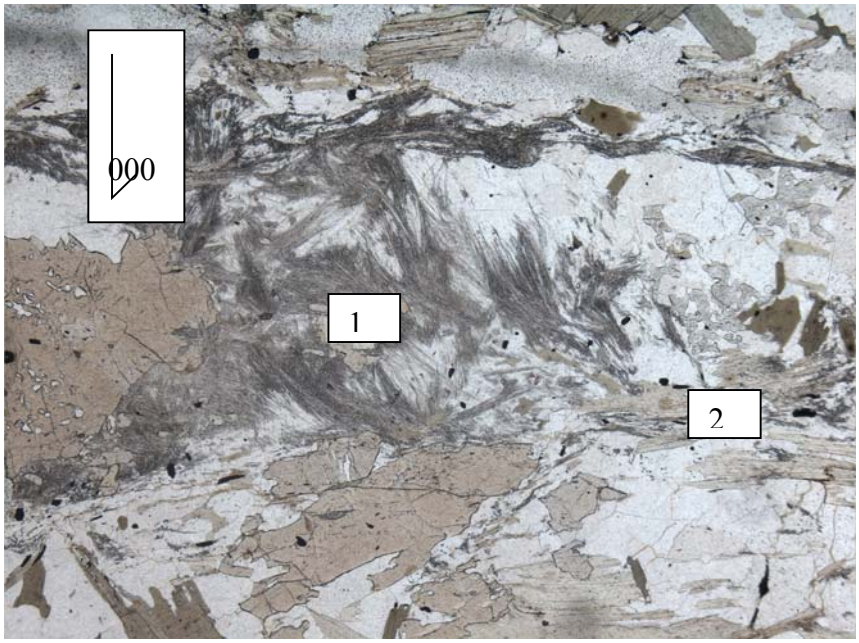

Fig. 14. Photo shows a crenulation cleavage with two stages of sillimanite growth (1, 2). The staurolite present also shows two growth stages. Sample 61476 (Lewthwaite, 2001). Length 5.6 mm.

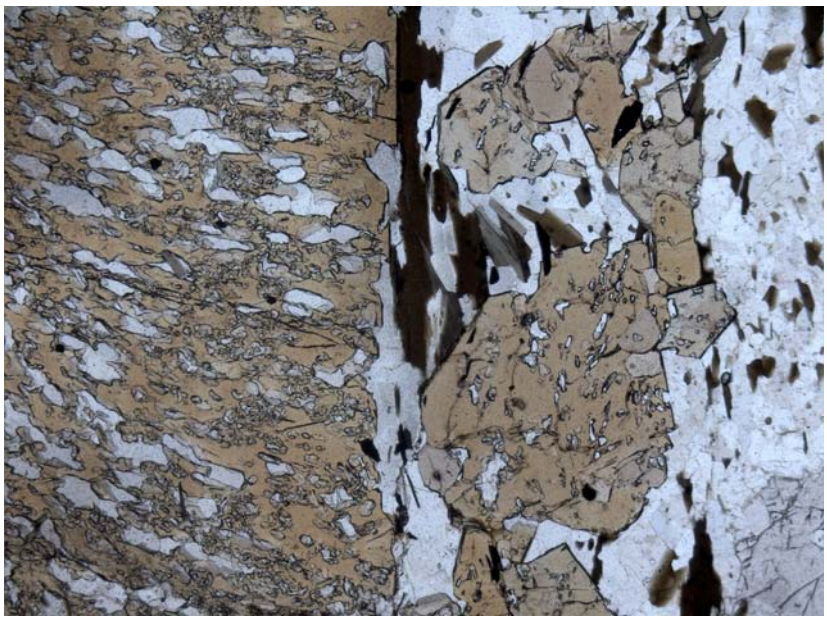

Fig. 15. Two generations of staurolite. The earlier one on the left has overgrown a shallow foliation, clearly truncated by the steep matrix foliation. The grains on the right have overgrown the matrix foliation, probably S_{3a}. The matrix consists of quartz, albite, biotite and chlorite, but albite inclusions occur in the later staurolite. A relict andalusite grain, which probably grew in D_1, is in the lower right corner. Sample 743B. Length 5.6 mm.

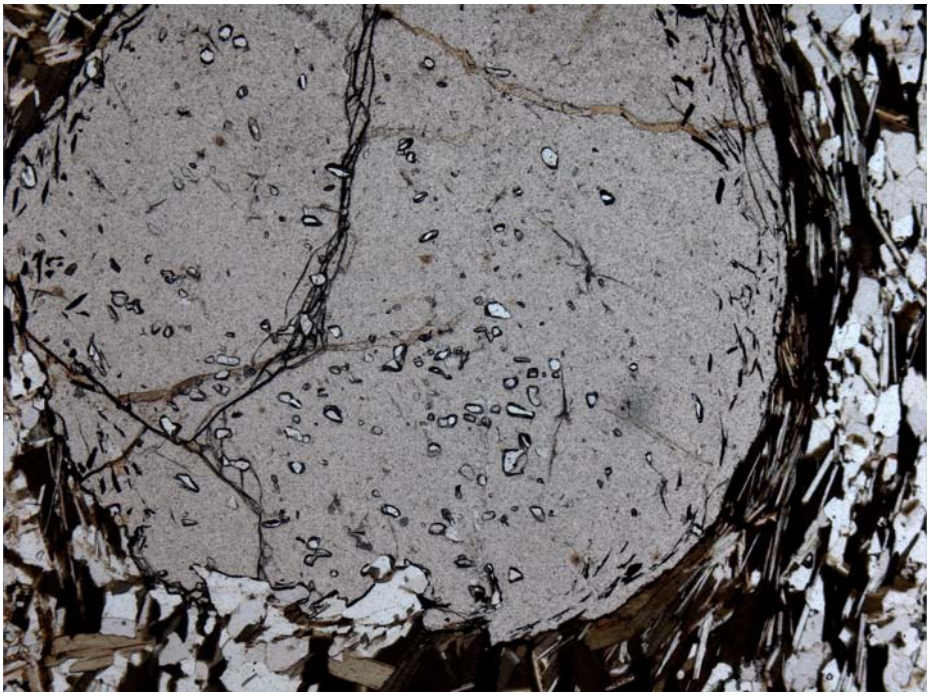

Fig. 16. The core of the late-growth garnet has overgrown a shallow foliation shown by quartz inclusions, whereas the rim has overgrown graphite aligned in steeply-dipping ? S3a. The sample also contains early cordierite pseudomorphs, andalusite, staurolite and sillimanite. Sample 814.2. Length 5.6 mm.

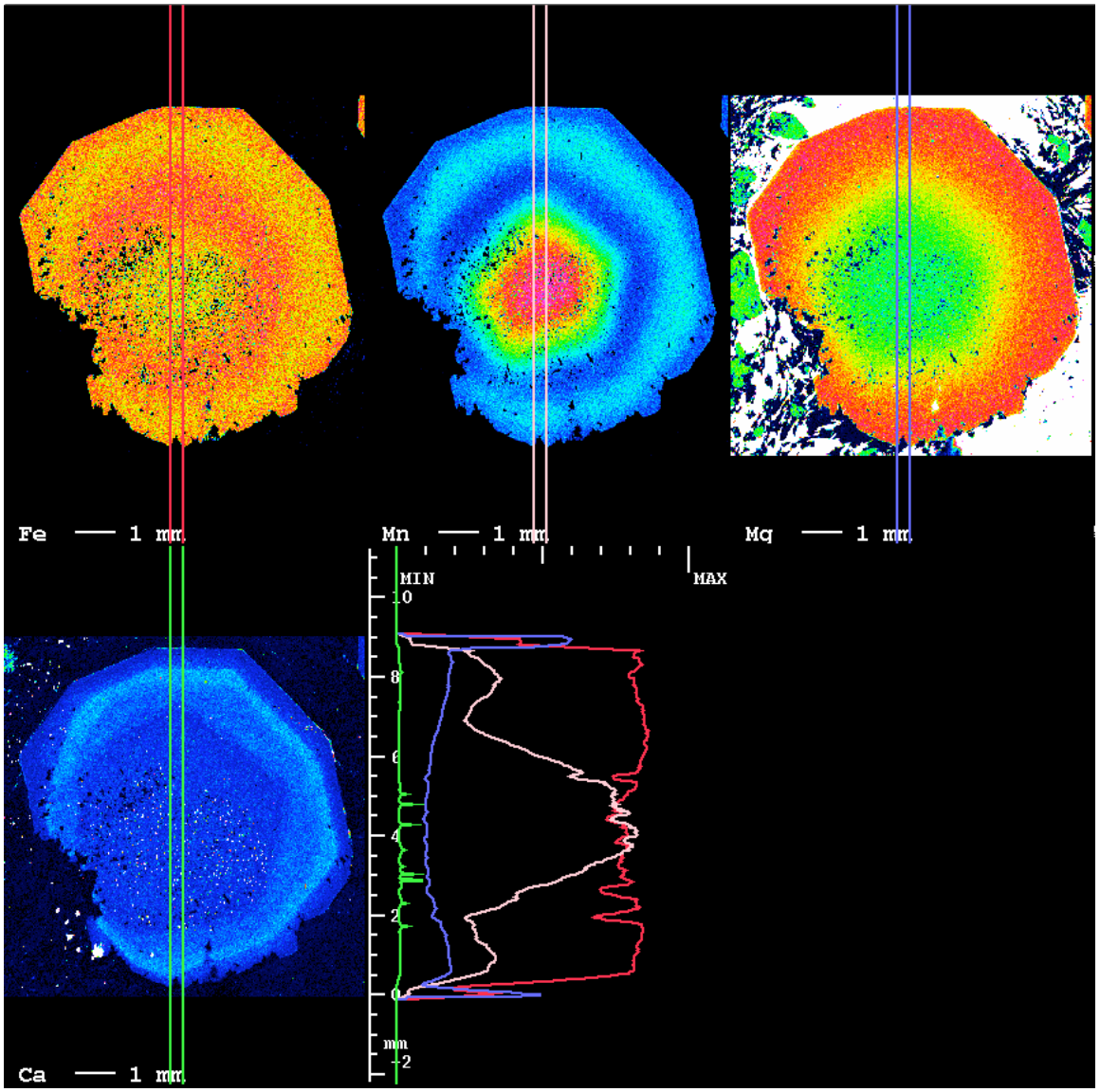

Fig. 17. X-ray maps of garnet in sample 109 (collected by Cameron Huddlestone-Holmes). The garnet shows at least two growth stages, best shown by the Ca map and the Mn map and profile. These are probably during D_1 and D_{2a}. Andalusite had grown before garnet, which has inclusions of chlorite. The matrix consists of biotite, quartz, albite, and contains small staurolite porphyroblasts. The Ca map shows small white spots of apatite in the garnet, and larger ones in the matrix. The apatite grains in the different growth stages and matrix show different populations of Cl and F, suggesting changing fluid compositions.

Garnet. In the Snake Creek Anticline garnet is typically small with poorly-developed inclusion trails and so are difficult to time. However many occur as inclusions in andalusite and staurolite, so they must be older or contemporaneous with the host porphyroblast. In many samples garnet inclusions in andalusite are smaller than those in the matrix, indicative of a second growth stage after andalusite. The chemical profiles through such garnets, however, generally show no hiatuses. In some rocks garnet does show good inclusion trails, commonly showing EW FIAs indicating growth in D_1 (Sayab, 2005). In other cases garnet occurs only the matrix and has overgrown S_2 or S_3 foliations (Fig. 16); such examples show only NS FIAs (Sayab, 2005, Section C). A few samples (SC104, 1117, 118) studied by Sayab show both NS and EW FIAs. Note that garnet does not occur

in cordierite-bearing rocks with the exception of a few samples where cordierite has been replaced and garnet grew late (e.g., Fig. 16).

Kyanite. Kyanite rarely has inclusion trails so is difficult to time. However, in several samples in the NW of the Snake Creek Anticline kyanite has overgrown the dominant NS foliation, i.e. S_2 or S_2 reactivated during D_3.

Albite. Albite is typically fine-grained, but limits on its timing can be deduced on its presence or absence inside particular porphyroblast growth stage or simply occurs in the matrix. Rubenach & Barker (1998) noted that albite veining occurred both pre- to syn-D_2. As it occurs as inclusions within early cordierite, the most important albitization event in the Llewellyn Creek Formation is interpreted as syn-D_{Ab}. However, albite veins occur parallel to the axial plane of a mesoscopic F_{1a} fold (Rubenach, 2005), and areas of albitite concentration are elongate NS (Fig. 1), suggesting that albitization also occurred during D_1 and D_2. This is supported by the lack of albite in some early-growth andalusite and staurolite porphyroblasts, with abundant albite in the matrix and/or porphyroblast rims. However, this is not absolute since albite, like muscovite, is an aluminous mineral so is prone to dissolution to supply local Al for the growing porphyroblast, even if it is not a direct reactant (Carmichael, 1969), so may not occur as porphyroblast inclusions even if it was in the matrix (muscovite only rarely occurs as inclusions in aluminosilicate porphyroblasts). The possibility that albite was dissolved as a result of shearing against micas during foliation development and then precipitated in nearby zones of low shear strain adds a possible further complexity in determining albitite timing. Widespread albitization of clasts occurs throughout the extensive breccias developed in the Corella beds west of the Cloncurry Fault. Small bodies of granite and gabbro are quite common along the Cloncurry Fault, and albitized calcsilicate breccias (with granite, gabbro and mingled/mixed clasts) occur as rims around some of the granites, even those extending into the Soldiers Cap Group. Breccia veins up to tens of metres wide also cut across the foliation in schists (Fig. 19), with a few narrow zones where muscovite has been replaced by albite extending over a hundred metres from the breccia vein. The small bodies of felsic granites along the Cloncurry Fault have been extensively albitized. Igneous zircons from a partly albitized granite from the NW corner of the main body of Saxby Granite yielded an age of 1527 ± 3Ma (this project), and this age also corresponds to the brecciation and late albitization, as well as to the D_{3b} event (Section 6).

Cl enrichment. Cl enrichment in biotite is common in many areas in the Snake Creek anticline, especially in schists subjected to biotite metasomatism that commonly accompanied albitization (Rubenach, 2005). As significant Cl is not expected in metasedimentary rocks of turbidite derivation, such as the Llewellyn Creek Formation, the chlorine is highly likely to be metasomatic. F enrichment also occurs, particularly in more Mg-rich biotite in the breccias, but not much work has been done on fluorine. Cl enrichment is higher in biotite inclusions in late-growth rims of andalusite porphyroblast and in biotite from the matrix of biotite-rich schists in many locations (Rubenach, 2005).

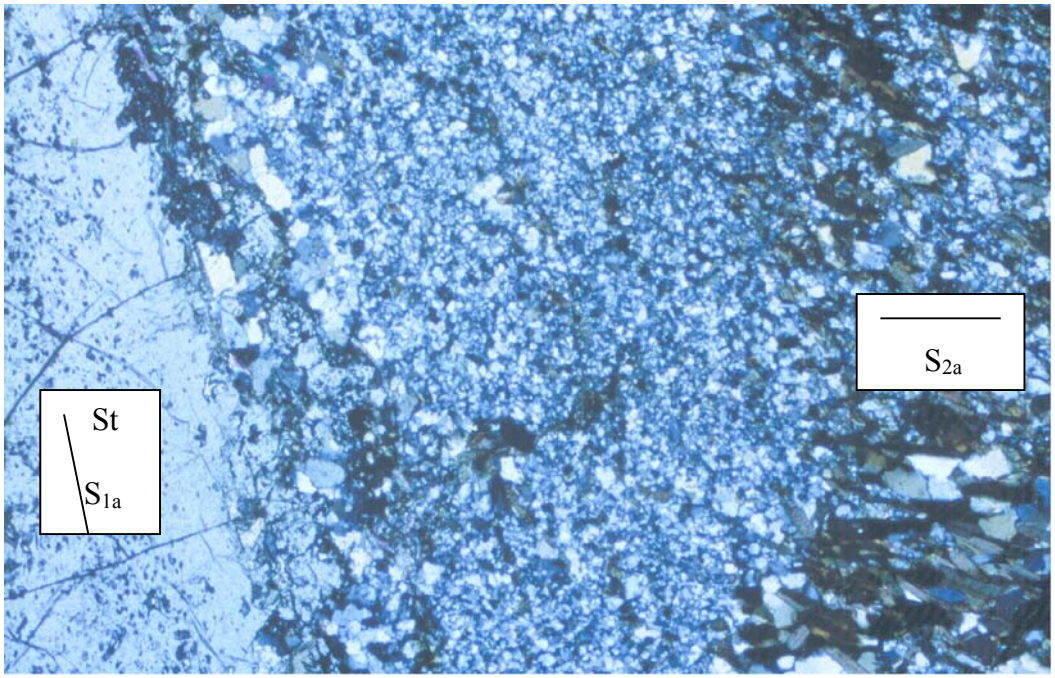

Fig. 18. The staurolite porphyroblast shows fine inclusions that define S_{1a} parallel to S_0, and are free of albite. Albite is abundant in the matrix, and occurs as inclusions in a narrow staurolite rim. Biotite grains inj the matrix are aligned in S_{2a}. It would appear that albitization in this specimen occurred after D_{1a} and before or during D_{2a}. Length 5.6mm.

5.2 Metamorphism elsewhere in the Eastern Fold Belt (other than Snake Creek)

Former work includes regional metamorphic studies (Jaques et al., 1982; Foster, 2003), the Eastern Selwyn Ranges (De Jong, 1995), the Fairmile area (Mares, 1998), the Eloise Mine (Baker, 1996) the Selwyn Range area (Adshead-Bell, 2000), the Gilded Rose area (Lewthwaite, 2001; Sayab, 2005) the Sandy Creek area (Sayab, 2005), and the Osborne Mine (Adshead, 1995; French, 1997; Banville, 1998). Other significant studies elsewhere in the Eastern Fold Belt (Wonga Belt, Tommy Creek Block) include those of Oliver et al. (1991), Reinhardt (1987, 1992a, 1992b), Reinhardt & Rubenach (1989), Bell et al. (1992), Hill et al. (1992), Lally (1997) and Sayab (2005). For pelitic rocks between the biotite and sillimanite zones the assemblages are quite similar. A common progression is garnet zone followed by staurolite/andalusite (Eastern Selwyn Ranges, Gilded Rose, Tommy Creek Block, Sandy Creek, White Blow Formation, Selwyn Ranges. Exceptions include much of the Mary Kathleen-Duchess zone, where the progression is biotite zone, cordierite zone and andalusite zone (Foster, 2003), with areas of unusual high-Mg rocks that metamorphosed to assemblages that include anthophyllite, talc, chlorite, biotite and cordierite (Reinhardt, 1987). As is the case at Snake Creek, some outcrops in the Selwyn Ranges, commonly with associated albitization, have localized cordierite + andalusite assemblages among the more common with garnet-staurolite-andalusite assemblages (Adshead-Bell, 2000). Such widespread low-pressure metamorphism, that also includes the Western Fold Belt (e.g., Rubenach, 1992; Foster, 2003), has important tectonothermal implications (see Section 8).

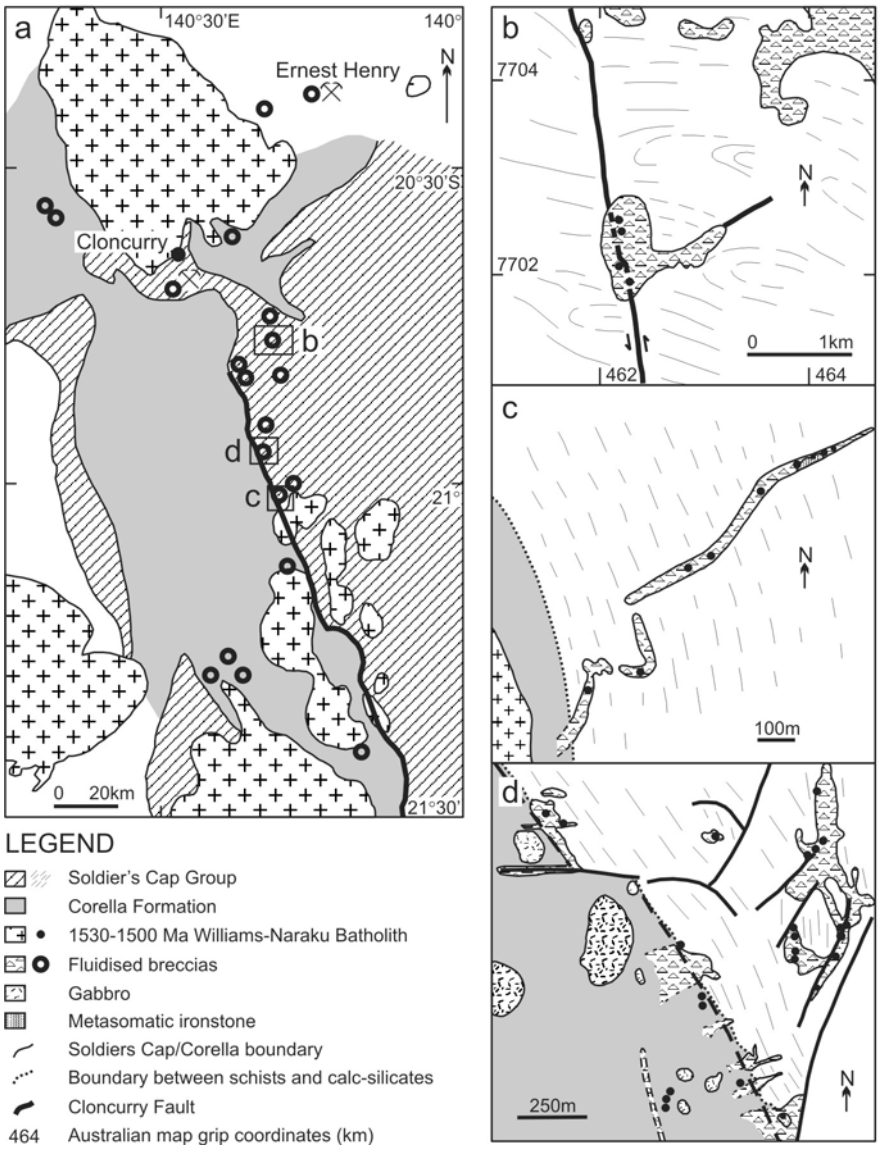

Fig. 19, from Oliver et al (2005). Breccias and hydothermal alteration, especially albitization, are abundant throughout the Corella Formation in the Cloncurry region, the localities showing "fluidised breccias" in this Fig. being representative. The breccias are dominated by calcsilicate clasts, even where hosted by the Soldiers Cap Group. Clasts of granite, gabbro/dolerite and mixed granite/mafic rocks are also common. The body of Saxby Granite SE of location C is dated at 1527±3 Ma. Note the breccia "dyke" in C that transects the regional foliation.

Determining metamorphic growth events in the middle to upper sillimanite zone and sillimanite K-feldspar zone is generally quite difficult, as inclusion trails do not occur in sillimanite and, with the exception of garnet in a few samples, there are generally no relicts of lower grade porphyroblasts. However, excellent inclusion trails occur in many garnet

samples from the Fairmile area (Mares, 1998). In this regard, the southern part of the Eastern Fold Belt, south of the Yellow Waterhole Granite, is quite important, as it shows the transition from andalusite zone rocks of the Selwyn Range to the sillimanite/K-feldspar rocks at the Osborne Mine (Fig. 2). Under cover just west of this area, the Plume Prospect (around 43600E, 75800W) contains andalusite showing two stages of growth with cordierite inclusions in the first stage, (Fletcher, 1999). At the nearby Houdini Prospect, Weston (2000) used oriented core to argue that andalusite grew in the D_1 to early D_{2b} events, garnet and staurolite show multiple growth stages from D_{2a} to D_3, while sillimanite, representing the peak, mainly grew in D_{2b}. In the Jasper Ridge subarea to the east of these prospects, Sayab (2005, Section A) found that andalusite grew early and was replaced by coarse muscovite overprinted by S_{2b} and S_{3a}, whereas staurolite shows NS FIAs and probably grew during D_{2b} and D_3. Sayab (2005) also interprets sillimanite in the area north of Osborne to have mainly grown during D_{2a}, with some in the Jasper Ridge domain possibly growing in D_3.

At Osborne the peak of metamorphism, defined mainly on migmatite development, was probably during D_{2a}/D_{2b}, based on the 1595 Ma titanite U-Pb dates (Gauthier et al., 2001; Rubenach et al., 2001). A sample of albitized gneiss collected by myself from drillhole OSB20A, 890.1 metres, clearly shows a large andalusite porphyroblast now totally replaced by sillimanite. This is important, as it shows a progression from low-P andalusite through to what is now a sillimanite/K-feldspar gneiss. Garnet and sillimanite are common in parts of the Osborne Mine, but mainly relate to post-peak metasomatism. However, Adshead (1995) records cordierite and garnet porphyroblasts in an albite-rich K-feldspar-free gneiss that preserve an older foliation at a high angle to the dominant gneissic foliation, again suggesting multiple metamorphic growth events. The history of metamorphic, metasomatic and partial melting events at Osborne is considered in Section 7.

Microstructural and FIA studies by Sayab (2005) have demonstrated a similar timing of metamorphic growth relative to deformation events over much of the Eastern Fold Belt (Fig. 2). Thus growth occurred during the D_1 events (EW FIAs) and D_2/D_3 events (NS FIAs) at Snake Creek, Fairmile (Mares, 1998), Gilded Rose, Cannington, Sandy Creek area, and the White Blow Formation near the Wonga Belt. The only exceptions are the Tommy Creek Block and the Camel Dam domain (Fig. 2), that appear to show only NS FIAs (Lally, 1997; Sayab, 2005). However, in the case of the latter garnet is too small and weathered for FIA studies, and the timing of early andalusite now replaced by muscovite is uncertain. Although she did no FIA studies, Adshead-Bell (2000) worked with oriented thin sections of schists from the Selwyn Range, and the porphyroblast timing in the D_1 to D_3 events is quite comparable those from with Snake Creek.

6. AGE DETERMINATIONS OF METAMORPHIC EVENTS

Table 1 summarizes previous work relevant to the metamorphic peak in the Eastern Fold Belt, while Table 2 presents new work on monazite using the JCU Jeol Superprobe. Previous work on Ar-Ar cooling ages is briefly discussed in Section 7.6. Regarding the microprobe dating, it was found that monazites in a given sample produced statistically the same results regardless of whether they occurred within a porphyroblast or in the matrix, and high Th/high U domains within an individual monazite gave very similar results to low Th/low U domains. Three repeat analyses (different days, different calibrations) were performed for sample 519.10, and as the results are quite similar they are pooled in Table 1. These dates will be subjected to more sophisticated statistical treatment, but are unlikely to change very much.

Sample	Location	Lithology	Method	Age Ma	Reference
92220.8004	35km N of Cannington	Gneiss	U-Pb, zircon	1587±17	Page & Sun (1998)
	Rosebud Syncline	Crd-Ath gneiss	U-Pb, Mnz	1570 1540 rim	Hand & Rubatto(2002)
	"	Crd-And Schist	"	1570 1510 rim	"
	"	Grt schist	Nd-Sm, Grt	1570	"
	Tommy Creek	Grt-St schist	"	1585, 1575	"
CAD159	Cannington	Migmatitic gneiss	U-Pb Mnz	1585±5	Giles & Nutman 2002
DGC96.3	"	Pegmatite	"	1585±5	"
DGC96.2	Middle Creek Anticline	Meta-psammite	"	1599±10 corrected	"
"	"	"	"	1630±7 uncorrected	"
	Osborne Mine	Albitized calcsilicate	U-Pb titanite	1595±6	Gautier et al. (2001)
	"	Albitite at pegmatite contact	"	"	"

Table 1. Published peak metamorphic ages for the Eastern Fold Belt

Sample	Location	Lithology	Age
OSB20A 890.1 m.	Osborne Mine	Bt-Ab-Sil gneiss	1659±15 D_{Ab}
C96-60 Mares (1996)	Fairmile	Ms-Bt-Grt schist	1617±21
490.4	Snake Creek Area 2	Crd-Ab-Bt-And-Sil albitite	1652±8 D_{Ab}
519.10a	Snake Creek Area 3	Ms-And-Bt-Crd-Ab schist	1631±12 D_{Ab}
430.4	Snake Creek Area 2	And-Bt-Ms-Ab-Crd Schist	1611±10
725.2	Snake Creek Area 3	Bt-Grt-St-Ab Schist	1608±8
773.3	Snake Creek, SE corner near granite	Ms-And-Bt schist	1609±9
52.2	Snake Creek NW corner Fig. 1	Bt-And-Ky-St-Grt schist	1588±18
408.3	Snake Creek Area 1	Ms-Bt-Grt schist And psuedomorphs	1545±13 ? D_{3a}
109	Snake Creek Area 3	Bt-Grt-Ab-St-And schist	1584±20

Table 2. U-Th-Pb dates of monazites using JCU Jeol Superprobe. Unless otherwise indicated the dates are assumed to relate to the peak metamorphic event.

Previous age dating (Table 1) indicates that the peak of metamorphism was ca. 1590 Ma, possibly slightly younger in the east. In dating monazites using the Superprobe, inclusions within porphyroblasts were chosen in the hope of dating events earlier or later than the metamorphic peak. However, in any given sample no significant differences were found between monazite inclusions and matrix monazite, even where the porphyroblast inclusion trails were S_1. Thus, except for a few rare single analyses, each rock produced a uniform age.

The significant findings are:

1. An early group of albitized samples from Snake Creek and Osborne gave 1631-1659 Ma. Unsuccessful attempts were made to confirm one of these with the SHRIMP at ANU (the monazites are too small). These dates overlap with the deposition of the Mt Norna Quartzite and Toole Creek Volcanics, so may represent an extensional basin-forming event. Since major albitization was synchronous with this event it has been labelled D_{Ab}. Cordierite with or without early andalusite occurs in the Snake Creek rocks, whereas the Osborne sample contains a large andalusite now replaced by sillimanite.
2. Most of the samples produced ages in the range 1584-1615 Ma, comparable with presumed metamorphic peak ages in the literature (Table 1). It was interesting that no distinction could be made between D_1 and D_2. One sample gave an age of 1545 Ma.

7 PRESSURE-TEMPERATURE-TIME (P-T-t) PATHS

7.1 Metamorphic reactions

Table 3 provides a list of important reactions relevant to the Eastern Fold Belt. It is not an exhaustive list, as many more reactions, either not seen by the rocks or judged not important, are implied by the pseudosections and other phase diagrams.

Table 3. Metamorphic reactions

1 kyanite = andalusite
2 andalusite = sillimanite
3 chlorite + muscovite + quartz = garnet + biotite + H_2O
4 chlorite + muscovite = staurolite + biotite + quartz + H_2O
5 chlorite + muscovite = cordierite + biotite + quartz + H_2O
6 chlorite + muscovite = andalusite + biotite + quartz + H_2O
7 chlorite + garnet + muscovite + quartz = staurolite + biotite + H_2O
8 staurolite + muscovite + quartz = andalusite + biotite + H_2O
9 staurolite + muscovite + quartz = sillimanite + biotite + H_2O
10 staurolite + muscovite + quartz = sillimanite + garnet + biotite + H_2O
11 cordierite + muscovite + quartz = andalusite + biotite
12 chloritoid + biotite + quartz = garnet + muscovite + H_2O
13 garnet + muscovite = andalusite + biotite
14 garnet + muscovite = kyanite + biotite
15 garnet + muscovite = sillimanite + biotite
16 paragonite + quartz = andalusite + albite + H_2O
17 muscovite + quartz = K-feldspar + andalusite + H_2O
18 muscovite + quartz = K-feldspar + sillimanite + H_2O
19 chloritoid + muscovite = staurolite + biotite + quartz + H_2O
20 cordierite + K-feldspar + H_2O = andalusite + quartz + biotite
21 cordierite + K-feldspar + H_2O = sillimanite + quartz + biotite
22 rutile + calcite + quartz + H_2O = titanite + CO_2
23 muscovite + calcite + quartz = K-feldspar + plagioclase +CO_2 + H_2O
24 tremolite + calcite + quartz = diopside + CO_2 + H_2O
25 phlogopite + calcite + quartz = tremolite + K-feldspar + CO_2 + H_2O
26 dolomite + K-feldspar + H_2O = calcite + phlogopite + CO_2

7.2 Critical observations relevant to the P-T-t path, Snake Creek

1 Garnet is very common in schists, but commonly forms small porphyroblasts with poor trails. Sayab (2005, Section C) however found a number of garnet samples that yielded either EW (D_1) or NS (D_2 or D_3) FIAs, with both FIAs present in a few examples. Sayab (2005, Section D) also obtained results of 4-5 Kbar for intersecting isopleths, applying THERMOCALC to garnet core compositions; samples with EW FIAs are around 5 kbar, whereas the one sample with a NS FIA for the core yielded 4 kbar. Andalusite + garnet assemblages are very common in the Snake Creek Anticline. Some show two stages of garnet growth, with an early stage preserved as smaller porphyroblasts within andalusite and a second stage occurring as overgrowths on matrix garnets; the second stage of garnet growth in such samples clearly postdates at least the early stage andalusite (e.g., sample 813). In some cases garnets occur only in the matrix and so are late (e.g., 507.2). Chemical zoning within the garnets is typically smoothly continuous with no reverse zoning from earlier- to later-stage garnet, with only rare examples (e.g., 109, Fig. 17) of distinctly different chemistry in the second stage. In some samples garnet is partly replaced by biotite according to reactions 13-15 (Fig. 20); these reactions show a very shallow slope on a P-T diagram, with the pressure dependant very much on the bulk composition, but in all cases indicate decompression or an in-part clockwise path. The initial growth of garnet is commonly defined by reaction 1, whereas a reaction such as 10 is a possibility for late-stage garnet present in some rocks.

2 Kyanite occurs sporadically in rocks from the northwest to the northern central parts of the Snake Creek Anticline (Fig. 1). Sample 52 is typical of those from the NW, and shows kyanite partly replaced by andalusite according to reaction 1 (Fig. 21). It was suggested by Rubenach & Barker (1998) that this may have occurred during isobaric heating and cooling, but the other possibility is a clockwise P-T-t path. The latter possibility is the most likely, as it is consistent with garnet core modelling of Sayab (2005, Section D) and the pseudosections discussed below. It is also most probable that the kyanite originally replaced earlier andalusite, as large andalusite grains replaced by randomly oriented blades of kyanite have been found in a number of localities.

3 Samples showing replacement of cordierite by andalusite and biotite are quite abundant (Figs. 7-10), implying reaction 11 was commonly crossed. This reaction (and its equivalent with sillimanite) is divariant in KFMASH (so it depends on Mg/(Mg+Fe) as well as P and T) and is commonly given a positive slope on P-T diagrams and P-T pseudosections. However, Pattison et al. (2002) convincingly argue that the slope is negative with a shallow gradient, the most compelling argument being that cordierite in the outer aureoles of granites is replaced by andalusite in the inner aureoles. Reaction 11, therefore, implies an anticlockwise P-T-t path. Several samples from albitite area 2 (Fig. 1) show cordierite replaced by biotite, kyanite and andalusite, but the relative timing of kyanite and andalusite is uncertain. The reaction of cordierite to kyanite implies overstepping of reactions and/or a relatively low a_{H2O}, as reaction 11 otherwise would not occur in the kyanite field.

4 Partial replacement of staurolite by andalusite according to reaction 8 occurs in numerous samples (Fig. 22). This can occur with isobaric heating and/or decompression. Many samples show the reverse reaction, particularly around albite areas 1 and 5. In these two areas early-growth andalusite has been replaced by coarse-grained muscovite (Fig. 23), whereas staurolite is unaltered. The reversal of reaction 8 implies isobaric cooling and/or an anticlockwise P-T-t path. Other rocks upgrade of areas 1 and 5, and elsewhere in the north of the Snake Creek Anticline, show early growth of andalusite followed by smaller grains of staurolite, which in turn show partial replacement by late-stage andalusite (Fig. 24). This alternation implies a complex P-T-t path.

5 The reaction of andalusite to sillimanite implies an isobaric or anticlockwise path. As discussed above, sillimanite represents the metamorphic peak and probably grew during D_{2a} and/or D_{2b}, and so probably grew during a thermal spike. In several samples sillimanite occurs as inclusions in staurolite as well as in the matrix, so there are possibly several growth stages of sillimanite. In the far SE of the anticline sillimanite, which in this area is restricted to the granite contact, occurs as inclusions in stage 3 andalusite (Fig. 13), suggesting a rise and fall in the aureole temperature during sillimanite and stage 3 andalusite growth.

6 In some rocks cordierite has been replaced by varying combinations of andalusite, sillimanite and staurolite (Figs. 8, 14, 25-27). This was also certainly the result of overstepping of several reactions along a P-T-t path (Pattison et al., 1999). In several samples, cordierite has been replaced by biotite, andalusite kyanite and staurolite, although the relative timing of andalusite and kyanite is uncertain (Fig. 28).

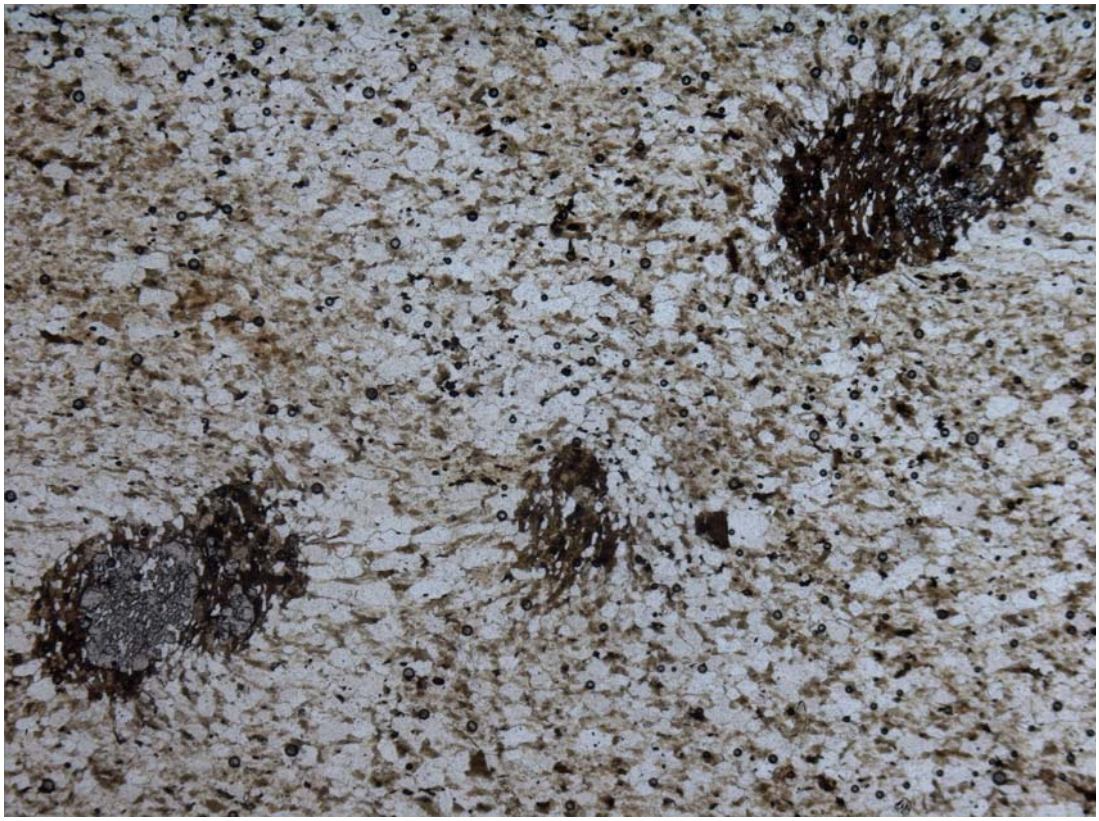

Fig. 20. Garnet partly (lower left) to totally (top right) replaced by biotite. Specimen 61461 (Lewthwaite 2001). Length 5.6 mm.

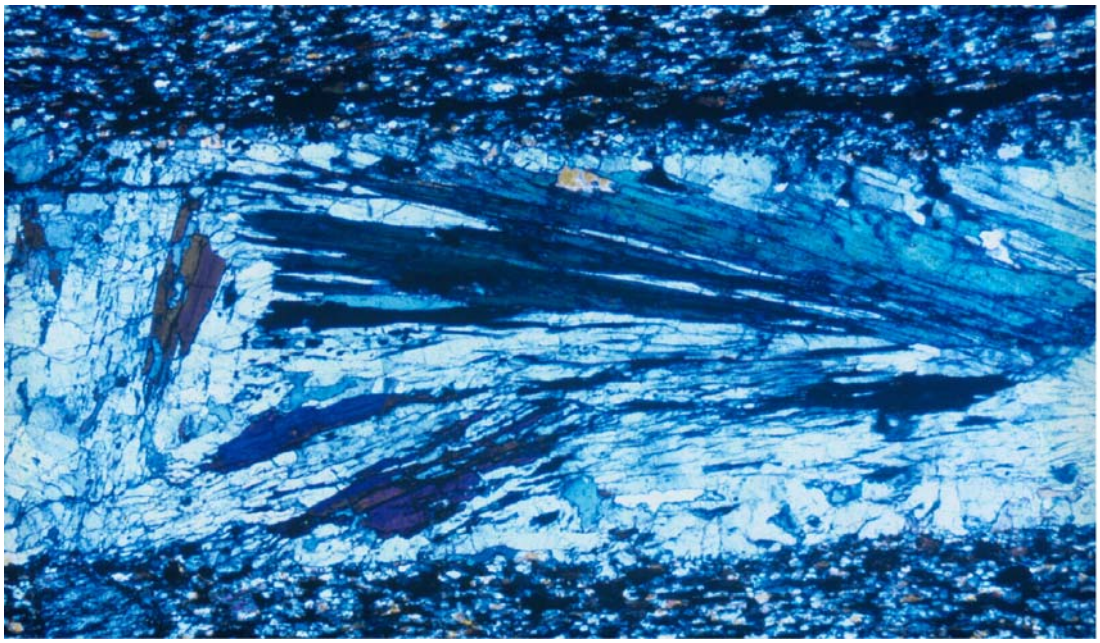

Fig. 21. Blades of kyanite partly replaced by andalusite, sample 52. The kyanite had probably replaced earlier andalusite. Inclusion trails are parallel to the matrix S_2, suggesting late-SW_{2a} to early S_{2b} growth of kyanite. Length of photo 5.6 mm.

Fig. 22. Staurolite partly replaced by andalusite, sample 52. Length 5.6 mm.

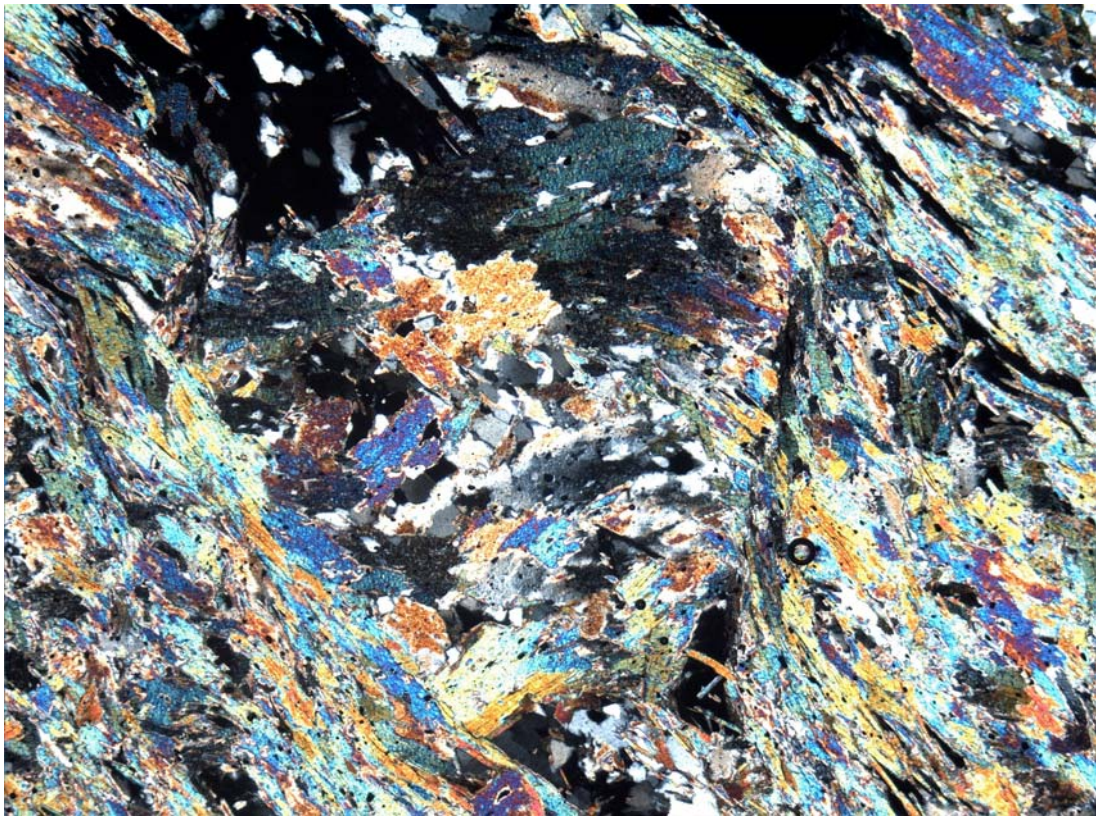

Fig. 23. Part of a large andalusite, now replaced by muscovite, in a staurolite-biotite-chlorite schist, sample 61475 (Lewthwaite, 2001). The andalusite grew early, as the muscovite is now aligned in S_2 and overprinted by subsequent F_3 crenulations.

Length 5.6 mm.

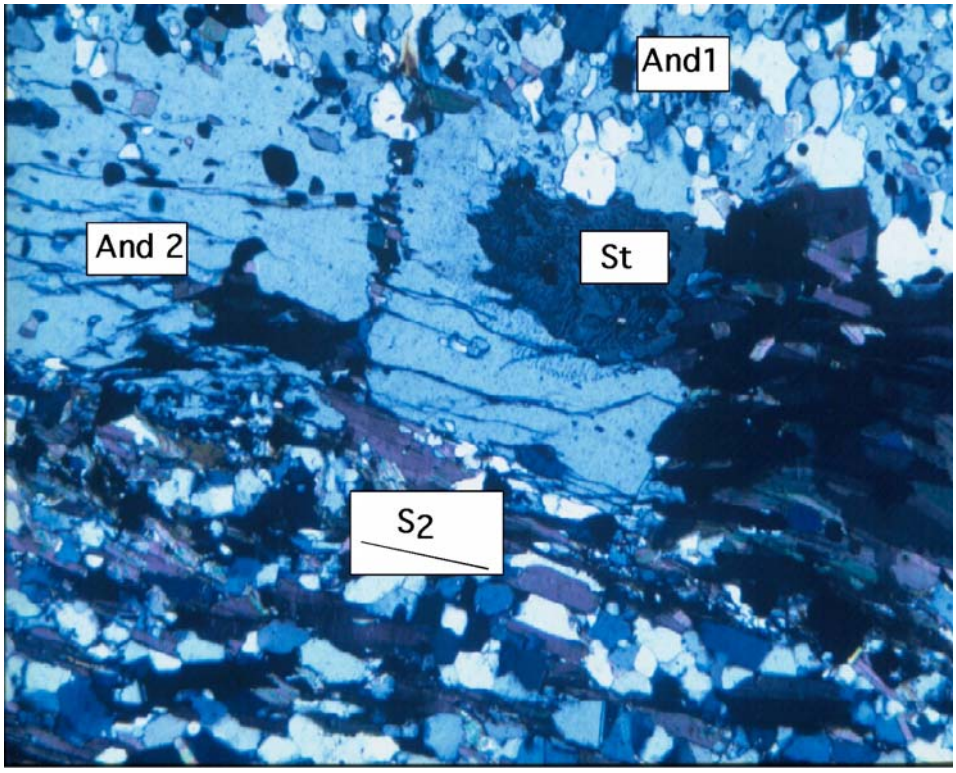

Fig. 24. Andalusite 1 preserves an earlier foliation, probably S_1. Andalusite 2 preserves the matrix foliation, probably S_2. Staurolite grew between the two stages, and is now partly replaced by andalusite 2. Length 5.6 mm.

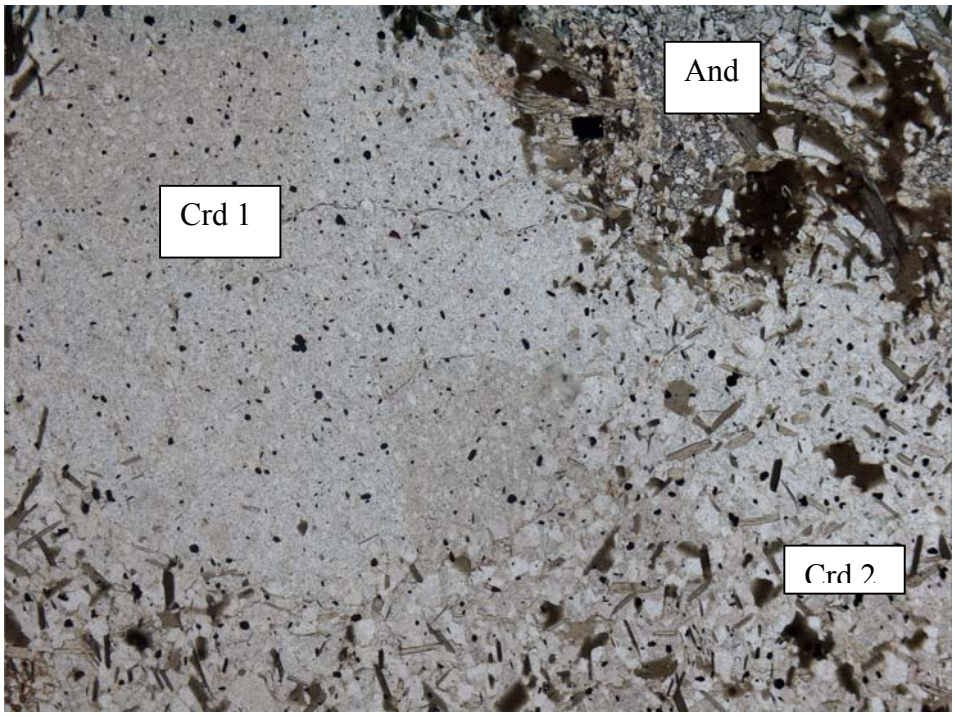

Fig. 25. Sample 61476 (Lewthwaite, 2001). Two stages of cordierite, partly replaced by andalusite and biotite. Note the poorly aligned inclusion trails in Crd 1. Length 5.6 mm.

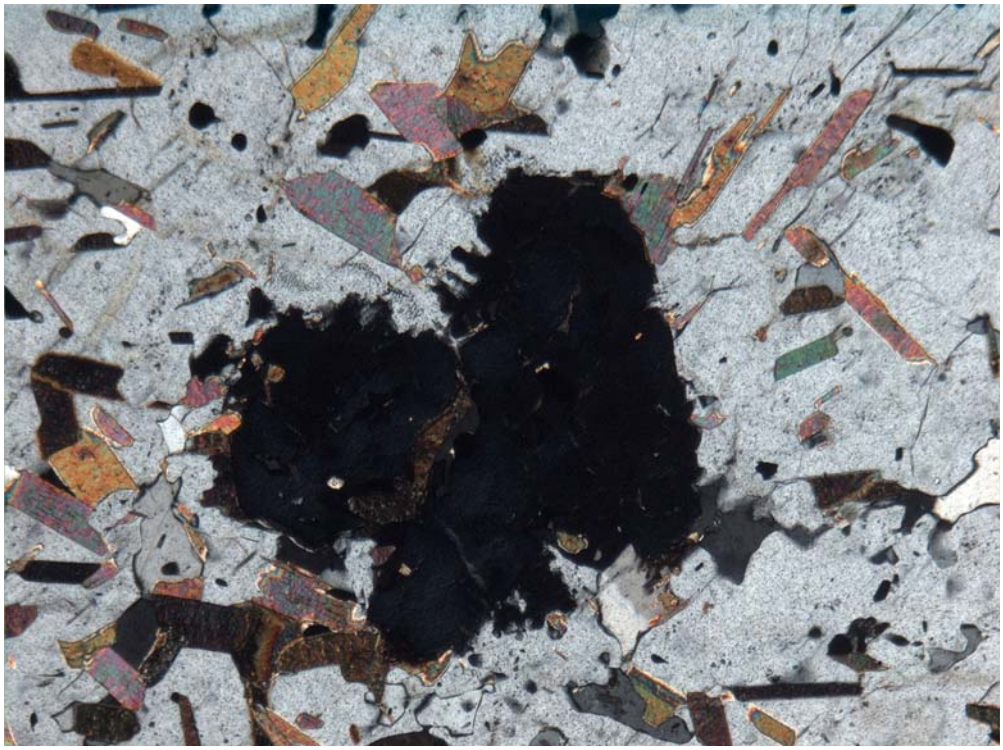

Fig. 26. Sample 61476. Staurolite (in extinction) partly replaced by andalusite that has biotite inclusions showing two orientations. Length 2.8 mm.

Fig. 27. Sample 519.3. The large cordierite on the right has been replaced by biotite (and elsewhere andalusite) Biotite within the replaced cordierite is aligned in two orientations. The matrix to the left contains biotite, sillimanite and staurolite aligned in the foliation (S_2 or reactivated in D_3). Length 5.6 mm

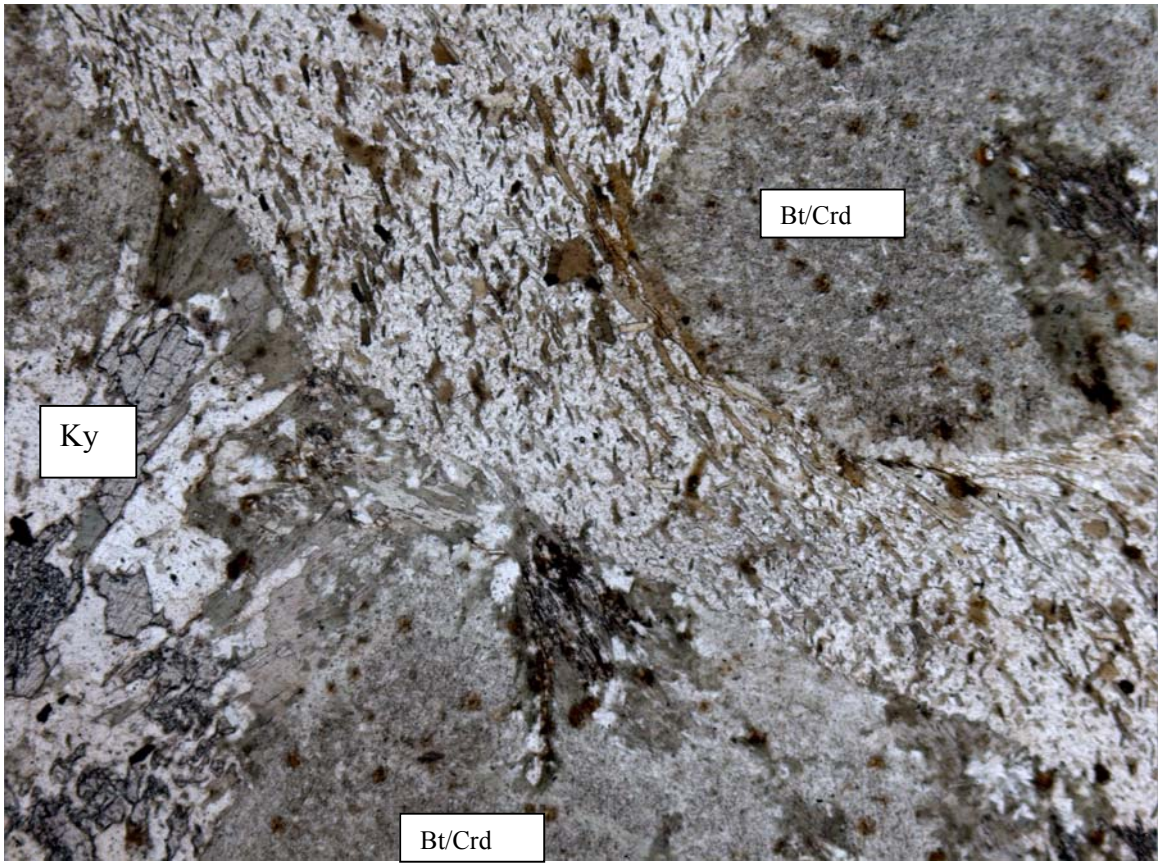

Fig. 28. Sample 252.5. The matrix consists of albite and biotite and shows S_2 that wraps around elliptical cordierite grains now pseudomorphed by fine-grained green biotite, some coarser brown biotite, and kyanite. Elsewhere in the same section andalusite and staurolite also replace cordierite. Length 5.6 mm.

7.3 Pseudosections and P-T-t paths, Snake Creek Anticline

Pseudosections are phase diagrams plotted for a particular whole rock composition. For all pseudosections discussed below the rock composition was determined using XRF at the Advanced Analytical Centre, James Cook University. Calculations were done using the THERMOCALC program of Powell & Holland (1988, and succeeding upgrades, e.g. Powell et al., 1998). Pseudosections allow solid solutions to be considered. The rocks discussed below were calculated in the MnNCKFMASH system (M, Na, Ca, K, Fe^{2+}, Mg, Al, Si, H_2O). Because of time constraints complete pseudosections were not completed, only parts relevant to the P-T-t paths. The THERMOCALC versions used for these calculations has the Holdaway (1971) aluminosilicate triple point built in. However, I agree with Pattison et al. (2002, and references therein) that the Holdaway andalusite-sillimanite reaction is inconsistent with data for many other reactions in low pressure metamorphic rocks, so I have also plotted the Pattison version on the following diagrams.

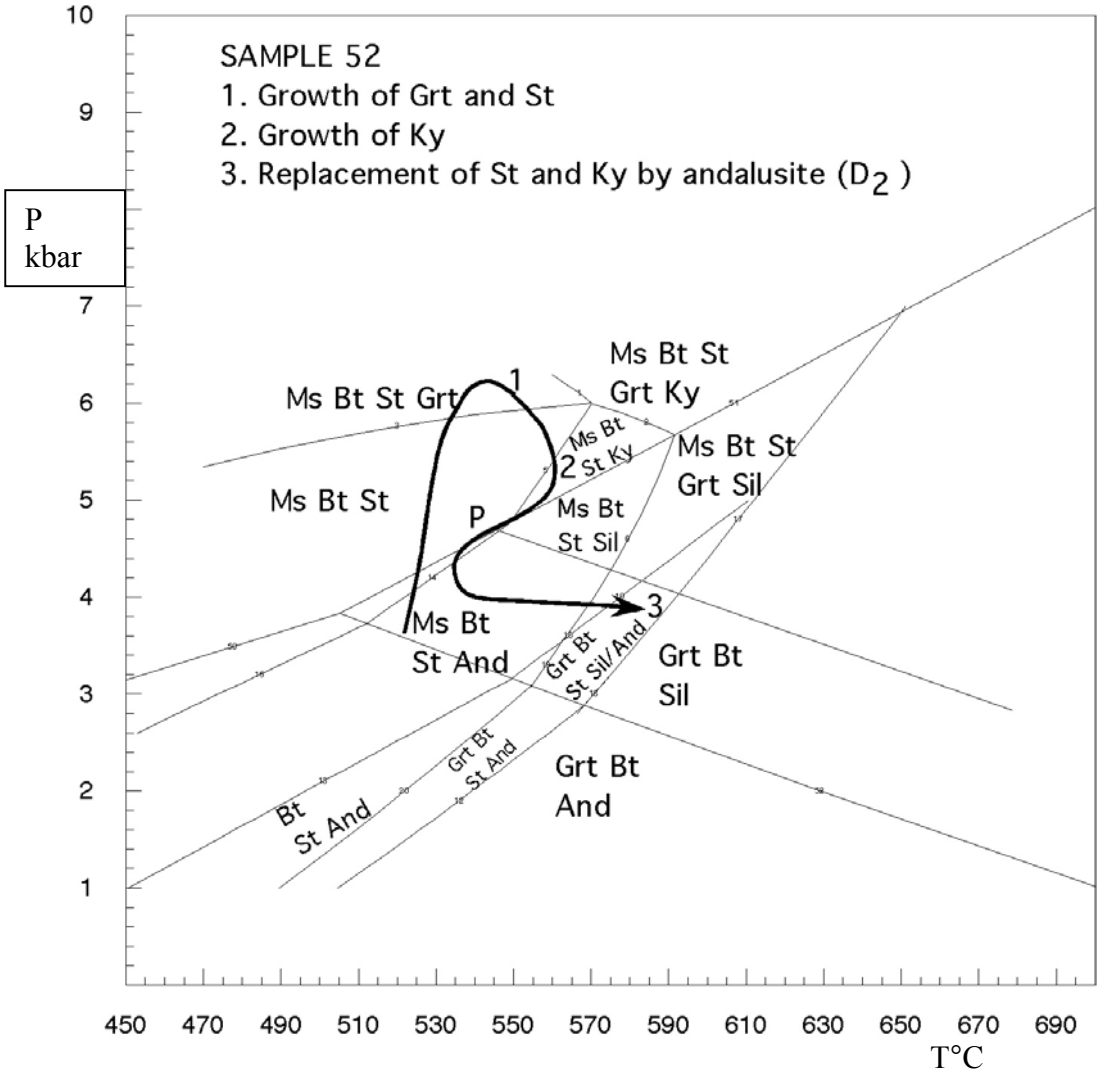

Fig. 29

Sample 52

This is a key rock because of the kyanite-andalusite-staurolite relationships. It occurs in the Mount Norna Quartzite, just NNW of Albite area 1 (Fig. 1). The full assemblage is Qtz-Bt-Ky-And-St-Grt-Ilm (and graphite), with only a small amount of muscovite (replacing andalusite) and very rare plagioclase. Of critical importance on the pseudosection (Fig. 29) is the early growth of andalusite and staurolite and the fact that kyanite exists only above 4.6 kbar. Garnet grew early, probably at 1. The location of garnet and kyanite fields shows that the suggestion of Rubenach & Lewthwaite (2002) of isobaric cooling into the kyanite field would not produce kyanite in this bulk composition, so that a clockwise loop into medium pressure is necessary. This loop also explains garnet, which along with kyanite is a relict after subsequent overstepping. The clockwise loop at 2 is also consistent with determinations of 5-6 Kbar determined using THERMOCALC (Sayab, 2005, Section D) for garnets in samples SC189 and 192 that occur just west of sample 52. There is no evidence in sample 52 for the drop in temperature after 2, and the isobaric rise to 3 (i.e., the other possibility is isothermal pressure decrease after 2), but the proposed loop in Fig. 28 is consistent with loops determined for other samples, as is discussed below. Note that muscovite reacts out of the rock in reaction near 3. P is the Pattison triple point.

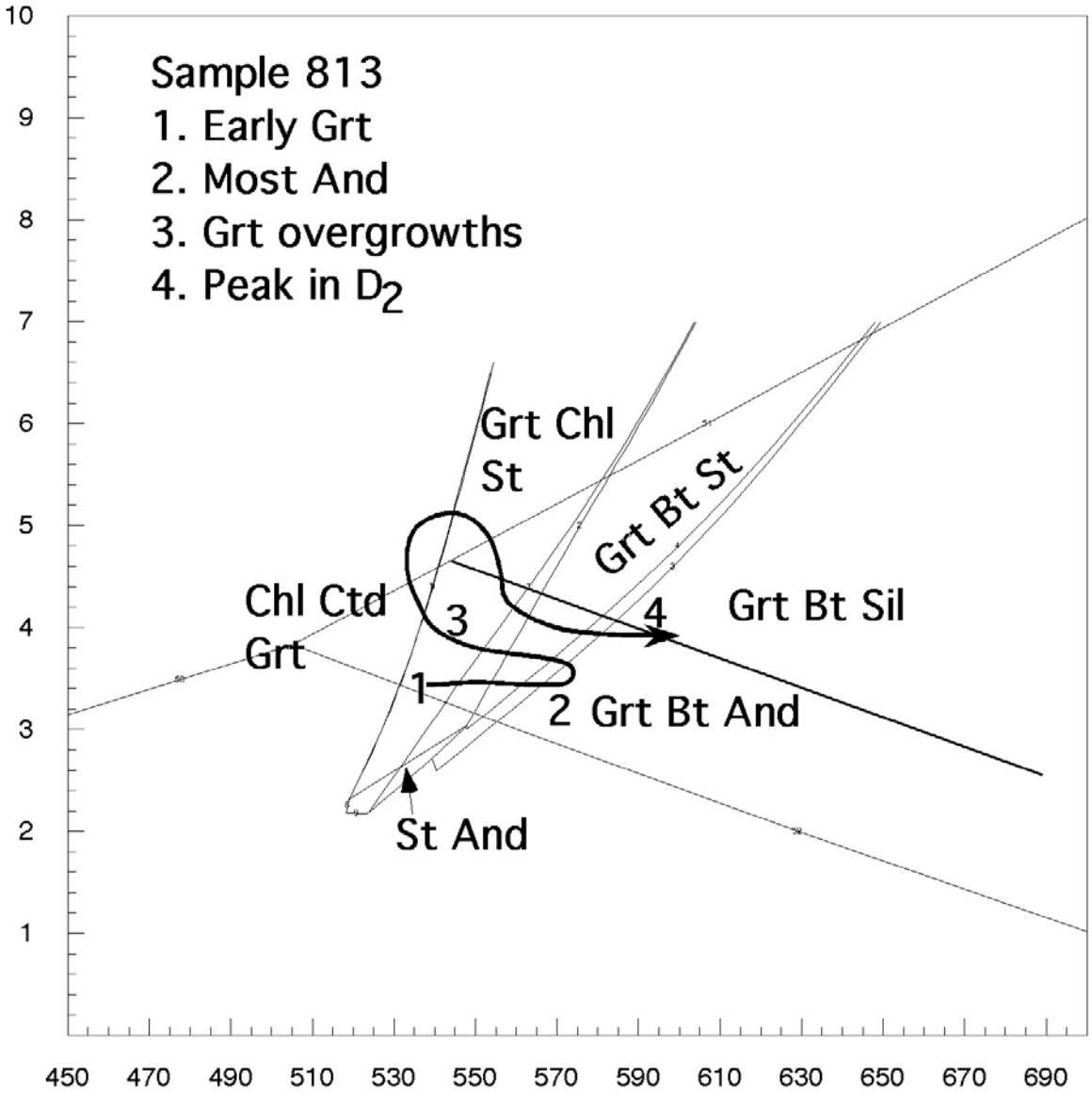

Fig. 30.

Sample 813

This was collected just west of Albite Area 2 (Fig. 1). It has the assemblage Ms-Qtz-Bt-And-Grt, with minor fibrolite, accessory ilmenite and a trace of graphite, and is representative of the most common schist type in the Snake Creek Anticline. A P-T-t loop for this rock (Fig. 30) has to explain early small garnets, early andalusite, and late overgrowths on garnet in the matrix, and any number of configurations would be possible. However, the loop has to be consistent with others for the anticline, particularly the adjacent cordierite-andalusite rocks (e.g., sample 244.1). Although kyanite would not occur in this bulk composition, it does occur in nearby rocks, especially in Albite Area 2, so the loop for sample 813 must go through the kyanite field, broadly analogous to sample 52.

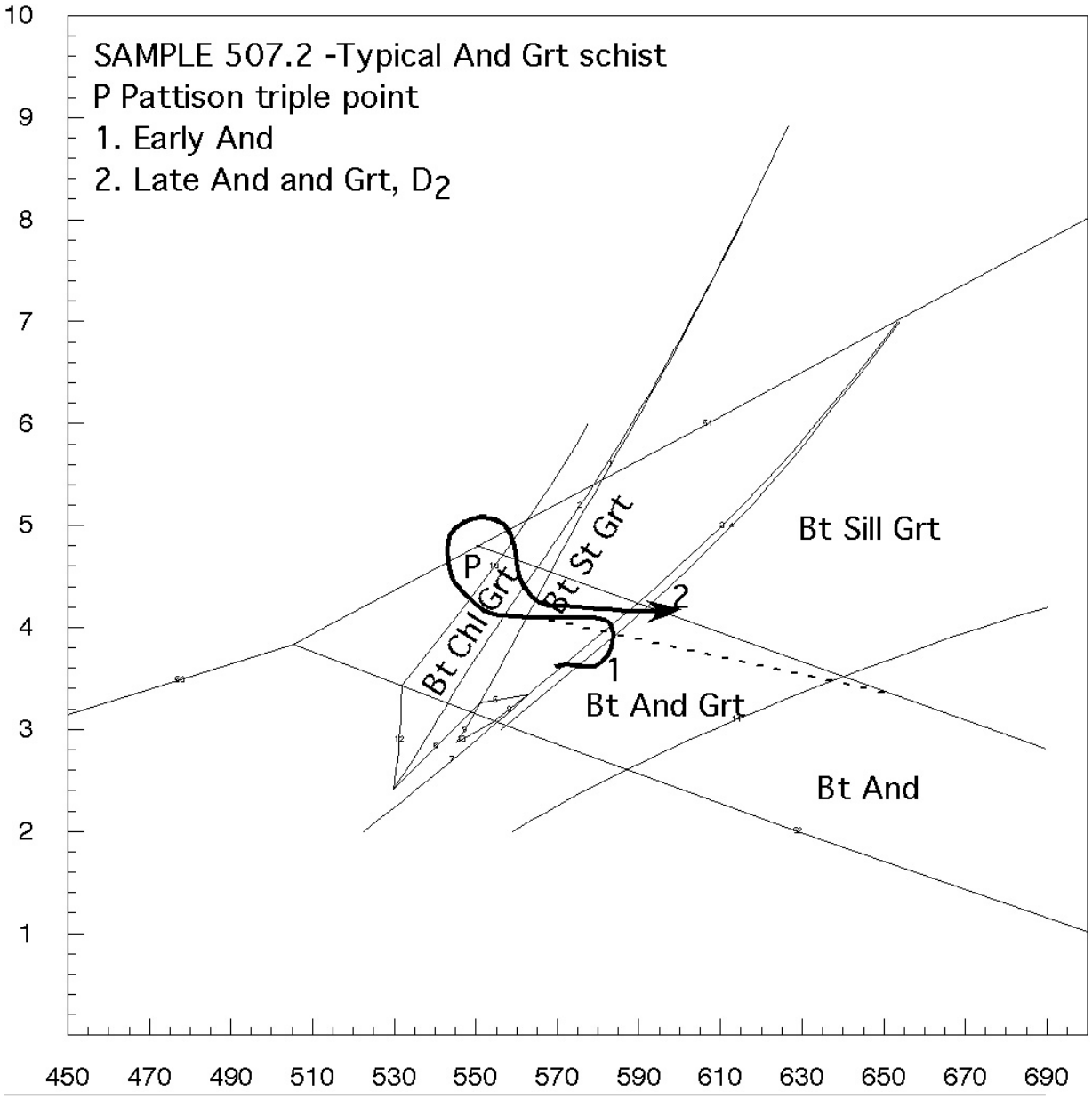

Fig. 31.

Sample 507.2

This sample was collected within Albite Area 2 from a patch of andalusite-garnet schist within mainly cordierite-andalusite schists affected by the early metasomatism related to albitization. It has the assemblage Ms-Qtz-Bt-And-Grt, with accessory ilmenite, minor albite and a trace of graphite. Very small garnet grains occur within the early stage of andalusite, with larger garnet porphyroblasts in the matrix that were contemporaneous with or post-dated a second stage of andalusite. Other rocks in the general area show staurolite grains between the two andalusite stages, consistent with the proposed loop (Fig. 31). Fibrolitic sillimanite, not present in this sample, occurs in the matrix of nearby rocks, so the loop must intersect the sillimanite field as shown. Similarly, relict kyanite occurs in nearby rocks (Fig. 28). Otherwise the loop is consistent with sample 244.1.
(Pseudosection by M. Cihan).

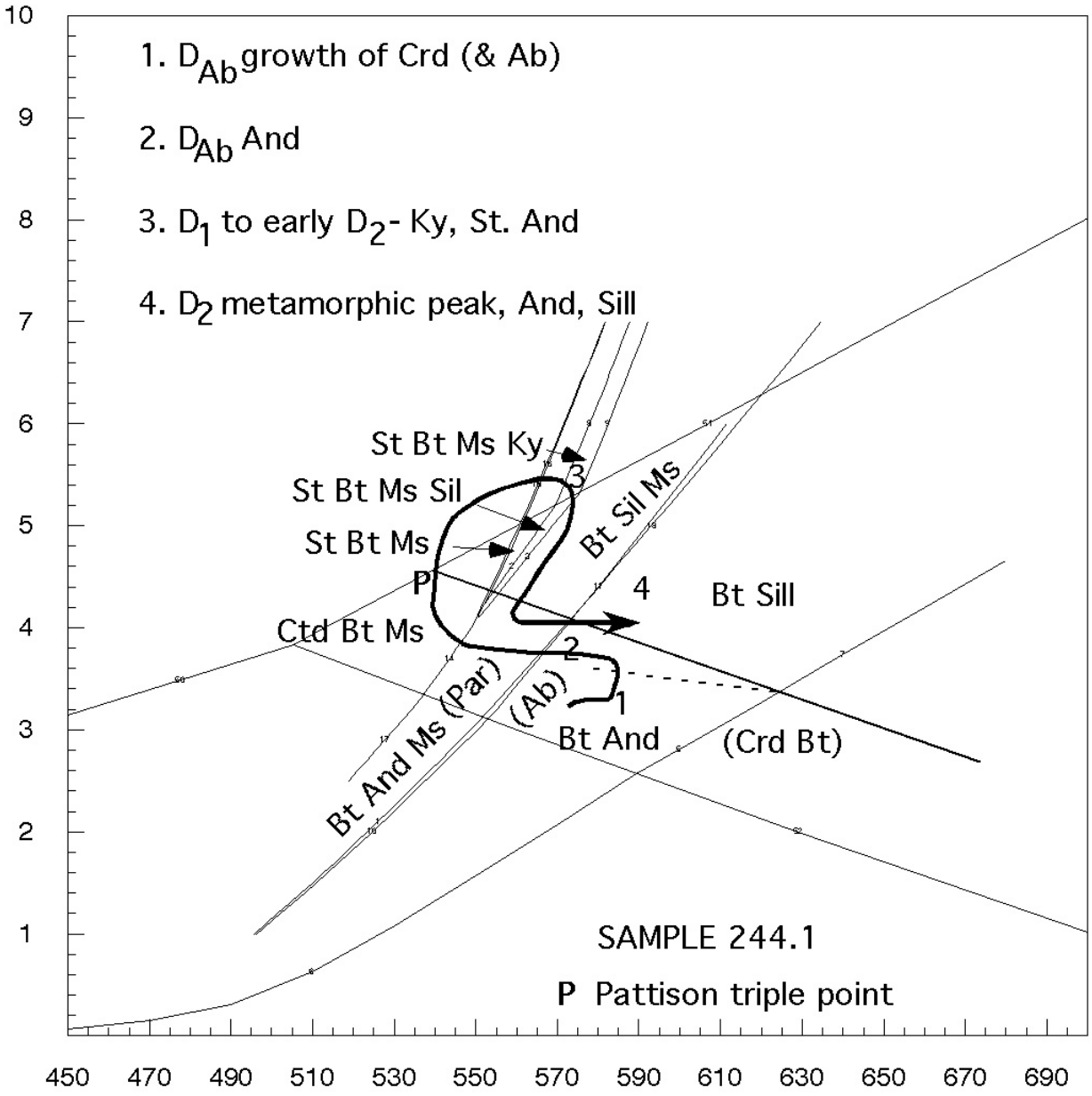

Fig. 32

Sample 244.1

This sample is from Albite Area 2, and consists of the assemblage Bt-Qtz-Ms-Ab-And-Tur, with abundant pseudomorphed cordierite, and accessory rutile, ilmenite and a trace of graphite. Cordierite replaced by andalusite, biotite and tourmaline occurs in early stage andalusite. A field for Crd-Bt as determined by THERMOCALC is shown, but the slope of this reaction is not consistent with observations in aureoles throughout the world, and Pattison et al. (2002) have calculated reaction with a negative slope. The dashed line represents an isopleth value of Mg/(Mg+Fe) for biotite of 0.50 (Pattison et al., 2002 for graphite-bearing samples), obtained for this rock for biotite that has replaced cordierite. Thirteen other samples from around Albite Area 2 show similar biotite chemistry. The loop must cross the isopleth. This rock does not contain kyanite, staurolite or sillimanite, but nearby samples, also rich in pseudomorphed cordierite, do. In one outcrop, for example, as well as cordierite replaced by andalusite, early andalusite has been pseudomorphed by an

aggregate of kyanite blades. The loop from 1 to 4 is therefore proposed for cordierite-andalusite samples from within or near Albite Area 2.

Also shown on this diagram is a line for the reaction

Paragonite + Qtz = Albite + Andalusite + H_2O

Paragonite is very rare in the Snake Creek Anticline, but andalusite + albite is a common assemblage.

Note that although the proposed loop does pass through fields with chloritoid, staurolite and kyanite, as these do not occur in sample 244.1. Such situations where minerals are not recorded along P-T-t are quite common in metamorphic rocks. Perhaps they reacted out, but more likely they did not grow because no active deformation occurred along such parts of the loop. Minerals tend to grow during deformation, the active strain helping nucleation to occur and assisting fluid infiltration, which in turn helps the reaction to proceed.

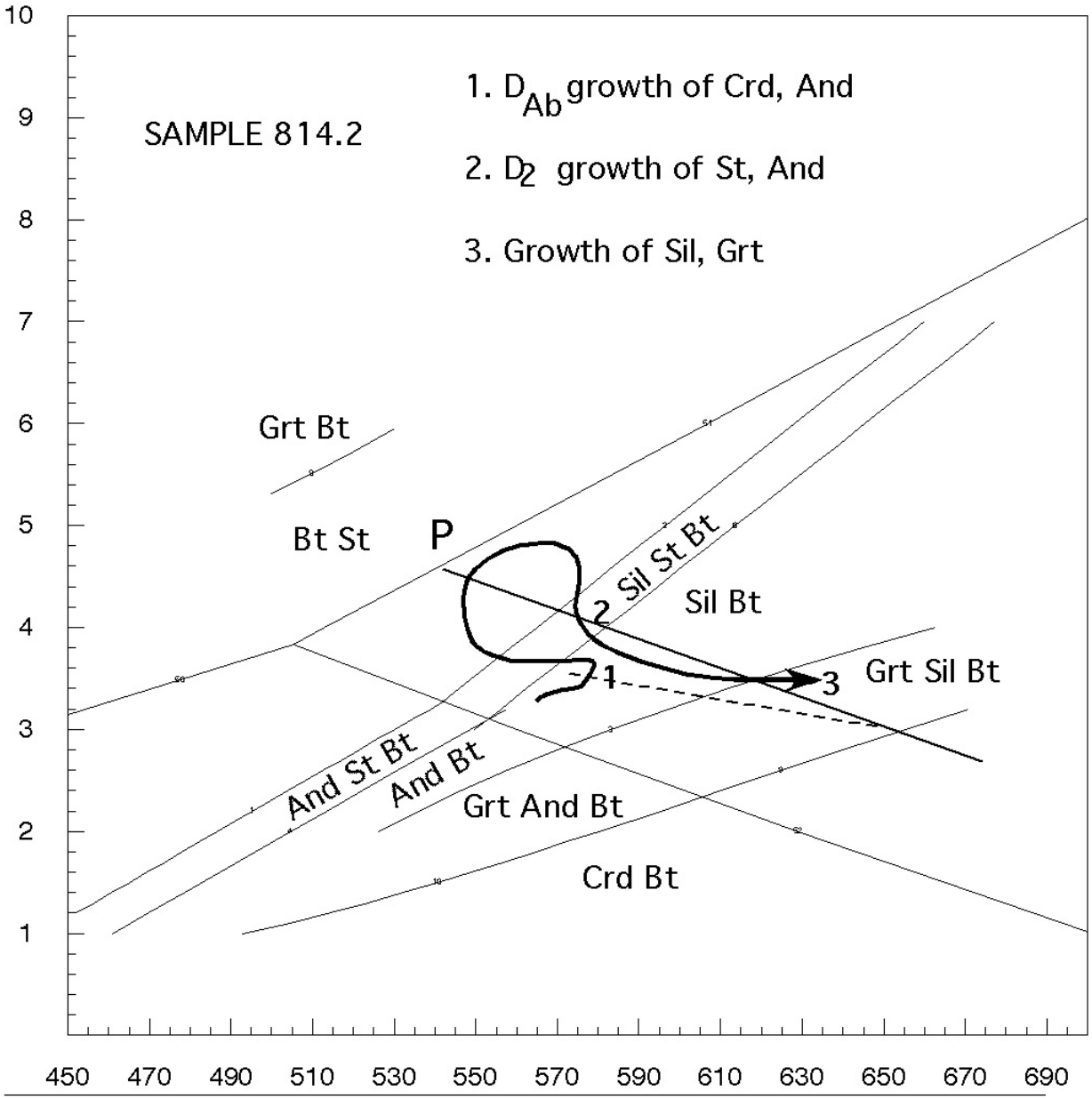

Fig. 33

Sample 814.2

This occurs in Albite Area 3, and consists of Bt-Qtz-And-St-Grt-Ab-Sil, with minor muscovite and accessory magnetite. Pseudomorphed cordierite is also present, and garnet occurs only as rare large grains in the matrix that clearly grew late. The rock is typical of the biotite-rich schists that formed in association with albitites (Rubenach, 2005). Two stages of andalusite are present, with the second stage partly replacing biotite. Sillimanite occurs only in the matrix. The dashed line represents the 0.50 isopleth for biotite after cordierite (Pattison et al., 2002). The higher pressure part of the loop is not extended into the kyanite field, as no kyanite has been found in area 3 or further south. Otherwise the loop fits the observed paragenesis quite well.

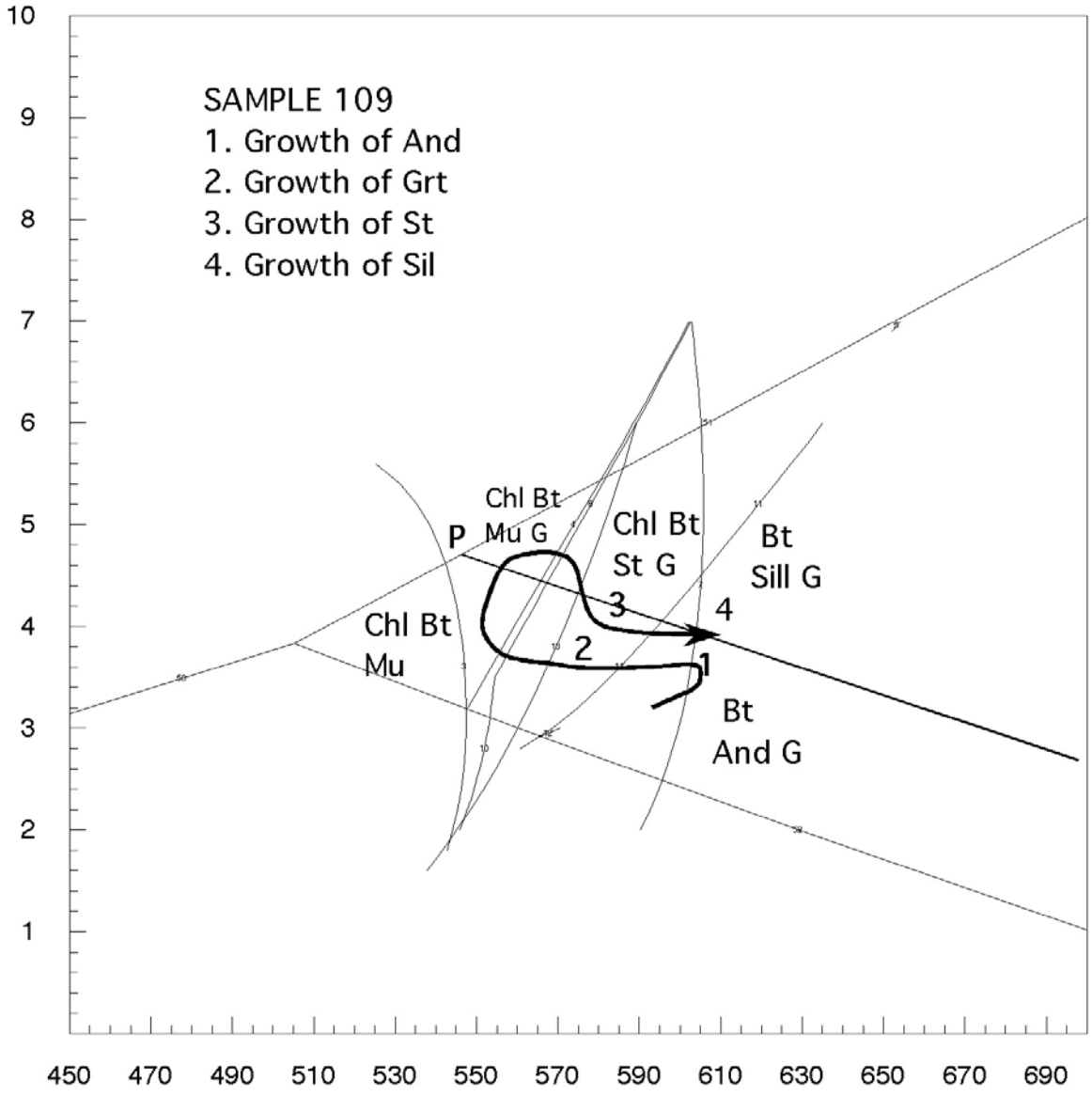

Fig. 34

Sample 109

This rock occurs just to the east of Albite Area 3, and was collected by Holmes (1991). It is a biotite-rich rock related to albitites, and consists of the assemblage Bt-Grt-Qtz-St-Ab and minor early andalusite that appears to precede garnet. Two stages of garnet are present (Fig. 17). Chlorite occurs as inclusions in garnet. No pseudomorphs after cordierite are present. There is no evidence that the loop extended into the kyanite field, the higher pressure portion of the path being added for consistency with rocks to the north. Otherwise the proposed path fits the paragenesis quite well.

Aureole rocks, Saxby Granite

Figure 1 shows a wide sillimanite/K-feldspar zone around the northwestern contact of the Saxby Granite. Migmatites also occur in this zone, as well as minor andalusite. The sillimanite/K-feldspar zone may be the result of greater abundance of gabbro and dolerite that has mixed and mingled with the western half of the granite. Around the northeastern contact, sillimanite occurs only within a few metres of the contact, as does K-feldspar in one sample. All these observations are consistent with heating at 3-3.5 Kbar in the aureole, implying a pressure drop from the metamorphic peak (Fig. 35). As discussed above, the granite intruded at 1527 Ma, synchronous with the D_{3b} event (NE-trending FIA).

In the far SW of the Snake Creek Anticline, close to the Cloncurry Fault, muscovite schist in contact with a calcsilicate breccia, in turn close to a small granite body, has the assemblage Kfs-And-Bt-Sil-Pl, with minor high-Zn staurolite, spinel, corundum (in plagioclase), and pseudomorphed cordierite. Biotite in the altered cordierite gave an isopleth of 0.32 (5 on Fig. 35), and it is proposed that the temperature rose from 5 to 6.

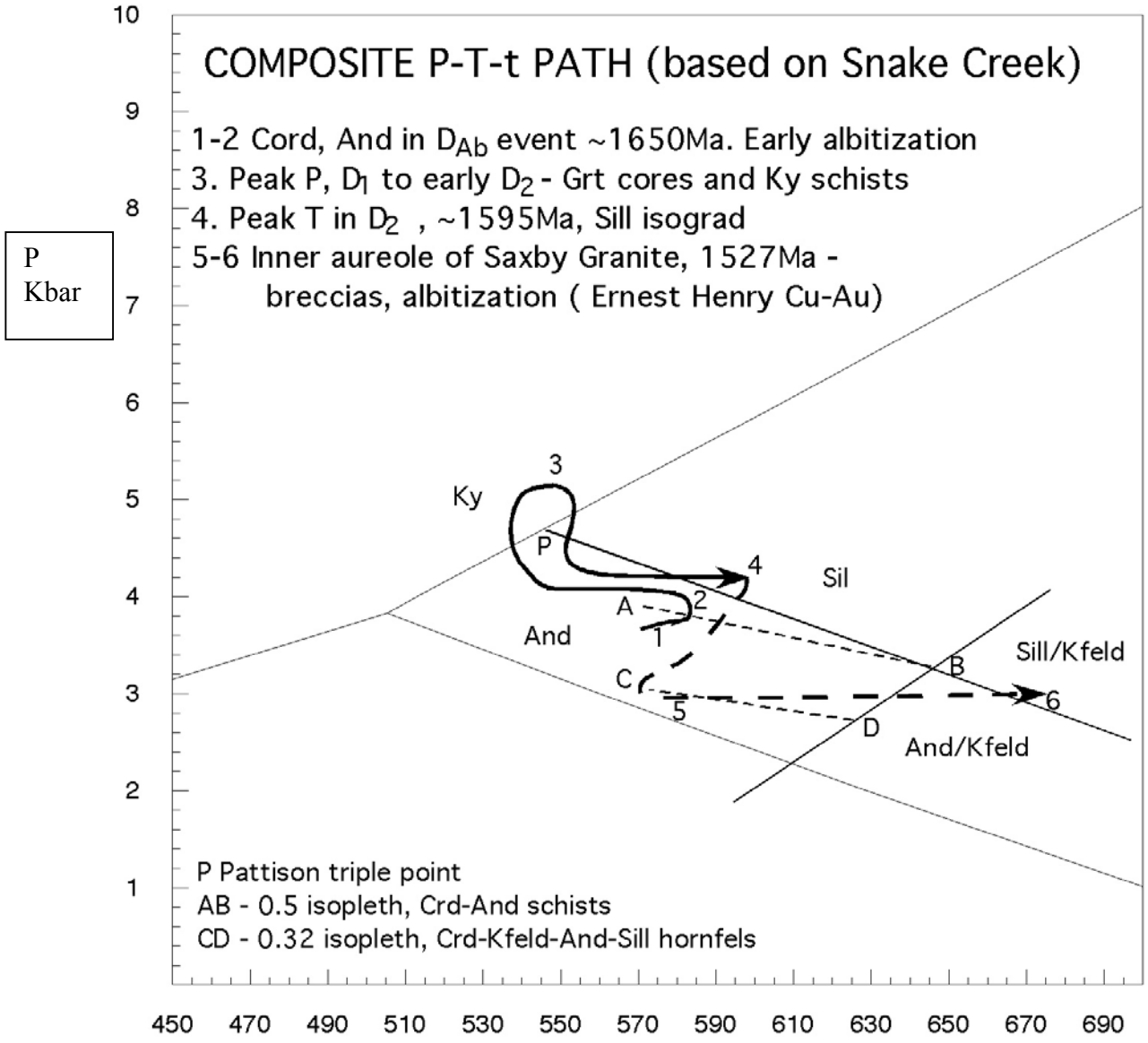

Fig. 35

Composite P-T-t path

Figure 35 is a composite P-T-t path, based on Figs. 29-34 and the aureole data. All the pseudosections are necessary, as any particular sample defines only part of the overall path. Part of the loop extends into the kyanite field, as proposed by Sayab (2005), but otherwise there are significant differences between this path and one proposed by Sayab. In addition to garnet core compositions and isopleths and reactions involving kyanite, of critical importance to the Snake Creek path is the abundant evidence of early cordierite replaced by andalusite (and staurolite, kyanite and sillimanite), andalusite to staurolite to andalusite reactions, and andalusite to sillimanite. Note that most samples studied were located close to the sillimanite isograd, as these define P-T-t paths better than rocks from either lower or higher grades as these commonly contain fewer phases. Note that the paths only work because of the metastable persistence of minerals that would have reacted out if strict equilibrium was maintained along the path. This in turn implies a type of "metamorphic fractionation" equivalent to igneous fractionation, so that strictly the bulk rock composition should be continually modified along the path.

As mentioned above, the restriction of kyanite to the north and northwest of the Snake Creek Anticline implies a field gradient such that maximum pressure decreased from the NW to the SE.

7.4 P-T-t paths for andalusite/staurolite zones elsewhere in the Eastern Fold Belt

Mary Kathleen Region

No detailed studies of pelites have been undertaken to distinguish between Wonga age (~1740Ma) and Isan Orogeny metamorphism in the Corella Formation. However most of the metamorphic assemblages studied by Reinhardt (1992a, b) are probably Isan age. Reinhardt (1992b) defined an anticlockwise P-T-t path from andalusite to sillimanite to kyanite (to andalusite), but this is schematic as there are uncertainties as to the precise pressures of crossings from andalusite, sillimanite and kyanite. Although Reinhardt studied a large number of oriented thin sections no FIA studies were undertaken in those days, so that the timing of growth relative to the various EW and NS foliations is uncertain. However, detailed studies by Sayab (2005) of staurolite-garnet schists in the White Blow Formation yielded EW and NS FIAs (four in total) in both garnet and staurolite, correlating reasonably well with the Snake Creek Anticline and Gilded Rose data. A garnet core composition produced estimates of 3.7-4.4Kbar/542-547°C for sample WB161 (Sayab, 2005), but the P-T-t path is uncertain for this rock. However, the occurrence of late andalusite and sillimanite in some localities in the White Blow Formation (not collected by Sayab) suggests isobaric heating to the metamorphic peak.

Tommy Creek Block

Spectacular spiral inclusion trail patterns occur in some garnets from the Tommy Creek Block, but surprisingly they relate only to NS FIAs (Lally, 1997; Sayab, 2005). P-T conditions of 2-2.5Kbar/500-525°C were obtained for a garnet core from sample TC186 (Sayab, 2005). Lally (1997) found staurolite partly replaced by andalusite and late fibrolite, indicating an anticlockwise path. However, he also found kyanite-staurolite schists, and Derrick (1980) describes andalusite pseudomorphed by an aggregate of blades of kyanite, suggesting a path similar to sample 52 from Snake Creek (Fig. 29) for the D_2 and perhaps younger events.

Gilded Rose Area

Rocks from the Gilded Rose area, just SSE of Cloncurry, have been studied by Lally (1997), Lewthwaite (2001) and Sayab (2005). Schists with combinations of garnet, staurolite and andalusite are common, but ones with garnet, chloritoid and andalusite are also present. Garnet and chloritoid show spectacular trails indicating overgrowths of several foliations (S_{1a}, S_{1b}; Figs. 36, 37), whereas andalusite and staurolite preserve only the steep S_{1b} foliation. Interestingly only EW FIAs are present in these rocks (Lally, 1997; Sayab, 2005). Sayab (2005) obtained garnet core conditions for sample GR76 of around 4kbar/510°C , while Fig. 38 is a pseudosection for sample 61471 (Lewthwaite, 2001; also see Fig. 37). Note that the details of the path are speculative.

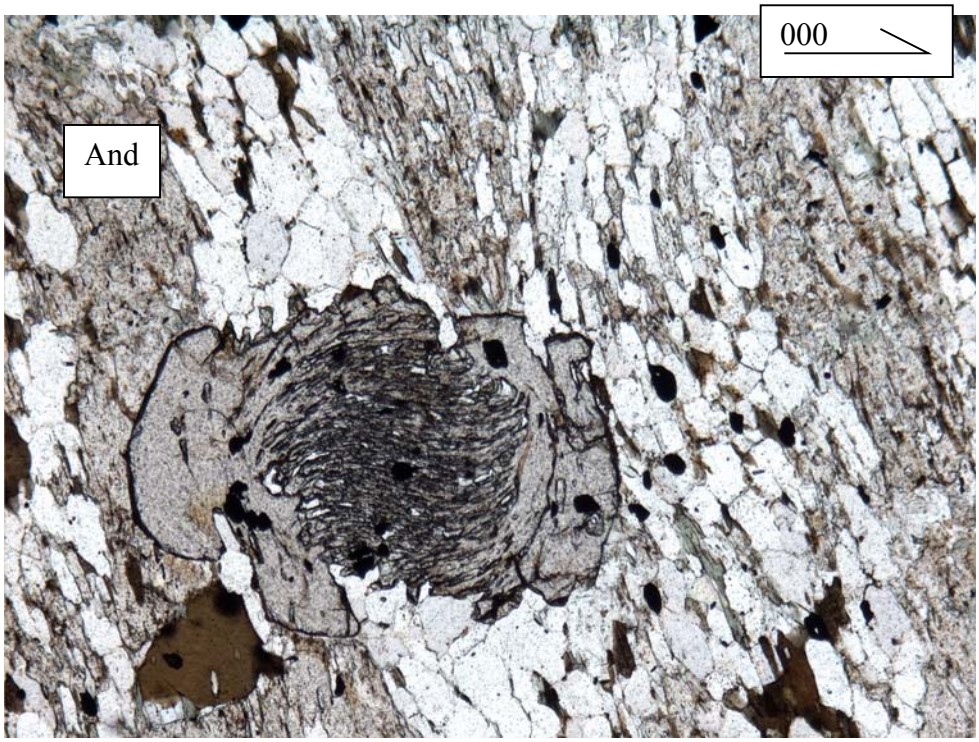

Fig. 36, sample 61468, Gilded Rose (Lewthwaite 2001). Two stages of garnet growth and one of andalusite. The steep foliation is S_{1b}, while the flat preserved in the garnet core is S_{1a}. Length 2.8 mm.

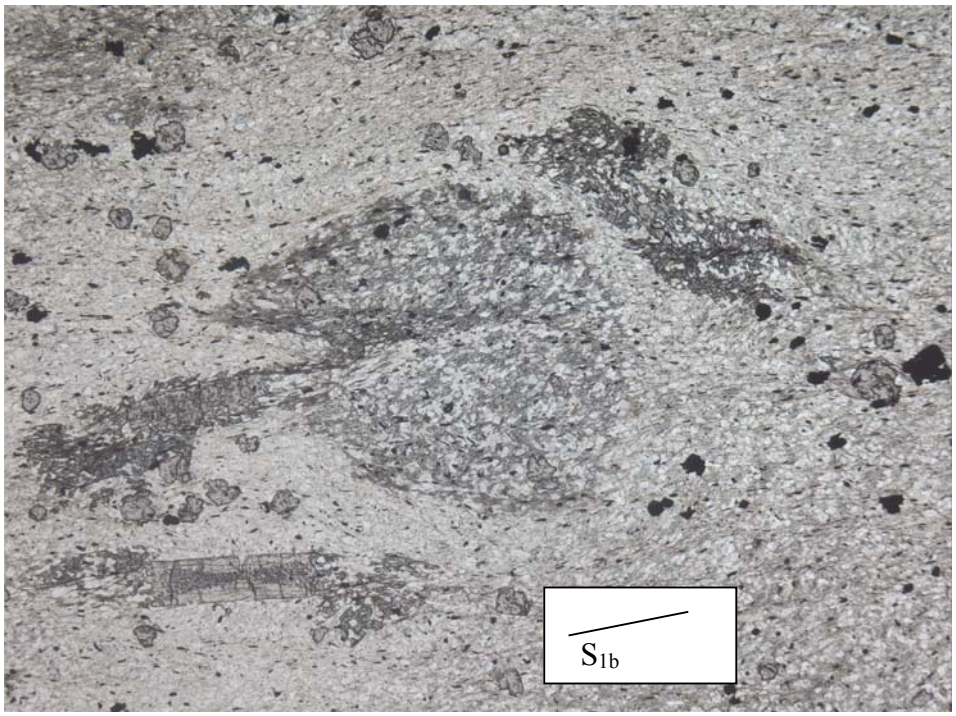

Fig. 37, sample 61471, Gilded Rose (Lewthwaite, 2001). The central large andalusite has overgrown the S_{1b} crenulation cleavage, whereas the chloritoid grains (lower left and top right of andalusite) show two growth stages, overgrowing S_{1a} and S_{1b} respectively. Small garnets are also present. Length 5.6 mmm.

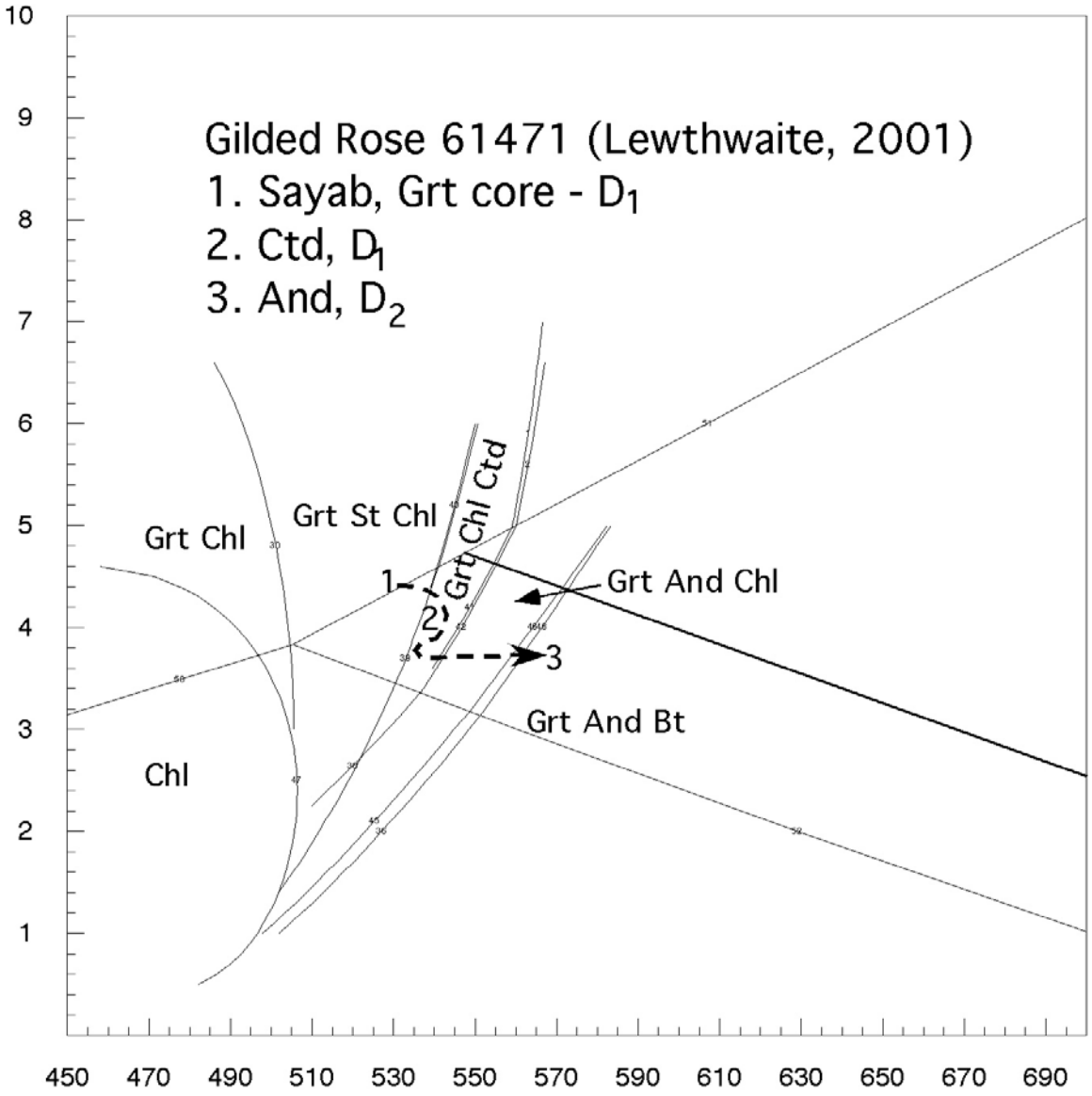

Fig. 38. Pseudosection for sample 61471

Fairmile area

The metamorphic rocks between Snake Creek and Cannington are described in general terms by Newberry (1990) and De Jong (1995), with isograds summarized in Fig. 2. There is a general increase in grade from andalusite zone rocks in the north and northeast at the Middle Creek Anticline (Ryburn et al., 1988) and Eloise (Baker, 1996), to sillimanite zone around Fairmile, with sillimanite/K-feldspar zone in the southern zone. Mares (1998) found EW and NS FIAs in garnets with well-developed spiral trails. Fig. 39 is a pseudosection for Mares' sample C96, but as is commonly the case in the sillimanite zone a P-T-t path cannot be constrained for muscovite-biotite-garnet schists from the sillimanite zone. A peak metamorphic age of 1615±17 was obtained for this specimen (Superprobe, monazite – Table 2)

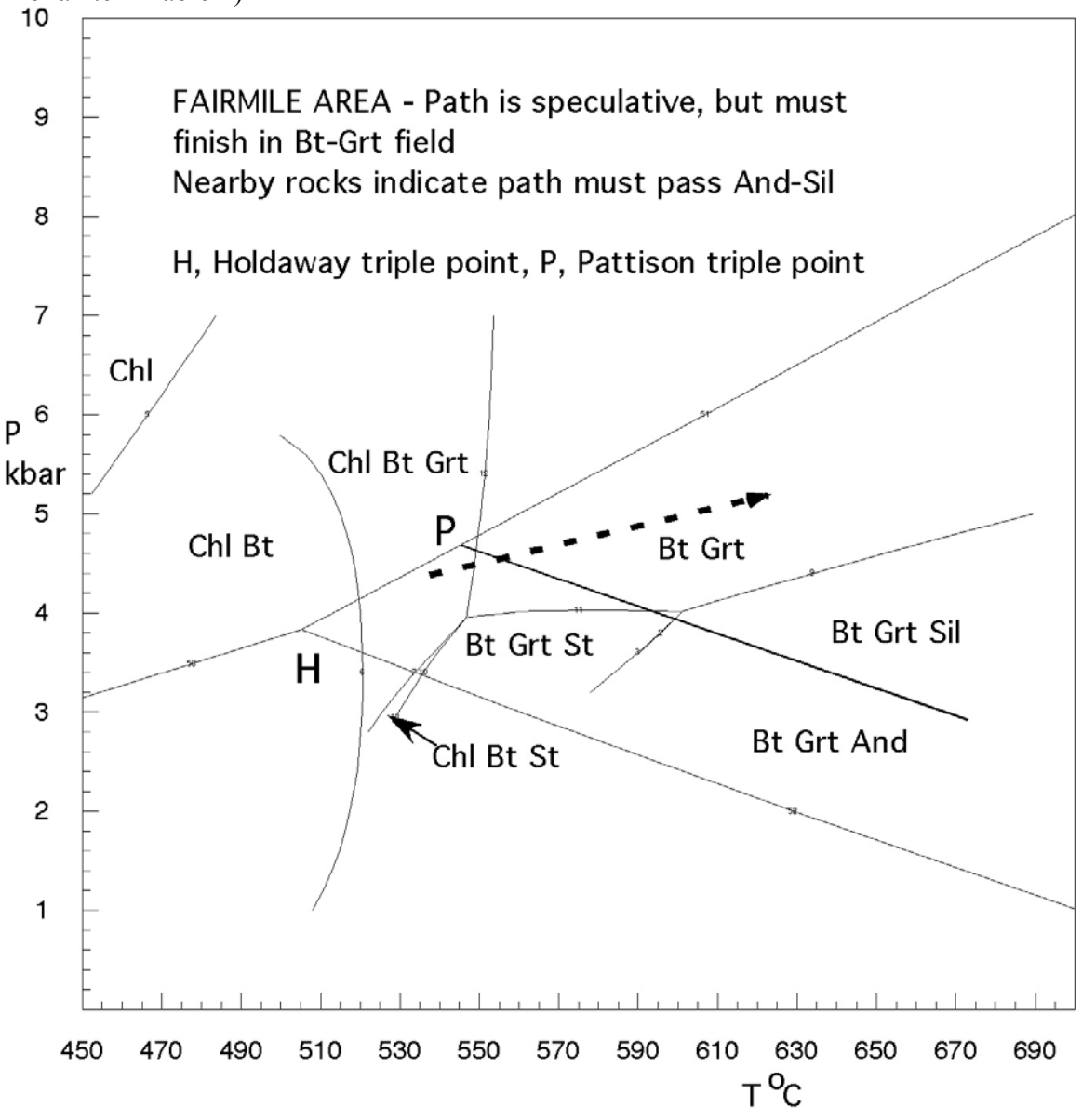

Fig. 39. Pseudosection of sample C96 of Mares (1998)

Cannington Mine

A very detailed study of some samples of gneiss and amphibolite from the Cannington Mine has been made by Kim & Bell (in press). The work includes FIA studies of garnet and gahnite (zincian spinel) and pseudosections. EW and NS FIAs are preserved in both the garnet and gahnite, while the metamorphic conditions were determined as 634±62°C and 4.8±1.3 Kbar. Again no path could be deduced. Peak metamorphic assemblages in pelitic compositions in the mine include biotite, sillimanite, K-feldspar and garnet, and migmatization is widespread (Mark et al., 1998). Dates of between 1585 and 1599 Ma for gneiss and migmatitic pegmatites were obtained by Giles & Nutman (2002).

Selwyn Ranges

The metamorphism in this area has been described in general terms by Beardsmore (1986), Switzer (1987) and Pocock (1992), and in more depth by Adshead-Bell (2000). Further south, between the Yellow Waterhole Granite and Osborne, the work of Fletcher (1999), Weston (2000) and Sayab (2005) is significant. Detailed P-T-t paths have not been determined. However a number of observations make it highly likely that the paths have much in common with those in the Snake Creek Anticline. Andalusite and staurolite show several growth stages and muscovite has replaced early andalusite in staurolite-bearing rocks in a number of localities (Weston, 2000; Adshead-Bell, 2000; Sayab, 2005). Cordierite pseudomorphs in andalusite are a common occurrence in a number of localities (Adshead-Bell, 2000; Fletcher, 1999). This is significant as it suggests similar P-T-t throughout at least the eastern part of the Eastern Fold Belt.

Osborne Mine

Metamorphism at the Osborne Mine has been described in Adshead (1995), French (1997), Banville (1998), and Kennedy (2000). I also did some petrographic work on gneisses and albitites with Dr Gregg Morrison (reports to Osborne Mines) along with subsequent petrographic and analytical studies. The deduced sequence of events is as follows:

1 As in the Snake Creek Anticline, the most important albitization event occurred early in the history. The exact timing of this relative to early metamorphism is uncertain, but samples of garnet-cordierite-albite-biotite gneiss studied by Adshead and French have quartz and no albite in the porphyroblasts whereas the matrix contains abundant albite and very little quartz. In contrast, Banville found albite in the rims but not the cores of some garnet porphyroblasts. Sample OSB20A-890.1m, dated at 1659 Ma, has been albitized but albite timing relative to the andalusite replaced by sillimanite is ambiguous (Table 2). The massive lens of albitization that encloses the ironstones, silica flooding and ore lenses at Osborne (Fig. 40) is early. However, the gneisses surrounding this zone also show albitization to varying degrees. Most of the albitite samples show granoblastic textures, commonly polygonal, as a result of grain boundary migration during the subsequent peak metamorphic event (Fig. 41). In the centre of the main albitite zones, “calcsilicate” albitites with pyroxene and grandite garnet are common.

2 The peak of metamorphism, which probably occurred during one of the D_2 events, has been dated at 1595 Ma (Table 1). The ore was also deposited close to the metamorphic peak (Gauthier et al., 2001). Peak assemblages in the gneisses include biotite, microcline, albite, and (in some) sillimanite. Garnet is not common. Cordierite is rare and only occurs with garnet in albitic gneisses free of microcline. French (1997) obtained values of 611-622° between 3-5 kbar for the garnet-cordierite thermometer, and 679-719°C for the same pressures for garnet-biotite. Some samples of gneiss from the Kulthor prospect show elliptical masses

of sillimanite that probably replaced cordierite. The pressure remains uncertain. A small body of peridotite at the mine have a metamorphic assemblage of orthopyroxene, olivine, anthophyllite, and tremolite, indicating temperatures between 700 and 800°C. Clinopyroxene occurs in some Osborne amphibolites, but orthopyroxene is absent, so the metamorphic grade at Osborne (and Cannington) did not achieve granulite facies. In situ melting in gneisses to form migmatites is common (Fig. 43). Melting probably would not have occurred unless albite was present. Larger bodies of pegmatite are common in the mine, and are at least in part synchronous with foliation development (Kennedy, 2000). Kennedy demonstrated that the pegmatites are simply larger equivalents of the partial melts in migmatites. They are variably albitized, but to what extent this is the result of self-albitization during their crystallization is uncertain (clearcut examples of both possibilities have been identified). A second generation of albitization occurs in the gneisses at some pegmatite contacts, and a titanite date from such a sample gave the same age as an albitized gneiss recrystallised in the metamorphic peak (Table 1). Some albite pegmatites have microcline rims on albite that are almost certainly magmatic (Fig. 44), and a few examples of albite antiperthites have been identified. These observations are interpreted as melting of already albitized gneisses during the metamorphic peak, producing albite-rich pegmatites. Quartz-albite would in fact melt under water-saturated conditions according to the above temperatures (Fig. 45).

3 Reactions following the metamorphic peak include the development of small sillimanite shears in migmatitic gneisses (Figs 41, 46-7). In places sillimanite has replaced microcline, implying hydrogen ion metasomatism according to the reaction

$$Kfs + H^+ = Sil + Qtz + K^+ \qquad \text{(or the equivalent with albite and } Na^+\text{)}$$

4 Garnet accompanies sillimanite in some of these shears. In many examples coarse late muscovite has partly overprinted the sillimanite (Fig, 47) suggesting that the temperature has dropped below the reaction of muscovite to Kfs + Sil. The path suggested in Fig. 45 has few pressure constraints, except for andalusite to sillimanite and cordierite to sillimanite, the latter having a positive slope indicating an anticlockwise path around the peak (Spear et al., 2002).

5 Minor late albitization occurs in the mine (French, 1997), but the timing is unknown.

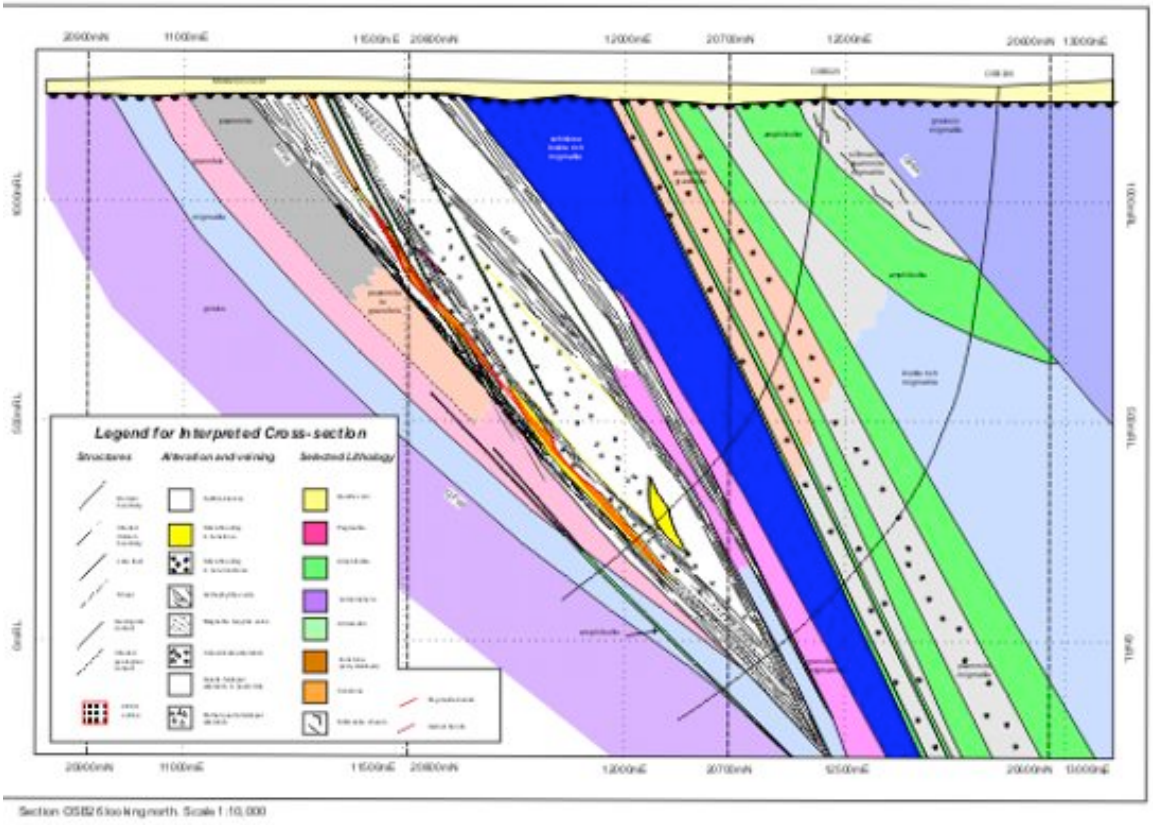

Fig. 40. Interpreted cross-section of the Osborne Mine, prepared by Dr G. Morrison. The central white zone are highly albitized rocks that host the silica-flooding and ironstones that in turn host the ore. The fine lines in the albitites are anthophyllite and cummingtonite veins. The enclosing rocks are variably albitized and migmatitic gneisses of pelitic to psammitic compostions. The green bodies are amphibolite.

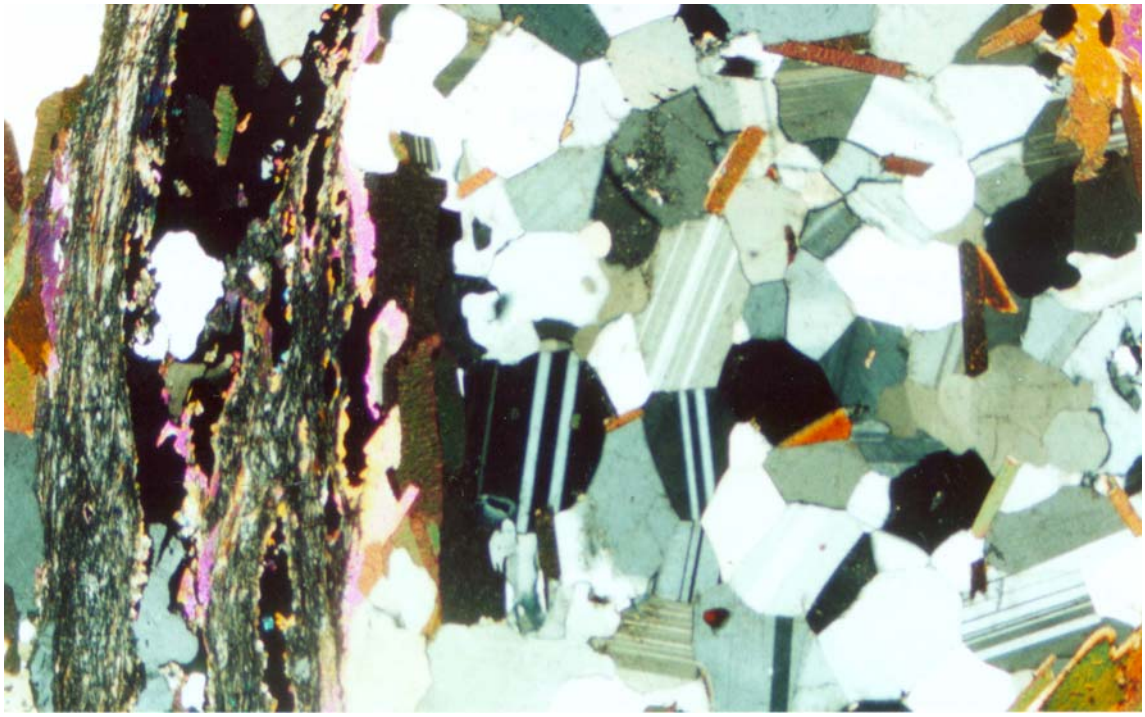

Fig. 41. Albitized gneiss, Osborne, showing a well-developed polygonal texture. Note sillimanite shear zones on the left. Length 5.6 mm

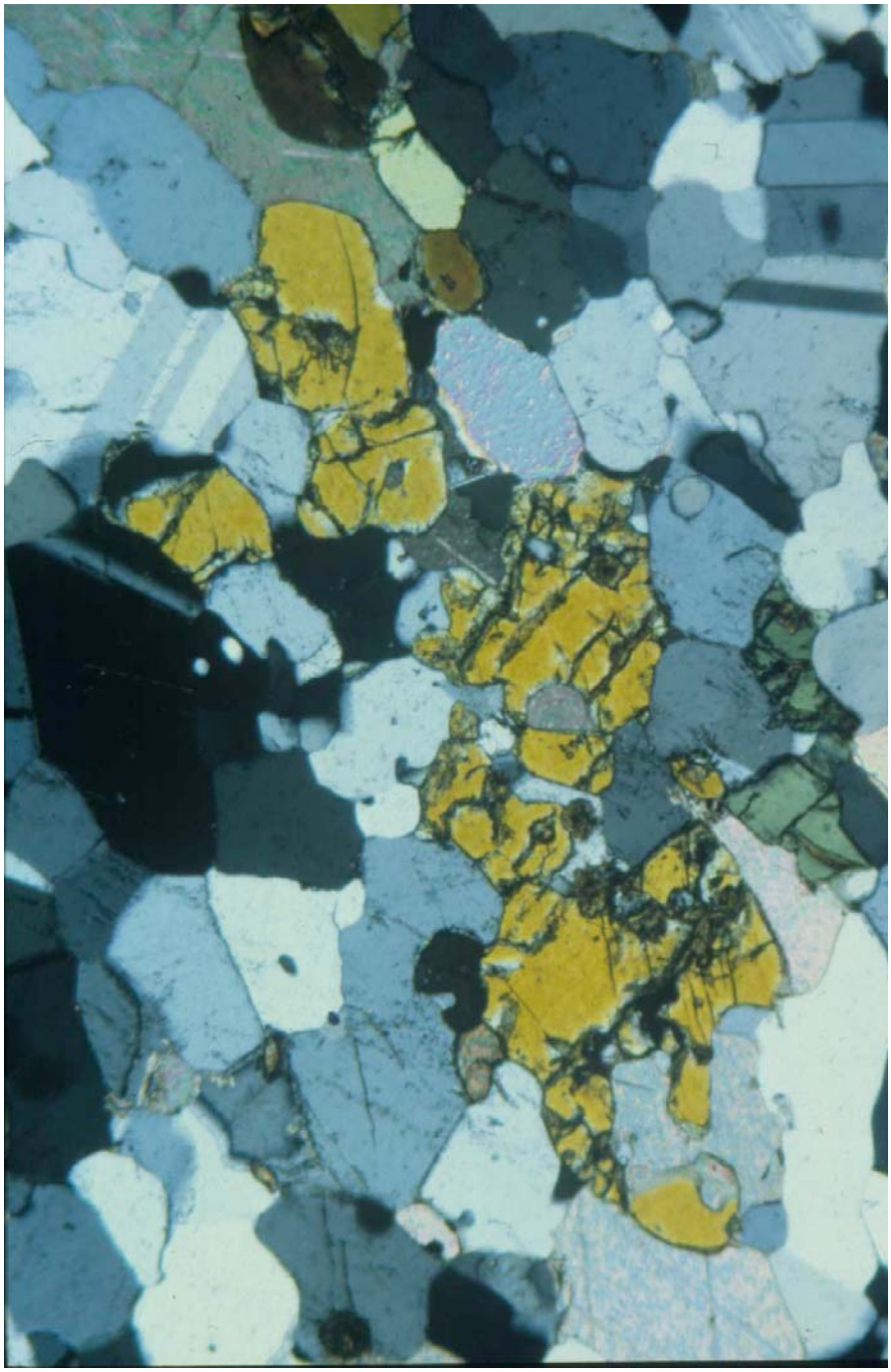

Fig. 42. Albitized gneiss, now consisting of albite, clinopyroxene, titanite and grossularite andradite (not shown). Osborne Mine. Note the polygonal texture of the albite, implying equilibration around the peak of metamorphism. Length 2.8 mm.

Fig. 43. Migmatitic gneiss, Osborne Mine. Hole Osb26a, 1679 m.

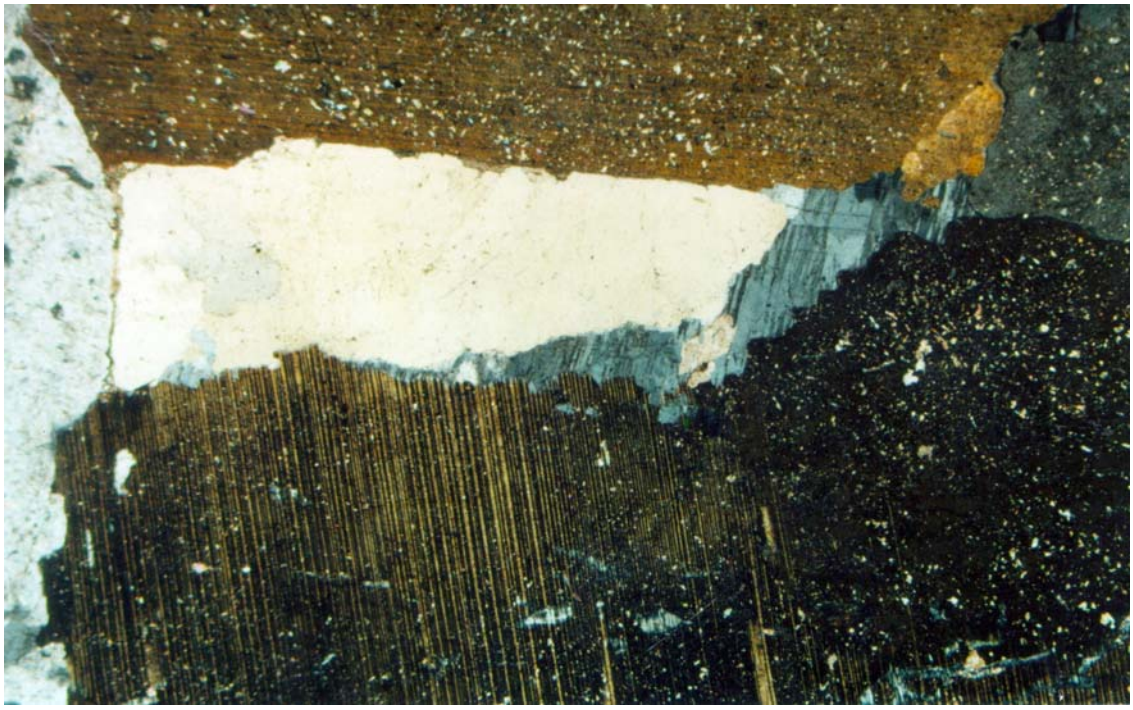

Fig. 44. Pegmatite from Osborne, showing magmatic albite partly rimmed by magmatic microcline, with interstitial quartz. Length 5.6 mm.

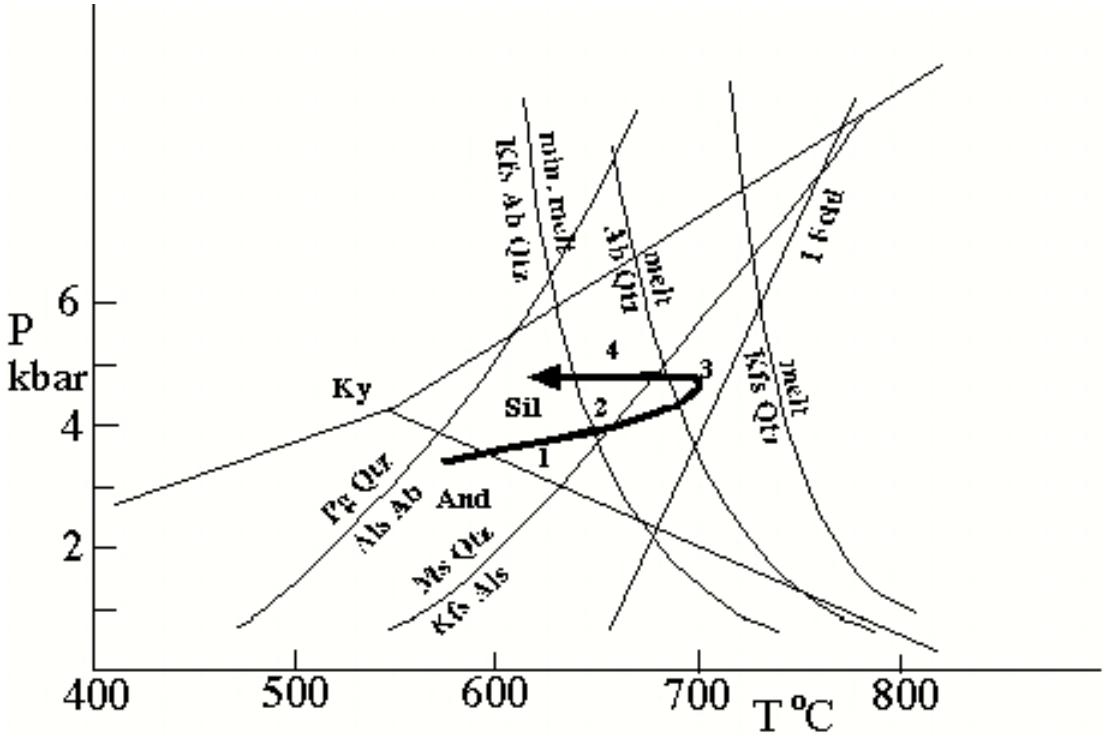

Inferred P-T path for migmatization at Osborne.

1. Large scale albitization
2. Melting of partly albitized gneisses
3. Metamorphic peak (1595 Ma).
   Melting of fully albitized gneisses.
   Pegmatite emplacement
   Cu-Au mineralization
4. Sillimanite alteration, followed by muscovite alteration

Fig. 45

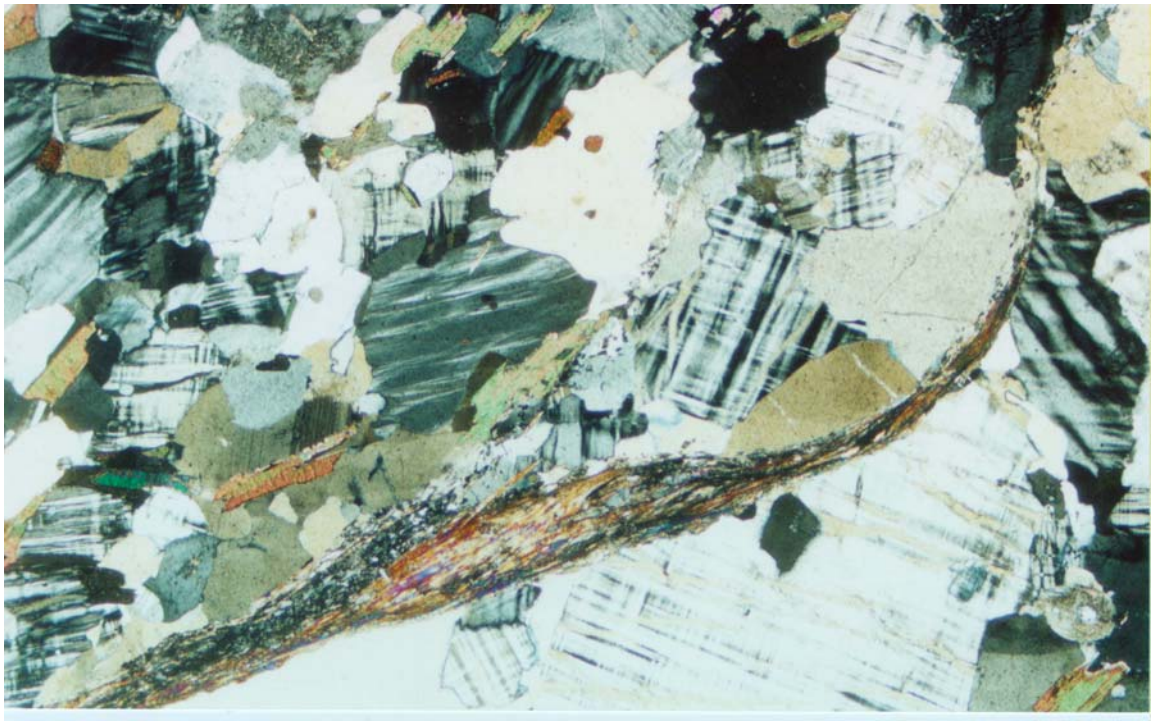

Fig. 46. Sillimanite shear zone on contact between a gneiss (upper) and pegmatite (lower), Osborne Mine. Note the truncation of quartz, microcline and albite grains on either side. Length 5.6 mm.

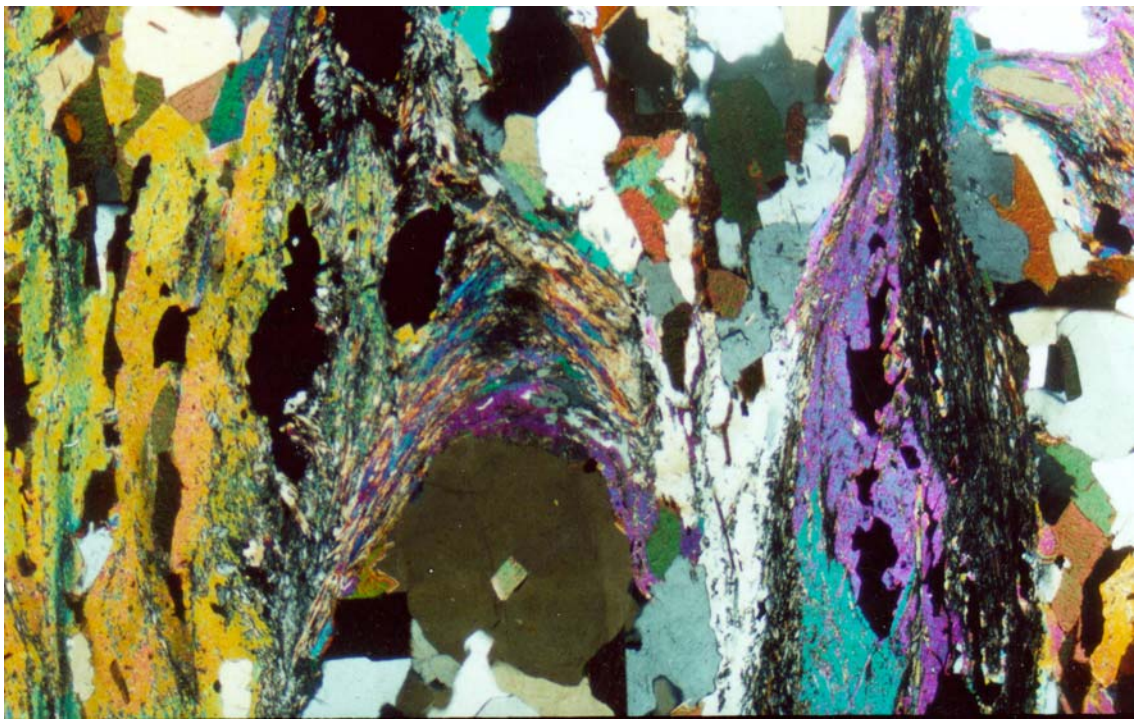

Fig. 47. Gneiss from Osborne, with sillimanite shear zones, including a fold. The sillimanite has been partly replaced by coarse muscovite. Length 5.6 mm.

7.5 Metamorphism of Corella beds, Snake Creek Anticline

Metamorphism of the Corella Formation in the Wonga Belt, and implication for fluid flow and metasomatic processes, has been considered by others (Oliver, 1995; Reinhardt, 1992a; Oliver et al., 1991), whereas detailed studies of calcsilicate breccias in the Cloncurry area have been made by Marshall (2004). Hingst (2002) studied calcsilicates and breccias near the Cloncurry area in the Snake Creek area. A problem with dealing with calcsilicate rocks is that pressures can only rarely be determined, and combined with solid solution uncertainties and the affect of X_{CO_2} on the temperature of reactions, P-T for calcsilicate reactions, let alone P-T-t paths, generally cannot be defined with any certainty. However, a pressure of 4 kbar can be inferred from the pelitic rocks in the Snake Creek area. Reactions 22-26 are important in the Corella rocks of the Snake Creek Anticline (Table 3).

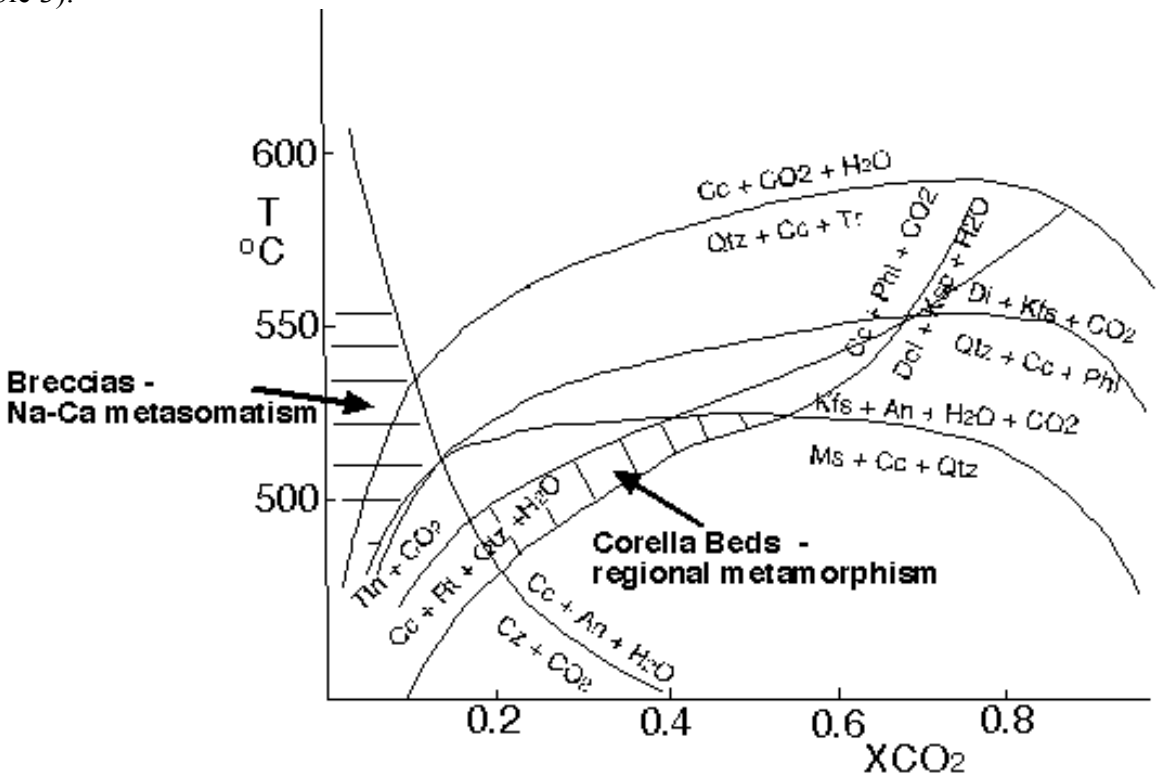

Fig. 48. T-XCO_2 plot for metasomatized and unmetasomatized Corella beds, Snake Creek area, determined at 4 kbar and end-member compositions using THERMOCALC. Modified from Hingst (2002).

Away from the breccias "rock-buffered" calcsilicate rocks contain assemblages with calcite, biotite, scapolite, muscovite, rutile, quartz and microcline, indicating temperatures of the order of 480-520°C (Fig. 48). These temperatures are lower than adjacent sillimanite-zone Soldiers Cap Group east of the Cloncurry Fault, indicating that not only did post-peak metamorphism movement occurr on the Fault but also that the stratigraphically lower Corella beds in this area were subjected to lower regional metamorphic temperatures. This is consistent with the pattern of elongate NS-oriented tongues of higher grade rocks alternating with lower grade zones, regardless of stratigraphy (Fig.2).

There are few constraints on the T- X_{CO_2} conditions for the brecciated and albitized Corella beds. X_{CO_2} conditions were probably low, based on the presence of clinozoisite in a few samples. Titanite is ubiquitous. Many samples contain clinopyroxene, generally diopside but hedenbergite in some samples. A significant acmite (aegerine) component is

present in a few samples. The presence of clinopyroxene is probably in part related to the proximity of gabbro and granite bodies (Fig. 19), and partly because it is relatively early in the thermal metamorphic/brecciation/retrograde fluid sequence (Fig. 49). In many samples, clinopyroxene is partly replaced by amphiboles (combinations of tremolite, actinolite, and rare magnesioriebeckite).

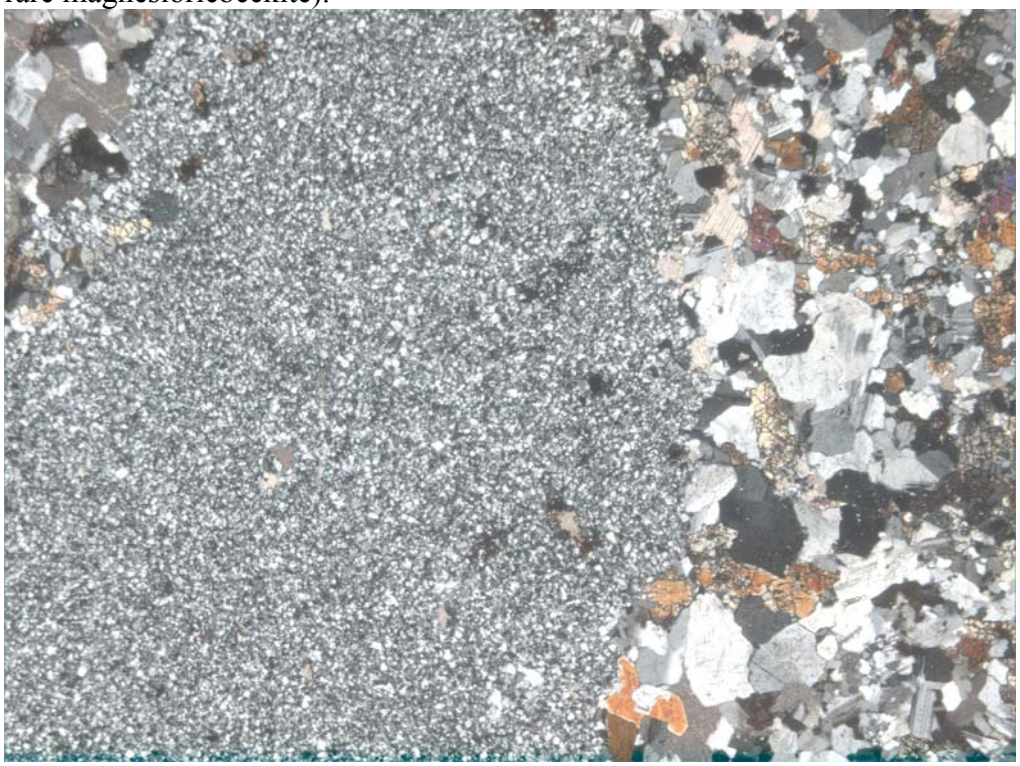

Fig. 49. Breccia sample collected close to a body of Saxby Granite, SW part of SW Snake Creek Anticline. The clast consists mainly of fine-grained albite. The matrix consists of coarser albite, clinopyroxene, calcite and titanite. Length 5.6 mm.

7.6 Cooling history of the Eastern Fold Belt

The cooling history of an orogenic belt is an integral part of its tectonothermal evolution. Igneous rocks that intrude after the metamorphic peak are crucial, not only because of their control on cooling temperatures but also in allowing pressure estimates from aureole assemblages. As mentioned above, pegmatites and migmatites at the Osborne and Cannington mines were produced by anatexis in the metamorphic peak (1584-1595 Ma; Giles & Nutman, 2002; Gauthier et al., 2001). One group of granitic rocks intruded at 1545-1552 Ma (Boorama Tank Gneiss, Maramungee Granite, Percol Planes Tonalite; Pollard and McNaughton, 1997; Page & Sun, 1998). Another group intruded at 1520-1536 Ma (Saxby Granites, Mount Margaret Granite, Mount Angelay Granite (Page & Sun, 1998; Pollard and McNaughton, 1997). A final group intruded between 1501 and 1516 Ma (e.g., Tea tree Granite, Wimberu Granite, Mount Dore Granite, Yellow Waterhole Granite; Page & Sun, 1998; Pollard and McNaughton, 1997).

As previously discussed, the Saxby Granites in the south of the Snake Creek Anticline intruded at 1527 Ma, at a pressure of ~3 kbar. This implies a pressure drop of only 1 kbar after the metamorphic peak at ~1590 Ma. Samples of hornfels collected by Adshead-Bell (2000) from the aureole of the Yellow Waterhole Granite (north of Osborne) consist of K-feldspar, cordierite, quartz, biotite, andalusite and sillimanite, suggesting a pressure of 3 kbar, although biotite Mg/(Mg+Fe) of 0.5 from one of these suggests a pressure of ~ 4 kbar. The Yellow Waterhole Granite is dated at 1510 Ma by Pollard and McNaughton (1997), so these data imply that the Eastern Fold belt was not significantly unroofed until after 1510 Ma, with perhaps only 3.5 km removed by 80 Ma after the metamorphic peak.

The closure temperatures for the various isotopic systems used to date the rocks are highly significant in considering the cooling history of the Eastern Fold Belt. There are uncertainties, but U-Pb closure temperatures for monazite and zircon are above 700°C, U-Pb for titanite ~500-600°C, Ar-Ar for hornblende ~450-525°C, Ar-Ar for muscovite ~325-375°C, and Ar-Ar for biotite ~250-350°C (Spear, 1993). Ar-Ar dates for various minerals from the Eastern Fold Belt can be found in Green (1975), Perkins & Wyborn (1998), Baker et al. (2001), and Spikings et al., (2001). Many of these are younger than 1500 Ma, whereas others are in the range 1530-1576. With the exception of Osborne, titanite ages for metasomatized Corella Formation are in the range 1524-1555 Ma (Oliver et al., 2005). The data suggests that cooling may have been strongly influenced by proximity to plutonic intrusions, with many samples located close to younger granites of the Williams-Naraku granites and so recording ages less than 1500 Ma. However, no granites of Williams-Naraku-Maramungee ages occur in the Wonga Belt where hornblende and titanite ages of over 1524 Ma are recorded. Also, there is scatter in the Ar-Ar data for amphibole and biotite for some localities, e.g. the Osborne Mine, suggesting processes such as ductile deformation, local high-temperature fluid infiltration and veining may be important in addition to simple cooling through closure temperatures.

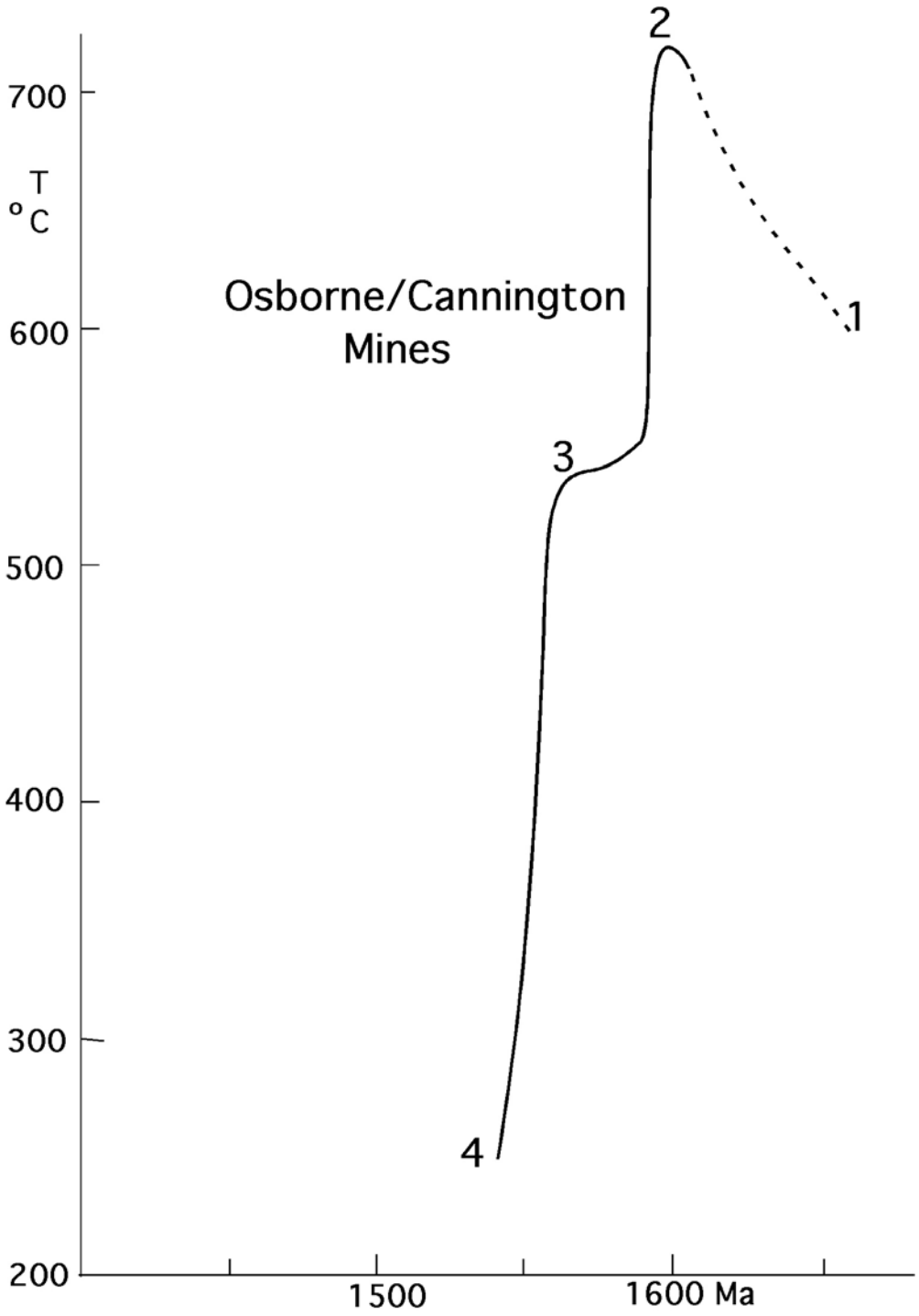

Fig. 50. Suggested T-t diagram, based mainly on the Osborne Mine and partly on the Cannington Mine. 1, D_{Ab} event. 2, metamorphic peak in D_2, followed by rapid cooling so that the 1595 Ma titanite ages were preserved. Ar-Ar ages between 1530 and 1590 Ma were also preserved. There was a possible minor temperature spike around 3. Otherwise, the younger intrusions of the Williams Batholith were too far away so that cooling ages less than 1500 Ma, common to the north, were not recorded at these mines.

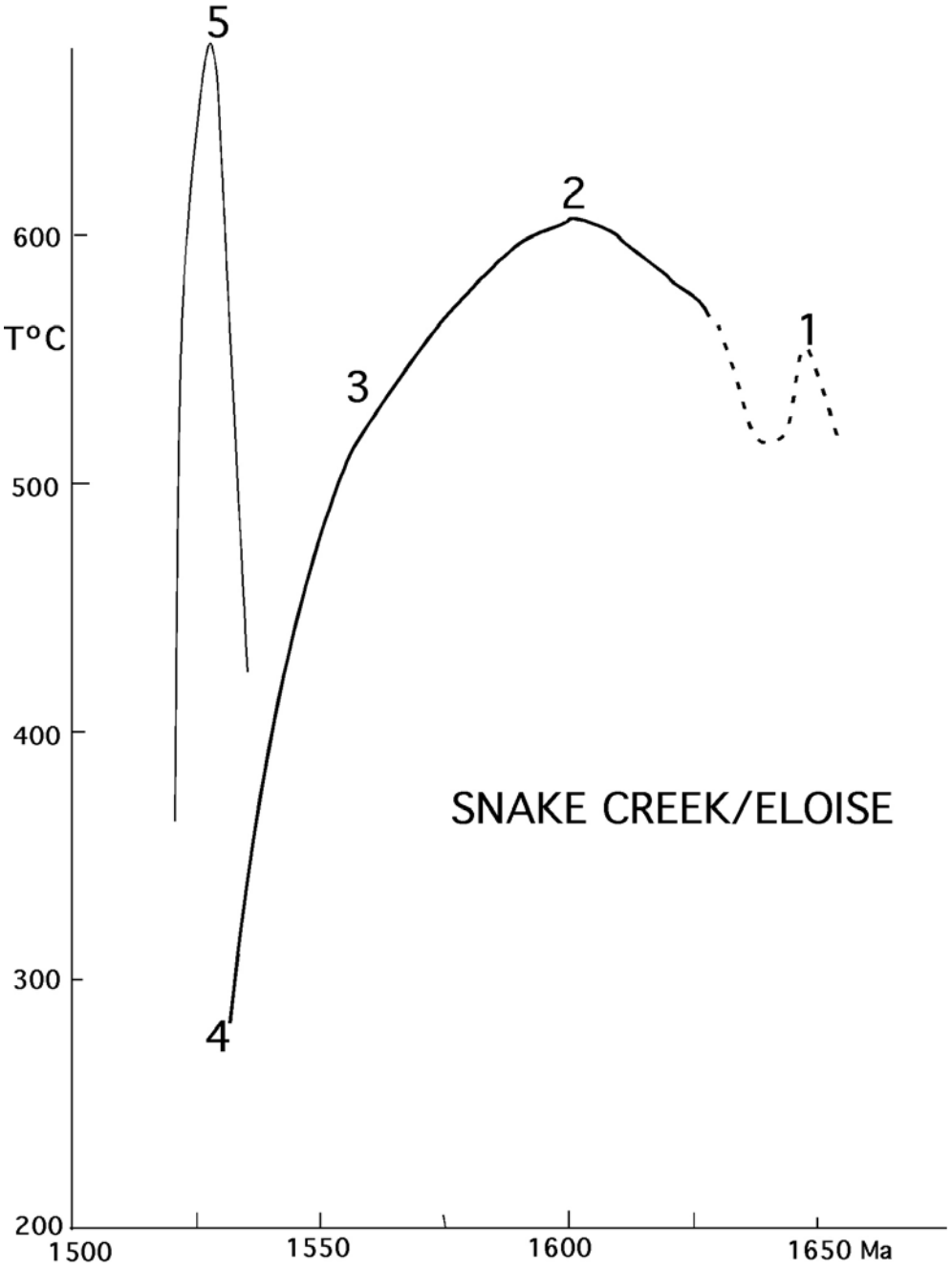

Fig. 51. Suggested T-t diagram mainly based on Snake Creek, partly on the Eloise Mine. 1, D_{Ab} event, with major albitization in the Soldiers Cap Group. 2, peak of metamorphism during D_2. 3, 1555 Ma closure for hornblende at Eloise. 4, 1530 Ma closure for biotite, Eloise (Baker et al., 2001). 5, intrusion of the Saxby Granites and gabbros in the southern part of the Snake creek Anticline, accompanied by massive brecciation and albitization around the Cloncurry Fault and further west. The Saxby Granite also corresponded to the D_{3b} event, and a NE-oriented FIA in andalusite and staurolite. Note that the rarer Ar-Ar cooling ages greater than 1500 Ma (Spikings et al., 2001), such as those at Eloise, are only recorded for locations far enough away from the influence of the Williams/Naraku Batholith.

8. SYNTHESIS, AND MODEL FOR THE TECTONOTHERMAL EVOLUTION

8.1 Summary of main points

1 Multiple regional metamorphic growth events occurred over a considerable time-span, from 1659 to at least 1527 Ma.

2 The main tectonothermal events were: D_{Ab}, a possible extensional event ca. 1530-59 Ma, accompanied by significant albitization and cordierite/andalusite growth; D_1 group of events, NS shortening, garnet, staurolite, kyanite, andalusite; D_2 events, EW shortening, highest grade up to sillimanite/K-feldspar zone, probably in D_{2b} (ca. 1590 Ma). Although kyanite probably grew in the D_{2a} event in the northern part of the Snake Creek anticline and in the Tommy Creek Block, the subsequent P-T-t path involved a pressure drop to around 4 kbar and a temperature rise, resulting in the sequence staurolite to andalusite to sillimanite. Migmatization and injection of pegmatites, along with intrusion of at least some dolerite dykes, occurred around the peak, A continuation of roughly EW shortening then lead to various D_3 events, resulting in folds, crenulations and/or reactivation of S_2. Around D_{3b} time saw the intrusion of the Saxby Granites (1527 Ma) and gabbros, major brecciation and albitization along the Cloncurry Fault and the Corella beds to the west (the Ernest Henry Cu-Au deposit, itself hosted in a breccia system, probably also formed at this time).

3 The P-T-t path in the Snake Creek Anticline is complex. Following cooling after the proposed extension and heating to form the D_{Ab} event, a clockwise path extending into medium-pressure metamorphic series to 5 kbar or greater during D_1. Continuation of the clockwise path earlier in D_2 saw a pressure drop flowed by an isobaric temperature increase to the metamorphic peak in D_{2b}. During subsequent cooling the path returned to clockwise, and the pressure was around 3 kbar during the D_{3b}event. However, significant unroofing did not ensue until after the 1510 Ma Yellow Waterhole Granite intruded.

4 There is good evidence that the P-T-t path deduced for Snake Creek area applied to the Soldiers Cap Group throughout the eastern part of the Eastern Fold Belt (i.e., Ernest Henry, Cloncurry, Snake Creek, Eloise, Fairmile, Cannington, Osborne, Starra, possibly Kuridala). It may apply to the Tommy Creek Block from D_2 onwards. However, in the Wonga Belt, the next higher grade belt to the west, there appear to be differences. Although the same FIAs are present in the White Blow Formation (Sayab, 2005) , the path determined by Reinhardt (1992b) is one of a simple anticlockwise from andalusite to sillimanite, followed by cooling into the kyanite field. A determination by Sayab (2005) of a pressure of around 4 kbar for a core of a garnet from the White Blow Formation is consistent with this.

5 An extraordinary observation that appears to apply across the Eastern Succession is that there appears to be only minor spatial shifts corresponding to the different events. In other words, if a particular area was subjected to lower amphibolite facies conditions in D_1 or D_{Ab} then such conditions were more or less maintained at least until the D_2 events. This implies that the same anomalous thermal pattern applied over a period of at least 50 Ma. Exceptions are the Tommy Creek Block, where only EW shortening events are recorded, and the Gilded Rose area that preserves porphryoblasts of D_1 association only.

8.2 A tectonothermal model

Low pressure metamorphism requires a substantial thermal anomaly in the mid- to lower-crust. Possible heat sources are as follows:

1 Self-heating, due to relatively high contents of heat-producing radioactive isotopes in the metasedimentary rocks or adjacent granites.
2 Extensional tectonics, involving major crustal thinning and mantle upwelling. This may be accompanied by mafic igneous activity.
3 Mantle delamination.
4 Igneous intrusions (gabbros and/or granites)

Various combinations of the above are also possible.

Self-heating as a result of high contents of heat producing elements in the Sybella Granite was proposed by McLaren et al. (1999) for the area west of mount Isa. They were able to model the metamorphic peak at the then-believed 1532 Ma, but subsequently peak ages of ca. 1575 were found at Mount Isa (Hand & Rubato, 2002). However, no older granites are found in the Soldiers Cap Group, and the older granites in the Wonga Belt are over 130 Ma older than the metamorphic peak, so self-heating cannot explain metamorphism peaking at 1575-1595 Ma across the inlier. A self-heating model would not by itself explain the multiple growth events extending over 100 Ma in the Eastern Fold Belt. However, older granites such as those in the Wonga Belt undoubtedly made a contribution to the overall thermal budget during the Isan Orogeny.

As mentioned above, it is suggested that the D_{Ab} event was extensional, as the monazite ages (Table 2) overlap with depositional ages of the Mount Norna Quartzite and Toole Creek Volcanics that overly the Llewellyn Creek Formation where the cordierite-andalusite-albite schists are located. D_{1a} produced a flat-lying foliation and recumbent folds, but is believed to be compressional (Loosveld, 1989; Sayab, 2005). Later folds and crenulations with shallow axial planes, such as those formed in D_{2b}, are interpreted as relaxation events in an overall compressional setting (Bell & Johnson, 1989; Mares, 1998; Sayab, 2005). So with the exception of the D_{Ab} event, the Isan Orogeny metamorphic events in the Eastern Fold Belt are interpreted as taking place in compressional settings.

Mantle delamination was proposed by Loosveld & Etheridge (1990) to explain low-pressure metamorphism in a compressional setting in the Eastern Fold Belt. Besides other limitations of the model (e.g., the requirement of instantaneous delamination), it fails to explain the multiple events taking place over 100 Ma, and also the pattern of alternating high and low-grade belts across the Mount Isa Inlier.

I propose that igneous intrusions offer the best explanation for the isograd patterns and longevity of metamorphism in the Eastern Fold Belt. It is clear that igneous activity was abundant throughout the evolution of the post-Wonga Eastern Fold Belt. It includes the 1686 Ma gabbros and tonalites at Snake Creek, a 1679 Ma unnamed granite at Cloncurry, the 1657-1660 Ma Ernest Henry Diorite, the 1658 Ma Toole Creek Volcanics, syn-D_2 dolerite dyke swarms parallel to the axial plane of the Snake Creek Anticline, 1585-1595 Ma migmatites and pegmatites around the metamorphic peak, post-peak granite and tonalite at 1547-1552 Ma (e.g., Maramungee Granite), and the 1500-1530 Ma period of Naraku and Williams Batholiths (including abundant gabbro and dolerite). However, despite the abundance of igneous rocks, a major problem with this hypothesis is the apparent lack of local large igneous intrusives corresponding to most of the metamorphic

events, although some igneous rocks have the right timing for nearby metamorphism. For example, the dolerite dyke swarms at Snake Creek could not by themselves explain the peak of metamorphism as they are volumetrically insignificant. However, they do indicate mafic intrusion was possible around the time of the peak, and as they are fractionated they could be linked to large bodies deeper in the crust. The migmatites at Osborne and Cannington are the product of the overall thermal anomaly rather than the cause of it. However, the aureole of the Saxby Granite at the SE end of the Snake Creek Anticline demonstrates metamorphic growth (andalusite and sillimanite) synchronous with reactivation of S_2 during the D_{3b} event. The wide sillimanite/K-feldspar aureole around the NW part of this granite (Fig. 1) also implies synchronous porphyroblast growth further north, which is consistent with the occurrence of thin rims of late andalusite or staurolite in many samples (Up to 10 km from this granite, but less than 5 km from smaller bodies of granite and gabbro along the Cloncurry Fault). It is possible, therefore, to make a case for "intrusives at depth" for the peak of metamorphism. However, no plutons correspond in timing with the metamorphic peak in either the Wonga belt or the eastern part of the Eastern Fold Belt on the scale, for example, of the gabbro and granite plutons that probably supplied the heat for the low-pressure overprint elsewhere, for example Connemara, Ireland, or the Cooma Granodiorite surrounded by low-pressure metamorphics of the Lachlan Zone.

Modelling of the evolution of the abundant high-Fe mafic rocks that characterize the Mount Isa Inlier suggests considerable fractionation in magma chambers below the current levels of emplacement (Oliver et al., 2005). A few of these fractionation products are exposed, for example the small thrust sheet of peridotite at the Osborne Mine and the Teatree layered gabbro north of Cloncurry. Modelling of geophysical data suggests considerable amounts of heavy material (averaging as diorite) in the lower crust (Blenkinsop et al, 2005). It is suggested that gabbros ponded in the lower crust during the metamorphic episodes (i.e., 1630-1660 Ma, and 1527-1610 Ma) causing considerable partial melting. During the later part of the Isan Orogeny when the ductile strain was less intense, larger bodies (i.e. plutons) of granite and gabbro were able to intrude (e.g., Maramungee Granite, and the Williams and Naraku Batholiths). However, during D_2 significant partial melting led to migmatites and mobilization as pegmatites, which intruded only as far as the sillimanite isograd as this corresponded to the depth of crystallization of water-saturated minimum melts (In contrast, the younger granites formed plutons that were not water-saturated and could intrude to shallower depths). I believe a model proposed by Miyazaki (2004) for a low-pressure metamorphic belt in Japan applies to the Mount Isa Inlier – heat was transported from deeper in the crust via melt migration, with heat transferred within the migmatite/pegmatite zones via advection and to the overlying lower grade zones via conduction. Thus the heat from abundant deeper mafic intrusions is carried upwards by the small bodies of crustal melts.

The two higher-grade zones occur within the Eastern Fold Belt, the Mary Kathleen/Duchess zone (including the Wonga Belt) and the Cloncurry/Osborne zone (also extends to the eastern edge of the Inlier), are located along significant long-lived linear features, namely the Wonga Belt and the Cloncurry Worm (Blenkinsop et al., 2005). Worms are defined in terms of gravity and magnetic gradients, and it is suggested that these zones were the locus of repeated mafic intrusions throughout the metamorphic episodes, which for the Cloncurry-Osborne zone extended from 1660 Ma through to 1500 Ma. Advective transfer of heat from the ponded gabbro intrusions lower in the crust was achieved via granites, either by pegmatites (S-type) during the metamorphic peak or by

mainly A-type plutons later in the Isan Orogeny. The Tommy Creek Block, which achieved amphibolite facies from D_2 onwards, was possibly the result of a more localized mafic "hotspot".

8.3 Implications for exploration

The tectonothermal evolution project was largely meant to provide a background framework for research directed at the genesis of ore deposits in the Eastern Fold Belt (e.g., Oliver et al, 2005; Rubenach & Oliver, 2005). However, it is probably not a coincidence that the main Cu-Au deposits of the Eastern Fold Belt are situated along Cloncurry/Osborne zone of amphibolite facies metamorphism. Their localization is probably controlled by structure (Blenkinsop et al., 2005), although fluids associated with the mafic rocks were probably an essential ingredient in the ore genesis (Oliver et al., submitted; Oliver et al, 2005). Note also that the ore deposition also occurred over a considerable time-frame, from around the metamorphic peak at Osborne to 1527 Ma at Ernest Henry and mafic rocks were emplaced in the period.

Acknowledgements

The author would like to thank the following CRC colleagues for numerous fruitful discussions: Tim Baker, Tom Blenkinsop, James Cleverley, Damien Foster, Bin Fu, Cam Huddlestone Holmes, Roger Mustard, Nick Oliver, and Pat Williams.

Similarly, students supervised by the author are gratefully acknowledged – Kris Butera (PhD in progress), Mohammad Sayab (PhD completed), and Richard Hingst (honours thesis, 2002).

Tim Bell and Bill Collins (non-CRC colleagues) are thanked for numerous stimulating discussions.

Geologists from Osborne Mines, in particular Frank Tullemans, are acknowledged for their assistance and discussions, both before and during the CRC. Some earlier work on gneisses, migmatites and albitites was done for Osborne Mines in collaboration with Gregg Morrison.

Most of the analytical work was done by the Advanced Analytical Centre at JCU, and Sharon Ness (director) is acknowledged for the overall excellent quality control. In particular, Kevin Blake is thanked for all his assistance with microprobe analyses and dating.

Two SHRIMP age dates were done by Dr Mark Fanning, ANU.

9. REFERENCES

Adshead, N.D., 1995. Geology, alteration and geochemistry of the Osborne Cu-Au8 deposit, Cloncurry district, NW Queensland. Unpubl. PhD thesis, James Cook University.

Adshead-Bell, N.S., 2000. Structural constraints of the ironstone hosted Au-Cu Starra deposit and Selwyn Range region, Eastern Fold Belt, Mount Isa Inlier. Unpublished PhD thesis, James Cook University, Townsville.

Baker, T., Perkins, C., Blake, K.L., & Williams, P.J., 2001. Radiogenic and stable isotope constraints on the genesis of the Eloise Cu-Au deposit, Cloncurry district, northwest Queensland. Economic Geology 96, 723-742.

Banville, G., 1998. Textural and geochemical investigation of the magnetite species at the Osborne Cu-Au deposit, Cloncurry district, Mount Isa I(nlier, NW Queensland. Unpubl. BSc hons thesis, James Cook University

Beardsmore, T.J., 1992. Petrogenesis of Mount Dore-style breccia-hosted copper ± gold mineralization in the Kuridala-Selwyn region of Northwestern Queensland. Unpubl. PhD thesis, James Cook University.

Bell T.H., & Johnson S.E., 1989. Porphyroblast inclusion trails: the key to orogenesis. J. Metamorphic Geol. 7, 297-310.

Bell, T.H., 1986. Foliation development and refraction in metamorphic rocks: reactivation of ealier foliation and decrenulation due to shifting pattern of deformation partitioning. J. Metamorphic Geol., 4, 421-444.

Bell, T.H., Reinhardt, J., & Hammond, R.L., 1992. Multiple foliation development during thrusting and synchronous formation of vertical shear zones. J. Structural Geology 14, 791-805.

Betts, P., Ailleres, L., O'Dea, M, & MacCready, T., 1997. Polyphase thrust-related deformation of the Mitakoodi Culmination: evidence along the eastern limb of the duck Creek Anticline. In, Ailleres & Betts (eds) Structural Elements of the Eastern Successions (Filed Guide). Australian Geodynamics Cooperative Research Centre, pp 17-36.

Blake, D.H., & Stewart, A.J., 1992. Detailed studies of the Mount Isa Inlier. AGSO Bull. 243.

Blenkinsop, T. G., Huddlestone-Holmes, C., Foster, D., Mark, G., Austin, J., Edmiston, M., Lepong, P., Ford, A., Murphy, F.C. 2005. 3-D model and crustal architecture of the Mt Isa Eastern Succession. I2+3 Final Report, pmdCRC.

Carmichael, D.M., 1969. On the mechanism of prograde metamorphic reactions in quart-bearing pelitic rocks. Contribs. Mineralogy Petrology 20, 244-267.

Connors, K.A. and Page, R.W., 1995. Relationships between magmatism, metamorphism and deformation in the western Mount Isa Inlier, Australia. Precambrian Research, 71: 131-153.

De Jong, G., 1995. Post metamorphic alteration and mineralization in a highly deformed Proterozoic terrain: the eastern Selwyn Ranges, Cloncurry District, NW Queensland. Unpublished PhD thesis, James Cook University, Townsville.

Derrick, G.M., 1980. Marraba, Queensland, 1:100.000 geological map commentary. Bureau of Mineral Resources, Canberra.

Fletcher, A.C., 1999. Geology, mineralisation and metamorphism of the Plume Prospect, northwest Queensland. Unpublished BSc Hons thesis, James Cook University, Townsville. 100 pp.

Foster, D.R.W, 2003. Proterozoic low-pressure metamorphism in the Mount Isa Inlier, northwest Queensland, Australia, with particular emphasis on the use of calcic amphibole chemistry as temperature-pressure indicators. Unpubl. PhD thesis, James Cook University.

Foster, D.R.W. and Rubenach, M.J., 2000. Comment: High radiogenic heat-producing granites and metamorphism - An example from the western Mount Isa Inlier, Australia. Geology, 28: 671.

French, T., 1997. Genesis of albitites and anthophyllite-bearing lithologies of the Osborne Cu-Au deposit, Cloncurry district, Mount Isa Inlier, NW Queensland. Unpublished BSc Hons thesis, James Cook University, Townsville. 98 pp.

Gauthier, L., Hall, G., Stein, H. and Schaltegger, U., 2001. The Osborne deposit, Cloncurry district: a 1595 Ma Cu-Au skarn deposit. In Williams, P.J. (ed.) 2001: a hydrothermal odyssey, new developments in metalliferous hydrothermal systems research, extended conference abstracts. EGRU contribution 59: 58-59.

Giles, D., Betts, P. and Lister, G., 2002. Far-field continental backarc setting for the 1.80-1.67 Ga basins of northeastern Australia. Geology, 30: 823-826.

Giles, D. and MacCready, T., 1997. The structural and stratigraphic position of the Soldiers Cap Group in the Mount Isa Inlier. In: Ailleres, L. and Betts, P.G., (eds.), Structural elements of the Eastern Succession-a field guide illustrating the structural geology of the eastern Mount Isa terrane, Australia. Australian Crustal Research Centre, technical publication 63: 61-73.

Giles, D. and Nutman, A.P., 2002. SHRIMP U-Pb monazite dating of 1600-1580 Ma amphibolite facies metamorphism in the southeastern Mt Isa Block, Australia. Australian Journal of Earth Sciences, 49: 455-565.

Green, D.C., 1975. Geochronology of the Cloncurry Complex, northwest Queensland, with particular emphasis on the later Carpentarian events, 1975 Field Conference, Mount Isa Region. Geological Society of Australia, Queensland Division: pp. 29-33.

Hand, M. and Rubatto, D., 2002. The scale of the thermal problem in the Mount Isa Inlier. In: Preiss, V.P., (ed.), Geoscience 2002: expanding horizons. Abstracts of the 16th Australian Geological Convention, Adelaide Convention Centre, Adelaide, SA, Australia. July 1-5, 2002, number 67. 475 pp.

Hill, E.J., Loosveld, R.J.H. and Page, R.W., 1992. Structure and geochronology of the Tommy Creek Block, Mount Isa Inlier. In: Stewart, A.J. and Blake, D.H., (eds.), Detailed studies of the Mount Isa Inlier. Australian Geological Survey Organization, Bulletin 243: 329-348.

Hingst, R., 2002. Geoloogy and geochemistry of the Cloncurry Fault. Unpubl. BSc hons thesis, James Cook University.

Holmes, C.R., 1992. The structural and metamorphic history of the Snake creek Anticline, Cloncurry, northwest Queensland. Unpublished BSc Honours thesis, James Cook University, Townsville.

Jaques, A.L., Blake, D.H. and Donchak, P.J.T., 1982. Regional metamorphism in the Selwyn Range, northwest Queensland. Journal of Australian Geology and Geophysics, 7: 181-196.

Kennedy., M.A., 2000. The si9gnificance of pegmatites in the Osborne Copper-Gold Deposit. Unpubl. BSc Hons thesis, James Cook University.

Kim, H. S, & Bell, T.H, in press. Multiple generations of sillimanite shear zones in the Cannington Ag-Pb-Zn deposit, Northwest queensland, Australia: implications for Zn mineralization. Gondwana research.

Kretz, R., 1983. Symbols for rock-forming minerals. American Mineralogist, 68: 277-279.

Lally, J.H., 1997. The structural history of the central Eastern Fold Belt, Mount Isa Inlier, northwest Queensland. Unpublished PhD thesis, James Cook University, Townsville.

Lewthwaite, K.J., 2000. The structural and metamorphic development of the Soldiers Cap Group SE of Cloncurry: implications for the orogenic development of the Eastern Fold Belt of the Mount Isa Inlier, Australia. Unpublished PhD thesis, James Cook University, Townsville.

Loosveld, R.J.H., 1989. The synchronism of crustal thickening and high T/low P metamorphism in the Mount Isa Inlier, NW Queensland, Australia. Part 1: an example, the central Soldiers Cap Group. Tectonophysics, 159: 173-190.

Loosveld, R.J.H. and Etheridge, M.A., 1990. A model for low-pressure facies metamorphism during crustal thickening. Journal of Metamorphic Geology, 8: 257-267.

Loosveld, R.J.H. and Schreurs, G., 1987. Discovery of thrust klippen, northwest of Mary Kathleen, Mount Isa Inlier, Australia. Australian Journal of Earth Sciences, 34: 387-402.

Mares, V.M., 1998. The Structural development of the Soldiers Cap Group within a portion of the Eastern Fold Belt of the Mount Isa Inlier: a succession of horizontal and vertical deformation events and large-scale shearing. Australian Journal of Earth Sciences, 45: 373-387.

Mark, G., 2001. Nd isotope and petrogenetic constraints for the origin of the Mount Angelay igneous complex: implications for the origin of intrusions in the Cloncurry district, NE Australia. Precambrian Research, 105: 17-35.

Mark, G., Phillips, G.N. and Pollard, P.J., 1998. Highly selective partial melting of gneiss at Cannington, Cloncurry district, Queensland. Australian Journal of Earth Sciences, 45: 169-176.

McLaren, S., Sandiford, M. and Hand, M., 1999. High radiogenic heat-producing granites and metamorphism - An example from the western Mount Isa inlier, Australia: Geology, 27: 679-682.

Miyazaki, K., 2005. Low-P-high-T metamorphism and the rolke of heat transport by melt migration in the Higo Metamorphic Complex, Kyushu, Japan. J. Metamorphic Geology 22, 793-810.

O'Dea, M.G., Lister, G.S., MacCready, T., Betts, P.G., Oliver, N.H.S., Pound, K.S., Huang, W. and Velenta, R. K., 1997. Geodynamic evolution of Proterozoic Mount Isa terrain. In: Burg, J.P. and Ford, M., (eds.), Orogeny through time. Geological Society of London, Special Publication 121: pp. 99-122.

Oliver, N.H.S., 1995. Hydrothermal history of the Mary Kathleen Fold Belt, Mount Isa Block, Queensland. Australian Journal of Earth Sciences, 42: 267-279.

Oliver, N.H.S., Holcombe, R.J., Hill, E.J. and Pearson, P.J., 1991. Tectono-metamorphic evolution of the Mary Kathleen Fold Belt, northwest Queensland: a reflection of mantle plume processes? Australian Journal of Earth Sciences, 38: 425-456.

Oliver, N.H.S, Mark, G., Pollard, P.J., Rubenach, M.J., Marshall, L.J., Williams, P.J, & Baker, T., 2005. Geochemistry and geochemical modelling of fluid-rock interaction in the eastern Mt Isa Block, Australia: Modelling of the role of sodic alteration in the genesis of iron oxide-copper-gold deposits, Eastern Mount Isa Block, Australia. Economic Geology 99, 1145-1176.

Oliver, N.H.S., Butera, K., Cleverley, J.S., Marshall, L.J., Rubenach, M.J., Collins, W.J., Fu, B., Mustard, R. & Baker, T., 2005. From source to sink: evolution of fluid systems in the Eastern Succession of the Mount Isa Block. I2+3 Final Report, pmdCRC.

Page, R.W. and Sun, S-s., 1998. Aspects of geochronology and crustal evolution in the Eastern Fold Belt, Mount Isa Inlier. Australian Journal of Earth Sciences, 45: 343-361.

Pattison, D.R.M, Spear, F.S., & Cheney, 1999. Polymetamorphic originj of muscovite + cordierite + staurolite + biotite assemblages: implications for the metapelitic petrogenetic grid and P-T paths. J. Metamorphic Geology 17, 685-703.

Pattison, D.R.M., Spear, F.S., Debuhr, C.L., Chesney, J.T., & C.V. Guidotti, 2002. Muscovite + cordierite→ Al_2SiO_5 + biotite + quartz +H_2O: constraints from natural assemblages and

implications for the metapelitic perogenetic grid. J.Metamorphic Geology 20, 99-118.

Pearson, P.J., Holcombe, R.J. and Page R.W., 1992. Synkinematic emplacement of the Middle Proterozoic Wonga Batholith into a mid-crustal extensional shear zone, Mount Isa Inlier, Queensland, Australia. In: Stewart, A.J. and Blake, D.H., (eds.), Detailed studies of the Mount Isa Inlier. Australian Geological Survey Organization, Bulletin 243: 289-328.

Perkins, C. and Wyborn, L.A.I., 1998. Age of Cu-Au mineralization, Cloncurry district, eastern Mount Isa Inlier, Queensland, as determined by $^{40}Ar/^{39}Ar$ dating. Australian Journal of Earth Sciences, 45: 233-246.

Pollard, P.J. and McNaughton, N.J., 1997. U/Pb geochronology and Sm/Nd characteristics of Proterozoic intrusive rocks in the Cloncurry district, Mount Isa Inlier, Australia. In: Pollard, P.J. (compiler) AMIRA P438 Cloncurry base metals and gold: final report.

Pollard, P.J. and Perkins, C., 1997. $^{40}Ar/^{39}Ar$ geochronology of alteration and Cu-Au-Co mineralization in the Cloncurry district, Mount Isa Inlier, Australia. In: Pollard, P.J. (compiler) AMIRA P438 Cloncurry base metals and gold: final report.

Reinhardt, J., 1987. Cordierite-anthophyllite rocks from northwest Queensland, Australia: metamorphosed magnesian pelites. Journal of Metamorphic Geology, 5: 451-472.

Reinhardt, J., 1992 a. The Corella Formation of the Rosebud Syncline (central Mount Isa Inlier): deposition, deformation and metamorphism. In: Stewart, A.J. and Blake, D.H., (eds.), Detailed studies of the Mount Isa Inlier. Australian Geological Survey Organization, Bulletin 243: 229-226.

Reinhardt, J., 1992 b. Low-pressure, high-temperature metamorphism in a compressional tectonic setting: Mary Kathleen Fold Belt, northeastern Australia. Geological Magazine, 129: 41-57.

Reinhardt, J. and Rubenach, M.J., 1989. Temperature-time relationships across metamorphic zones: evidence from porphyroblast-matrix relationships in progressively deformed metapelites. Tectonophysics, 158: 141-161.

Rubenach, M.J., 1992. Proterozoic low-pressure/high-temperature metamorphism and anticlockwise P-T-t path for the Hazeldene area, Mount Isa Inlier, Queensland, Australia. Journal of Metamorphic Geology, 10: 333-346.

Rubenach, M.J., 2005. Relative timing of albitization and chlorine enrichment in biotite in Proterozoic schists, Snake Creek Anticline, Mount Isa Inlier, northeastern Australia. Canadian Mineralogist 43, 349-366.

Rubenach, M.J., Adshead, N.D., Oliver, N.H.S., Tullemans, F., Esser, D. and Stein H., 2001. The Osborne Cu-Au deposit: geochronology, and genesis of mineralization in relation to host albitites and ironstones. In Williams, P.J. (ed.) 2001: a hydrothermal odyssey, new developments in metalliferous hydrothermal systems research, extended conference abstracts. EGRU contribution 59: 172-173.

Rubenach, M.J. and Barker, A.J., 1998. Metamorphic and metasomatic evolution of the Snake Creek Anticline, Eastern Succession, Mount Isa Inlier. Australian Journal of Earth Sciences, 45: 363-372.

Rubenach, M.J. and Foster, D.R.W., 1996. Interrelationships between multiple metamorphic episodes, high strain zones, granites and metasomatism, Mount Isa Inlier. In: Buick, I.S. and Cartwright, I., (eds.), Evolution of metamorphic belts. Geological Society of Australia, Abstracts 42: pp. 40-41.

Rubenach, M.J. and Lewthwaite, K.J., 2002. Metasomatic albitites and related biotite-rich schists from a low-pressure polymetamorphic terrane, Snake Creek Anticline, Mount Isa Inlier, north-eastern Australia: microstructures and P-T-d paths. Journal of Metamorphic Geology, 20: 191-202.

Rubenach, M.J., & Oliver, N.H.S., 2005. Geochemical and stable isotope studies of albitites and associated metasomatic rocks, Soldiers cap Group, and implications concerning fluid sources and mineralization. I2+3 Final Report, pmdCRC.

Ryburn, R., Wilson, I.H., Grimes, K.G. and Hill, R.M., 1988. Cloncurry, Queensland, 1:100 000 geological map commentary. Bureau of Mineral Resources, Canberra.

Sayab, M., 2005. N-S shortening during orogenesis in the Mt Isa Inlier: the preservation of W-E structures and their tectonic and metamorphic significance. Unpubl. PhD thesis, James Cook University. Pmd-CRC report

Southgate, P.N, et al., 2000. Chronostratigraphic basin framework for Palaeoproterozoic rocks (1730-1575) in northern Australia and implications for base metal mineralization. Australian J. Earth Sciences 47, 461-483.

Spear, F.S., 1995. Metamorphic phase equilibria and pressure-temperature-time paths. Mineralogical Society of America Monograph, Washington. 799 pp.

Spikings, R.A., Foster, D.A., Kohn, B.P. and Lister, G.S., 2001. Post-orogenic (<1500 Ma) thermal history of the Proterozoic Eastern Fold Belt, Mount Isa Inlier, Australia. Precambrian Research, 109: 103-144.

Weston, R., 2000. An overview of the structure, metamorphism, petrology, paragenesis and geochemistry of the Houdini Prospect, Cloncurry District, Mount Isa Inlier, NW Queensland. Unpubl. BSc Hons. Thesis, James Cook University

Williams, P.J., 1998 a. Metalliferous economic geology of the Mount Isa Eastern Succession, Queensland. Australian Journal of Earth Sciences, 45: 329-342.

Williams, P.J., 1998 b. Magmatic iron enrichment in high-iron metatholeiites associated with 'Broken Hill-type' Pb-Zn-Ag deposits, Mount Isa Eastern Succession. Australian Journal of Earth Sciences, 45: 389-396.

Revised chronostratigraphy for the Mount Isa Inlier with emphasis on the Eastern Succession

Damien Foster, James Austin
School of Earth Sciences, James Cook University, Townsville QLD 4811

ABSTRACT

The chronostratigraphic and magmatic framework for the Proterozoic Mount Isa Inlier, northwest Queensland has been substantially revised to match insights provided by radiometric age constraints accumulated over recent years. This material and existing chronometric constraints is used to construct a new time-space plot for the Inlier and to compare Eastern Succession volcanosedimentary accumulations with temporally equivalent units in the Western Fold Belt. The accumulation of volcanosedimentary sequences in the Eastern Succession occurred in four main periods: namely 1890-1850 Ma, 1800-1725 Ma, 1710-1690 Ma, and 1680-1610 Ma. Temporally equivalent units can be identified in the Western Fold Belt. Periods of sedimentary accumulation were immediately preceded by bimodal igneous activity across the Inlier. The locus of bimodal volcanism migrates from west to east with time.

The majority of the Soldiers Cap Group was deposited between ca. 1675-1650 Ma with the exception of units in the Boomarra Horst now known to belong to older sequences (deposited ca. 1775-1750 Ma), and the Llewellyn Creek Formation at Snake Creek that is likely to be overlain unconformably by the Mount Norna Quartzite. Upper amphibolite facies rock units in the southwest (e.g. the Gandry Dam Gneiss) are likely to be higher metamorphic grade, temporal equivalents of the Soldiers Cap Group. Five rock units previously assigned to the cover sequence 2 Mary Kathleen Group; namely, the Answer Slate, Kuridala Formation, Staveley Formation, Marimo Slate and Agate Downs Siltstone are now known to have been deposited between ca. 1675-1610 Ma. These units (bar the Kuridala Formation) have been removed from the cover sequence 2 Mary Kathleen Group and given the informal name 'Young Australia Group'. The Kuridala Formation has been included in the Soldiers Cap Group. The rock units within the Young Australia Group are likely to be lateral facies equivalents of the Soldiers Cap Group. Rock units within the mount Albert Group (although undated) are considered likely to be temporal equivalents of the Soldiers Cap Group and the Young Australia Group. The Roxmere Quartzite is included here in the Young Australia Group that it tectonically overlays. The Ballara Quartzite and Mitakoodi Quartzite represent a single regionally extensive sequence deposited at ca. 1755 Ma. The Double Crossing Metamorphics (previously mapped as basement) are likely to correlate with the Argylla Formation and Mitakoodi Quartzite. EMP (electron microprobe) U-Th-Pb dating of the Quamby Conglomerate supports deposition of this unit after ca. 1640 Ma and prior to ca. 1500 Ma.

Most of the Eastern Succession to the west of the Pilgrim Fault is likely to have been a topographic high between ca. 1780-1755 Ma, prior to the Ballara Quartzite unconformably overlying the ca. 1780 Ma Argylla Formation. Detrital zircons of 'Argylla' and 'Wonga'

ages indicate that the Mary Kathleen Belt is likely to have been a topographic high at least periodically during accumulation of the Soldiers Cap and Young Australia Groups. Soldiers Cap Group units in the southeast contain numerous detrital zircons giving ages between ca. 1730-1710 indicating a possible siliciclastic source to the east. The host rocks to the Pb-Zn-Ag deposits are restricted to cover sequence 3 units deposited between ca. 1680-1590 Ma and, with the exception of Century, young from the southeast towards the northwest. Cu ± Au deposits and prospects are hosted in units from all the major periods of volcanosedimentary accumulation, however many of the most significant deposits are found within the younger sequences.

Keywords. Mount Isa Inlier, stratigraphy, geochronology, time-space plot

1. INTRODUCTION

The construction of any 3D model of the crust is heavily dependent on the temporal and spatial relationships of the various elements that make up the upper crust. The serial cross section approach used for building the model of the Eastern Succession (Blenkinsop et al., 2005) required the best available understanding of the chronostratigraphic framework for the region. This framework is also of critical importance in placing the host rocks to the major mineralising events within discrete temporal and stratigraphic windows. Of recent times, the standard reference template for the Mount Isa Inlier has been the chronostratigraphic compilation (and 1:500,000 map) of Blake (1987). However, a sustained effort over the last decade has garnered a considerable body of new depositional, magmatic, and metamorphic age constraints for the Mount Isa Inlier. These new data allow a comprehensive re-evaluation of the stratigraphic relationships within the Inlier. Recent publications have gone some way towards this (e.g. Page and Sun, 98; Page et al., 2000; Southgate et al., 2000a; and the Proterozoic event stratigraphy compilation of Hinman within the North-west Queensland Mineral Province Report of 2000). However, of these, only the Mineral Province Report addresses the Inlier as a whole, and significant new data has been obtained since this publication. Additionally, no new maps have been produced to reflect our changing understanding of the chronostratigraphy. The following report presents a new chronostratigraphic framework for the Mount Isa Inlier that takes advantage of all the currently available age constraints. The report is focused on stratigraphic relationships within the Eastern Succession but includes discussion of possible links with the Western Fold Belt.

2. PREVIOUS STRATIGRAPHIC DIVISIONS

The Mount Isa Inlier is an extensive area of exposed mid-Proterozoic rocks in northwest Queensland, the formation of which has been attributed to two early-mid Proterozoic tectonostratigraphic cycles (Etheridge et al., 1987). Remnants of cycle one form the basement to the inlier and were metamorphosed to amphibolite facies during the Barramundi Orogeny at *ca*. 1900-1870 Ma (Blake, 1987). Basement units include the Plum Mountain Gneiss in the east and the Yaringa Metamorphics, Saint Ronans Metamorphics and Kurbayia Migmatite in the west (Figure 1). The basement rocks were overlain by a sequence of sediments and volcanics that were subsequently deformed and metamorphosed by the Isan Orogeny of *ca.* 1600-1500 Ma (Blake and Stewart, 1992; Page and Sun, 1998). The inlier has conventionally been divided into three north-south trending tectonic units on the basis of major faults or fault zones (Blake, 1987; Blake and Stewart, 1992), namely: the Western Fold Belt (comprised of the Lawn Hill Platform and the Leichhardt River Fault Trough); the central Kalkadoon-Leichhardt Belt; and the Eastern Fold Belt (Figure 1).

The post-Barramundi Orogeny sedimentary and volcanic accumulations have been interpreted as the result of three periods of intracratonic rifting and divided into three cover sequences on the basis of regional scale unconformities (Blake, 1987; Blake and Stewart, 1992). Recent geochronological, sequence stratigraphic and structural studies within the western half of the inlier have led to suggestions that basin formation and sedimentation was more complicated than the three discrete cover sequences model (Page and Sweet, 1998; Betts et al., 1998; Page et al., 2000; Southgate et al., 2000a, b). Cover sequence 1 (ca.1870-1850 Ma) is restricted to the Kalkadoon-Leichhardt Belt and is dominated by felsic volcanics. Cover sequence 2 (ca.1790-1690 Ma) includes the calc-silicate rocks of the Corella Formation, and felsic volcanics of the Argylla Formation (Tewinga Group) that

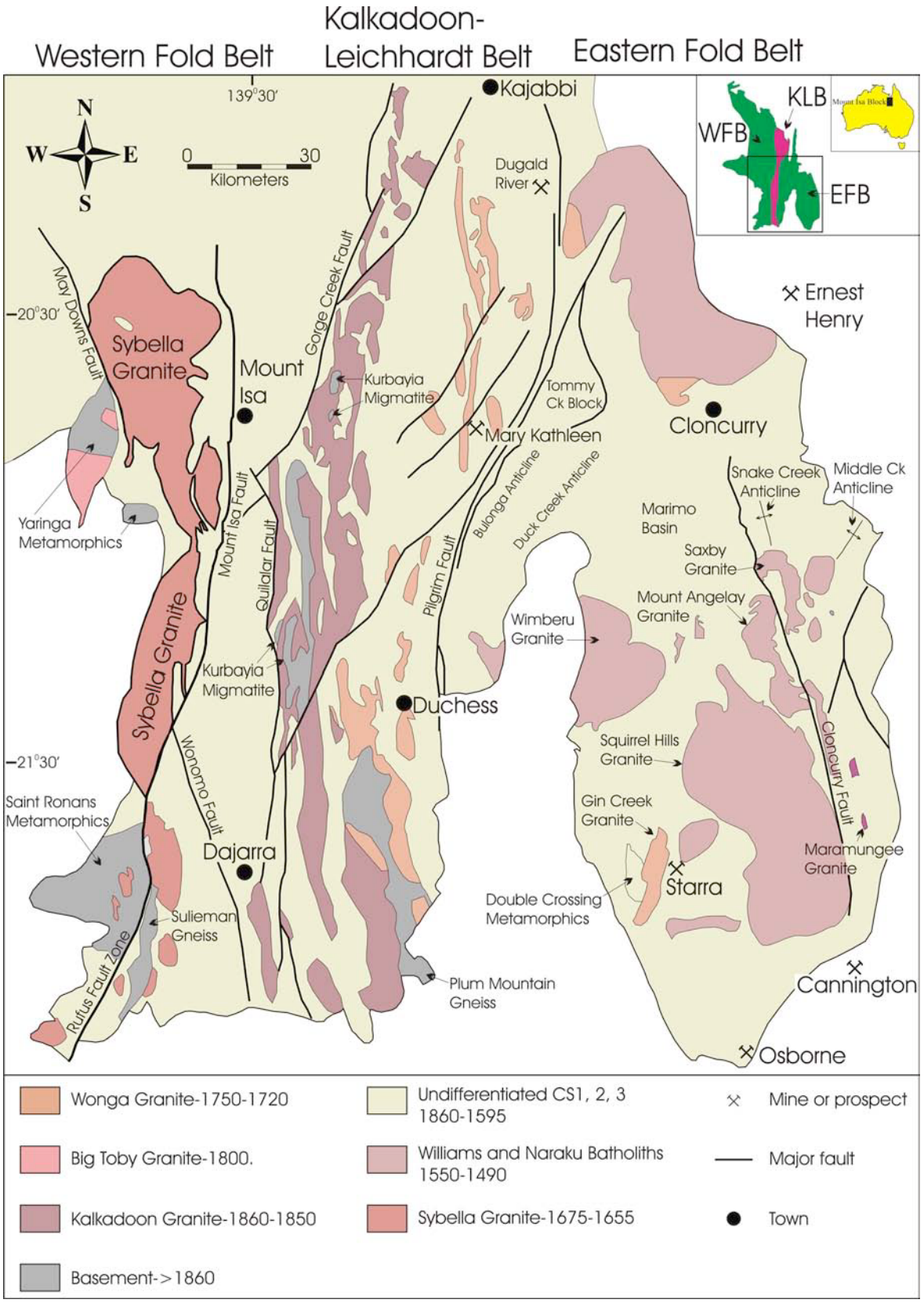

Figure 1. Simplified Geology of the southern Mount Isa Inlier showing the location (inset) and the threefold division into north-south trending zones marked out by major faults and/or granitic batholiths. Also highlighted is the distribution of basement, granite suites, major mines and prospects and key locations referred to in the text. Geology adapted from Blake (1987).

outcrop over a large part of the Eastern Fold Belt (Figure 2). The Eastern Creek Volcanics of the Haslingden Group are one of the most extensive components of cover sequence 2 in the Western Fold Belt. Important components of cover sequence 3 (1680-1610 Ma) include the Mount Isa Group in the West and the Soldiers Cap Group (formally assigned to cover sequence 2) in the East. A series of linear batholith scale granitic intrusives were emplaced contemporaneously with the deposition of the cover sequences (Figures 1, 2). These include the Kalkadoon Granite (cover sequence 1), Wonga Granite (cover sequence 2), and the Sybella Batholith (cover sequence 3). Additionally, the Williams and Naraku Batholiths crop out over a large area in the Eastern Fold Belt and were emplaced in late-syn to post Isan Orogeny time. Mafic dykes are a ubiquitous component of the Mount Isa Inlier and range in age from pre Barramundi to 1100 Ma (Blake and Stewart 1992).

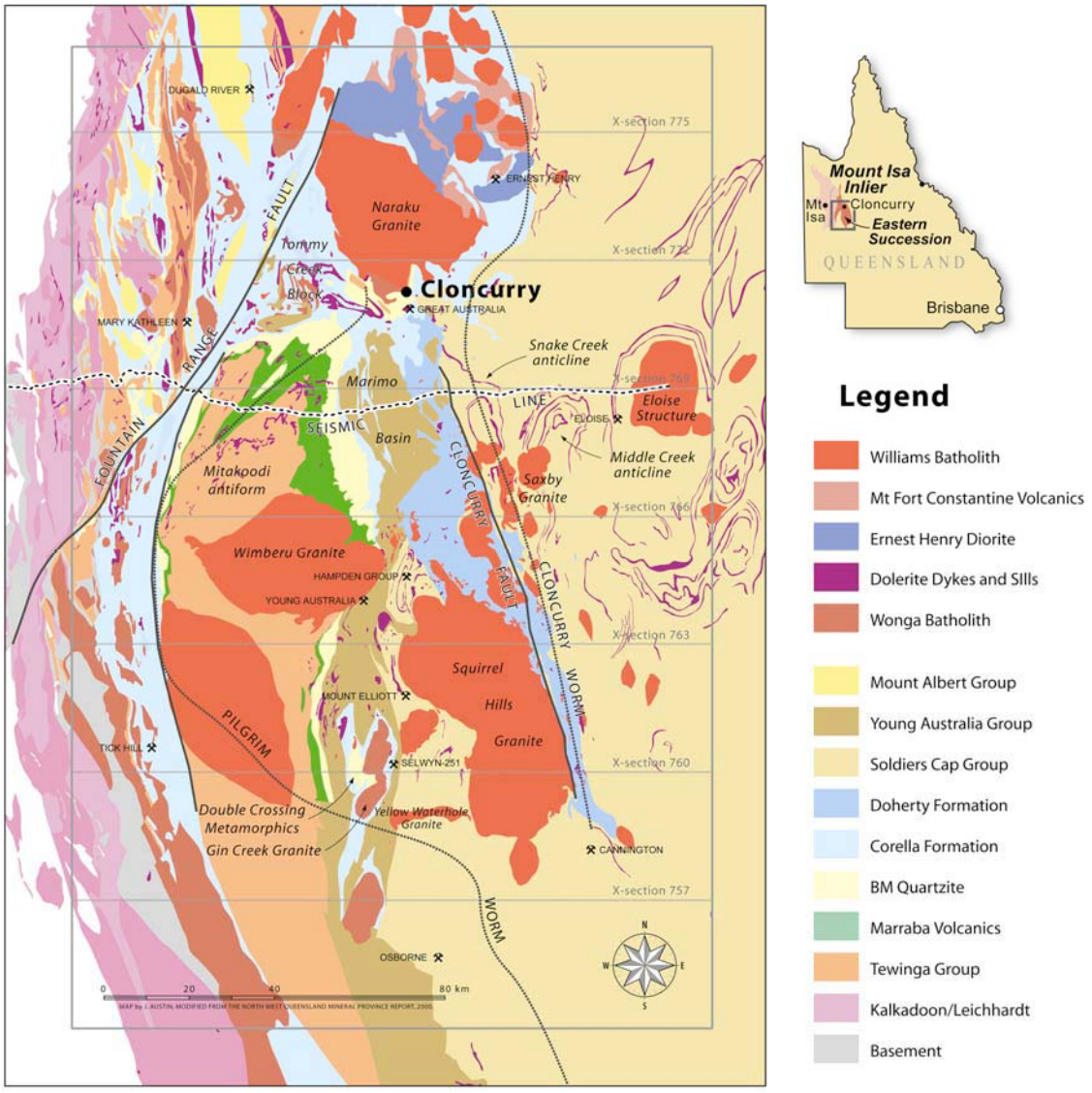

Figure 2. Simplified geology of the Eastern Fold Belt, modified from the NWQMPR (original geology after Blake, 1987) to incorporate new geochronological data. The 'Young Australia Group' is an informal name assigned here to units in the Marimo-Staveley area, previously assigned to the Mary Kathleen Group (cover sequence 2) but now known to belong to the much younger cover sequence 3 (discussed below). The Ballara and Mitakoodi Quartzites are combined into a single unit on the map (BM Quartzite). The grey east-west lines refer to cross-sections discussed in Blenkinsop et al. (2005). The 'Pilgrim Worm' and 'Cloncurry Worm' refer to geophysical features discussed in Blenkinsop et al. (2005).

3. CHRONOSTRATIGRAPHIC CHART

A revised chronostratigraphic chart for the Mount Isa Inlier is presented in Figure 3. The stratigraphic template of Blake (1987), and the compilations of Blake and Stewart (1992), Page and Sun (1998), Page and Sweet (1998), and Page et al. (2000) were used as the starting point for the construction of the new chronostratigraphy. The chart coverage is that of the 1:500,000 Mount Isa Inlier map of Blake (1987) with the exception of the South Nicholson Basin in the far northwest of the map sheet. The geology is simplified somewhat by omission of some of the smaller units with only limited exposure, e.g. the Makbat and Stanbroke Sandstones (possible correlatives of the Ballara Quartzite) that crop out in the southern Kalkadoon-Leichhardt Belt. The nomenclature of units, and stratigraphic relationships, are as described in Blake (1987) except where new age constraints render these obsolete. The division of the stratigraphy into 3 cover sequences is after Blake (1987), whereas the division into the Leichhardt, Calvert and Isan supersequences and delineation of the "Big", "Gun", "River" and "Wide" events is after Jackson et al. (2000), Scott et al. (2000), and Southgate et al. (2000a, b).

Age determinations shown on the figure represent a summary of all available published material and are drawn from a range of sources although the majority come from the vast body of work done by Rod Page in this terrane. Age determinations that add little to the summary have been omitted from the figure e.g. where they contain large errors that overlap with more precise ages for the same unit, and/or where they duplicate results for the same unit. Age determinations for individual stratigraphic units or intrusions are all U-Pb zircon determinations (mostly via SHRIMP) bar the pegmatites at Osborne (U-Pb titanite) and anatexis at Cannington (SHRIMP U-Pb monazite). Metamorphic ages (Mt) include U-Pb zircon and monazite (SHRIMP), and Sm-Nd garnet determinations. Depositional ages for sedimentary units have been obtained from felsic tuffs or extrusive felsic volcanics. Ages obtained from zircon populations that are considered by the authors to be detrital in origin constrain only the maximum possible age for the unit and are indicated in the figure by the addition of less than '<' at the front of the age. More detailed information about the age determinations can be found in Page et al. (2000), Page and Sun (1998), Page and Sweet (1998), Page (1978, 1983, 1998), Page and Bell (1986), Connors and Page (1995), Blake (1987), Blake and Stewart (1992), Pollard and McNaughton (1997), Pollard et al. (1998), Pearson et al. (1992), Gunter (1996), Mark et al. (2001, 2005), Davis et al. (2001), Rubenach et al. (2001), Hoadley et al. (2001), Giles and Nutman (2002, 2003), Hand and Rubatto (2002), Bierlein and Black (2005), Neumann et al. (2005), and Rubenach (2005).

4. MAJOR CHANGES

This section describes the stratigraphic changes necessitated by the recently acquired geochronological data (Figure 3), and suggests some other possible correlations between units for which there is as yet, no or limited chronometric support. The most significant changes to the Eastern Succession include the age and distribution of the Soldiers Cap Group, the delineation of the informally named Young Australia Group, removal of the Double Crossing Metamorphics from a basement classification, a probable Proterozoic age for the Quamby Conglomerate, and the (uncertain) status of the Mount Albert Group.

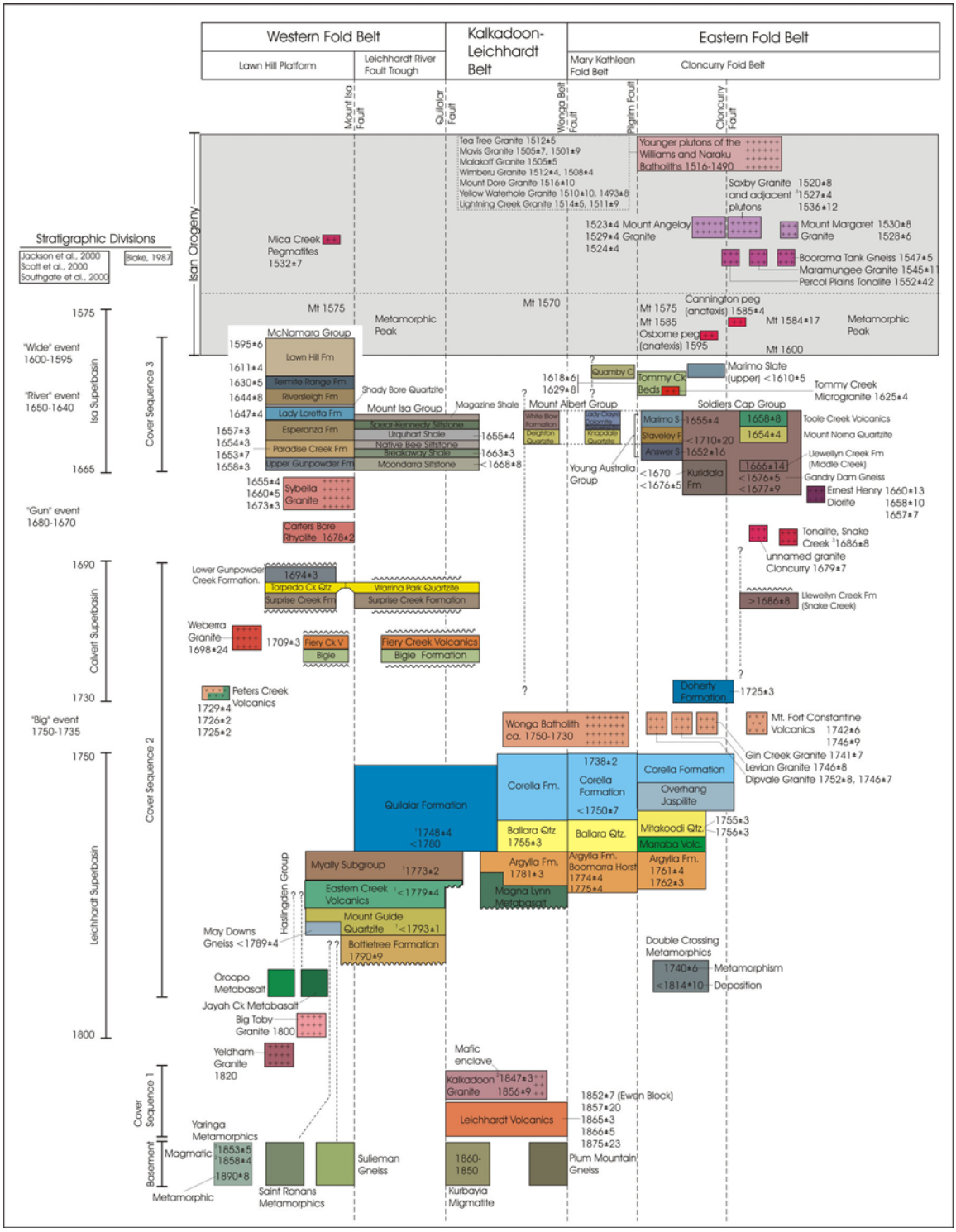

Figure 3. Revised chronostratigraphic framework (time-space plot) for the Mount Isa Inlier. Modified from the compilations of Blake (1987), Blake and Stewart (1992), Page and Sun (1998), Page and Sweet (1998), Page et al. (2000), and Foster (2003). The division of the stratigraphy into three cover sequences is after Blake (1987), whereas the division into the Leichhardt, Calvert and Isan supersequences and delineation of the 'Big', 'Gun', 'River' and 'Wide' events is after Jackson et al. (2000), Scott et al. (2000), and Southgate et al. (2000a, b). [1]New ages of Neumann et al. (2005), [2]new ages of Bierlein and Black (2004), [3]new ages of Rubenach (2005).

4.1 Soldiers Cap

4.1.1 Previous interpretations

Rock units assigned to the Soldiers Cap Group occupy the largest portion of the Eastern Fold Belt, although outcrop is generally poor in the east and south, and much of the area assigned to this unit in Figure 2 is interpreted. The Soldiers Cap Group consists of (from oldest to youngest): the Llewellyn Creek Formation, the Mount Norna Quartzite, and the Toole Creek Volcanics. These formations are delineated in the Snake Creek area between Cloncurry and the Saxby Granite (Figure 2) with a large proportion of the remainder mapped as undifferentiated Soldiers Cap. The poor outcrop in many areas, and generally tectonic contacts elsewhere (Blake, 1987) made it difficult to place this unit within the overall stratigraphic succession. The approximate parallelism of bedding across the calc-silicate breccias marking the contacts with the Corella and Doherty Formations indicated a possible conformable or disconformable relationship (Blake, 1987). In light of this the Soldiers Cap Group was placed within Cover Sequence 2, and considered likely to be older than the Corella and Doherty Formations (Blake, 1987).

Based on mapping in the Cloncurry-Selwyn area, Beardsmore et al. (1988) divided the undifferentiated Soldiers Cap between the three named units within the Group, namely the Llewellyn Creek Formation, the Mount Norna Quartzite, and the Toole Creek Volcanics, and assigned the rest (high-grade metamorphic rocks in the southwest) to a feldspathic metasedimentary unit they termed the Fullarton River Group. The Fullarton River Group as defined by these authors consists of the Gandry Dam Gneiss (oldest) overlain by the Glen Idol Schist. In this scheme the Fullarton River Group is considered to be conformably overlain by the Soldiers Cap Group. Previous workers (e.g. Blake, 1987) had suggested that the Kuridala Formation (belonging to the Mary Kathleen Group to the west) merged into the Soldiers Cap Group in the south. Beardsmore et al. (1988) continued this theme by removing the Kuridala Formation from the Mary Kathleen Group and dividing it into four units, correlating the upper three with the named units within the Soldiers Cap Group, and the lowermost unit (termed the New Hope Arkose) with the newly defined Glen Idol Schist.

Beardsmore et al. (1988) placed the expanded Soldiers Cap Group (including the upper three units of the Kuridala Formation) and the Fullarton River Group (including the basal Kuridala unit) into a conformable sequence they termed the Maronan Supergroup. The Double Crossing Metamorphics and adjacent Gin Creek Granite (Figure 1) were inferred to have been tectonically emplaced, with the Double Crossing Metamorphics correlating with the Fullarton River Group. On the basis of perceived differences in the range of contained lithologies, metamorphic grade, and the geochemistry and geophysical response of volcanic units, Beardsmore et al. (1988) suggested that the newly defined Maronan Supergroup formed in an early volcanosedimentary cycle that probably predated others in the Mount Isa Inlier. They suggested that it was deposited in the interval 1890-1810 Ma. Lang and Beardsmore (1986) and Lang (1990) further suggested that the Maronan Supergroup was an allochthonous terrane (linked to the Broken Hill and Georgetown blocks) and that it had been thrust over the younger Mount Isa terrane from the east.

4.1.2 Current status

U-Pb-zircon age determinations obtained in the last seven years from the Soldiers Cap Group (including the Gandry Dam Gneiss of Beardsmore et al., 1987) and the Kuridala

Formation indicate an unequivocally young (Cover Sequence 3) depositional age for these units (Page and Sun, 1998; Page 1998; Giles and Nutman, 2003). Depositional ages (or maximum depositional ages) from the Toole Creek Volcanics (1658 ± 8 Ma), Mount Norna Quartzite (1654 ± 4 Ma, <1693 ± 5 Ma), Llewellyn Creek Formation (<1666 ± 14 Ma), Kuridala Formation (<1676 ± 5 Ma), and the Gandry Dam Gneiss (< 1676 ± 5 Ma, <1677 ± 9 Ma) point to deposition of the majority of the Maronan Supergroup of Beardsmore et al. (1988) between ca. 1675-1650 Ma. This renders obsolete the suggestion by Beardsmore et al. (1988) that the Soldiers Cap formed part of an earlier volcanosedimentary cycle deposited in the interval 1890-1810 Ma. Depositional ages of 1775 ± 4 Ma and 1774 ± 4 Ma have been obtained from units previously mapped as undifferentiated Soldiers Cap in the Boomarra Horst, a north-trending structural unit, starting to the northeast of Dugald River (Page and Sun, 1998). These units consist of quartzite, schist, amphibolite, and minor calc-silicates and felsic metavolcanics and are thought to be overlain, possibly conformably, by calc-silicate units mapped as Corella Formation (Blake, 1987). The age constraints, relationship with the Corella Formation, and lithological units present, indicate that these units are likely correlatives of the Argylla Formation and Ballara Quartzite (Cover Sequence 2) and can be safely removed from the Soldiers Cap Group.

The Llewellyn Creek Formation in the core of the Snake Creek Anticline (Figure 1) may be older than the range suggested by the depositional ages above. At this location the Llewellyn Creek Formation is intruded by a tonalite that has recently been dated via the U-Pb SHRIMP technique at 1686 ± 8 Ma (Rubenach, 2005). The tonalite mingles with a layered gabbro and other intrusive rocks. This relationship indicates a *minimum* depositional age of ca. 1680 Ma for this Formation. However, a maximum depositional age of <1666 ± 14 Ma has been obtained from a unit mapped as Llewellyn Creek Formation in the Middle Creek Anticline to the east-southeast of the Snake Creek Anticline (Giles and Nutman, 2003). A maximum depositional age of <1676 ± 5 Ma obtained for the probably correlative Kuridala Formation supports the younger age above. Although the latter two ages are within error of the age for the tonalite, they are strictly *maximum* ages obtained from the youngest groupings of detrital zircons analysed. Both the samples contain numerous older detrital grains indicating that the ages obtained from the youngest concordant groupings are unlikely to be actual depositional ages for these units which may be nearer to the ca. 1660-1650 Ma ages obtained for the overlying Mount Norna Quartzite and Toole Creek Volcanics. The age populations of detrital zircons from the above two samples overlap with those obtained from the Gandry Dam Gneiss (Figure 7) indicating a shared source and the likelihood of similar depositional ages (e.g. Page and Sun, 1998; Giles and Nutman, 2003). If this is the case then the depositional age of the Llewellyn Creek Formation, Kuridala Formation and the Gandry Dam Gneiss would need to be near the maximum depositional ages common to several of the samples (ca. 1676 Ma) in order to accommodate the age of the tonalite intrusion at Snake Creek. This would imply a considerable time gap of ca. 20 my between deposition of these units and the overlying Mount Norna Quartzite and Toole Creek Volcanics (ca. 1655 Ma). This would require either slow sedimentation rates or, more likely, the presence of an unconformity located somewhere within the upper Llewellyn Creek Formation or the lower Mount Norna Quartzite (Figure 3; inset in Figure 4). An alternative hypothesis would be that the Llewellyn Creek Formation in Snake Creek is an older unit and does not correlate with lithologies mapped as Llewellyn Creek Formation in the Middle Creek Anticline, nor with the Kuridala Formation and Gandry Dam Gneiss. This hypothesis would also indicate the presence of an unconformity in this area. A third hypothesis is that the preferred magmatic

crystallisation age of the Snake Creek tonalite may not be an accurate reflection of its emplacement age. If this is the case then there would be no requirement for an unconformity within this unit, or for a large time gap between this and overlying units.

4.1.3 Stratigraphic nomenclature

The term 'Maronan Supergroup' was originally conceived to describe a conformable sequence that had the three mapped units within the Soldiers Cap (Toole Creek Volcanics, Mount Norna Quartzite and Llewellyn Creek Formation) overlying the older and newly defined Fullarton River Group (New Hope Arkose, Glen Idol Schist and Gandry Dam Gneiss). The geochronology to date does not support this division of the original Soldiers Cap into older (Fullarton River Group) and younger (Soldiers Cap Group) segments of a conformable sequence although it does not preclude it entirely (Figure 3). However it does support correlations suggested between the Kuridala Formation and the Soldiers Cap Group (e.g. Blake, 1987; Beardsmore et al. 1988). The approach taken in this report is to continue usage of the term 'Soldiers Cap Group' with the three sub-units as defined by Blake, but expanded to include the Kuridala Formation as a lateral continuation of this group. As the geochronology indicates that the proposed 'Fullarton River Group' is likely to be high metamorphic grade lateral equivalents of the named subunits of the Soldiers Cap Group, the use of this term is avoided here. Usage of the term 'Maronan Supergroup' is also avoided for the same reason. The three subunits of the Fullarton River Group (New Hope Arkose, Glen Idol Schist and Gandry Dam Gneiss) might be retained as geographically separate map units as delineated by Beardsmore et al. (1988) subject to future stratigraphic mapping and geochronology. If these do indeed turn out to be older than and overlain conformably by the Llewellyn Creek Formation then the names 'Fullarton River Group' and 'Maronan Supergroup' may be reinstated.

4.2 Young Australia Group

The Mary Kathleen Group as defined by Blake (1987) is the other major lithological grouping (along with the Soldiers Cap and the Tewinga Group) in the Eastern Succession. Recent geochronology has revealed that much of the Mary Kathleen Group is younger than previously thought. The younger elements of this group are reassigned here (as described below) into the informally named 'Young Australia Group'.

4.2.1 Previous interpretations

Lithological units previously mapped as members of the Mary Kathleen Group outcrop extensively between the Kalkadoon-Leichhardt Belt and the Pilgrim Fault, and east of the Pilgrim Fault (Figures 1, 2). West of the Pilgrim Fault this group consists of the Ballara Quartzite and the Corella Formation. Units outcropping to the east of the Pilgrim Fault are: the Overhang Jaspilite, the Answer Slate, the Kuridala Formation, the Staveley Formation, the Marimo Slate, the Agate Downs Siltstone, the Doherty Formation, and the Corella Formation. The calc-silicate dominated Corella and Doherty Formations are the most prominent units in the group.

The Mary Kathleen Group was assigned to Cover Sequence 2 in the scheme of Blake (1987). The Doherty and Corella Formations were thought to be the youngest members of the group. These two units were thought to possibly overlie the Soldiers Cap Group in the east (discussed above). The Overhang Jaspilite was considered to be a basal unit in the Mary Kathleen Group. The remainder of the Mary Kathleen Group in the east (the Answer Slate, the Kuridala Formation, the Staveley Formation, the Marimo Slate, and the Agate Downs Siltstone) outcrop in a narrow north-south trending belt starting just to the south of

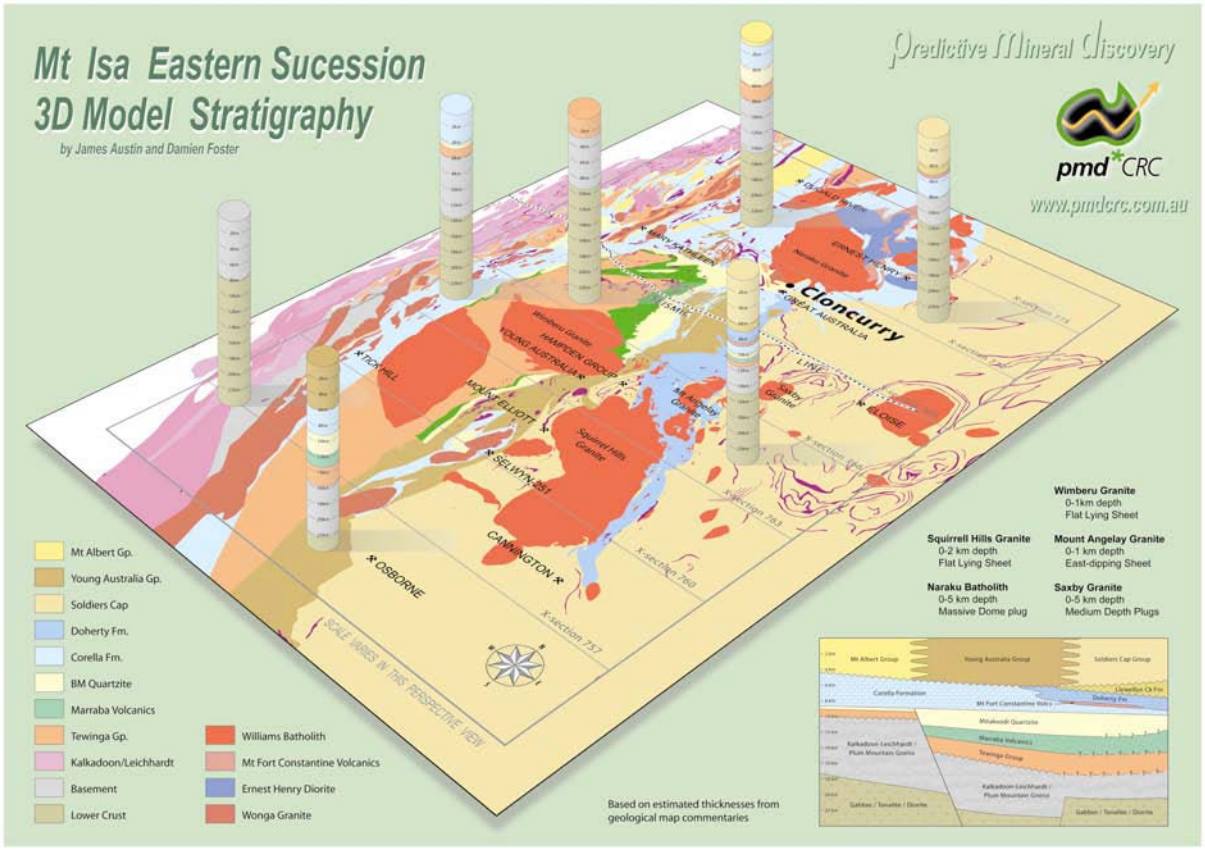

Figure 4. Mount Isa Eastern Succession 3D model stratigraphy. The inset shows schematic depositional model for cover sequence 2 and 3 sedimentary units in the east prior to tectonic shortening. The relative thickness of individual units are consistent with published maximum thicknesses from the literature.

Cloncurry and extending to south of the Gin Creek Granite and Double Crossing Metamorphics (Figures 1, 2). The basal unit was considered to be the Answer Slate which was thought to merge laterally with the Kuridala Formation in the east, with both inferred to be overlain by the Stavely Formation, which was in turn overlain conformably (or interfingered with) the Marimo Slate. The Stavely Formation was also overlain conformably by the Agate Downs Siltstone in the centre-west of the belt (likely to be a lateral facies equivalent of the Marimo Slate). The Marimo Slate was thought to be overlain conformably by the Corella Formation. The Corella Formation is intruded by various plutons of the Wonga Batholith in the Mary Kathleen Belt indicating that much of this unit was deposited prior to ca. 1740-1730 Ma.

4.2.2 Current status

Recent depositional age determinations for the Mary Kathleen Group demonstrate that it contains units of both Cover Sequence 2 and Cover Sequence 3 age (Figure 3). The calc-silicate dominated Corella Formation and Doherty Formation (and the Ballara Quartzite) belong to Cover Sequence 2, whereas all the remaining units appear to belong to Cover Sequence 3. The exception to the above is the Tommy Creek sequence (Figure 1) where units mapped as Corella Formation give Cover Sequence 3 ages (including some of the youngest ages in the Mount Isa Inlier). A depositional age of 1755 ± 3 Ma was obtained from the basal Ballara Quartzite in the west, whereas ages of <1750 ± 7 Ma and 1738 ± 2 Ma were obtained from the Corella Formation in the Mary Kathleen Fold Belt (Page, 1998; Page, Geoscience Australia Ozchron database). The Overhang Jaspilite and the Chumvale Breccia are assumed to correlate with the Corella Formation in this system (Figure 5). The Doherty Formation (1725 ± 3 Ma; Page and Sun 1998) in the east appears to be slightly younger than the Corella Formation in the west and is interpreted here as a lateral facies equivalent of the Corella Formation that it probably overlies in the east (Figure 5).

A depositional age of <1676 ± 5 Ma has been obtained from the Kuridala Formation (Page, Geoscience Australia Ozchron database). The Kuridala Formation outcrops between the Squirrel Hills Granite and the Gin Creek Granite and, as indicated above, is included here in an expanded Soldiers Cap Group (Figure 2). The removal of the Kuridala Formation (and the Cover Sequence 2 units) leaves the Answer Slate, the Staveley Formation, the Marimo Slate, and the Agate Downs Siltstone (and parts of the Tommy Creek sequence) outcropping in a northerly trending belt between the Doherty and Kuridala Formations in the east, and the Overhang Jaspilite in the west (Figure 2). Depositional ages for the basal Answer Slate (<1652 ± 16 Ma), Staveley Formation (<1710 ± 20 Ma) and Marimo Slate (1655 ± 4 Ma), place this group within Cover Sequence 3. However a depositional age of 1610 ± 5 Ma has also been obtained from the Marimo Slate indicating a more complicated depositional history than outlined here. This complexity also occurs within the Tommy Creek Block (Figure 1) which yields maximum depositional ages of 1758 ± 4 Ma and 1762 ± 5 Ma near the base of the sequence, an age of 1650 ± 3 Ma in the west of the Block, and ages of 1629 ± 8 Ma and 1618 ± 6 Ma in the south (Page, 1998; Page and Sun, 1998).

4.2.3 The informal 'Young Australia Group'

The unequivocally young (Cover Sequence 3) ages of the Answer Slate, the Kuridala Formation, the Staveley Formation, the Marimo Slate, and (by inference) the Agate Downs Siltstone necessitates their removal from the Mary Kathleen Group as previously defined. The term 'Mary Kathleen Group' is best retained for the older (Cover Sequence 2) group as the Corella Formation is by far the most extensively outcropping unit within the Group, and it outcrops in the Mary Kathleen zone (unlike the younger units above). The rump

Mary Kathleen Group would then consist of the Corella and Doherty Formations, the Overhang Jaspilite, the Chumvale Breccia, the Ballara Quartzite, and the temporally equivalent Mitakoodi Quartzite (see below). In this report the informal term 'Young Australia Group' is used for the younger (Cover Sequence 3) grouping of the Answer Slate, the Staveley Formation, the Marimo Slate, and the Agate Downs Siltstone (Figures 2-6). The Lalor Beds within the Tommy Creek Block are included within this group in the interpreted geology map (Figure 2). The name is taken from the former Young Australia mine located in the Answer Slate to the southeast of the Wimberu Granite (Figure 2). The Young Australia Group is considered here to be lateral facies equivalents of the Soldiers Cap Group.

4.3 Mitakoodi Quartzite, Ballara Quartzite equivalence

The Mitakoodi Quartzite is a thick quartzite- and sandstone- dominated unit (also containing minor metabasalt and felsic porphyry) that crops out to the east of the Pilgrim Fault where it helps to define the Mitakoodi Antiform, the most prominent structural feature of the Eastern Succession (Figure 2). This unit has an estimated maximum thickness in the east of ca. 3000 metres, and thins towards the Pilgrim Fault in the west (Blake, 1987). Units mapped as Ballara Quartzite crop out between the Kalkadoon-Leichhardt Belt and the Wonga Belt, and between the Wonga Belt and the Pilgrim Fault (Figures 1, 2). There are lithological similarities between the Mitakoodi Quartzite and the Ballara Quartzite with the latter also being predominantly sandstone and quartzite, with minor metabasalt and felsic tuff. The Ballara Quartzite is thickest (ca. 1250 metres) in the west, but is as thin as 80 metres between the Wonga Belt and the Pilgrim Fault in the east (Blake, 1987).

Previous workers have suggested that the Pilgrim Fault may represent a terrane boundary with probable transcurrent displacement of several hundred kilometres (Blake and Stewart, 1988). There is some support for this idea in the geophysics where the gravity data delineates a prominent worm (Pilgrim worm) that appears to link with the Pilgrim Fault to the west of the Mitakoodi Antiform (Figure 2; and see discussion in Blenkinsop et al., 2005). However, U-Pb SHRIMP depositional ages obtained from a tuff and two felsic volcanics in these two major quartzite units that crop out to the east (Mitakoodi) and to the west (Ballara) of the fault are indistinguishable in age. A depositional age of 1755 ± 3 Ma was obtained from the basal Ballara Quartzite in the far west, adjacent to the Kalkadoon-Leichhardt Belt whereas ages of 1756 ± 3 Ma (west limb) and 1755 ± 3 Ma (east limb) were obtained from the Mitakoodi Quartzite exposed in the Duck Creek Anticline in the east (Page, 1998). This data supports the contemporaneous deposition of these two units which can now be elevated to the status of a single (regionally significant) fluvial, near shore beach, and shallow marine sequence (Blake, 1987). In this report, these two units are combined on the stratigraphic map and in the cross-sections (Blenkinsop et al. 2005) to form a single unit, the Ballara-Mitakoodi Quartzite (Figures 2, 7). This association aided considerably in construction of the cross-sections (e.g. Figure 8; Blenkinsop et al., 2005).

4.4 Double Crossing Metamorphics

The Double Crossing Metamorphics crop out to the east of the Gin Creek Granite (Figure 1). This unit consists of micaceous and feldspathic gneiss and schist, migmatitic gneiss, and minor augen gneiss, amphibolite and quartzite. It has concordant (possibly tectonic) contacts with the overlying Answer Slate and Stavely Formation that are much less deformed, and of lower metamorphic grade (Blake, 1987). For these reasons, this unit was considered to be possibly basement (deformed and metamorphosed during the Barramundi

Orogeny at *ca*. 1900-1870 Ma) and generally mapped as such, although Blake (1987) suggested that it might correlate with the Tewinga Group of Cover Sequence 2. Beardsmore et al. (1988) as discussed above, inferred that the Double Crossing Metamorphics may correlate with the high metamorphic-grade Fullarton River Group within their proposed Maronan Supergroup deposited between ca 1890-1810 Ma, and that both it and the Gin Creek Granite had been tectonically emplaced.

The geochronology of the Gin Creek Block has been clarified by the work of Page and Sun (1998). Detrital zircons from a paragneiss from the Double Crossing Metamorphics yielded age populations ranging from 2600-2500 Ma to 1850-1830 Ma and included a group at 1900-1860 Ma. Inherited zircons within a felsic leucosome that cross-cut the gneiss contained a similar range of ages, with 12 grains giving a maximum depositional age of 1814 ± 10 Ma. Magmatic crystallisation of the leucosome was timed at 1740 ± 6 Ma, within error of an age of 1741 ± 7 Ma obtained for the Gin Creek Granite to the east (Page and Sun, 1998). The age populations from the detrital zircons indicate source terranes consistent with the Mount Isa Barramundi basement, and the Kalkadoon-Leichhardt belt, both of which outcrop to the west. The probable Barramundi basement and Kalkadoon-Leichhardt belt source terranes, the maximum depositional age of ca. 1814 Ma, and the absence of any inherited zircons of Argylla Formation (ca 1780-1760 Ma) or Wonga Granite (ca 1740-1730 Ma) age indicates that the Double Crossing Metamorphics belong to Cover Sequence 2. Units mapped as Argylla Formation, Marraba Volcanics, and Mitakoodi Quartzite outcrop ca. 7 km to the west of the Double Crossing Metamorphics (Figure 2) supporting possible correlations with these lithologies as suggested by Blake (1987).

The new data demonstrate that the Double Crossing Metamorphics, along with the Gin Creek Granite, is not a tectonically emplaced basement block that correlates with the southern Soldiers Cap Group (Beardsmore et al., 1988; Laing, 1990). Rather, it forms part of Cover Sequence 2 (probable Argylla formation and Mitakoodi Quartzite correlatives) and was metamorphosed to upper amphibolite facies (with local migmitisation) by the intrusion of the Wonga Granite- aged Gin Creek Granite. These high-grade metamorphics and the Gin Creek Granite were subsequently overlaid by the Cover Sequence 3 Answer Slate and Stavely Formation. These relationships removed some of the complexity from this area with regard to construction of the geological cross-sections (Blenkinsop et al. 2005). In this report, the Double Crossing Metamorphics are shown as Mitakoodi Quartzite grading into Corella Formation on the simplified geological map (Figure 2). These units are shown extending south from the Gin Creek Granite to an interpreted (undercover) intrusion. The magnetic response of this interpreted intrusion and its margins are remarkably similar to the ca. 1740 Ma Gin Creek Granite, and unlike the younger Yellow Waterhole Granite (1493 ± 8 Ma) and Mount Dore Granite (1516 ± 10 Ma). It is interpreted here to be related to the Gin Creek Granite with both mapped as part of the ca. 1740 Ma intrusions of the Wonga Batholith (Figure 2).

4.5 Mount Albert Group

Lithological units mapped as Mount Albert Group crop out in three different zones within the Eastern Succession. In the west between the Kalkadoon Granite and the Wonga Granite, it consists of the Deighton Quartzite (feldspathic-, lithic- and quartz- sandstone) overlaid conformably and locally unconformably by pelitic and calcareous rocks of the White Blow Formation (Blake, 1987). In the Dugald River area it consists of the Knapdale Quartzite (feldspathic, quartzose, calcareous and micaceous sandstone and quartzite)

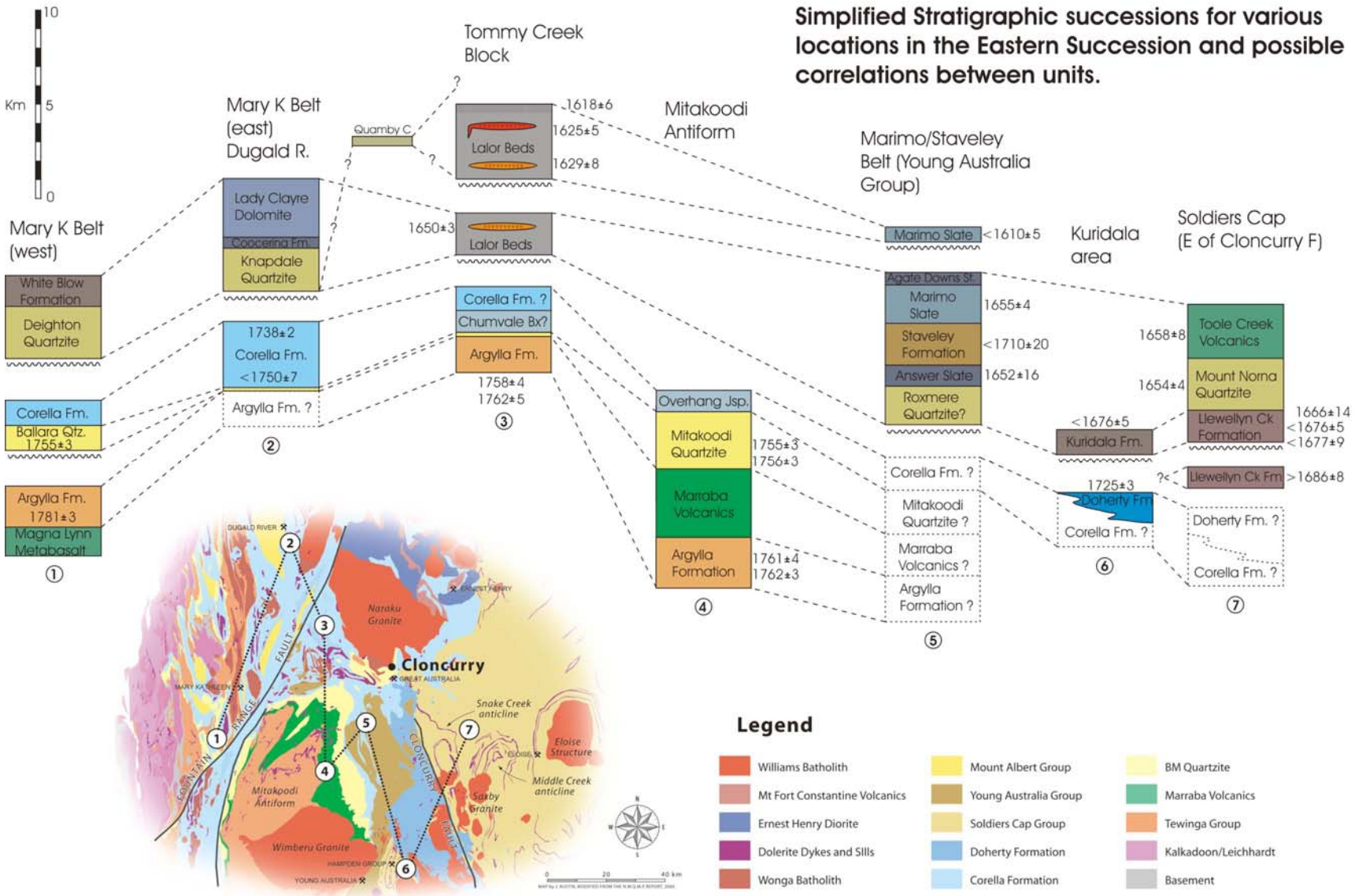
Simplified Stratigraphic successions for various locations in the Eastern Succession and possible correlations between units.
Km
10
5
0
Mary K Belt (west)
White Blow Formation
Deighton Quartzite
Corella Fm.
Ballara Qtz. 1755±3
Argylla Fm. 1781±3
Magna Lynn Metabasalt
①
Mary K Belt (east) Dugald R.
Lady Clayre Dolomite
Coccerinna Fm.
Knapdale Quartzite
1738±2
Corella Fm.
<1750±7
Argylla Fm. ?
②
Quamby C.
Tommy Creek Block
1618±6
1625±5
Lalor Beds
1629±8
1650±3
Lalor Beds
Corella Fm. ?
Chumvale Bx?
Argylla Fm.
1758±4
1762±5
③
Mitakoodi Antiform
Overhang Jsp.
Mitakoodi Quartzite
1755±3
1756±3
Marraba Volcanics
Argylla Formation
1761±4
1762±3
④
Marimo/Staveley Belt (Young Australia Group)
Marimo Slate
<1610±5
Agate Downs Sst.
Marimo Slate
1655±4
Staveley Formation
<1710±20
Answer Slate
1652±16
Roxmere Quartzite?
Corella Fm. ?
Mitakoodi Quartzite ?
Marraba Volcanics ?
Argylla Formation ?
⑤
Kuridala area
<1676±5
Kuridala Fm.
1725±3
Doherty Fm
Corella Fm. ?
⑥
Soldiers Cap (E of Cloncurry F)
1658±8
Toole Creek Volcanics
1654±4
Mount Norna Quartzite
1666±14
<1676±5
<1677±9
Llewellyn Ck Formation
?<
Llewellyn Ck Fm
>1686±8
Doherty Fm. ?
Corella Fm. ?
⑦
DUGALD RIVER
ERNEST HENRY
Naraku Granite
Cloncurry
GREAT AUSTRALIA
MARY KATHLEEN
FAULT
MOUNTAIN RANGE
Snake Creek anticline
Eloise Structure
ELOISE
Middle Creek anticline
CLONCURRY
Saxby Granite
Mitakoodi Antiform
Wimberu Granite
HAMPDEN GROUP
YOUNG AUSTRALIA
0
20
40 km
Legend
Williams Batholith
Mt Fort Constantine Volcanics
Ernest Henry Diorite
Dolerite Dykes and Sills
Wonga Batholith
Mount Albert Group
Young Australia Group
Soldiers Cap Group
Doherty Formation
Corella Formation
BM Quartzite
Marraba Volcanics
Tewinga Group
Kalkadoon/Leichhardt
Basement

Figure 5 (above). Simplified stratigraphic successions for various locations in the Eastern Succession showing possible correlations between units and available depositional age data. The inset map shows locations of the schematic stratigraphic columns (the legend applies to the inset location map). Thicknesses shown for the units are maximum thicknesses derived from the literature (mostly from Blake, 1987).

overlain conformably by calcareous black shale and scapolitic metasiltstone of the Coocerina Formation, with the latter overlain by the Lady Clayre Dolomite (Blake, 1987). In the Marimo area, several small, generally fault-bounded blocks of feldspathic and quartz sandstone are included within the Mount Albert Group as the Roxmere Quartzite (not differentiated on the map in Figure 2). The Roxmere Quartzite is considered to be either conformable, or disconformable on (or thrust over) the Corella Formation, Staveley Formation and the Marimo Slate.

There are no direct age constraints for the geographically disparate units of the Mount Albert Group other than inferences from underlying units. As they overlay the Corella Formation, and other units formally placed within the Mary Kathleen Group (Staveley Formation and Marimo Slate, now known to belong to Cover Sequence 3), they are generally taken to belong to Cover Sequence 3 and are depicted this way in the 1:500,000 map of Blake (1987). However the nature of the contacts between the basal units of the Mount Albert Group and the underlying units are generally uncertain. The contact beneath the Deighton Quartzite was considered to be an unconformity by Derrick et al. (1980) who correlated the Mount Albert Group with the Surprise Creek Formation (deposition ca. 1700-1690 Ma) in the Western Fold Belt. However, Blake (1987) reported that this contact was invariably tectonic and might represent a thrust surface. Blake (1987) also noted striking similarities between the Deighton Quartzite and overlying White Blow Formation, and the Ballara Quartzite and Corella Formation. He suggested that the Deighton Quartzite and White Blow Formation may be correlatives of the Cover Sequence 2 units, but had been thrust into their present position. The Knapdale Quartzite is apparently conformable on the Corella Formation in the Dugald River area and, along with the overlying Coocerina Formation, exhibits lithological similarities with the Corella Formation. The basal contacts of the Roxmere Quartzite in the east are commonly faults or breccia zones and may also be tectonic (Blake, 1987).

The approach taken in this report is to place the Mount Albert Group within Cover Sequence 3, and treat them as possibly lateral facies equivalents of the Soldiers Cap Group and Young Australia Group (e.g. Figures 5, 6). In the absence of any geochronological constraints, this correlation remains tentative; however, it is reasonably consistent with the present stratigraphic position of these units and lithological similarities between the groups. The fault-bounded contacts beneath the Roxmere Quartzite may indicate that these small blocks have been thrust into their current position overlying the Staveley Formation and Marimo Slate and may in fact represent the base of the Young Australia Group in this area (Figures 5, 6). This suggestion is supported by two U-Pb SHRIMP ages obtained by Page (1998) from units mapped as Marimo Slate that gave ages of 1655 ± 4 Ma and 1610 ± 5 Ma (indicating unrecognised structural complexity within this area). In this report, the Roxmere Quartzite has been removed from the Mount Albert Group and included with the Young Australia Group (Figures 2, 5, 6). If the Roxmere Quartzite does represent a basal Young Australia Group unit, then tentative correlations can be drawn between the Mount Norna Quartzite (Soldiers Cap Group), Roxmere Quartzite (now in the Young Australia Group), and the Knapdale Quartzite and Deighton Quartzite (Mount Albert Group)

4.6 Quamby Conglomerate

The Quamby Conglomerate crops out in two small fault-bounded units to the south of Dugald River adjacent to the Fountain Range Fault and the Mount Roseby Fault. It consists of ca. 300 metres of conglomerate, arkose, hematitic quartz sandstone, and greywacke, and is thought to unconformably overlie units mapped as Corella Formation (Blake, 1987). The conglomerate contains clasts of metasiltstone, schist, slate, quartzite and vein quartz (Blake, 1987). This unit was considered to have been deposited after the Isan Orogeny by Derrick (1980). Idnurm and Wyborn (1998a, b) suggested a Mesoproterozoic age of ca. 1500 Ma based on palaeomagnetic dating of arenite lenses within the Quamby Conglomerate.

A recent study by Wilde et al. (in prep.) examined samples from the abandoned Quamby gold mine (a minor Au occurrence hosted in the Quamby Conglomerate) under the petrological microscope and via scanning electron microscopy. A thin section of the pebble conglomerate was found to contain a number of ca. 100 μm monazite grains. Five of these grains were dated at James Cook University using the EMP (electron microprobe) U-Th-Pb technique. The age spectrum obtained from a total of 41 analyses indicates that these may be complex grains consisting of multiple age domains. The calculated ages cluster about three main groupings: ca. 1640 Ma (22 % of all analyses), ca. 1580 Ma (62 %), and ca. 1500 Ma (15 %). These groupings are statistically valid and supported by variable trace element chemistry. However, it is still possible that they form a single population as there are no clear textural differences representing the age groups other than weak core-rim relationships. The 1640 Ma analyses show a narrow range in trace element concentrations and include the core of the only grain to exhibit concentric zoning. The ca. 1640 domains are interpreted here as inherited components of probable igneous origin. If this interpretation is correct than it provides a maximum depositional age for the Quamby Conglomerate. The ca. 1580 Ma grouping exhibits the widest range in trace element chemistry and is likely to be of either metamorphic or hydrothermal origin. This age could reflect either 1), inherited grains of regional metamorphic affinity (peak in the Eastern Succession at ca. 1580-1600 Ma), or 2), peak metamorphic or hydrothermal monazite growth in situ in the Quamby Conglomerate, possibly associated with the crystallisation of the specular hematite. The ca. 1500 Ma age may relate to a hydrothermal event that produced thin veinlets of oxy-chlorite and finer-grained Fe-oxides that overprint the coarse-grained hematite and monazite, possibly related to the intrusion of the ca. 1500 Ma plutons of the Williams Batholith (perhaps correlating with the magnetic overprint event found by Idnurm and Wyborn, 1998b). Alternatively, it could relate to diagenetic overprinting of detrital monazite grains at this time.

If the ca. 1580 Ma monazites are the result of in situ hydrothermal or metamorphic mineral growth then the Quamby Conglomerate must be considerably older than previously supposed. The conglomerate is believed to unconformably overlie units mapped as Corella Formation. This would imply a maximum age of ca. 1740 Ma. However, in the Fountain Range Fault zone the conglomerate abuts subunits of the Corella Formation that have recently given a depositional age of 1650 ± 3 Ma (forming part of the Cover Sequence 3 rocks within the Tommy Creek Block originally mapped as Corella Formation) (Page, 1998). This relationship and the possible detrital monazite age of ca. 1640 Ma (above) indicate that, if of a Mesoproterozoic age, then the conglomerate is likely to have been deposited within Cover Sequence 3. The conglomerate is unlikely to belong to older units than this as the fault-bounded outcrops underwent only low-grade metamorphism (probably sub-greenschist) but abuts a coarse-grained andalusite schist near the southern

end of the outcrop (in the ca. 1650 Ma lithology previously mapped as Corella). The large difference in metamorphic grade implies that the Quamby Conglomerate has shifted down relative to the adjacent schist after the peak of metamorphism. Possible correlatives of the conglomerate could be: 1), the Knapdale Quartzite (the base of the Mount Albert Group) that crops out 5-10 km to the west of the Quamby Conglomerate, 2), sequences deposited between ca. 1650 Ma to 1615 Ma in the Tommy Creek Block, and 3), sequences deposited at ca. 1610 Ma in the Marimo Basin to the east (Figure 5).

In summary, the preliminary EPMA U-Th-Pb monazite study supports a Mesoproterozoic age for the Quamby Conglomerate that was probably deposited sometime after ca. 1640 Ma and before ca. 1500 Ma. The data is insufficient to determine whether the ca. 1580 Ma ages that dominate in the monazites are an inherited (detrital) component or are a result of in situ metamorphic or hydrothermal processes associated with hematite growth. The palaeomagnetic data of Idnurm and Wyborn (1998b) has to be considered carefully in answering this question. When these authors applied bedding (dip) corrections to their magnetic remanence measurements from hematite (the two Quamby Conglomerate outcrops form synclines), they halved the directional scatter. This implies that the magnetism (and hematite growth) was acquired prior to the folding event. If the Quamby Conglomerate had then been deformed and metamorphosed during the early Isan Orogeny, some resetting of the palaeomagnetism might have been expected.

5. DISCUSSION

5.1 Temporal groupings and correlations with the Western Fold Belt

The revised chronostratigraphic chart highlights four distinct temporal groupings of magmatism and sedimentary accumulation within the Eastern Succession. These groupings have time equivalents in the Western Fold Belt indicating links between the two terranes (e.g. Page, 1998). Our present understanding of the geochronology of the Eastern Succession allows direct correlations with the well-constrained age divisions applied to the Western Fold Belt by Jackson et al. (2000), Scott et al. (2000), and Southgate et al. (2000a, b).

5.1.1 Barramundi basement and Kalkadoon-Leichhardt Belt between ca. 1890 Ma (metamorphism) to 1850 Ma

The only basement units that crop out in the Eastern Succession are the Plum Mountain Gneiss and the Kurbayia Migmatite (shown as undifferentiated basement in Figure 2). The Kurbayia Migmatite crops out along the western edge of the Kalkadoon-Leichhardt Belt whereas the Plum Mountain Gneiss crops out on the south-eastern flank of this belt. The other basement units in the west are the Yaringa Metamorphics, and possibly the Saint Ronans Metamorphics and the Sulieman Gneiss (Figures 1). Metamorphism within the Yaringa Metamorphics has been dated at 1890 ± 8 Ma by Page and Williams (1988) whereas an igneous crystallisation age of 1857 ± 5 Ma was obtained from a leucosome in gneiss within the Kurbayia Migmatite (Page and Sun, 1998), although McDonald et al. (1997) argued for an early Proterozoic and late Archean component to this unit. The ca. 1860 Ma and ca. 1890 Ma ages may indicate a substantial time difference between metamorphism of the Yaringa Metamorphics in the west, and the Kurbayia Migmatite along the central Kalkadoon-Leichhardt Belt. However, recently obtained crystallisation ages of ca. 1860-1850 Ma for igneous phases within the Yaringa Metamorphics (Bierlein and Black, 2005) suggest that this was the age of migmitisation in both these basement blocks. This age overlaps with the deposition of the Leichhardt Volcanics (ca. 1870-1850

Ma) indicating that the thermal event responsible for the melting out of these voluminous felsic volcanics was responsible for the high-grade metamorphism and migmatite formation in the older sequence, and that the intrusion of the Kalkadoon Granite (ca. 1860-1850 Ma) immediately post dated this event.

5.1.2 1800-1725 Ma sequence

Volcanics and sediments of this age encompass the majority of the material now included in Cover Sequence 2 of Blake (1987). This age range corresponds with the Leichhardt Superbasin (ca. 1800-1750 Ma) defined in the Western Fold Belt, although expanded to 1725 Ma to include the Doherty Formation (Figure 3). This sequence is preceded by the intrusion of the Big Toby Granite in the Western Fold Belt at ca. 1800 Ma. The western sequence begins with the bimodal (felsic-dominated) volcanism of the Bottletree Formation at ca. 1790 Ma followed by the accumulation of the Haslingden Group (Mount Guide Quartzite, Eastern Creek Volcanics, and Myally Subgroup) between ca. 1790 Ma and 1770 Ma. The sequence begins in the east at ca. 1780 Ma with the bimodal volcanism of the Magna Lynn Metabasalt and Argylla Formation adjacent to the Kalkadoon Leichhardt Belt. The sequence continues in the Eastern Succession with the eruption of the Marraba Volcanics (mafic) and subsequent accumulation of the Mitakoodi Quartzite and Ballara Quartzite between ca. 1760-1750 Ma. The variably calcareous Quilalar Formation, Corella Formation and Doherty Formation are then deposited probably across the entire Mount Isa Inlier between ca. 1750-1725 Ma.

The emplacement of the various intrusions of the Wonga Batholith into the above sequence, and eruption (or shallow intrusion) of the felsic Fort Constantine Volcanics takes place between ca. 1750-1740 Ma (most intrusions probably ca. 1740-1730 Ma). This predates the deposition of the Doherty Formation in the east (Figure 3). It could be argued that the Doherty Formation should be placed in a younger (separate) age grouping. However, in this report we have considered this unit to represent an overall younging to the east of the calcareous sequence (e.g. Figures 5, 6). Subsequent east-west shortening during the Isan Orogeny may have juxtaposed these younger units against the older Corella Formation.

5.1.3 ca. 1710 Ma to 1690 Ma

Sediments of this age are known only from the Western Fold Belt and are grouped in the Calvert Superbasin of Jackson et al. (2000). The Calvert Superbasin extends from ca. 1730 Ma to ca. 1690 Ma to include the bimodal Peters Creek Volcanics (ca. 1725-1730 Ma) in the far northwest of the Mount Isa Inlier. Felsic volcanics in this unit are the same age as a rhyolite that gives the depositional age of the Doherty Formation in the Eastern Succession. The 1710-1690 Ma sequence can be further subdivided into groups (separated by an unconformity) deposited at around 1710 Ma and ca. 1700-1690 Ma. The older group consists of the Bigie Formation (sandstone and conglomerate) and the bimodal Fiery Creek Volcanics (1709 ± 3 Ma, co-magmatic with the Weberra Granite). The younger group consists of quartz sandstone, feldspathic sandstone, siltstone and shale. The Llewellyn Creek Formation in the core of the Snake Creek Anticline (Figure 1) in the Eastern Succession is a possible time equivalent unit of these 1710-1690 Ma sequences (Figure 3). At Snake Creek the Llewellyn Creek Formation has been intruded by a tonalite with a magmatic crystallization age of 1686 ± 8 Ma (Rubenach, 2005).

5.1.4 ca. 1680 Ma to 1610 Ma

Sediments of this age in the Eastern Succession include the Soldiers Cap Group, the Young Australia Group, and, if the correlations drawn above are correct, the Mount Albert Group (e.g. Figure 5). These units may be assigned to Cover Sequence 3 in the scheme of Blake (1987). The Soldiers Cap Group has the most extensive outcrop and is the dominant unit found in the eastern half of the Eastern Succession (Figure 2). Depositional ages for these units can be divided into two main groups, namely, ca. 1680-1650 Ma, and ca. 1630-1610 Ma. The majority of the ages gathered to date indicate deposition between ca. 1680-1650 Ma. Ages from tuffs or rhyolites thought to directly date deposition cluster ca. 1665-1650 Ma, therefore the majority of these older units may have been deposited in this interval. However maximum ages of ca. 1675-1680 Ma obtained from a number of different samples in the southeast may be indicating that this is close to the depositional age for part of the Soldiers Cap Group. The second group of depositional ages of between 1630-1610 Ma are restricted to the Tommy Creek Block and the Marimo Slate. Ages of ca. 1630-1620 Ma from the Tommy Creek Block, and one (max) age of ca. 1610 Ma from the Marimo Slate indicate the presence of minor younger sequences in the Eastern Succession.

The ca. 1665-<1610 Ma depositional ages in the Eastern Succession invite direct comparison with the well constrained Mount Isa Group and McNamara Group (Isa Superbasin, Jackson et al., 2000) in the western Mount Isa Inlier (e.g. Page, 1998; Page and Sun, 1998; Page et al., 2000). The Breakaway Shale near the base of the Mount Isa Group has a depositional age of 1663 ± 3 Ma, whereas sedimentation in the McNamara Group extends from ca. 1660 Ma (upper Gunpowder Formation near the base) to as young as 1595 ± 6 Ma in the upper Lawn Hill Formation at the top of this sequence. Most of the Mount Isa Group was deposited at ca. 1665-1650 Ma, the same time interval as the majority of the Cover Sequence 3 units in the Eastern Succession (Figure 3). The Urquhart Shale at Mount Isa (host to the Pb-Zn-Ag-Cu mineralization) has a well constrained depositional age of ca. 1655 Ma, within error of the age of 1655 ± 4 Ma obtained from the Marimo Slate (carbonaceous slate, shale and siltstone) and of ages obtained from the Mount Norna Quartzite (1654 ± 4 Ma) and the Toole Creek Volcanics (1658 ± 8 Ma).

Possible correlations between the Soldiers Cap Group and Young Australia Group

As noted above, the informally-named Young Australia Group is treated in this report as possible lateral facies equivalents of the Soldiers Cap Group (including the Kuridala Formation) to the east. Although there is broad geochronological support for this hypothesis, correlating particular subunits is a tenuous process due to significant lithological differences between the two groups (e.g. the voluminous mafic magmatism of the Toole Creek Volcanics has no counterpart in the Young Australia Group). However, allowing for the effects of shortening during the Isan Orogeny, and the generally lower metamorphic grade of the Young Australia Group, tentative correlations can be drawn between units based on shared lithological components, particularly between the Answer Slate and the Kuridala Formation, and between the Staveley Formation and The Mount Norna Quartzite (Figures 3, 5, 6). Lithological descriptions below are drawn from Blake (1987).

The Answer Slate at the base of the Young Australia Group has many lithological similarities to the Kuridala Formation to the east. Blake (1987) observed that the Kuridala Formation appeared to merge laterally with the Answer Slate. The dominant lithologies in the Answer Slate are slate, siltstone and phyllite whereas the Kuridala Formation is predominantly comprised of schist, metagreywacke and slate. Lithological units within the

Answer slate are commonly graphitic and pyritic, as too are some siltstones and slates within the Kuridala Formation. Marble is a minor component of the Answer Slate, as is banded calc silicate in the Kuridala Formation. One significant difference between the units is the presence of minor mafic volcanics and banded iron formation in the Kuridala Formation (although both units contain some quartz-hematite rock). The Kuridala Formation has only a maximum depositional age from detrital zircons of 1676 ± 5 Ma whereas the Answer Slate has a depositional age of 1652 ± 16 (Geoscience Australia Ozchron database).

The Mount Norna Quartzite of the Soldiers Cap Group is dominated by quartzite, feldspathic quartzite and schist. Although more massive, these lithologies are not dissimilar to the (generally lower metamorphic grade) Staveley Formation of the Young Australia Group which is predominantly comprised of interbedded sandstone, siltstone, phyllite, shale and mudstone (variably calcareous, ferruginous, feldspathic and siliceous). Both units contain minor metabasalt, conglomerate and felsic metavolcanics. Marble and banded iron formation are a minor constituent of the Mount Norna Quartzite, as is marble, banded calc-silicate, and banded quartz-hematite-magnetite rock in the Staveley Formation (Figure 6). The most significant differences between the two units is the greater abundance of calcareous lithologies and finer interbeds in the Staveley Formation compared to the Mount Norna Quartzite although this comparison is complicated by the higher metamorphic grade, and the degree of deformation and silicification within the Mount Norna Quartzite. Indeed, isolated blocks of Roxmere Quartzite that overlie the Doherty Formation, Staveley Formation and Marimo Slate locally resemble silicified calc-silicate, or calcareous quartzite. It has been suggested above that these may correlate with the Mount Norna Quartzite, but have been thrust up from basal units of the Young Australia Group. It is also possible some of the blocks are calcareous sandstones derived from the Staveley Formation near the base of this group (cf. Figure 6). The Staveley Formation has only a maximum depositional age of ca. 1710 Ma, however it is presumed to overlie the Answer Slate (1652 ± 16 Ma) and be overlain by the Marimo Slate (1655 ± 4 Ma). These constraints provide a depositional interval that is in agreement with that obtained for the Mount Norna Quartzite (1654 ± 4 Ma).

The most significant difference between the Young Australia Group and the Soldiers Cap Group to the east is the absence of the mafic volcanics of the Toole Creek Volcanics in the western group. The Toole Creek Volcanics at the top of the Soldiers Cap Group are dominated by basalts (and related sills and dykes) with some intercalated metasediments including siltstone, phyllite, schist and quartzite. Minor banded calc-silicates, banded iron formation, chert, jaspilite and slate also occur within the unit. In contrast, the Marimo Slate at the top of the Young Australia Group (along with the Agate Downs Siltstone) is predominantly a package of carbonaceous slate, shale and siltstone, and contains no mafic (or felsic) volcanics, banded calc-silicates, and banded iron formation. Mafic sills and dykes that cut the Marimo Slate are generally absent. The depositional ages of ca. 1610 Ma and ca. 1655 Ma obtained from the Marimo Slate indicates that at least part of this unit is much younger than the Toole Creek Volcanics (1658 ± 8 Ma). However, the inferred relationships with underlying units and the older age of ca. 1655 Ma indicate that the deposition of part of this unit is likely to have overlapped with that of the Soldiers Cap Group. One possibility is that the underlying Staveley Formation correlates with both the Mount Norma Quartzite and the Toole Creek Volcanics. The Staveley Formation contains minor metabasalt, and, like the Toole Creek Volcanics contains minor banded iron-rich rocks and banded calc-silicates. The main depositional centre for the mafic volcanics must

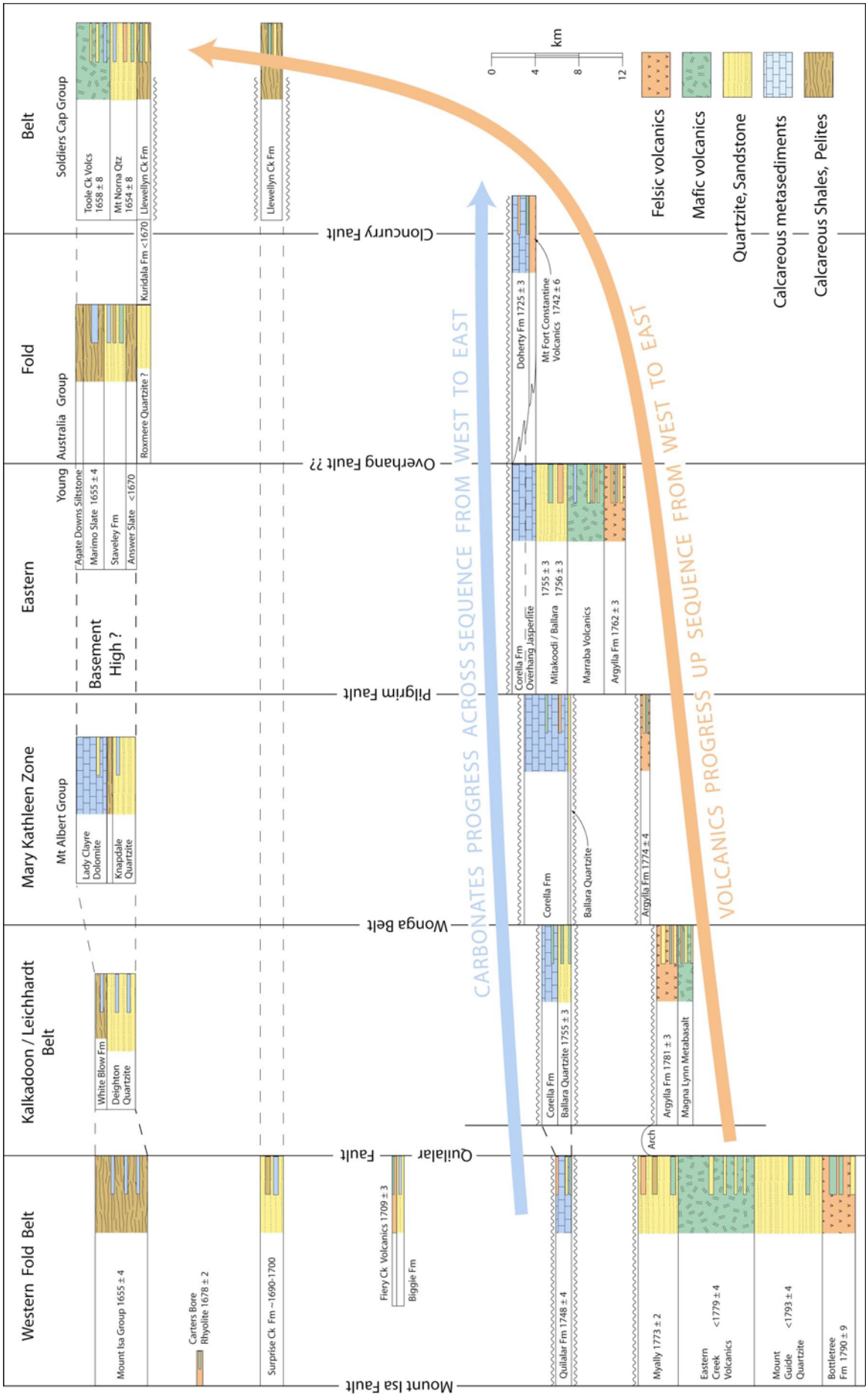
Western Fold Belt
Kalkadoon / Leichhardt Belt
Mary Kathleen Zone
Eastern
Fold Belt
Mount Isa Fault
Quilalar Fault
Wonga Belt
Pilgrim Fault
Overhang Fault ??
Cloncurry Fault
Mt Albert Group
Young Australia Group
Soldiers Cap Group
Basement High ?
Lady Clayre Dolomite
Knapdale Quartzite
White Blow Fm
Deighton Quartzite
Agate Downs Siltstone
Marimo Slate 1655 ± 4
Staveley Fm
Answer Slate <1670
Roxmere Quartzite ?
Kuridala Fm <1670
Toole Ck Volcs 1658 ± 8
Mt Norma Qtz 1654 ± 8
Llewellyn Ck Fm
Mount Isa Group 1655 ± 4
Carters Bore Rhyolite 1678 ± 2
Surprise Ck Fm ~1690-1700
Fiery Ck Volcanics 1709 ± 3
Biggie Fm
Quilalar Fm 1748 ± 4
Corella Fm
Ballara Quartzite 1755 ± 3
Corella Fm
Overhang Jasperlite
Mitakoodi / Ballara
1755 ± 3
1756 ± 3
Marraba Volcanics
Argylla Fm 1762 ± 3
Doherty Fm 1725 ± 3
Mt Fort Constantine Volcanics 1742 ± 6
Argylla Fm 1774 ± 4
Argylla Fm 1781 ± 3
Magna Lynn Metabasalt
Arch
Myally 1773 ± 2
Eastern Creek Volcanics <1779 ± 4
Mount Guide Quartzite <1793 ± 4
Bottletree Fm 1790 ± 9
CARBONATES PROGRESS ACROSS SEQUENCE FROM WEST TO EAST
VOLCANICS PROGRESS UP SEQUENCE FROM WEST TO EAST
km
0
4
8
12
Felsic volcanics
Mafic volcanics
Quartzite, Sandstone
Calcareous metasediments
Calcareous Shales, Pelites

Figure 6 (above). Simplified time-space plot for the Mount Isa Inlier showing only the volcanosedimentary units in cover sequences 2 and 3. The approximate proportions of various rock types are shown schematically for each unit or group. Note the preponderance of bimodal volcanism and siliciclastics in the basal cover sequence 2 units, and the temporal progression of volcanism from west to east , extending up into cover sequence 3. The interpreted lateral facies relationships between cover sequence 3 units are also shown, and the position of a possible emergent zone (basement high) during deposition (as indicated by detrital zircon populations). Thicknesses of units are to scale and based on estimates of maximum thickness in Blake (1987).

have been to the east (possibly controlled by rift-related growth faults) with only minor occurrences within the Staveley Formation being deposited to the west. The absence of basalt flows, sills and dykes within the Marimo Slate indicates that this unit was deposited after the mafic volcanism had ceased.

Young calcareous sequences in the Tommy Creek Block?

The generally fault-bounded Tommy Creek Block (Figure 1, 2) remains one of the most puzzling areas within the Eastern Succession. It contains both east-west dominant (southern section) and north-south dominant (central and northern section) structural grains evident in the orientation of fold axial traces and in the outcrop pattern of felsic igneous rocks. The felsic igneous rocks range from rhyolite to porphyritic rhyolite, to minor microgranite and have been variously interpreted as flows or shallow intrusive bodies (generally sills) at differing localities in the block. These felsic rocks (and some mafic dykes and sills) intrude or are overlain (or intercalated with) metasedimentary rocks comprised predominantly of calcareous sandstone, slate, schist, marl, and calc-silicate. These metasedimentary units have been mapped previously as part of the Corella Formation (deposited ca. 1750 Ma). Igneous zircon crystallisation ages obtained from rhyolite in the southwest of the block (1758 ± 4 Ma) and in the east (1762 ± 5 Ma) are identical to those obtained from Argylla Volcanics in the core of the Mitakoodi Antiform to the south (Page, 1998). These ages from the structurally lowest part of the Tommy Creek sequence are consistent with an interpretation that the overlying calcareous metasediments belong to the Corella Formation. However ages obtained from two felsic (possibly extrusive) igneous rocks in the south of the block of 1629 ± 8 Ma and 1625 ± 4 Ma (Tommy Creek Microgranite), substantiated by an age of 1618 ± 6 Ma from a tuffaceous volcaniclastic attest to a much younger depositional time for much of this sequence. Additionally, a felsic metavolcanic from the northwest of the block constrained that part of the sequence to ca. 1650 ± 3 Ma (Page, 1998).

In view of the range of ages presented above, an important question is, how much of the calcareous sequence in the Tommy Creek block (if any) is temporally equivalent to the Cover Sequence 2 Corella Formation? Are the rhyolites actually extrusive, or are they shallow intrusions and sills? The approach taken in this report is to place the subunits within which the younger ages occur within the Young Australia Group, whereas the remainder has been left in the Corella Formation (Figure 2). However, further geochronological work may reveal that some of these ‘Corella’ units correlate with much younger rocks in the east. The generally calcareous metasedimentary rocks within much of the Tommy Creek Block are not that dissimilar to parts of the Staveley Formation to the southeast. The ca. 1650 Ma age from the western part of the Tommy Creek Block is within error of that estimated for the Staveley Formation from the ages of overlying and underlying units. Two linear belts of calcareous metasediments that crop out in the middle of the Marimo Basin (previously mapped as Corella, and shown as such in Figure 2) may be other temporally correlative units.

5.2 Temporal and spatial progression in magmatism

One of the striking features of the reconstructed chronostratigraphy for the Mount Isa Inlier is the occurrence of significant (usually bimodal) igneous activity immediately prior to, and sometimes overlapping with the onset of the accumulation of the temporally discrete sedimentary sequences (Figure 3). This igneous activity includes batholith-scale felsic intrusions (usually interpreted as emplaced in an extensional setting), voluminous felsic and mafic volcanics, and the emplacement of large mafic sills and dyke swarms. Mingling and mixing between felsic and mafic magmas is commonly observed in the intrusive phases. These discrete magmatic events and the elevated heat flow that produced them are likely to be intimately associated with the basin-formation mechanisms for the Mount Isa Inlier. The felsic magmatism is predominantly anorogenic I-type and has a chemistry that plots as within plate on tectonic discrimination diagrams (e.g. Wyborn, 1988; Wyborn et al., 1988, 1998). The mafic magmas most closely resemble continental tholeiites, with intercontinental rifting suggested as the most likely tectonic setting (Ellis and Wyborn, 1984; Williams, 1998b). Intracontinental rifting has been the accepted paradigm for the formation of the sedimentary basins in the Mount Isa Inlier, however recent publications have suggested the involvement of continental-margin arc magmatism (McDonald et al., 1997), and far-field responses to a distant southern subduction zone (Scott et al., 2000, dynamic tilting; Giles et al., 2002, continental backarc basins).

The earliest igneous activity in the Mount Isa Inlier that postdates the Barramundi Orogeny is manifest by the Kalkadoon Granite and the co-magmatic Leichhardt Volcanics, formed ca. 1870-1850 Ma (Figure 3). However, as noted above, the Kalkadoon Granite probably followed closely in time behind the migmitisation of the basement units. Other than the felsic volcanics, no significant sedimentary sequences of this age are preserved. Only rare sedimentary units and minor metabasalt occur within the Leichhardt Volcanics. Both the Kalkadoon Granite and the Leichhardt Volcanics are cut by numerous mafic dykes (Blake, 1987). The intrusion of the late mafic dyke swarm (of continental tholeiite affinity) is probably indicating an extensional tectonic setting for the Kalkadoon Granite and associated volcanics (cf. Wyborn, 1988), although McDonald et al. (1997) suggested they represented a continental arc.

The accumulation of the Leichhardt Superbasin between ca. 1800-1750 Ma in the west is preceded by the emplacement of the Yeldham Granite (ca. 1820 Ma) and Big Toby Granite (ca. 1800 Ma). The volcanosedimentary sequence begins in the west with the extrusion of the felsic (and minor mafic) volcanics of the Bottletree Formation between ca. 1800-1790 Ma. A hiatus in volcanism during the deposition of the siliciclastics of the Mount Guide Quartzite (with minor basalt) is followed by the extrusion of the mafic lavas of the Eastern Creek Volcanics and Magna Lynn Metabasalt to the east and west of the Kalkadoon-Leichhardt Belt. Volcanism continues in the east with the felsic lavas of the Argylla Formation overlain in the far east by the mafic lavas of the Marraba Volcanics.

The main accumulation of Cover Sequence 2 sediments in the Mary Kathleen and Wonga Belts of the Eastern Succession was terminated by the intrusion of the Wonga Batholith and coeval mafic intrusions into an extensional shear zone between ca. 1750-1730 Ma (Pearson et al., 1992). However the deposition of calcareous sediments continued further to the east (the Doherty Formation). The Doherty Formation and the felsic Mount Fort Constantine Volcanics are the only volcanic or sedimentary accumulations remaining in the east that overlap with or closely postdate the emplacement age of the Wonga Batholith. However, the Peters Creek Volcanics (basalt, rhyolite) was deposited in the far northwest

of the Mount Isa Inlier between ca. 1730-1725 Ma. The subsequent ca. 1710-1690 Ma sequences in the Western Fold Belt include the bimodal Fiery Creek Volcanics (1709 ± 3 Ma) and the co-magmatic Weberra Granite.

Cover Sequence 3 (the Isa Superbasin in the west) was preceded by the Carters Bore Rhyolite (ca. 1678 Ma) and then the extensive felsic intrusions (and coeval dolerite) of the Sybella Batholith which were emplaced between ca. 1674-1655 Ma. Several small intrusions of this age (including the Ernest Henry Diorite) have been identified in the Eastern Succession. The earliest phases of the Sybella Granite were emplaced into an amphibolite facies shear zone, almost certainly related to development of the sedimentary basin (Hoadley et al., 2001). Felsic and mafic volcanism is absent from the Mount Isa Group sediments in the Western Fol Belt (although felsic tuffs are present in the sequence). However voluminous mafic volcanics, and related sills and dykes occur within the Soldiers Cap Group in the east at this time (most intense in the Toole Creek Volcanics). However, unlike the older cover sequences, only minor felsic volcanism is reported.

One interesting outcome of the revised chronostratigraphy is an apparent west to east migration of volcanism with time (changing locus of rifting?) that begins at the base of Cover Sequence 2 (Page, 1998). This progression is shown schematically in Figure 6 where bimodal magmatism begins in the Bottletree Formation at ca. 1790 Ma, and is followed by the mafic-dominated Eastern Creek Volcanics and Magna Lynn Metabasalt, the latter overlain by Argylla Formation felsic volcanics at ca. 1780 Ma. Volcanics within the Boomarra Horst (part of the Mary Kathleen Zone) have given ages of ca. 1775 Ma, whereas the felsic volcanics of the Argylla Formation east of the Pilgrim Fault give ages of ca. 1760 Ma (and are overlain by a thick sequence of mafic volcanics, the Marraba Volcanics). The Mount Fort Constantine Volcanics were erupted further to the east at ca. 1745 Ma, and finally, the mafic volcanics of the Toole Creek Volcanics were erupted still further to the east at ca. 1655 Ma.

5.3 Sediment providence and detrital zircons

5.3.1 Cover Sequence 2

The Bottletree Formation and Haslingden Group (lower Cover Sequence 2 and Leichhardt Superbasin) in the Western Fold Belt were laid down in north-south trending rift basins or half-grabens during east-west directed extension (Glikson et al., 1976; Derrick, 1982; Blake, 1987; Eriksson et al., 1993). Sediments were derived from (and generally coarsened towards) an emergent Kalkadoon-Leichhardt and basement block to the east that formed the eastern margin of the basin (Blake, 1987). Early workers favoured a single stage rift-sag model for the Haslingden Group and the overlying Quilalar Formation (Derrick, 1982; Blake, 1987), however later researchers favoured multiple rift-sag events (e.g. Eriksson and Simpson, 1990; O'Dea et al., 1997; Betts et al., 1998; cf. review in Jackson et al., 2000). Eriksson et al. (1993) interpreted the Myally Subgroup as filling from the east in a similar manner to the underlying Eastern Creek Volcanics, however O'Dea et al. (1997) and Betts et al. (1998) favoured infilling of half-grabens during north-south extension. Recent basin architecture and geochronological studies support the former hypothesis. Geochronological work by Neumann et al. (2005) demonstrates that the Eastern Creek Volcanics and Myally Subgroup form a single supersequence. McIntyre et al. (2005) show that the Myally sediments are predominantly continental to shallow restricted marine in origin and were laid down in a NNW-trending basin (with linked local depocentres) that

opened out to the north and was sourced from a basin margin to the east. Detrital zircons from the May Downs Gneiss, Mount Guide Quartzite, and Lena Quartzite (Eastern Creek Volcanics) are entirely consistent with sediment derivation from the Kalkadoon-Leichhardt Belt to the east (and the Bottletree Formation on its western flank) (Figure 7). Significant age populations occur at ca. 1780-1790 Ma (Bottletree), ca. 1850-1860 Ma (Kalkadoon-Leichhardt), and ca. 1870-1880 Ma (Barramundi basement). An additional age grouping near 2000 Ma is consistent with zircon populations within the Pothole Creek Gneisses in the Kurbayia Migmatite (McDonald et al., 1997).

Most authors equate the Quilalar Formation with sedimentation in a sag phase and suggest a blanket-like geometry with possible links to similar units (Ballara Quartzite and Corella Formation) to the east of the Kalkadoon-Leichhardt Belt and in the Eastern Fold Belt (Derrick et al., 1980; Blake, 1987; Jackson et al., 1990, 2000). Blake (1987) suggested that a marine transgression led to the Quilalar Formation spreading eastward across the eastern margin of the Leichhardt River Fault Trough. Jackson et al. (1990, 2000) proposed sedimentation in meridionally trending sub-basins. Recent geochronology supports the correlations between the Quilalar Formation (1748 ± 4 Ma) and the Ballara Quartzite and Mitakoodi Quartzite (1755 ± 3 Ma) and Corella Formation (Page 1998; Page and Sun, 1998; Page, Geoscience Australia Ozchron database; Neumann et al., 2005; Figures 3, 6). That the Quilalar Formation was widespread across the Mount Isa Inlier is supported by McIntyre et al. (2005) who described the deposition of the Quilalar Formation in a northwest-southeast trending basin that was open to the southeast.

Depositional (or maximum depositional) ages obtained by Neumann et al. (2005) from the Myally (1773 ± 2 Ma) and the overlying Quilalar Formation (1748 ± 4 Ma) indicate that a significant hiatus in sedimentation may have occurred between the two. The same relationship is shown to the east of the Kalkadoon-Leichhardt Belt where the Ballara Quartzite (1755 ± 4 Ma) is some 20-25 m.y. younger than the underlying felsic volcanics of the Argylla Formation (1781 ± 3 Ma) (Page, 1998). It is likely that most of the Eastern Succession to the west of the Pilgrim Fault was predominantly a topographic high between ca. 1780-1755 Ma (shown schematically in Figure 6), perhaps caused by doming related to the voluminous felsic magmatism of the Argylla Formation (cf. Scott et al., 2000; Southgate et al., 2000a). Minor sedimentary units (fluvial sandstones) occur within the ca. 1780 Ma Argylla Formation on the eastern flank of the Kalkadoon-Leichhardt Belt, however these are much more common within the younger (ca. 1760 Ma) Argylla Formation to the east of the Pilgrim Fault (Blake, 1987). Additionally, locally occurring pillow basalts have been reported from near the base of the overlying Marraba Volcanics, whereas calcareous sandstones and siltstones become more common in the upper units (Blake, 1987). Both of these factors indicate subaqueous trending to shallow marine conditions during the eruption of the bimodal volcanics. The available geochronology indicates a window of ca. 5 m.y. for the eruption of the upper Argylla Volcanics, Marraba Volcanics, and the beginning of the accumulation of the Mitakoodi Quartzite to the east of the Pilgrim Fault (Figure 6). Accommodation for this thick sequence in the east may have been related to the existence of a major growth fault on the western boundary as is postulated by Blenkinsop et al. (2005) as a possible explanation for the Pilgrim gravity worm (cf. inset in Figure 4).

The relationships shown in Figure 6 suggest that the Ballara Quartzite and Mitakoodi Quartzite, and the overlying Corella Formation (and Quilalar Formation) are likely to have been partially sourced from a north-south trending topographical high consisting of the

Magmatic Event or orogeny	Sybella Granite Ernest Henry Dior	Fiery Ck Vol. Peters Ck V.	Wonga Granite	Argylla Fm volcanics	Bottletree F volcanics	Yeldham Granite	Kalk-Leich + Nicholson Gr	Barramundi Orogeny										
Age	<1700	1700-1730	1730-1750	1760-1780	1780-1800	1800-1840	1840-1870	1870-1900	1900-2000	2000-2100	2200	2300	2400	2500	2600	2700	2800	2900+
CS2-Western Fold Belt																		
Quilalar Fm					1780+-20		*1840	*1860-1890	1940-2000	2100				2520		2690		3110
Quilalar Fm					1780+-20		*1840	*1900			2200			2540	2610		2800	
Lena Qtz (ECV)				1779+-4[d]			*1860											
Mt Guide Qtz					*1793+-1		*1860											
May Downs Gn					*1789+-4		*1851+-4	1870	1910,1950	2020					2560	2690		
May Downs Gn						1815+-7	1848+-24	*1877+-6	*1999+-6									
CS2-Eastern Fold belt																		
Corella Fm			1740+-20[d]	1780			1830-1870		1940					2530				
Corella Fm						1820			1941									
Argylla Fm (BH)				1775+-4[d]			1855		1980									
Double Cr. Met.						*1814+-10	1870				2200-2300				2540-2600			
Double Cr. Met.							1830-1850	1860-1900	1930,1990		2170				2500-2600			
CS2-Western Fold Belt																		
Lady Loretta Fm	1680-1690			1760		1820	1870				2205			2513				
Lady Loretta Fm	1650+-20[d]			1770					1970							2730		
Lady Loretta Fm		1701+-4		*1765+-10	1790									2480				
Paradise Ck. Fm	*1654+-4[d]	1724				#1803		#1880										
Paradise Ck. Fm	*1658+-3[d]		1731+-11															
Urquhart Shale	*1654+-5[d]	1710			1786													
Breakaway Shale	*1663+-3[d]		1754		1788		1867											
Moondarra Silt	1668+-8[d]		1745		1785+-5		1850	1870-1880										
CS3-Eastern Fold Belt																		
Marimo Slate(up)	*1610[d],1646,1689			1770														
Staveley Fm		*1710	1750	1774														
Staveley Fm					1796+-9													
Staveley Fm							1858+-9											
Answer Slate	1652+-16[d]			1755														
Toole Ck. Vols								1900+-20			2230					2680		
Toole Ck. Vols	*1658+-8[d]				1790		1850		1940	2070		2350			2580			
Mt Norna Qtz [Fm]	*1693		*1733+-8	*1765+-25										2452				
Mt Norna Qtz [Fx]	1654+-4[d]		1740	1780			1850					2300			2600			
Mt Norna Qtz [GR]	1690+-20		1750															
Mt Norna Qtz [Mn]				1770+-7														
Kuridala Fm	*1676+-5	*1720		1770												2674		
Llewellyn Ck Fm	*1666+-14	*1721+-7											2400		2600			
Gandry DG [Mar]	*1677+-9		*1734+-6			1830						2320		2550				
Gandry DG [Can]	*1676+-5	*1715+-5				1820							2400					3250
Gandry DG [Can]		*1712+-6		1750-1770										2530-2565				
Gandry DG [Can]	1678+-18	*1720+-16												2497+-18				

Figure 7 (above). Detrital zircon populations from metasediments in the Eastern Fold Belt and Western Fold Belt of the Mount Isa Inlier. The age population in the columns are grouped via regional magmatic events (potential zircon sources). [Fm]Fairmile, [Fx]Foxes Creek, [GR]Gilded Rose, [Mn]Monakoff, [Mar]Maramungee, [Can]Cannington, *significant number of grains or analyses, [#]single grains from different samples from the same sedimentary unit, [d]probable depositional age.

older (ca. 1780 Ma) Argylla Formation volcanics and possibly Kalkadoon-Leichhardt Belt material (consistent with the meridionally trending sub-basins model of Jackson et al., 2000). The existence of this unconformity between the Ballara Quartzite and the underlying felsic volcanics of the Argylla Formation to the west of the Pilgrim Fault can also be postulated for the volcanosedimentary units of the Boomarra Horst in the northeast (previously mapped as Soldiers Cap, discussed above). A felsic tuff and a mafic tuff gave ages of 1774 ± 4 Ma and 1775 ± 4 Ma (Page and Sun, 1998) indicating some sedimentary accumulation at this time in the Eastern Succession. However, the most prominent outcropping units in the Boomarra Horst are a quartzite (probable Ballara Quartzite equivalent) and calc-silicates mapped as Corella Formation. These units are likely to unconformably overlie the older tuffs that are the source of the age dates. Interestingly the ages obtained from these tuffs are indistinguishable from a depositional age of 1773 ± 2 Ma obtained from a volcaniclastic in the Myally Subgroup at the top of the Haslingden Group in the Western Fold Belt (Neumann et al., 2005). That an unconformity exists above the western Argylla Formation is evidenced by the occurrence of Argylla type volcanic clasts in the basal fluvial units of the Ballara Quartzite (Blake, 1987). These basal fluvial units grade up sequence into shallow marine deposits consistent with a marine transgression across the Inlier depositing the Quilalar and Corella Formations. Detrital zircons from the Quilalar Formation give age groupings that are consistent with derivation from the Argylla and/or Bottletree Formations, Kalkadoon-Leichhardt Belt, and Barramundi basement (including groupings at ca. 2000 Ma and ca. 2500-2600 Ma) (Figure 7). However these ages are also consistent with derivation from the Murphy Inlier and Kamarga Dome in the northwest where the Nicholson Granite (1845 ± 3 Ma, 1856 ± 3 Ma), Cliffdale Volcanics (1851 ± 3 Ma) and Kamarga Volcanics (probable Eastern Creek Volcanics equivalents) display the same age groupings. This latter providence for the Quilalar Formation is supported by the basin analysis of McIntyre et al. (2005) who inferred an east-to-southeast dipping shelf basin geometry, with sediment transport being from the west. An almost identical spread of ages is found within the Corella Formation in the Eastern Succession (Figure 7) supporting the shared depositional history of these two Formations. No detrital zircon data has been collected from the Ballara Quartzite and Mitakoodi Quartzite, however the Double Crossing Metamorphics (a possible correlative as argued above) has a similar spread of ages although missing any of Argylla or Bottletree age (Figure 7).

There is no published detrital zircon data for the ca. 1710 to 1690 Ma deposits of the Calvert Superbasin in the west (nor from the Llewellyn Creek Formation at Snake Creek, a possible temporally correlative unit in the Eastern Succession). Sequence stratigraphic and basin analysis research conducted by Domagala et al. (2000), Southgate et al. (2000b) and McIntyre et al. (2005) revealed that the Calvert Superbasin sediments were predominantly marine in origin, and that the depositional basin had no eastern or south-eastern margin. Domagala et al. (2000) interpreted locally rapid lateral facies changes within the Calvert Superbasin sediments as indicative of deposition within a tectonically active intracratonic basin where depocentres were separated by basement highs. The inference that the depositional basin was open to the east increases the likelihood that temporally correlative

units were deposited in the Eastern Succession and underlines the importance of constraining the age of the Llewellyn Creek Formation at Snake Creek.

5.3.2 Cover Sequence 3

Detailed basin analysis and sequence stratigraphic research hasn't been carried out on the Cover sequence 3 rocks in the Eastern Succession. However temporally equivalent (and lower metamorphic grade) units in the Western Fold Belt have been studied in great detail, particularly by the North Australian Basins Resource Evaluation (NABRE) project in the mid to late 1990's (e.g. Scott et al., 2000; Southgate, 2000a, b; Domagala et al., 2000). Early models for the Mount Isa Group favoured their deposition into a predominantly post-rift sag basin (e.g. Blake and Stewart, 1992; O'Dea et al., 1997; Betts et al., 1998). The results of the NABRE project led Southgate et al. (2000b) to argue for periodic tectonism and magmatism throughout the life of the Isa Superbasin as an alternative to the rift-sag model. These researchers identified repeated episodes of paired uplift and subsidence, and suggested that these were incompatible with a rift-sag model. They proposed that these episodes of paired uplift and subsidence were related to strike-slip faulting, coincident with compressive tectonics in central Australia (Southgate et al., 2000b; and cf. Scott et al., 2000). Southgate et al. (2000b) interpreted the Gun Supersequence sediments (most of the Mount Isa Group and western equivalents) as being deposited on a broad southeast-facing ramp in a marine basin that extended from the Murphy Inlier in the northwest to the Gorge Creek Fault to the east of Mount Isa. These researchers inferred that the general absence of shoreline facies sediments in the Mount Isa Group (and deeper water basinal deposits in the east and south) indicated that the depositional systems probably crossed the Kalkadoon-Leichhardt Belt. Southgate et al. (2000b) inferred that a siliciclastic providence to the west of the Mount Isa Group underwent periodic rejuvenation. An emergent siliciclastic province to the east is indicated by the presence of rhythmically laminated turbidite deposits in the upper Native Bee Siltstone adjacent to the Kalkadoon-Leichhardt Belt, however the scarcity of coarse siliciclastics material near the eastern margin of the preserved sediments indicates that any siliciclastics providence is likely to have been of a transient nature (Southgate et al., 2000b).

Although scarce in number, detrital zircon populations from the Mount Isa Group and temporally equivalent members of the McNamara Group reflect known magmatic events in the area (Figure 7). Ages between ca. 1730-1700 Ma most likely reflect reworking of material related to the Peters Creek Volcanics, Weberra Granite and Fiery Creek Volcanics in the northwest. Grains dated at ca. 1880-1850 Ma, and ca. 1785 Ma are consistent with derivation from the Murphy Inlier and Eastern Creek Volcanics or equivalents in the west or, alternatively, from the Kalkadoon-Leichhardt Belt and Argylla and Bottletree Formations to the east.

The majority of the Cover Sequence 3 units sampled in the Eastern Succession are characterised by detrital grains that give 'Argylla' ages of between 1780-1760 Ma, and by a general absence of ages coincident with those of the Kalkadoon-Leichhardt Belt (Figure 7). Additionally, three out of four Mt Norna Quartzite samples, a Stavely Formation sample, and one out of four Gandry Dam Gneiss samples have detrital grains with 'Wonga' type ages of between 1750-1730 Ma. This data suggests that the Mary Kathleen Zone to the west may have formed a local topographic high during the deposition of at least part of the Soldiers Cap Group (shown schematically in Figure 6). There are significant differences between dated samples attributed to the Mount Norna Quartzite and

the older Llewellyn Creek Formation and Kuridala Formation, and undifferentiated Soldiers Cap in the south (i.e. the Gandry Dam Gneiss). All three samples of Gandry Dam Gneiss from Cannington contain numerous detrital grains giving ages between ca. 1730-1710 Ma, contain no 'Wonga' type ages, and only one sample yielded detrital grains of 'Argylla' age. A Kuridala Formation sample and Llewellyn Creek Formation sample (from the Middle Creek Anticline) also lack 'Wonga' type ages, but contain numerous grains giving ages of ca. 1720 Ma. The numerous detrital zircons giving ages of ca. 1730-1710 in the south-eastern Soldiers Cap Group may indicate a fairly proximal source at the time of sedimentation. The only known magmatic source of this age in the Eastern Succession is the ca. 1725 Ma rhyolite within the Doherty Formation (also in the southeast of the Eastern Succession). Although the contacts between the Doherty Formation and the Soldiers Cap Group are invariably tectonic, it might be expected that the latter would have unconformably overlain the former. Therefore it is tempting to speculate that the ca. 1720 Ma ages reflect reworking of felsic volcanics in the Doherty Formation or related volcanics to the east or southeast. That a siliciclastic providence existed to the east is supported by the general decrease in grain size and feldspar content from east to west (Blake, 1987), although this inference is complicated by the uncertain age relationship between the various units (i.e. the postulated unconformity in the upper Llewellyn Creek Formation at Snake Creek).

Although we have emphasised the differences between the Mount Norna Quartzite and the Gandry Dam Gneiss, Kuridala Formation and Llewellyn Creek Formation, it is by no means certain that all four Mount Norna Quartzite samples correlate with this particular unit. One sample from near Gilded Rose (GR) and one from Monakoff (Mn) are within units mapped as Mount Norna Quartzite however the remaining two samples are usually included as 'undifferentiated Soldiers Cap' by most researchers. The sample from just east of the Fairmile Pb-Zn prospect (Fm) was included as Mount Norna Quartzite on the basis of mapping by Beardsmore et al. (1988). These researchers placed Fairmile near the boundary between undifferentiated Mount Norna Quartzite and Toole Creek Volcanics, and Llewellyn Creek Formation. This possibly tuffaceous sample contains numerous grains that define a maximum depositional age from 51 analyses of 1693 ± 5 Ma (Page and Sun, 1998). This age is either the time of deposition of the unit at this locality, or represents reworking of a probably proximal source. The latter is the more likely scenario as the host to the Pb-Zn prospect at Fairmile is probably of a similar age to that of the Maramungee Pb-Zn prospect some 30 km to the south, and that of the Cannington Pb-Zn-Ag mine some 30 km further south. The host rocks at the latter two Pb-Zn occurrences have maximum depositional ages of ca. 1677 Ma. The 1693 ± 5 Ma detrital zircon age grouping from Fairmile is indistinguishable from that of a tuff (1694 ± 3 Ma) near the younger limit of the Calvert Supersequence (lower Gunpowder Creek Formation) in the Western Fold Belt. The Calvert Supersequence basin is interpreted as having continued across the Kalkadoon-Leichhardt Belt, therefore 1693 Ma falls within the expected age range for any temporally correlative units. It is also within error of the age of 1686 ± 8 Ma obtained for a tonalite that intrudes the Llewellyn Creek Formation at Snake Creek (Rubenach, 2005). If the Mount Norna Quartzite does unconformably overlie the Llewellyn Creek Formation at Snake Creek, then ca. 1693 Ma is a useful best guess as to the age of the latter at that locality.

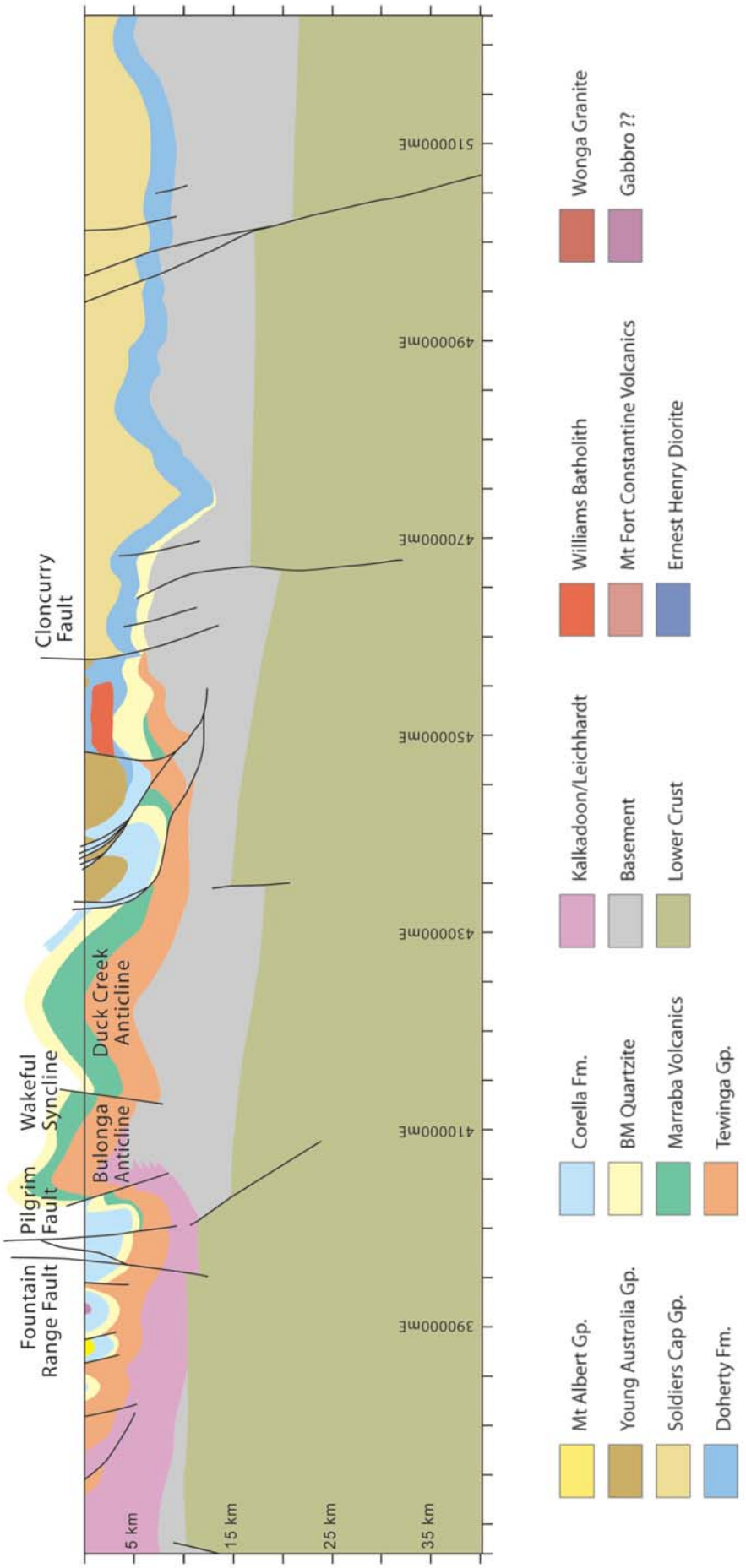

Figure 8. Example of cross-sections constructed for the Eastern Fold Belt (Blenkinsop et al., 2005) showing the interpreted relationships between the major rock units (cf. Figures 4, 5, 6). East-west section along line 769000 (location of line shown in Figures 2, 4).

5.4 Temporal and stratigraphic position of major deposits

5.4.1 Pb-Zn-Ag deposits

The revamped stratigraphy for the Mount Isa Inlier confirms that the host rocks to the major Pb-Zn-Ag deposits or prospects are entirely confined to the younger sequences. Assuming that the Dugald River resource is hosted by Cover Sequence 3 sediments, than every Pb-Zn-Ag deposit or prospect of any note in the entire Inlier (and including the HYC deposit in the McArthur Basin) is hosted by sediments deposited between ca. 1680 Ma to 1590 Ma. If Century is ignored, the remainder were deposited between ca. 1680-1640 Ma. The upper age limit (ca. 1680 Ma) from Cannington is poorly constrained and it remains possible that the host at that deposit was formed in the same interval as all of the Western deposits (minus Century), i.e. between ca. 1655-1640 Ma (Page and Sweet, 1998). The host rocks to the Pb-Zn-Ag deposits become progressively younger from the southeast to the northwest. Although only maximum depositional ages exist for the host sediments at Cannington, they are likely to be as old as or slightly older than the host rocks at Dugald River, and the Mount Isa and Hilton deposits in the Western Fold Belt (ca. 1655 Ma). The Lady Loretta deposit in the central Lawn Hill Platform is hosted by slightly younger sediments deposited at ca. 1647 Ma. The host sediments to the Walford Creek deposit on the southern flank of the Murphy Inlier and the HYC deposit in the McArthur Basin were deposited ca. 1640 Ma. The Century deposit in the northwest Lawn Hill Platform is the exception to the general westerly younging trend and is hosted in sediments deposited at ca. 1595 Ma. Galena Pb isotope values vary systematically between deposits (Sun et al., 1994) as do model Pb-Pb ages. Model Pb-Pb ages calculated for Mount Isa (1653 Ma), McArthur River (1640 Ma), and Century (1575 Ma) shift systematically towards younger ages with the age of the host rocks, attesting to the robustness of this technique (Carr and Sun, 1996; Carr et al., 1996). The westward progression of host rock ages for the Pb-Zn-Ag deposits and the systematic younging of the Pb-Pb model ages for galena in the deposits imply that the time of sulphide precipitation was intimately linked to depositional processes (Page and Sweet, 1998). Southgate et al. (2000a, b) proposed a model in which the Pb-Zn-Ag deposits in northern Australia were formed by migration and focussing of metal-bearing fluids into evolving sub-basin depocentres, and that these major fluid flow events were a response to changes in intraplate stress during major tectonic events that coincided with bends on the apparent polar wander path for northern Australia. However, in the case of the 'Broken Hill type' deposits of the Eastern Succession (e.g. Cannington and Maramungee, hosted in upper amphibolite facies rocks) it has been argued that the majority of the Pb-Zn-Ag mineralisation postdates peak-metamorphic assemblages (e.g. Williams and Smith 2003).

The westerly to north-westerly younging direction for the host rocks to the Pb-Zn-Ag deposits can be extended to include deposits in the Broken Hill Block and the Georgetown Block (e.g. Page and Sun, 1998; Southgate et al., 2000a). Broad geochronological and lithological similarities suggest the possibility of tectonostratigraphic connections between the Eastern Fold Belt and the Broken Hill Block and the Georgetown Inlier in southern Australia and northeast Queensland respectively (e.g. Derrick, 1976; Laing, 1990; Blewett and Black, 1998; Black et al., 1998; Blewett et al., 1998; Page and Sun, 1998). Laing (1996) proposed that the Eastern Fold Belt was an allochthonous terrane that formed part of this eastern Australian 'Diamantina Orogeny', and was rafted on to the rest of the Mount Isa Inlier during the younger east-west events. However, the recent geochronology

of basin phases described above has demonstrated the contemporaneous accumulation of sedimentary sequences in the Western Fold Belt and the Eastern Fold Belt (Page and Sun, 1998) and it has been suggested that the two terranes represent a tectonic continuum of crustal shortening rather than discrete orogenic events (Giles and MacCready, 1997). The host rocks to the Broken Hill Deposit were laid down at ca. 1690 Ma (Page and Lang, 1992) and galena yielded a Pb-Pb model age for the mineralization of ca. 1675 Ma (Carr et al., 1996). Similar Pb-Pb isotope ratios were obtained from the Cannington deposit, and the Mount Misery and Railway Flat deposits in the Georgetown Block. The Georgetown deposits are hosted in the Einasleigh Metamorphics. The precise age of the host rocks is not well defined, although it is likely to be between ca. 1700-1675 Ma (Black et al., 1998).

5.4.2 Cu ± Au deposits

The stratigraphic range of the host rocks to the Cu ± Au deposits is much more widespread than that of the Pb-Zn-Ag deposits although many of the most significant deposits are hosted in the younger rock sequences. The majority of the medium to large tonnage Cu ± Au deposits (e.g. Mount Isa Copper, Osborne, Starra) in the Mount Isa Inlier are hosted in Cover Sequence 3 rocks with the notable exception of Ernest Henry, the largest deposit in the Eastern Succession. The latter deposit is hosted by volcanic rocks presumed to be equivalent to the nearby Fort Constantine Volcanics that were erupted (or emplaced as shallow intrusions) at ca. 1745 Ma. The Fort Constantine Volcanics overlap in age with the Wonga Batholith and thus can be considered as occurring at the end of the major Leichhardt Superbasin equivalent deposits in the Eastern Succession (Figure 3; although note the rather enigmatic Doherty Formation postdates the Fort Constantine Volcanics). Despite the preponderance of Cover Sequence 3 rock units as hosts to the economically significant deposits, there are literally thousands of Cu ± Au occurrences throughout the Mount Isa Inlier. Perhaps the highest concentration of these occurs within the Mary Kathleen Fold Belt to the west of the Pilgrim Fault, with the majority hosted in Cover Sequence 2 rocks (i.e. the Corella Formation, Argylla Formation, and Ballara Quartzite). Several significant resources and/or former mines occur within this belt including small to medium tonnage deposits such as Trekelano and Wee MacGregor, and also low tonnage but high grade deposits e.g. Duchess (205,000 tonnes at 12.3 % Cu) and Tick Hill (470,000 tonnes at 27 g/t Au) (Williams, 1998a). The districts only significant uranium deposit (the now abandoned Mary Kathleen mine) is also located in this belt. Cu ± Au deposits also occur within the older rocks of the Kalkadoon-Leichhardt belt with the most significant being Mount Cuthbert to the northeast of Kajabbi that is hosted in Leichhardt Volcanics.

In summary, the age of the host rocks is much less significant for the Cu ± Au deposits than for the Pb-Zn-Ag deposits. Suitable host rocks also appear to be a significant factor in the formation of the deposits. Indeed, in the Western Fold Belt, McIntyre et al. (2005) highlighted a possible association between Cu occurrences and local depocentres within the Myally Formation (ca. 1775 Ma), Quilalar Formation (ca. 1748 Ma) and Surprise Creek Formation (ca. 1695 Ma). These researchers attributed this association to the prevalence of (and role as a reductant) of deeper-water facies carbonaceous siltstones in the depocentres.

6. Main Points

- Accumulation of new stratigraphic and igneous age dates allows a substantial revision of the stratigraphic framework for the Mount Isa Inlier.
- Majority of Soldiers Cap Group deposited ca. 1675-1650 Ma.

- Geochronology doesn't support the division of the Soldiers Cap into an older (Fullarton River Group) and younger (Soldiers Cap Group).
- Probable unconformity separating Llewellyn Creek Formation at Snake Creek from Mount Norna Quartzite. Llewellyn Creek Formation at Snake Creek possibly temporal equivalent of Calvert Superbasin in the west (deposited ca.1694 Ma?)
- Units in Boomarra Horst previously mapped as Soldiers Cap removed from this group, likely to consist of Argylla Formation volcanics (ca. 1774 Ma) unconformably overlain by Ballara Quartzite (ca. 1755 Ma) and Corella Formation.
- The Answer Slate, Kuridala Formation, Staveley Formation, Marimo Slate and Agate Downs Siltstone were deposited between ca. 1675-1610 Ma. These units (bar the Kuridala Formation) have been removed from the cover sequence 2 Mary Kathleen Group and given the informal name 'Young Australia Group'. The Kuridala Formation has been included in the Soldiers Cap Group.
- The Young Australia Group likely to be lateral facies equivalents of the Soldiers Cap Group. Possible links between the Answer Slate and the Kuridala Formation, and between the Staveley Formation and the Mount Norna Quartzite.
- Although unconstrained by geochronology, the Mount Albert Group is likely to have been deposited during the major depositional period that produced the Soldiers Cap Group and the Young Australia Group (ca. 1675-1610 Ma).
- Distribution and extent of younger sequences deposited between ca. 1630 -<1610 Ma (mostly calcareous and/or carbonaceous units) within the Tommy Creek Block, Marimo Basin and possibly elsewhere relatively unconstrained.
- Mitakoodi Quartzite and Ballara Quartzite likely to represent a single regionally extensive sequence deposited at ca. 1755 Ma.
- The Double Crossing Metamorphics (and Gin Creek Granite) isn't a tectonically emplaced basement block. Rather, it was deposited after ca. 1815 Ma, and most likely correlates with the Argylla Formation and Mitakoodi Quartzite that outcrop to the west of this unit.
- EMP (electron microprobe) U-Th-Pb dating of the Quamby Conglomerate supports deposition of this unit after ca. 1640 Ma and before ca. 1500 Ma.
- The accumulation of volcanosedimentary sequences in the Eastern Succession can be divided into four distinct age groupings, namely: ca. 1890-1850 Ma, ca. 1800-1725 Ma, ca. 1710-1690 Ma (possible age of Llewellyn Creek Formation at Snake Creek), and ca. 1680-1610 Ma.
- The periods of sedimentary accumulation in the Eastern Succession broadly coincide with temporally equivalent accumulations in the Western Fold Belt.
- Significant (usually bimodal) igneous activity immediately precedes (and often overlaps with) the beginning of each period of sedimentary accumulation.
- The locus of bimodal vulcanism in the southern Mount Isa Inlier migrates progressively from the west to the east with time.
- Most of the Eastern Succession to the west of the Pilgrim Fault is likely to have been a topographic high between ca. 1780-1755 Ma, until the Ballara Quartzite unconformably overlay the ca. 1780 Ma Argylla Formation.
- Detrital zircon populations in the cover sequence 3 sediments in the Eastern Succession are generally characterised by 'Argylla' (ca. 1789-1760 Ma) and 'Wonga' (ca. 1750-1730 Ma) type age groupings indicating that the Mary Kathleen Belt may have been a topographic high during accumulation of these units.
- Detrital zircons from high metamorphic grade sediments in the southeast contain numerous grains with ages between ca. 1730-1710 Ma, possibly indicating an emergent siliciclastic source terrane to the southeast.

- Host rocks to the Pb-Zn-Ag deposits and prospects are restricted to cover sequence 3 units across the Mount Isa Inlier and, with the exception of hosts to the Century deposit, young from the southeast towards the northwest.
- Cu ± Au deposits and prospects are hosted within units representing all the major periods of volcanosedimentary accumulation. However, many of the most significant deposits are found within the younger sequences.

6. REFERENCES

Beardsmore, T.J., Newbery, S.P. and Laing, W.P., 1988. The Maronan Supergroup: an inferred early volcanosedimentary rift sequence in the Mount Isa Inlier, and its implications for ensialic rifting in the middle Proterozoic of northwest Queensland. Precambrian Research, 40/41: 487-507.

Betts, P.G., Lister, G.S. and O'Dea, M.G., 1998. Asymmetric extension of the Middle Proterozoic lithosphere, Mount Isa terrane, Queensland, Australia. Tectonophysics, 296: 293-316.

Bierlein, F.P. and Black, L., 2004. SHRIMP U-Pb dating of zircons in 3 samples of pre-Barramundi Basement rocks in the Western Fold Belt of the Mount Isa Inlier. In pmdCRC Architecture A1 annual project report to 30/06/04, pp. 5-7.

Black, L.P., Gregory, P., Withnall, I.W. and Bain, J.H.C., 1998. U-Pb zircon age for the Etheridge Group, Georgetown region, north Queensland: implications for relationship with the Broken Hill and Mt Isa sequences. Australian Journal of Earth Sciences, 45: 925-935.

Blake, D.H., 1987. Geology of the Mount Isa Inlier and environs. Bureau of Mineral Resources, Geology and Geophysics, Bulletin 225, Canberra. 83 pp.

Blake, D.H. and Stewart, A.J., 1988. Block and possible terrane boundaries in the Mount Isa Inlier. Bureau of Mineral Resources, Geology and Geophysics, Research Newsletter, 9: 2-3.

Blake, D.H. and Stewart, A.J., 1992. Stratigraphic and tectonic framework, Mount Isa Inlier. In: Stewart, A J. and Blake, D.H., eds. Detailed studies of the Mount Isa Inlier. Australian Geological Survey Organization Bulletin, 243: pp. 1-12.

Blenkinsop, T.G., Huddlestone-Holmes, C., Foster, D.R.W., Mark, G., Austin, J., Edmiston, M., Lepong, P., Ford, A. and Murphy, F.C., 2005. 3-D model and crustal architecture of the Mt Isa Eastern Succession. I2-3 Final Report, pmdCRC.

Blewett, R.S. and Black, L.P., 1998. Structural and temporal framework of the Coen Region, north Queensland: implications for major tectonothermal events in east and north Australia. Australian Journal of Earth Sciences, 45: 597-609.

Blewett, R.S., Black, L.P., Sun, S-s., Knutson, J., Hutton, L.J. and Bain, J.H.C., 1998. U-Pb zircon and Sm-Nd geochronology of the Mezoproterozoic of North Queensland: implications for a Rodinian connection with the Belt supergroup of North America. Precambrian Research, 89: 101-127.

Carr, G.R. and Sun, S-S., 1996. Lead isotope models applied to Broken Hill-style terrains-syngenetic vs epigenetic metallogenesis. In: Pongiatz, J. and Davidson, G., eds. New developments in Broken Hill-type deposits. pp. 77-88. CODES Key Centre, University of Tasmania Special Publication 1.

Carr, G.R. and Sun, S-S., Page, R.W. and Hinman, M., 1996. Recent developments in the use of lead isotope model ages in Proterozoic terrains. In: Baker, T., Rotherham, J., Mark, G. and Williams P.J., eds. MIC 96: New developments in metallogenic research: The McArthur, Mt Isa, Cloncurry minerals province, pp. 33-35. James Cook University Economic Geology Research Unit Contribution 55.

Connors, K.A. and Page, R.W., 1995. Relationships between magmatism, metamorphism and deformation in the western Mount Isa Inlier, Australia. Precambrian Research, 71: 131-153.

Davis, B.K., Pollard, P.J., Lally, J.H., McNaughton, N.J., Blake, K. and Williams, P.J., 2001. Deformation history of the Naraku Batholith, Mt Isa Inlier, Australia: implications for pluton ages and geometries from structural study of the Dipvale Granodiorite and Levian Granite. Australian Journal of Earth Sciences, 48: 113-129.

Derrick, G.M., 1976. Some insights into old and new zinc mineralization at Dugald River and Squirrel Hills, and uranium at Mary Kathleen, Queensland. Journal of Australian Geology and Geophysics, 1: 251.

Derrick, G.M., 1980. Marraba, Queensland, 1:100.000 geological map commentary. Bureau of Mineral Resources, Canberra.

Derrick, G.M., 1982. A Proterozoic rift zone at Mount Isa, Queensland, and implications for mineralisation. Journal of Australian Geology and Geophysics, 7: 81-92.

Domagala, J., Southgate, P.N., McConachie, B.A. and Pidgeon, B.A., 2000. Evolution of the Palaeoproterozoic Prize, Gun, and lower Loretta Supersequences of the Surprise Creek Formation and Mt Isa Group. Australian Journal of Earth Sciences, 47: 485-507.

Ellis, D.J. and Wyborn, L.A.I., 1984. Petrology and geochemistry of Proterozoic dolerites from the Mount Isa Inlier. Journal of Australian Geology and Geophysics, 9: 19-32.

Eriksson, K.A. and Simpson, E.L., 1990. Recognition of high-frequency sea-level fluctuations in Proterozoic siliciclastic tidal deposits, Mount Isa, Australia. Geology, 18: 474-477.

Eriksson, K.A., Simpson, E.L. and Jackson, M.J., 1993. Stratigraphical evolution of a Proterozoic syn-rift to post-rift basin: constraints on the nature of lithospheric extension in the Mount Isa Inlier, Australia. In: Frostick, L.E. and Steel, R.J. eds. Tectonic controls and signatures in sedimentary successions, pp. 203-221. International Association of Sedimentologists Special Publication 20.

Etheridge, M.A., Rutland, R.W.R. and Wyborn, L.A.I., 1987. Orogenesis and tectonic processes in the Early to Middle Proterozoic of northern Australia. In: Kroner, A. (ed.) Precambrian lithospheric evolution. American Geophysical Union, Geodynamics series, 17: 131-147.

Foster, D.R.W., 2003. Proterozoic low-pressure metamorphism in the Mount Isa Inlier, northwest Queensland, Australia, with particular emphasis on the use of calcic amphibole chemistry as temperature-pressure indicators. Unpubl. PhD thesis, James Cook University.

Giles, D., Betts, P. and Lister, G., 2002. Far-field continental backarc setting for the 1.80-1.67 Ga basins of northeastern Australia. Geology, 30: 823-826.

Giles, D. and MacCready, T., 1997. The structural and stratigraphic position of the Soldiers Cap Group in the Mount Isa Inlier. In: Ailleres, L. and Betts, P.G., (eds.), Structural elements of the Eastern Succession-a field guide illustrating the structural geology of the eastern Mount Isa terrane, Australia. Australian Crustal Research Centre, technical publication 63: 61-73.

Giles, D. and Nutman, A.P., 2002. SHRIMP U-Pb monazite dating of 1600-1580 Ma amphibolite facies metamorphism in the southeastern Mt Isa Block, Australia. Australian Journal of Earth Sciences, 49: 455-565.

Giles, D. and Nutman, A.P., 2003. SHRIMP U-Pb zircon dating of the host rocks of the Cannington Ag-Pb-Zn deposit, southeastern Mt Isa Block, Australia. Australian Journal of Earth Sciences, 50: 295-309.

Glikson, A.Y., Derrick, G.M., Wilson, I.H. and Hill, R.M., 1976. Tectonic evolution and crustal setting of the middle Proterozoic Leichhardt River fault trough, Mount Isa region, northwestern Queensland. Journal of Australian Geology and Geophysics, 1: 115-129.

Hand, M. and Rubatto, D., 2002. The scale of the thermal problem in the Mount Isa Inlier. In: Preiss, V.P., (ed.), Geoscience 2002: expanding horizons. Abstracts of the 16th Australian Geological Convention, Adelaide Convention Centre, Adelaide, SA, Australia. July 1-5, 2002, number 67. 475 pp.

Hoadley, E., Rubenach M.J., Coleborn, D., Sisois, I. and Fanning, M., 2001. Significance of an amphibolite facies shear zone event synchronous with the emplacement of the Sybella Batholith, Mount Isa. In: Davidson, G. and Pongratz, J., (eds.), 2001: a structural Odyssey. Geological Society of Australia, Abstracts 64. p. 83.

Idnurm, M. and Wyborn, L., 1998a. Palaeomagnetism and mineral exploration related studies in Australia: a brief overview of Proterozoic applications. AGSO Journal of Australian Geology and Geophysics, 17: 277-284.

Idnurm, M. and Wyborn, L., 1998b. A Mesoproterozoic age for the gold-bearing Quamby Conglomerate, Queensland. AGSO Research Newsletter 28.

Jackson, M.J., Scott, D.L. and Rawlings, D.J., 2000. Stratigraphic framework for the Leichhardt and Calvert Superbasins: review and correlations of the pre-1700 Ma successions between Mt Isa and McArthur River. Australian Journal of Earth Sciences, 47: 381-403.

Jackson, M.J., Simpson, E.L. and Eriksson, K.A., 1990. Facies and sequence stratigraphic analysis in an intracratonic, thermal relaxation basin: the early Proterozoic, Lower Quilalar Formation and Ballara Quartzite, Mount Isa, Australia. Sedimentology, 37: 1053-1078.

Laing, W.P., 1990. The Cloncurry terrane: an allochthon of the Diamantina orogen rafted on to the Mount Isa orogen, with its own distinctive metallogenic signature. In: Mount Isa Inlier Geology Conference abstracts, Victorian Institute of Earth and Planetary Sciences, Melbourne. 19-22.

Laing, W.P., 1996. The Diamantina orogen linking the Willyama and Cloncurry terranes, eastern Australia. In: Pongratz, J. and Davidson G.J., eds. New developments in Broken Hill type deposits. University of Tasmania Centre for Ore Deposit Studies special publication 1: 67-72.

Laing, W.P. and Beardsmore, T.J., 1986. Stratigraphic rationalisation of the eastern Mount Isa block, recognition of key correlations with Georgetown and Broken Hill Blocks in an Eastern Australian Proterozoic terrain, and their metallogenic implications. Proceedings of the 8th Australian Geological Convention, Adelaide. pp.114-115.

McDonald, G.D., Collerson, K.D. and Kinny, P.D., 1997. Late Archean and Early Proterozoic evolution of the Mount Isa block, northwest Queensland, Australia. Geology, 25: 1095-1098.

McIntyre A., Debenham, S., Gibson, G., Henson, P., Lambeck, A., Hutton, L. and Southgate, P., 2005. Basin analysis and sequence stratigraphy. I1 Project Final Report, pmdCRC.

Mark, G., Foster, D.R.W., Oliver, N.H.S., Richmond, J.M., Pollard, P.J. and Tolman, J.L., 2001. The role of magmatism in regional sodic-calcic alteration in the Cloncurry district, northern Australia. In: Mark, G., Oliver, N.H.S., Foster, D.R.W. and Marshall, L.J., (eds.), Mineralisation, alteration and magmatism in the Eastern Fold Belt, Mount Isa Block, Australia. Geological Society of Australia Specialist Group in Economic Geology, Special Publication number 5: pp. 46-63.

Mark, G., Pollard, P., Mustard, R., Foster, D., and McNaughton, N. 2005b. Episodic syn-tectonic magmatism in the Cloncurry district, NW Queensland, Australia: Implications for the origin, derivation and tectonic setting of "A type" magmas. I2+3 Final Report, pmdCRC.

Neumann, N., Southgate, P. and McIntyre, A., 2005. Chronostratigraphy and Geodynamics of the Western Fold Belt, Mount Isa Inlier. In, I1-Western Succession 3D architecture and ore systems final report, pmdCRC.

O'Dea, M.G., Lister, G.S., MacCready, T., Betts, P.G., Oliver, N.H.S., Pound, K.S., Huang, W. and Velenta, R. K., 1997. Geodynamic evolution of Proterozoic Mount Isa terrain. In: Burg, J.P. and Ford, M., (eds.), Orogeny through time. Geological Society of London, Special Publication 121: pp. 99-122.

Page, R.W., 1978. Response of U-Pb zircon and Rb-Sr total-rock and mineral systems to low grade regional metamorphism in Proterozoic igneous rocks, Mount Isa Inlier, Australia. Journal of the Geological Society of Australia, 25: 141-164.

Page, R.W., 1983. Chronology of magmatism, skarn formation and uranium mineralisation, Mary Kathleen, Queensland, Australia. Economic Geology, 78: 838-853.

Page, R.W., 1998. Links between eastern and western fold belts in the Mount Isa Inlier, based on SHRIMP U-Pb studies. Geological Society of Australia Abstracts, 49: 349.

Page, R.W. and Bell, T.H., 1986. Isotopic and structural responses of granite to successive deformation and metamorphism. Journal of Geology, 94: 365-379.

Page, R.W., Jackson, M.J. and Krassay, A.A., 2000. Constraining sequence stratigraphy in north Australian basins: SHRIMP U-Pb zircon geochronology between Mount Isa and McArthur River. Australian Journal of Earth Sciences, 47: 431-459.

Page, R.W. and Laing, W.P., 1992. Felsic metavolcanic rocks related to the Broken Hill Pb-Zn-Ag orebody, Australia: geology, depositional age, and timing of high-grade metamorphism. Economic Geology, 87: 2138-2168.

Page, R.W. and Sun, S-s., 1998. Aspects of geochronology and crustal evolution in the Eastern Fold Belt, Mount Isa Inlier. Australian Journal of Earth Sciences, 45: 343-361.

Page, R.W. and Sweet, I.P., 1998. Geochronology of basin phases in the western Mt Isa Inlier, and correlation with the McArthur Basin. Australian Journal of Earth Sciences, 45: 219-232.

Page, R.W. and Williams, I.S., 1998. Age of the Barramundi Orogeny in northern Australia by means of ion microprobe and conventional U-Pb zircon studies. Precambrian Research, 40/41: 21-36.

Pearson, P.J., Holcombe, R.J. and Page R.W., 1992. Synkinematic emplacement of the Middle Proterozoic Wonga Batholith into a mid-crustal extensional shear zone, Mount Isa Inlier, Queensland, Australia. In: Stewart, A.J. and Blake, D.H., eds. Detailed studies of the Mount Isa Inlier. Australian Geological Survey Organization, Bulletin 243: 289-328.

Pollard, P.J. and McNaughton, N.J., 1997. U/Pb geochronology and Sm/Nd characteristics of Proterozoic intrusive rocks in the Cloncurry district, Mount Isa Inlier, Australia. In: Pollard, P.J. (compiler) AMIRA P438 Cloncurry base metals and gold: final report.

Pollard, P.J., Mark, G. and Mitchell, L.C., 1998. Geochemistry of post-1540 Ma granites spatially associated with regional sodic-calcic alteration and Cu-Au-Co mineralisation, Cloncurry district, northwest Queensland. Economic Geology, 93: 1330-1344.

Queensland Department of Mines and Energy, Taylor Wall & Associates, SRK Consulting Pty Ltd & ESRI Australia, 2000. North-west Queensland Mineral Province Report, Queensland department of mines and energy, Brisbane.

Rubenach, M. 2005. Tectonothermal evolution of the Eastern Fold Belt, Mount Isa Inlier. I2+3 Final Report, pmdCRC.

Rubenach, M.J., Adshead, N.D., Oliver, N.H.S., Tullemans, F., Esser, D. and Stein H., 2001. The Osborne Cu-Au deposit: geochronology, and genesis of mineralization in relation to host albitites and ironstones. In Williams, P.J. (ed.) 2001: a hydrothermal odyssey, new developments in metalliferous hydrothermal systems research, extended conference abstracts. EGRU contribution 59: 172-173.

Scott, D.L., Rawlings, D.J., Page, R.W., Tarlowski, C.Z., Idnurm, M., Jackson, M.J and Southgate, P.N., 2000. Basement framework and geodynamic evolution of the Palaeoproterozoic superbasins of north-central Australia: an integrated review of geochemical, geochronological and geophysical data. Australian Journal of Earth Sciences, 47: 341-380.

Southgate, P.N., Bradshaw, B.E., Domagala, J., Jackson, M.J., Idnurm, M., Krassay, A.A., Page, R.W., Sami, T.T., Scott, D.L., Lindsay, J.F., McConachie, B.A. and Tarlowski, C., 2000. Chronostratigraphic basin framework for Palaeoproterozoic rocks (1730-1575) in northern Australia and implications for base-metal mineralisation. Australian Journal of Earth Sciences, 47: 461-483.

Southgate, P.N., Scott, D.L., Sami, T.T., Domagala, J., Jackson, M.J., James, N.P. and Kyser, T.K., 2000. Basin shape and sediment architecture in the Gun Supersequence: a strike-slip model for Pb-Zn-Ag ore genesis at Mount Isa. Australian Journal of Earth Sciences, 47: 509-531.

Sun, S-S., Page, R.W., and Carr, G., 1994. Lead-isotope-based stratigraphic correlations and ages of Proterozoic sediment-hosted Pb-Zn deposits in the Mount Isa Inlier. AGSO Research Newsletter, 20: 1-2.

Wilde, A., Evins, P., McKnight, S., Foster, D.R.W. and Blenkinsop, T.G., in prep. Age and significance of the Quamby Conglomerate.

Williams, P.J., 1998 a. Metalliferous economic geology of the Mount Isa Eastern Succession, Queensland. Australian Journal of Earth Sciences, 45: 329-342.

Williams, P.J., 1998 b. Magmatic iron enrichment in high-iron metatholeiites associated with 'Broken Hill-type' Pb-Zn-Ag deposits, Mount Isa Eastern Succession. Australian Journal of Earth Sciences, 45: 389-396.

Williams, P.J. and Smith, M.J., 2003. Pb-Zn-(As) enrichments in amphibolites from Broken Hill-type ore systems, NW Queensland: products of retrograde hydrothermal dispersion. Geochemistry: Exploration, Environment, Analysis, volume 3: 245-261.

Wyborn, L.A.I., 1988. Petrology, geochemistry and origin of a major Australian 1880-1840 Ma felsic volcano-plutonic suite: a model for intracontinental felsic magma generation. Precambrian Research, 40/41: 37-60.

Wyborn, L.A.I., 1998. Younger *ca*.1500 Ma granites of the Williams and Naraku Batholiths, Cloncurry district, eastern Mount Isa Inlier: geochemistry, origin, metallogenic significance and exploration indicators. Australian Journal of Earth Sciences, 45: 397-411.

Wyborn, L.A.I., Page, R.W. and McCulloch, M.T., 1988. Petrology, geochronology and isotope geochemistry of the post-1820 Ma granites of the Mount Isa Inlier: mechanisms for the generation of Proterozoic anorogenic granites. Precambrian Research, 40/41: 509-541.

Section 3

Architecture

Detailed Reports

3D Model and Crustal Architecture of the Mt Isa Eastern Succession

Tom Blenkinsop, Cameron Huddlestone-Holmes, Damien Foster, Geordie Mark[1], Jim Austin, Mark Edmiston, Piter Lepong, Arianne Ford, Barry Murphy[2], Michelle Stark

School of Earth Sciences, James Cook University, Townsville QLD 4811
[1]School of Geosciences, Monash University, Melbourne, Victoria 3168
[2]School of earth Sciences, University of Melbourne, Victoria 3010

ABSTRACT

A preliminary 3D geological of the Eastern Succession of the Mount Isa Inlier model has been made from serial cross-sections constructed using geological map data, revised chronostratigraphy, gravity, magnetics, worms (multiscale wavelet edges of potential field data) and seismic data. The revised chronostratigraphy and the model suggest that the depositional basin architecture was controlled by major North-South crustal structures, which are interpreted to have had a prolonged history originating during east-west extension and deposition of Cover Sequence 2 and 3 rocks. These structures also localize upper crustal structures such as the Cloncurry Fault and Mitakoodi Anticlinorium. Positive inversion may have been a key process in the evolution of the inlier. The dominant role of North-South structures was established at least as early as Cover Sequence 1 and continued throughout the crustal evolution.

Keywords. Mount Isa Inlier, Crustal Architecture, Mitakoodi Anticlinorium, Inversion Tectonics, 3D model, Positive Inversion

1. INTRODUCTION

This report focuses on the crustal-scale geometry and relationships between rock units in the Eastern Succession of the Mt Isa Proterozoic inlier, referred to as the "Architecture" of the inlier. This focus was chosen because:

- Least is known about this scale of structural geology
- The only previous crustal scale models (e.g. MacCready et al., 1998) were based on a single interpretation of the Mt Isa seismic section
- Reinterpretation of the seismic section has lead to questions about this interpretation
- Worms (multiscale wavelet edges of potential field data) have provided a new method of interpreting crustal structure which is especially useful on large scales
- Revisions to the basin stratigraphy carried out in this project have resulted in new insights to depositional basin architecture

The geographic focus of the report is on the area for which a 3D model was constructed (370000mE, 7540000mN to 520000mE, 7770000mN MGA 94, Zone 54 – Fig. 1). This model is regional in scale and attempts to resolve the architecture of the crust down to the Moho. Building it has helped to identify shortcomings in our understanding of the area and highlighted where data is lacking. Information on the 3D geometries at this scale is restricted to geophysical data and as a result, the model is "expert driven". The report describes the construction of the 3D model, its current status and discusses the crustal architecture of the Eastern Succession. Particular attention is payed to the central part of this model south of Cloncurry, because this is the best-exposed area and the seismic section was obtained here.

2. 3D MODEL INPUT DATA

A large amount of geological data available for the Mount Isa inlier is available from Geoscience Australia (GA) and the Queensland Department of Natural Resources. The majority of this data is digital, typically in a GIS format and either free or at low cost. Published papers and unpublished theses are another source of publicly available data that has been utilized in the construction of the model. In addition to these public data sources this project has had access to detailed aeromagnetic and radiometric data collected by MIM Holdings Ltd. (now Xtrata) and Worms derived from this data. Below are descriptions of the main data elements that were used for this project.

2.1 Geology map data

1:100,000 Geology Maps compiled by the BMR are available for all of the area in which Proterozoic rocks crop out. They are the Cloncurry (Ryburn et al., 1988), Dajarra (Blake et al., 1982), Duchess (Blake et al., 1984), Kuridala (Donchak et al., 1984), Marraba (Derrick, 1980), Mary Kathleen (Derrick et al., 1977), Prospector (Derrick & Little, 1979), Quamby (Wilson et al., 1980), and Selwyn (Blake et al., 1983) sheets. These maps are also available as part of a GIS for the Mount Isa Inlier. GA have two versions of this dataset, a 1997 edition and a 2001 edition, the later version utilising more recent GIS formats. The geological data in these digital datasets are from the original 1:100,000 geology maps some of which are over 20 years old. Although some of the information and interpretations are incorrect or outdated, the data does provide a good representation of the surface geology at the 1:100,000 scale. There are some inconsistencies between map sheets as the result of the maps being produced over a long time period by different authors.

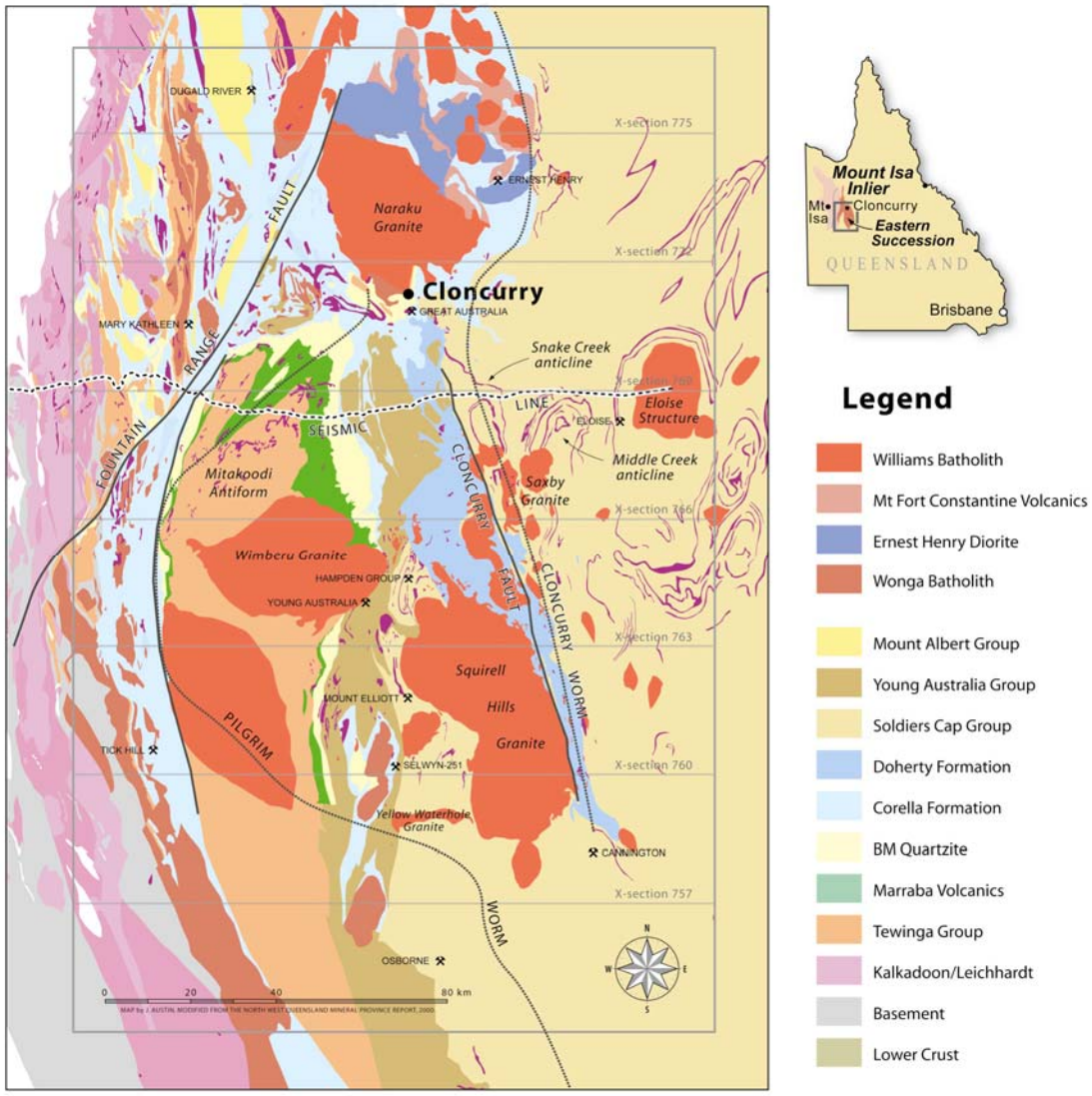

Fig. 1. Locality Map. Geology shown here is modified from the NWQMPR. The approximate surface traces of the Cloncurry and Pilgrim Worms are shown as dotted lines.

The 1:500,000 "Mount Isa Inlier & Environs Qld & NT geological map" by Blake (1987a) was useful in providing a broad scale overview of the geology of the region. A companion volume (Blake 1987b) contains useful information such as formation thicknesses. The chronostratigraphy in this report is outdated and unreliable.

2.2 North West Queensland Mineral Province Report

The North West Queensland Mineral Province Report (NWQMPR) (Queensland Department of Mines and Energy et al., 2000) was compiled by a team of industry consultants, ESRI Australia and the Queensland Department of Natural Resources and Mines (QDNRM, then the Department of Mines and Energy). The goals of this report were to provide a review of the geology of the Mount Isa Inlier, particularly with regard to mineralisation; new conceptual models for exploration and specific targets for base and precious metals; and to provide a comprehensive digital dataset. It provides an excellent starting point for studies in this terrain.

The components of the NWQMPR that proved most valuable to this project were an interpreted solid geology map/GIS at 1:250,000 scale and an attributed fault GIS dataset. This geology map was based on integrated interpretation of published 1:100,000 geology maps, open source geophysical data, MIM Holdings' airborne geophysical data and DME and GA gravity data. The map units are based on an updated "Time-Space Chart" that corrected some of the problems in Blake's (Blake 1987a) map. This interpreted geology provided the base geology from which the 3D model is being constructed.

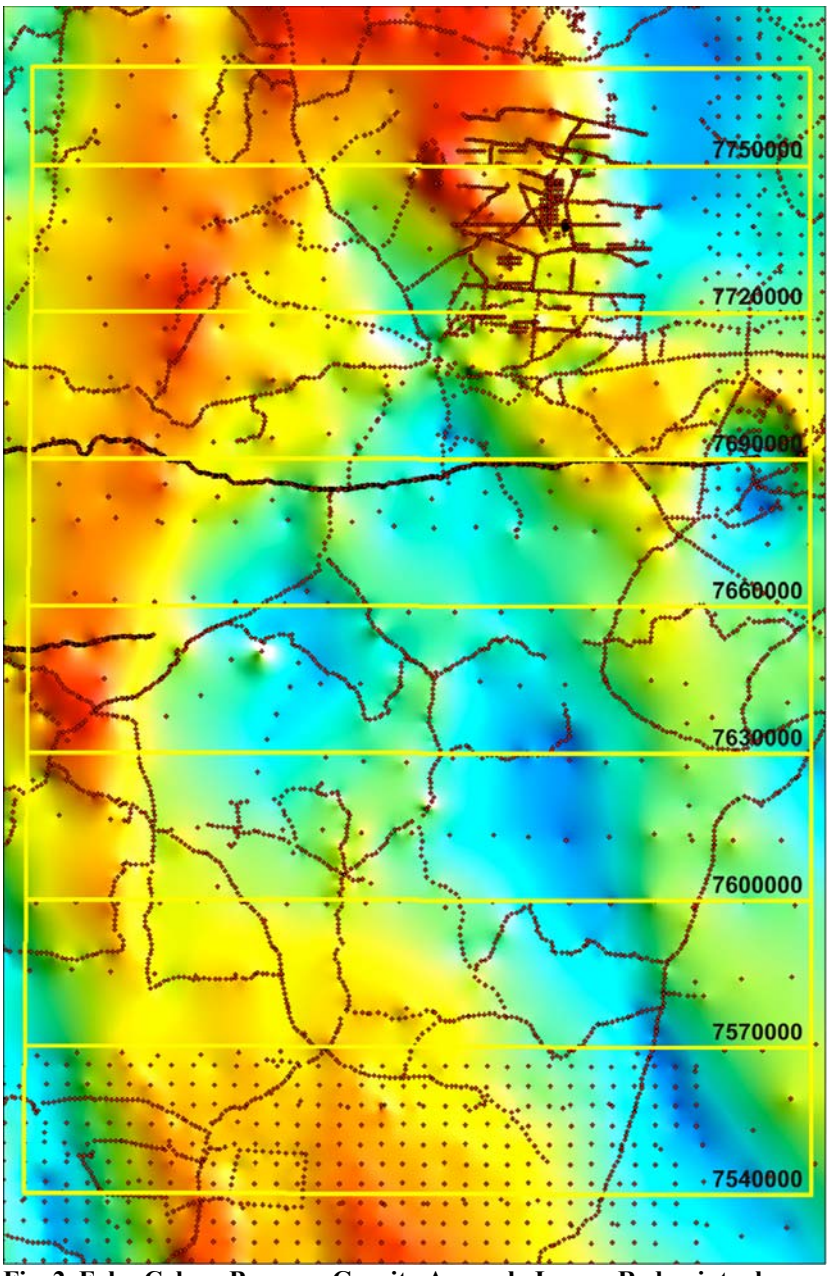

Fig. 2. False Colour Bouguer Gravity Anomaly Image. Red points show observation locations. The yellow box and lines show the 3d Model area and cross-section lines.

2.3 Gravity data

Gravity data was sourced from GA's "Gravity Anomaly Grid of the Australian Region". The grid cell size of the data is 0.5 minutes of arc (ca. 800m) and the cell values are Bouguer anomalies, density 2670 kgm^{-3}. Because of the size of the grid, the lowest wavelength anomalies that can be seen in the data are 1600m. However, the data used to generate the grid in the study area have highly variable spacing (see Fig. 2) that ranges from hundreds of metres to over 10 km. This further limits the scale of the anomalies that can be seen. The gravity observations are also available from GA in the "Australian National Gravity Database 2004". A false colour Bouguer anomaly map was produced for the area as well as anomaly profiles at various levels of upward continuation. These profiles help to separate different wavelength anomalies.

2.4 Magnetic data

Magnetic data used here are MIM Holdings Ltd.'s (now XStrata) aeromagnetic data (Fig. 3) This data was collected in 1994 for the whole of the Mount Isa Inlier in an airborne geophysics survey that included radiometrics. The dataset is confidential to researchers in the pmd*CRC. The survey was flown at a height of 70m and a 200m - 400m line spacing. The total magnetic intensity dataset is grided at a 50 m cell size. This is a high quality dataset that shows good detail. A greyscale total magnetic intensity map was produced for the area as well as anomaly profiles at various levels of upward continuation.

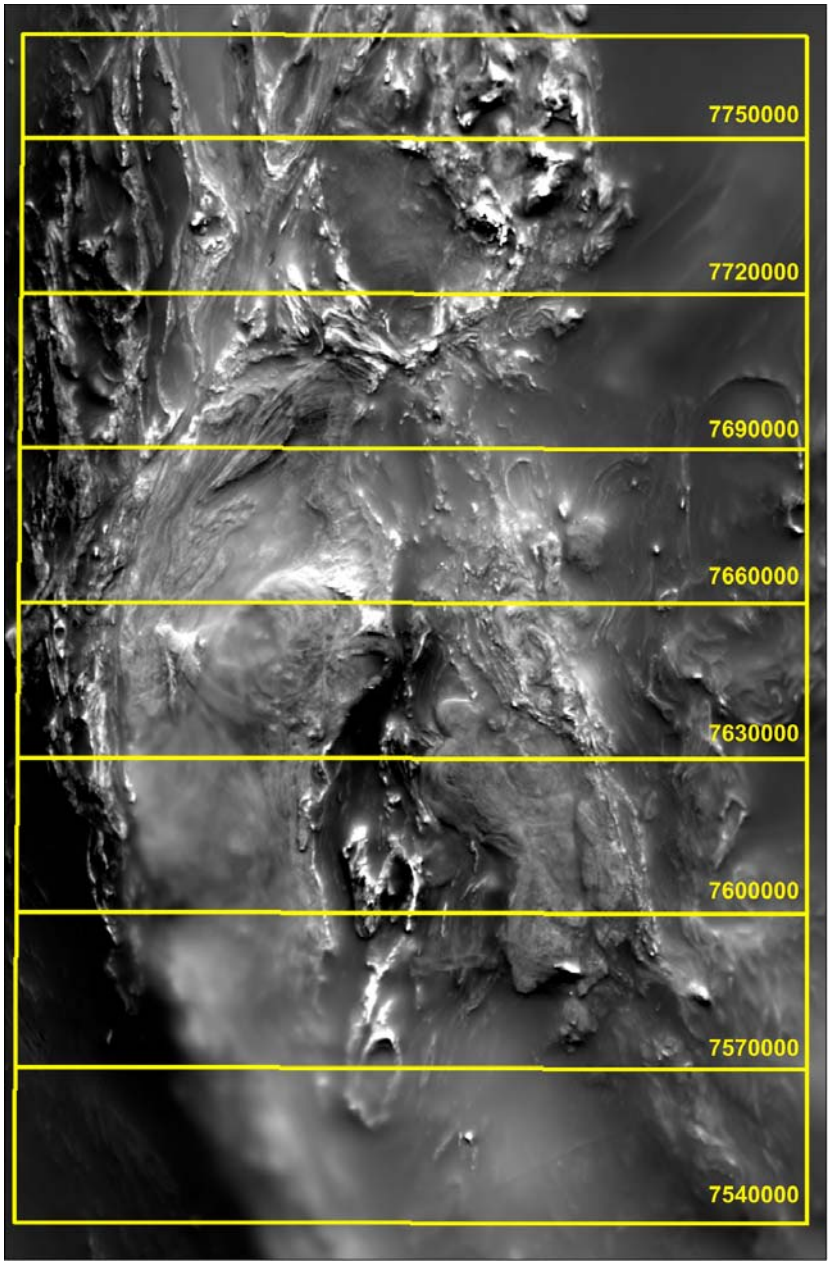

Fig. 3. Greyscale Total Magnetic Intensity image. The yellow box and lines show the 3D Model area and cross-section lines.

2.5 Worms

Both gravity and magnetic worm (multiscale wavelet edges of potential field data) datasets provided key data for this project (Fig. 4). The worm processing was done by Fractal Geosciences using the MIM aeromagnetics and gravity data provided to the pmd*CRC by BHP- Billiton, Placer, QDNRM and GA. Both "MAX" and EFVD worm types were produced, the former from the standard input data and the later from the enhanced first vertical derivative data. The magnetic data were regrided to a 200m cell size and upwardly continued to just under 30km. The gravity data were regrided to 500m and upwardly continued to just over 60km. Murphy (2002) provides a detailed report on these worm datasets.

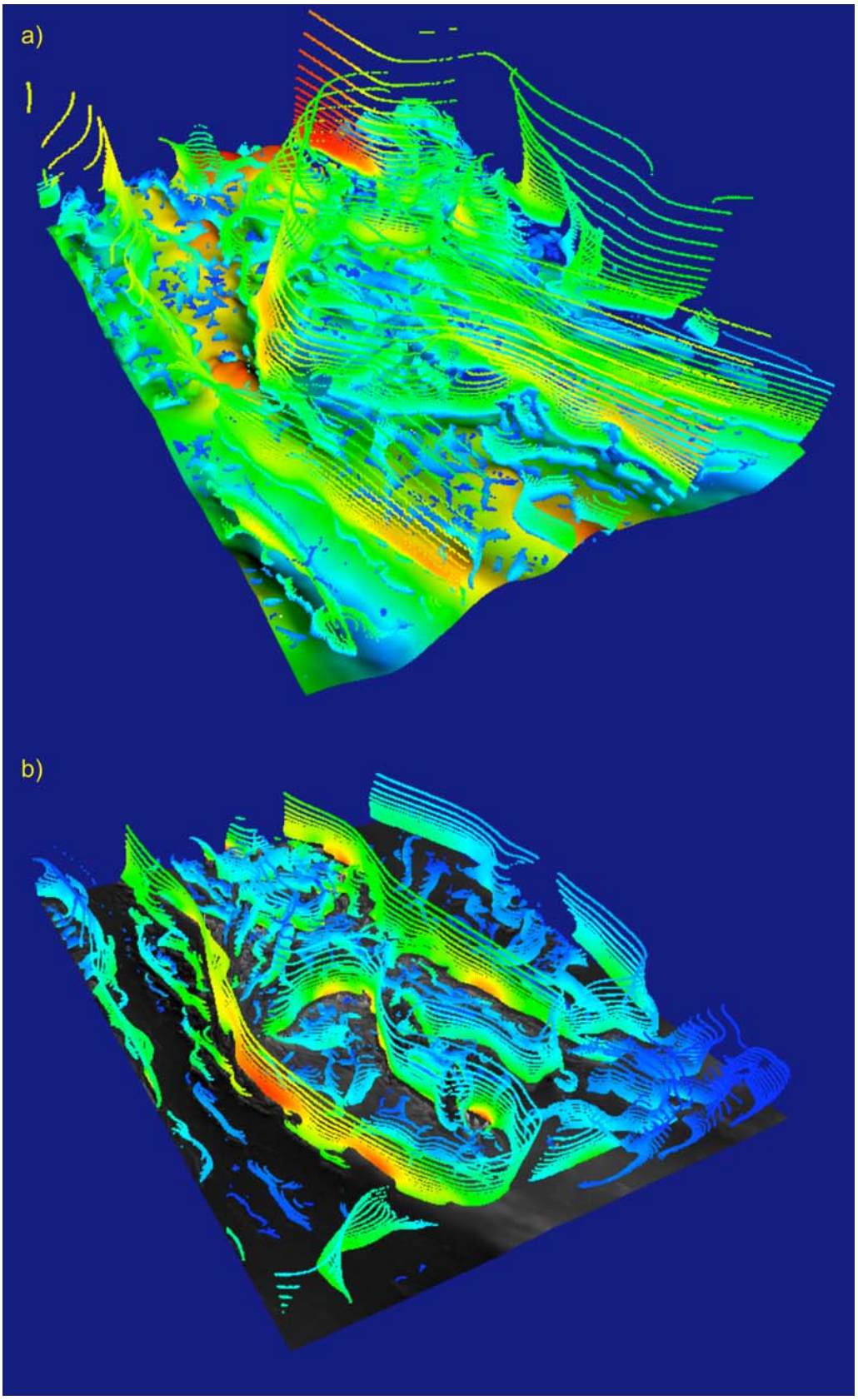

Fig. 4. Perspective views of (a) gravity worms and (b) magnetic worms.

Worms provide a way of viewing geophysical data in 3D and they were used in the interpretation of the 3D geology of the area imaged. They enhance edges in the dataset and

resolve high frequency, small wavelength anomalies (low levels of upward continuation) from low frequency, large wavelength anomalies (higher levels of upward continuation). An anomaly contrast at a particular level of upward continuation is generally thought to be the result of a geological feature at half the equivalent depth. The "W" value gives a measure of the magnitude of the contrast. Worms are particularly useful at defining the dips on structures and their level of continuity both at depth and along strike. It is important to note that worms will only be present where there is a contrast in the petrophysical properties being measured either side of a fault or lithological contact, and that a very strong anomaly at the surface may result in high levels of upward continuation that do not represent a deep source (e.g. magnetic worms around the Naraku Batholith).

The magnetic worms provide information on structures near the surface to approximately 10 km depth because of the fine scale of the original data and the maximum height of upward continuation. Deeper levels tend to be swamped by near surface contrasts. On the other hand, because of the coarse nature of the original dataset, the gravity worms provide more information on structures in the 2km to 20km range.

2.6 Seismic data

The Mount Isa seismic survey was done in 1994 as part of the Australian Geodynamics CRC (Goleby et al., 1998; Goncharov et al., 1998: Fig. 1). It consists of a 250km seismic reflection line and a coincident seismic refraction line that extends east and west of the reflection line for a total length of 500km. In the study area, the seismic line runs east-west at approximately 7690000mN (AMG 94, Zone 54). The seismic reflection line has been reprocessed as part of the I2+3 project (Lepong & Blenkinsop, 2005). The reprocessing made significant improvements in signal to noise ratio, continuity of reflectors, and collapsed some diffractions. However the section below approximately 3 seconds two-way travel time (approximately 9 km) remained almost devoid of information. The refraction data was collected to provide regional velocity data. Because of its course shot and receiver spacing it reveals little structural data and is more useful as an indicator of lithology and crustal composition at depth. Unfortunately it has not been possible to source a digital version of the velocity data.

2.7 Stratigraphic Data

A revised chronostratigraphy constructed by (Foster & Austin, 2005) for the I2/3 project was used for this model (Appendix 2). The revisions were made on the basis of all available age dates and reinterpretation of stratigraphic relationships. The main changes to that of the NWQMPR are:

- Including the Kuridala Formation with the Soldiers Cap Group;
- Moving the Lewellyn Creek formation out of and below the Soldiers Cap Group;
- Assigning an age of 1720Ma for the Doherty Formation (younger than the Corella Formation or the Wonga Batholith and Mount Fort Constantine Volcanics);
- Grouping the siliciclastic rocks of the Mary Kathleen Group (Answer Slate, Marrimo Slate, Stavely Formation) together as the informal Young Australia Group as a lateral facies variations to the Soldiers Cap Group and Mount Albert Group;
- Grouping the Ballara and Mitakoodi Quartzites as age equivalent;
- Putting the Quamby Conglomerate in the Mount Albert Group (based on new monazite age date in a conglomerate sample for peak metamorphism at ~1590Ma).

These changes are reflected in a revised version of the NWQMPR geology map (Fig. 1, an additional field has been added to the GIS file called "model unit"). Some other

modifications that were made to the geology map of the NWQMPR based on newer age data and reinterpretation of stratigraphy are:

- Removing the Double Crossing Metamorphics and replacing them with Ballara/Mitakoodi Quartzite. This makes more sense stratigraphically because the former has an inherited zircon population that matches that of the Ballara/ Mitakoodi quartzites;
- Assigning Wonga Batholith ages to the Levian Granite (southern end of the Naraku Batholith) and interpreted granites to the south of the Gin Creek Granite;
- Dividing the Capsize Creek Granite into the Dipvale Granite (southern end - Wonga Batholith) and the Mavis Granite (northern end - Williams Batholith);
- Separating the Doherty Formation from the Corella Formation;
- Including the Tommy Creek Beds and Roxmere Quartzite in the Young Australia Group.

3. METHODS

The first step in the model building process was to construct a series of east west cross-sections at thirty-kilometre spacing. A base sheet for each cross-section was made showing the worm data for a 600m wide swath centred on the section northing and the location of

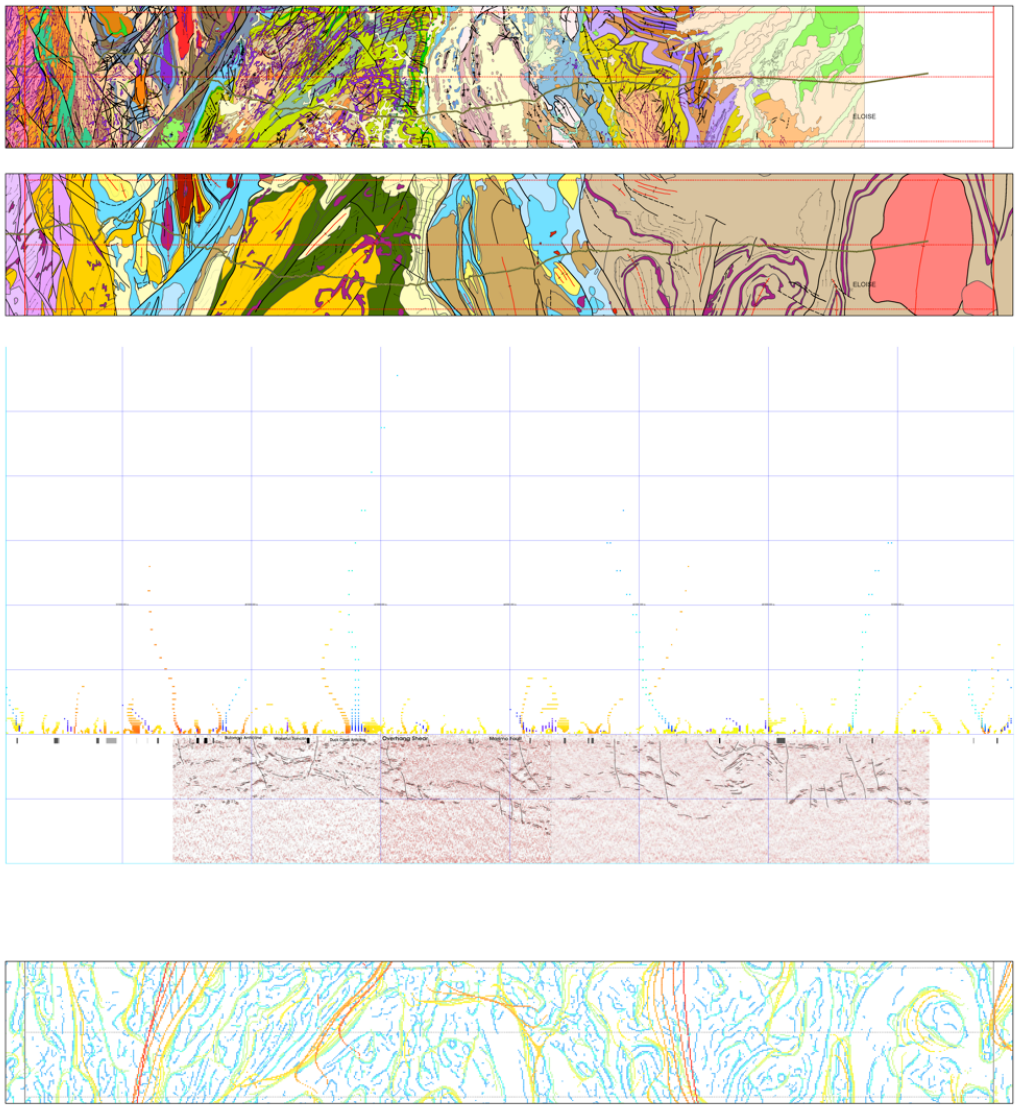

Fig. 5. Template used for construction of the 769 cross-section. Top panels: geology from 1: 100 000, and NWQMPR: Central panel: projections of magnetic worms (yellow and orange) and gravity worms (blue and green), seismic section, and lowest panel, magnetic worm strip map

fault intersections with the section, strip maps from the 1:100,000 geology GIS, the NWQMPR geology map and a strip map of the magnetic worms (Fig. 5). A Fracsis database containing all available digital data was used to provide a 3D context while constructing the sections. This was very important for tracing structures and maintaining consistent interpretations between sections.

Unconstrained inversions of the gravity and magnetic data were attempted in ModelVision; however they were deemed to be of little value. Forward modelling of gravity data for various geometries were used in a qualitative sense to check if the interpreted cross-sections were feasible. A more rigorous review of the 3D model using forward modelling and constrained inversions needs to be done to refine the model.

Once the cross-sections had been drawn they were digitised and imported into GoCad and Fracsis. Surfaces were built in GoCad for major faults and the lower crust. Surfaces for lithological contacts and intrusions need to be constructed.

3.1 Assumptions

The main difficulty in constructing a 3D model of this part of the Earth's crust is the lack of data in the third-dimension. Information about sub-surface geology can only be interpreted from surface geology and geophysical data. It is difficult to incorporate multiple hypotheses into a single 3D model and as a result some assumptions have to be made. The key assumptions in the model presented here are-

- the chronostratigraphy is as in Foster and Austin (2005),
- the Moho is at 50-55km and a 15km thick transition zone sits immediately above the Moho (Goncharov et al., 1998),
- a lower crust of mixed tonalite/diorite/gabbro underlies the basement. This material has a density in the range of 2850 to 3000 km/m^3. Melting of this material produces magmas that form the Williams Batholith (I and A type intrusives, Mark, 2001),
- the Bouguer anomaly distribution reflects mainly the depth to the top of the lower crust rather than the intrusion of large amounts of mafic rocks into the upper crust,
- a basement of granitic composition (i.e. silica rich) underlies the rocks of the three cover sequences (CS1 – 3). This crops out in the south-west of the area as the Plum Mountain Gneiss and Kurbaiya Migmatite. The density of these rocks will be in the range 2.6 to 2.8gm/cm^3,
- gravity worms with high levels of upward continuation represent crustal scale structures.

4. RESULTS AND GEOLOGICAL INTERPRETATION

Seven east-west cross-sections of the model area have been completed from 7570000mN to 7750000mN at 30km spacing (the 7570000mN section is referred as 757, etc). These sections show the crustal architecture from the top of the transition zone to the current land surface, and are presented in Appendix 1.

4.1 Basement architecture

Basement architecture has been interpreted on the basis of the long-wavelength gravity features and the gravity worms. There are three major gravity worms referred to as the KL (Kalkadoon-Leichhardt), Pilgrim and the Cloncurry worms (Fig. 6), all trending generally

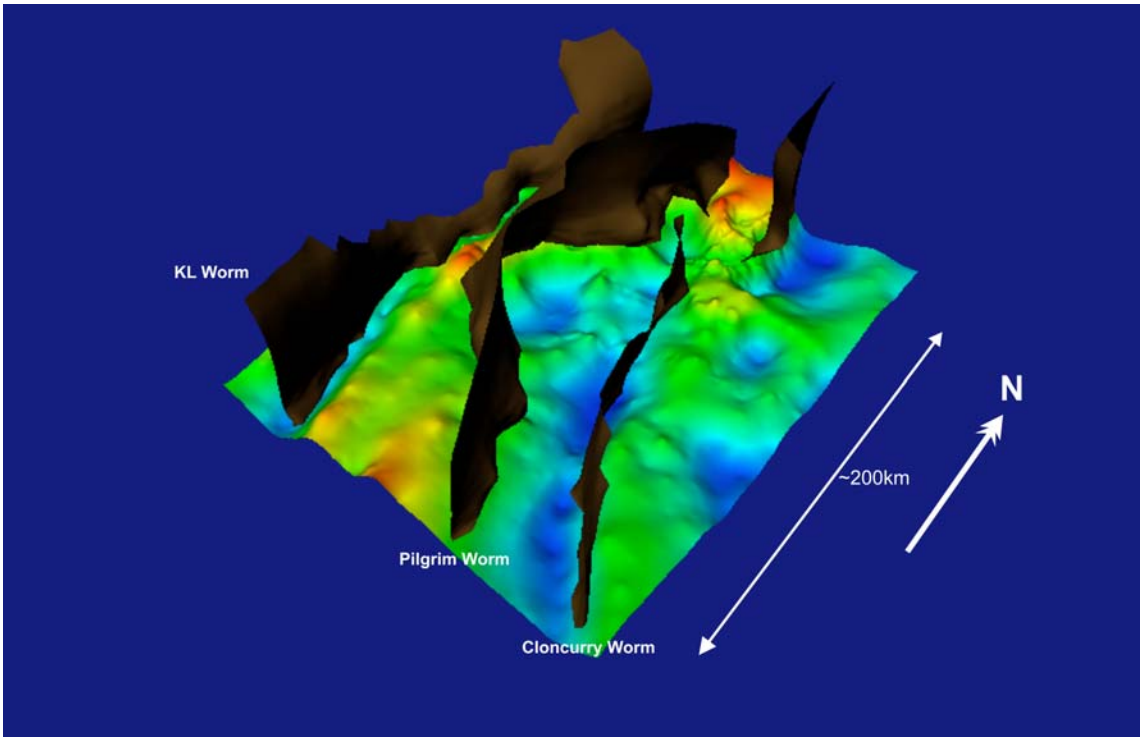

Fig. 6. Bouguer gravity anomaly as a 3D surface overlain by surfaces corresponding to the three major gravity worms.

NS. The KL worm is a steeply dipping structure that occurs at the surface near the western edge of outcrop of Eastern Succession rocks. The Pilgrim worm is readily defined at high levels of upward continuation, but is less readily defined as a discrete structure near the surface, and there is no surface structure that corresponds to the Pilgrim worm, although it is nearly coincident with the Pilgrim fault in its central section. It dips generally to the west (indicating an east dipping density contrast). In the southern part of the area, the NW-trending section of the Pilgrim worm (Figs. 1, 6) is likely to be due to the merging at high levels of upward continuation between the worm to the north, and separate, N- to NNW-trending worms through Selwyn and Osborne. The Cloncurry gravity worm dips steeply either to the west or east. It does not persist to the highest levels of upward continuation south of about 7700000mN. The Cloncurry gravity worm differs from the KL and Pilgrim worms in that it does have a coincident magnetic anomaly.

The major gravity worms are interpreted in the 3D model as steps in the lower crust because they separate long-wavelength anomalies of different magnitudes. Elevated gravity anomalies suggest a basement high. An alternate hypothesis would be that these gravity highs are caused purely by the intrusion of a large volume of mafic rocks in the regions that are now gravity highs. This is considered unlikely for several reasons. Firstly, the area of mafic outcrop is not high enough to increase the average density at the surface; secondly, the seismic refraction study suggests the density of the crust down to 18-20km is "granitic" (i.e. metasedimentary rocks, felsic volcanic rocks, granite) in terms of its silica content (Goncharov et al., 1997); finally, if a large volume of mafic rocks was intruded into crust with a "granitic" composition melting should occur producing granites with an S-type geochemical signature for which there is no evidence.

At the latitude of Cloncurry a subtle but consistent change in strike occurs in the gravity and magnetic anomalies, which are deflected to more easterly strikes over a zone approximately 20 km wide striking NE which is referred to as the Cloncurry Flexure. This feature is most pronounced in the magnetic image (Fig. 7). The Cloncurry worm cannot be

recognised as a discrete structure in this zone; however, to the north of the Cloncurry Flexure, a N-striking worm with similar continuity to the Cloncurry worm and higher levels of upward continuation can be seen. However, this worm separates gravity lows to the west from highs to the east, the opposite of the Cloncurry worm. If this worm is correlated with the Cloncurry worm, it indicates a dextral deflection or displacement of approximately 20 km. The distribution of gravity highs and lows also changes across this structure, with a broad central high to the north and the two ridges to the south. The lack of a direct surface expression of this flexure, combined with the above observations suggest that it is a deep and fundamental crustal structure. It may have been a transfer zone during basin formation that has been active from early stages of basin formation through orogenesis.

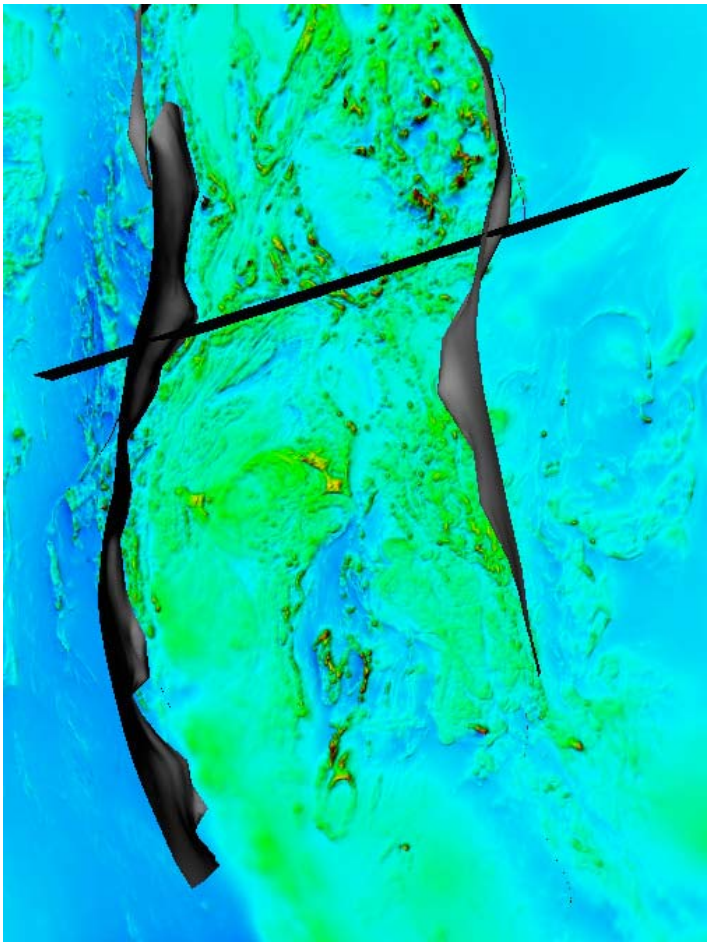

Fig. 7. TMI Aeromagnetic image superimposed with surfaces representing the major magnetic worms showing a change in strike of major features at Cloncurry, represented by the ENE trending vertical surface.

4.2 Depositional basin architecture and stratigraphy

The basin architecture has been established by compiling stratigraphic thickness estimates on 1: 100 000 sheets and analysing their geographical variation. The results are discussed in detail in Foster and Austin (2005). Fig. 8 is a schematic cross-section showing the stratigraphic relationships in the study area. It shows the structures in the lower crust that are interpreted to influence the location of faults that were active during the deposition of the three cover sequences. The western most structure is interpreted to control the location of a growth fault during the deposition of early CS2 rocks and the relationships between the Mt Albert, Young Australia and Soldier's Cap Groups of CS3.

The Eastern Succession rocks are interpreted to represent the western margin of a sedimentary basin that had a depocentre to the east of where Proterozoic rocks now crop out. This basin formed as the result of E-W extension and the Pilgrim and Cloncurry Worms and Cloncurry Flexure, are interpreted as formed by basement–cutting structures that were active during basin formation. CS1 rocks were deposited early during basin formation and outcrop only on its western margin. The lateral extent of CS1 and CS2 to the east is unknown. As basin formation progressed in CS2 the depo-centre migrated to the east.

4.3 Upper Crustal Structure

Major new insights into upper crustal structure have come from reprocessing the Mt Isa seismic section and from building the 3D model, in particular from the use of aeromagnetic worms to constrain dips of contacts.

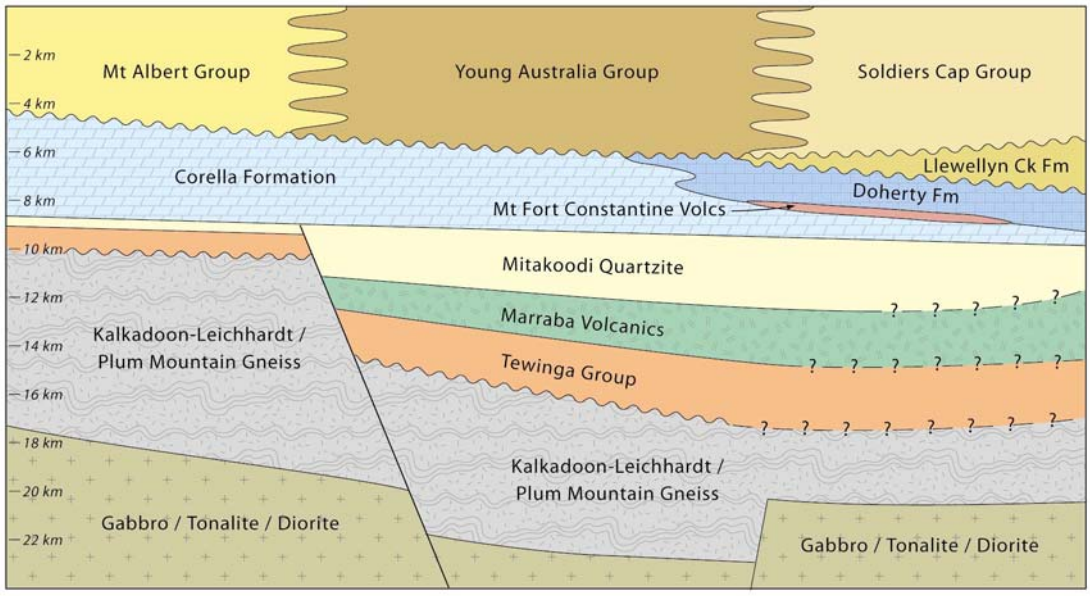

Fig. 8. Cartoon of the Stratigraphic Relationships in the Eastern Succession: from Foster and Austin (2005).

The newly processed seismic section (Lepong & Blenkinsop, 2005) suggests that a correlation of one reflector could be made with the base of CS2 on the west limb of the Mitakoodi anticlinorium (Fig. 1), and this was used to constrain the shape of the fold: a similar reflector on the East limb was interpreted as the other limb. An important result from the reprocessed section is that a sub-horizontal surface, previously interpreted as a detachment (MacCready et al., 1998), could not be seen across the whole section (see Fig. 9).

The largest upper crustal folds on the crustal-scale cross-sections are the Mitakoodi anticlinorium, the Snake Creek Anticline, the Weatherly Creek Syncline, the Middle Creek Anticline and a feature to the east of Eloise referred to as the Eloise structure (Fig. 1). Significant faults include the Fountain Range Fault, the Pilgrim Fault, the Overhang shear, the Cloncurry Fault and a number of N-S faults inferred to be under cover in the eastern part of the area.

All the folds identified above have upright to steeply east dipping, approximately NS axial surfaces (Fig. 1, Appendix 1). The Mitakoodi anticlinorium, which is the largest fold, plunges gently N to NE and changes northward into the Wakeful Syncline and the Bulonga and Duck Creek Anticlines. The Pilgrim worm at surface follows approximately the axial surface of the Mitakoodi anticlinorium in the northern part. The Snake Creek Anticline is markedly different in the respects that its fold hinge plunges subvertically in the northern part of the structure, and that much of the structure consists of overturned beds. The Cloncurry worm structure coincides with part of the Snake Creek Anticline, which is separated by the tight angular Weatherly Creek Syncline from the Middle Creek Anticline; the latter appears to have a similar geometry to the Snake Creek Anticline.

The Eloise structure is delineated on the aeromagnetic interpretation by almost continuous high susceptibility thin units, commonly in a pair, which are readily interpreted as mafic sills by analogy with their signature around the Snake Creek and Middle Creek structures. The structure has been modelled as a doubly plunging synform on the basis of dips suggested by aeromagnetic worms over the mafic sills in the limbs (agreeing with the interpretation in NWQMPR, Queensland Department of Mines and Energy et al., 2000).

The Mitakoodi, Snake Creek, Middle Creek and Eloise structures are all intruded by plutons of the Williams Naraku batholith (respectively the Wimberu granite, the Saxby granite and the unnamed granite in the Eloise structure, see Fig. 1 and Appendix 1).

All the major faults are subvertical at surface on the basis of dips given by worms, and strike approximately NS. Their depth can be inferred to some extent by the levels of upward continuation in worms corresponding to the faults. NE trending faults of generally shorter strike length appear to offset the Cloncurry Fault and worm dextrally in places.

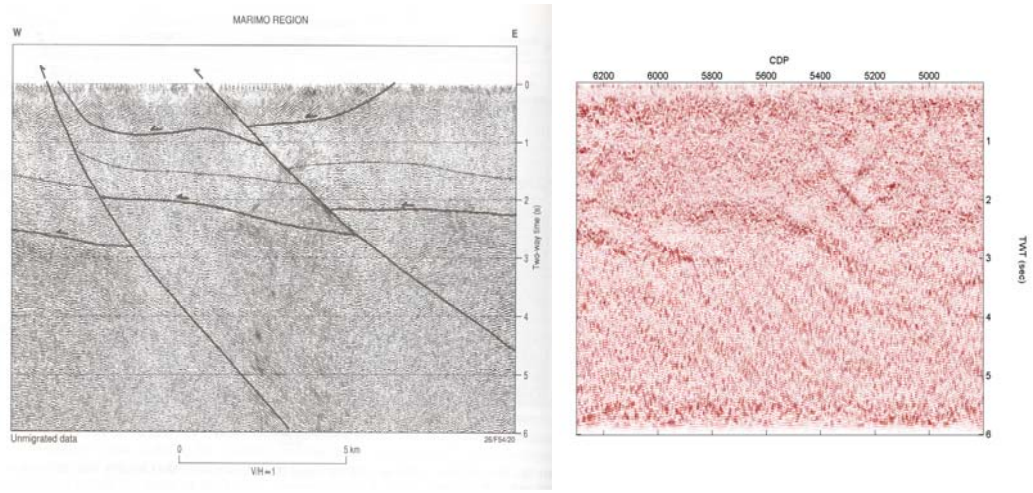

Fig. 9. Seismic sections showing previous interpretation by MacCready et al. (1998) (left) compared to reprocessed section by Lepong et al. (2005) (right). The reprocessed section does not show the sub-horizontal reflector previously interpreted as a decollement by MacCready et al. (1998).

A major regional structure is defined on the eastern edge of the Mt Isa inlier by both gravity and aeromagnetic worms, extending from Cannington in the south to north of Ernest Henry mine, a distance of over 200 km (Fig. 1). These worms trends NNW and generally dip steeply to the east but also to the west in places. Because the worms are seen in high levels of upward continuation, their depth extent is inferred to be greater than 20 km. The surface trace of the magnetic worms is referred to as the Cloncurry Lineament, and was studied in detail (Austin, 2005) in order to understand the geological significance of major worms.

The worms that generate the Cloncurry Lineament, like other major worms, are continuous and relatively straight at high levels of upward continuation, but have a complex geometry at low levels. The gravity contrast across the worm shows that it marks an elevation of basement to the east. The Cloncurry Lineament does not have a unique or diagnostic expression in the surface geology, but it is a zone of highly folded metasediments, breccias, mylonites, and numerous granitic to mafic intrusions. The Cloncurry Lineament corresponds to three geological features: 1) the boundary between the Doherty formation

and the Soldiers Cap group 2) contacts of plutons of the Saxby Granite and Maramungee Granite 3) NE-trending faults with dextral separations. Variations in the orientation and occurrence of these features are reflected in the complex geometry of the worm at low levels of upward continuation; at higher levels, they are simplified by the smoothing effect of upward continuation. Gravity data suggest that the structure corresponding to the Cloncurry Lineament cuts and displaces basement with an east side up sense, and it also coincides with part of the Snake Creek Anticline. Because of the crustal scale of the worms, the Cloncurry Lineament is interpreted as the surface trace of a major crustal fault.

The Cloncurry Lineament and the Cloncurry Fault are coincident around latitude 21.7 º S but diverge to the north so that the Cloncurry Fault is 10 km west of the lineament at 21º S. The Cloncurry Fault does not have a clear expression on the seismic line; the most likely orientation is sub-vertical, as judged by terminations of reflectors.

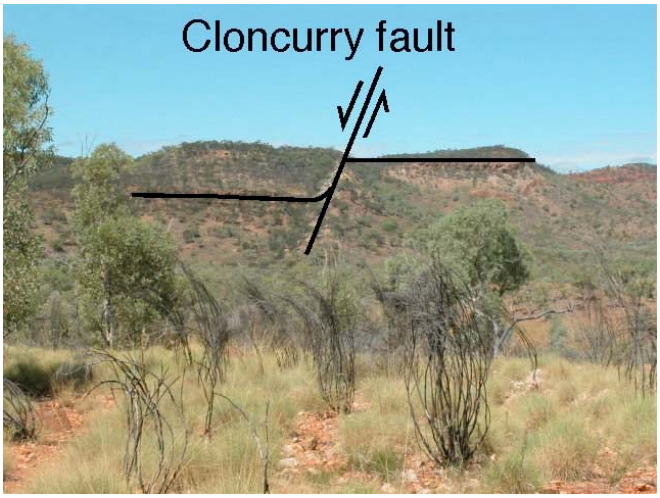

Fig. 10. The Cloncurry Fault at 471667mE 7653031mN showing the normal displacement of the Jurassic sandstones.

An important aspect of the Cloncurry Fault discovered in this project is that there has been a component of post-Jurassic displacement. Near the Fullarton River Gorge, a 20-50 m wide, topographically protruding, quartz-dominated ridge marks the fault trace. The fault dips at 70º to the east. The fault cuts sub-horizontal Jurassic sediments that are preserved as mesas unconformable on the Proterozoic sediments, giving a normal separation of 50 – 100 m to prominent beds of sandstone (Fig. 10). Within the Jurassic sandstones there is a dramatic change in fault fill. The fault fill changes from red, well cemented cataclasite, which is a regionally recognised type of fault fill, to a less consolidated fault breccia at the contact with the Jurassic sediments, which includes clasts of Jurassic sediment and is cut by lenses of fault gouge 2-4 m long. Bedding in the hangingwall of the fault is tilted to the same dip as the fault plane in a normal drag sense.

4.4 Intrusions

The largest intrusions are all bodies of the Williams-Naraku batholith (including the Squirrel Hills, Wimberu, Mt Angelay, Naraku, Saxby and Yellow Water Hole granites, and the unnamed interpreted granites south of the Wimberu granite and under the Eloise structure). Geophysical modelling of shallow crustal cross sections indicate that the edges of these granites generally dip steeply, but that the granites are no more than a few km thick (Barlow 2005). They have been shown as tabular bodies in the 3D model. Both radiometrics and aeromagnetic patterns show clearly that the larger bodies such as the Wimberu and Squirrel Hills granites are composite, containing several discrete intrusions which may have approximately internal concentric zones, and they contain a wide range of compositions (Wyborn, 1998).

5. RELATION BETWEEN BASEMENT, BASINS AND UPPER CRUSTAL STRUCTURES: POSITIVE INVERSION

5.1 Positive Inversion: general aspects

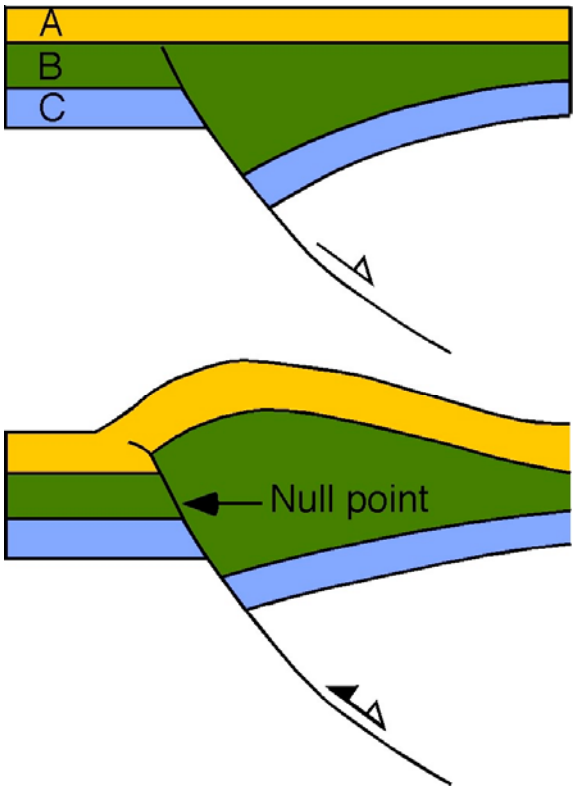

Fig. 11. Geometry of inversion. A, B and C are post-, syn- and pre-rift sequences. From Williams et al. (1987).

Positive inversion is the reversal of extensional fault movement during contractional tectonics (Williams et al., 1987, Fig. 11). If the extensional fault has been associated with pre- syn- and post-rift deposition, post-rift sequences will always show reverse movements, while syn- and pre-rift sequences may show either or both extensional or contractional movements. The point at which contractional movements change to extensional is called the Null point (Fig. 11).

Typical features of inversion are:

1. Reactivation of normal faults as thrusts: Reversal of slip direction at null point (Fig. 11)
2. Localization of folds (synforms/ antiforms) above faults
3. The Buttressing effect: Localization of folds and strain in the hangingwall of a normal fault because of the presence of a relatively rigid footwall
4. Reversals in fault dip direction.

Inversion can be classified into three types:

1. Inversion on faults exclusively within sedimentary or cover sequences
2. Inversion within cover sequences and passive behaviour of faults cutting into basement
3. Inversion involving displacement of basement

The first two types of inversion can be classified as “thin-skinned” inversion, and the latter as “thick-skinned inversion”.

5.2 Inversion In the Eastern Succession – A Working Hypothesis

A striking feature on the largest scale brought to light by the 3D model is the relationship between the major gravity worms and the major fold structures. The Mitakoodi anticlinorium coincides with the Pilgrim worm and the Snake Creek anticline corresponds to part of the Cloncurry worm. Cross-sections 763, 766 and 769 (Appendix 1) show this relationship clearly. Stratigraphic evidence shows that the Pilgrim worm structure served as a major locus of thickening to the east from CS2 to CS3 times. This structure is likely to have been of fundamental significance since before the Isan orogeny, because it marks a contrast in lower crustal isotopic signatures (Mark et al., 2005). The worm corresponds to a structure with a normal separation of basement. These observations are strong evidence that the Pilgrim worm structure represents a basement fault that controlled the architecture

of the depositional basins in CS2 and CS3, with thickening to the east in its hangingwall if its dip direction has not changed. The Pilgrim worm also coincides with the axial trace of the largest fold in the model, the Mitakoodi anticlinorium. This suggests the hypothesis that the fault has been inverted, and that the Mitakoodi anticlinorium may have developed in response to reverse movement on a fault corresponding to the Pilgrim worm. In places the surface expression of the Pilgrim worm may be the Pilgrim fault itself.

Typical features of inversion that can be seen in the above relations are:

1. A change from extensional displacements at depth to contractional at surface
2. The existence of a null point somewhere above the mid-lower crust at which the change from extensional to contraction occurs
3. The localisation of folds above the normal fault

Although the cross-sections apparently show a type 2 inversion in which the a fault cutting the basement has been passively reactivated, a component of active behaviour by reverse movement of the basement may have occurred, but this can not be determined since the original extensional component of the Pilgrim worm fault is not known.

Inversion is compatible with some features of the fault inferred to mark the Cloncurry worm. The relationship of this structure to sedimentation is not as clear as for the Pilgrim worm, but it may have played a role in the thickening of CS3 to the east. The coincidence of the Snake Creek anticline with the Cloncurry worm may be due to the localizing effect of a structure in the basement. The steep and changeable dip direction of the Cloncurry worm suggests that the separation of the basement may be extensional and contractional. The possibility of reorientation of the Cloncurry Fault during positive inversion can be raised to explain the variability in dip direction.

Other structures have also been inferred in the basement between the Cloncurry and Pilgrim worms. Because of their more limited strike extent, it has not been possible to link these so positively with surface structures, but at least one example could link to the Overhang shear. These structures may have played a role in the facies changes observed in CS2 and 3 (i.e. the change from Corella to Doherty formation in CS2 and from Young Australia to Soldiers Cap group in CS3), and the thickening of CS3 to the east.

In summary, the relationship between major basement structures, stratigraphy and contractional structures suggests the hypothesis that positive inversion is a key process in the evolution of the inlier. The dominant role of NS structures was established at least as early as CS2 and continued throughout the crustal evolution.

5.3 Implications of positive inversion for crustal structure and basement-cover relations in the Eastern Succession

The alignment between stratigraphic changes, extensional and contractional structures has an important implication for the relationship between the basement and cover in the Eastern Succession over the Pilgrim worm structure. This alignment would not be preserved if large-scale nappe structures or décollement had occurred either in extension or shortening. The cover appears to be broadly autochthonous relative to the Pilgrim worm structure. Decoupling on the order of a maximum of 10 km may have occurred.

This conclusion is not necessarily so surprising for D2 EW shortening, which is generally manifest in the form of upright folding. However, it is a significant constraint on any earlier deformation, generally supposed to have involved NS shortening (Rubenach 2005).

The parautochthonous relationship of the cover to the basement implies that shortening must also have occurred in the basement. A simple line length balance over the Mitakoodi anticlinorium as drawn in cross-section 768 indicates a stretch of 0.44 (or 56% shortening), which must also have occurred in the basement. The present thickness of the crust is approximately 40 km, but evidence from the Ce/Y ratios indicates that it was only 8 km at 1686 Ma, giving a thickening factor of 5 (Butera et al., 2005). Underplating, thrust stacking (possibly on reactivated normal faults) and penetrative deformation are all ways in which the crust may have thickened, and thickening may have occurred in more than one event.

6. CONCLUSIONS

1. A preliminary 3D model of the Mt Isa Eastern Succession, constructed to the base of the crust, allows important conclusions to be drawn about the crustal evolution of the inlier from sedimentation of the cover sequences to the events of the Isan orogeny.
2. The major lower crustal structure in the model area is a depression in the central part of the area between basement highs to the west and east. The boundaries of this structure are structures that correspond to worms known as the Pilgrim and Cloncurry worms.
3. A clockwise deflection in strike of all crustal features around Cloncurry occurs along an ENE zone, called the Cloncurry Flexure.
4. Upper crustal structure is dominated by kilometre- to tens of kilometre- wavelength upright folds, and north to northeast trending steeply dipping faults such as the Fountain Range, Pilgrim and Cloncurry faults.
5. Intrusions of the Williams-Naraku batholith have tabular shapes no more than a few km thick.
6. There is an important relationship between the structure corresponding to the Pilgrim gravity worm and the depositional basin architecture: major thickness increases occur to the east over this structure in some of the Cover Sequence 2 and 3 rocks.
7. The major Mitakoodi anticlinorium and Snake Creek anticline occur over the structures corresponding to the Pilgrim and Cloncurry worms
8. The relationships between changes in depth to the lower crust (which cause the major gravity worms), depositional basin architecture and major folds suggest the hypothesis that basin margin faults exerted a fundamental control on sedimentation and contractional deformation during the geological history of the inlier. The Pilgrim worm can be interpreted as a basin margin fault that was positively inverted to localise the largest fold structure in the inlier – the Mitakoodi anticlinorium. Likewise the Snake Creek anticline overlies the Cloncurry worm and appears to have been localised by it.
9. If the structure corresponding to the Pilgrim Worm was a basin-forming structure over which depositional architecture is still located, then there has been less than 10 km of displacement between the cover and basement in any deformational event. The cover is parautochthonous with respect to the basement.

7. RECOMMENDATIONS

This report has raised important questions about architecture and tectonostratigraphy that need to be followed up.

7.1 Architecture

The most important further work on architecture is the completion of the 3D model by creation of volumes for all rock units, and by incorporation of infill cross-sections between the existing skeleton. Geophysical forward modelling and inversion of the resultant model are urgent tasks to verify the basement architecture.

As a result of building the 3D model it has become apparent that several major structures need detailed field-based, modern structural investigation in the Eastern Succession. These have important implications for one or more aspects of new ideas for IOCG deposits presented in Butera et al. (2005).

1. The major crustal-scale structure of the Eastern Succession corresponds to the Pilgrim worm. A field program with detailed mapping at carefully chosen localities is needed to contrast the tectonic history across the Pilgrim fault where it coincides with the Pilgrim worm with places that is does not. This investigation needs to be paralleled by mapping of the Mitakoodi anticlinorium, which is localised on top of the gravity worm.
2. The significance of the Cloncurry Flexure needs to be understood. In this area the CS 2/3 contact appears to be gently dipping and may preserve some of its least reactivated character, with attendant implications for localisation of CuAu occurrences along this contact
3. The magnetic worm on the margin of the Wonga belt requires a geological explanation that can be established by several detailed cross-sections.
4. Mapping around and to the northwest of Ernest Henry, using Xstrata, and other drilling data, needs to be incorporated into the 3D model.
5. The Starra-Selwyn corridor is a north-south shear zone, which partly corresponds to an important gravity worm. A deformation chronology, linked to mineralization, is needed for this zone.

All the above structures are in NS or NE orientations that also correspond to the dominant orientations of faults associated with mineralization. They have the potential to be fluid pathways.

7.2 Tectonostratigraphy

The creation of the model also emphasised the need for a better stratigraphic understanding of the Eastern Succession based on high calibre new geochronological work. Our review of the tectonostratigraphy of the Eastern Succession, raised several critical issues:

1. The age and significance of the Double Crossing metamorphics. This is very important to the 3D model and understanding the deeper architecture of the Eastern Succession. The Double Crossing metamorphics are the only possible candidate for a basement to the cover sequences: If they are indeed such a basement, this places a major constraint on the model.

2. Diachroneity of the Corella/Doherty Formation. Meagre radiometric evidence suggests that the Doherty formation may be 20 Ma younger than the Corella formation.
3. Facies changes in CS 3. There appear to be major facies changes from E to W in CS3. This have been recognised in the 3D model by the definition of a new group (the Young Australia group), that encompasses cover sequence three rocks in the region of Young Australia. A clear definition and date for these rocks needs establishing. Furthermore the possibility that the Mt Albert group is a western facies of CS 3 has been raised by the 3D model and needs further testing.

Both the above points are important because of the recognition that the CS 2/3 contact is a major factor in localising Cu-Au mineralization (Mustard et al. 2005). However, the stratigraphic and the tectonic investigations are important in a broader sense – it will not be possible to choose between several viable alternatives for the basic architecture of the Eastern Succession unless the stratigraphy is better understood. Map patterns cannot be correctly interpreted at present, even on a 1: 500 000 scale, because of the fundamental uncertainties in the stratigraphic relations of the major cover sequences.

Acknowledgments
Thanks to Pat Williams for a critical reading of a draft.

8. REFERENCES

Austin, J. 2005. The Cloncurry worm. I2+3 Final Report, pmdCRC.

Barlow, M., 2005. Potential field modelling of geological cross-sections duchess- urandangi region Mt Isa basin. I2+3 Final Report, pmdCRC.

Blake, D. H. 1987a. Geology of the Mount Isa inlier and environs, Queensland and Northern Territory. 1:500,000 Map. Australian Geological Survey Organization

Blake, D. H. 1987b. Geology of the Mount Isa Inlier and Environs, Queensland and the Northern Territory. Bureau of Mineral Resources, Geology and Geophysics. Bulletin 225. 83.

Blake, D. H., Bultitude, R. J. & Donchak, P. J. T. 1982. Dajarra, Queensland. 1:100,000 Map. Australian Bureau of Mineral Resources, Geology and Geophysics

Blake, D. H., Bultitude, R. J., Donchak, P. J. T., Wyborn, L. A. I. & Hone, I. G. 1984. Geology of the Duchess-Urandangi region, Mount Isa Inlier, Queensland. 1:250,000 Map. Australian Geological Survey Organization

Blake, D. H., Jaques, A. L. & Donchak, P. J. T. 1983. Geology of the Selwyn region. 1:100,000 Map. Australian Government Publishing Service.

Butera, K., Oliver, N., Collins, W., & Cleverley, J. 2005. Multiple generations of metal and sulphur contribution from mafic rocks to the IOCG budget of the Mount Isa Eastern Succession. I2+3 Final Report, pmdCRC.

Derrick, G. M. 1980. Marraba, Queensland. 1:100,000 Map. Australian Government Publishing Service

Derrick, G. M. & Little, M. R. 1979. Prospector, Queensland. 1:100,000 Map. Australian Government Publishing Service

Derrick, G. M., Wilson, I. H., Hill, R. M., Glikson, A. Y. & Mitchell, J. E. 1977. Geology of the Mary Kathleen area, Northwest Queensland. 1:100,000 Map. Australian Geological Survey Organization

Donchak, P. J. T., Blake, D. H., Noon, T. A. & Jaques, A. L. 1984. Kuridala region, Queensland. 1:100,000 Map. Australian Government Publishing Service

Foster, D. R. W. & Austin, J. 2005. Revised chronostratigraphy for the Mount Isa Inlier with emphasis on the Eastern Succession. I2+3 Final Report, pmdCRC

Goleby, B. R., MacCready, T., Drummond, B. J. & Goncharov, A. 1998. The Mount Isa geodynamic transect - crustal implications. In: Structure and Evolution of the Australian Continent (edited by Braun, J., Dooley, J. C., Goleby, B. R., van der Hilst, R. D. & Klootwijk, C. T.). Geodynamic Series 26. American Geophysical Union, Washington, 109-118.

Goncharov, A., Lizinsky, M. D., Collins, C. D. N., Kalnin, K. A., Fomin, T. N., Drummond, B. J., Goleby, B. R. & Platonenkova, L. N. 1998. Intra-crustal "Seismic Isostasy" in the Baltic Shield and Australian Precambrian Cratons from the Deep Seismic Profiles and the Kola Superdeep Bore Hole Data. In: Structure and Evolution of the Australian Continent (edited by Braun, J., Dooley, J. C., Goleby, B. R., van der Hilst, R. D. & Klootwijk, C. T.) 26. American Geophysical Union, Washinston, 119-138.

Goncharov, A., Sun, S.-s. & Wyborn, L. 1997. Balanced petrology of the crust in the Mount Isa region. AGSO Research Newsletter, 26, 13-16.

Lepong, P., and Blenkinsop, T.G. 2005. Reprocessing and Reinterpretation of the Mount Isa Seismic Section. I2+3 Final Report, pmdCRC

MacCready, T., Goleby, B. R., Goncharov, A., Drummond, B. J. & Lister, G. S. 1998. A framework of overprinting orogens based on interpretation of the Mount Isa deep seismic transect. Metallogeny of the McArthur River-Mount Isa-Cloncurry minerals province, 93(8), 1422-1434.

Mark, G. 2001. Nd isotope and petrogenetic constraints for the origin of the Mount Angelay igneous complex; implications for the origin of intrusions in the Cloncurry District, NE Australia. Precambrian Research, 105(1), 17-35.

Mark, G, Pollard, D., Pollard, P., Damien Foster, D., McNaughton, N., and Mustard, R. 2005. Episodic syn-tectonic magmatism in the Eastern Succession, Mount Isa Block, Australia: implications for the origin, derivation and tectonic setting of 'A-type' magmas. I2+3 Final Report, pmdCRC

Mustard, R., , Blenkinsop, T., Foster, D., Mark, G., McKeagney, C., Huddelston-Holmes1, C., Partington, G., and Higham, M. 2005. Critical ingredients in Cu-Au ± iron oxide deposits, NW Queensland: An evaluation of our current understanding using GIS spatial data modelling. I2+3 Final Report, pmdCRC.

Murphy, F.C. 2002. Structural Framework and Target Generation in the Osborne District, Mt Isa region, Queensland, through analysis of Aeromagnetic Multiscale Wavelets ("Worms"). Report to pmdCRC.

Queensland Department of Mines and Energy, Taylor Wall and Associates, SRK Consulting Pty Ltd & ESRI Australia. 2000. North-west Queensland Mineral Province Report. Queensland Department of Mines and Energy, Brisbane.

Rubenach, M. 2005. Tectonothermal Evolution of the Eastern Fold Belt, Mount Isa Inlier. I2+3 Final Report, pmdCRC.

Ryburn, R. J., Wilson, I. H., Grimes, K. G. & Hill, R. M. 1988. Cloncurry, Queensland. 1:100,000 Map. Australian Government Publishing Service

Williams, G. D., Powell, C. M. & Cooper, M. A. 1987. Geometry and kinematics of inversion tectonics. In: Inversion Tectonics (edited by Cooper, M. A. & D., W. G.). Special Publication of the Geological Society of London 44. Geological Society, London, 3-16.

Wilson, I. H., Little, M. R. & Robertson, A. 1980. Quamby, Queensland. 1:100,000 Map. Australian Bureau of Mineral Resources Geology and Geophysics.

Wyborn, L.A.I., 1998. The younger ~1500 Ma granites of the Williams and Naraku Batholiths, Cloncurry district, eastern Mount Isa Inlier: geochemistry, origin, metallogenic significance and exploration indicators. Australian Journal of Earth Sciences, 45, 397-412.

9. APPENDIX 1 – CROSS SECTIONS

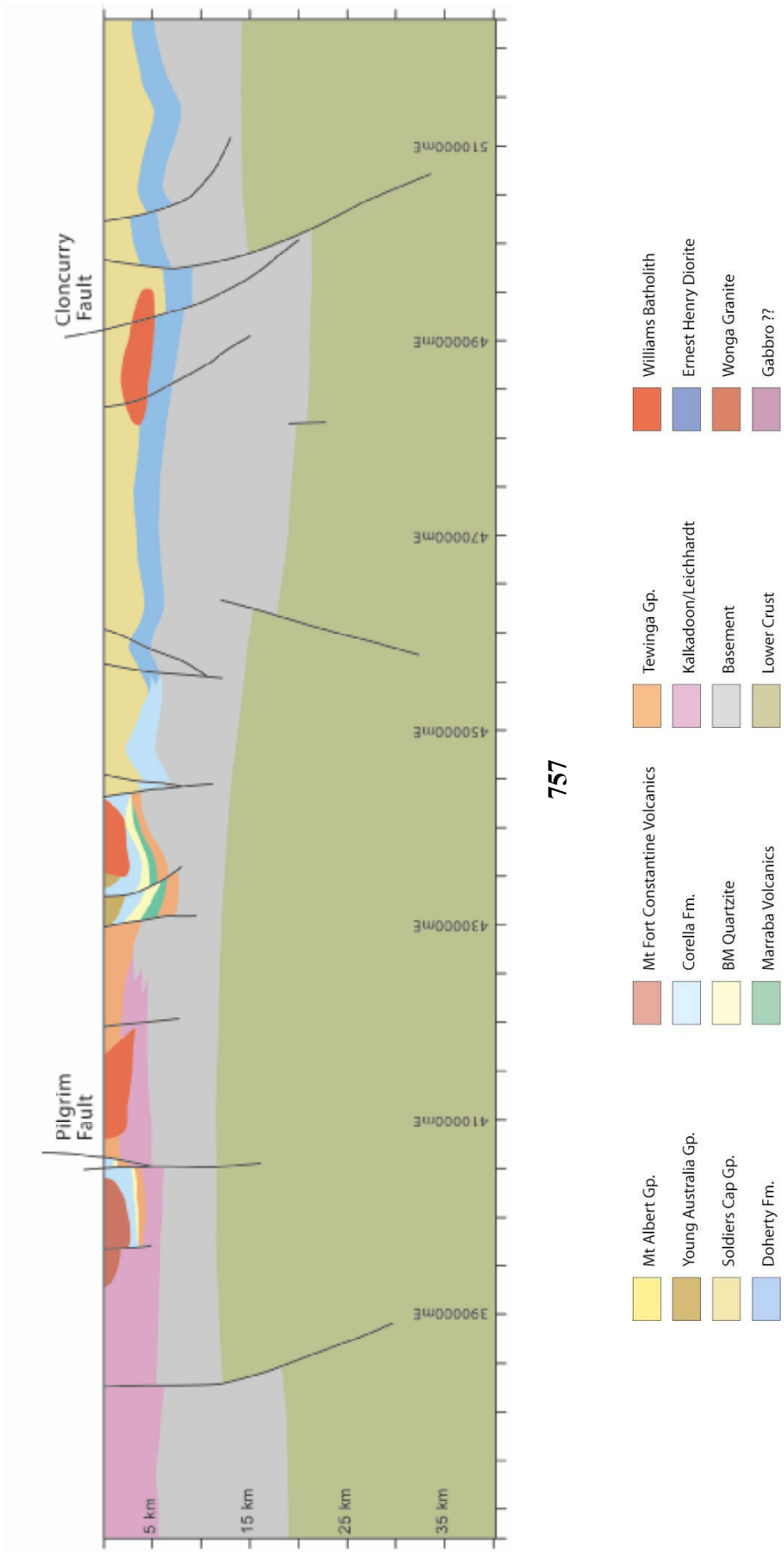
Cloncurry Fault
Pilgrim Fault
510000mE
490000mE
470000mE
450000mE
430000mE
410000mE
390000mE
5 km
15 km
25 km
35 km
Williams Batholith
Ernest Henry Diorite
Wonga Granite
Gabbro ??
Tewinga Gp.
Kalkadoon/Leichhardt
Basement
Lower Crust
Mt Fort Constantine Volcanics
Corella Fm.
BM Quartzite
Marraba Volcanics
Mt Albert Gp.
Young Australia Gp.
Soldiers Cap Gp.
Doherty Fm.

757

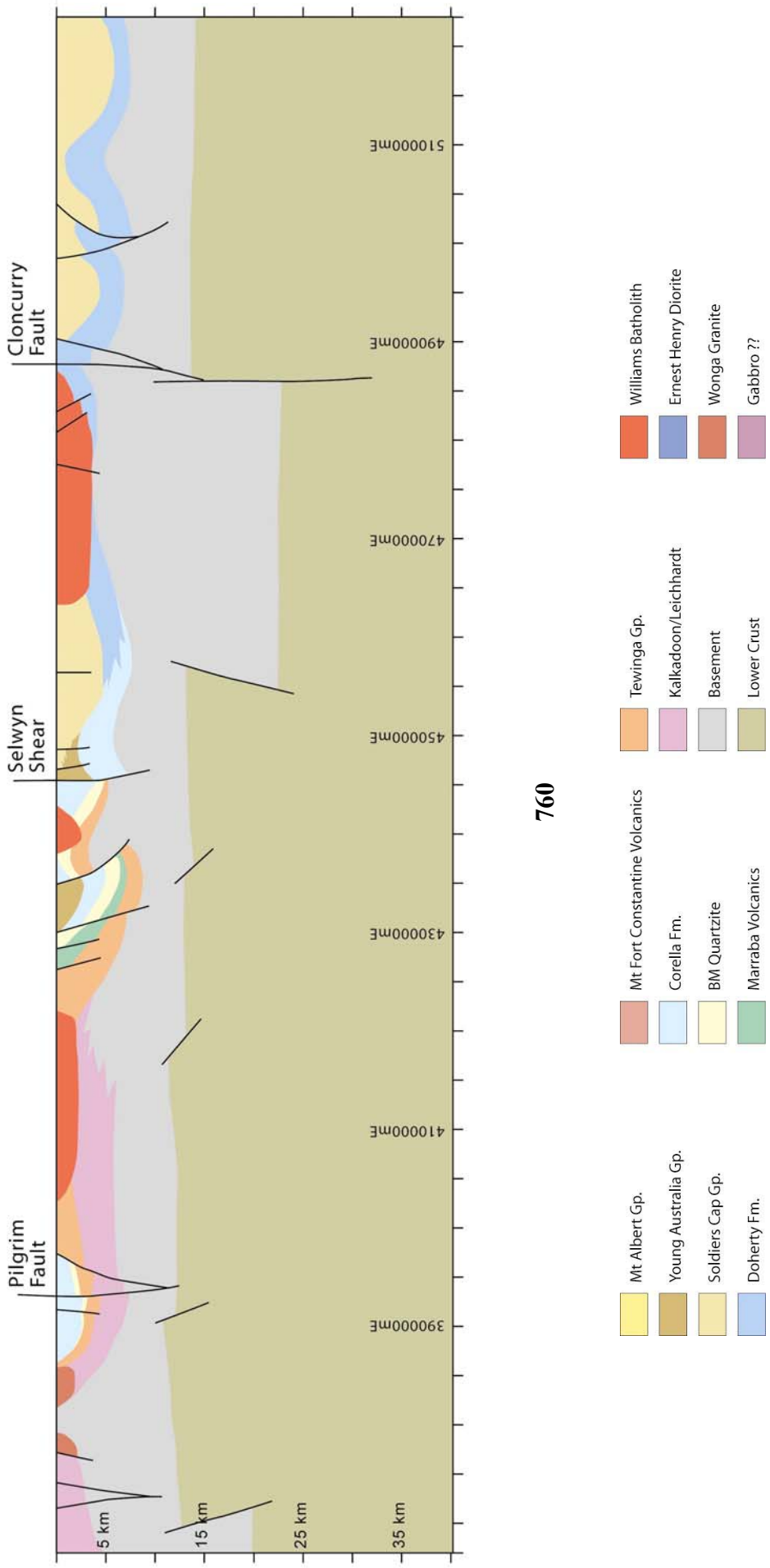
Cloncurry Fault
Selwyn Shear
Pilgrim Fault
510000mE
490000mE
470000mE
450000mE
430000mE
410000mE
390000mE
5 km
15 km
25 km
35 km
760
Williams Batholith
Ernest Henry Diorite
Wonga Granite
Gabbro ??
Tewinga Gp.
Kalkadoon/Leichhardt
Basement
Lower Crust
Mt Fort Constantine Volcanics
Corella Fm.
BM Quartzite
Marraba Volcanics
Mt Albert Gp.
Young Australia Gp.
Soldiers Cap Gp.
Doherty Fm.

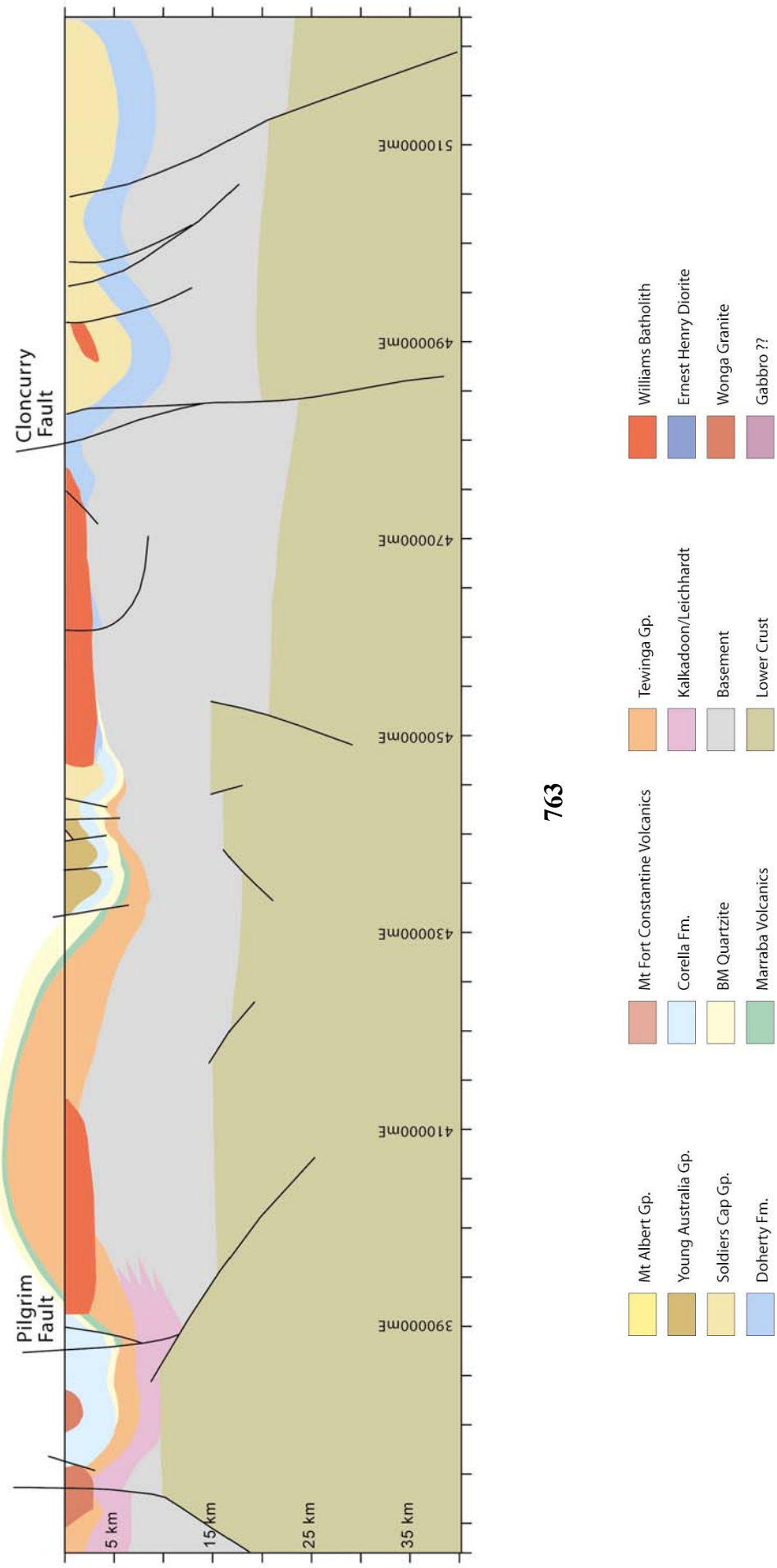
Cloncurry Fault
Pilgrim Fault
510000mE
490000mE
470000mE
450000mE
430000mE
410000mE
390000mE
5 km
15 km
25 km
35 km
Williams Batholith
Ernest Henry Diorite
Wonga Granite
Gabbro ??
Tewinga Gp.
Kalkadoon/Leichhardt
Basement
Lower Crust
Mt Fort Constantine Volcanics
Corella Fm.
BM Quartzite
Marraba Volcanics
Mt Albert Gp.
Young Australia Gp.
Soldiers Cap Gp.
Doherty Fm.

763

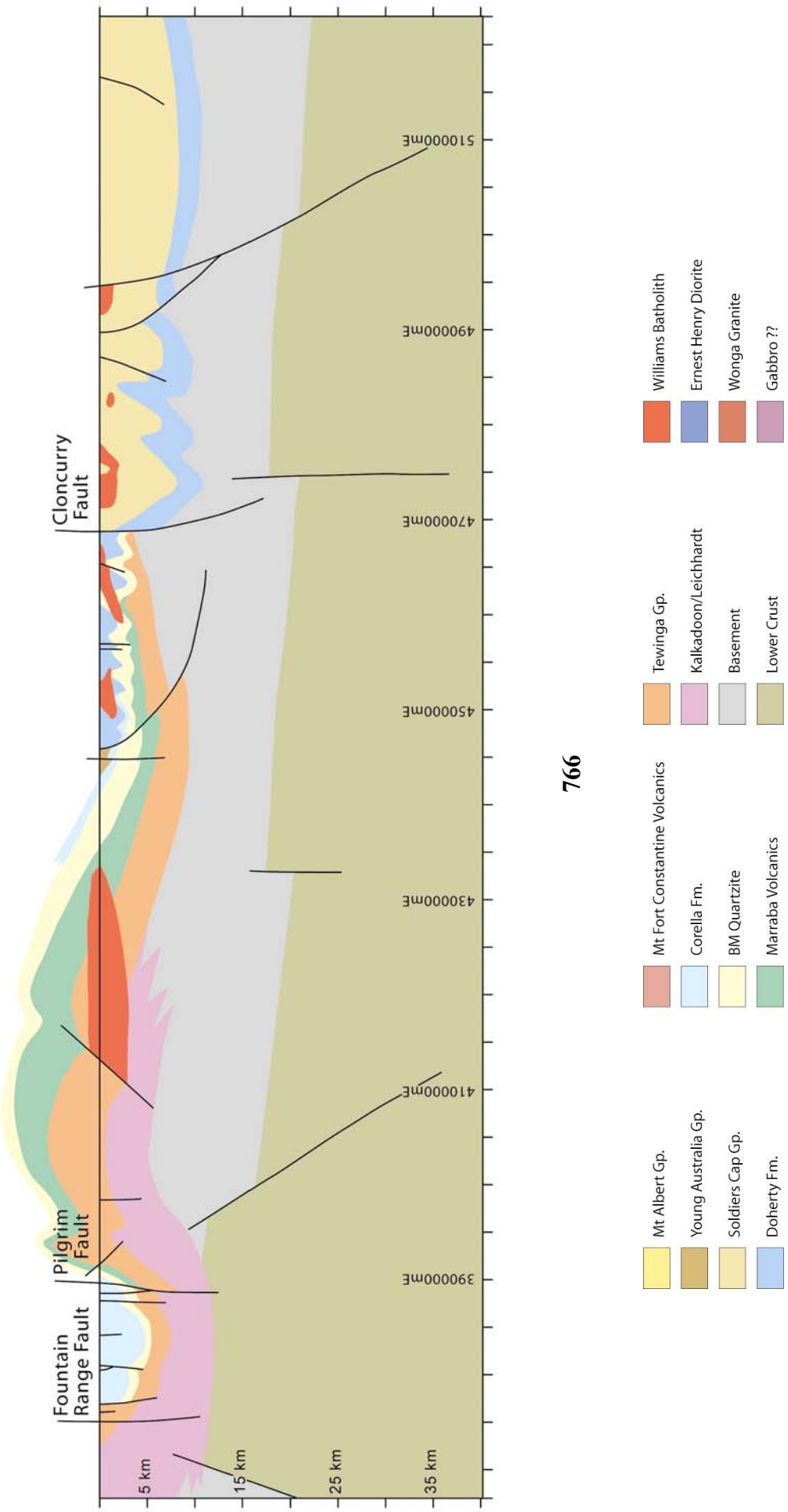
Cloncurry Fault
Pilgrim Fault
Fountain Range Fault
5 km
15 km
25 km
35 km
510000mE
490000mE
470000mE
450000mE
430000mE
410000mE
390000mE
766
Williams Batholith
Ernest Henry Diorite
Wonga Granite
Gabbro ??
Tewinga Gp.
Kalkadoon/Leichhardt
Basement
Lower Crust
Mt Fort Constantine Volcanics
Corella Fm.
BM Quartzite
Marraba Volcanics
Mt Albert Gp.
Young Australia Gp.
Soldiers Cap Gp.
Doherty Fm.

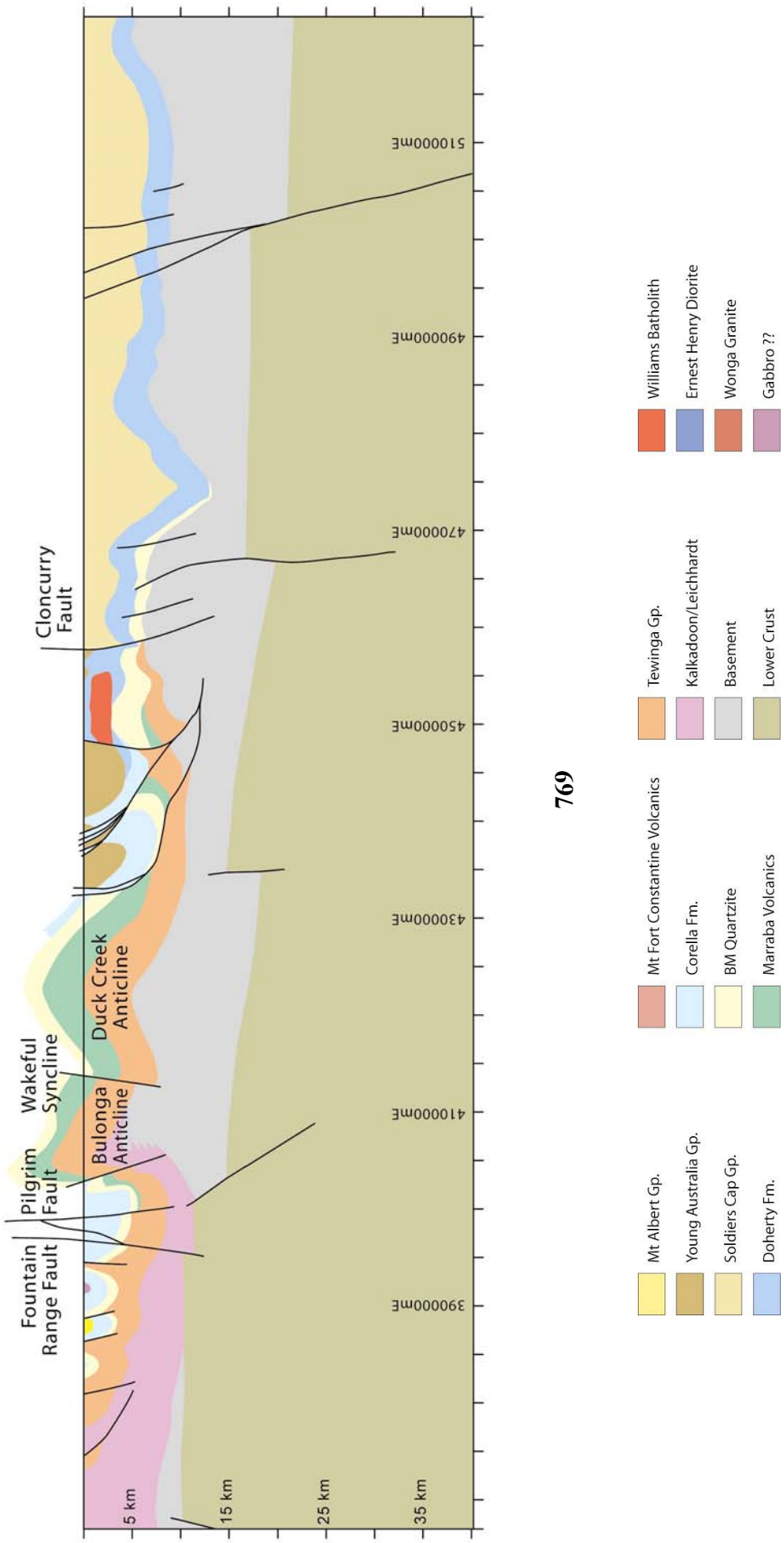
Fountain Range Fault
Pilgrim Fault
Wakeful Syncline
Bulonga Anticline
Duck Creek Anticline
Cloncurry Fault
5 km
15 km
25 km
35 km
390000mE
410000mE
430000mE
450000mE
470000mE
490000mE
510000mE
Mt Albert Gp.
Young Australia Gp.
Soldiers Cap Gp.
Doherty Fm.
Mt Fort Constantine Volcanics
Corella Fm.
BM Quartzite
Marraba Volcanics
Tewinga Gp.
Kalkadoon/Leichhardt
Basement
Lower Crust
Williams Batholith
Ernest Henry Diorite
Wonga Granite
Gabbro ??

769

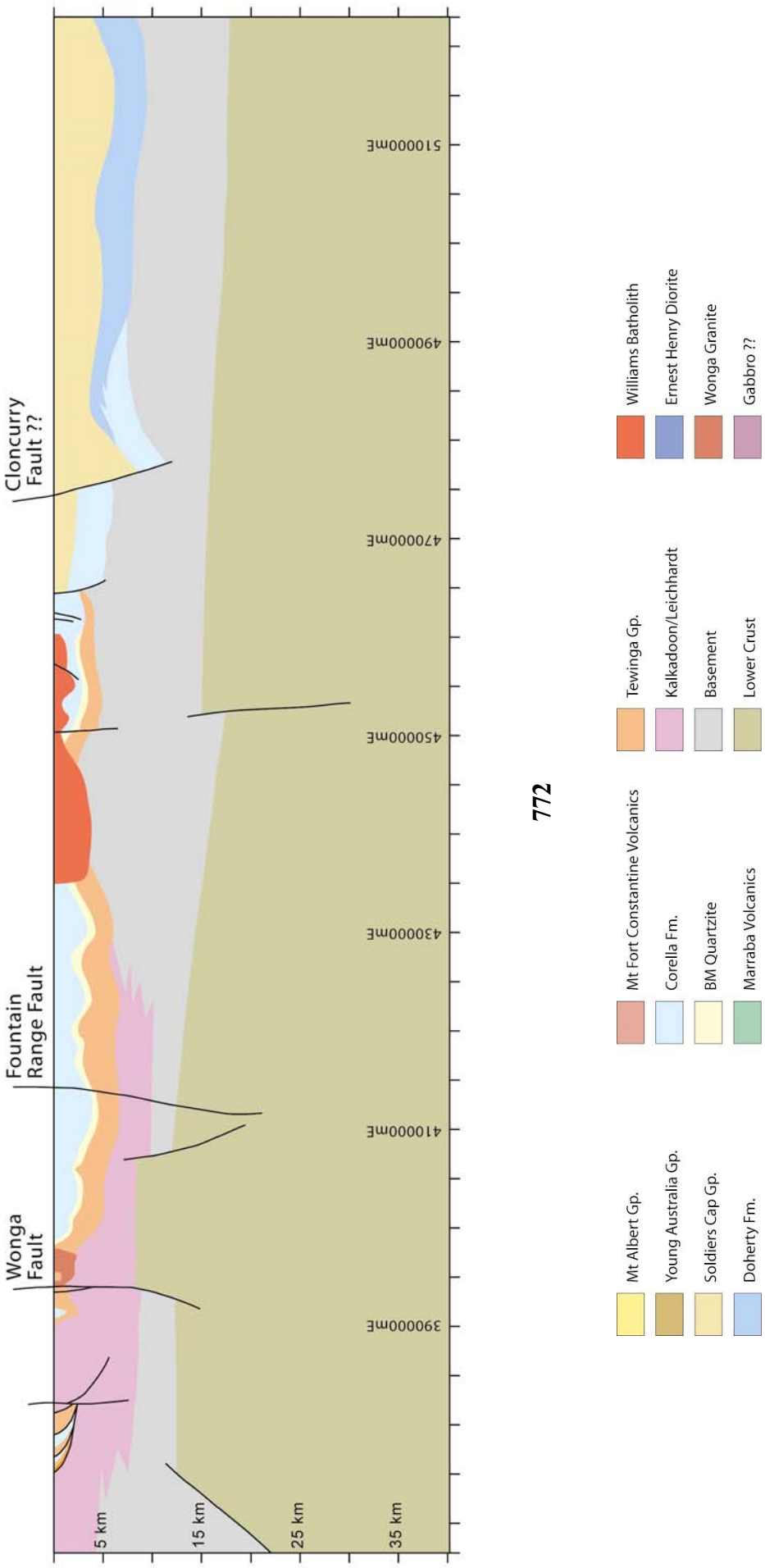
Cloncurry Fault ??
Fountain Range Fault
Wonga Fault
510000mE
490000mE
470000mE
450000mE
430000mE
410000mE
390000mE
5 km
15 km
25 km
35 km
772
Mt Albert Gp.
Young Australia Gp.
Soldiers Cap Gp.
Doherty Fm.
Mt Fort Constantine Volcanics
Corella Fm.
BM Quartzite
Marraba Volcanics
Tewinga Gp.
Kalkadoon/Leichhardt
Basement
Lower Crust
Williams Batholith
Ernest Henry Diorite
Wonga Granite
Gabbro ??

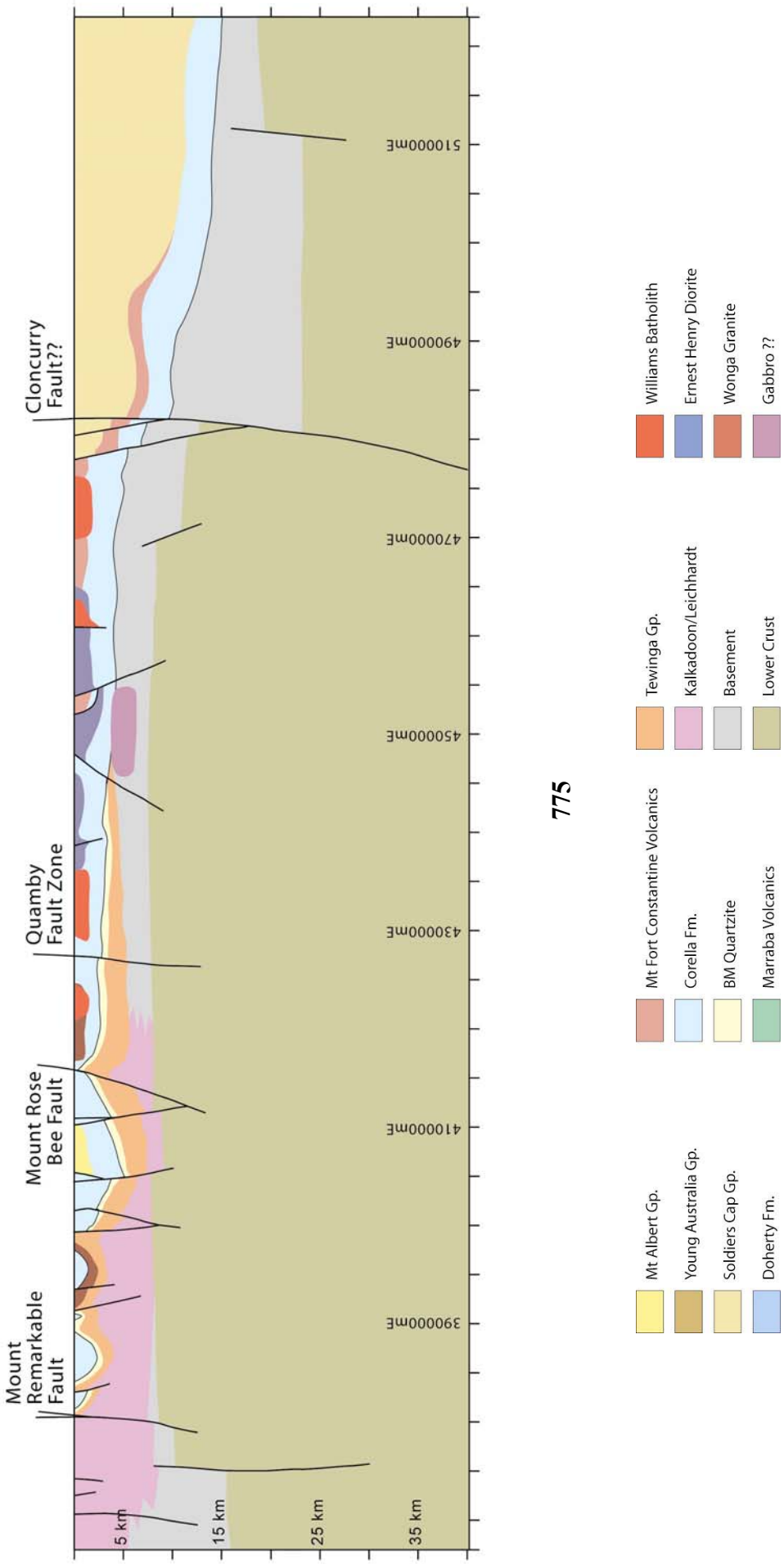
Cloncurry Fault??
Quamby Fault Zone
Mount Rose Bee Fault
Mount Remarkable Fault
510000mE
490000mE
470000mE
450000mE
430000mE
410000mE
390000mE
5 km
15 km
25 km
35 km
775
Williams Batholith
Ernest Henry Diorite
Wonga Granite
Gabbro ??
Tewinga Gp.
Kalkadoon/Leichhardt
Basement
Lower Crust
Mt Fort Constantine Volcanics
Corella Fm.
BM Quartzite
Marraba Volcanics
Mt Albert Gp.
Young Australia Gp.
Soldiers Cap Gp.
Doherty Fm.

10. APPENDIX 2 – REVISED CHRONOSTRATIGRAPHY

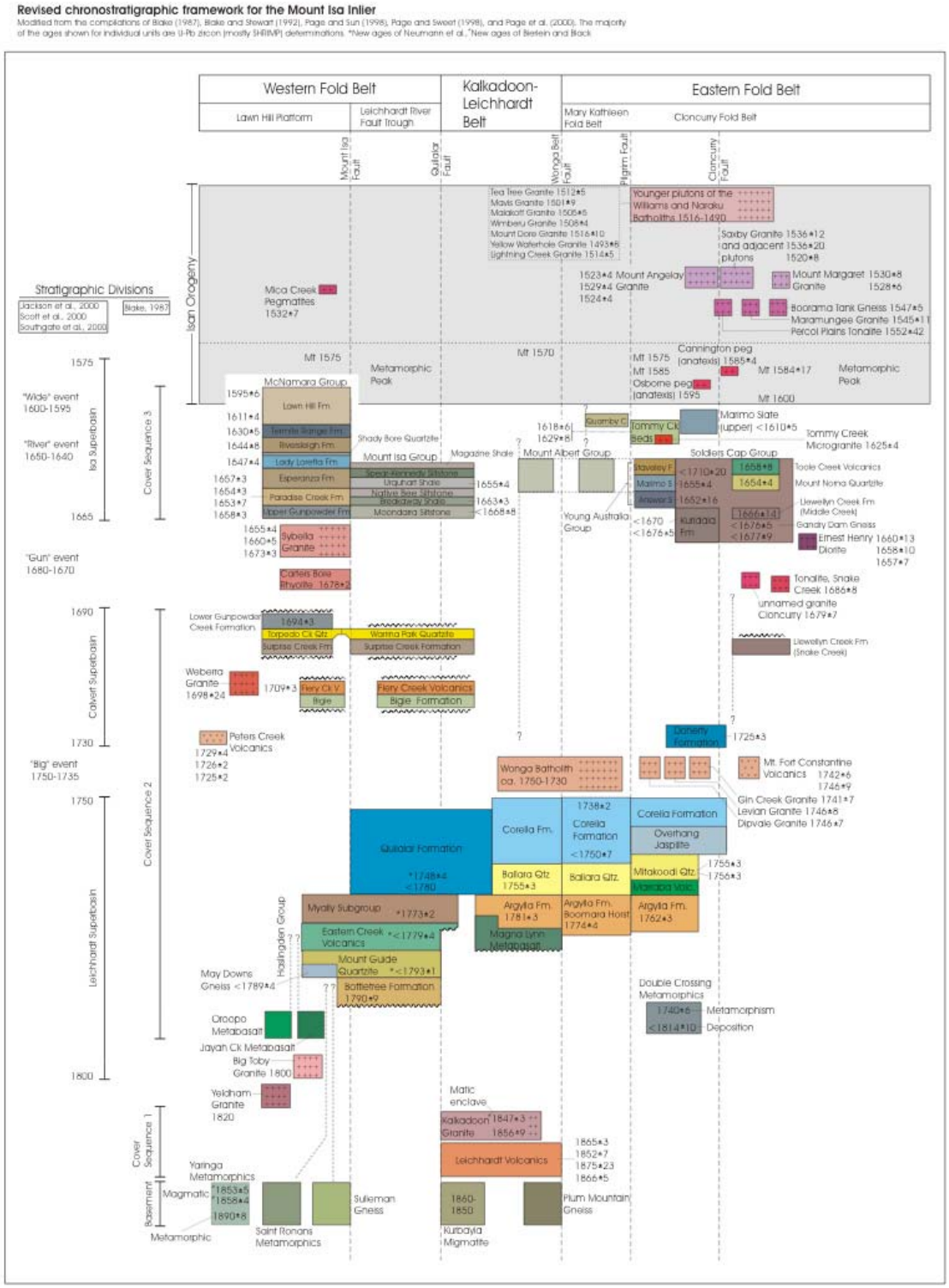

Composition of multi-scale wavelets (worms) in the potential field of the Mt Isa region.

F. C. Murphy[1]

[1]predictive mineral discovery*CRC, School of Earth Sciences, The University of Melbourne, Parkville, Vic 3010, Australia. (bmurphy@unimelb.edu.au)

ABSTRACT

Potential field data over the Mt Isa region and its environs provide key insights into its structural, magmatic and mineralisation architecture. To help reduce the inherent bias in interpretation of such data, an automated multi-scale edge detection technique, called worms, was applied to the regional gravity and aeromagnetic data. Through a process of wavelet transformation and upward continuation, this provides information on the positions and strengths of gradients in 3D space, thereby informing 3D models and has potential value to explorers as area selection filters. Recent advances in post-processing of the 3D worm points, using nearest neighbour and vectorisation procedures, have added to the parameter space by which these gradients may be better constrained geologically in 2D GIS platforms. The original worm data and post-processed outputs are supplied as a data release, and the component features of these data are outlined here. The analysis and integration of these data into a coherent geological framework is on-going. Preliminary analysis of such data suggests a crustal scale deflection of major gradients through the Mt Isa region in response to NE trending dextral shearing of at least D2 age.

Keywords. Multi-scale edge detection, worms, gravity, aeromagnetic, gradient, geophysics

1. INTRODUCTION

Regional scale potential field data sets are a critical input to understanding the structural architecture of the Mt Isa region. Arising from the impetus to advance this understanding and to derive terrane scale mineralisation controls, the gravity and aeromagnetic data sets were wormed. These data sets are being released as part of the Isa project outputs and their component features are outlined here. Worms are points of maximum gradient that derive from a process of wavelet transformation and upward continuation of the potential field. A considerable body of research by CSIRO in the 1990's addressed the ambiguity problem with the interpretation of potential field data and from this emerged a multiscale wavelet-based edge detection technique, called "worms" (Hornby *et al.* 1999). The technique constrains the location and strength of gradients, and yields information on the 3D shape and persistence of related geological contacts. The procedure is optimized using FRACWORMER™ by Fractal Graphics Pty. Ltd. Visually, through multi-scaling, worm points coalesce to form worm sheets and these can be fine to coarse scale, reflecting increasing height in upward continued space (Archibald *et al.* 1999). A reasonable assumption underlying the interpretation of worms is that singularities in the mass density distribution of the sources correspond *lit-par-lit* with apparent edges in the potential field and such singularities can be ascribed a geological meaning (Archibald *et al.* 1999).

The point data records the 3D position (*xyz*) and amplitude (*w*) of gradients. Fine scale worms are high frequency/short wavelength gradients that relate to shallow sources, whereas coarse scale worms are low frequency/long wavelength gradients that typically (but with exception) correspond to deeper level and more persistent crustal sources. Holden *et al.* (2000) show synthetic models where the dip direction of a worm sheet may mirror image its related geological contact (e.g. folds, faults, intrusive bodies), up to the amplitude maxima. A rule of thumb used in interpreting the nature of such gradients, more so for gravity data, is that the depth extent of the source is proportional to the height of the worm sheet. Naturally, this data represents a mixed and complex population of geological sources, being responses to density variations in a 3D crustal volume. The worming process is blind to dipping geological contacts with no associated density contrast across them (e.g. stratigraphic units, faults). However, the existence of such structures can be inferred from their interaction with adjacent worm sheets, for example faults that effect truncations and offsets in worm gradients. Shallow dipping density contrasts within the crust that do not have a near surface expression are problematical, and are best imaged with seismic data. As the worming process requires a regular grid of data, and regional surveys rarely conform to this, data may be introduced to pad out the grid and, in some instances, the survey boundary may create an artificial worm.

2. GEOSCOPE PROCESSING

The gravity and aeromagnetic worm data sets for the Mt Isa region represent a 3D gradient field of circa 18 million km^3. Early analysis of the worms (Murphy 2000) involved visual interpolation of the 3D data to derive a 2D interpretation of the fault architecture. The objective was to determine the influence of fault-related worms on the distribution of major ore systems. While the approach shows some promise, constraints were encountered both in a computational sense in viewing, manipulating and plotting millions of points in 3D and 2D GIS platforms, and in an interpretation sense of reliably ascribing a geological source to the worms. Worm points have no connection to their neighbour, yet

the eye of the interpreter is drawn to making such connections through the morphology of the worm sheet and visual correlations with mapped geology. To optimise the processing of worms in a GIS analysis, a series of nearest neighbour algorithms were developed through the pmd*CRC and are implemented in a software routine, called Geoscope. This firstly applies nearest neighbour processing of points across successive levels of upward continuation along the worm sheet. This height migration yields a point data set that is attributed with the maximum height of upward migration of the worm sheet (zwt), the amplitude maxima (wmax) and the height of the amplitude maxima (wzmax). The process also generates an image of the original worms ("data" bitmap), an image of the level to which the migration is mapped to ("near surface" bitmap), and an image of the height weighted points ("migrated" bitmap). This allows the 3D data to be visualised effectively in a 2D platform. A second nearest neighbour algorithm is then applied horizontally to the height migrated points. This delineates the connectivity of points in map view and generates vector lines from the point data. Worm lines are attributed with the maximum height (zwt) of the associated points, together with the length, trend and straightness of the individual line segment. These attributes can then be mapped thematically in a 2D GIS platform.

The values derived from the post-processed worms represent a six-fold increase in parameter space, and are potentially useful descriptors to guide subsequent geological interpretation. For example, highly curved worm vectors are typically associated with intrusive bodies, whereas long, relatively straight worm vectors are more likely to represent fault boundaries. Further analysis of the vector data involves joining of contiguous line segments (concatenation) and attributing the lines with a geological descriptor. The data described below, and released as a data package, have not been concatenated or geologically attributed. This analysis of the data will be undertaken as an input to developing a coherent structural architecture in the emerging Isa project (I7).

3. GRAVITY WORM DISTRIBUTIONS

Newly generated worms using an updated network of gravity stations were generated for the Mt Isa region by Fractal Graphics Pty. Ltd in AGD 66 Zone 54. The data covers an area of 480 km by 780 km and was upward continued to 55 km from a 500m grid (Fig. 1). Two types of worms were produced, MAX and EFVD. The MAX worms represent the points of maximum horizontal gradient while the EFVD worms are points of effective first vertical derivative. The latter provide more information on fine scale gradients. The distribution of the MAX worms is show in Figure 2, colour coded by height of upward continuation.

Geoscope outputs at 500m, 1km, 2km, 5km, 10km, 20km and 40km intervals have been made from the MAX and EFVD worms. An example of the height migration algorithm is shown at 10 km upward continuation height for the MAX worms (Fig. 3). Other height intervals are shown in Murphy (2005). These are used to help determine the positions of individual gradients at varying heights of upward migration, such as the Barramundi Worm (Hobbs et al., 2000), and to visualise how such gradients change spatially over successive levels. As height is a proxy for depth of penetration, this provides a way of highlighting the major bounding surfaces of relevance to 3D geological modelling. Outputs from the 2D delineation and vectorisation algorithm applied to the migrated MAX worm points at the 2km level of upward continuation are shown as a series of thematic maps of length, trend

and straightness parameters respectively (Figures 4, 5, 6). Given these parameters, a range of possible thematic distributions can be explored.

4. AEROMAGNETIC WORM DISTRIBUTIONS

Using MIM's aeromagnetic data, Fractal Graphics Pty. Ltd derived worms on a 200m grid that was upward continued to 30 km, in AGD 66 Zone 54. As with the gravity data, two types of worms were provided, MAX and EFVD. The data was processed in two overlapping groups, one for the Eastern Succession and one for the Western Succession. In addition, the EFVD processing of the Eastern Succession worms was divided into northern and southern areas because of the large size of the files. An example of the MAX worms colour coded by height of upward continuation (Fig. 7) shows a number of coarse to fine scale features, and varying relationships to major metallic deposits. The nature and significance of these relationships are explored elsewhere in this volume (Austin 2005, Edmiston 2005), and will be further evaluated in on-going research in I7. Note that the boundaries of the data have generated artificial worms.

Post-processing outputs of the MAX worms have been made for Eastern and Western Successions, at 200m, 500m, 1km, 2km, 5km and 10km intervals. An example of the migrated gradients at 5km height is shown in Figure 8. At this regional scale, an association of some deposits with coarse scale worms is apparent and, as such, may have an impact on area selection decisions by the explorer. Examples of the vector outputs at 2km height of upward continuation are shown as thematic maps of length, trend and straightness (Figs. 9, 10, and 11 respectively). Note that the survey boundary worms have been deleted.

5. CONCLUSIONS

A complex distribution of potential field gradients is revealed through multi-scale wavelet processing (worms) of the Mt Isa region. These 3D data sets and their post-processed 2D derivatives are provided as part of a data release on completion of the Isa projects (I1 and I2). Over the course of the research, significant advances have been made in the ability to manipulate and interpret these gradients through nearest neighbour algorithms in Geoscope software. This process increases the parameter space of the worm gradients, allows the data to be manipulated in a 2D GIS framework, and augments the richness of the 3D data.

Slicing though the data at selected height intervals provides a basis for determining the positions and depth persistence of gradients, and aids the delineation of major bounding surfaces for subsequent 3D modelling. Thematic mapping of vector parameters is also a useful aid in determining the geological nature of the gradients. An example is shown (Fig. 12) of the combined gravity and magnetic vector lines at 2km upward continuation. This data was filtered by straightness (>0.5) and length (>4km) and, from this, three selected trends have been displayed: 180-210 ^{o}, 300-330 ^{o} and 330-360 ^{o}. Notwithstanding the differing nature of the gravity and magnetic responses, there is a reasonable degree of coherence in the data, and the majority of the vector gradients may be fault-related. The distribution of the differing trends within discrete domains is strongly apparent. For example, the 300-330 ^{o} trending gradients are more evident to the west of the Isa Valley, within the Proterozoic and beneath the Georgina Basin, and in the Eastern Succession to

the east of the Pilgrim-Fountain Range fault systems. Conversely, the 330-360 ^{o} trend is more pronounced within the central region, in part following the Kalkadoon-Leichhardt Belt. The 180-210 ^{o} trend is also contained in discrete domains, in this instance occupying the central region of Mt Isa. Its distribution is correlated with fault systems such as the Fountain Range and Mt Gordon Faults. It appears significant that this distribution overlaps in large part with that of the 330-360 ^{o} trend. The overall geometry, and based on similar patterns in the regional scale mapped faults (Murphy 1997), suggest a model of crustal scale rotation of the 300-330 ^{o} trend into the Isa region where it is expressed as the 330-360 ^{o} trend, and this dextral rotation is determined by the presence of the 180-220 ^{o} trend. The timing of dextral deflection appears at be relatively late stage in the Isan orogeny (D2). Naturally, this is a simplification of a complex system, and further work is being directed towards unravelling the structural architecture and geodynamic history. However, it serves to illustrate the potential application of the data for researchers and explorers alike.

Acknowledgements
Fractal Graphics Pty. Ltd. (now Geoinformatics Exploration Australia Ltd) is thanked for supplying the terrane scale Fracworms to the pmd*CRC. MIM provides access to the regional aeromagnetics, and additional gravity data was provided as in-kind contributions by BHP Billiton and Placer. Information regarding the Geoscope software tool and its availability to researchers and sponsors of the pmd*CRC is provided via the Twiki website.

6. REFERENCES

Archibald, N. J., Gow, P. and Boschetti, F. 1999. Multi-scale edge analysis of potential field data. *Exploration Geophysics*, 30, 38-44.

Austin, J. 2005. The Cloncurry Lineament: Interpretation of a major crustal worm. I2+3 Final Report, pmdCRC

Edmiston, M. 2005. The role of geophysics in the exploration for iron oxide copper gold deposits. I2+3 Final Report, pmdCRC

Hobbs, B. E. H., Ord, A., Archibald, N. J., Walshe, J. L., Zhang, Y., Brown, M. and Zhao, C. 2000. Geodynamic modelling as an exploration tool. In *After 2000- The Future of Mining*, Sydney, p34-49.

Holden, D., Archibald N. J., Boschetti, F. and Jessell, M. W. 2000. Inferring geological structures using wavelet-based multiscale edge analysis and forward models. *Exploration Geophysics*, 31, 617-621.

Hornby, P., Boschetti, F. and Horowitz, F. 1999. Analysis of potential field data in the wavelet domain. *Geophysics Journal International*, 137, 175-196.

Murphy, F. C. 1997. Pattern of faulting and controls on mineralisation in the Mt Isa region, Queensland. Abstract in "Faulting, fluid flow and mineralisation", Dave Johnston Memorial Meeting, Trinity College Dublin.

Murphy, F. C. 2002. Structural framework and target generation in the Proterozoic Mt Isa region, Queensland, through analysis of potential field multi-scale wavelets (worms). pmd*CRC internal report.

Murphy, F. C. 2005. The Barramundi gravity worm in relation to crustal structure of the Mt Isa region. I1 Final Report, pmdCRC

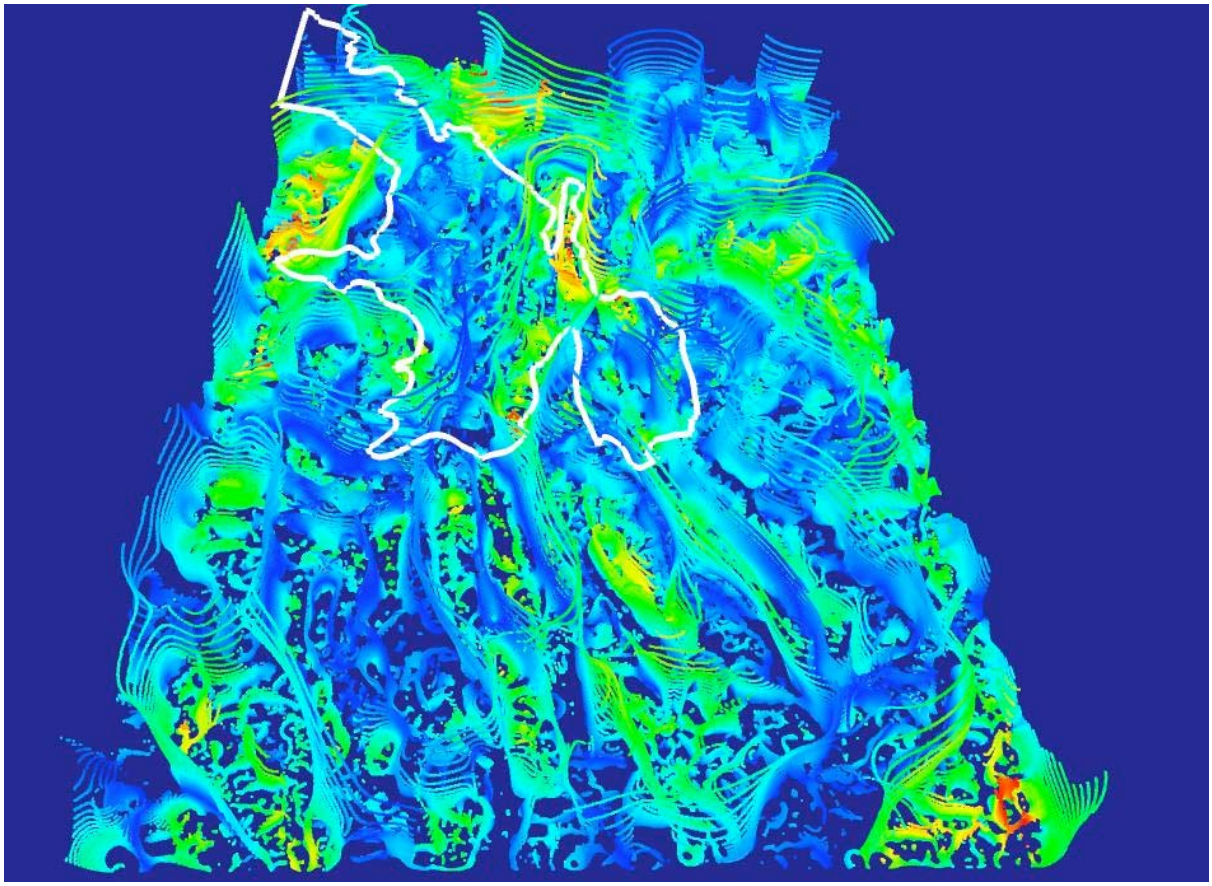

Fig. 1: Perspective view to north of gravity (EFVD) worms, colour coded by amplitude, and showing outline of the Mt Isa Proterozoic inlier (white).

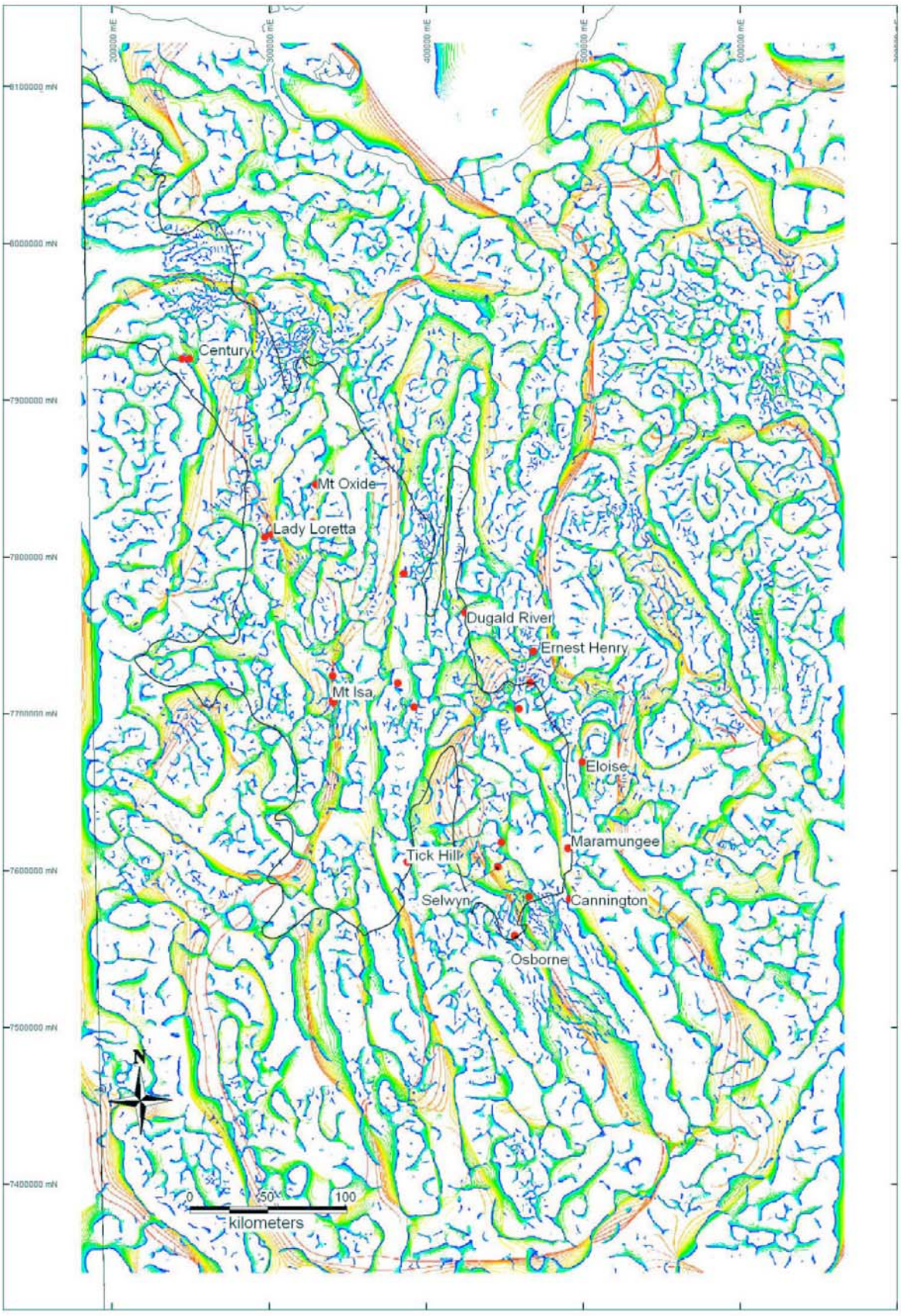

Fig. 2: Gravity MAX worm data coloured by height of upward continuation (blue 500m to red 55km) with outline of Proterozoic Mt Isa region (black) and major metallic deposits (red).

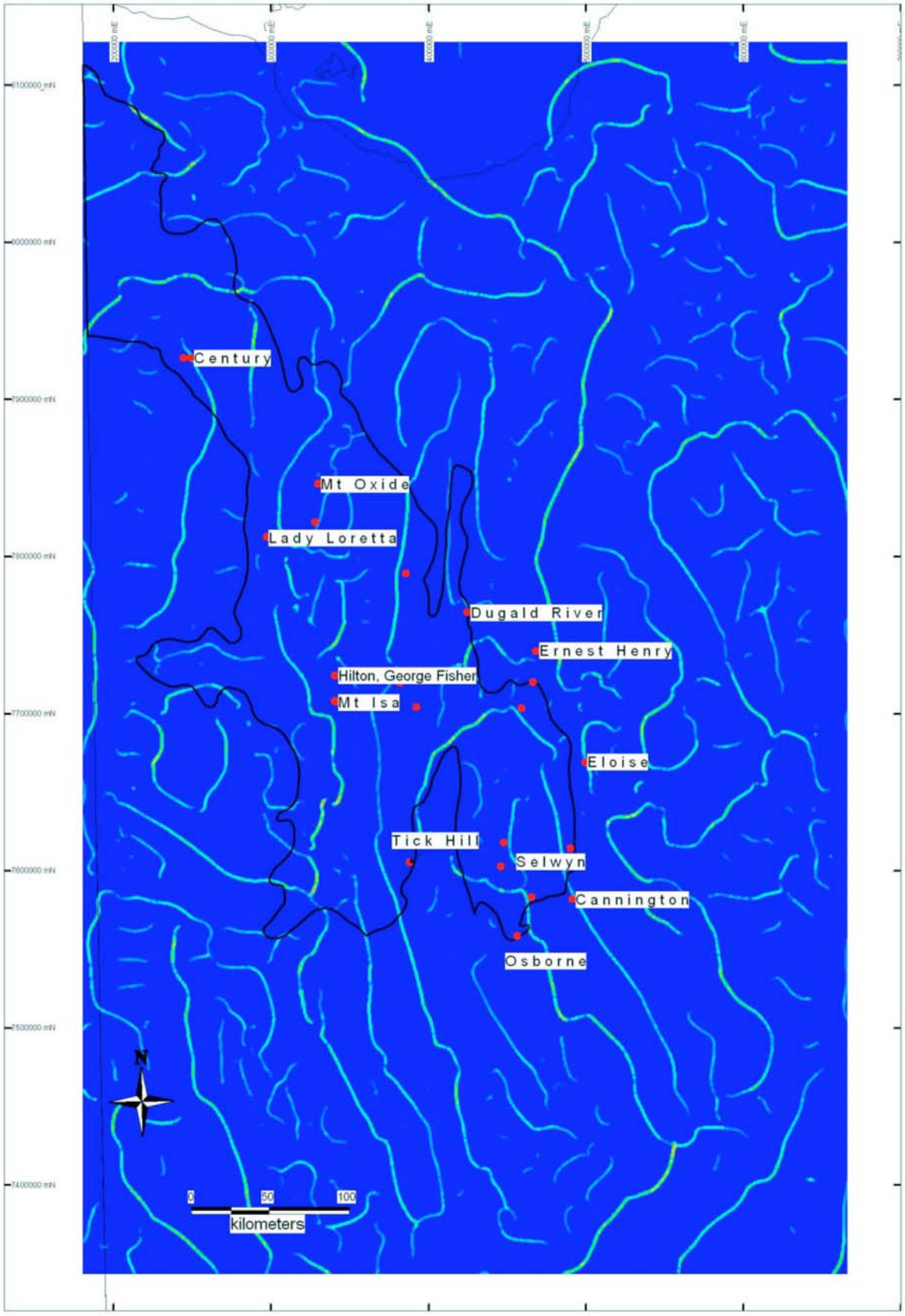

Fig. 3: Image of migrated gravity worms at 10 km height of upward continuation, with outline of Proterozoic Mt Isa region (black) and major metallic deposits (red).

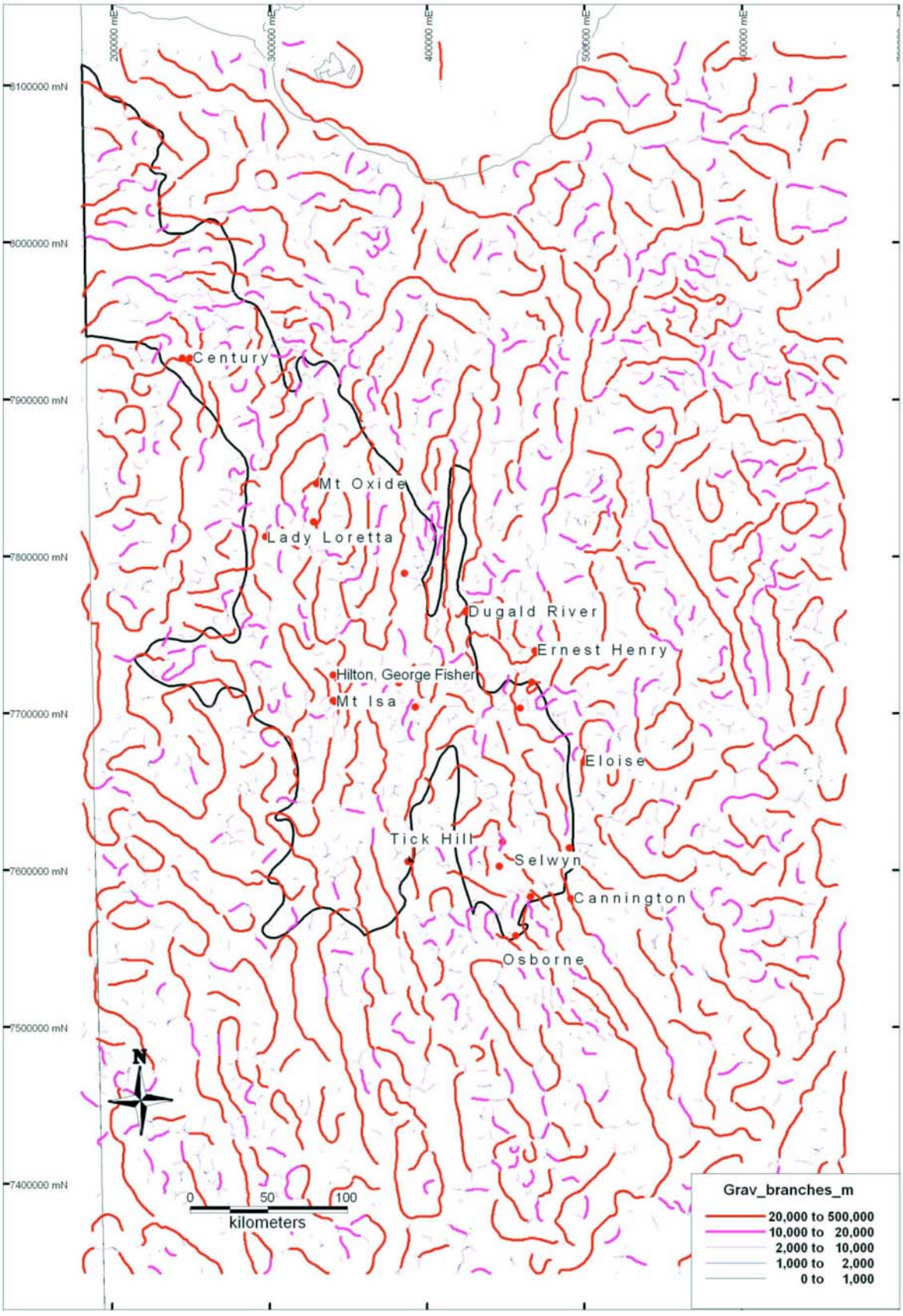

Fig. 4: Thematic map of gravity MAX worm vector line length, at 2 km height of upward continuation.

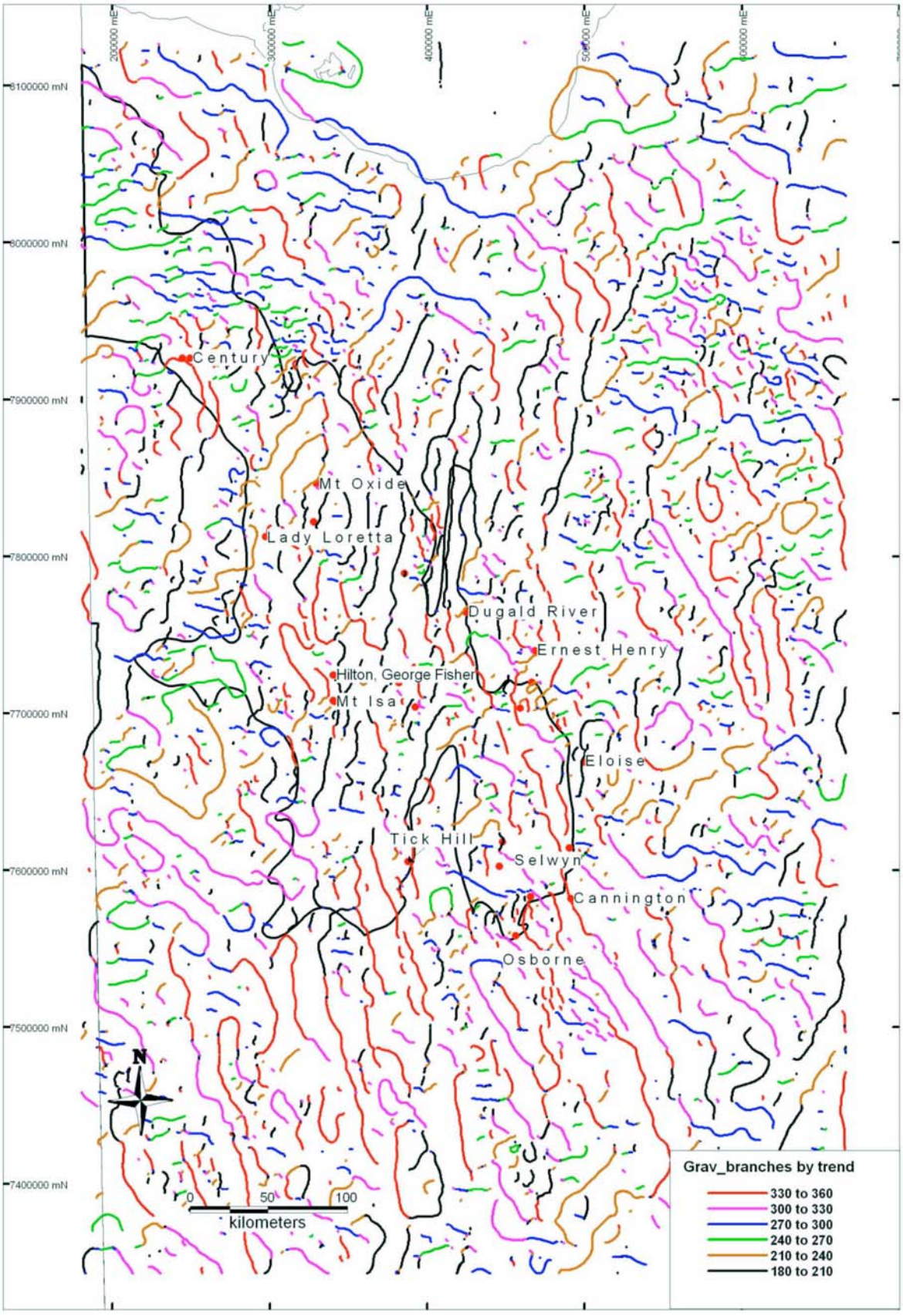

Fig. 5: Thematic map of gravity worm vector line trend, at 2 km height of upward continuation, in 30^{o} increments.

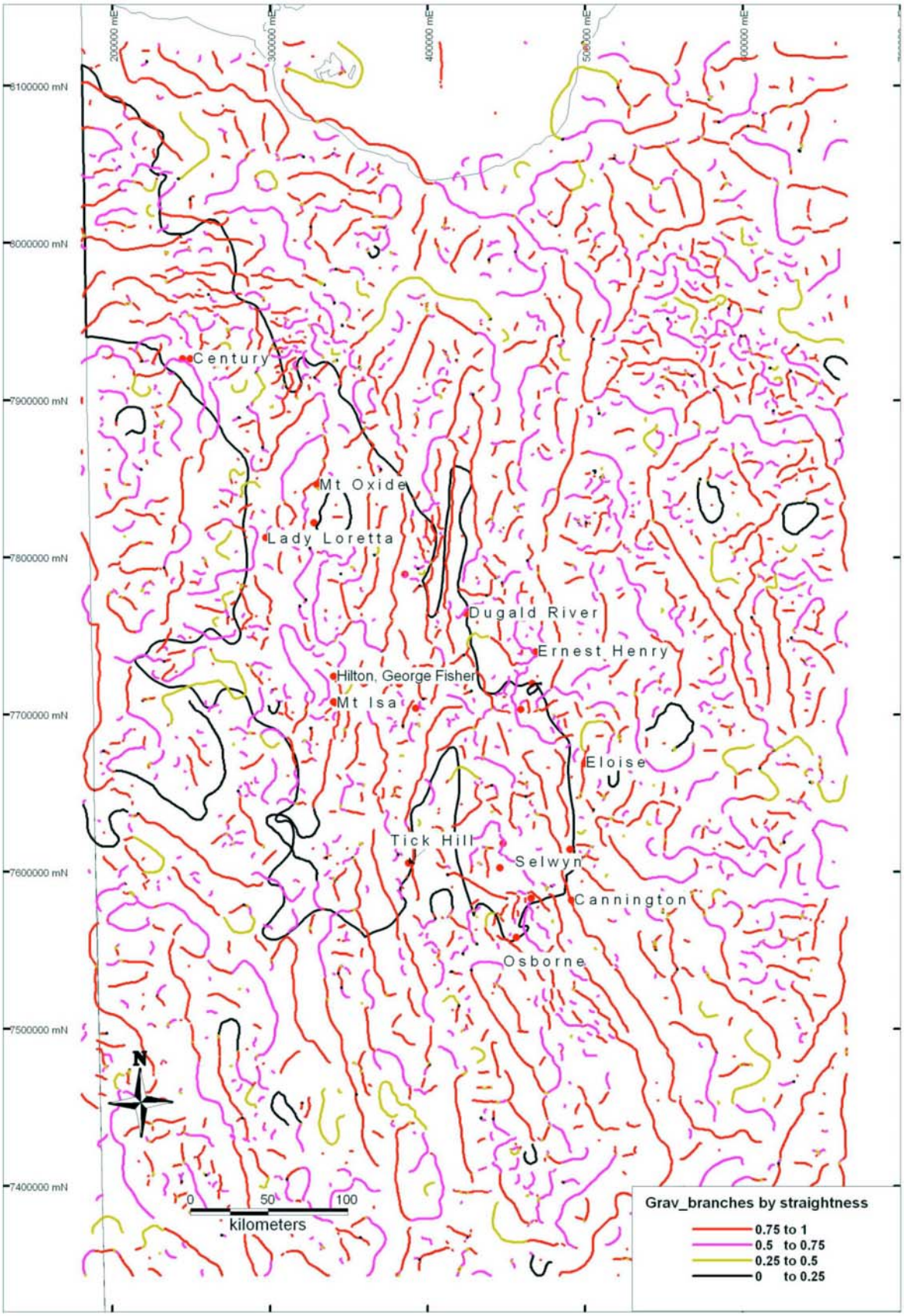

Fig. 6: Thematic map of gravity worm vector line straightness, at 2 km height of upward continuation, 1 = straight, 0 = sub-circular.

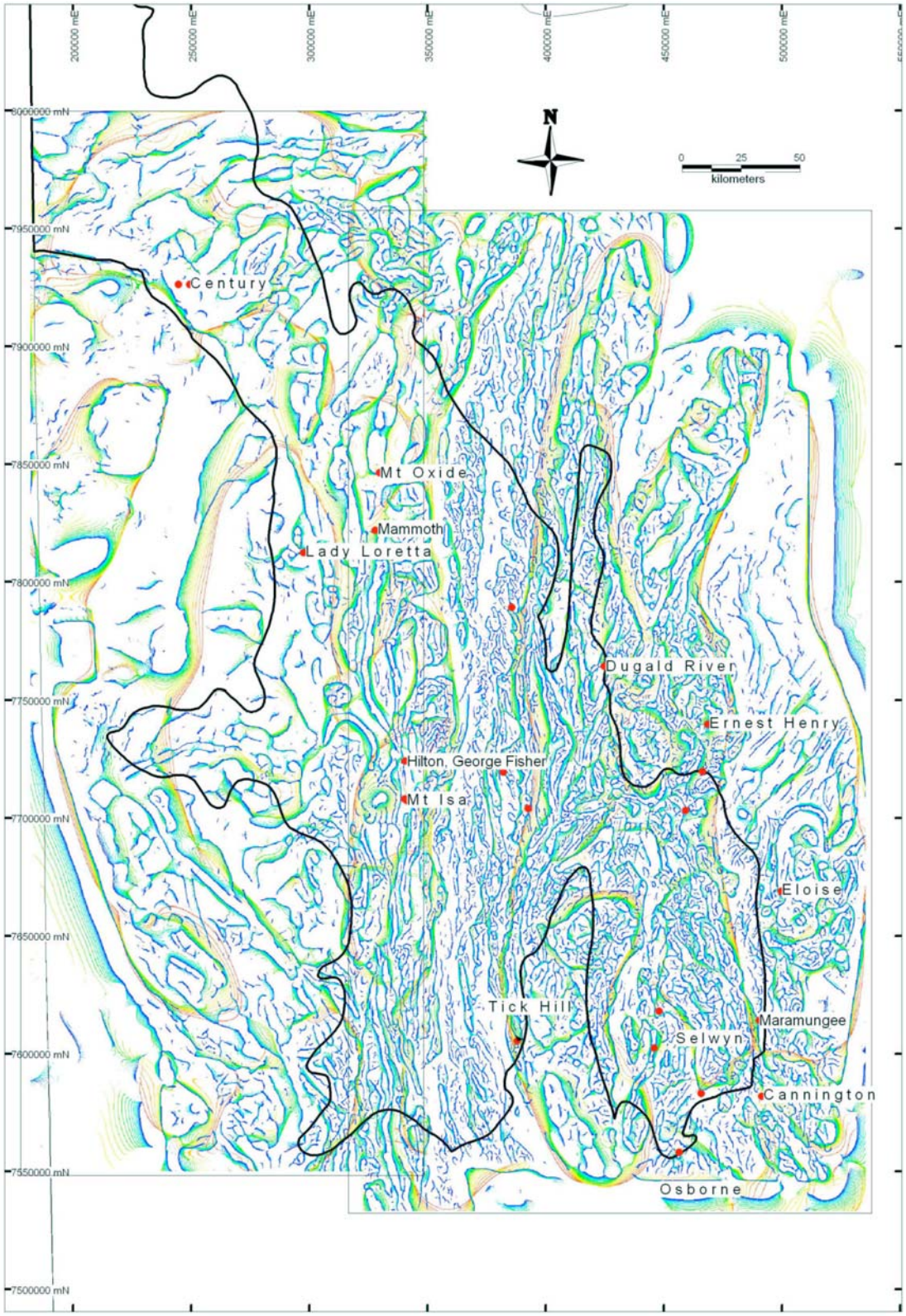

Fig. 7: Aeromagnetic worms for Eastern and Western Successions, coloured coded by height from 1 km (blue) to 30 km (red), with outline of Proterozoic Mt Isa region (black) and major metallic deposits (red).

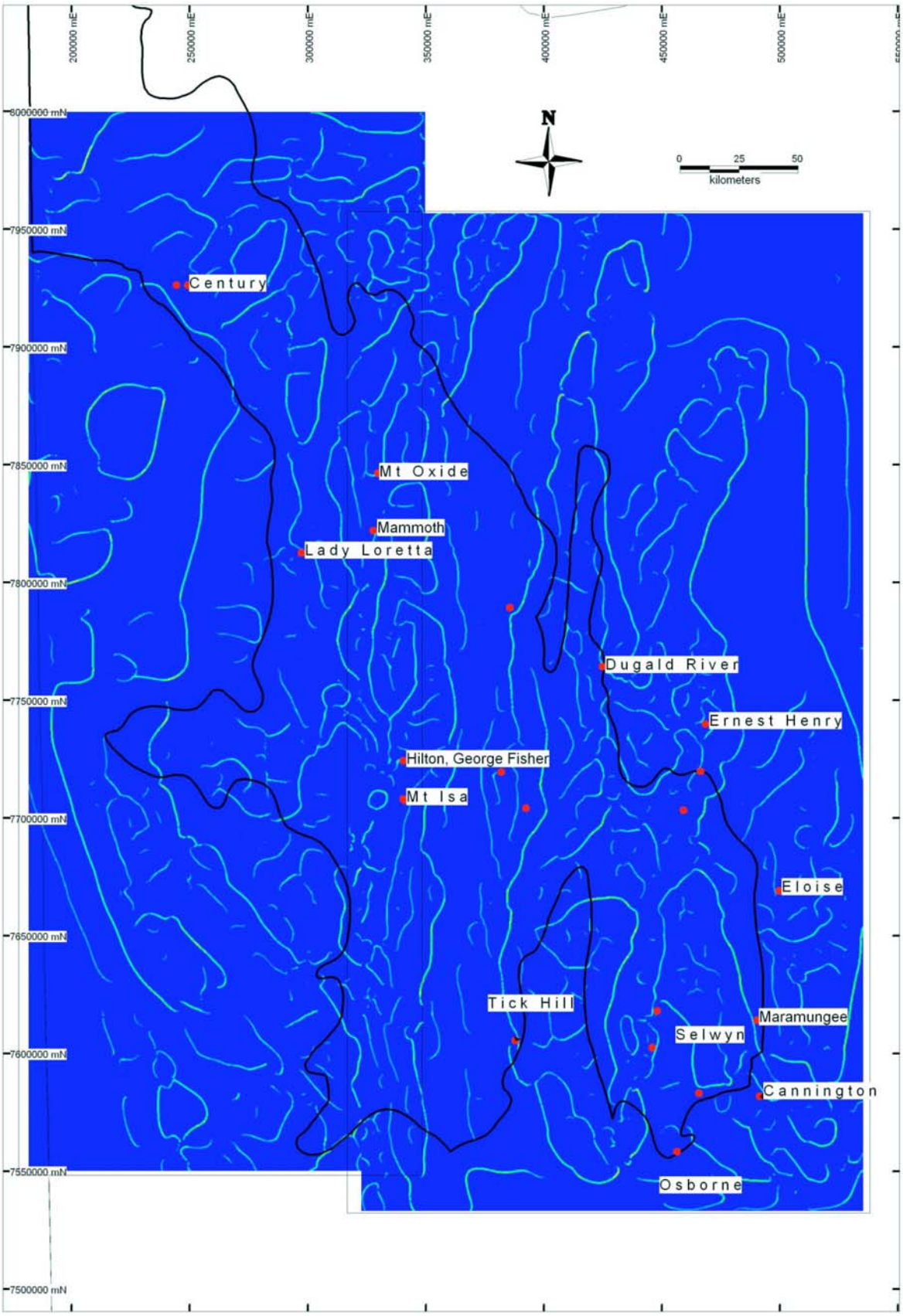

Fig. 8: Image of migrated magnetic worms at 5 km height of upward continuation, with outline of Proterozoic Mt Isa region (black) and major metallic deposits (red).

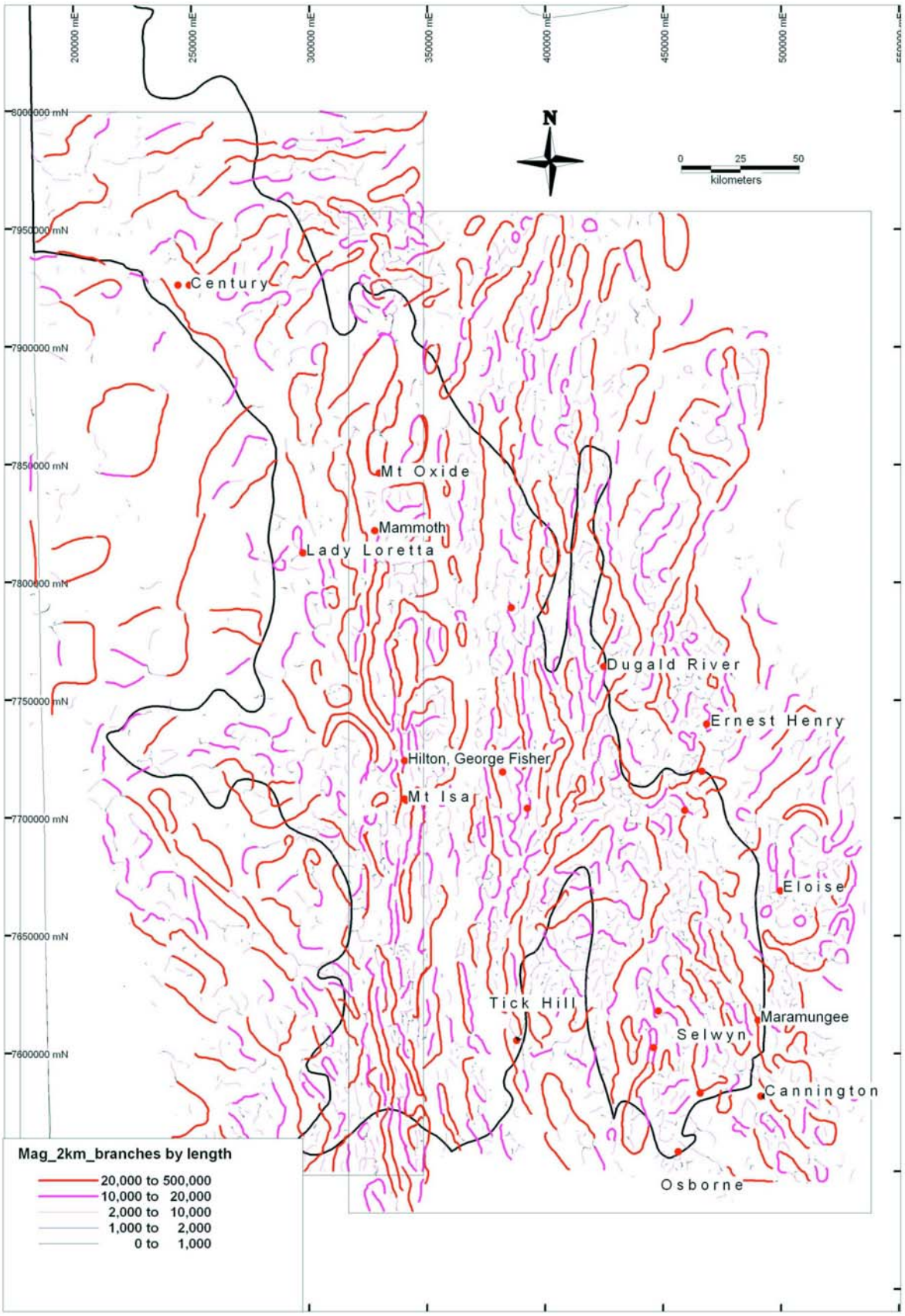

Fig. 9: Thematic map of magnetic worm vector line length (m), at 2 km height of upward continuation.

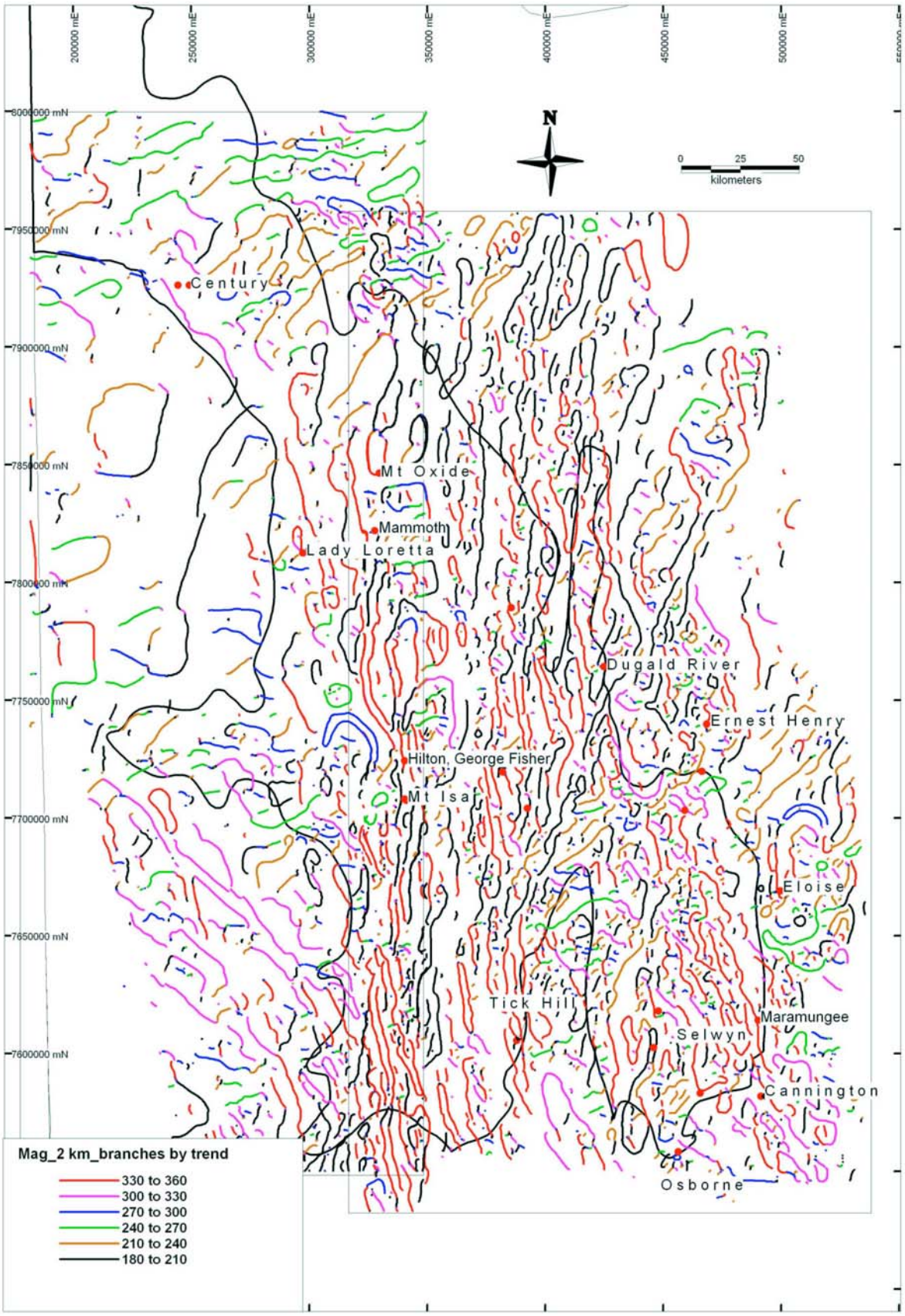

Fig. 10: Thematic map of magnetic worm vector line trend, at 2 km height of upward continuation, in 30^{o} increments.

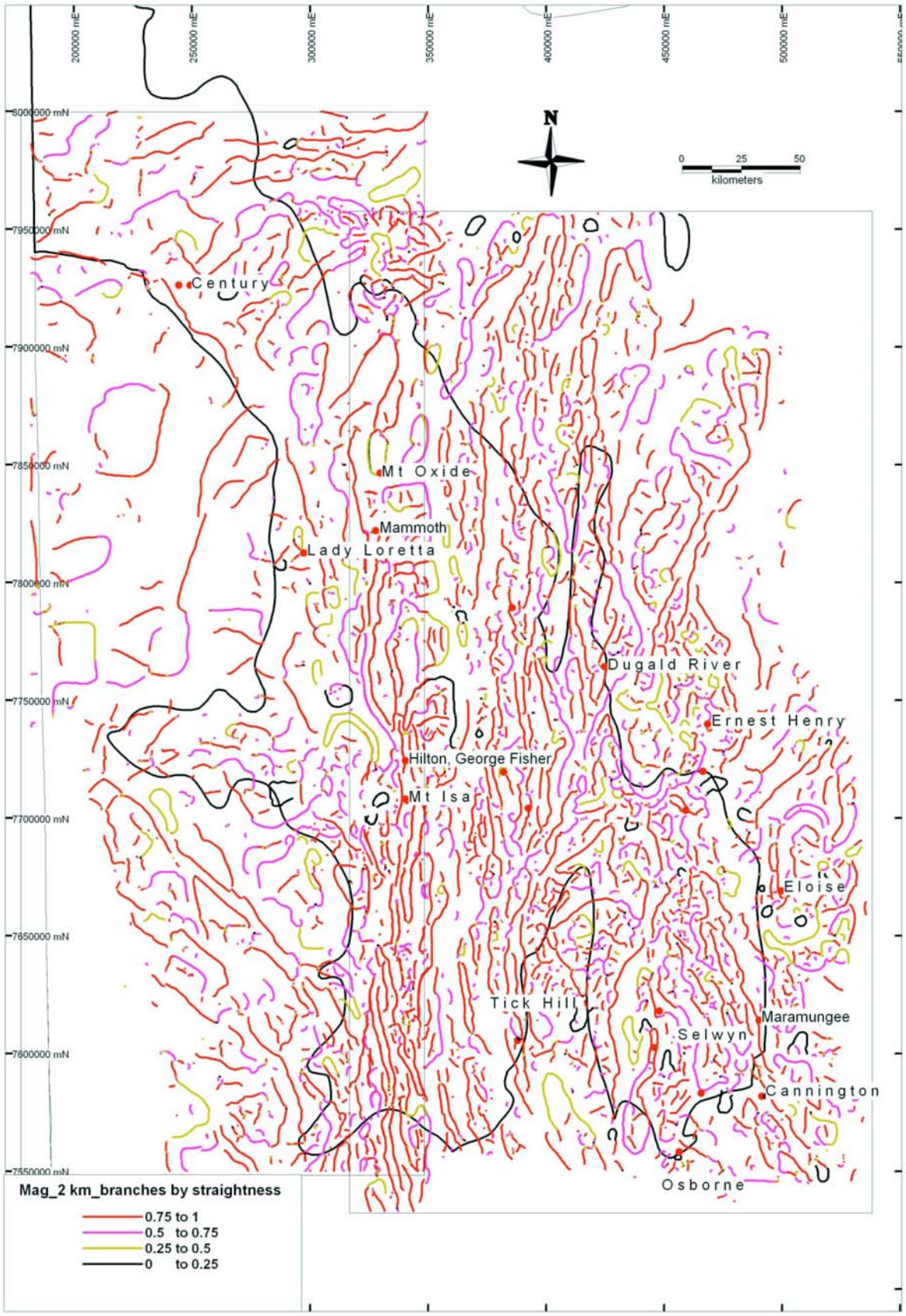

Fig. 11: Thematic map of magnetic worm vector line straightness, at 2 km height of upward continuation, 1 = straight, 0 = sub-circular.

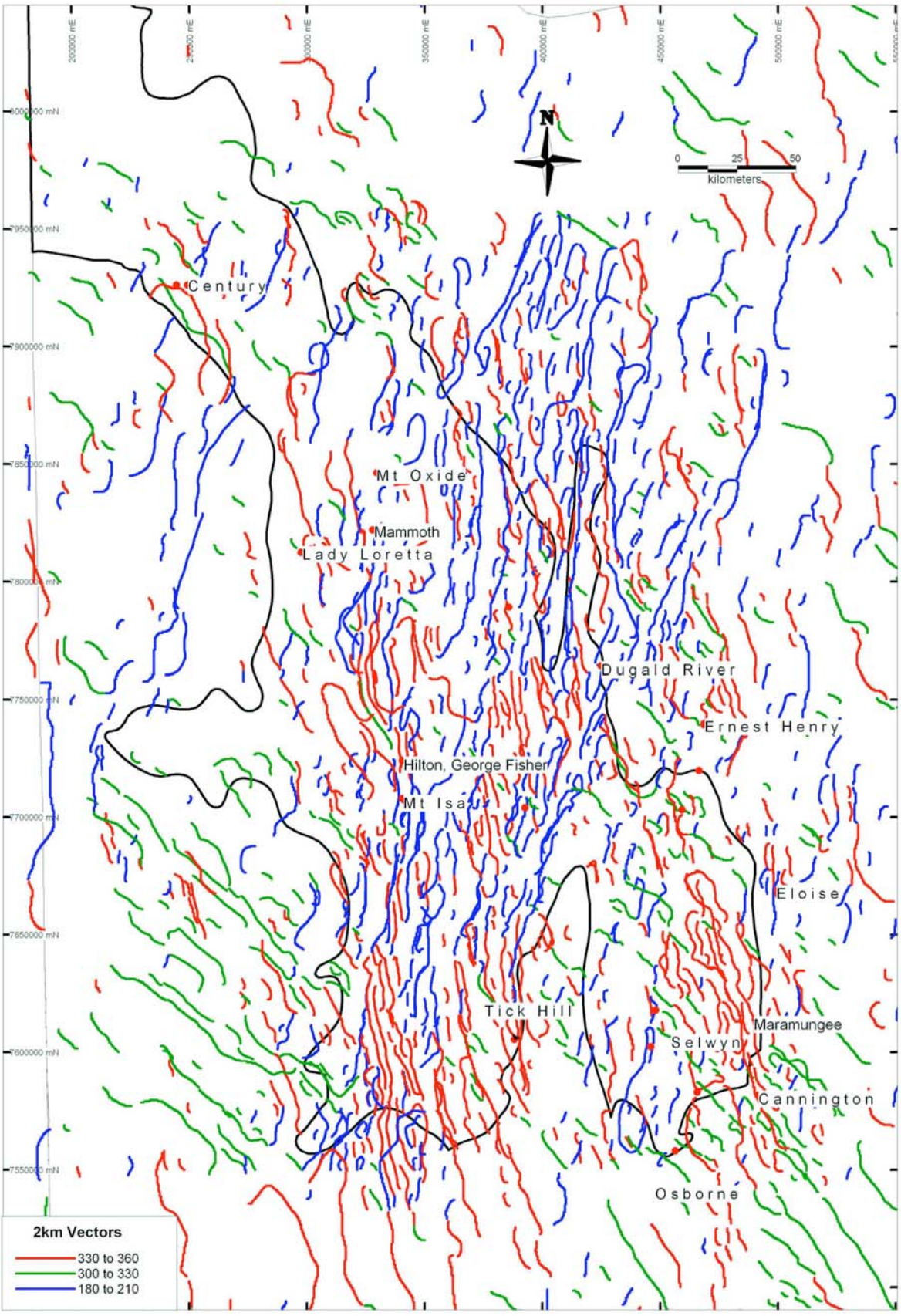

Fig. 12: Thematic map of combined gravity and aeromagnetic vectors showing selected trends, filtered by length and straightness.

Reprocessing and Reinterpretation of the Mt Isa Seismic Transect

Piter Lepong[1], Tom Blenkinsop[1]

[1]School of Earth Sciences James Cook University, Townsville QLD 4811, Australia

ABSTRACT

Reprocessing of the Mt Isa Seismic transect utilized the processing facilities at Geoscience Australia in Canberra. Updated techniques and processing algorithms were applied, including a dip moveout correction and Kirchhoff Migration. New seismic profiles with improved in temporal and spatial resolution facilitate more accurate interpretation of the data, especially in the Mt Isa Eastern Succession. Geologic interpretation incorporated potential field data and advanced geological knowledge obtained by related studies during the I2+3 project. New profiles indicate structural styles with steeply dipping faults, including the Cloncurry and Marimo Faults, and upright folds. This contrasts with interpretations based on the previously processed section that emphasized a detachment surface separating cover sequences from crystalline basement.

Keywords: Seismic reflection, reprocessing, reinterpretation, Mt Isa Eastern Succession, folds, faults

1. INTRODUCTION

The Mt Isa deep seismic section (Fig.1) was acquired and processed in the last decade. Interpretation of the deep seismic transect indicates that the Eastern Fold Belt is dominated by large-scale horizontal offsets of supracrustal rocks that were decoupled from the basement along a subhorizontal detachment that spawned numerous east-dipping thrust faults (MacCready et al., 1998). This west-directed fold and thrust system was then broadly warped and dissected by a number of reverse and strike-slip faults that involve the basement and may link to a major mid-crustal structure (inferred from alignment of high-velocity rocks interpreted from seismic refraction).

On the other hand, surface geology and potential field data (i.e. gravity and aeromagnetic) indicate that the major structure of the Mt Isa Eastern Succession is generally steeply dipping and extends down to the base of the crust in contrast to the shallowly dipping seismic interpretation. The resolution of this paradox is a vital for understanding the formation of mineral deposits and depends essentially on understanding the deep structure of the crust.

Seismic sections can not directly image structures with steep to vertical dips. Any interpretation of the crustal structure from seismic sections alone may therefore be biased towards shallow-dipping structures. The Mt Isa area offers a unique opportunity to evaluate true crustal structure by combining interpretation of seismic sections with potential field data and advanced geological knowledge. This article describes reprocessing of the Mt Isa seismic section to investigate if it is possible to increase temporal and spatial seismic resolution, followed by reinterpretation of the data.

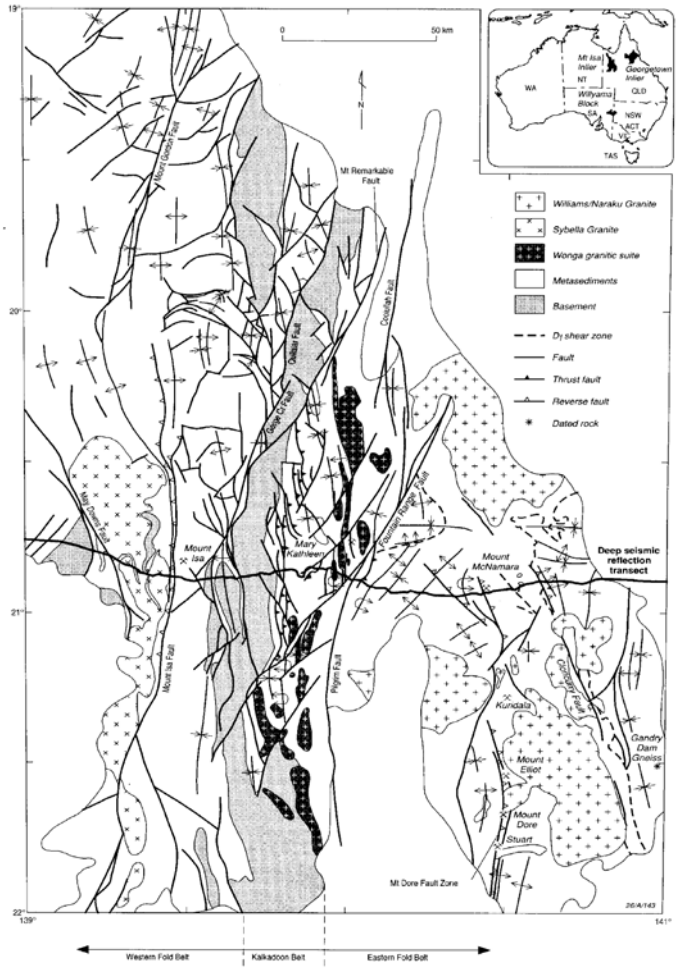

Fig.1.Seismic line and the major structure of the Mt Isa inlier (MacCready et al, 1998)

2. REPROCESSING OF DEEP SEISMIC TRANSECT

The Mt Isa deep seismic reflection data were reprocessed using Disco/Focus seismic data processing system using updated techniques and processing algorithms. Reprocessed was done used the processing facilities at Geoscience Australia in Canberra. Processing sequences and parameters used by Goleby et al. (1996) provided a useful starting point for designing the processing sequence. The data were reprocessed through a basic sequence of noise attenuation, spiking deconvolution, dip moveout and scaling prior to stack. The post-stack data were subsequently migrated using the Kirchhoff algorithm. Further filtering was applied post-migration. Preprocessing including demultiplex, editing, gain recovery, field geometry and field static mostly adopted from previous processing. This reprocessing focused on increasing the signal to noise ratio within the seismic records and improving continuity of the reflector events. The following is a summary of the updated techniques and parameters used in this current reprocessing sequence.

2.1 Deconvolution (Pre-Stack)

To increase temporal resolution and sometimes, to remove the effects of multiples, deconvolution is applied before stack. The Wiener-Levinson algorithm was used to sharpen seismic events and extend the frequency bandwidth. Spiking deconvolution used 160-millisecond operator length and 0.1% pre-whitening parameters applied to all traces over two gates window, near and far offset.

2.2 Spectrum Balancing

Spectrum Balancing is particularly useful for balancing the spectrum of the data contaminated by source generated noise. The input is prestack data, sampled at 4 milliseconds. Spectral whitening is achieved using four frequency bands.

2.3 Bandpass Filter

Filtering for temporal frequency (in time) and also for spatial frequency (in wavenumber) is applied in this processing. Band filters with slopes in decibels per octave, including band pass, are applied to traces in all shots. A Four time gate is designated for filtering with a 160 millisecond length. Lower frequencies are attenuated at 18 decibels per octave and higher frequencies are attenuated at different ranges of decibels per octave.

2.4 Dip Moveout

The dip moveout (DMO) correction applied before stack used the F-K DMO algorithm as described by Cabera and Levy (1989). The input to this DMO routine are NMO corrected shot records. The group interval for this data is 20 meters. The maximum frequency of the data is approximately 75 Hz. The minimum time start of DMO operation is 150 milliseconds.

2.5 Kirchhoff Migration

The objective of migration is to move (migrate) data from an observed point of reference to the point of actual origin. Implemented ideally, this procedure essentially collapses diffractions to a single point, and spatially orients dipping events to their correct position.

A poststack data set is migrated for all traces using time space Kirchhoff migration. The imaging operation is based on an algorithm derived from the description of Kirchhoff migration in Stolt and Benson (1986). The CDP trace spacing is 20 meters and the dip limit is 70º with an interpolation filter. The velocity model used for the migration has previously been stored in the database.

3. NEW PROCESSED SEISMIC SECTION

The reprocessing methodology described here resulted in seismic profiles with increased temporal and spatial resolution, which should facilitate more accurate interpretation of the data. Clearly visible improvements in places in the new profiles are:

1) Much better signal to noise ratio
2) Greater length and continuity of reflectors in some areas
3) More reflectors visible in the interval from 4 to 10 s two way travel time, which is characterized on both the former and newly processed sections by homogeneity.
4) Apparent reflectors on the previous sections are not visible on the newly processed sections because they may be diffractions removed by the new migration technique.

The major difference in the sections between the original processing and current processing is attributed to the applied of spiking deconvolution, dip moveout and Kirchhoff migration. The application of DMO eliminated the dip dependency of the NMO velocity field and removed the midpoint noise on dipping events. The DMO technique appeared to be very efficient in areas of the Mt Isa where structure is associated with steeply dipping features. The overall quality of the reprocessed data shows better noise suppression and increases of continuity reflector events, especially after DMO and post-stack Kirchhoff migration section as shown in Fig.2 compare to original processing of the unmigrated section in Fig.3.

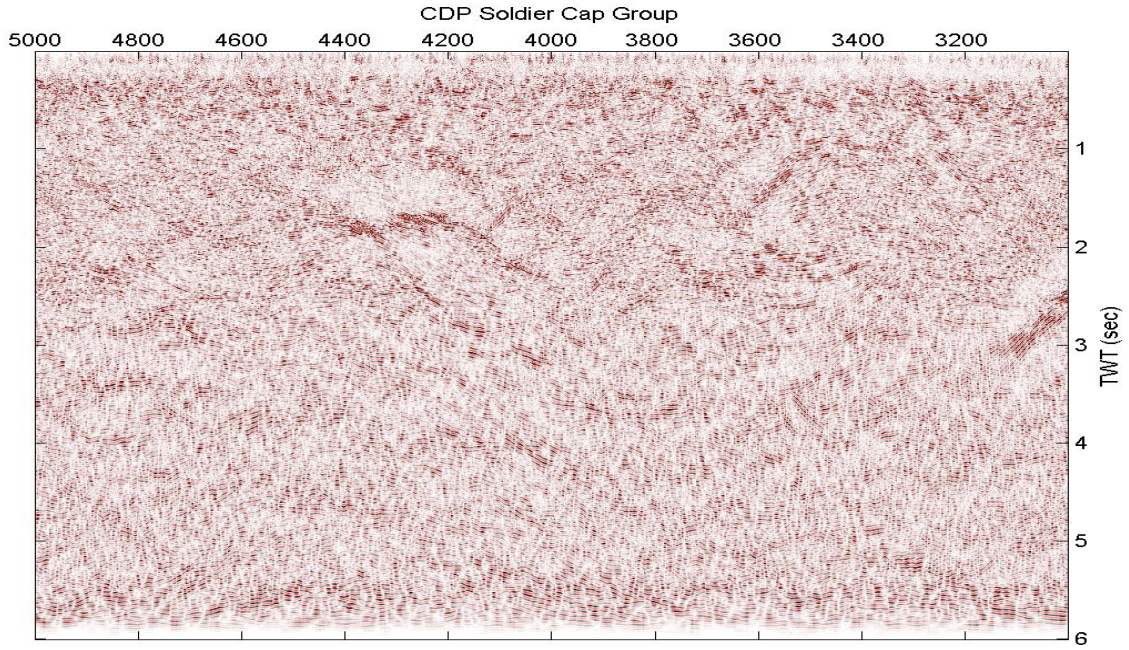

Fig.2. Migrated Seismic Section in the Soldiers Cap Group. Dominant Reflector below CDP 4200 and 4400 is correlated to the Snake Creek Anticline and reflector below the CDP 3600 is correlated to the west limb of the Middle Creek Anticline.

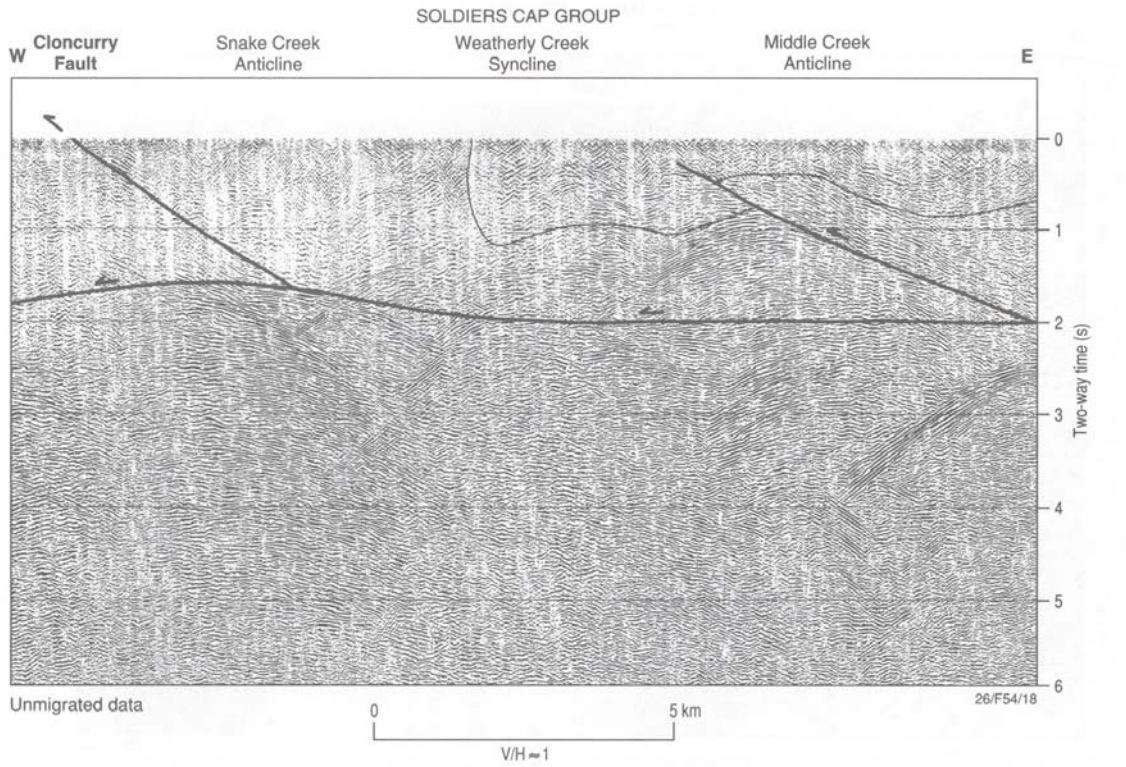

Fig. 3.Previous Unmigrated and Interpreted Section in the Soldiers Cap Group (Goleby et al, 1998).

4. INTERPRETATION OF THE NEW SECTION

Reprocessed seismic reflection data across the Proterozoic region in the Mt Isa provides better images that lead to more detailed interpretation of the data. The prominent feature of the reprocessed profile is a number of dipping reflective zones found between 1-3s two way travel time (TWT), corresponding to 3 - 6 km in depth. These reflectors do not clearly show a widespread sub-horizontal detachment surface separating cover sequences from crystalline basement as previously interpreted by MacCready et al. (1998). The detachment was interpreted to mark a major D2 decollement between basement and the cover sequences.

The following interpretations do not merely rely on the seismic profile but also incorporated the potential field data and modelling, and advanced geological understanding obtained by related studies during the I2+3 project. The interpretation of the upper crustal structure was derived from the seismic profile, geological knowledge and potential field data, and in the lower crust down to ~ 30 km depth, interpretation is derived from potential field worms, gravity modelling and geological inference.

4.1 Interpretation of the Soldiers Cap Group

Two prominent reflectors in Soldiers Cap Group may correlate to the limbs of the Middle Creek Anticline and Snake creek Anticline. Those two reflectors separate the Weatherly syncline (W) from Middle Creek Anticline (M) to the East and the Snake Creek anticline (S) to the West as described in Fig.4. Truncation reflectors separating the boundary between Doherty Formation (DF) and the Soldiers Cap Group (SCG) can be traced along the section in this area. A significant gradient of the gravity was used to infer the Eloise fault (F) that links or cuts in to the lower crust. This fault was not mentioned in the

previous interpretation. Moderate reflectors together with the magnetic worm are used to infer the Cloncurry fault (CF) as steeply dipping fault rather than shallowly dipping fault (Goleby et al., 1998).

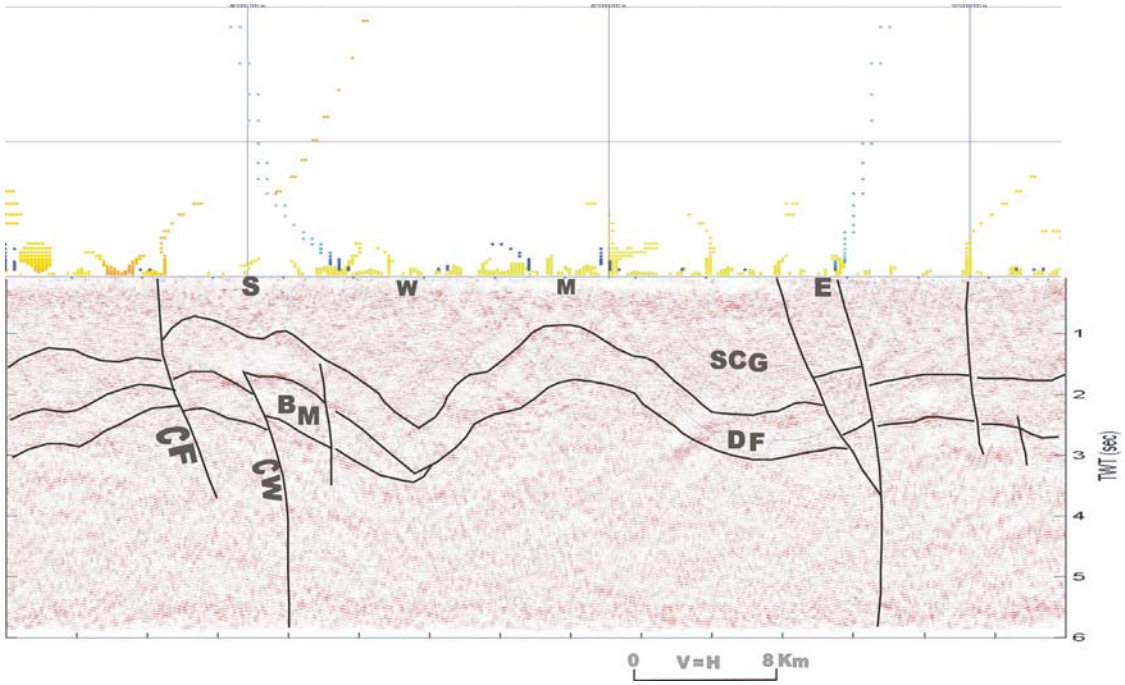

Fig. 4. Seismic Interpretation along the Soldiers Cap Group. Top section showing gravity (blue) and magnetic (yellow) worm used to draw the Cloncurry worm (CW) and Eloise fault (E) down to lower crust.

4.2 Interpretation of the Marimo Slate

The dominant subhorizontal reflectors in the vicinity of Marimo region are interpreted to represent the base of Tewinga group (TG) as showing in Fig.5. The Marimo fault (MF) is marked as a straight reflective zone dissecting the Young Australia group in the western part and Mitakoodi Quartzite in the eastern part, indicating it is a last generation structure and the reflectivity is thought to be enhanced by hydrothermal alteration along the fault zone (MacCready et al., 1998). The Overhang shear (OS) zone can be followed from its surface trace along gently dipping reflections to ~3 s twt.

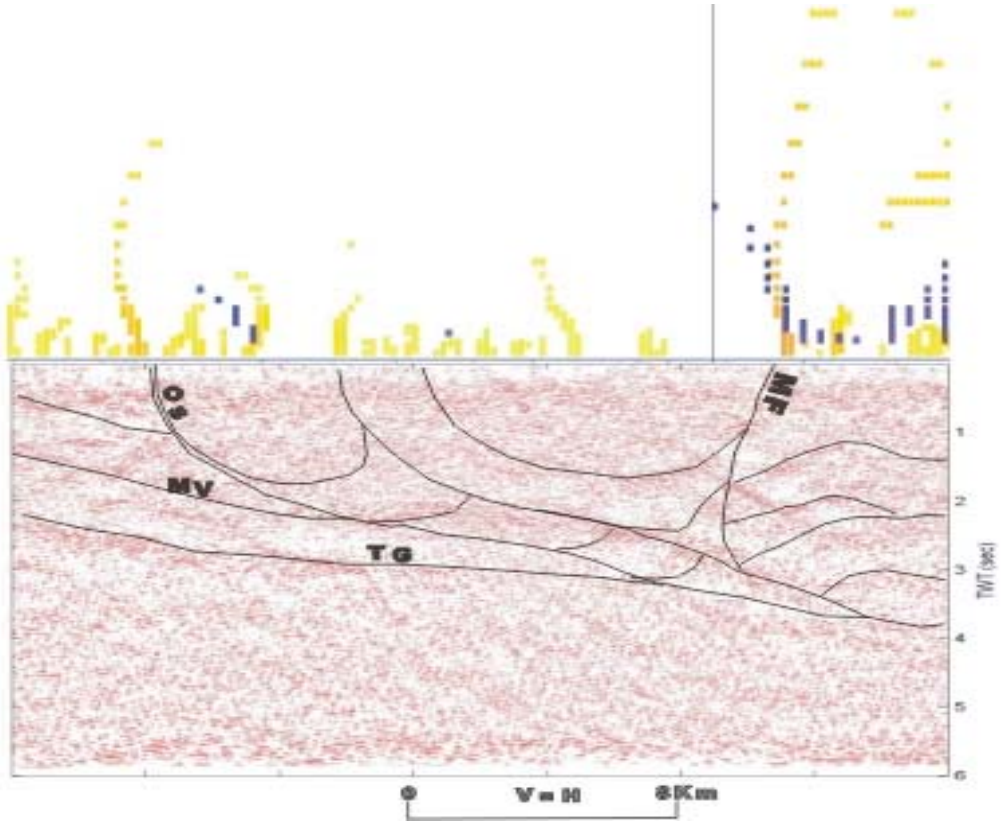

Fig.5. Seismic Interpretation in the Marimo region. Marimo Fault and Overhang Shear were interpreted based on the strong reflectors and the mirror of the gravity (blue) and magnetic (yellow) worm.

4.3 Interpretation of the Mitakoodi Fold Belt

In the Mitakoodi Fold Belt, the openly folded Duck Creek Anticline (DA) and the overturned Bulonga anticline (BA) are separated by the Wakeful syncline (WS) and a fault plane in Fig.6. Three different stratigraphic groups including Kalkadoon Leichhardt Basement (KB) in the western part of this profile, Tewinga group (TG) and Marraba Volcanics (MV) are interpreted in this region. Greater contrast of the gravity worm is inferred to correlate to the broad body of the Duck Creek anticline. MacCready et al. (1998) interpreted that the D2 Bulonga thrust splays off the decollement and documented it as a low angle fault. However, gravity and magnetic worms and the reflector features show that the fault is steeply dipping to the east and extended down to the detachment surface.

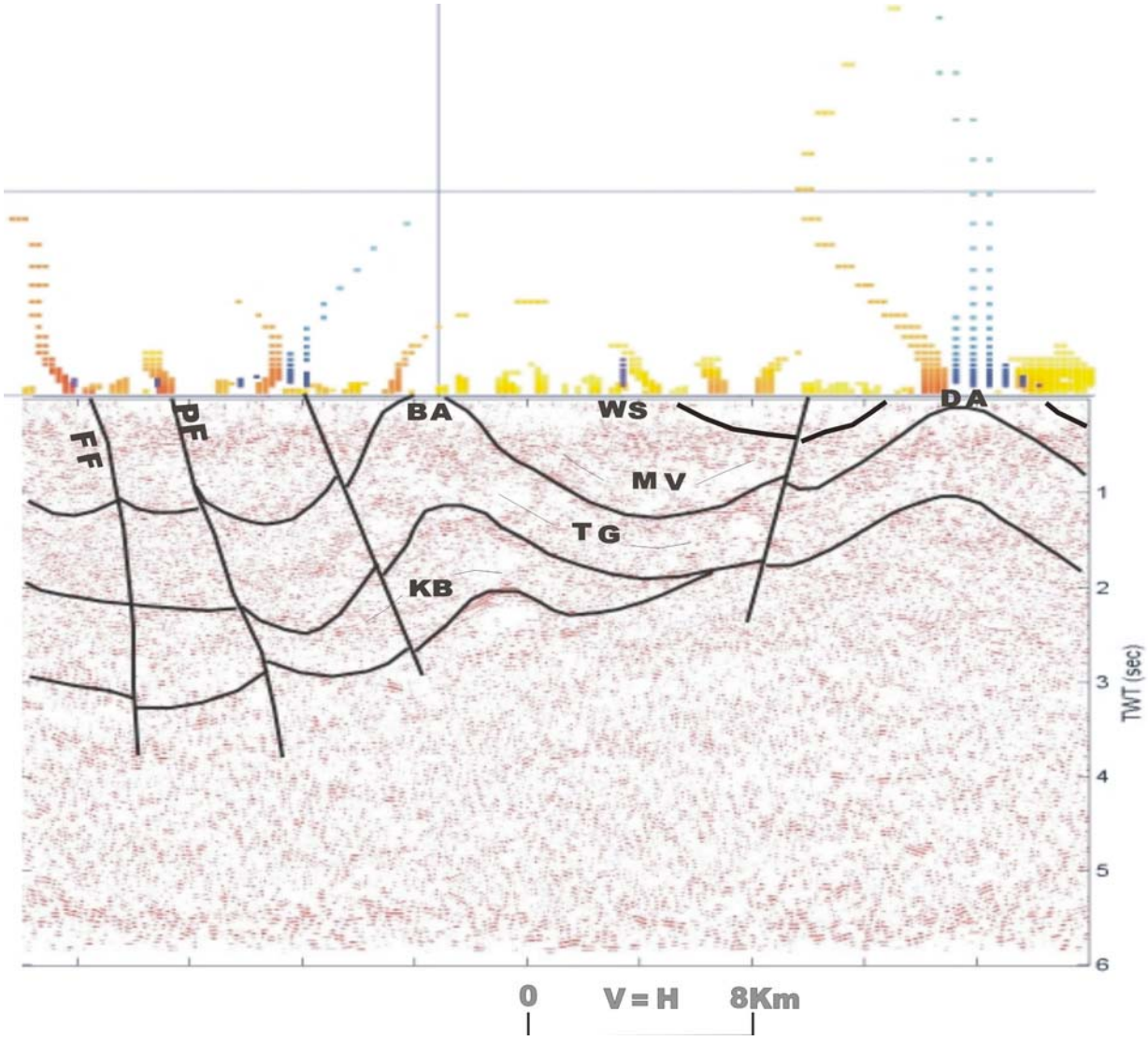

Fig.6.Seismic Interpretation of Miktakoodi Fold Belt. The strongest gravity (blue) and magnetic (yellow) worm in the eastern part of this section inferred as reflected from the dense body across the Duck Creek Anticline (DA). Pilgrim Fault (PF) and Fountain Range Fault (FF) showing in the western section.

5. CONCLUSIONS

The reprocessed section has offered a new perspective on the upper crustal structure of the Mt Isa seismic section. Improvements in the processing indicate that some sub-horizontal surfaces interpreted in earlier work may be diffractions. The dominant structural style of the reinterpreted section consists of upright folds and steeply dipping faults – which correlate with the surface geology. This style is also reflected in the construction of the I2+3 3D model (Blenkinsop et al., 2005), and is part of the evidence for a close relationship between major faults, basin architecture and contractional structures that implies that positive inversion has been a fundamental process in the evolution of the crustal architecture of the inlier.

Acknowledgments
Bruce Goleby is thanked for his invaluable help in data processing.

6. REFERENCES

Blenkinsop, T. G., Huddlestone-Holmes, C., Foster, D., Mark, G., Austin, J., Edmiston, M., Lepong, P., Ford, A., Murphy, F.C. 2005. 3-D model and crustal architecture of the Mt Isa Eastern Succession. I2+3 Final Report, pmdCRC.

Cabera, J., and Levy, S., 1989, Shot Dip Moveout with Logarithmic Transform, Geophysics, 54: 1038-1041

Goleby, B. R., MacCready, T., Drummond, B. J., and Goncharov., 1998. The Mount Isa Geodynamic Transect-Crustal Implications. In: Braun, J., Dooley, J., Goleby, B., Van der Hilst, R., Klootwijik, C., (Eds), Structure and Evolution of the Australian continent, Published by American Geophysical Union, Geodynamic 26, 109-117.

Goleby, B.R., Drummond, B.J., and MacCready, T., 1996, The Mount Isa Deep Seismic Transect, Australian Geological Survey Organization, Research Newsletter, 24:6-8

MacCready, T., Goleby, B.R., Goncharov, A., Drummond, B.J., and Lister,G.S., 1998, A Framework of Overprinting Orogens Based on Interpretation of the Mount Isa Deep Seismic Transect, Economic Geology, 93:1422-1434

Stolt, R.H., and Benson, K.H., 1986, Seismic Migration, London , geophysical Press Ltd..

The Cloncurry Lineament: Interpretation of a Major Crustal Worm

J. R.Austin
Pmd*CRC, School of Earth Sciences, James Cook University, Townsville, Qld, 4811

ABSTRACT

The Cloncurry Lineament (CL) is a prominent feature of magnetic and gravity worm data over the structurally complex Mt Isa Eastern Succession. The Cloncurry Lineament primarily delineates the contact between the Cover Sequence 2 (CS_2) Doherty Formation and the CS_3 Soldiers Cap Group which is thought to be a pre-CS_3 basin-bounding normal fault. This is seen convincingly in an area in the south of the study area. However the CL also displays evidence of later tectonic activity. Widely described NE trending dextral faults that developed syn-post D3 offset the Doherty/Soldiers Cap contact at several locations. These are identified where the 150° trend in low upward continuation (UC) worms are dextrally offset along a ~NE trend, or where worms appear to truncate along a consistent ~NE trend. Work by Mustard et al. (2005) identifies the Doherty/Soldiers Cap contact and NE trending strike-slip faults as highly prospective to Cu-Au mineralisation in the Mt Isa Inlier. Williams-Naraku intrusions also have a great effect on worm trends in the study area. The margins Saxby Granite for example is traced very closely by low UC magnetic worms. At higher levels of UC the granites are not delineated, implying that they sit at fairly shallow levels in the crust. Neither the Saxby Granite contact nor the Doherty/Soldiers Cap contact are delineated in the north of the study area suggesting that the high UC worm is tracing a magnetic response cause by a fusion of both contacts. A tectonic hypothesis to explain the Cloncurry Lineament is: 1) ~NE-SW extension created a basin-bounding fault and allowing deposition of the Soldiers Cap Group. 2) E-W shortening caused ~N-S folding to occur during D2. 3) This shortening continued during D3 before ~NE trending dextral faults developed allowing the crust to be extended N-S. 4) Intermediate magmas intruded into the crust along fault intersections generated by 1 and 3. Continued research focus on the Doherty/Soldiers Cap contact and later NE dextral faulting will help unravel the tectonic implications of the Cloncurry Lineament and its importance to mineralisation in the Mt Isa Eastern Succession.

Keywords: Cloncurry, Worm, Doherty Fm, Soldiers Cap Fm, Williams-Naraku Batholith

1. INTRODUCTION

The Mount Isa Inlier has been the subject of research for decades. However there still remains a need to understand the crustal scale structure of the inlier, particularly in the east where the structural framework is least well understood (Loosveld, 1989, Betts et al, 2000). "Attempts to place localised structural observations into an inlier-wide deformation scheme have led to conflicting interpretations of the nature and significance of the deformation history" (Betts et al., 2000). Seismic coverage is limited to one transect across the entire inlier and reveals a paucity of information about the deep crustal structure. There are limitations in traditional surface mapping particularly in complex terranes where crustal to regional scale observations may be obscured by smaller scale features. Seismic methods and surface mapping give 2 dimensional insights into crustal structure, whereas multiscale edge detection (worming) provides an opportunity to look at deep crustal structures in three dimensions. The aim of this project is to investigate the geological reasons for a major geophysical structure, the Cloncurry Lineament. What crustal components define its architecture and what is its role in the mineralisation and tectonic history of the Mt Isa Eastern Succession?

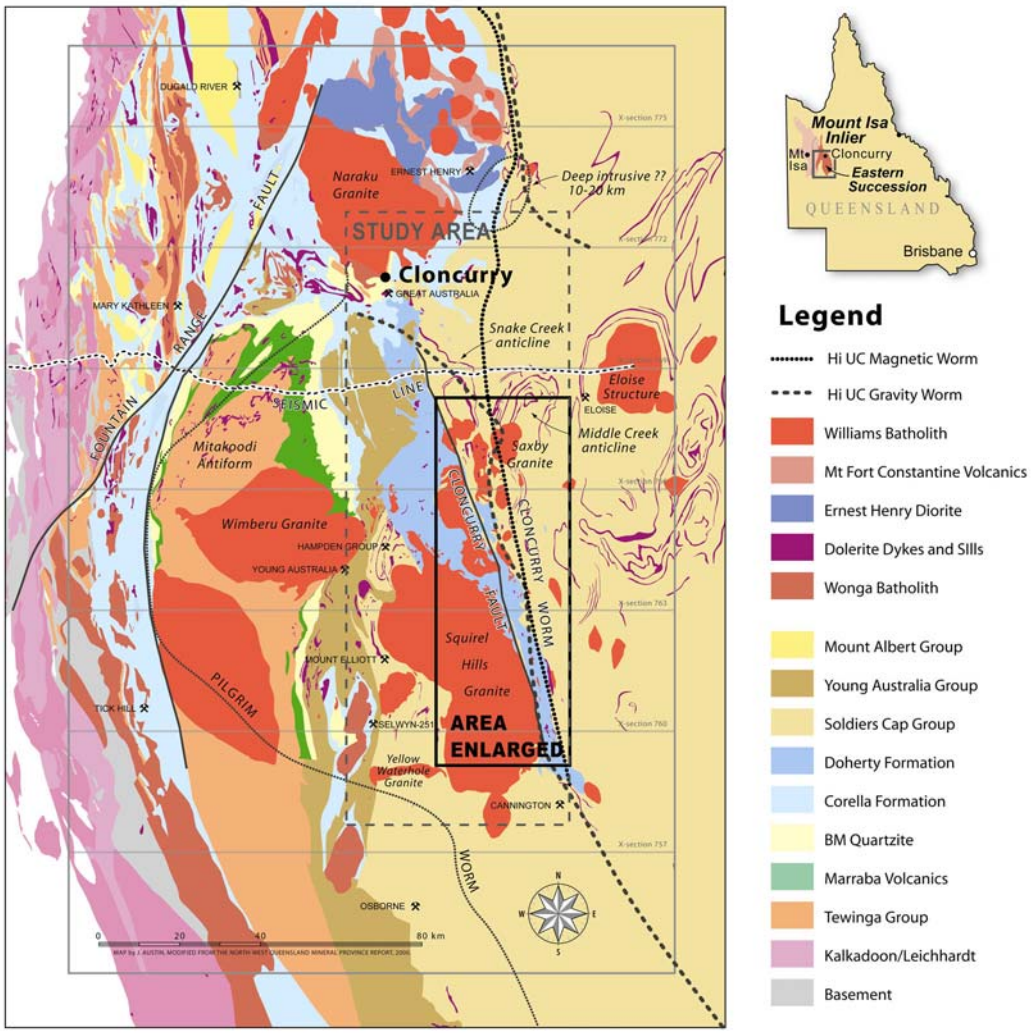

Fig. 1: The Mt Isa Eastern Succession model area showing geological units, cross-section lines, major structures, faults, and high UC worms. The detailed study area of this project is boxed.

The Cloncurry Lineament

The Cloncurry worm, a major regional magnetic and gravity anomaly, is a dominant feature of the wavelet processed potential field data (worms) over the Mt Isa Eastern Succession. The Cloncurry Lineament (CL) is defined as the surface trace of the Cloncurry worm, delineated from the high upward continuation (UC) levels of the magnetic worm dataset. This ~30 km level of UC indicates that the anomaly can be traced to a depth of about 15 km. The gravity worm maybe traced deeper, but with less reliability. The worm lies sub-parallel to the eastern edge of the Mount Isa Inlier and extends 200km north of Cannington and under cover east of Ernest Henry (See figure 1). The 30km UC worm is a continuous line oriented approximately 160°-170°. Lower levels of UC are progressively more variable in both their orientation and their continuity.

The CL coincides with a complex geological zone of highly folded metasediments, breccias, mylonites, and numerous granitic to mafic intrusions ; specifically it runs through the Soldiers Cap Group, Doherty Formation and plutons of the Williams-Naraku Batholith. Although the CL appears, at least in part, to mark the poorly understood boundary between the CS_2, Doherty Fm. and the CS_3, Soldiers Cap Group it generally lacks a distinctive surface expression in mapped geology, aerial photography, ASTER or magnetic potential. Its surface expression is also masked by Jurassic mesas that occur throughout the area.

2. BACKGROUND

2.1 Worming

Multiscale edge detection using potential field geophysics (worming) was developed by researchers working for Fractal Graphics (now Geoinformatics) and CSIRO Exploration and Mining. The 1998 paper by Archibald et al. first introduced the concept which was then developed through successive papers by Hornby et al. (1999) and Holden et al. (2001). Multiscale edge detection highlights geological edges such as faults and contacts in three dimensions using an algorithm to upward continue data to higher altitudes. The higher the Upward Continuation (UC) the deeper the origin of the contrast in geophysical properties that causes the edge. For detailed worm theory see the aforementioned papers.

Worms have a number of applications but the most important is to aid in mapping, and investigation of crustal architecture. Worms will easily identify surface features such as faults, contacts, granitic intrusions and mafic dykes provided there is significant petrophysical contrast to generate an anomaly in magnetic or gravity potential. Different levels of UC allow examination of structure with increasing depth; the actual depth being about half the UC height. One important aspect of this breakthrough is that it allows us to see deep structures (e.g., along the Cloncurry Lineament) even though their expression in magnetic potential data is not obvious. Because there are several different levels of UC, we can trace the “edge” from surface to depth thus giving important information about the 3-D orientation of planar structures, and the depth extent of intrusive bodies.

The Cloncurry lineament provides an opportunity to study a crustal scale worm lying within a structurally complicated, highly metamorphosed terrain, where the geological interpretation of worms may not be straightforward.

2.2 Regional Geology

The Mount Isa Inlier is amongst the world's most productive mineral provinces and contains copper, IOCG, Ag-Pb-Zn and uranium deposits. The majority of its complex tectonic development took place from 1.9 to 1.5 Ga and it is overlain in places by Cambrian, Jurassic and Cenozoic basins.

The oldest basement rocks in the inlier are Archean in age with the earliest documented tectonic activity occurring during the Barramundi Orogeny 1.9-1.85 Ga (Etheridge et al., 1987). This was followed by rifting which resulted in the deposition of Cover Sequence 1 (CS_1, D_{E1}) and intrusion of the Kalkadoon Granite at 1.87-1.85 Ga. Following initiation of a second rifting phase, Cover Sequence 2 (CS_2, D_{E3}) was deposited from 1.8-1.72 Ga with the Wonga Granite intruding at about 1.74 Ga. A third rifting phase from 1.7-1.6 Ga allowed deposition of Cover Sequence 3 (CS_3, D_{E3}) and intrusion of the Sybella Granite at ~1.70 Ga (Page and Bell, 1986, Betts et al, 1998).

The Isan Orogeny, occurring from ~1600-1500 Ma, was the major contractional deformation event in the Isa Inlier. Contention exists over the style and sequence of sub-events, with some researchers proposing one or two protracted events (eg, MacCready et al ., 1998, Holcombe et al., 1992) with heterogeneous deformation, while others propose up to seven separate homogeneous events (eg, Mares, 1998). It is generally accepted that there are three main events within the Isan Orogeny, D_1, D_2 and D_3 (called D_4, post-1998). D_1, is proposed by Bell (1983) to be a N-S thrusting event. However it is not easily observed at most localities in the Eastern Succession. Oliver et al. (1998) suggest that during D1 the *ca* 1670 Soldiers Cap Gp. was "interleaved" with the *ca* 1750 Corella (Doherty) Fm. D_2 and D_3 are both roughly E-W shortening events that have formed the dominant ~N-S structural grain of the Eastern Succession. D_2 produced upright folding, shearing and veins associated with peak metamorphism, while the D_3 event led to increased kinking and brecciation events (Oliver et al., 1998). More recent events generally formed crenulation cleavages and faulting.

Plutons of the Williams-Naruku Batholith intruded large areas of the Eastern Succession from 1545 to 1480 Ma. There is a progression from tonalitic compositions to normal I-type chemistries over this period (Mark, 2001). Doleritic dykes and sills of various ages intrude the area. Many are sills that have intruded into CS_3 units and been amphibolised and extensively folded. Many others are post-Isan, unaltered, small intrusions aged ~1100 Ma.

Metamorphism in the inlier is high temperature, low pressure and follows an anti-clockwise P-T-t path (Rubenach and Lewthwaite, 2002) with peak metamorphism commonly thought to be syn-D2 (Rubenach and Barker, 1998). Three metamorphic peaks are commonly quoted in the literature. One at 1584+/-17 Ma (Page and Sun, 1998) is proposed as syn-D1 in the Eastern Succession by Rubenach and Barker (1998). The other is 1544+/-12 Ma (Page and Bell, 1986) which is proposed to be the syn-D2 peak at Mt Isa (Rubenach, 1993). However, more recent work of Rubenach (2003) puts the peak of metamorphism at 1595 Ma for schists of the Soldiers Cap Fm in the Snake Creek anticline. It is possible that the metamorphic peak has migrated from east (~1595 Ma) to west (1530 Ma) (Oliver et al, 1998). Several mechanisms are proposed to explain these high temperature/low pressure metamorphic peaks including mantle under-plating (Oliver et al., 1998) and large mafic / felsic mid-crustal intrusions.

Various styles of mineralisation occur throughout the inlier. The main styles of mineralisation are copper and IOCG, however there is wide variation within this group. Other common deposit types include Ag-Pb-Zn and Uranium. Mineralisation ages vary widely from deposit to deposit. Many are synchronous with the intrusion of the Sybella and Williams-Naraku Batholiths. However there are anomalies such as the ~1600 Ma mineralisation age for the Osborne deposit.

3. OBSERVATIONS

3.1 Petrophysics

To understand the CL's origin, petrophysical properties (in this case magnetic susceptibility) of relevant units should be examined with reference to magnetic potential. Magnetic susceptibility (K) is the ratio of the strength of induced magnetisation in a given rock to the strength of the magnetic field that causes it. K can be measured in situ or hand sample with a magnetic susceptibility meter.

There are 6 main rock units in the area; (1) Soldiers Cap Group, (2) Williams–Naraku Batholith, (3) Breccias and (4) laminated to massive calc-silicates of the Doherty Formation (5) Undifferentiated granites (6) Dolerite dykes and/or sills. 1-4 are most voluminous and are most spatially associated with the CL.

Petrophysical data obtained by the BMR, Xstrata, and by the author can be used as a basis for petrophysical subdivision. The BMR / Xstrata database covers the whole Mt Isa Inlier but has few readings for the areas adjacent to the Cloncurry Lineament. These data suggest a high K average of 8000 x 10^{-5} SI for Soldiers Cap rocks. The author's data, as shown in table 1 is concentrated along the CL and suggests that the Soldiers Cap psammite, quartzite and schist is generally devoid of magnetic material. Readings taken thus far give a K value of 0 x 10^{-5} SI. The Doherty Formation has more variable lithology and a wide range of K values from 0 to ~30,000 x 10^{-5} SI. Doherty Fm. rocks including breccias, calc-silicates, amphibolites and granites have high K values and average about 6000 x 10^{-5} overall. Readings taken in the Saxby Granite taken from several distinct plutons vary from

Magnetic Susceptibility (K)

Stratigraphic Unit	Rock type	Sample Count	Mag Sus (x 10^{-5} SI)	
			avg mag	max mag
Doherty	Amphibolite	12	13048	28647
Doherty	Breccia	18	5051	11817
Doherty	Calc-Silicate	3	3042	6517
Doherty	Granite	10	395	747
Saxby	Dolerite	4	2609	4000
Saxby	Granite	29	1780	3026
Soldiers Cap	Schist, Quartzite	14	0	0

Table 1: The magnetic susceptibility of units adjacent to the Cloncurry lineament a strongly contrasting. Soldiers Cap rocks are basically un-magnetic, the Saxby granite is moderately magnetic and the Doherty Formation which is generally highly magnetic.

about 100 to 4,000 x 10^{-5} SI and average ~2,000 x 10^{-5} SI. In general we see a marked magnetic contrast between the Soldiers Cap Group which has low K values and units 2-4 which have much higher K values.

3.2 Worms

Figures 2-7 show the Magnetic and Gravity worms at high and low levels of UC and the Cloncurry lineaments 3D surface in Magnetic and Gravity data. There are several similarities and differences between magnetic and gravity lineaments and these occur for a number of reasons, including data resolution and the physical property being measured. The worm data reveals important aspects of the nature of the Cloncurry lineament.

In the south of the study area the gravity and magnetic worms strike differently and follow different surface contacts. The magnetic lineament strikes ~160° and its surface trace follows the Doherty/ Soldiers Cap contact, then deviates through the Saxby granite to the north and bends eastward through the Cloncurry flexure (defined in Blenkinsop et al., 2005) to trace the eastern margin of the Corella formation in the north. In contrast the gravity lineament strikes ~150° in the south and initially traces the western margin of the Doherty Fm along the contact with the Squirrel hills granite. It then follows a similar trend to the magnetic lineament towards the Saxby granite before deviating westward and terminating in the Vicinity of the Cloncurry Flexure. The gravity Worm then re-appears north of the Cloncurry flexure and follows a similar trend to the magnetic lineament.

The near surface disparity between the two sorts of worms partly reflects the difference in the property being measured but is mostly due to data resolution. Because gravity data is so broadly sampled, the worms generated are less well constrained than the magnetic data which has 40m line spacing. Low UC magnetic worms trace the eastern side of the Soldiers Cap/Doherty contact because there is a large magnetic contrast between the Soldiers Cap Group and the Doherty calc-silicates. The gravity worm broadly traces the same contact however the near surface trace of the gravity worms does not trace the Soldiers Cap/Doherty contact very well. This is due to the sparse sampling of the gravity data which will detect edges at deeper levels than aeromagnetic data.

Many of the 1550-1500 Ma aged granites have a magnetic susceptibility similar to that of the Doherty Fm, which causes magnetic worms to deviate from the Doherty/ Soldiers Cap contact through the Saxby granite as illustrated in figure 8. This is seen particularly well in the low UC magnetic worms which trace parts of the Saxby, Wimberu and Squirrel Hills granites closely. The worms can also be used to infer the presence of intrusions at depth, eg, a possible intrusion at 10-20km depth, east of Ernest Henry (see figs 1 & 2). At shallow levels of UC the granite contacts are traced by the magnetic worms, but the high UC worm delineates neither granites nor the Doherty/Soldiers Cap contact, but lies in an intermediate position.

Another important feature highlighted in figure 8 is that two dominant trends are observed in low UC worms at about 150° and 050°. However the high UC Cloncurry worm corresponds to neither, striking about 160°. At several locations low UC worms appear to run along 150° trends and deflect sharply to a 050° trend. Published geology maps (e.g.,

Donchak et al, 1984) and unpublished mapping by the author suggest that 150° is the dominant structural grain in Eastern Succession rocks east of the Cloncurry Fault. The 050° trend corresponds to relatively late (D_3) dextral faulting that is observed widely throughout the inlier. This trend generally only shows up where it cuts the contact of two magnetically contrasting units.

Figure 2: Model area with high level (~20-30 km) UC worms. These worms correspond to the major magnetic anomalies in model area and delineate major lithological contacts eg, granite contacts, and the Soldiers Cap Fm/ Doherty Fm contact.

Figure 3: Model area with low level (~2-5 km) UC worms. These worms -highlight gravity anomalies caused by near surface features such as contacts, and doleritic dykes.

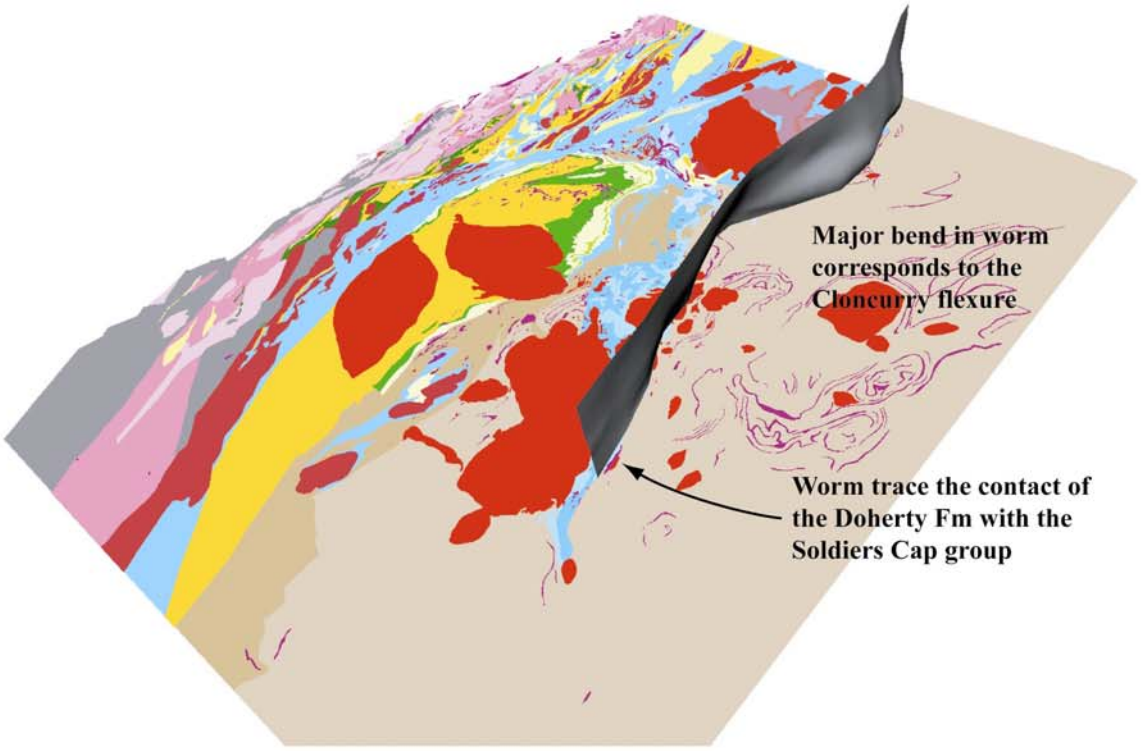

Figure 4: Model area in perspective view showing a surface that traces the Cloncurry magnetic worm from surface up through progressively higher levels of upward continuation to ~30 km

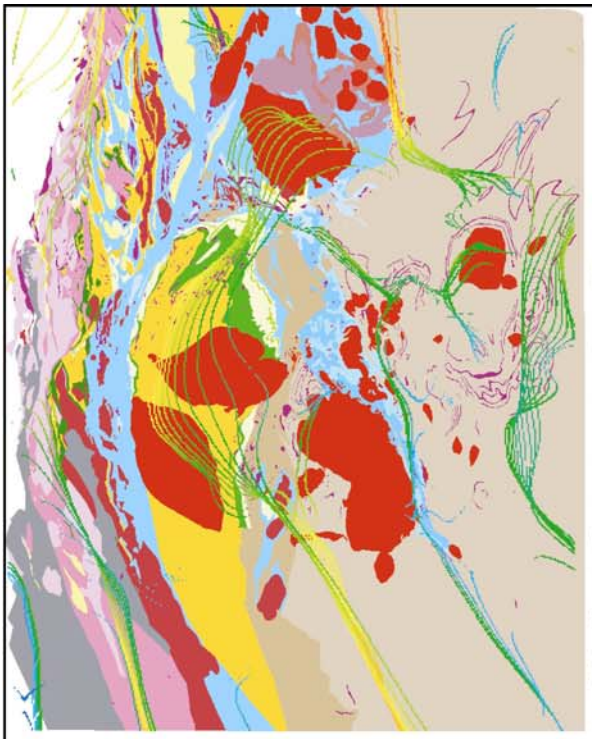

Figure 5: Model area with high level (~40-60 km) UC worms. These worms correspond to the major gravity anomalies in model area and are interpreted to be basement faults.

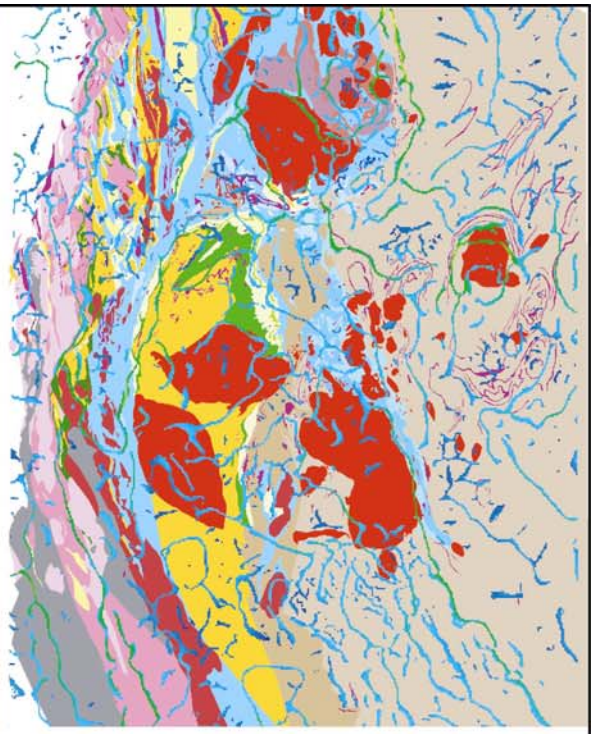

Figure 6: Model area with low level (~5-10 km) UC worms. These worms -highlight gravity anomalies caused by near surface features.

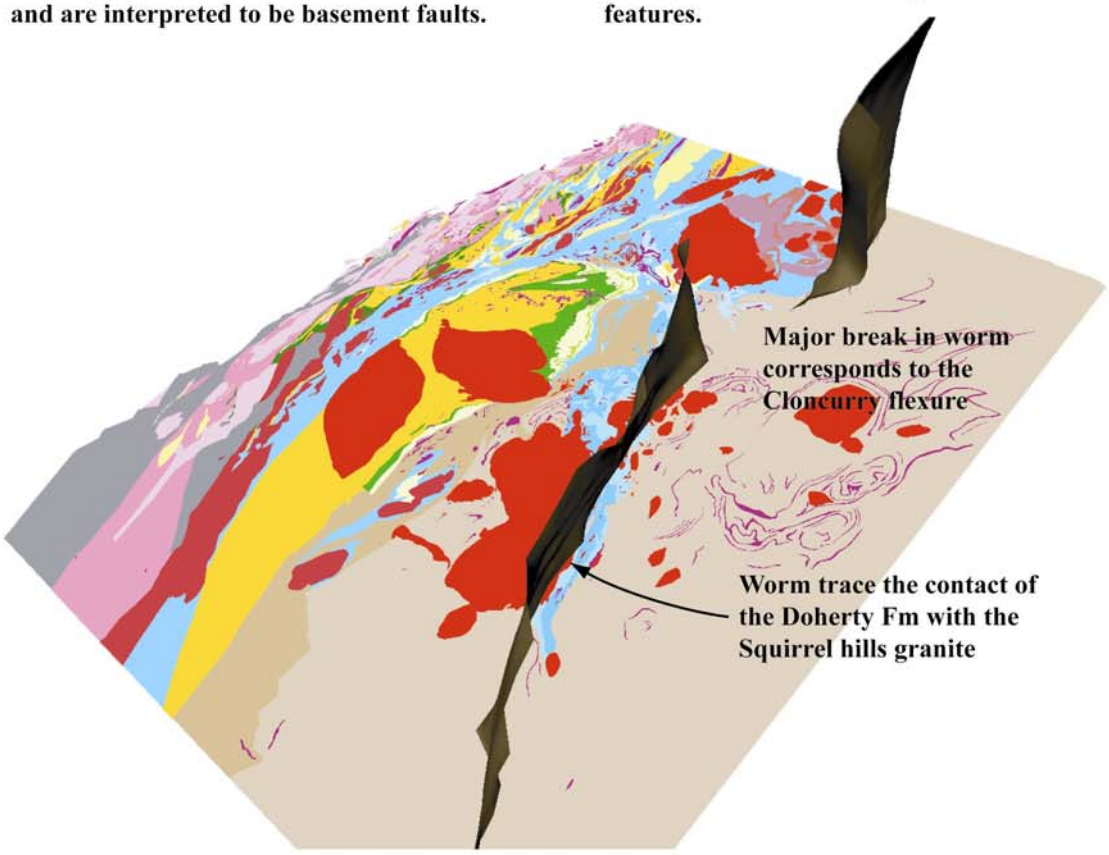

Figure 7: Model area in perspective view showing a surface that traces the Cloncurry gravity worm from surface up through progressively higher levels of upward continuation to ~60 km

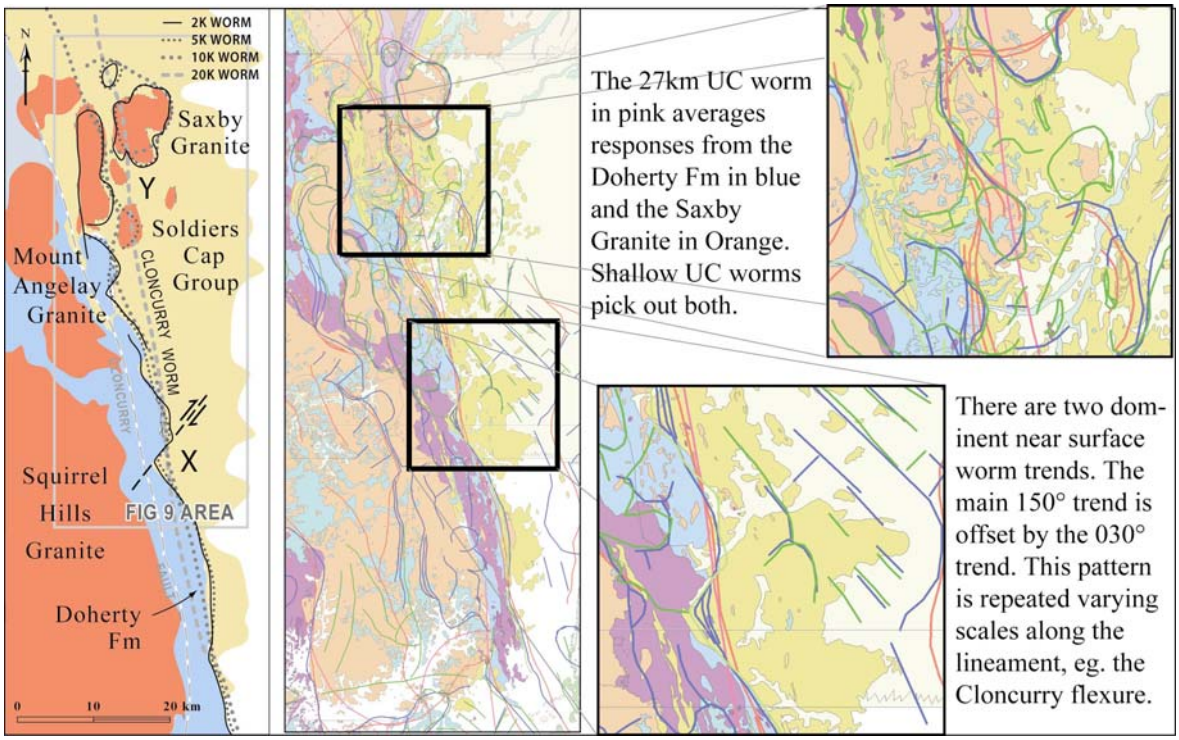

Figure 8: Shows the study area of this project with simplified geology, and worms at varying UC. The maps on the right hand side zoom in on areas of importance and illustrate two important observations of the Cloncurry worm; 1) that the high UC response may reflect a fusion of several lower UC worms 2) that a high UC may round a zig-zaging worm into a smooth continuous one.

It is interpreted that the 150° structural grain which parallels to the Doherty/Soldiers Cap contact has been cut by 050° trending dextral strike-slip faults. The resultant zig-zagging low UC worm is represented at high UC as a smooth line of best fit.

It is proposed here that there are many such dextral offsets along the Cloncurry lineament. Most are small in scale and some are overprinted by granites that appear to intrude at the intersection of the faults with the Doherty/Soldiers Cap contact which is proposed to be an earlier generation fault. The Cloncurry flexure may be a large scale example where the Cloncurry lineament appears to be dextrally offset by about 50km east of Cloncurry.

The interpreted dextral offsets have a good correlation with several mineral deposits in the study area, such as shown in figure 9, an auto-correlation plot. The correlation of Copper Gold mineral deposits with both, the Soldiers Cap/ Doherty (Corella) contact and ENE striking dextral faulting is a very important one. Mustard et al. (2005) identify these two structures as highly prospective to Copper Gold deposits in the Mount Isa Inlier. The two minor trends observed in the figure 9 correspond to the two major foliations observed in mylonites within Fullarton Gorge as shown in figure 10.

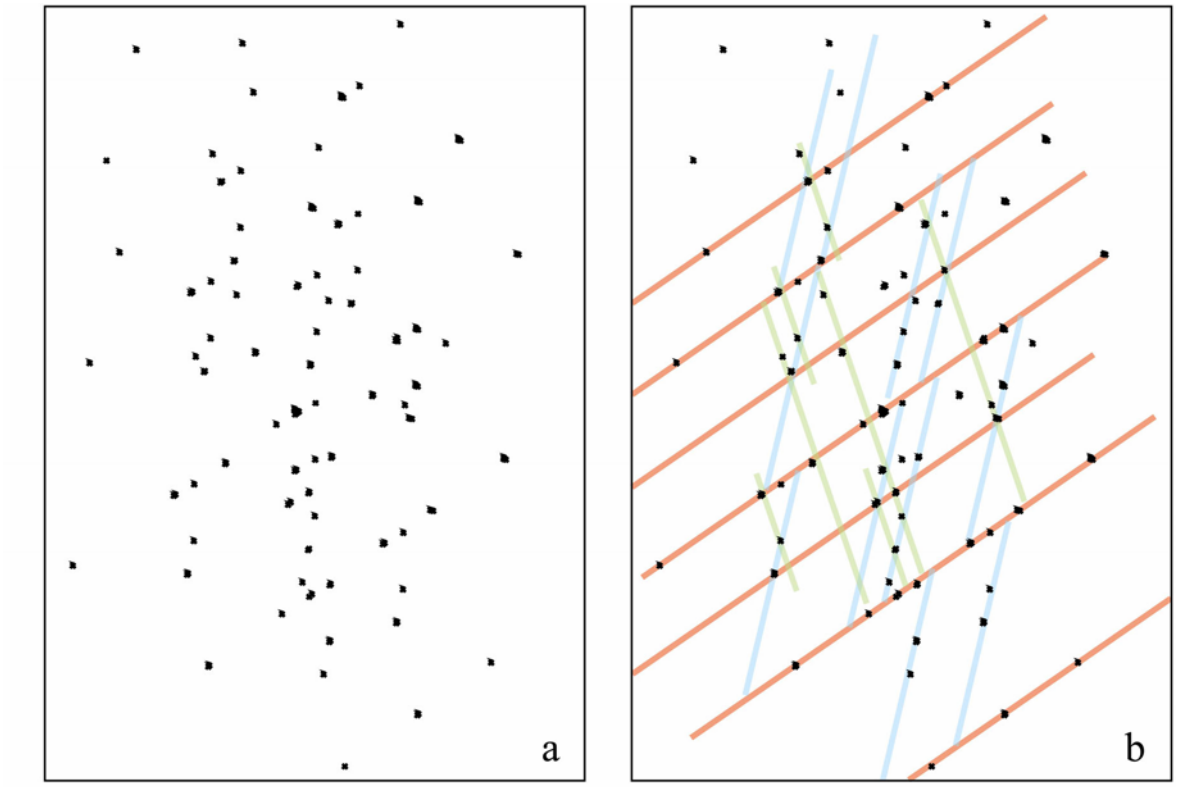

Fig. 9: a) An auto-correlation plot of major mineral deposits in the Mt Isa Eastern Succession shows b) a major NE-SW mineralisation trend and two minor mineralisation trends of 150° and 030°.

4. INTERPRETATION

The Cloncurry Lineament is defined by high UC worms, thus it highlights a distinct regional contrast in susceptibility. The high UC worms suggest a linear structure. However low UC worms suggest the near surface is more complicated and that the CL may correspond to several structures rather than one.

The major problem in defining the CL's origin is that it is difficult to trace high UC worms to the surface through successively lower levels of UC. At some locations lower UC worms lie approximately parallel to higher ones suggesting that a single structure is being traced. In other areas the high to low UC pattern is more varied indicating that the structure either becomes more complicated toward the surface or that other petrophysically contrasting bodies are present near the surface (e.g., plutons). In the case of the CL both scenarios appear to be true in different places. However this may be in part due to resolution loss with progressive levels of upward continuation that effectively smooths out the ground response.

By visualising worms projected over 1:100,000 scale geology, a basic understanding of petrophysical contrasts allows the inference that the Cloncurry Lineament is the contact between the Soldiers Cap Group and the Doherty Fm. The low UC worms trace the contact almost perfectly in the south of the study area, where there is minimal granitic intrusion near the contact. In the north however, this primary structure is complicated by several secondary sources including the Saxby Granite, post-Isan cross-cutting faults and dolerite dykes. The CL is thus a composite of several different structures and rock units that broadly correspond to the Doherty/ Soldiers Cap contact.

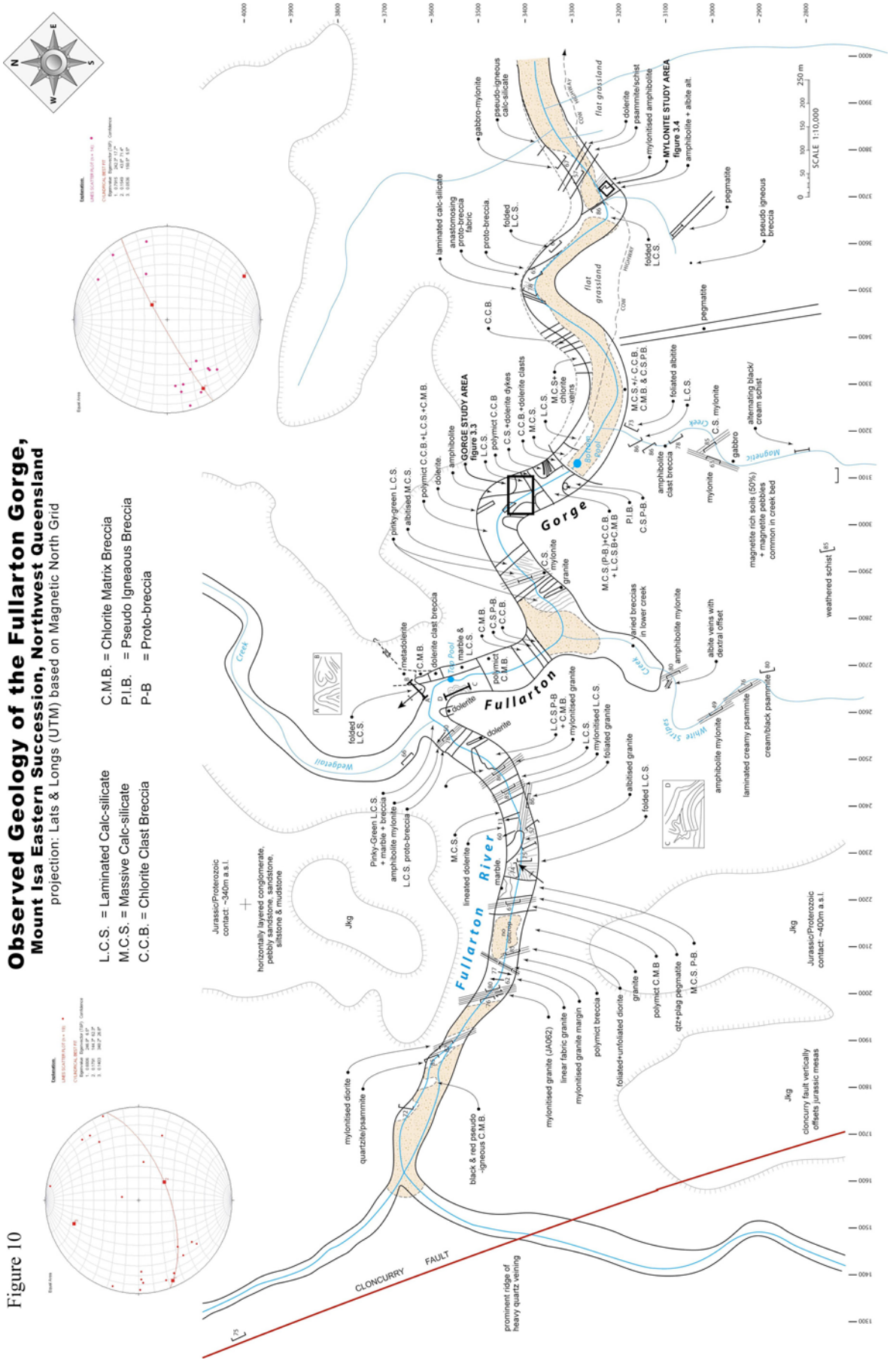
Observed Geology of the Fullarton Gorge,
Mount Isa Eastern Succession, Northwest Queensland
projection: Lats & Longs (UTM) based on Magnetic North Grid
L.C.S. = Laminated Calc-silicate
M.C.S. = Massive Calc-silicate
C.C.B. = Chlorite Clast Breccia
C.M.B. = Chlorite Matrix Breccia
P.I.B. = Pseudo Igneaous Breccia
P-B = Proto-breccia
GORGE STUDY AREA figure 3.3
MYLONITE STUDY AREA figure 3.4
Fullarton River
Fullarton Gorge
CLONCURRY FAULT
Jurassic/Proterozoic contact: ~340m a.s.l.
Jurassic/Proterozoic contact: ~400m a.s.l.
horizontally layered conglomerate, pebbly sandstone, sandstone, siltstone & mudstone
Jkg
SCALE 1:10,000

Figure 10

4. 1 Structural Hypothesis

A hypothetical tectonic history is proposed to explain the features observed in worm data over the Cloncurry Lineament. It aims to explain the composite nature of the CL: how one high UC worm represents several near surface worms and how a broad regional trend can be a function of several potentially un-related structural units. It ties proposed events into the current structural model of the Eastern Succession. While the history does make use of field observations it will primarily be used as a working model and will evolve as more structural data is generated. This structural hypothesis is illustrated in figure 11.

The history must include at least 4 separate structural events. Firstly extension lead to rift development (normal faulting) and deposition of cover sequence 3 units (eg Soldiers Cap Gp.) in the resulting graben and or half-graben. It is proposed that this primary structure is the main contact between the Doherty Fm and Soldiers Cap Gp. If the above is true then it is probable that the primary structure formed during CS_2 (~1800, D_{e1} or ~1750, D_{e2} of Loosveld, 1989) or at the onset of CS_3 (~1680, D_{e3} of Loosveld, 1989). The highly mylonitised nature of the Doherty Fm adjacent to the Cloncurry Lineament suggests that it was deformed extensively as the primary structure formed. Therefore it is likely that the structure formed after the deposition of the Doherty Fm, at the commencement of CS_3 to allow deposition of CS_3 sediments until about 1.6 Ga. The second event known as D_2 (Bell, 1983) is widely documented and occurs throughout the inlier at an age of 1590-1550 Ma. It produced macro- to micro-scale folds oriented just west of north that form the dominant structural grain of this area. The third event produced N-S trending folds, kinks and brecciation in response to E-W compression during D_3 (1550-1500). At this time Epidote-Actinolite-Albite-Calcite Breccias formed (Oliver, 1995) in the Doherty Fm adjacent to the margin of the CL as seen in Fullarton Gorge. Oliver (1995) proposes dextral faulting and brecciation during D_4 (1500-1100 Ma). Such dextral faulting appears to offset the primary normal fault along NE-SW planes creating a boudinage outcrop pattern along the Doherty/Soldiers Cap Contact in the south of study area. Such late faulting is not seen to cut breccias in the Fullarton Gorge area (Figure 10), suggesting that dextral faulting may have started earlier than as proposed by Oliver (1995). Such faulting is one of a number of deformation mechanisms operating during E-W shortening (D_2 -D_3). E-W compression may have initially generated large-scale folding (D_2) but as the already tightly folded crust began to lock-up, kinking then brecciation occurred as dextral faults propagated thus allowing the competent Corella Fm to be extended vertically, then N-S. The higher metamorphic grade east of the Cloncurry Fault (Foster, D.R.W. and Rubenach M.J., 2005) suggests that this episode also caused positive inversion and reverse movement along the primary structure. The dextral faulting of the CL formed crustal weaknesses at the fault intersections, which made paths for emplacement of plutons of the Williams-Naraku Batholith, in particular the Saxby Granite and Mount Angelay Granite, which intruded from late D_2 to post D_3. The Maramungee Granite has an earlier emplacement age of ~1545 Ma indicating that its emplacement was not influenced by dextral faulting. It crops out directly adjacent to the CL indicating that it may simply have risen along the primary structure and crystallised in the early stages of E-W shortening.

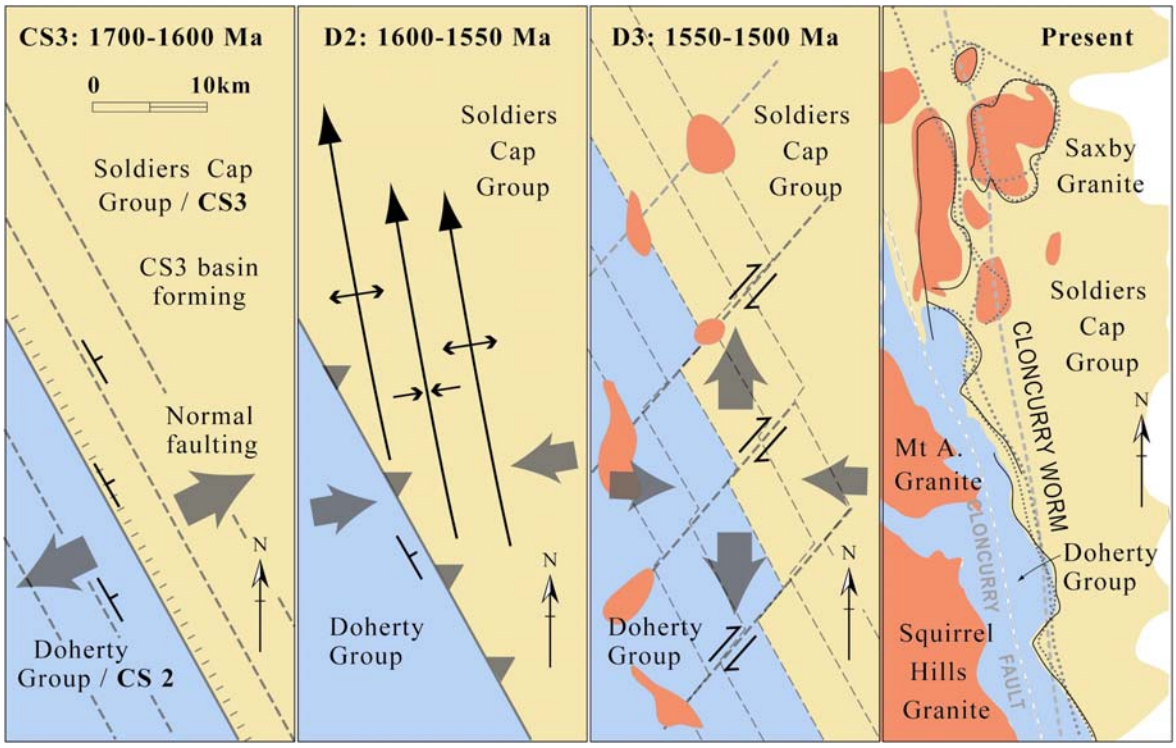

Figure 11: A hypothetical history of the Doherty/Soldiers Cap contact in the South-eastern Mt Isa Inlier that illustrates a potential scenario to explain structures observed along the Cloncurry lineament.

5. CONCLUSIONS

The previously unrecognised Cloncurry Lineament is an important structure in the context of the structural evolution of the Eastern Succession and the whole Mount Isa Inlier. Worm data suggest that it is continuous to at least 20km depth. It is broadly associated with a major lithological contact, separating cover sequence units CS_2 and CS_3. The CL traces the Soldiers Cap (CS_3) / Doherty (Corella) Fm (CS_2) boundary very closely in the south of the field area, suggesting that the lineament is primarily caused by this contact. However, the CL is also generated by other structures. The main elements of this composite feature are: 1) The Soldiers Cap/Corella boundary, 2) NE-SW dextral faults 3) Intermediate plutons of the Saxby Granite and Maramungee Granite.

The CL must be a major crustal boundary given its depth of penetration and its location between two distinct Cover Sequence groups. In general the worms indicate a structure that dips steeply to the east, suggesting it may have originated as a normal fault. Both CS_2 and CS_3 deposition were initiated by rifting/extension so this structure may have formed early in an extensional phase during the deposition of CS_3. The E-W extension generated a depositional basin that was subsequently filled with Soldiers Cap sediments.

The outcrop pattern of the Soldiers Cap / Corella Fm boundary is jagged with apparent dextral offsets striking NE-SW at several locations in the study area. This indicates that that the initial fault structure has been affected by a later series of faults which have caused N-S stretching, effectively boudinaging the Corella Fm. This offset occurred in response to E-W compression during D3.

The Saxby, Marramungee and Blackeye granites that sit along the contact also complicate the magnetic response. Their intrusion is syn-post D3 and it is possible that they intruded up points of weakness at fault intersections. 150° / 050° fault intersections generated along the Cloncurry lineament may have acted as an important corridor for pluton emplacement in the Eastern Succession.

Previous accounts of the Cloncurry Fault and the Soldiers Cap/Corella contact have proposed a moderate easterly dipping thrust (Blake and Stewart, 1992; McCready et al., 1998; Drummond et al., 1998; the Cloncurry Overthrust of Loosveld 1989). It is proposed that such movement fits into the tectonic history proposed above in a reactivation or positive inversion phase, following the initial development of some structures during extension.

Other events may have influenced the worm expression of the CL. The most important questions relate to the structural nature of the original ~1.7 Ga structure and proposed NE-SW dextral faulting. Further field work on with emphasis on mylonites, breccias and intrusive rocks will generate more structural data which will be used to test the above and develop variant hypotheses.

Acknowledgments

Tom Blenkinsop, Mike Rubenach, Barry Murphy, Pmd*CRC, Xstrata, Mark Edmiston, Sayab Mohammad, Kris Butera, Michelle Stark, Roger Mustard, Cameron Huddleston-Holmes, Janine Josey.

6. REFERENCES

Archibald, N., P. Gow, et al. (1999). "Multiscale edge analysis of potential field data." Exploration Geophysics (Melbourne) 30(1-2): 38-44.

Bell, T. H. (1983). "Thrusting and duplex formation at Mount Isa, Queensland, Australia." Nature 304: 493-497.

Betts, P. (1998). Is the Paleoproterozoic Mount Isa Basin a result of asymmetric extension? 14th Australian geological convention. Anonymous, Geological Society of Australia. 49: 30.

Betts, P. (2000). "Asymmetric extension of the lithosphere and its influence on Palaeoproterozoic Pb-Zn deposits of the Western fold belt, Mount Isa Terrane." Journal of the Virtual Explorer 1.

Blake, D. H. (1980). "The early geological history of the Proterozoic Mount Isa Inlier, northwestern Queensland; an alternative interpretation." BMR Journal of Australian Geology and Geophysics 5(4): 243-256.

Blake, D. H. (1987). Geology of the Mount Isa inlier and environs, Queensland and Northern Territory. Canberra, A.C.T., Australian Geological Survey Organization.

Blake, D. and A. Stewart (1988). "Block and possible terrane boundaries in the Mount Isa Inlier." BMR Research Newsletter 9: 2-3.

Blenkinsop, T. G., Huddlestone-Holmes, C., Foster, D., Mark , G., Austin, J., Edmiston, M., Lepong, P., Ford, A., Murphy, F. ,Stark, M. 2005. 3D model and crustal Architecture of the Mt Isa Eastern Sucession. I2+3 Final Report, pmdCRC

Donchak, P. J. T., D. H. Blake, et al. (1984). Kuridala region, 1:100,000 Geology, Queensland. Canberra, A.C.T., Australian Government Publishing Service.

Drummond, B. J., B. R. Goleby, et al. (1998). "Crustal-scale structures in the Proterozoic Mount Isa Inlier of North Australia; their seismic response and influence on mineralisation." Tectonophysics 288: 43-56.

Etheridge, M.A., Rutland, R.W.R., and Wyborn, L.A., 1987, Orogenesis and tectonic process in the Early to Middle Proterozoic of northern Australia, *in* Kroner, A., ed. Proterozoic Lithosphere Evolution, American Geophysical Union Geodynamic series 1. p. 131-147.

Foster, D.R.W. and Rubenach M.J., 2005. Isograd pattern and regional low-pressure, high-temperature metamorphism of pelitic, mafic and calc-silicate rocks along an east-west section through the Mount Isa Inlier. Australian Journal of Earth Sciences. In press.

Goleby, B. R., T. MacCready, et al. (1998). The Mount Isa geodynamic transect - crustal implications. Structure and Evolution of the Australian Continent. J. Braun, J. C. Dooley, B. R. Goleby, R. D. van der Hilst and C. T. Klootwijk. Washington, American Geophysical Union. 26: 109-118.

Holcombe, R. J., P. J. Pearson, et al. (1987). The Mary Kathleen fold belt, Northwest Queensland; geometry and timing of deformation. International conference on Deformation of crustal rocks. Anonymous, Geological Society of Australia. 19: 35-36.

Holden, D. J., Archibald, N. J., et al. (2000) "Inferring geological structures using wavelet-based multiscale edge analysis and forward models." Exploration beyond 2000; conference handbook
Preview, Australian Society of Exploration Geophysicists.

Hornby, P., F. Boschetti, et al. (1999). "Analysis of potential field data in the wavelet domain." Geophysical Journal International 137(1): 175-196.

Loosveld, R. J. H. (1989). "The intra-cratonic evolution of the central eastern Mount Isa Inlier, Northwest Queensland, Australia." Precambrian Research 44(3-4): 243-276.

MacCready, T., B. R. Goleby, et al. (1998). "A framework of overprinting orogens based on interpretation of the Mount Isa deep seismic transect." Metallogeny of the McArthur River-Mount Isa-Cloncurry minerals province 93(8): 1422-1434.

Mares, V. M. (1998). "Structural development of the Soldiers Cap Group in the Eastern Fold Belt of the Mt Isa Inlier; a succession of horizontal and vertical deformation events and large-scale shearing." Geological framework and mineralisation in the Mt Isa Eastern Succession, Northwest Queensland 45(3): 373-387.

Mark, G. (2001). "Nd isotope and petrogenetic constraints for the origin of the Mount Angelay igneous complex; implications for the origin of intrusions in the Cloncurry District, NE Australia." Precambrian Research 105(1): 17-35.

Mustard, R., Blenkinsop, T., Foster, D., Mark, G., McKeagney, C., Huddlestone-Holmes, C., Partington, G., and Higham, M. 2005. Critical ingredients in Cu-Au ± iron oxide deposits, NW Queensland: an evaluation of our current understanding using GIS spatial data modelling. I2+3 Final Report, pmdCRC.

O'Dea, M. G. and G. S. Lister (1995). "The role of ductility contrast and basement architecture in the structural evolution of the Crystal Creek Block, Mount Isa Inlier, NW Queensland, Australia." Journal of Structural Geology 17(7): 949-96

Oliver, N. H. S. (1995). Hydrothermal history of the Mary Kathleen fold belt, Mt Isa Block, Queensland. Mid- to lower-crustal metamorphism and fluid-rock interaction. N. H. S. Oliver, I. Cartwright and M. J. Rubenach, Blackwell. 42: 267-279.

Oliver, N. H. S., G. M. L. J. Mark, et al. (1998). Mineralisation, alteration and magmatism in the Eastern fold belt, Mount Isa Block, Australia; geological review and field guide, Geological Society of Australia Specialist Group in Economic Geology.

Page, R. W. and T. H. Bell (1986). "Isotopic and structural responses of granite to successive deformation and metamorphism." Journal of Geology 94(3): 365-379.

Page, R. W. and S. S. Sun (1998). "Aspects of geochronology and crustal evolution in the Eastern Fold Belt, Mt Isa Inlier." Geological framework and mineralisation in the Mt Isa Eastern Succession, Northwest Queensland 45(3): 343-361.

Rubenach, M. J. (1993). Petrogenesis of a variety of metasomatic lithologies west of Mount Isa. Mid- to lower-crustal metamorphism and fluids conference, Mount Isa. Anonymous, Geological Society of Australia. 35: 60.

Rubenach, M. J. and A. J. Barker (1998). "Metamorphic and metasomatic evolution of the Snake Creek Anticline, Eastern Succession, Mt Isa Inlier." Geological framework and mineralisation in the Mt Isa Eastern Succession, Northwest Queensland 45(3): 363-372.

Rubenach, M. J. and K. A. Lewthwaite (2002). Metasomatic albitites and related biotite-rich schists from a low-pressure polymetamorphic terrane, Snake Creek Anticline, Mount Isa Inlier, north-eastern Australia; microstructures and P-T-d paths. Ron Vernon symposium; 15th Australian geological convention. G. L. Clarke and M. Brown, Blackwell. 20: 191-202.

Section 4

Fluids & Metals: Drivers, Sources, Pathways, Sinks

Detailed Reports

Critical ingredients in Cu-Au ± iron oxide deposits, NW Queensland: An evaluation of our current understanding using GIS spatial data modelling

Roger Mustard[1]*, Tom Blenkinsop[1], Damien Foster[1], Geordie Mark[2], Cathy McKeagney[1], Cameron Huddelstone-Holmes[1], Greg Partington[3] and Martin Higham[4].

1. predictive mineral discovery Cooperative Research Centre, Economic Geology Research Unit, School of Earth Sciences, James Cook University, Townsville, Q4811, Australia
2. School of Geosciences, Monash University, Clayton Campus, Melbourne, Victoria, 3168
3. Kenex Knowledge Systems Ltd, Ballinger Gdns, 39B Oroua St, Wellington, New Zealand
4. Avantra Geosystems, 11 Milroy St, Brighton East, Vic 3187

ABSTRACT

Current understanding of the critical processes involved in the formation of Cu-Au± iron oxide-bearing Cu-Au deposits in the Mt Isa Inlier, NW Queensland is based on more than 20 years of research on these Proterozoic hydrothermal systems and their environs. A current popular model for the formation of IOCG deposits in the Mt Isa Inlier involves magmatic fluids derived from the post metamorphic (1550-1500 Ma) Williams-Naraku batholith granites, either mixing with a second external fluid source or reacting with favourable wallrocks to form Fe- (commonly magnetite-) rich alteration zones that contain vein stockwork, breccia, dissemination or replacement style mineralization. However, recent dating studies at Osborne have highlighted a potential syn-peak metamorphic timing to mineralization (based on 1595 Ma Re-Os age dates on molybdenite and a 1595 ± 6 Ma U-Pb age date on hydrothermal titanite), with no apparent proximal major intrusion. There is also a potential link between mineralization and widespread mafic intrusive activity, which spans the entire range of known mineralization ages. In other terrains where spatially and temporally related intrusions are not present, alternative models in which the fluids are entirely intra-basinal and amagmatic in origin are favoured.

In order to investigate the considerable range of potential geological controls on IOCG mineralization, a GIS was developed allowing us to evaluate our current understanding of critical ingredients, statistically rank the relative importance of the parameters, and gain new insights into potential controls currently unrecognised or considered less important. A 'weights of evidence' approach was adopted for the processing due to the data rich nature of the region, and the degree of uncertainty about the role played by particular ingredients such as mafic and felsic intrusives.

Using Contrast (a measure of association of training sites with the predictor features or patterns), the patterns were ranked from best to worst predictor. Rockchip geochemistry including copper (>249 ppm) and gold (>0.11 ppm) were the strongest predictors, returning C values of 2.50 and 2.38 respectively. Proximity to the Corella Formation

contacts is the next highest predictor of known Cu-Au occurrences with a C value of 1.87, and is the highest ranking geological layer. Aero-magnetic highs are a strong predictor of known Cu-Au occurrences with a C value of 1.82. N-S and ENE orientated faults are the next best predictor of Cu-Au occurrences with a C value of 1.45. Proximity to mafic intrusions, lithology, gravity and fault bends associated with N-S and ENE orientated faults are all moderately strong predictors of know Cu-Au occurrences, with C values greater than 1, except metamorphic grade. Radiometrics (U/Th ratio) is a weak predictor of know Cu-Au occurrences, with C value of 0.83. Distance to the Williams and Naraku intrusives (4km buffer) had the lowest C value of 0.63.

New geological or exploration models for the formation of IOCG deposits in the Mt Isa Inlier, must incorporate the critical ingredients highlighted in this study: (1) the significant role that the Corella Formation - Soldiers Cap contact played, possibly by localizing faulting, fluid flow, and juxtaposing lithologies of contrasting rheology, geochemical character, and oxidation state (2) the district scale control that reactivated D2 age? NS and ENE orientated basement structures have on localizing fluids responsible for the Cu-Au mineralisation, (3) the potential role that mafic intrusives play in providing rheological contrast and/or a potential source of sulphur causing Cu-Au deposition, (4) the presence of major basement crustal structures delineated by abrupt gravity gradients, (5) the presence of significant mafic intrusions of dioritic? composition in the underlying crust/mantle reflecting gravity highs, (6) if magmatic fluids are considered to the ultimate source of metals, they have traveled significant distances (commonly >4km) from their source prior to deposition.

12-layer and 9-layer posterior probability maps for predicting the distribution of Cu-Au ±iron oxide deposits in the Mount Isa Inlier were produced. The 9-layer posterior probability map deliberately excluded data that was restricted to areas of surface outcrop (Cu and Au rockchip geochemistry and radiometrics) with the aim of targeting through cover. The two maps generated similar patterns, with 12-layer posterior probability map highlighting specific areas within broader anomalous regions outlined by the 9-layer posterior probability map. Verifying the posterior probability map against the known gold deposits, it can been seen that the Ernest Henry deposit (the largest single deposit) produced by far the largest anomalous region within the area and the second most richly endowed region (the Selwyn Line) defined the single largest anomalous linear trend extending for 40km, of which the southern most 10km was located under cover.

The 9 and 12-layer posterior probability maps were evaluated by comparing with the expert driven targeting for Cu-Au deposits completed by the Queensland Department of Mines and Energy as part of the North West Queensland Mineral Province Report. The weights of evidence model delineate permissive areas comparable to the expert delineation, but much more restricted in area. Additional discrete areas of high potential were highlighted that do not coincide with expert targets, are under cover and are likely to have not been subject to exploration. The weight of evidence model has additional characteristics that it is well defined, reproducible, objective, and provides a quantitative measure of confidence.

Keywords: weights of evidence, Cu-Au ± iron-oxide deposits, Mount Isa Inlier.

1. INTRODUCTION

The Mount Isa Inlier is a world class minerals district, richly endowed with major sediment-hosted Pb-Zn deposits (Mount Isa, Hilton, George Fisher, Century, Cannington) and the Mount Isa Cu deposit. With the discovery of deposits such as Ernest Henry, Starra (formerly Selwyn), Osborne, Mt Elliot, and Eloise, the Mt Isa Inlier and in particular the Eastern Fold Belt emerged as a major province for Fe-Oxide Cu-Au deposits (Pollard, 1998; Williams, 1998). The Cu-Au ± iron-oxide deposits of the Mt Isa Inlier have yielded more than 900,000 t copper, 27 t gold, and 28 t silver from the deposits exploited to date, with 3,300,000 t copper, 167 t gold in global resources and reserves. Readers are referred to Williams and Pollard (2001) for concise descriptions of individual deposit geology.

The large study area (>80,000km^2) was selected to assess the distribution of all known Cu-Au deposits and significant occurrences within the Mt Isa Inlier, including the Eastern Fold Belt, the Kalkadoon-Leichardt Fold Belt and the Western Fold Belt. Fifteen data layers were selected for analysis that may have had a significant influence on the Proterozoic 1550-1500Ma Fe-oxide Cu-Au deposits. The fifteen perameters are: (1) Lithostratigraphy, (2) Corella Formation-Soldiers Cap Group contact, (3) mafic intrusives, (4) Williams-Naraku batholiths, (5) Metamorphic zones, (6) Faults, (7) Fault bends, (8) Magnetics, (9) Gravity, (10) Radiometrics, (11-15) Rockchip Geochemistry (Cu, Au, Co, Ni and As).

The main aims of the study were to: (1) Determine the critical processes/ ingredients potentially involved in the localisation of Cu-Au mineralisation within the Mt Isa Inlier by studying the spatial association of fifteen parameters to the location of Cu-Au ±iron oxide deposits; (2) Rank the relative importance of the 15 data layers based on contrast values, to gain new insights into potential controls currently unrecognised or considered less important; (3) Discuss the results in relation to a geological/ exploration model, with the aim of improving it; (4) Provide exploration companies a set of ranked perameters that they can use to help in ranking targets; (5) Generate a set of posterior probability maps for the Mt Isa Inlier including a 9-layer model (that sees through cover) and a 12-layer model that includes surface rock chip geochemistry (Cu and Au) and radiometrics; (6) Compare the results of the data driven posterior probability maps with an expert driven study for the same area.

2. STUDY AREA – MOUNT ISA INLIER

The study area occupies 82,733 km^2 and is located between 325,000mE to 525,000mE and 7,955,000mN to 7,535,000mN. It extends from 17km west of Mount Isa township to 75km east of Cloncurry, and from 23km south of Osborne to 110km north of Mount Oxide. The selected area encompasses three 1:250,000 sheets areas including Dobbyn (SE54-14), Cloncurry (SE54-2) and Duchess (SE54-6), as well as portions of the surrounding sheets. The area includes all of the exposed Eastern Fold Belt (12,455 km^2, 15%), Wonga Fold Belt (3,924 km^2, 5%), Kalkadoon-Leichardt Fold Belt (6,879 km^2, 8%) and eastern parts of the Western Fold Belt (12,410 km^2, 15%, Fig. 1). 47,065 km^2 or 57 % of the area comprises post-mineralisation cover belonging to Phanerozoic basins. A large portion of this (16,162 km^2) or 20 % of the study area where it is <100m deep, and much of the potential of the region is located.

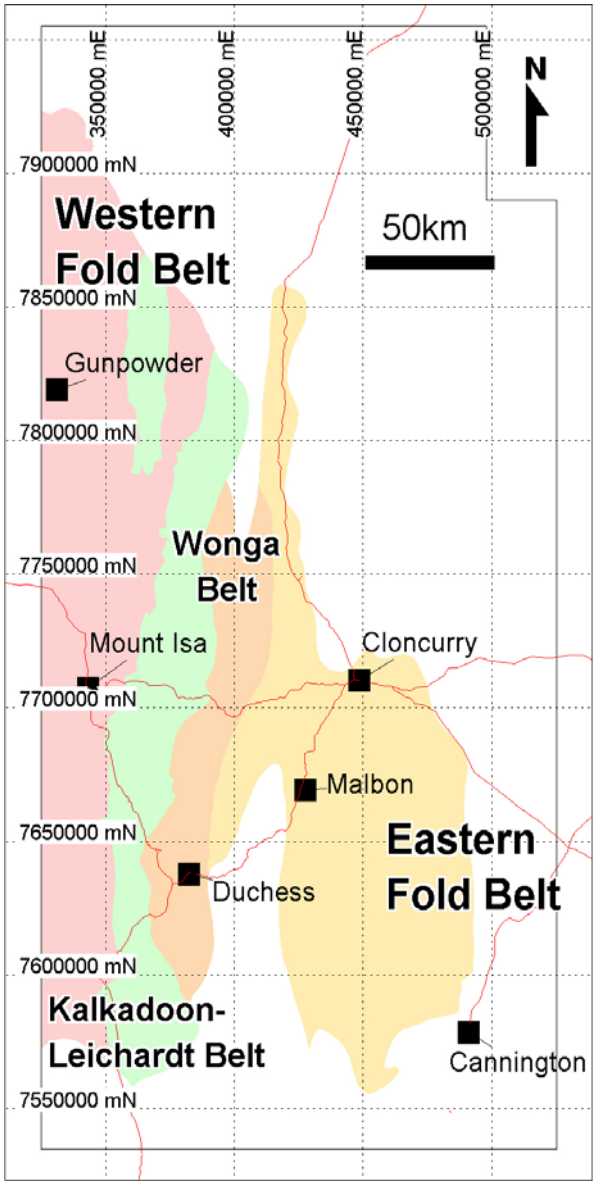

Fig. 1. Location diagram displaying the limits of the Mount Isa study area, as well as foldbelts and area of post-mineralisation cover (white). Projection: AMG Zone 54 (AGD66).

3. CU-AU ± IRON-OXIDE DEPOSIT GEOLOGICAL MODEL

Iron oxide Cu-Au deposits worldwide display great variability (Hitzmann, 2000; Skirrow and Walshe, 2002) and occurrences in the Mount Isa Inlier are no exception. The diverse range of Cu-Au deposit styles found in the Mount Isa Inlier (Fig. 2) includes magnetite-rich breccias (Ernest Henry), ironstone hosted (Osborne-magnetite rich, Starra-hematite rich), skarn hosted (Mt Elliot, SWAN, Trekelano), and carbonaceous metasediment hosted (Mt Dore, Victoria, Stuart). The key variable that gives rise to differences in Cu-Au ± iron oxide deposits within the Mount Isa Inlier may be the local host rock types which are very diverse. These can produce a spectrum of structural styles (vein, breccia, replacement), Fe oxide association (magnetite, hematite), alteration and Fe sulphides ore mineral assemblage (pyrite, pyrrhotite or both), minor element association (±Co ±Ni ±Ag ±F ±As ±Mo ±Ba ±REE ±U), and Cu:Au:Ag ratios.

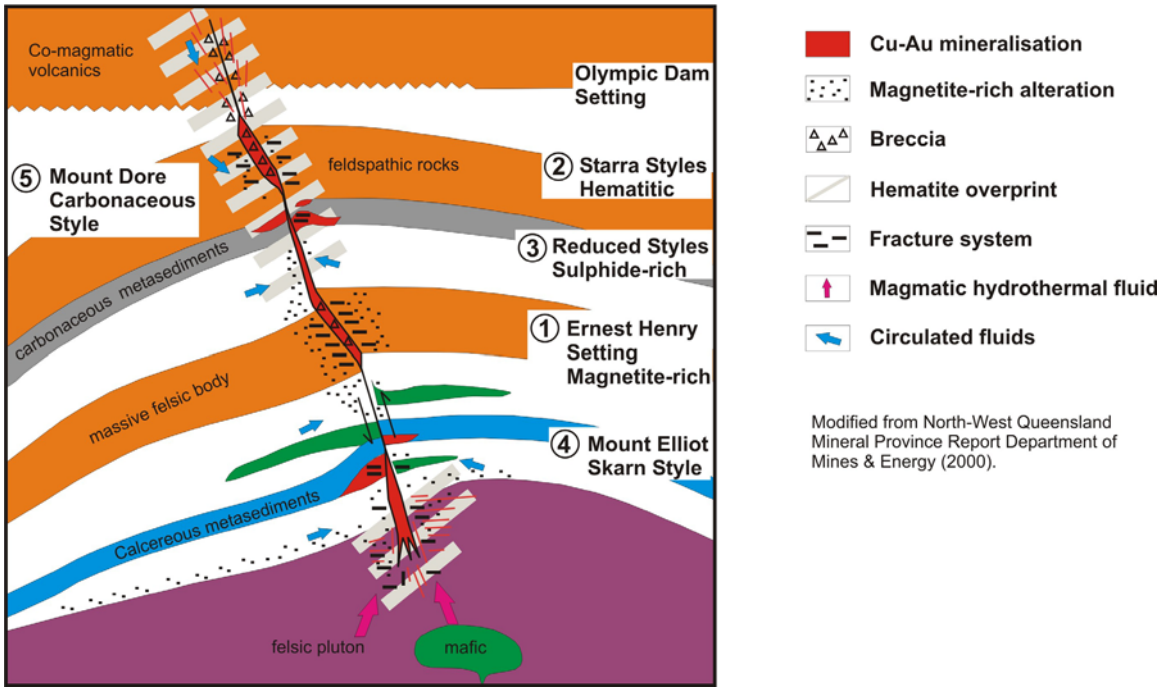

Fig. 2. The diverse range of Cu-Au ± Fe oxide deposit styles found in the Mount Isa Inlier. (Modified from the Northwest Queensland Mineral Deposit Report).

A number of shared characteristics have been considered as common to the Cu-Au ± iron-oxide deposits in the Mount Isa Inlier, including: (1) regional temporal association with intrusions of the 1550-1500 Ma Williams-Naraku batholiths, but lack of a local intimate spatial relationship such as porphyry and skarn deposits (Budd et al., 2001;Williams et al., 2004); (2) alteration sequence from early sodic-calcic, to Fe and K-rich alteration, to muscovite (Williams et al., 1993; Williams, 1994); (3) Brines (200-500°C) directly associated with ore deposition; and (4) Strong structural controls, localised by a range of brittle-ductile and brittle shear zones (Laing, 1998). These similar characteristics has been interpreted to imply a common genesis for many of the Cu-Au ± iron-oxide deposits.
Intense exploration over the last decade for iron-oxide-associated Cu-Au deposits has led to great interest in the genesis of this ore deposit class. Numerous genetic models have been proposed. Specific published ore-genesis models for Au-Cu-iron-oxide deposits in the Mt Isa Inlier range from a single-stage hydrothermal system with one evolving fluid source, to complex multiple-stage hydrothermal systems involving two or more fluid sources (Mark et al., 2004).

A review of available literature (prior to this spatial analysis study) suggests a favoured deposit model for the genesis of Cu-Au-iron-oxide deposits in the Mount Isa Inlier that involves:

- Metal-rich, sulfur-poor, moderately oxidised, aqueocarbonic brines were derived from oxidised alkaline-intermediate intrusions of the (1550-1490 Ma) Williams-Naraku batholith, which were emplaced at mid-crustal levels (~200 MPa; 8-15km depth).
- As the ore fluids moved away from their source they were focussed along ductile-brittle shear zones, interacting to various degrees a range of different rock types partly modifiying their character.
- Initial fluid-wallrock interaction (between degassed magmatic fluids and country rocks) produced early, barren, regionally extensive Na-Ca alteration. Subsequent

areally restricted K-Fe rich alteration ± later rare carbonate-muscovite was intimately associated with Cu-Au mineralisation. OR There is a general sequence from (1) sodic alteration to (2) potassic alteration to (3) sericitic alteration and silicification with time.

- Within an overall compressional tectonic setting, ore bodies were formed locally at favourable trap sites where either chemical reaction and / or a rapid change in physical conditions (↓P, ↓T, ↓fO_2, fS?pH?) occurred.
- Cu-Au ore precipitation involved one or a combination of depositional mechanisms including i) cooling; ii) a number of wall-rock reactions (reduction by magnetite or carbonaceous matter, sulphidation of Fe silicates, sulphur-rich rock (mafic intrusives); iii) unmixing of a magmatic fluid into low salinity CO_2 bearing aqueous fluid and brines; and iv) fluid mixing between magmatic and one or more fluids of a different origin (mantle /metamorphic /basinal evaporate /meteoric).

It should be noted that the deposits discussed in the Mt Isa Inlier are considered to represent deep seated Cu-Au systems with a depth of formation around ~200 MPa or 8-15km depth. Many workers believe that this will greatly restrict fluid convection, resulting in single pass systems (Hitzman, 2000). In contrast, other terrains possess systems developed at shallower levels ranging from 4-6km to near surface. As a result models involving hybrid, or dominantly amagmatic fluid sources are realistic.

Yet researchers do not agree on major issues such as (1) the relationships between early sodic-calcic alteration, later potassic alteration and Cu-Au mineralisation, (2) sources of fluid responsible for ironstone formation, (3) the role of magmas versus other sources of ore metals and fluids, (4) the role of mafic intrusions as a source of ore metals and fluids (Mark et al., 2004).

4. CU-AU ± IRON-OXIDE DEPOSITS IN THE MT ISA INLIER (TRAINING DATA SET)

A total of 567 Cu-Au occurrences are recorded in the Mineral Occurrence 2002 database within the study area. A subset of 181 occurrences were selected as the training data set based on the presence of both commodities (Cu and Au), and either recorded historical production or the existence of a cited geological resource (Fig. 3, Appendix 1). Some of the main occurrences include Ernest Henry (167 Mt @ 1.1% Cu; 0.54 g/t Au), Eloise (3.2 Mt @5.8% Cu; 1.5g/t Au; 19g.t Ag), Osborne (11.2 Mt @ 3.51% Cu; 1.49 g/t Au), Mt Elliot (3.3 Mt @ 3.6% Cu; 1.8 g/t Au), Starra (6.9 Mt @ 1.65% Cu; 4.8 g/t Au) and Mount Dore (26 Mt @ 1.1% Cu; 5.5 g/t Au; Williams and Skirrow, 2000).

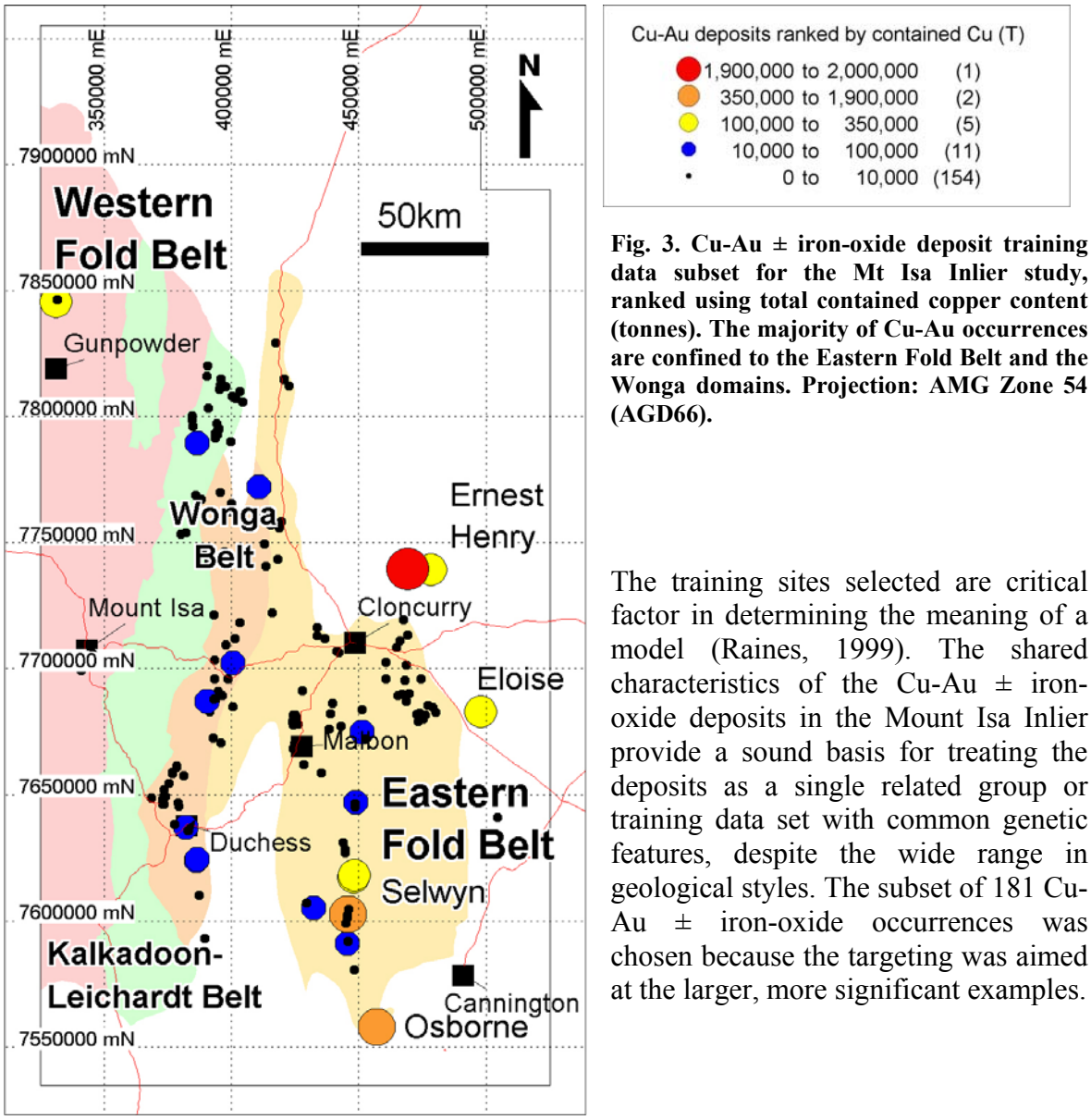

Fig. 3. Cu-Au ± iron-oxide deposit training data subset for the Mt Isa Inlier study, ranked using total contained copper content (tonnes). The majority of Cu-Au occurrences are confined to the Eastern Fold Belt and the Wonga domains. Projection: AMG Zone 54 (AGD66).

The training sites selected are critical factor in determining the meaning of a model (Raines, 1999). The shared characteristics of the Cu-Au ± iron-oxide deposits in the Mount Isa Inlier provide a sound basis for treating the deposits as a single related group or training data set with common genetic features, despite the wide range in geological styles. The subset of 181 Cu-Au ± iron-oxide occurrences was chosen because the targeting was aimed at the larger, more significant examples.

5. SPATIAL DATA ANALYSIS

In order to investigate the considerable range of potential geological controls on IOCG mineralization, a spatial data analysis was undertaken, aimed at evaluating the relative importance of a range of spatial variables including: host rock type, proximity to particular stratigraphic contacts, proximity to mafic intrusives or the Williams-Naraku batholiths, metamorphism, structure, geophysics (including aero-magnetics and gravity), radiometrics, and rockchip geochemistry (Cu, Au, Co, Ni and As). A data driven approach was taken in view of the considerable uncertainty in genetic models for IOCG deposits. Spatial correlations were calculated using the Weights of Evidence technique (cf. Bonham-Carter, 1994) using the Spatial Data Modeller extension developed for Mapinfo software. A unit

area of 0.25 km^2 was used in these calculations assuming the known deposits have a 0.25 km^2 area of influence.

Geological data such as lithological and structural information was derived from the Northwest Queensland Mineral Province Report (Queensland Department of Mines and Energy, 2000). The report provides a solid geology map of Proterozoic basement and structural framework based on an integrated interpretation of outcropping geology combined with aero-magnetics and gravity. As a result, this data potentially enables us to look under cover. The high resolution regional aero-magnetic and radiometric data was obtained from Xstrata. Regional gravity data was provided by Geoscience Australia. Surface rock chip geochemistry was obtained from the Geological Survey of Queensland geochemical database (Queensland Department of Natural Resources and Mines, 2003) and the Rockchem database from Geoscience Australia.

The creation of binary evidence maps is described briefly below:

- Buffers (proximity to a feature). The procedure used was to generate a series of buffer zones around the feature being tested for spatial association. The buffer zone with the maximum contrast is defined as the optimal buffer distance. In the instance of Williams-Naraku batholith the first buffer or granite polygon was excluded. In the case of mafic intrusives, the first buffer or mafic intrusion polygon was included.
- Presence within a grid feature (magnetic, gravity and radiometrics). Grids were subdivided into a number of classes using the MI-SDM> grid analysis tool> classify grid by histogram tool. Weights of evidence were run on the classified grid to determine the contrast for each class. The classes producing a contrast of 0.5 or greater were then combined in a final reclassified grid. The patterns were used without buffering.
- presence within a polygonal feature (lithologies, metamorphism) For regions such as lithologies, and metamorphic zones.All features with a contrast value of 0.5 or greater were combined in a reclassified map.

Parameter 1- Host-rock lithostratigraphy

The digital basement geology map was subdivided into 22 lithological groups (Appendix 1 - Table 1). The most favourable lithologies that have contrast values >0.5 include: Siliciclastics-carbonaceous shale to siltstone, mafic intrusives, felsic extrusives, very fine to fine grained carbonates, mafic extrusives, jaspilite/chert, intermediate intrusives, and medium to fine grained carbonates. The binary map produced from the grouped lithologies is shown below (Fig. 4).

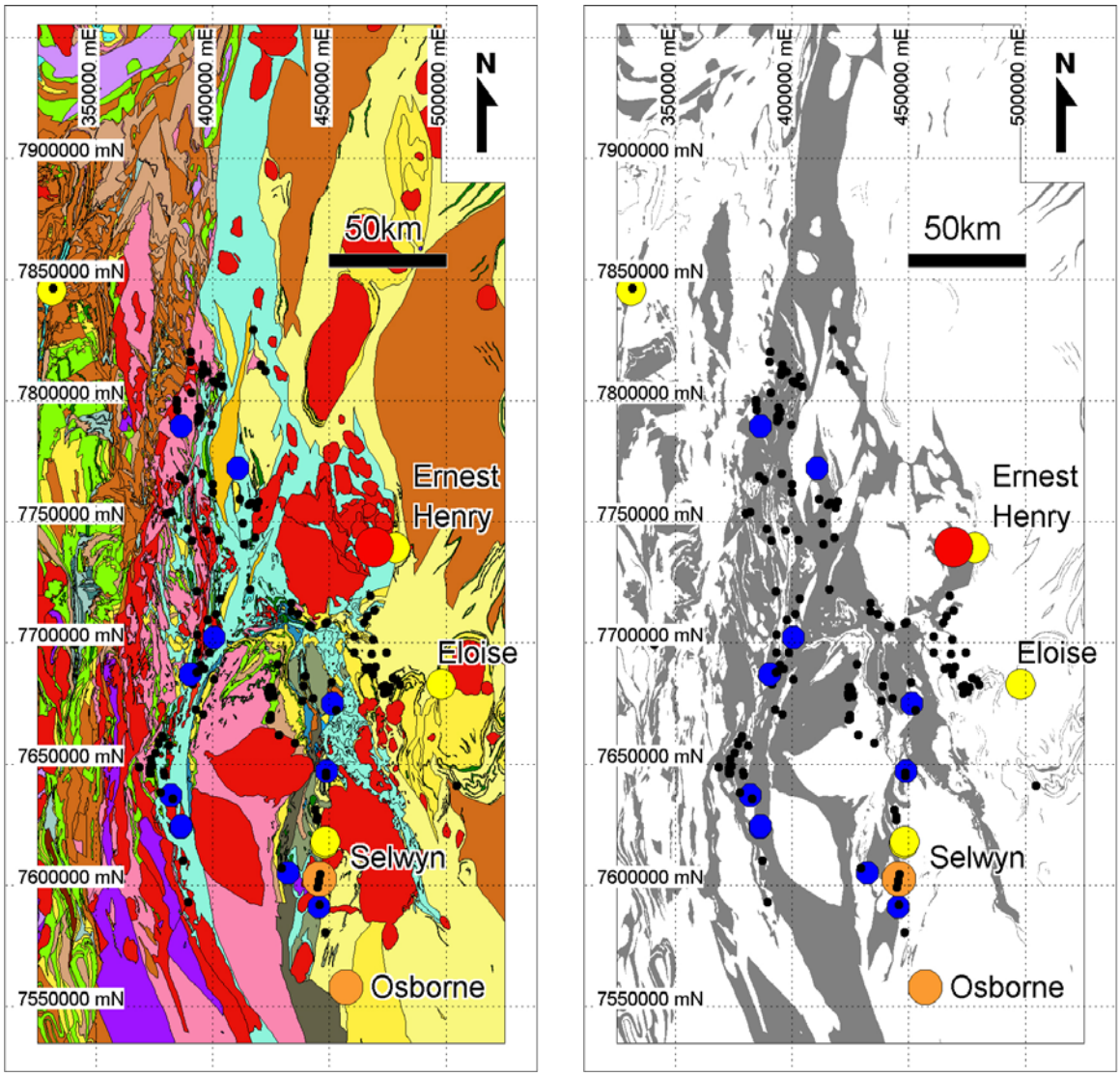

Fig. 4A. Simplified geology of the Mt Isa Inlier derived from the Northwest Queensland Mineral Province Report, overlain with the Cu-Au ± iron-oxide deposit training dataset. 4B. Binary map of favourable lithologies highlighted in grey. Projection: AMG Zone 54 (AGD66).

Parameter 2- Lithological Boundaries

A statistical review of proximity of Cu-Au ± iron-oxide training data lithological boundaries highlighted a significant number of total occurrences located within 750m of the contact between the Corella Formation and these other lithologies, with many of the larger known occurrences close to the contact with the Soldiers Cap Group. The binary map produced for the Corella Formation boundary is shown below (Fig. 5).

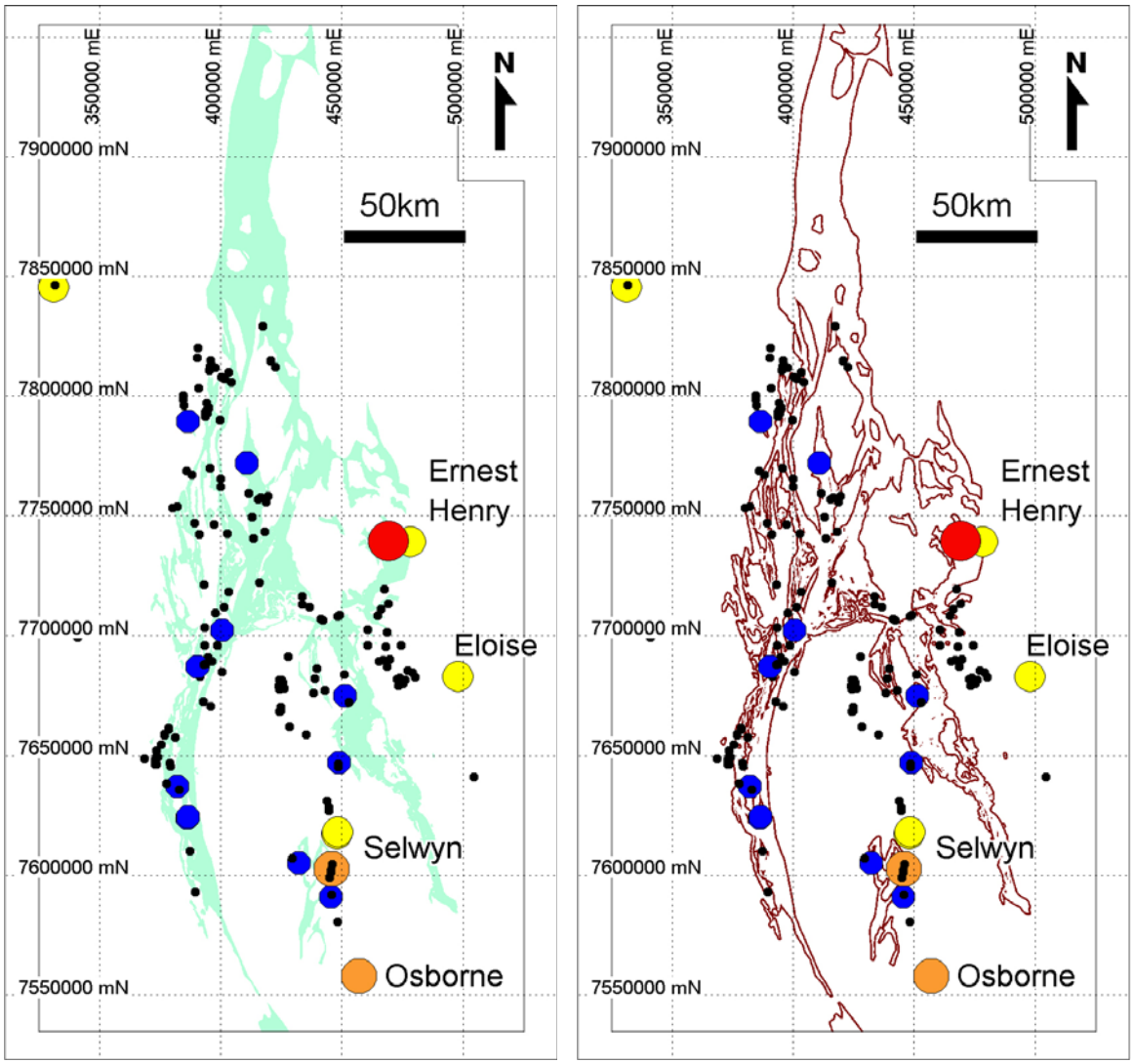

Fig. 5A. Distribution of Corella Formation within the Mount Isa study area highlighted in pale green. B. A binary map of 750m buffer from the Corella Formation contact. The location of Cu-Au training data is plotted (refer to Fig. 3 for legend). Projection: AMG Zone 54 (AGD66).

Parameter 3- Mafic intrusives

Mafic intrusives occur throughout the Mt Isa Inlier. Many of the known Cu-Au deposits have a spatial association with mafic intrusives (such as metadolerite, amphibolites, mafic dykes, diorites, and minor gabbro intrusives). A 750m buffer provides best contrast value, and a binary map produced for the mafic intrusives is shown below (Fig. 6).

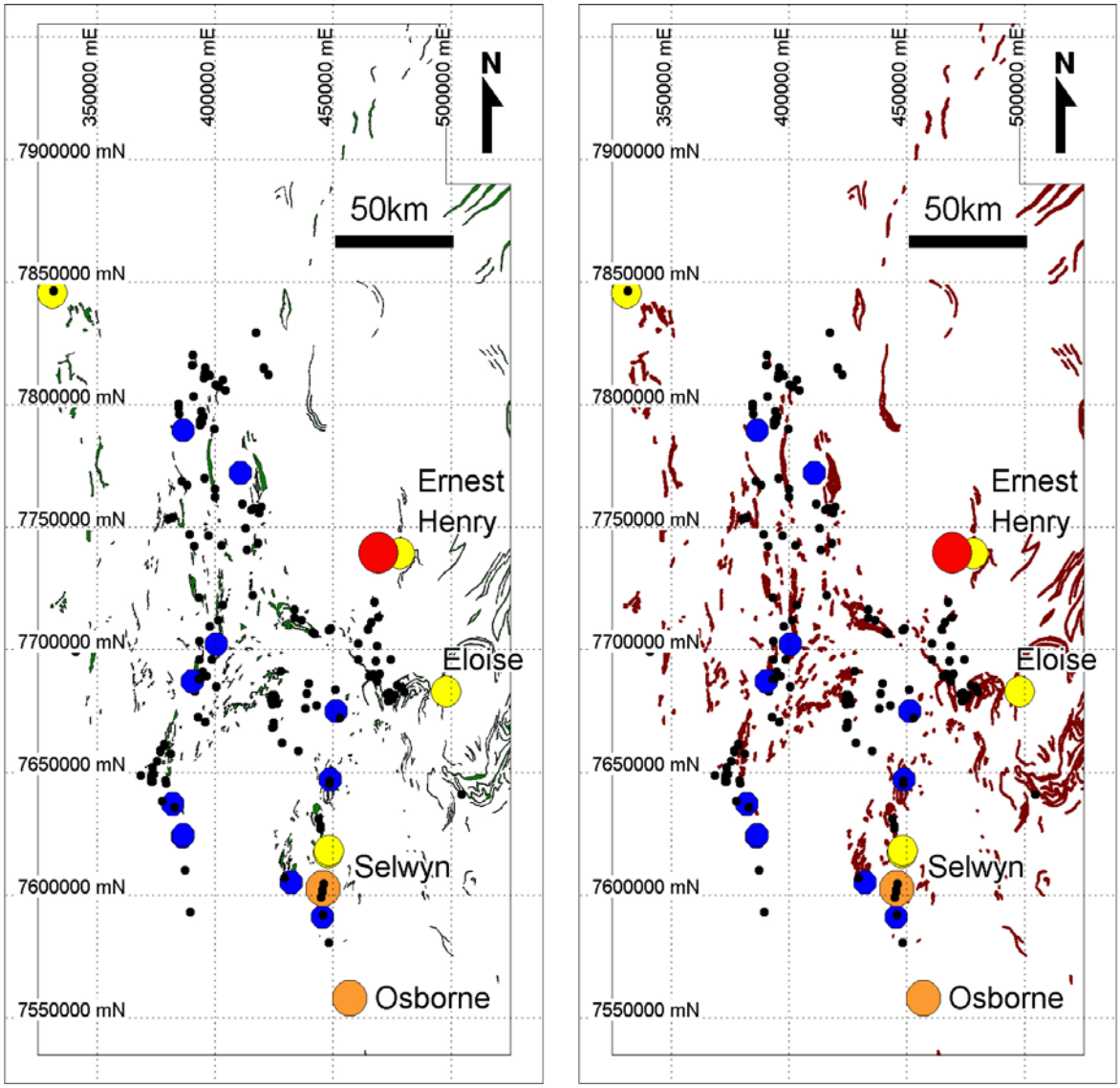

Fig. 6A. The distribution of mafic intrusives within the Mount Isa study area. The location of Cu-Au training data is plotted (refer to Fig. 3 for legend). Projection: AMG Zone 54 (AGD66).

Parameter 4- Williams-Naraku batholiths

The late stage (post-D_2) intrusives of the Williams and Naraku Batholiths crop out over at least 2400km^2, range in age from 1520 to 1490Ma and show a spatial association with Cu±Au mineralisation (Wyborn, 1998; Wyborn and Heinrich 1993a and 1993b, Budd et al., 2002). Using a data driven proximity analysis, Budd et al (2002) concluded that fractionated F-poor I-type granites are most commonly spatially associated with Cu-Au deposits in their study of the metallogenic potential of Australian Proterozoic granites. In their synthesis of the Mount Isa Inlier they concluded that the Williams Supersuite, comprising the post D2 (Post-1550 Ma) plutons of the Williams and Naraku Batholiths, had the best metallogenic potential, whereas the Burstal Suite, Sybella Suite, Nicholson Suite and the Kalkadoon suite had little or no potential.

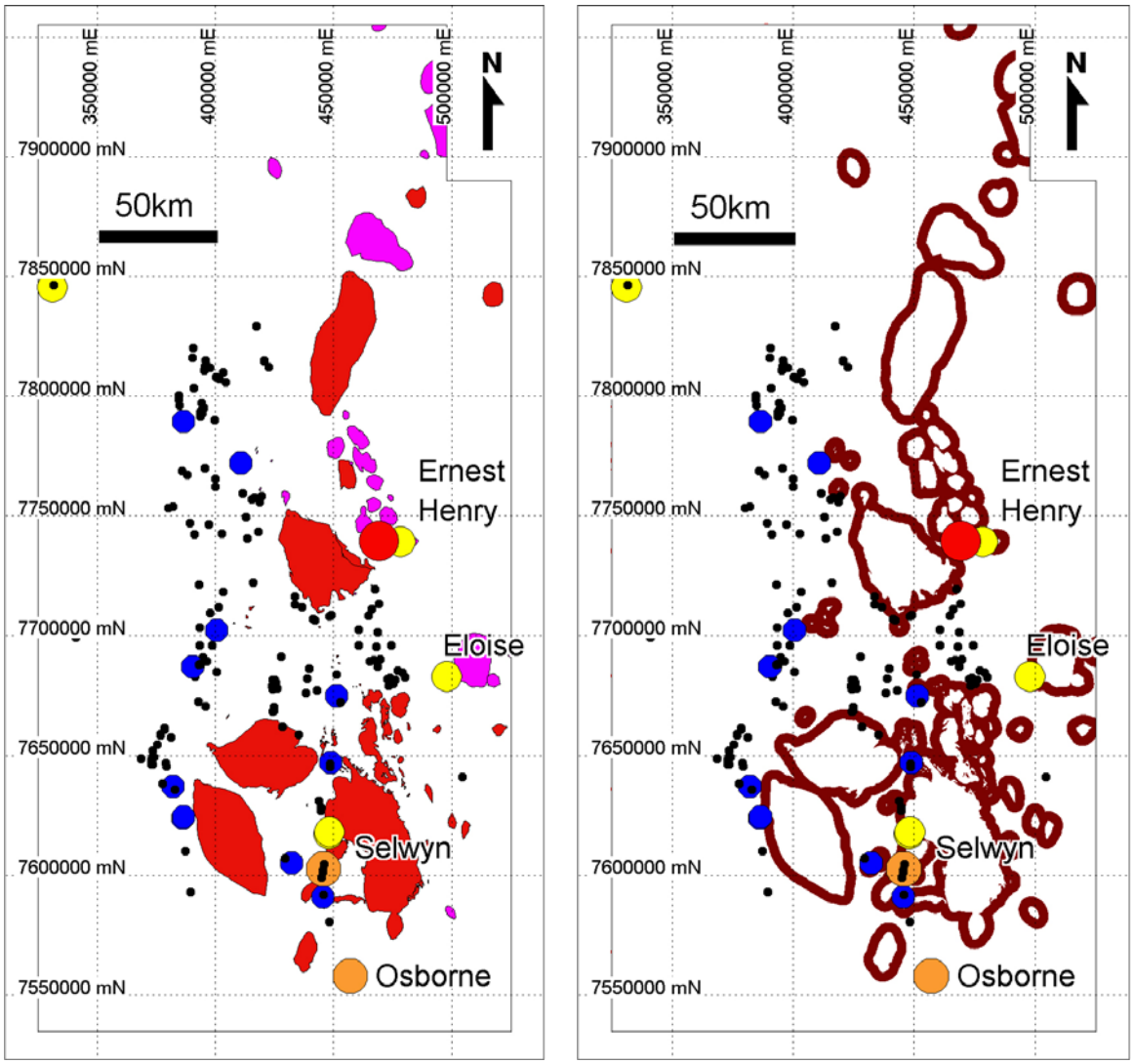

Fig. 7A. The distribution of Williams (red) and Naraku batholiths within the Mount Isa study area. The location of Cu-Au training data is plotted (refer to Fig. 3 for legend). B. Binary map showing optimal 4km buffers to Williams-Naraku batholiths. Projection: AMG Zone 54 (AGD66).

Parameter 5- Metamorphic zones

Published age constraints indicate that the metamorphic peak in most areas occurred ca. 1600-1580 Ma across much of the district (Page and Sun, 1998; Giles and Nutman, 2002; Hand and Rubatto, 2002). Regional metamorphism ranges in grade from greenschist to upper amphibolite facies. This generalised metamorphic map was compiled from studies by Foster (2003) and has been subdivided into greenschist facies, lower to middle amphibolite facies (staurolite, andalusite, cordierite zones), sillimanite zone (Upper Amphibolite Facies) and sillimanite/k-feldspar zone (Upper Amphibolite Facies). The Cu-Au deposits occur mainly in Lower to Middle Amphibolite facies rocks, with Osborne as the exception hosted by upper amphibolite rocks.

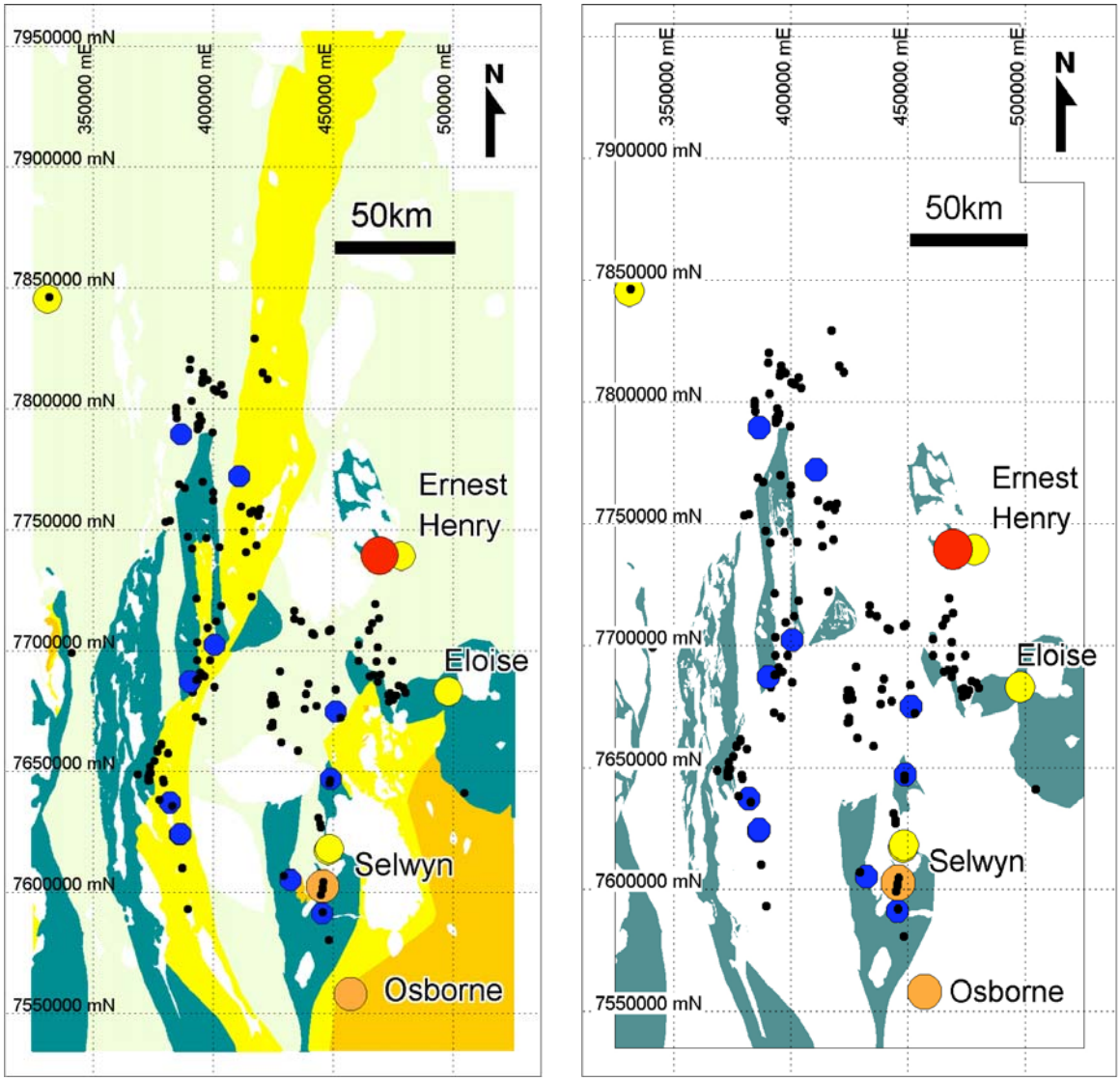

Fig. 8A. Distribution of metamorphic zones within the Mount Isa study area. Pale green = greenschist facies, dark green / grey = amphibolite facies, yellow = sillimanite zone, gold = sillimanite / K-feldspar zone, white = post-metamorphic intrusions (Modified from Foster (2003). The location of Cu-Au training data is plotted (refer to Fig. 3 for legend). Projection: AMG Zone 54 (AGD66).

Parameter 6- Structure

The relatively young age of most gold-copper mineralisation (1550-1500 Ma) excluding Osborne (~1595 Ma) means that all faults in the database were included in the analysis, because protracted deformation and metamorphism of the Isan Orogeny (ca. 1600-1500 Ma) could have reactivated earlier faults (formed between 1800-1600Ma). All faults within the study area were plotted on a rose diagram, and based upon their distribution, they were subdivided into 7 groups including N-S (350-15°), NNE (15-40°), NE (40-75°), E-W (75-100°), ESE (100-130°), SE (130-150°) and SSE (150-170°) (Fig. 9). It was note that many of the significant deposits are associated with either NS faults (Osborne, Selwyn, Eloise) or NE faults (Ernest Henry).

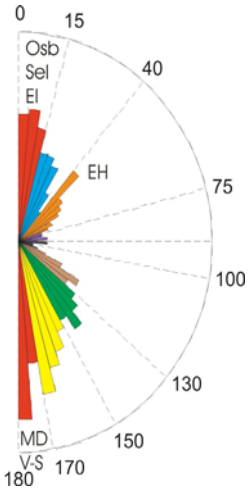

Fig. 9. Rose diagram of total faults (n=3,500) within the Mount Isa study area.

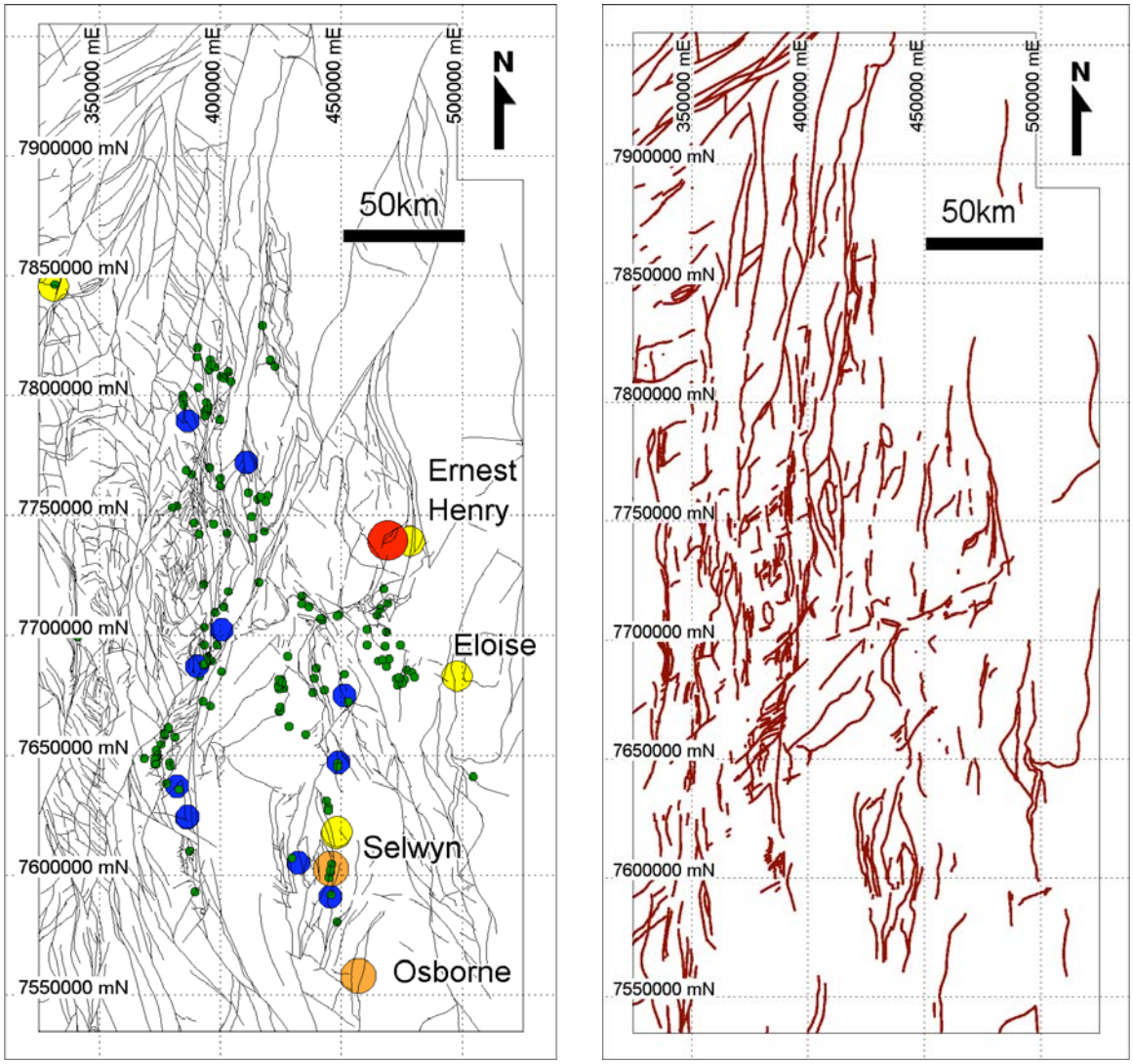

Fig. 10A. Distribution of major and moderate sized faults within the Mount Isa study area (derived from the NWQMDR). The location of Cu-Au training data is plotted (refer to Fig. 3 for legend). B. Binary map of NS (350-15°) and NE (40-75°) trending faults buffered to 600m. Projection: AMG Zone 54 (AGD66).

Parameter 7- Magnetic highs

Magnetic highs were extracted from regional aeromagnetic data obtained from Xstrata (Fig. 11A). This involved inspection of the cumulative histogram plots of the geophysical data for upper breakpoints and thresholding the data above this limit, producing a map of magnetic highs. The binary magnetic anomaly map used in the data driven modelling is shown in Fig. 11B.

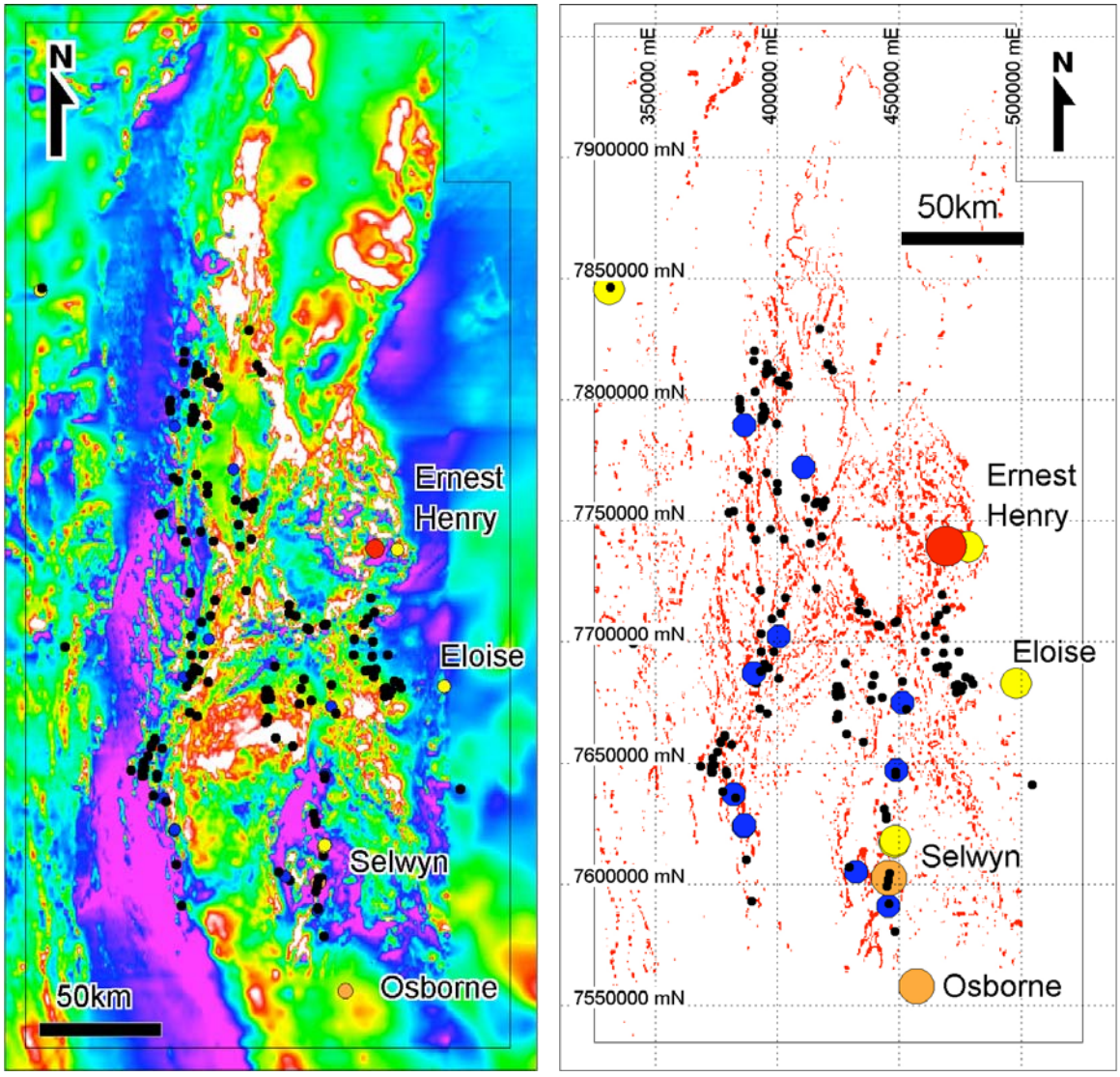

Fig. 11A. Regional aeromagnetic image of the Mount Isa study area (Data obtained from Xstrata). The location of Cu-Au training data is plotted (refer to Fig. 3 for legend). B. Binary map of magnetic highs. Projection: AMG Zone 54 (AGD66).

The simplified geology of the Selwyn region modified from Sleigh 2004 is overlain on a corresponding aeromagnetic image (Fig. 12A). This image highlights the Starra ironstones and iron-rich lithologies within the Selwyn fault zone and hydrothermal magnetite alteration associated with the Mt Elliot and SWAN deposits. The final binary image of the magnetic highs used in the modelling is highlighted in Fig. 12B.

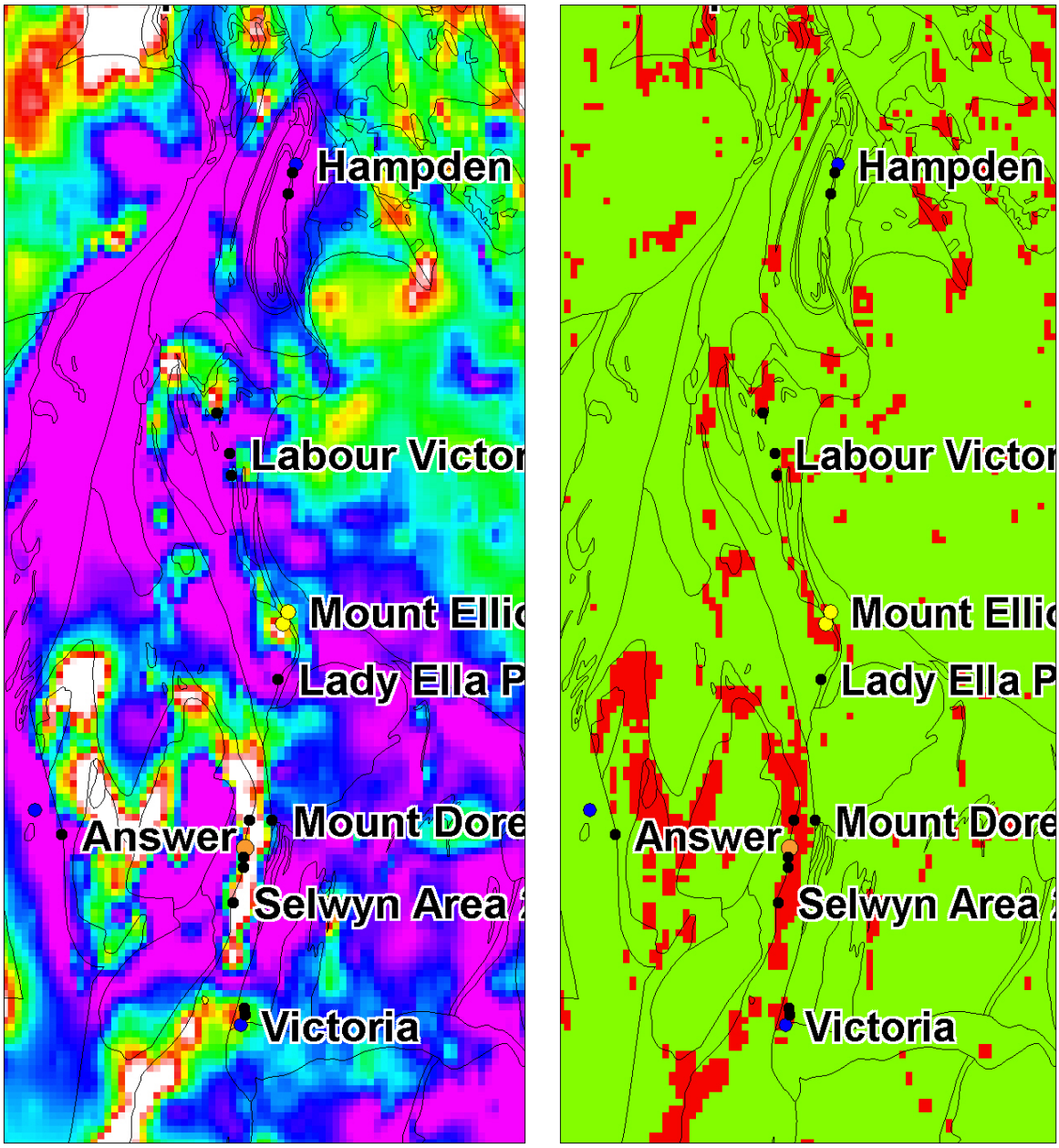

Fig. 12A. Aeromagnetic image for the Selwyn region with an outline of geological boundaries. B. Binary image of the magnetic highs for the Selwyn region used in the modelling. Projection: AMG Zone 54 (AGD66).

Parameter 8- Gravity highs and gradients

The gravity data was subdivided into 5 classes using MI-SDM > grid analysis tools > classify grid by histogram (Fig. 13B). Weights of evidence for the 5 classes indicated gravity highs and steep gradients adjacent to gravity highs and gravity lows have a strong spatial association with the Cu-Au occurrences. The gradients showing good contrast have been combined to produce the binary map

.

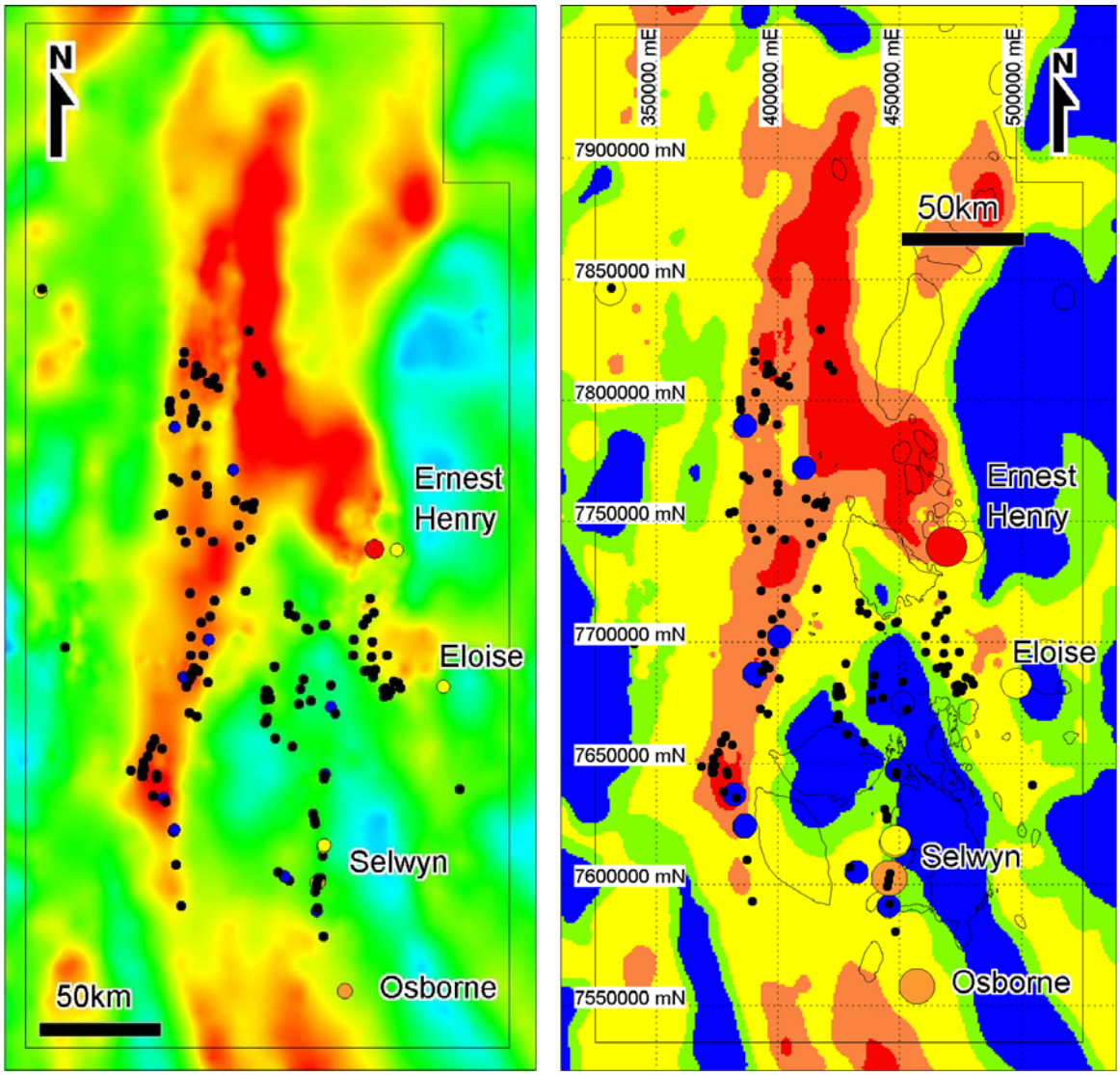

Fig. 13A. Regional gravity image of the Mount Isa study area (Data obtained from Geoscience Australia). The location of Cu-Au training data is plotted (refer to Fig. 3 for legend). B. Classified gravity image with the location of Williams-Naraku batholith outlined for reference. The gravity highs (red and orange) and the steep gradients adjacent gravity lows (green) were incorporated into a binary map based on statistics. Projection: AMG Zone 54 (AGD66).

Parameter 9- Radiometrics (U/Th anomalies)

After trying a variety of ratios it was determined that the U/Th ratio radiometric image provided the strongest correlation with the Cu-Au occurrences. A subset of the U/Th image covering the Selwyn region demonstrates that it has been relatively successful in highlighting the Selwyn group of deposits, Mt Dore, Victoria, Stewart and Stuart South (Fig. 14). Uranium has been documented as an accessory in several Cu-Au occurrences including Ernest Henry (Oliver et al., 2004). One of the limitations of the radiometric data is that its effectiveness is restricted to areas of outcrop. The data was clipped to areas of known outcrop to eliminate false anomalies located in areas of cover.

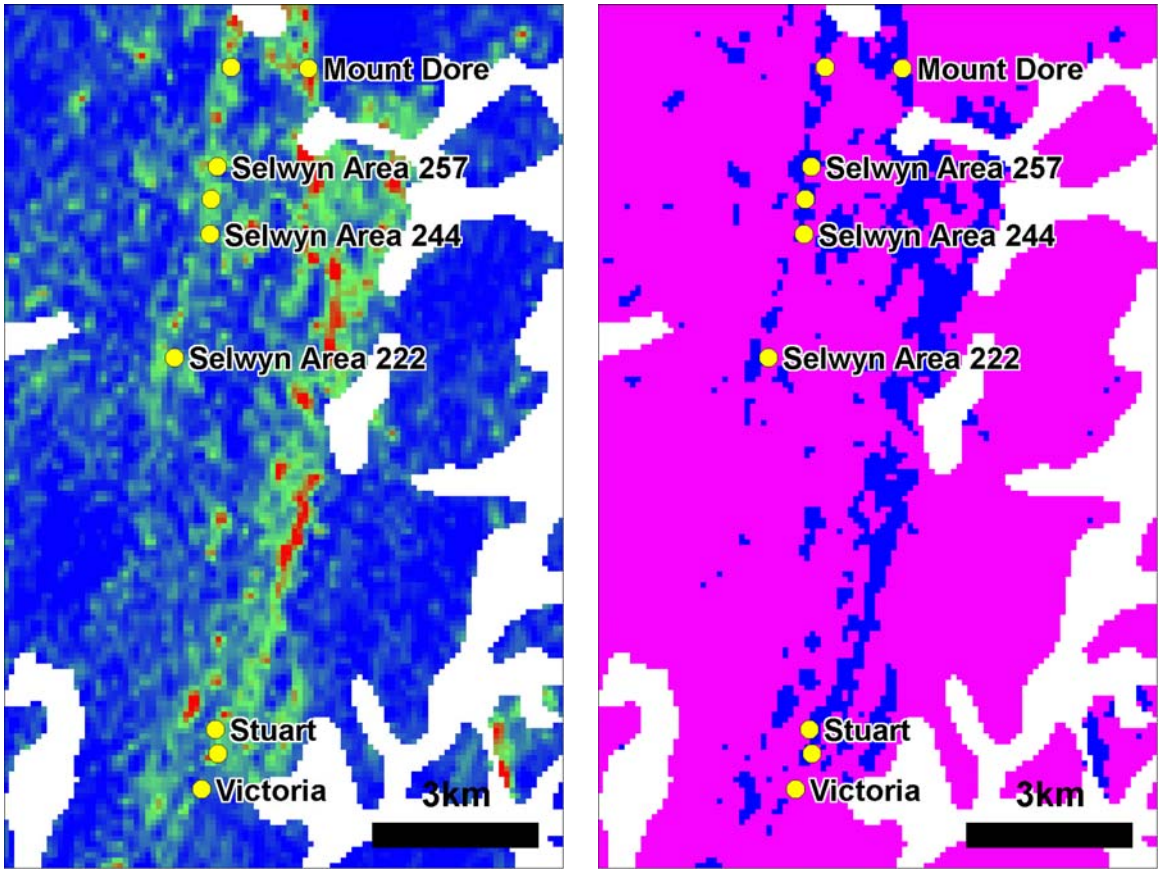

Fig. 14A. U/Th radiometric image for the Selwyn region showing the location of Cu-Au training data. White areas represent areas of cover and have been clipped from the image. B. Binary U/Th map produced, showing dark blue areas(included), purple (outside) and white (null data). Projection: AMG Zone 54 (AGD66).

Parameter 10- Rockchip geochemistry

Rockchip geochemistry may be used to identify areas of outcropping mineralisation. The Department of Natural Resources and Mine's exploration geochemistry dataset covering Mount Isa Inlier and Geoscience Australia's Geochemical database (OZCHEM) were combined into a single database. Gstats analysis (statistical analysis software program in ArcSDM) was used to create a cumulative probability plots to analyse the assay data for each element. The data was reclassified according to bottom cut, lower threshold and upper thresholds. Spatial statistics were run to determine the spatial correlations with the Cu-Au occurences. Binary files were then created above and below an optimal threshold value (ie. for gold in rockchips it was over 0.11 ppm and < 0.11 ppm).

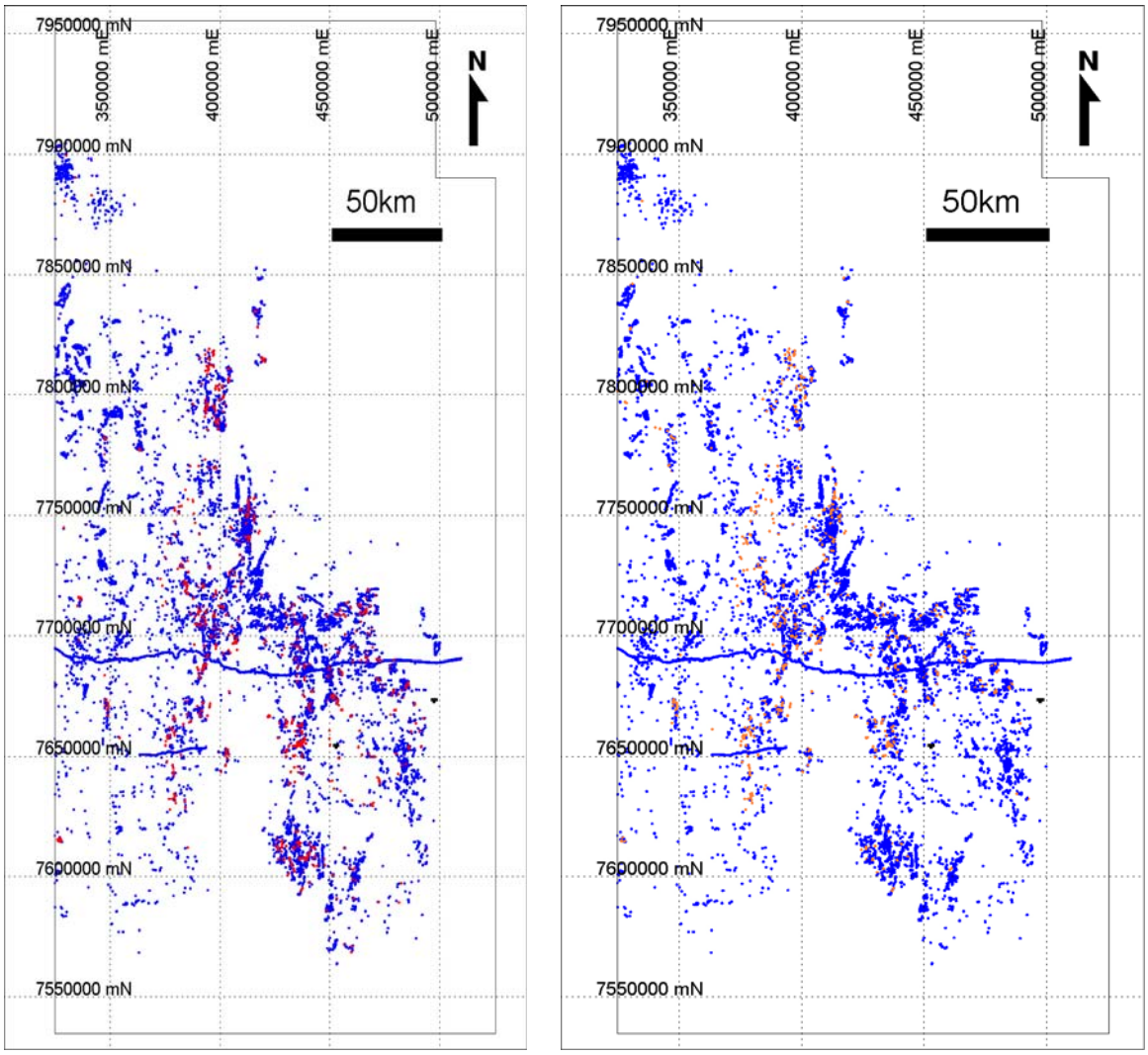

Fig. 15. Distribution of rockchip samples within the Mount Isa study area. Fig. 15A displays rockchip samples analysed for gold (n = 20,431) with values above a anomalous threshold of 249 ppm Cu highlighted in red and values below marked in blue. Fig. 15B displays rockchip samples analysed for copper (n = 30,161) with values above a anomalous threshold of 0.11 ppm Au highlighted in yellow and values below marked in blue. Projection: AMG Zone 54 (AGD66).

6. RESULTS

All 7 fault groups were tested separately and the weights of evidence indicated that NS and NE orientated faults had the strongest spatial association with the Cu-Au occurrences based on contrast values of around 1.4 and confidence of 9 (Table 1). All NS and NE orientated faults were selected to produce the binary map.

Orientation	Area (km^2)	Mineral Occurrences	Contrast	Confidence
NS (350-15)	21,265	108	1.45	9.59
NE (40-75)	8,339	58	1.43	9.02
SSE (150-170)	16,834	102	0.95	6.26
NNE (15-40)	11,851	53	0.91	5.55
EW (75-100)	2,389	9	0.56	1.65
ESE (110-130)	5,935	21	0.53	2.28
SE (130-150)	9,434	29	0.39	1.94

Table 1. Weights of evidence statistics for the seven fault orientations.

The Contrast and Confidence values indicate that there is a very strong spatial association with rockchips assaying ≥ 249 ppm Cu, ≥ 0.11 ppm Au with the known occurrences (Table 2). Co (≥ 85 ppm) and Ni (≥ 43 ppm) also possess a strong spatial association with contrast values of 1.85 and 1.65 respectively. However significantly less Co and Ni samples have been collected and coverage is less extensive. Arsenic (≥33 ppm) has a low contrast and weak spatial association.

	Cu	Au	Co	Ni	As
Count	30,161	20,431	17,511	7,717	14,038
Maximum	9,910,000	133	10,300	4,100	103,000
Minimum	0.00001	0.00001	0.00001	0.00001	0.00001
Mean	4,459	0.262	49.2	46.9	70.42
StnDev	60,671	2.12	154.9	117.6	934.5
Threshold	**249**	**0.11**	85	43	33
Anom	2,160	0.64	178	128	125
UA	8300	3.1	274	364	300
Contrast	**2.5**	**2.38**	1.85	1.65	0.26
Confidence	12.37	11.97	7.66	4.76	0.65
Association	V Strong	V Strong	Strong	Strong	Weak

Table 2. Summary statistics including confidence and contrast for Cu, Au, Ni, Co and As in rockchip samples from the Mount Isa study area.

6.1 Evaluation of best Cu-Au parameters

Ranking	Key Ingredient	Contrast	Confidence
1	Copper in rockchips (>249 ppm Cu)	2.50	36.31
2	Gold in rockchips (>0.11ppm Au)	2.38	26.45
3	Corella-Soldiers Cap Contact (750m buffer)	1.87	13.98
4	Aeromagnetics (magnetic highs)	1.82	14.36
5	N-S and ENE faults (650m buffer)	1.45	17.20
6	Mafic Intrusives (750m buffer)	1.25	7.47
7	Lithologies (dominantly Cycle 3)	1.21	5.09
8	Gravity (Gradients)	1.03	15.91
9	Bends on N-S and ENE faults	1.03	2.33
10	Metamorphic Grade (Amphibolite Facies)	0.98	7.85
11	Radiometrics (U/Th)	0.83	4.46
12	Williams and Naruku batholiths (4km buffer)	0.64	3.36

Table 3. Ranking of critical ingredients for the Mount Isa Cu-Au study based on Contrast values.

Table 3 ranks the parameters analysed from one to twelve in terms of their spatial association with the Cu-Au deposits. The higher the contrast (C) the better the spatial association. As a rule of thumb Contrast values above 0.5 are considered reasonable (pers. comm. G. Partington, 2004) and Confidence values above 1.5 considered better than random (pers. comm. G. Partington, 2004).

Rockchip geochemistry is clearly the best parameter for Cu-Au occurrences. Cu and Au in rockchip geochemistry are the only two parameters that produced C values above 2, returning 2.5 and 2.38 respectively. Note however that geochemistry is restricted to areas of outcrop. Proximity to the Corella Formation contacts is the next highest parameter of known Cu-Au occurrences with a C value of 1.87 (and a rank of 3). It represents the highest ranking geological layer. Aeromagnetic highs are also strong predictor of known Cu-Au occurrences with a C value of 1.82. This is by far the highest ranking geophysical parameter, well above that of gravity and radiometrics. The combined N-S and NE orientated faults is the next best parameter for Cu-Au occurrences with a C value of 1.45.

Proximity to mafic intrusions, lithology, gravity and fault bends associated with N-S and NE orientated faults and metamorphic grade are all moderately strong predictors of know Cu-Au occurrences, with contrast (C) values greater than 1, except metamorphic grade. Radiometrics (U/Th ratio) is a weak predictor of know Cu-Au occurrences, with a contrast (C) value of 0.83. Proximity to the Williams-Naraku batholith (4km buffer) had the lowest contrast (C) value of 0.63 and is a weak predictor of know Cu-Au occurrences.

6.2 Cu-Au Posterior Probability Maps

The weights of evidence maps generated for each criterion were combined to create to different cumulative posterior probability Cu-Au maps for the Mount Isa Inlier, northwest Queensland, Australia.

The first posterior probability Cu-Au map consists of 9 weighted map patterns including favourable lithostratigraphy, proximity to the Corella Formation - Soldiers Cap Group contact, proximity to mafic intrusives, proximity to the Williams-Naraku batholith, metamorphic zones, fault orientations, fault bends, magnetics and gravity (Fig. 16). The 9 layer model excluded surface geochemistry and radiometrics so as to look through the cover to some degree.

Several observations can be made about the 9 layer model:

- The Ernest Henry deposit which is the largest known Cu-Au deposit in the Mount Isa Inlier with a resource 167 Mt @ 1.1% Cu and 0.54 ppm Au (Ryan, 1998), produced the largest single anomalous region within the study area. There are some analogous Ernest Henry type targets to the north and west.
- The Selwyn group defined the single largest anomalous linear trend extending for 40km strike length, of which southernmost ~10km is located under cover. Interesting areas in this same region include: NW of Labour victory, north of Answer and north of Hampton.
- The Eloise deposit is also highlighted, with several Eloise type targets are located NNE to NNW of Ernest Henry.
- The Osborne deposit is not strongly highlighted and is considered to reflect the lack of detailed geology in the interpretation as a result of cover.
- Mt Elliot, Mt Dore and Victoria-Stewart deposits are highlighted.
- Trekalano and SE Duchess and areas NW of Lady Ethleen are highlighted in the Wonga belt.
- Numerous areas are highlighted particularly around Cloncurry township and to the west.

The second posterior probability Cu-Au map consists of 12 weighted map patterns including those present within the 9-layer model as well as outcrop based data for Cu and Au rockchip geochemistry, and radiometrics (Fig. 17). The effect of addition of the extra 3 layers was to further highlight areas anomalous geochemistry around Cloncurry Fold Belt and Wonga belt, without significantly reducing areas previously highlighted in the 9 layer model.

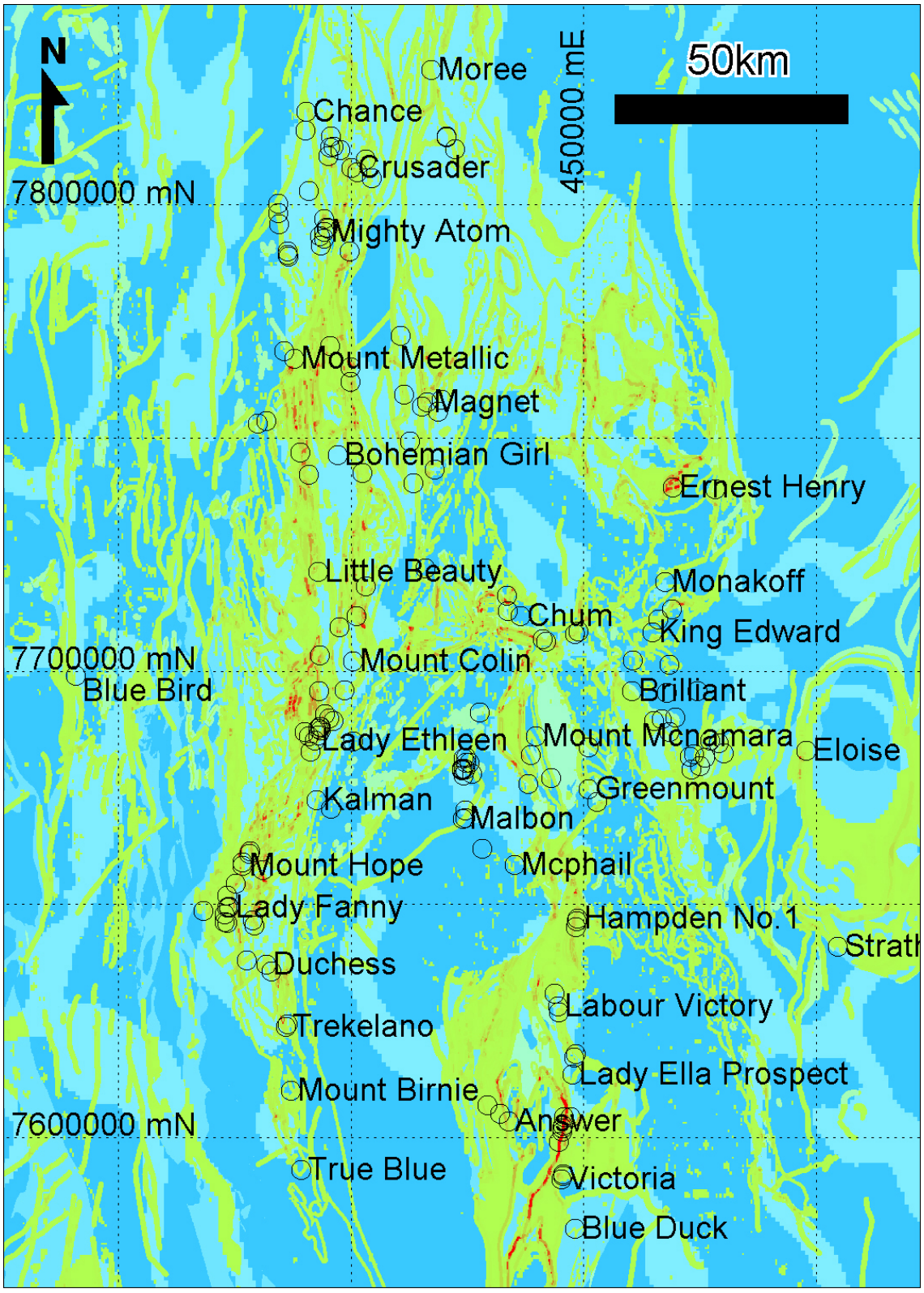

Fig. 16. The 9 Layer Cu-Au posterior probability map for the Mount Isa Inlier, NW Queensland. Projection: AMG Zone 54 (AGD66).

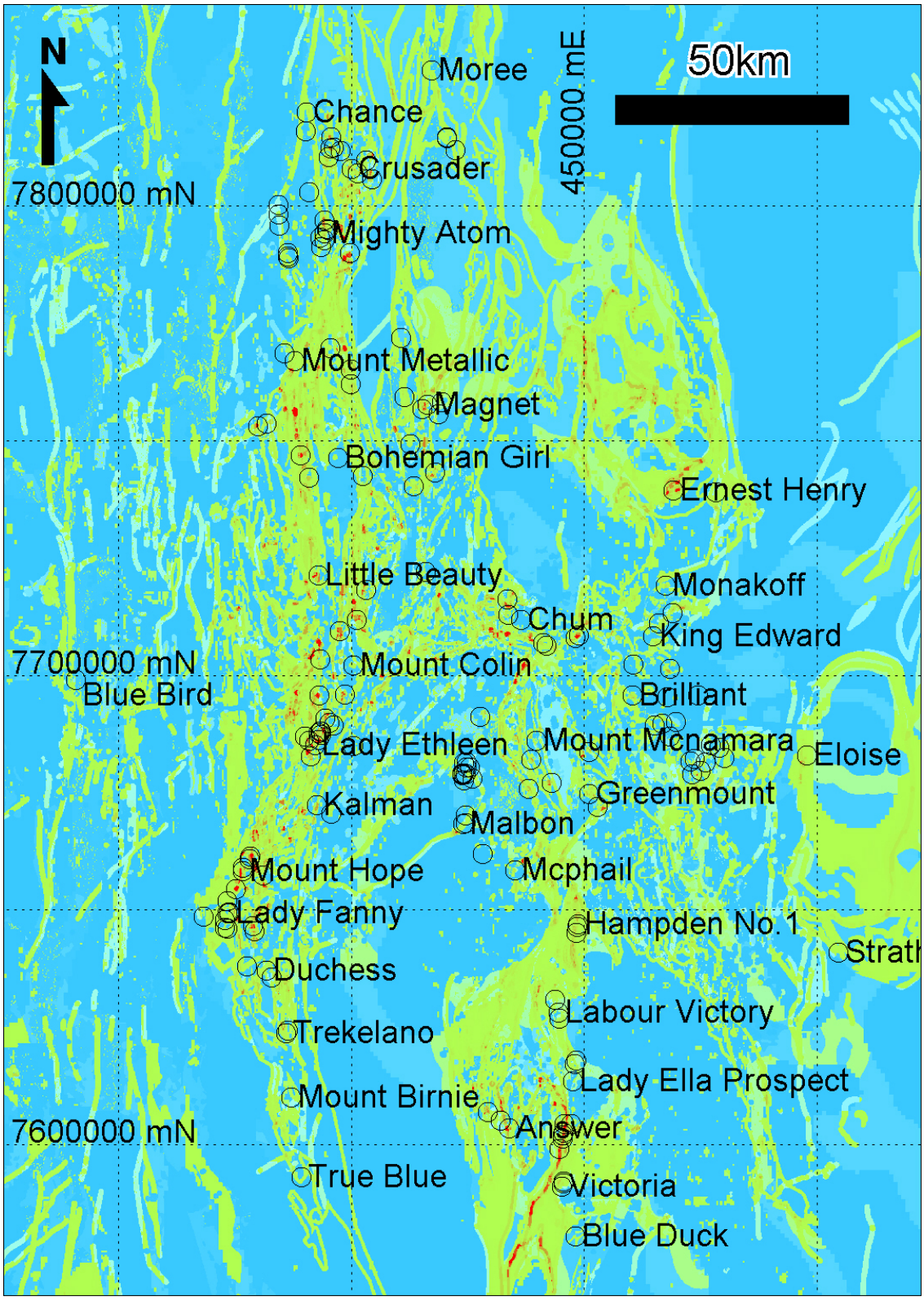

Fig. 17. The 12 Layer Cu-Au posterior probability map for the Mount Isa Inlier, NW Queensland. Projection: AMG Zone 54 (AGD66).

6.3 Comparison with expert targeting

Expert driven targeting has been completed over the Mount Isa Inlier previously by SRK Consulting and forms part of the North-West Queensland Mineral Province Report for the Queenland Government Department of Mines and Energy. 103 expert driven Cu-Au targets (CGM1 to 103) were listed in Table 11.4 (pp 98 to 110) of the report. Their overall ranking (1 - high priority, 2 – medium priority, and 3 - lower priority) was determined from a combination of favourable regional and local structural setting, lithostratigraphic setting, alteration/mineralisation indicators and thickness of cover.

A comparison between the data driven method of the 9 and 12 layer Cu-Au posterior probability maps and the expert driven targeting can be made from overlaying the expert area polygon (Figs. 18 and 19). The data driven models delineate permissive areas comparable to expert delineation, however they are much more restricted in area. The weight of evidence model has additional characteristics that it is well defined, reproducible, objective, and provides a quantitative measure of confidence.

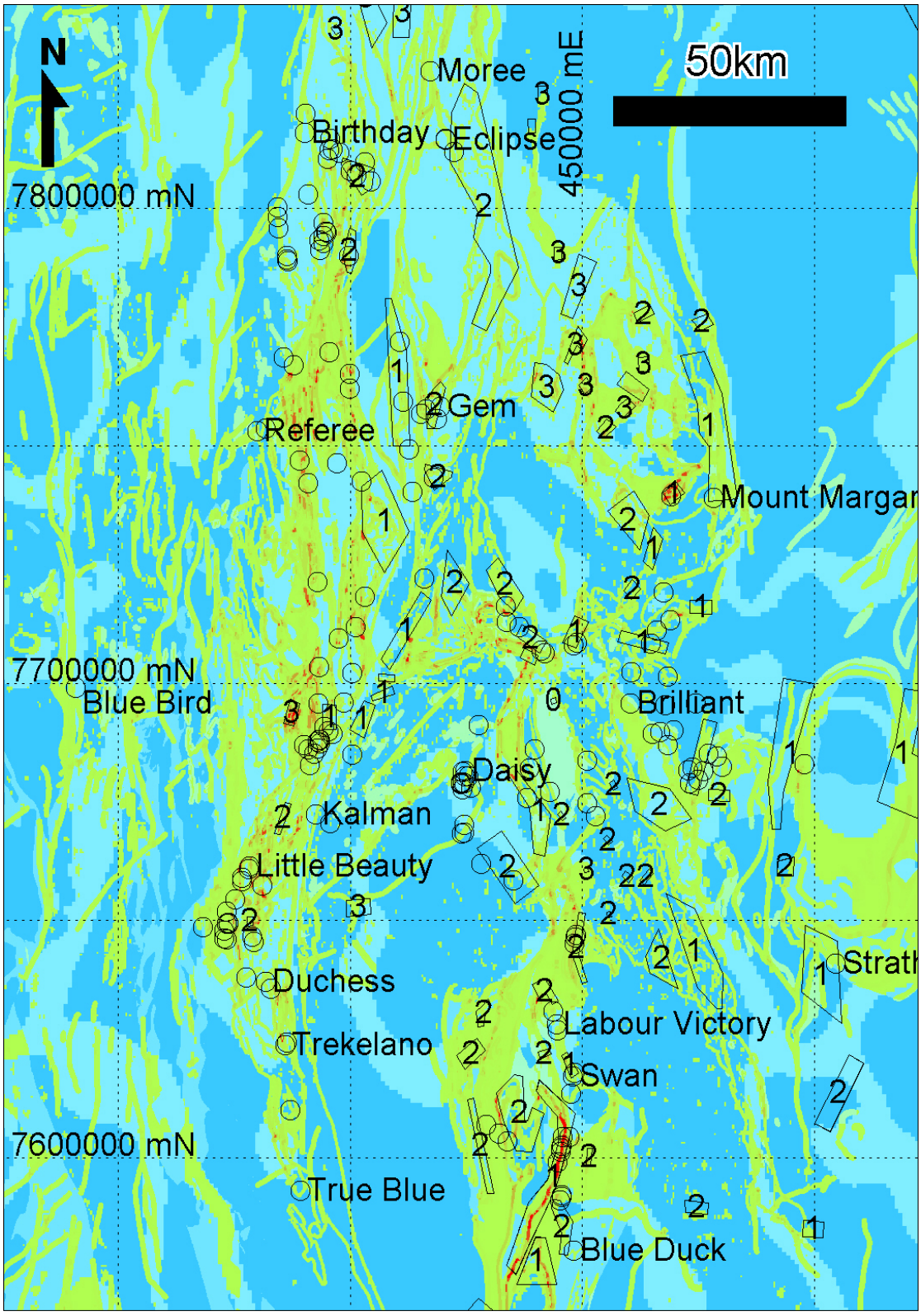

Fig. 18. Expert driven targets (ranked as 1 - high priority, 2 – medium priority, and 3 - lower priority) overlain on the 9 Layer Cu-Au posterior probability map for the Mount Isa Inlier, NW Queensland. Projection: AMG Zone 54 (AGD66).

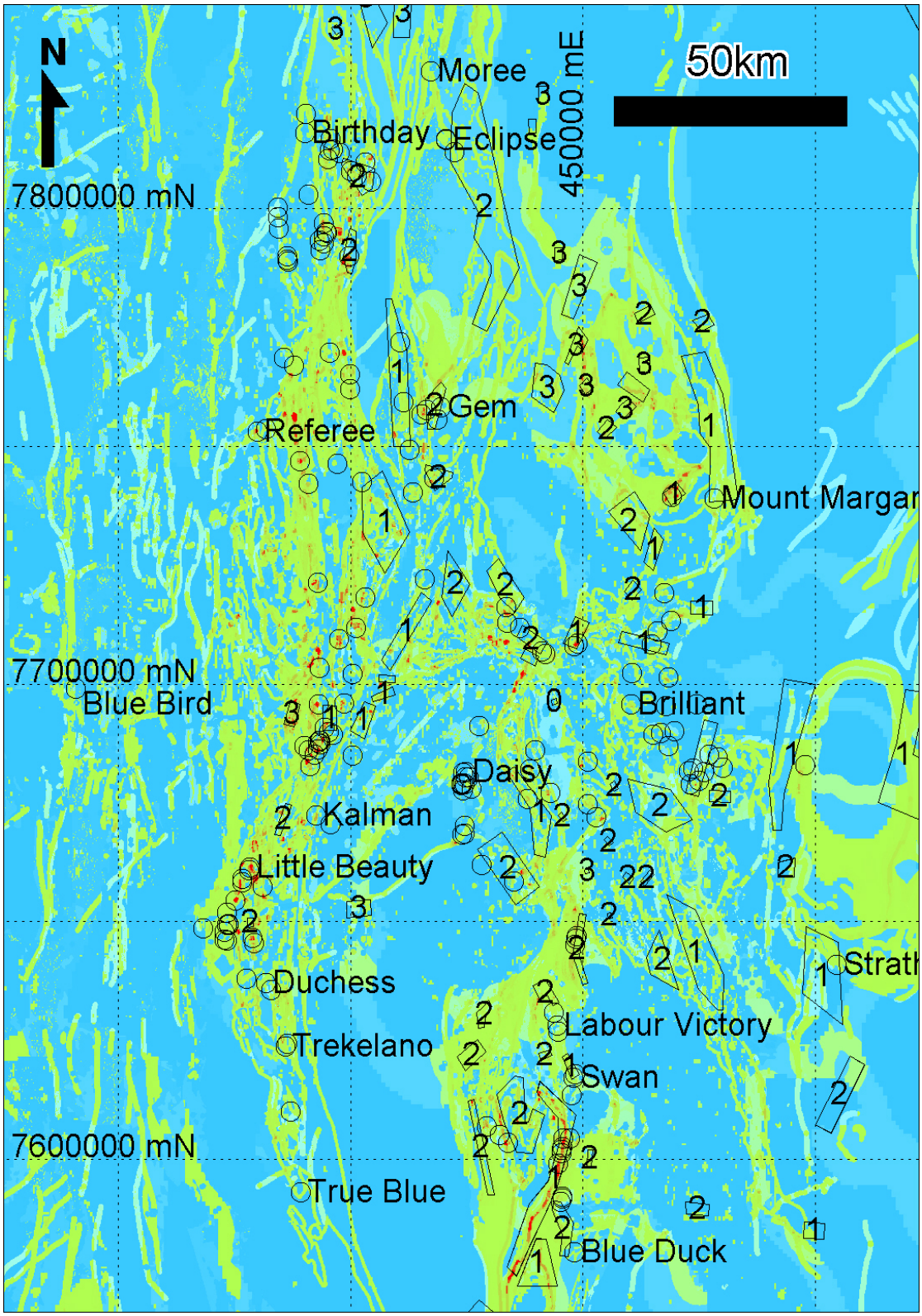

Fig. 19. Expert driven targets (ranked as 1 - high priority, 2 – medium priority, and 3 - lower priority) overlain on the 12 Layer Cu-Au posterior probability map for the Mount Isa Inlier, NW Queensland. Projection: AMG Zone 54 (AGD66).

7. DISCUSSION

7.1 Corella Formation / Soldiers Cap Group contact

The results of this study indicate a significant proportion of the Cu-Au mineral occurrences were located less than 750m from the contact between the Corella Formation (cover sequence 2) and Soldiers Cap Group (cover sequence 3). This boundary represents a regional unconformity between Soldiers Cap Group (ca.1680 to 1650 Ma) and other units of similar age (including Kuridala Formation, Staverly Formation and the Marimo Slate) and the Corella Formation (ca. 1750-1720 Ma, including Doherty Formation). The regional unconformity was attributed to basin subsidence and tectonism by Blake and Stewart (1992). D_1 of the Isan Orogeny has been inferred to be responsible for the emplacement of younger cover sequence 3 rocks over older cover sequence 2 rocks through normal faulting or reactivation of normal faults as thrust faults (O'Dea et al., 1997; Betts et al., 2000).

The field observation that the Corella Formation - Soldiers Cap Group contact is consistently faulted and has intense localized alteration (pers. comm. D. Foster) suggesting that this boundary has been active during the main metasomatic events, and consequently played a key role in focusing metasomatic fluids responsible for Cu-Au mineralisation.

The Corella Formation consists of calc-silicate rocks, marbles and minor pelitic and volcanic rocks, whereas the Soldiers Cap Group consists of siliciclastic metasedimentary rocks and mafic metavolcanics. The juxtaposing of these different rock types may provide: (1) a physical barrier to upward directed fluid flow from the more permeable metasedimentary rocks into the less permeable calc-silicate rocks, (2) favourable sites for fluid mixing or fluid-wallrock reaction, (3) regions of significant chemical and/ rheological contrast.

7.2 Aeromagnetics

Magnetic highs, which may reflect areas of magnetite ± pyrrhotite precipitation, also have a strong correlation with Cu-Au occurrences. Magnetics has been a major tool used in exploration for Fe-oxide Cu-Au deposits in the Isa Inlier, and played an integral role in the discovery of significant deposits located under shallow cover, including, Osborne, Ernest Henry and Eloise (Williams and Blake, 1993; p56). Williams and Pollard (2001) concluded that "there is no simple geophysical model that can be relied on when exploring for Fe-oxide Cu-Au deposits at regional to prospect scale" based on the complex and varied spatial and temporal relationship between magnetite and Cu-Au ore in the Cloncurry District.

Many of the magnetic highs in the Mount Isa region are generated from the formation of hydrothermal magnetite ± pyrrhotite. However, the spatial relationship between Cu-Au deposits and iron oxides (reflected by magnetic highs) is not simple. This is because:

1) Not all Cu-Au deposits are associated with Fe oxides. Magnetite is absent from some deposit styles such as the graphitic schist hosted deposits (Mount Dore, Victoria and Stuart).
2) Some deposits occur within more reduced pyrrhotite rich zones which are less or non-magnetic (Eloise).

3) Not all ironstones are mineralised. At Lightning Creek the largest single accumulation of hydrothermal magnetite is Cu-Au poor, and many ironstones and magnetite-bearing alteration zones are barren.
4) Several generations of magnetite may be present. At Ernest Henry an earlier (barren) generation of magnetite is overprinted by a later (mineralised) generation.

Despite these problems, the high contrast values generated in the weights of evidence study indicates that aeromagnetics is a very effective exploration tool for targeting Cu-Au mineralisation in the Mt Isa inlier. It provides targets that are potentially mineralised and significantly reduces the area that requires exploration.

7.3 Structure

The ENE and NS orientated fault sets have a strong to moderate association with Cu-Au occurrences. All significant Cu-Au deposits in the study area are associated with at least one of these two orientations. Williams and Blake (1993; p29) described a N-S trend located at longitude 140 30' which formed a 100km long corridor extending from Stuart (south of Selwyn) to Great Australia (at Cloncurry) as the most striking evidence of structural control on Cu±Au±Ag±Co deposits in the Cloncurry district. The importance of NS and ENE structures is considered to reflect continued east-west directed shortening during D_2 and D_3 has been accommodated by movement along pre-existing fault zones in the older basement architecture.

7.4 Mafic Intrusives

The Cu-Au deposits within the Mount Isa study area have a strong spatial association with mafic intrusives (such as metadolerite, amphibolites, mafic dykes, diorites, and minor gabbro intrusives) with a significant proportion located <650m from or within these rock types.

Mafic igneous rocks occur throughout the Mount Isa Inlier range in style from sills to layered sills, dykes, plugs, phase of composite intrusions, net veining and other magma mingling textures. Based on field relationships and age dating, the mafic igneous rocks were emplaced over nearly 740 Ma of earth history, between 1850 Ma and 1116 Ma. This age range is based on:

- Net-veining documented by Blake (1992) indicating synchronous with emplacement with the Kalkadoon granite (~1850 Ma).
- Net-veining documented by Blake (1981) indicating synchronous with emplacement with the Mount Erle and Myubee Igneous complexes (~1740 Ma).
- Pre-dating metamorphism of >1590 Ma including (Page and Sun, 1998)
- Net-veining documented by Blake (1981) indicating synchronous with emplacement of the Sybella Granite (1655±4 Ma, 1660 5, 1673±3 Ma; Connors and Page, 1995)
- Ernest Henry Diorite (1660 ± 13 Ma, 1658 ± 10 Ma, 1657 ± 7 Ma).
- Synchronous with emplacement of the Williams-Naraku batholith ~1550-1500 Ma (Mark, 2000).
- Unmetamorphosed dykes cutting the Williams-Naraku batholith all regional structures and rock types. Including the Lakeview Dolerite Rb/Sr age 1116±12 Ma (Page, 1983).

There are many documented Cu-Au deposits spatially associated with mafic intrusives such as Ernest Henry (Mark et al., 2000), Osborne (Adshead, et al., 1998), Eloise (Baker, 1998), Mount Elliot and SWAN (Sleigh, 2002). Drabsch (1998) recorded a close spatial and temporal association between intra-ore trachyandesite dykes and Cu-Au mineralisation in the Corbould Zone at the Mount Elliot deposit. Wholerock analysis of these dykes by Wang and Williams (2001) indicated a distinct affinity with the Eureka Suite (cf. Pollard et al., 1998). Similarly, Adshead-Bell (2000) recorded a non-foliated diorite intrusion within the Starra 276 orebody that was spatially and temporally associated with mineralisation.

It is interesting to note that distance to mafic intrusives (650m buffer) has a much higher contrast C values than does distance to Williams and Naraku intrusives (4km buffer). This raises the question as to what role does mafic intrusions play in the genesis of Cu-Au deposits. The suggested role of mafics intrusives in IOCG deposits includes: (1) A potential source of sulphur ± metals (leached during hydrothermal activity or contributing directly), and (2) Rheological and chemical contrast (reduced). Butera (2004) implied a genetic link between mafic rocks and iron oxide Cu-Au deposits, based on spatial data analysis using weights of evidence and fractal analysis, with older pre-D_1 mafic intrusives being a source of sulphur ± metals.

7.5 Gravity

Weights of evidence indicated that gravity highs and steep gradients adjacent to gravity highs or gravity lows have a strong spatial association with the Cu-Au occurrences. The gravity highs are considered to reflect large volumes of mafic rock within the middle to upper crust. The gravity gradients are interpreted to reflect a combination of crustal scale basement architecture as well as the margins of large felsic intrusions.

Eloise, Starra, and Mt Elliot are located on the margins of gravity lows interpreted to represent the margins of Williams-Naraku type batholiths. An analogous scenario has been described by Skirrow (2000) where observed several of the major Au-Cu-Bi deposits of the Tennant Creek District lying broadly within or near a regional gravity gradient interpreted to represent a deep seated contact with low-density granitic material. Ernest Henry is located on the flanks of a gravity high considered to reflect a significant component mafic intrusive rock in the upper to middle crust. Many of the smaller occurrences within the Wonga Belt overly a gravity high. The gravity high does not reflect the surface geology, which is dominated by calc-silicates and felsic volcanics, and contains only a few % mafics. This suggests that there is potentially a significant component of mafic rock within the middle to upper crust of the Wonga Belt that is not exposed at surface.

7.5 Felsic Intrusives

O,C,H,S isotope studies suggest that magmatic fluids provide a dominant component to IRCG deposits, however they only have a moderate spatial association with coeval granites. If the Williams-Naruku granitoids are the source of the mineralising fluids, then the magmatic fluids must have travelled 4 kilometres or greater prior to deposition (whilst retaining their isotopic signature). Mafic intrusives cannot be ruled out as a fluid source since the isotopic signatures cannot discriminated between felsic and mafic derived fluids.

8. CONCLUSIONS

The main conclusions of this study are:

1) The weights-of-evidence method provides a simple and effective technique to test the spatial association of a diverse range of geologic information with Cu-Au ± iron oxide deposits in the Mount Isa Inlier, Australia. This is particularly effective due to the large amount of publicly available digital data and good exposure.

2) The weights-of-evidence method allows us to rank the best Cu-Au predictors, refine our current geological understanding of the potential critical ingredients involved in Cu-Au deposit formation and accordingly modify geological/exploration models.

3) The data driven approach highlights importance of:

    a. Proximity to the Corella Formation contact, particularly with Soldiers Cap Group.
    b. Proximity to magnetic highs, despite the complex spatial relationships between Cu-Au ore and magnetite described by Williams and Pollard, (2001).
    c. Proximity to N-S (350-15°) and ENE (40-75°) structures (potentially reactivated older basement architecture).
    d. Proximity to mafic intrusive rocks (amphibolites) providing S or reducing environment.
    e. Proximity to gravity gradients (interpreted to reflect crustal scale basement architecture) and gravity highs ().

4) The data driven approach highlighted the relatively weak spatial association between Cu-Au occurrences and intrusions Williams-Naraku Batholiths. If these granites were considered a source of metals in many of the deposits, then the magmatic fluids would have travelled significant distances from their source (commonly more than 4 km) prior to deposition.

5) The posterior probability Cu-Au maps generated clearly highlight the main deposits as well as new areas including ‘Ernest Henry’ and ‘Eloise’ type analogues.

6) The data driven 9 layer and 12 layer posterior probability Cu-Au maps delineate prospective areas comparable to expert knowledge driven analyses, however they are much more site specific. They have the additional characteristics of being well defined, reproducible, objective, and providing a quantitative measure of confidence.

7) The study has progressed our understanding on the critical ingredients involved the formation of Cu-Au deposits in the Mount Isa Inlier far beyond a simple empirical approach.

8) The results imply that fluid pathways and sites of fluid mixing are much more important than fluid sources for controlling the distribution of IOCG deposits. This understanding can possibly explain some of the diversity in the range of IOCG deposit types and models. A common mineralizing process could generate deposits

in a variety of host rocks depending on the fluid pathways. The dominance of the fluid pathways means that fluid sources cannot be clearly recognized from spatial associations of the deposits alone, and mineralizing fluids may be complex and heterogeneous in view of their possible interactions with a variety of wall rocks. A detailed understanding of fluid pathways and structures at all scales is the most important direction for future research. Mechanical modeling directed at understanding fluid flow in the Mt Isa Eastern Succession based on this structural knowledge will also be an important tool.

9) It is recommended that a technique with regional coverage that can effectively determine the distribution of extensive sodic-calcic alteration and more proximal potassic alteration would be a useful additional layer for the model (remote sensing such as ASTER derived mineral maps may potentially be a useful technique for mapping alteration patterns).

Acknowledgements

The research was supported by the predictive mineral discovery Cooperative Research Center (pmd*CRC) as part of the I2/3 Project: Total systems analysis, Eastern Succession, Mt Isa Project. We would like to thank David A-Izzeddin from Xstrata for helpful comments.

9. REFERENCES

Adshead N.D., Voulgaris P., Muscio V.N. (1998) Osborne copper-gold deposit. In (Eds.) Berkman D.A. and Mackenzie DH. Geology of Australian and Papua New Guinean Mineral Deposits. The Australasian Institute of Mining and Metallurgy, Melbourne. 793-800.

Adshead-Bell N.S. (2000) Structural constraints of the ironstone hosted Au-Cu Starra Deposit and Selwyn Range Region, Eastern Fold Belt, Mt Isa Inlier. Unpublished PhD thesis. James Cook University.

Bonham-Carter, G., 1994, Geographic information systems for geoscientists : modeling with GIS: Oxford, England, Pergamon, 1st ed.

Blake D.H. (1981) Intrusive felsic-mafic net-veined complexes in North Queensland. BMR Journal of Australian Geology and Geophysics. 6(1): 95-99.

Blake D.H. and Stewart A.J. (1992) Straigraphic and tectonic framework, Mount Isa Inlier. In (eds. Stewart AJ and Blake DH) Detailed studies of the Mount Isa Inlier. AGSO Bulletin 243. pp1-11.

Budd, A.R., Wyborn A.I. and Bastrakova I.V. (2002) The metallogenic potential of Australian Proterozoic granites. Geoscience Australia Record 2001/12.

Butera K (2004) The role of mafic rocks in the genesis of IOCG and base metal deposits. Mount Isa Eastern Succession, NW Queensland, Australia. In (eds.) Barnicoat A.C. and Korsch R.J. Predictive Mineral Discovery Cooperative Reseach Centre. Extended Abstracts from the June 2004 Conference. Record 2004/09. p21-22.

Carew M., Mark G. and Oliver N. (2004) Orthomagmatic processes and Fe oxide-rich 'ironstones' in the eastern fold belt, northwest Queensland. . In: McPhie, J. and McGoldrick, P. (editors), 2004. Dynamic Earth: Past, Present and Future. Abstracts of the 17th Australian Geological Convention, Hobart, Tasmania. Geological Society of Australia, Abstracts No. 73, p.59.

Connors K.A. and Page R.W. (1995) Relationships between magmatism, metamorphism and deformation in the western Mount Isa Inlier, Australia Precambrian Research 71: 131-153.

Davidson G.J. (1998) Variation in copper-gold styles through time in the Proterozoic Cloncurry goldfield, Mt Isa Inlier: a reconnaissance view. Australian Journal of Earth Sciences 45, no.3: 445-462

Ellis D.J. and Wyborn L.A.I. (1984) Petrology and geochemistry of proterzoic dolerites from the Mount Isa Inlier. BMR Journal of Australian Geology and Geophysics. 9: 19-32.

Foster D R W (2003) Proterzoic low-pressure metamorphism in the Mount Isa Inlier, northwest Queensland, Australia, with particular emphasis on the use of calcic amphibole chemistry as temperature-pressure indicators. Unpublished PhD thesis. James Cook University.

Giles D. and Nutman A.P. (2002) SHRIMP U-Pb monazite dating of 1600-1580 Ma amphibolite facies metamorphism in the southeastern Mount Isa block, Australia: Australian Journal of Earth Sciences, v. 49, p.455-466.

Hand M. and Rubatto D. (2002) The scale of the thermal problem in the Mount Isa Inlier. Geoloigical Society of Australia Abstracts. V. 67, p. 173.

Haynes D.W. Iron Oxide (-Gold) Deposits: Their Position in the Ore Deposit Spectrum and Modes of Origin; in Porter, T.M. (Ed.), Hydrothermal Iron Oxide Copper-Gold & Related Deposits: A Global Perspective, Volume 1; PGC Publishing, Adelaide, pp 71-90.

Hitzman M.W. (2000) Iron Oxide-Cu-Au Deposits: What, Where, When and Why; in Porter, T.M. (Ed.), Hydrothermal Iron-Oxide Copper-Gold & Related Depsoits: A Global Perspective, Volume 1; PGC Publishing, Adelaide, pp 9-25

Laing W.P. (1998) Structural-metsomatic environment of the East Mt Isa Block base-metal-gold province. Australian Journal of Earth Sciences 45, no.3: 413-428

Mark G., Oliver N.H.S., Williams., P.J., Valenta R.K. and Crookes R.A. (2000) The evolution of the Ernest Henry hydrothermal system. In Hydrothermal Iron Oxide Copper-Gold and Related Deposits: A Global Perspective. Edited by T.M. Porter. Australian Mineral Foundation, p. 123-136.

Mark G., Williams P., Ryan C., Van Achterbergh E. and Prince K. (2004) A coupled microanalytical approach to resolving the origin of fluids and the genesis of ore formation in hydrothermal deposits. In: McPhie, J. and McGoldrick, P. (editors), 2004. Dynamic Earth: Past, Present and Future. Abstracts of the 17th Australian Geological Convention, Hobart, Tasmania. Geological Society of Australia, Abstracts No. 73, p.97.

McLaren S., Neumann N., Sandiford M. and Wyborn (1999) Post-intrusion heating associated with high-heat-producing Proterozoic granites – implications for mineralisation? AGSO Research Newsletter 30: 23-30

Nye, P.B. and Rayner, E.O. (1940) The Cloncurry copper deposits, with special reference to the gold-copper ratios of the ores. Aerial, Geological and Geophysical Survey of Northern Australia, Report Queensland, No. 35, 38pp.

Oliver N.H.S. (1995) Hydrothermal history of the Mary Kathleen Fold Belt, Queensland, Australia. Australian Journal of Earth Sciences. Vol. 42: 267-279.

Page R. W. and Sun S.S. (1998) Aspects of geochronology and crustal evolution in the Eastern Fold Belt, Mount Isa Inlier. Australian Journal of Earth Sciences. 45: 341-361.

Perkins C., Wyborn L.A.I. (1998) Age of Cu-Au mineralisation, Cloncurry district, eastern Mt Isa Inlier, Queensland, as determined by 40Ar/39Ar dating. Australian Journal of Earth Sciences 45, no.2: 233-246

Pollard, P.J. (1998) Geological framework and mineralisation in the Mt Isa Eastern Succession, northwest Queensland. Australian Journal of Earth Sciences. Vol. 45: 327.

Queensland Department of Mines and Energy 2000, Northwest Queensland Mineral Province Report, Queensland Department of Mines and Energy, Brisbane.

Queensland Department of Natural Resources and Mines 2002. QMIN - Queensland Mineral Resource Database MINOCC 2002 - Microsoft Access Database, Version 3.0, December 2002, Department of Natural Resources and Mines.

Queensland Department of Natural Resources and Mines 2003. Geoscience data: Queensland surface and drill hole geochemistry data. Mount Isa Eastern and Western Block Exploration. January 2004, Department of Natural Resources and Mines.

Ryan A (1998) Ernest Henry copper-gold deposit. In (eds.) Berkman DA, Mackenzie DH. Geology of Australian and Papua New Guinean Mineral Depsoits. Australasian Inst Mining Metall 22: 759-768.

Skirrow R.G. Gold-copper-bismuth deposits of the tenant creek district, Australia: a reappraisal of diverse high-grade systems; in Porter, T.M. (Ed.), Hydrothermal Iron Oxide Copper-Gold & Related Deposits: A Global Perspective, Volume 1; PGC Publishing, Adelaide, pp 149-160.

Skirrow R.G. and Walshe J.L. (2002) Reduced and oxidised Au-Cu-Bi Iron Oxide Depsoits of the Tennant Creek Inlier, Australia: An integrated Geologic and Chemical Model. Economic Geology, Vol. 97 (6): 1167-1202

Skirrow, R., 2004. Iron oxide Cu-Au deposits: An Australian perspective on their unifying characteristics. In: McPhie, J. and McGoldrick, P. (editors), 2004. Dynamic Earth: Past, Present and Future. Abstracts of the 17th Australian Geological Convention, Hobart, Tasmania. Geological Society of Australia, Abstracts No. 73, p.121

Sleigh, D.W.W. (2002) The Selwyn Line tabular iron-copper-gold system, Mount Isa Inlier, NW Queensland, Australia. In: (Eds.) Porter T.M. Hydrothermal iron oxide copper-gold & related deposits: A global perspective. PGC Publishing, Adelaide. vol. 2. 77-93.

Williams, P.J., De Jong, G., Verran, T. (1993) Evolution of Na-K-Fe-Si metasomatism and mineralisation associated with the Cloncurry Fault, SE Mount Isa Inlier: a comparison of Kiruna –Olympic type systems. Geol. Soc. Aust. Abstr. 35: 56-57.

Williams, P.J. (1994) Iron mobility during synmetamorphic alteration in the Selwyn Range area, NW Queensland: implications for the origin of ironstone-hosted Au-Cu deposits. Mineralium Deposita 29: 250-260.

An introduction to the Metallogeny of the McArthur River-Mount Isa-Cloncurry Minerals Province. Economic Geology. Vol. 93: 1120-1131

Wyborn, L.A.I., Heinrich, C.A., and Jaques, A.L., 1994 Australian Proterozoic mineral systems: Essential ingredients and mappable criteria. The Australasian Institute of Mining and Metallurgy, Publication Series, 5/94, 109-115.

Multiple generations of metal and sulphur contribution from mafic rocks to the IOCG budget of the Mount Isa Eastern Succession.

Kris Butera[1], Nick Oliver[1], Mike Rubenach[1], Bill Collins[1] & James Cleverley[1]

[1]Predictive Mineral Discovery Cooperative Research Centre and Economic Geology Research Unit
School of Earth Sciences, James Cook University, Townsville, QLD 4811

ABSTRACT

One of the most perplexing issues in the understanding of Iron Oxide Copper Gold deposits is the source of their metals and sulphur. Equally complex is an emerging picture of a protracted history and spatial complexity of sulphide precipitation, which is masked by the complicated history of multiple structural-metamorphic and hydrothermal events. The main outcome of this study is the realisation that although some metals were probably supplied by the crystallisation of the ca.1530Ma Williams-Naraku batholith, other, older sources of S and metals are highly apparent. Protracted mafic magmatism and associated exsolved S and metal bearing NaHCOS phases, particularly at 1686Ma and 1660Ma, and subsequent repeated leaching cycles (1640Ma, 1600-1580Ma and 1530Ma) were probably responsible for all of the sulphur and much of the metals now residing in the IOCGs. We cannot readily tell whether, or by how much, 1600Ma to 1530Ma ores derived most of their S (and at least some metals) by leaching of previous disseminated 1686Ma sulphides, except that the prospectivity analysis reveals that these components were likely sourced from an area <1km from the present deposits (mafic bodies). The strong possibility also remains that some of the deposits were derived by short distance remobilisation of actual 1686Ma orebodies.

Keywords. IOCG, mineralisation, weights of evidence, fractal analysis, mafics, exsolution, metamorphism, remobilisation

1. INTRODUCTION

The search for economically significant iron oxide-Cu-Au (IOCG) mineralisation in the Mount Isa Eastern Succession has proven to be an elusive task for explorationists over recent years. Exploration has been partly hampered by an inadequate set of ore genesis models. One of the most perplexing issues in the understanding of these deposits is the source of their metals and sulphur. Equally complex is an emerging picture of a protracted history and spatial complexity of sulphide precipitation, which is masked by the complicated history of multiple structural-metamorphic and hydrothermal events. The sustained, and to some extent renewed, focussing of exploration on these deposits is an immediate necessity, in order to overcome ever-depleting reserves.

What were the source(s) of metals and sulphur, via what processes did they contribute to the ores, and at what stage of the geological history were they incorporated into the IOCG budget? Can we predict the potential for significant new IOCG mineralisation, and identify where new deposits are most likely to be?

Paramount to recent investigations in the determination of metal and sulphur sources, is the discovery of a number of pieces of evidence that implicate mafic magmas and rocks as potential significant contributors to the overall deposition of IOCG ore. In this report, we outline the critical processes involving mafic rocks that contributed to the metal and sulphur budget of the Eastern Succession, we review the evolution of multistage fluid migration and structural controls on metal remobilisation, and we attempt to unify the spatial, temporal and geochemical progression of IOCG components from source to sink. Finally, in the context of exploration, we summarise the potential for significant undiscovered IOCG mineralisation in the Eastern Succession.

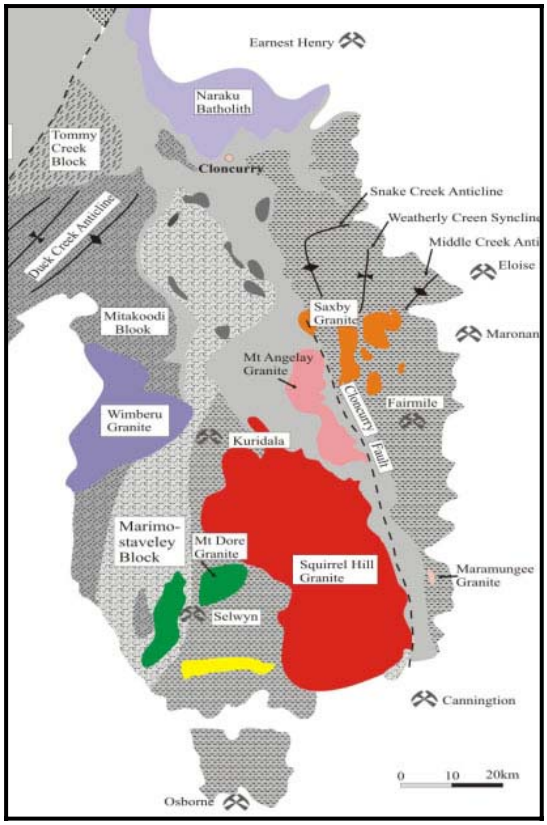

Figure 1. Geological map of the Mount Isa Eastern Succession, outlining different granites, key structural features and significant mineralisation, mostly discovered in the early 1990s. ***After Williams et al, 1998***

2. GEOLOGICAL BACKGROUND

The supracrustal sequences of the North Australian share a history of episodic rifting, sedimentation and volcanism between *c.* 1800 and 1620Ma (Beardsmore et al., 1988; Page et al, 1997; Page and Sun, 1998). At the core of the North Australian Craton is the Mount Isa Block, divided into three north-south trending fold belts, the Western Succession, the central older Kalkadoon-Leichhardt Belt and the Eastern Succession, cut by regional reverse and/or strike-slip faults (Blake, 1987; Blake and Stewart, 1992; O'Dea et al., 1997; MacCready et al., 1998).

The Eastern Succession of the Mount Isa Inlier is comprised predominantly of c. 1760 to 1730 Ma Mary Kathleen Group, and the c. 1690Ma to 1640 Ma Soldiers Cap Group. The latter in particular hosts numerous mineralisation styles, but is most noted for its world class IOCG and Broken Hill type Ag-Pb-Zn deposits (Williams, 1998; Williams and Pollard, 2003). Cu, Cu-Au, Au-only and minor other types of deposits are scattered throughout the Soldiers Cap Group.

Multiple episodes of bimodal magmatism occurred during both extensional and compressional events, leading to the complicated structural and thermal evolution now observed in the Eastern Succession (Fig. 2). Mafic tholeiitic intrusives (1686Ma) and volcanics (1660Ma Toole Creek Volcanics) were emplaced predominantly during and soon after the deposition of the Soldiers Cap sediments in an extensional basin setting. Less voluminous mafic intrusions were emplaced during E-W shortening and regional metamorphism at 1600Ma, preserved in the core of the Snake Creek Anticline, and at c. 1530Ma along the Cloncurry Fault and nearby around Mt Angelay, intimately associated with voluminous I- to A-type felsic magmatism of the Williams-

Naraku batholith. Most of the mafic rocks of the Eastern Succession were amphibolitised during peak metamorphism at ~1600Ma.

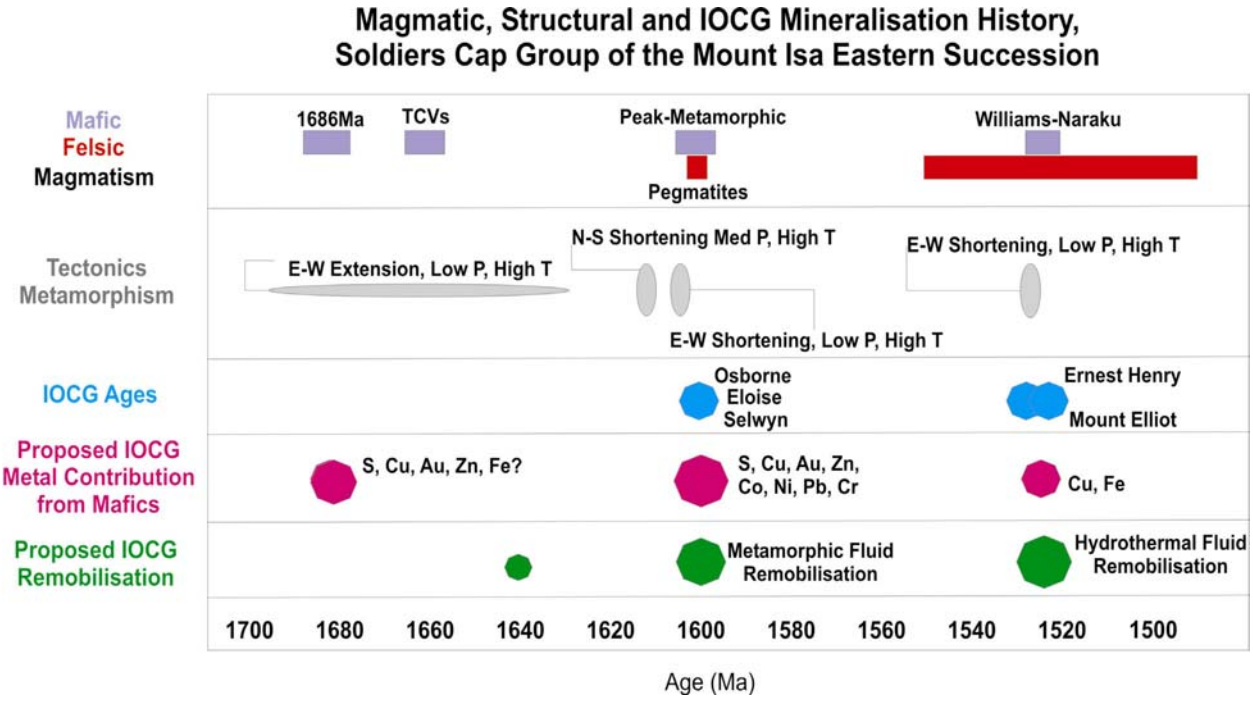

Figure 2. Summary of the magmatic, structural and IOCG mineralisation history of the Soldiers Cap Group, with proposed timing of metal and sulphur contributions from mafic rocks, and proposed IOCG remobilisation events. TCV = Toole Creek Volcanics.

3. NATURE OF MAFIC MAGMATISM

The geochemistry of tholeiitic intrusive and basaltic mafic rocks gives an insight into the nature of the underlying mantle, which in turn can help to constrain fundamental geodynamic, tectonic and deep metal source region controls for the varying mineralisation types. Scott et al (2000) made a number of interpretations of the nature of mafic magmas and the source regions of mafic melts of the Mount Isa Western Succession and McArthur River Basin. They concluded that the chemistries of these magmas were typical of continental flood basalts, and that they were not derived from plume- or rift- related processes. Rather, they were thought to be generated by a long-lived thermal anomaly, via convection initiated by subduction events in the Arunta Block of central Australia, melting the lithospheric mantle. Evidence for this reasoning includes the unlikelihood of continual lithospheric melting by a plume head over a 225 My period. Ellis & Wyborn (1984) studied multiple generations of mafic rocks from the Mount Isa Block and their conclusion as to the origin of the Eastern Succession mafics was in agreement with Scott et al (2000).

However, our geochemical study reveals that the mafic rocks of the Soldiers Cap Group most likely developed in a back-arc basin. Irrespective of the age of the mafic rocks within and emplaced into the Soldiers Cap Group, their chemistry is remarkably similar, indicating that they were all derived via similar processes from parental magmas of a common composition. We infer a back-arc basin basalt chemistry on the basis of decoupled spider-gram patterns that indicate a mix between an enriched MORB source that has undergone high degrees of partial

melting (flat REE pattern) and a steeper slope for lighter elements reflecting a subducted slab component (Figure 3). A distinctive feature of the chemistry of the mafic rocks is a consistently high Pb content (25-30ppm). We interpret this as a consequence of a chlorine flux during partial melting of a contaminated subducted slab.

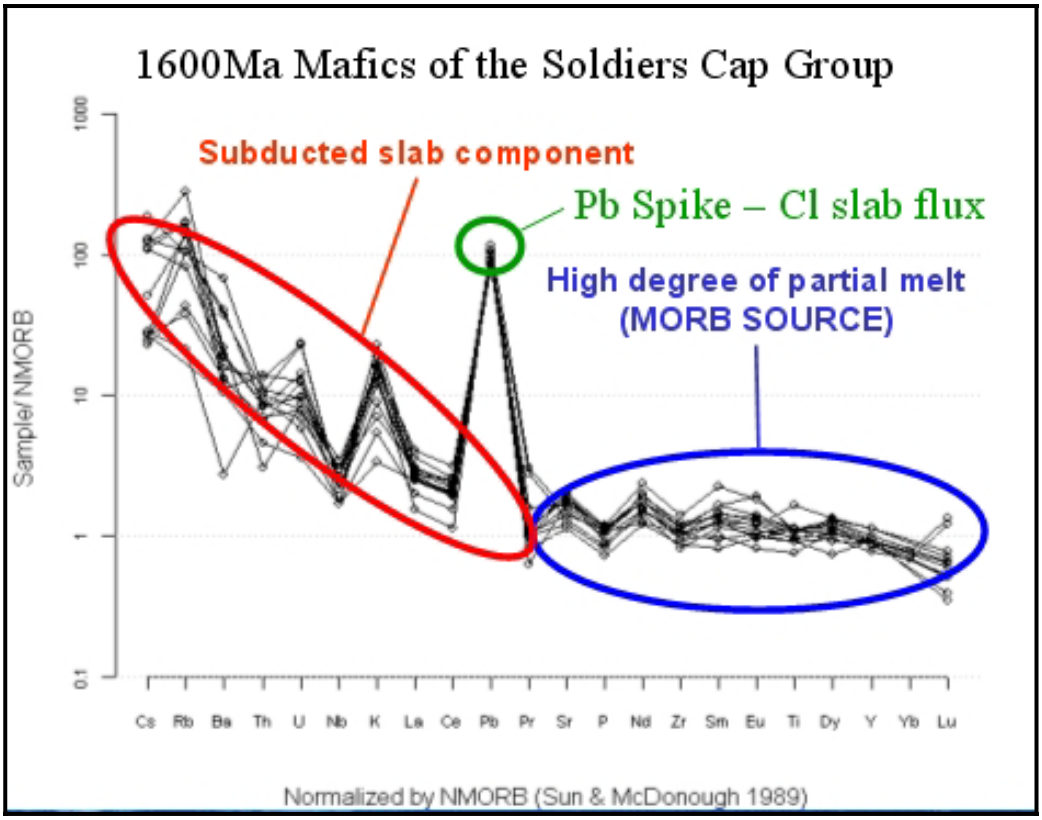

Figure 3. Typical spider diagram (multi-element plot) of 1600Ma mafic rocks from the Eastern Succession, normalised to NMORB (after Sun & McDonough, 89). Highlighted are the flat REE patterns, indicating high degrees of partial melting of an EMORB source, high Pb spike typical of magmas that have had a significant Cl contribution from subducted slabs, and the variability of the more mobile LILE and HFSE elements also typical of back-arc basalts. Mafic rocks at 1686 and 1530 Ma show similar trends.

Ce/Y ratios were used to determine the depth at which the mafics fractionated, based on the technique of Collins and Mantle (submitted). For the 1686 Ma mafics, a pressure of ~2.2kb was determined, corresponding to a source depth of as shallow as 8km. Thermodynamic modelling using the pMelts software of Ghiorso et al (2002) indicates that these mafic rocks were derived via the fractionation (to 58%) of a high Fe-picrite parental magma, with an initial liquidus temperature of 1377^{o}C at 2.2kb, and an initial H_2O content of 0.5wt% (Table 1).

The Ce/Y ratios of 1660, 1600 and 1530Ma mafic rocks indicate they formed at pressures greater than 2.2kb, reflecting intermittent crustal thickening, and hence deeper mafic source regions, during the post-1686 orogenic events. Modifying the pressure appropriately in the pMelts models yields similar results to the 1686 Ma model regarding Fe-rich picritic parental magmas and a high % fractionation. All the models require a contribution of H_2O in the source region in order to converge upon the real compositions. True continental rift basalts would be completely anhydrous, thus supporting our hypothesis of a hydrous (and Cl-bearing) subducted slab component to the magma.

T (C)	P (kbars)	Fractionation %	SiO2	TiO2	Al2O3	Fe2O3	FeO	MnO	MgO	CaO	Na2O	K2O	P2O5	H2O
1377	2.2	0.01	48.28	0.51	9.25	1.34	9.07	0.15	16.95	12.33	1.03	0.08	0.03	0.51
1357	2.2	2.79	48.5	0.53	9.51	1.37	9.07	0.15	16.03	12.67	1.06	0.08	0.03	0.53
1337	2.2	5.36	48.71	0.54	9.77	1.41	9.05	0.15	15.13	13	1.09	0.09	0.03	0.54
1317	2.2	7.75	48.91	0.56	10.02	1.45	9.02	0.15	14.27	13.32	1.11	0.09	0.03	0.56
1297	2.2	9.97	49.12	0.57	10.27	1.48	8.97	0.15	13.44	13.64	1.14	0.09	0.03	0.57
1277	2.2	12.03	49.32	0.58	10.51	1.52	8.92	0.15	12.65	13.95	1.17	0.09	0.04	0.58
1257	2.2	13.96	49.52	0.6	10.75	1.55	8.85	0.15	11.88	14.25	1.19	0.1	0.04	0.6
1237	2.2	21.25	49.37	0.64	11.5	1.6	9.15	0.16	10.93	13.96	1.3	0.1	0.04	0.65
1217	2.2	31.92	48.93	0.72	12.76	1.64	9.81	0.18	9.81	13.06	1.48	0.12	0.05	0.75
1197	2.2	40.07	48.55	0.8	13.95	1.66	10.39	0.21	8.76	12.2	1.66	0.14	0.05	0.86
1177	2.2	46.49	48.24	0.86	15.08	1.67	10.9	0.23	7.77	11.36	1.85	0.15	0.06	0.96
1157	2.2	51.69	48	0.92	16.14	1.68	11.34	0.26	6.85	10.54	2.03	0.17	0.06	1.06
1137	2.2	58.01	47.99	1.03	16.31	1.79	12.07	0.29	6	9.72	2.21	0.19	0.07	1.22
			Composition typical of 1686Ma Soldiers Cap Group Mafics											

Table 1. pMelts thermodynamic modelling of the fractionation of an H_2O-bearing Fe-picrite primary magma composition. At about 58% fractionation, the chemistry of the remaining liquid reflects the observed geochemistry of 1686Ma mafic rocks of the Soldiers Cap Group.

4. SPATIAL RELATIONSHIPS OF MAFICS AND MINERALISATION

In trying to determine the sources of sulphur and metals for IOCGs and base metal mineralisation for the Soldiers Cap Group, we conducted Weights of Evidence and Fractal Analysis of spatial data. These two methods were applied over a study area of the Mount Angelay and Selwyn 1:100000 Geological Map Sheets (Figure 4).

4.1 Weights of Evidence

Weights of Evidence has been used in recent years to measure the spatial relationships of geological units and mineralisation, and to evaluate and rank the most significant geological features in order to help build process models for the genesis of a number of deposit types. Weights of Evidence measures the strength of a spatial relationship of a set of 'training data points' i.e. mineral deposits, with any spatial data set such as lithological or structural units. The basis for the method is the "chance of a mineral deposit falling within an area surrounding the studied unit (i.e. within a buffer of a certain radius around that unit), over the chance that it does not sit within that area." The parameter derived from this ratio, which measures the strength of spatial relationship of a deposit to the studied data set, is termed the Contrast Value, while the statistical strength of the contrast value is referred to as the Confidence. In this study we consider a Contrast Value > 1 significant.

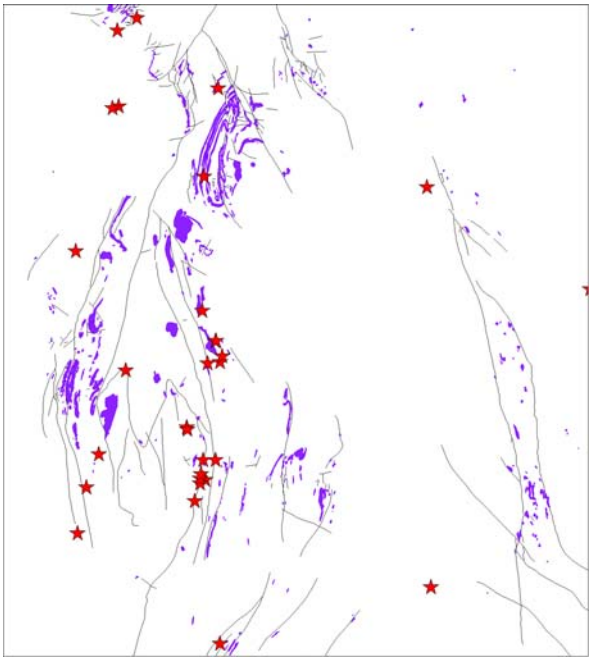

Figure 4. Map of spatial association of deposits, mafic rocks and faults in the study area – Mount Angelay and Selwyn 1:100000 sheets. Lines are faults, blue areas are mafics, red stars are IOCGs, black lines are faults.. Area ~75km x 85km.

This study has applied the Weights of Evidence test to IOCG deposits, Cu Deposits, all metalliferous deposits, large deposits (>500t metal), Au-only deposits and some rock chip geochemistry in the Mount Angelay and Selwyn 1:100K Geological Sheet Areas. Results are summarised in Table 2.

Ranking	Key Ingredient	Contrast	Confidence
1	Faults that intersect areas of mafics (0-250m)	7.8	18.7
2	Major Faults (0-100m)	2.18	4.76
3	Mafic Rocks (0-250m)	1.71	3.48
4	Medium Faults (0-100m)	1.53	2.1
5	Granites (all scales)	Insignificant	Insignificant
6	Minor Faults (all scales)	Insignificant	Insignificant

Table 2. Summarised results of WOE of lithological and structural units for IOCGs of the Selwyn-Angelay Study Area. [define medium vs minor faults]

IOCG deposits display a similar strength in spatial relationship to mafics (4 deposits, contrast= 2.24, confidence = 4.46 at 200-300m) compared with major faults (6 deposits, contrast = 2.18, confidence = 4.75 at 0-100m). There are 7 IOCG deposits within 500m of mafic rocks compared to 8 IOCG deposits within 500m of major faults. Most of the IOCG deposits optimally distanced 0-100m from major faults are concenctrated along the older Mount Dore Fault, whereas the IOCGs related to mafics are more regionally distributed.

Faults that intersect area of mafic rocks provide the best predictors for IOCG deposits (8 deposits, contrast = 7.78, confidence = 18.73 at 0-250m). These results are permissive of a model whereby mafic rocks may be the dominant source, or trap, of metals and sulphur for these deposits. Faulting is implicated as a process that may have enabled concentration or transport. Mafic rocks are also implicated in the genesis of both Cu-deposits and large deposits, and may act as the source of sulphur for all deposits. [we need to consider the meaning of the association a little more – source or trap, role of faults, mafics chemically favourable to sequester S and metals that happen to be moving through from elsewhere?]

These results are supported by the WOE study of Mustard et al (2005) whereby mafics demonstrate the strongest spatial association with IOCGs of all lithological units over the whole of the Eastern Succession. These results are also consistent with those of Ford and Blenkinsop (in prep) whereby mafic rocks of the Eastern Succession have an 88.5% correlation to IOCG deposits.

4.2 Fractal Analysis

Following Mandelbrot's (1983) hypothesis that minerals in the crust might have fractal distributions, several studies have demonstrated this by applying the box counting technique to analyse the spatial distribution of mineral deposits (e.g. Carlson, 1991; Blenkinsop, 1994; Agterberg et al. 1996; Blenkinsop and Sanderson, 1999). Genetic implications about mineralising systems can be drawn from the box counting fractal dimension, which measures the degree of clustering of the deposits. In this study the spatial distribution of metal deposits and the distribution of mafic rocks were analysed using binary images in the freeware program ImageJ. An image of the spatial distribution of deposits was produced with each deposit occupying one pixel, and box counting of this image was compared to box counting of a binary image of the distribution of mafic rocks. Box counting was initially performed over a range of box sizes from 0.34 km to 34.2 km. These data showed typical patterns of roll-off at small box sizes. The range of box sizes over which the data were linear was 8.53 km to 34.2km. Regression between these limits was used to derive the fractal dimensions, standard errors of regression and correlation coefficients. The results (Table 1) show that the fractal dimensions of mafic dykes (D = 1.43 ± 0.036) and mineral deposits (D = 1.43 ± 0.047) are effectively identical (Table 3). The results are consistent with those of Ford et al (2005) who obtained a fractal dimension of 1.42 ± 0.11 for IOCGs in the Eastern Succession.

	Regression Limits (km)		Number (Deposits)	Fractal Dimension	Standard Error	Correlation Coefficient
	Min	Max	N	D	E	R
Mafics	8.53	34.2	-	1.4345	0.0357	0.997221
Deposits	8.53	34.2	240	1.432	0.0468	0.99523

Table 3. Results of Fractal Analysis study of mafic rocks and mineral deposits over the Angelay-Selwyn study area

4.3 Summary of Spatial Associations

The strength of the spatial relationships of mafic rocks to IOCGs and base metal deposits is strongly permissive of a genetic relationship between the two, and as such has led us to undertake a comprehensive study of the role of mafic rocks in IOCG mineralisation.

5. 1686MA EVENT

The 1686Ma mafic intrusions, most of which have been amphibolitised by varying degrees of metamorphism at 1600-1580Ma are by far the most voluminous of the mafic rocks of the Eastern Succession, and are the rocks that display the strong spatial relationship to IOCG mineralisation. The 1686Ma (and similarly the 1660Ma Toole Creek Volcanics) mafic rocks of the Soldiers Cap Group were derived via the strong fractionation of an Fe-picrite parental magma at pressures of about 2-2.5kb (depths of about 8km). This may reflect fractionation in the mid to upper crust, or, more likely, that the crust was very thin, and the magmas fractionated just below the Moho. Given a typical modern day oceanic crust thickness of 5 km, this implies that the basalts were generated in a highly attenuated rifted continental environment that almost resulted in generation of oceanic crust.

One of the most intriguing features of the geochemistry of these mafic rocks is the consistent decrease in S, Cu, Au and Zn with increasing total Fe (Figure 6). The total Fe of the rock reflects the increasing degree of fractionation. It is a primary geochemical feature and is not a function of metamorphic or hydrothermal chemical overprinting (Foster, 2003), as indicated by Figure 7, which highlights the consistent immobility of Fe between igneous textured and amphibolitised mafic rocks from the Snake Creek Anticline.

The remarkably high levels of S (1500ppm) and metals at lower degrees of fractionation (~11wt% Fe2O3T) are also inferred to be primary features. Primary sulphides are present in the mafics only as late crystallisation stage interstitial pyrite and chalcopyrite associated with magnetite. These sulphides reflect the composition of a fluid that has exsolved from the system during cooling. For a given Fe content, levels of S and metals below the maximum are inferred to represent depletions caused by the passage of metamorphic or hydrothermal fluids at 1600 Ma or younger. Points lying close to the indicated line are samples that best preserve igneous textures and are least altered. The systematic decrease in the S and metal concentrations of these magmas with increasing Fe content can not be explained by orthomagmatic sulphide precipitation, because these melts lie well below the sulphide saturation values at 2.2kb (Mavrogenes and O'Neil, 1999). Additionally, we have made no field observations of orthomagmatic sulphide cumulates in any rocks of this age anywhere in the Mount Isa Eastern Succession. We propose that the decrease in S and metal concentrations with increasing fractionation reflects the increasing ability of exsolved aqueous fluid to transport these elements out of the magmatic system. Some of the Fe-oxides and Au-bearing iron and iron-copper sulphides present in the mafic rocks as interstitial minerals to late stage magmatic silicates were most likely precipitated from this exsolving fluid.

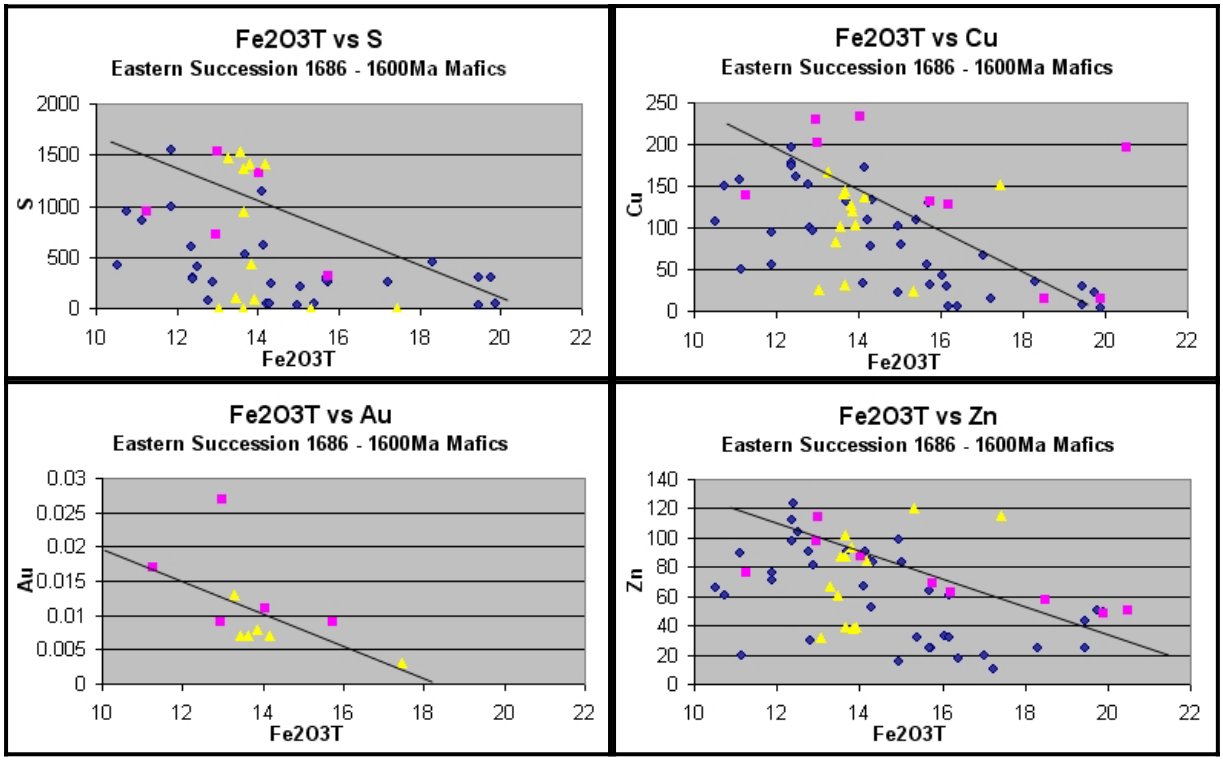

Figure 6a-d. Fe2O3T vs S, Cu, Au, Zn displaying consistent decreases in S and metals with increasing Fe, fractionation. The slope of the line on each graph indicates the elemental loss with increasing fractionation. Points below the lines represent elemental loss during metamorphism, while points above the lines represent enrichment associated with hydrothermal alteration. Data from KB 1686MA (pink), KB 1600Ma (yellow) and Ozchem Database 1686Ma (blue).

We can estimate the minimum amount of S, Cu and Au that has been exsolved from the mafics and potentially contributed to the overall IOCG budget, by taking into account that the mafic rocks intimately associated with IOCG mineralisation average around 15.6wt% Fe_2O_3 (total). We can also determine the amount of S and metals in the melt at around 11wt% (initial Fe content of pre-fractionated magma), which appears to correlate with the peak of the S, Cu, Au and Zn concentrations (Fig 6a-d). Along with ~1.22wt% H_2O available to leave the system at 15.6wt% Fe_2O_3 (total) (Table 1) are ~350ppm S, ~10ppb Au, and ~55ppm Cu. For the measured volume of ~$2x10^{11}$ m^3 down to 2000m depth for mapped 1686Ma mafic rocks of the Angelay-Selwyn area, this corresponds to ~$2.1x10^8$t S, ~$3x10^7$tCu and ~6000tAu, or an IOCG deposit @ 1% Cu and 0.5g/t Au of ~3Bt. This is ~10 times more mineralisation than has been thus far discovered in the area (334Mt). Conservatively then, the observed surface outcrop of mapped mafic rocks of this age, extrapolated to 200m depth, can account for the total Cu budget of the district, if Cu was extracted and deposited at 100% efficiency at the time of final crystallisation of the mafic magmas. Even if transport and deposition processes were inefficient, the calculated maximum amounts of metals and sulphur that could have been derived in this manner are extraordinarily high compared to the known deposits.

Mafic Pluton - S and Metal Exsolution									
Pluton diameter	10000	5000	2500	1000	500	15000	20000	30000	40000
Pluton radius	5000	2500	1250	500	250	7500	10000	15000	20000
Pluton volume (assuming spherical)	5.2E+11	6.5E+10	8.2E+09	5.2E+08	6.5E+07	1.8E+12	4.2E+12	1.4E+13	3.3E+13
Pluton mass @3t/m3	1.6E+12	2E+11	2.5E+10	1.6E+09	2E+08	5.3E+12	1.3E+13	4.2E+13	1E+14
S loss from 11 - 15.6wt% Fe Fractionation (ppm)	350	350	350	350	350	350	350	350	350
Cu loss from 11 - 15.6wt% Fe Fractionation (ppm)	55	55	55	55	55	55	55	55	55
Au loss from 11 - 15.6wt% Fe Fractionation (ppm)	0.01	0.01	0.01	0.01	0.01	0.01	0.01	0.01	0.01
Zn loss from 11 - 15.6wt% Fe Fractionation (ppm)	26	26	26	26	26	26	26	26	26
S exsolved via fluid (tonnes)	5.5E+08	6.9E+07	8585916	549499	68687.3	1.9E+09	4.4E+09	1.5E+10	3.5E+10
Cu exsolved via fluid (tonnes)	8.6E+07	1.1E+07	1349215	86349.8	10793.7	2.9E+08	6.9E+08	2.3E+09	5.5E+09
Au exsolved via fluid (tonnes	15700	1962.5	245.312	15.7	1.9625	52987.4	125600	423899	1004797
IOCG deposit size max based on S (t ore)	2.7E+10	3.4E+09	4.2E+08	2.7E+07	3398751	9.2E+10	2.2E+11	7.3E+11	1.7E+12
IOCG deposit size max based on Cu (t ore)	8.6E+09	1.1E+09	1.3E+08	8634978	1079372	2.9E+10	6.9E+10	2.3E+11	5.5E+11
IOCG deposit size max based on Au (t ore)	3.1E+10	3.9E+09	4.9E+08	3.1E+07	3924990	1.1E+11	2.5E+11	8.5E+11	2E+12

Table 4. Approximate guide to the capability of various sized mafic plutons to exsolve S, Cu, Au. Calculations for pluton volume assume that the pluton is spherical. Mass based on average density of 3t/m^3 for mafic rocks. IOCG deposit size is based on 100% efficiency from source to sink and average IOCG deposit grade of 1% Cu and 0.5g/t Au.

6. **1600-1580MA EVENT**

Mafic magmatism occurred during the peak of metamorphism at c.1600Ma – 1580Ma, locally along the axial planar foliation of the Snake Creek Anticline, and in the Rosebud Syncline. Minor contributions of metals and sulphur may have occurred via the same exsolution process mentioned for the 1686Ma event, but the apparent extent of these syn-metamorphic intrusions is quite restricted.

The nature of the metamorphic fluids associated with this event are not well constrained, but a detailed study of mafic rocks over the Soldiers Cap Group has outlined another potentially significant process by which mafic rocks have contributed to the overall metal and sulphur budget of the Eastern Succession at this time.

Geochemical investigations of mafic rocks that have undergone varying degrees of metamorphism reveals that S and certain metals are scavenged from the rocks, proportional to the degree of metamorphic recrystallisation (or amphibolitisation). Figure 7 shows an isocon plot (after Grant, 1986) comparing igneous-textured dolerites retaining clinopyroxene and magnetite, compared with hydrothermally altered and/or amphibolitized and variably foliated equivalents. Clearly outlined is the significant loss of S, Cu, Au, Ni, Zn and Cr, while additions to the rocks via metamorphic fluids include Ba, U, Sn, Sb.

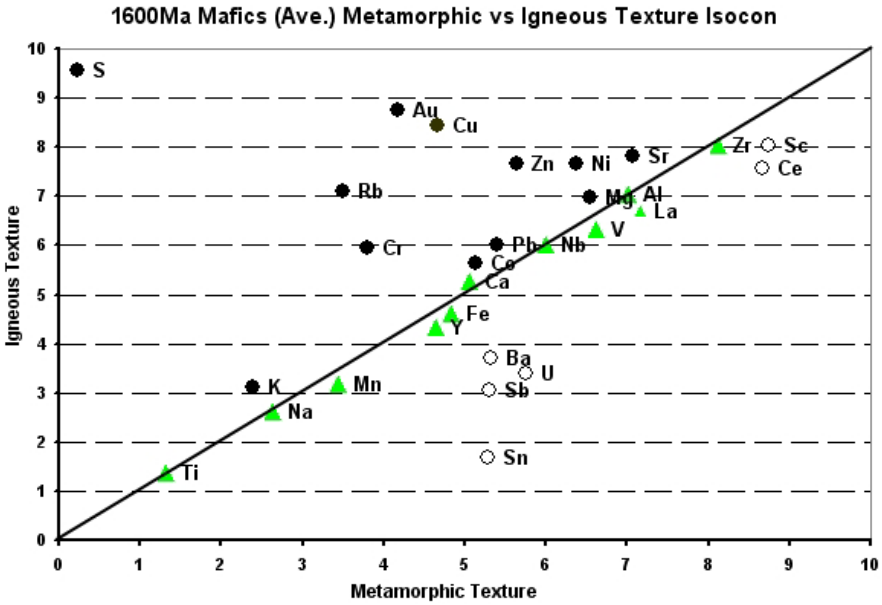

Figure 7. Isocon plot (with individual elements multiplied by factors which distribute them from 0 to 10) of average geochemical analysis for elements of igneous textured vs metamorphic textured dolerites from the Snake Creek Anticline. Significant loss of S, Au and Cu during metamorphism (black dots) have potentially contributed important amounts to the IOCG metal and sulphur budget. Green triangles are inferred immobile elements, including Fe; open circles are gains.

A semi quantitative analysis of the S and metal loss via metamorphic leaching process highlights the potential for mass contribution to the IOCG budget. Table 5 outlines the approximate loss of S, Cu and Au from primary igneous concentrations, to post metamorphic concentrations in mafic rocks. For the volumetrically significant 1686Ma mafic rocks, this represents leaching of 747ppm S, 53ppm Cu and 6ppb Au, or 66%, 26% and 37.5% respectively. For an assumed 2000m depth for mafic rocks over the Selwyn Angelay study area, and 70% amphibolitisation of all 1686Ma mafic rock (Foster, 2003), a minimum addition to the IOCG sulphur and metal budget via this process would be ~300Mt S, 21Mt Cu and 2470Mt of Au. On a 2 to 1 py:cpy ratio, and an average grade of 1% Cu, 0.5g/t Au, this addition could be capable of directly forming a minimum ~2Bt of IOCG ore, quite comparable to the amounts of these elements released by the aforementioned syn-magmatic volatile release (Table 4).

1686Ma Mafics			
Sample	**S**	**Cu**	**Au**
Average Igneous	1131.25	200.75	0.016
Average Metamorphic	383.67	148.00	0.010
Leached (ppm)	747.58	52.75	0.006
% Loss	66.08	26.28	37.50

1600Ma Mafics			
Sample	**S**	**Cu**	**Au**
Average Igneous	1435.00	126.75	0.004
Average Metamorphic	32.50	70.00	0.002
Leached (ppm)	1402.50	56.75	0.002
% Loss	97.74	44.77	52.38

Table 5. Average loss of S, Cu and Au from 1686Ma and 1600Ma mafic rocks during peak metamorphism at ~1600-1580Ma, highlighting significant leaching of S and metals.

7. 1530-1500MA EVENT

Many of the district's IOCG deposits have Ar-Ar and some U-Pb ages synchronous with the 1530-1500Ma Williams-Naraku Batholith of felsic to intermediate intrusions (e.g. Williams, 1998; Oliver et al., 2004), leading to hypotheses of a direct magmatic-hydrothermal connection between these granitoids and the IOCG deposits (e.g. Perring et al., 2000; Pollard, 2001). Other deposits such as Osborne have a clearly protracted history and major enrichments in Cu and S at or before 1580 Ma (Rubenach et al., 2001). A less direct connection between 1530 Ma magmas and IOCG deposits was drawn by Williams (1998) and Oliver et al. (2004) who demonstrated that some of the ingredients found in the deposits may have been leached from various country rocks by the passage of magmatic-hydrothermal brines. Albitisation of mafic rocks that had not previously been metamorphically recrytsallised, especially in the Northern portions of the Soldiers Cap may have contributed significant S and metals via leaching. However, S contents were not systematically analysed in previous work, and Oliver et al. (2004) reported no systematic Cu decrease by syn-1530 Ma albitizing fluids, despite clear evidence for leaching of Pb, Zn, Fe, K, Rb, Ba, Mn, Ni and Co, elements that are commonly found to be enriched in the deposits.

Recent studies have demonstrated that the most effective mechanism by which Cu and Fe may partition into a granitic-derived hydrothermal fluid is via magma mixing with mafic magmas (Kress, 1997); Edmonds et al, 2001; Hattori & Keith, 2001). Magma mixing and mingling is evident throughout the Williams-Naraku Batholith, with a large proportion of the batholiths comprised of dioritic and monzo/grano-dioritic intrusions. Further evidence is supported by magnetic highs at the base of the felsic plutons that we interpret to be large, underlying mafic bodies. The addition of this Cu and Fe into the IOCG district, along with remobilisation of pre-existing ores, has resulted in partial or complete destruction of recognisable pre-1530Ma ore characteristics and the possible accumulation of new ores. We interpret this age to be the final remobilisation age for most of the deposits, many of which initially began their lives as 1686Ma Cu-Au orebodies or proto-ores. An important observation by Perring et al (2000) at the Lightning Creek ironstone prospect, was the presence of high Ba, Cu and Fe contents in oxidised granite related fluids, yet an absence of barite and chalcopyrite – indicating sulphur absence in these fluids. If the felsic related hydrothermal fluids did play a part in IOCG deposition, it remains likely that earlier events were still responsible for the predominantly magmatic sulphur in the systems.

8. UNIFIED MODEL FOR IOCG GENESIS

In light of the new understanding of the critical processes involving mafic rocks in the contribution of significant concentrations of sulphur and metals, the consensus among many pmd*CRC researchers has recently detached from the notion that the granites were the key source of metals for IOCG mineralisation.

Spatial, temporal and geochemical evidence now supports a much more important role for mafic magmas and rocks than previously recognised. Complications in the attempt to directly link mafic rocks to IOCG mineralisation arise due to the nature of multiple periods of metamorphic and hydrothermal remobilisation. These hydrothermal, albitisation and metamorphic events at 1640Ma, 1600-1580Ma and 1530-1500Ma were all capable of remobilising pre-existing sulphide concentrations, from deposits, proto-ores or disseminated country rock metal accumulations, at

scales comparable to the degree of mafic-deposit fit in the prospectivity analysis, i.e. along 1640 to 1500 Ma fault zones.

At 1686Ma metal and sulphur accumulations in the upper crust were deposited via the exsolution of a metal-volatile rich fluid from mafic magmas. These concentrations were potentially focussed proximal to the mafic rocks, possibly in large, early extensional fault systems such as the Mt. Dore Fault Zone, or in disseminations at the top of the 1686 magma chambers. A localised metamorphic event with a possible association with albitisation at 1640Ma (M. Rubenach pers. comm.) may have had a minor remobilising effect on the metals and sulphur in the Snake Ck area. 1600Ma to 1580Ma metamorphism played a key role in scavenging sulphur and metals both from pre-(1686Ma) and syn-(1600Ma) mafic rocks, in addition to pre-existing accumulations from the earlier 1686Ma mafic rocks, leading to the formation of Osborne, and possibly Eloise. Oxidised hydrothermal brines and albitic fluids associated with the 1530Ma felsic-mafic mixed Williams-Naraku Batholith may have leached further metals, and potentially added more copper to the system directly, but probably did not directly contribute sulphur. These fluids and the associated structural regime at 1530-1500Ma provided the final spatial controls on ore genesis. Fluids derived from both the Williams Batholith and a direct or indirect primitive mafic source are implicated in the genesis of the Ernest Henry deposit (Cleverley & Oliver, (in revision); Oliver & Cleverley, 2004; this report).

A protracted history of uranium and REE remobilisation at 100m to km-scales was inferred at Mary Kathleen by Maas et al. (1988) and Oliver et al. (1999), with primary enrichment at 1740 Ma culminating in eventual ore accumulation by remobilisation at c. 1530 Ma. We infer similar processes for copper in the Eastern Succession. Despite the multiple additions of sulphur and metals, episodic remobilisation and ore precipitation, the results of the spatial association studies suggest that for the most part, the scale of overall IOCG remobilisation is on the order of less than ~750m. This explains the presence of mineralisation in c. 1590 Ma S2 folds in the Selwyn-Starra area, and at Eloise, older than the apparent 1550-1500Ma Ar-Ar age dates for mineralisation. Mixed ages at Ernest Henry include a c. 1650 Ma Re-Os age on bulk ore (Mark, pers. comm.), a 1600Ma Pb-Pb age for chalcopyrite (K. Bassano pers. comm.), and 1530 Ma U-Pb on ore stage titanite and a similar Re-Os age on molybdenite (Oliver et al., 2004; Mark et al., unpubl. data), suggesting that sulphur at least may have been derived from local mafic rocks (e.g. the Ernest Henry Diorite) or even pre- to syn-1600 Ma proto-ores, during a 1530Ma magmatic-hydrothermal brecciation and magnetite precipitation event. A summary diagram of the processes leading to IOCG ore deposition is given in Figure 8.

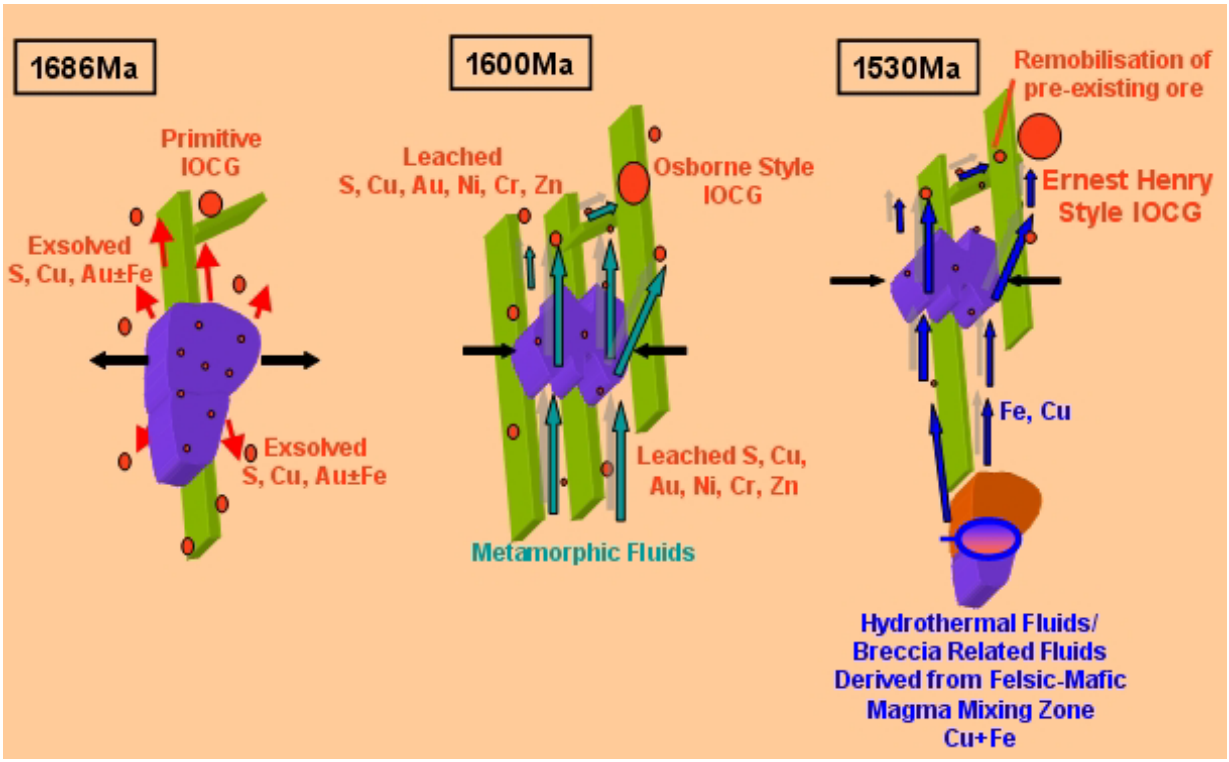

Figure 8. Evolutionary model of the contribution of S and metals via direct exsolution from mafic magmas at 1686Ma, metamorphic leaching at 1600Ma, and hydrothermal remobilisation with addition of Cu and Fe from mixed felsic-mafic magmatic fluids at 1530Ma.

9. EXPLORATION POTENTIAL AND TARGETING FOR IOCG DEPOSITS

We estimate that the total possible contribution of sulphur and metals from mafic rocks over the Selwyn-Angelay study area is grossly in excess of known ores, potentially being capable of forming a minimum 7Bt of IOCG ore. The inferred relative addition of new components during the evolution of the accumulated metal history was moderate to strong via direct exsolution of mafic magmas at 1686Ma, moderate via metamorphic leaching at 1600Ma and potentially moderate via hydrothermal fluids from the Williams-Naraku Batholith. The amount of IOCG and Cu mineralisation that has thus far been discovered is around 334Mt (based on all mineralisation in the GA Minocc database, with a cutoff of 500t contained Cu). Taking into account the present erosion level, and current exploration and mining capabilities down to a depth of ~1km, we believe that there is the potential for >1.5Bt of IOCG ore yet to be discovered in the area, especially for non-ironstone hosted Cu-Au, assuming ~75% transport and deposition efficiency of metals and sulphur.

In exploration terms, particularly for regions under cover, gravity highs (reflecting mafics) should be singled out as the first step for target generation. Figure 9 shows the relationship of some IOCGs with gravity. Following from mafics and gravity highs, are the critical ingredients for IOCGs as outlined by Mustard et al (2005), and for areas under Mesozoic cover would include magnetic highs and N-S and NE faults (mag worms or lineaments) for undercover exploration.

The main outcome of this study is the realisation that although some metals were probably supplied by the crystallisation of the Williams-Naraku batholith, other, older sources of S and

metals are highly apparent. Protracted mafic magmatism and subsequent repeated leaching cycles were probably responsible for all of the sulphur and much of the metals now residing in the IOCGs. We cannot readily tell whether, or by how much, 1600Ma to 1530Ma ores derived most of their S (and at least some metals) by leaching of previous disseminated 1686Ma sulphides, except that the prospectivity analysis reveals that these components were likely sourced from an area <1km from the present deposits (mafic bodies). The strong possibility also remains that some of the deposits were derived by short distance remobilisation of actual 1686Ma orebodies.

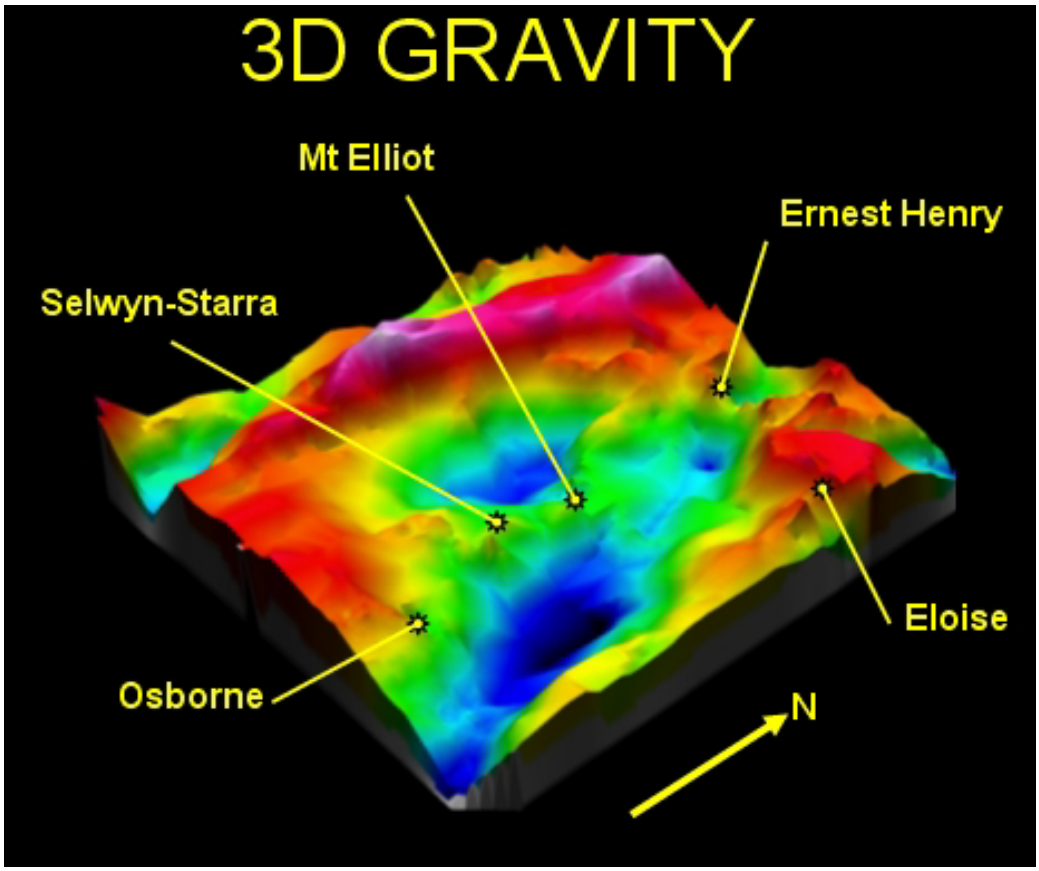

3D view of the gravity of the Mount Isa Eastern Succession, and associated IOCGs. Note the strong correlations of gravity highs and IOCG deposits.

10. REFERENCES

Agterberg, F. P., Cheng, Q., & Wright, D. F. 1996. Fractal modelling of mineral deposits. In:: Elbrond, J. and Tang, X. (eds) Proceedings of the International Symposium on the Application of Computers and Operations Research in the Minerals Industries. Montreal, Canada, 43-53.

Barnicoat, A.C. and Korsch, R.J. eds. Predictive Mineral Discovery Cooperative Research Centre – Extended Abstracts for the June 2004 Conference, Barossa Valley, 1-3 June 2004. Geoscience Australia Record 2004/9, pp. 21-22.

Beardsmore, T. J., Newberry, S. P. and Laing, W. P. 1988. The Maronan Supergroup; an inferred early volcanosedimentary rift sequence in the Mount Isa Inlier, and its implications for ensialic rifting in the middle Proterozoic of Northwest Queensland. Precambrian Research 40/41, 487–507.

Betts, P.G., Giles, D., Lister, G.S., Frick, L., 2002. Evolution of the Australian lithosphere. Australian Journal of Earth Sciences 49, 661– 695.

Blake, D.H., 1987. Geology of the Mount Isa Inlier and environs, Queensland and Northern Territory. Bureau Miner. Res. Geol. Geophys. Bull. 225, 83.

Blenkinsop, T.G. 1994. The fractal distribution of gold deposits. In : Kruhl, J.H. (ed) Fractals and Dynamic systems in Geosciences. Springer, Berlin, 247-258.

Blake, D.H., Stewart, A.J., 1992. Stratigraphic and tectonic framework, Mount Isa Inlier. In: Stewart, A.J., Blake, D.H. (Eds.), Detailed Studies of the Mount Isa Inlier. Australian Geological Survey Organisation Bulletin, vol. 243, pp. 1– 11.

Blenkinsop, T.G. and Sanderson, D.J. 1999. Are gold deposits in the crust fractals ? A study of gold mines in the Zimbabwe craton. Special Publication of the Geological Society of London, 155, 141-151.

Butera, K.M., and Blenkinsop, T.G., 2004. Fractal analysis of the spatial distributions of mafic rocks and mineralisation in the Eastern Succession, Mount Isa Inlier, Australia: Apossible genetic link. 4th International Conference, Fractals and Dynamic Systems in Geoscience. Technische Universität München, Germany, 19-22 May 2004. Abstracts16-19.

Butera, K.M., 2004. The role of mafic rocks in the genesis of IOCG and base metal deposits, Mount Isa Eastern Succession, NW Queensland, Australia. In: pmdCRC Focus On Science Conference. Barossa Valley. Abstracts. p21

Carlson, C. A. 1991. Spatial Distribution of Ore Deposits. Geology, 19, 111-114.

Cleverley, J.S., Oliver, N.H.S. (in revision) Equilirbium dynamic modelling of fluid-rock interaction concepts using HCh: Examples from K-alteration in Fe-oxide Cu-Au systems

Collins, W.C. and Mantle, G. (submitted). Moho control on arc basalt trace element geochemistry. Nature.

Edmonds, M., Pyle, D., and Oppenheimer, C., 2001. A model for degassing at Soufriere Hills Volcano, Monsterrat, West Indes, based on geochemical data. Earth and Planetary Science Letters, 186, 159-173

Ellis, D.J. & Wyborn, L.A.I., 1984. Petrology and geochemistry of Proterozoic dolerites from the Mount Isa Inlier. BMR Jounal 9, 19-32

Ford, A. and Blenkinsop, T.G., (in prep). Factors Controlling Base and Precious Metal Deposits, Mt Isa Inlier, Australia:
A new approach using Fractal Analysis and Weights of Evidence

Giles, D., Betts, P.G., Lister, G.S., 2002. Far-field continental backarc setting for the 1.80– 1.67 Ga basins of northeastern Australia. Geology 30, 823–826.

Ghiroso, M.S., Hirschmann, M.M., Reiners, P.W. and Kress, V. 2002. The pMELTS: A revision of MELTS for improved calculation of phase relations and major element partitioningrelated to partial melting of the mantle to 3 GPa. Geochem.Geophys. Geosyst., 3(5), 10.1029/2001GC000217

Giles, D., Betts, P.G. and Lister, G.S., 2004. 1.8–1.5-Ga links between the North and South Australian Cratons and the Early–Middle Proterozoic configuration of Australia. Tectonophysics 380, 27-41.

Hattori, H.H., and Keith, J.D., 2001. Contribution from mafic melt to porphyry copper mineralisation: evidence from Mount Pinatubo, Philippines, and Bingham Canyon, Utah, USA. Mineralium Deposita, 36, 799-806

Humphries, S.E., Thompson, G., Schilling, J.G. and Kingsley, R.A., 1985. Petrological and geochemical variations along the Mid-Atlantic Ridge between 46ºS and 32ºS: influence of the Tristan da Cuhna mantle plume. Geochimica et Cosmochimica Acta 49, 1445-1464.

Karlstrom, K.E., Harlan, S.S., Williams, M.L., McLelland, J., Geissman, J.W., Ahall, K.I., 1999. Refining Rodinia: Geologic evidence for the Australia –western US connection in the Proterozoic. GSA Today 9, 1 – 7.

Karlstrom, K.E., Ahall, K.-I., Harlan, S.S., Williams, M.L., McLelland, J., Geissman, J.W., 2001. Long-lived (1.8– 1.0 Ga) convergent orogen in southern Laurentia, its extensions to Australia and Baltica, and implications for refining Rodinia Precambrian Research 111, 5– 30.

Kress, V., 1997. Magma mixing as a source for Pinatubo sulphur. Nature, 389, 591-593

Laing, W.P., Beardsmore, T.J., 1986. Stratigraphic rationalization of the Eastern Mount Isa Block, recognition of key correlations with Georgetown and Broken Hill Blocks in an eastern Australian Proterozoic terrrain, and their metallogenic implications. Geological Society of Australia Abstracts 15, 114–115.

Laing, W.P., 1990. The Cloncurry terrane: an allochthon of the Diamantina orogen rafted onto the Mount Isa orogen, with its own distinctive metallogenic signature. Mount Isa Inlier Geology Conference. Victorian Institute of Earth and Planetary Sciences, Melbourne, Australia, pp. 19– 22.

Laing, W.P., 1996. The Diamantina orogen linking the Willyama and Cloncurry terranes, Eastern Australia. In: Pongratz, J., Davidson, G.J. (Eds.), New Developments in Broken Hill type deposits. University of Tasmania Centre Ore Deposit Studies Special Publication, vol. 1, pp. 67–72.

Maas, R., M. T. McCulloch, & Campbell, I.H. (1988). "Sm-Nd isotope systematics in uranium rare-earth element mineralization at Mary Kathleen uranium mine, Queensland." Econ. Geol. 82: 1805-1826.

MacCready, T., Coleby, B.R., Goncharov, A., Drummond, B.J. and Lister, G.S., 1998. A framework of overprinting oregens based on interpretation of the Mount Isa deep seismic transect. Economic Geology 93, 1422-1434.

Mandelbrot, B. B. 1983. The fractal geometry of nature. New York, W.H. Freeman and Company, pp. 468.

Mustard, R., Blenkinsop, T., Foster, D., Mark, G., McKeagney, C., Huddleston-Holmes, C., Partington, G., and Higham, M., 2005. Critical ingredients in Cu-Au±iron oxide deposits, NW Queensland:an evaluation of our current understanding using GIS spatial data modelling. Confidential report to the Cooperative Research Center for Predictive Mineral Discovery.

Myers, J.S., Shaw, R.D., Tyler, I.M., 1996. Tectonic evolution of Proterozoic Australia. Tectonics 15, 1431– 1446.

Nutman, A. P. & Ehlers K., 1998. Evidence for multiple Palaeoproterozoic thermal events and magmatism adjacent to the Broken Hill Pb–Zn–Ag orebody, Australia. Precambrian Research90, 203–238.

O'Dea, M.G., Lister, G.S., MacCready, T., Betts, P.G., Oliver, N.H.S., Pound, K.S., Huang, W., Valenta, R.K., 1997. Geodynamic evolution of the Proterozoic Mount Isa terrain. In: Burg, J.P., Ford, M. (Eds.), Orogeny Through Time. Geological Society Special Publication, vol. 121, pp. 99– 122.

Oliver, N. H. S., Pearson, P. J., Holcombe, R. J. & Ord, A. 1999. Mary Kathleen metamorphic-hydrothermal uranium-REE deposit: ore genesis and numerical model of coupled deformation and fluid flow. Australian Journal of Earth Sciences, 46, 467-484.

Oliver, N.H.S., and Cleverley, J.J., 2004. The role of sodic alteration in the genesis of iron-oxide copper gold deposits, eastern Mount Isa Block, Australia. Econ. Geol. 99, 1145-1176

Page R.W., Sun S-S. and MacCready, T., 1997. New geochronological results in the central and eastern Mt Isa Inlier and implications for mineral exploration. In: Geodynamics and Ore Deposits Conference, Australian Geodynamics Cooperative

Research Centre, February19–21, pp. 46–48. University of Ballarat, Ballarat.

Page, R. W. and Sun, S-S. 1998. Aspects of geochronology and crustal evolution in the Eastern Fold Belt, Mt Isa Inlier. Australian Journal of Earth Sciences 45: 343-361.

Perring, C. S., Pollard, P. J., Dong, G., Nunn, A.J. & Blake, K.L. 2000. The Lightning Creek sill complex, Cloncurry District, Northwest Queensland; a source of fluids for Fe oxide Cu-Au mineralization and sodic-calcic alteration, Economic Geology, 95, 1067-1089

Pickering, G., Bull, J. M. & Sanderson, D. J. 1995. Sampling power-law distributions. Tectonophysics , 248, 1-20.

Queensland Department of Mines and Energy, Taylor Wall & Associates, SRK Consulting Pty Ltd & ESRI Australia, 2000. North-west Queensland Minerl Province Report, Queensland department of mines and energy, Brisbane.

Raetz, M., Krabbendam, M. and Donaghy, A.G., 2002. Compilation of U–Pb zircon data from the Willyama Supergroup, Broken Hill region, Australia: evidence for three tectonostratigraphic successions and four magmatic events? Australian Journal of Earth Sciences 49, 965–983.

Scott, D.L., Rawlings, D.J. & Page, R.W., Tarlowski, C.Z., Idnurm, M., Jackson, M.J. and Southgate, P.N., 2000. Basement framework and geodynamic evolution of the Palaeoproterozoic superbasins of north-central Australia: an integrated review of geochemical, geochronological and geophysical data. Australian Journal of Earth Sciences 47, 341–380.

Sun, S. S. & McDonough, W. F., 1998 Chemical and isotopic systematics of oceanic basalts: implications for mantlecomposition and processes in: Magmatism in the ocean basins, Geological Society Special Publications 42, 313-345

Williams, P.J., and Blake, K.L., 1993. Alteration in the Cloncurry District; roles of recognition and interpretation in exploration for Cu-Au and Pb-Zn-Ag deposits. Contributions to the Economic Geology Research Unit 49

Williams, P.J. and Pollard, P.J., 2001. Australian Proterozoic Iron Oxide-Cu-Au deposits: an overview with New Metallogenic and Exploration Data from the Cloncurry district, Northwest Queensland. Explor. Mining. Geol. 10. 191-213

Williams, P.J., 1998. An introduction to the Metallogeny of the McArthur River-Mount Isa-Cloncurry Minerals Province. Economic Geology 93, 1120-1131

Geochemistry of albitites and related metasomatic rocks, Eastern Succession of the Mount Isa Block

M. J. Rubenach, N.H.S Oliver
Predictive Mineral Discovery Cooperative Research Centre @ Economic Geology Research Unit, JCU School of Earth Sciences, Townsville, Qld, Australia 4811.

ABSTRACT

Albitites and related metasomatic rocks (such as biotite-rich schists) are locally abundant in the Eastern Succession. They formed from infiltrating fluids over an extended period, the most important being 1630-1660 Ma and 1500-1530 Ma. The early group occur in the Soldiers Cap Group as veins and in shear zones, and are especially abundant in the Snake Creek Anticline and at the Osborne Mine. The second group occur as veins and replacement, and are particularly abundant in breccias of Corella beds, especially near the Cloncurry Fault, and are also spatially associated with intrusives of the Williams and Naraku batholiths. Chemical changes with albitization include addition of Na and removal of K, Fe, Mn, Cu, Pb and Zn. It is not known whether such removal of base metals contributed to mineralization, but a source of Fe is necessary for the metasomatic ironstones in the region and Mn occurs as a gangue mineral in some deposits. Isocon diagrams for the Osborne Mine are poorly defined in comparison with those for Snake Creek, and imply that many albitites in the Mine have a large component of infill. Metasomatic changes in the formation of biotite-rich schists include addition of Na and Mg, and biotite in such rocks was commonly enriched in Cl.

In any particular locality, similar values of $\delta^{18}O$ were obtained for albitites, metasomatic biotite-rich schists and unmetasomatized schists. 8 and 10‰ contours of the Snake Creek Anticline are not related to the stratigraphy or isograds, but are related to abundance of albitites, to metasomatized cordierite-bearing schists, and to the abundance of porphyroblasts in schists. Possible fluid sources are up-temperature infiltration from the Corella beds, or mantle-derived fluids, possibly related to distal carbonatites. The latter hypothesis is preferred.

Keywords: Cloncurry, metasomatism, albitites, isocons, oxygen isotopes

1. INTRODUCTION

This report deals with aspects of metasomatism and fluid-rock interaction during metamorphism of the Soldiers Cap Group and Corella beds in the period 1660-1500 Ma. The tectonothermal evolution is dealt with in the pmd*CRC Tectonothermal Evolution Report Rubenach (2005b). This report presents data and conclusions concerning geochemical changes during albitization and related biotite alteration and the sources of metasomatising fluids from an oxygen isotope perspective. More details as to the compositions and sources of the various fluids, and their implications regarding the genesis of cooper-gold deposits, can be found in the pmd*CRC report of Oliver et al. (2005).

2. CHEMICAL CHANGES ASSOCIATED WITH ALBITIZATION

In the Eastern Succession, albitization occurs sporadically in the amphibolite facies. Mary Kathleen/Duchess zone (although scapolitization is far more abundant there, Oliver et al., 1992). Albitization is more abundant in the Cloncurry/Osborne zone (e.g., Williams, 1994), in the amphibolite facies Soldiers Cap Group and in the greenschist to amphibolite facies Corella beds.

This section is mainly concerned with geochemical changes associated with albitization in the Cloncurry-Osborne zone. In particular it examines elemental losses and gains using isocon diagrams.

2.1 Albitization in the Snake Creek Anticline area

This has been considered in a number of publications (Rubenach & Barker, 1998; Rubenach & Lewthwaite, 2002; Rubenach, 2005a; Oliver et al., 2005). Albitization is widespread in the Soldiers Cap Group of the Snake Creek Anticline, particularly in the north and west (Fig. 1). It is particularly concentrated in the five albitite areas shown on Fig. 1. Although there is evidence of albitization in later events, most occurred early in the deformation history, D_1 according to Rubenach (2005a) but interpreted in this report as syn-D_{Ab} (1630-60 Ma- Tectonothermal Evolution Report). In contrast, albitization associated with breccias in the adjacent Corella beds and Mount Norna Quartzite close to the Cloncurry Fault occurred in the D_{3b} event, penecontemporaneous with emplacement of gabbros and the Saxby Granite at 1527 Ma. Within 2 km of the Cloncurry Fault, well over 50% of the Corella beds have been brecciated and albitized.

Albitites in the Soldiers Cap Group occur as veins (infill and replacement veins) and as replacement of beds of metapsammite or, less commonly, metapelite. Some veins are along shear zones, and Fig. 2 is a typical example. Muscovite has been selectively replaced, and with more extreme albitization biotite and quartz have also been replaced. Albite is typically fine-grained, and compositionally is An_{0-7}, with An_{2-5} most common. Albitite assemblages include combinations of biotite, staurolite, cordierite, andalusite, sillimanite, garnet, tourmaline and gedrite. Quartz is common in albitized metapsammite, and less common to absent in albitized metapelite. Apatite and rutile are common accessories, while ilmenite occurs in place of rutile in less albitized samples. Muscovite may be present as relicts or (rarely) as a late overprint. Biotite-rich/muscovite-absent schists commonly have replaced muscovite-rich schists and muscovite-rich metapsammitic rocks adjacent to albitites (generally on a scale of metres to tens of metres, e.g. Fig. 2). These have the same

assemblages as in albitites, but the proportion of biotite is much higher and the albite content lower.

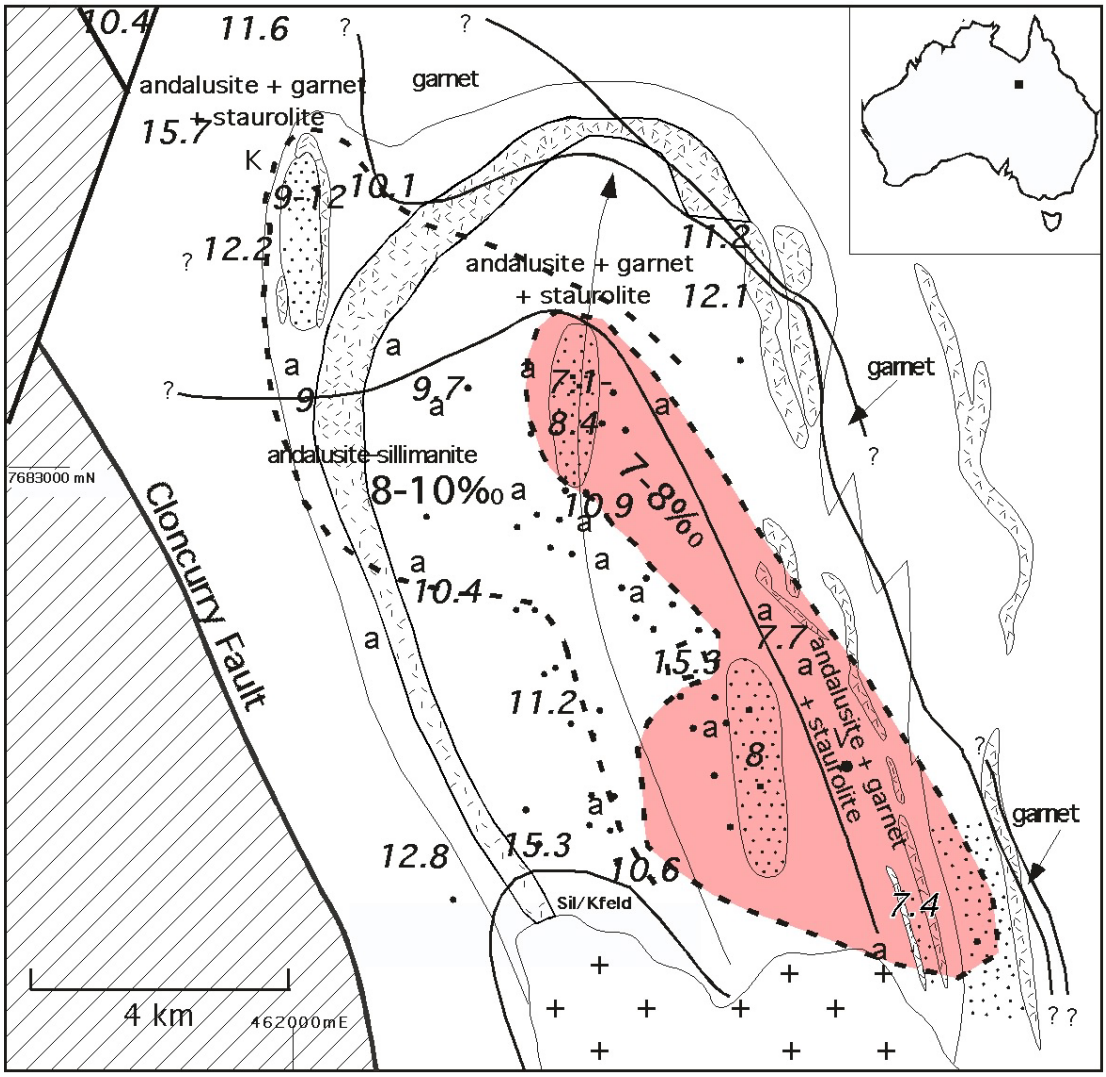

Fig. 1. Snake Creek Anticline, modified from Rubenach (2005b). Lined unit, Corella Beds. No pattern, Soldiers Cap Group. Areas with light dots represent main albitization areas, while additional early albitite localities are designated "a". Heavy dots are cordierite localities. Late albitites associated with breccias of Corella beds or Soldiers Cap rocks close to the Cloncurry Fault are not shown. Short line symbol, pre-D1 metagabbro/metadolerite/tonalite sills. Crosses, Saxby Granite. Numbers in italics are whole rock oxygen isotope values, with no distinction made between albitites, schists and biotite-rich schists. Contours at 8 and 10‰ are indicated – note that the contours are not parallel to either the stratigraphic contacts or the isograds, but instead appear related to early albitization.

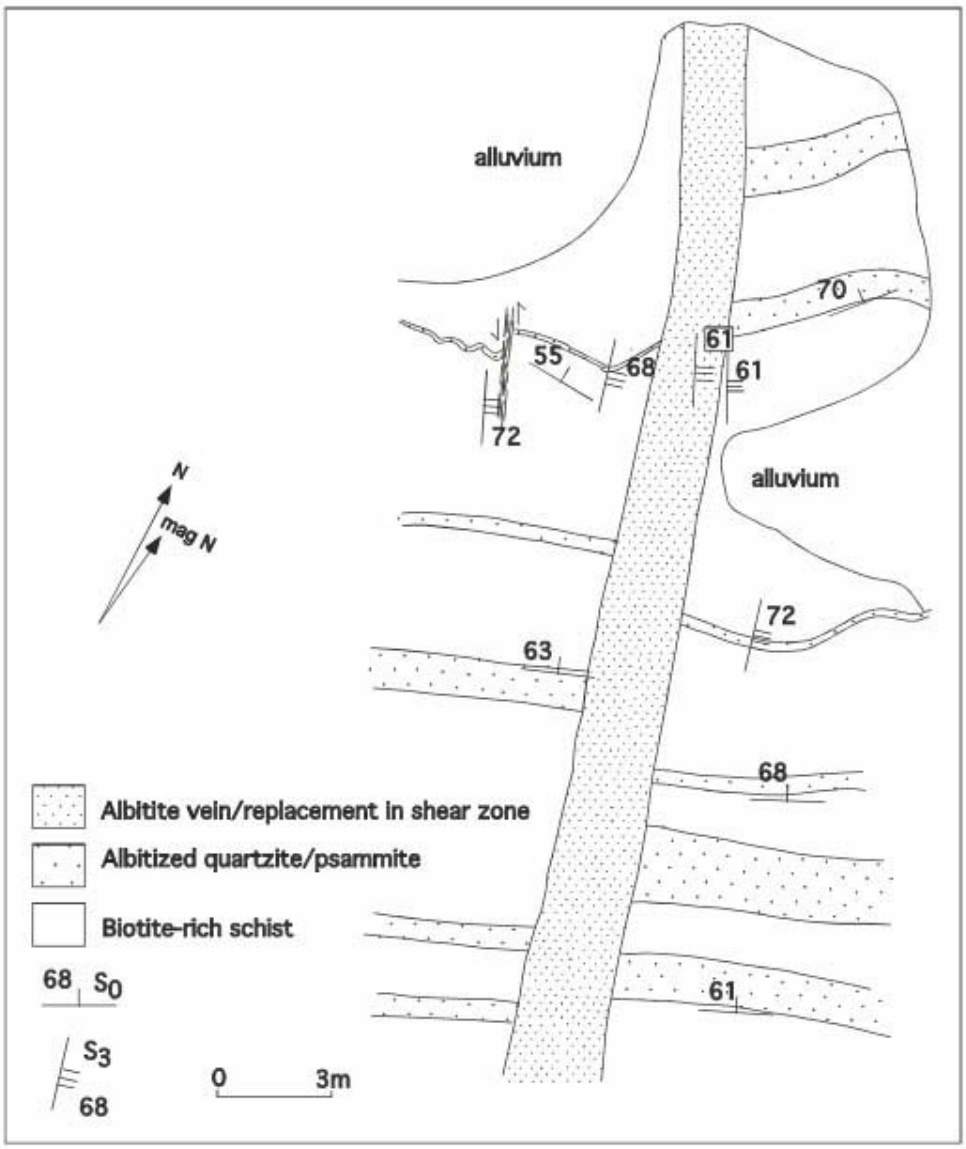

Fig. 2. Albitite outcrop from albitite area 2 (north-central Snake Creek Anticline - modified from Rubenach & Lewthwaite (2002). S_3 on the map is referred to as S_2 in this report. The main vein occupies a shear zone, and the albitite is largely a replacement of country rocks and only minor infill. Thin veins of albitite, parallel to the main body, occur in the country rocks mainly within 3 metres of the main albitite contacts. These veins are probably mainly infill. Many of the metapsammite layers have been albitized for at least 10 metres from the contact. In contrast the metapelitic and muscovite-rich metapsammitic layers have been largely converted to biotite-rich/muscovite-free schists, commonly with cordierite now replaced by andalusite and biotite. Although orientation of the albitite is consistent with it forming in D_2, detailed microstructural studies suggest it formed in D_1 (Rubenach, 2005b).

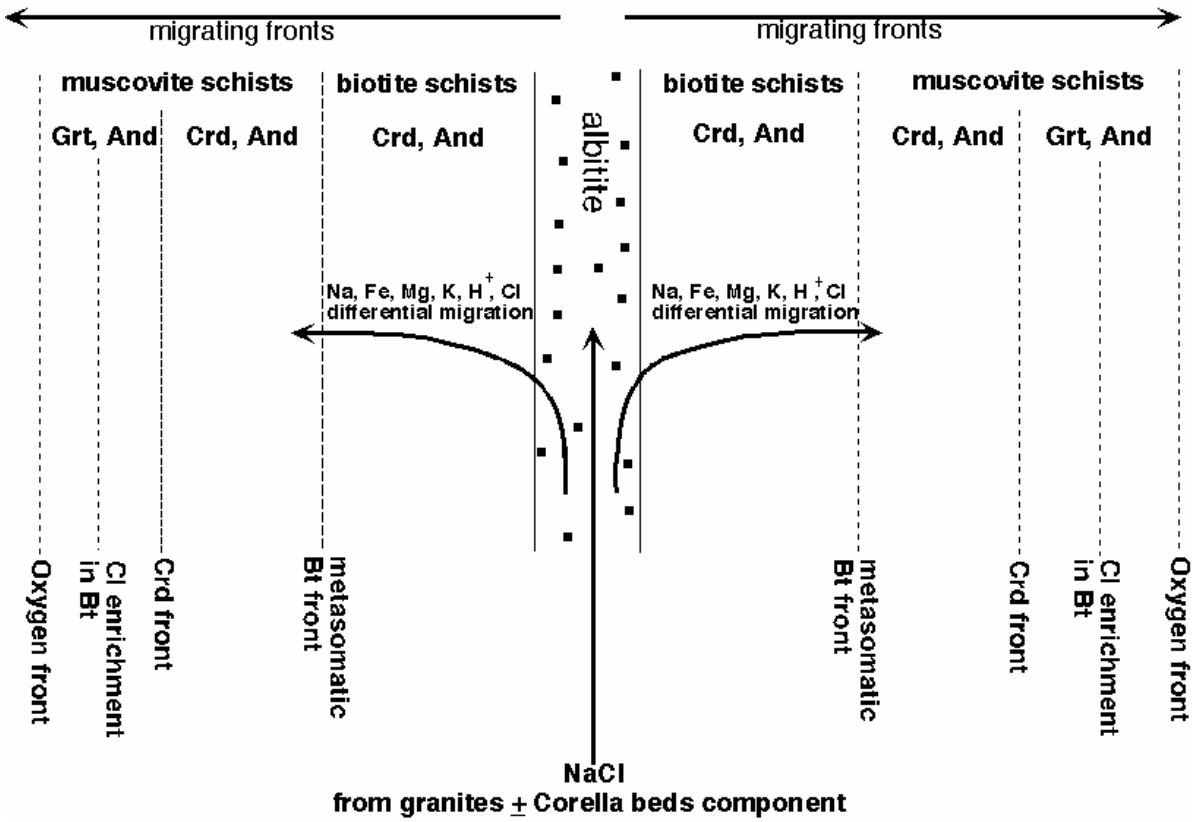

Fig. 3. Schematic diagram illustrating fluid processes related to albitization, Snake Creek Anticline (Rubenach, 2005a). In this report fluids originating from the mantle are thought more likely to be the ultimate source rather than fluids from granites as proposed on the Figure. The model is in part based on the albitite body in Fig. 2. External fluids with NaCl infiltrated fractures, shear zones and certain metapsammite beds to form albitites, removing K, Mg and Fe. In adjacent schists muscovite was destroyed and Na, Mg and Cl added to form biotite-rich schists with substantial Cl enrichment in biotite. The biotite fronts are typically metres to tens of metres distant from significant albitite shear zones or vein swarms. Further out are cordierite fronts, most of the original cordierite being now replaced by andalusite and biotite. Schists typically contain garnet in addition to andalusite or staurolite, but early alteration associated with albitization resulted in increased Mg/(Mg+Fe) in schists near albitites, precluding garnet and resulting in cordierite growth. Resetting of oxygen isotopes occurred over distances of hundreds of metres to kilometres away from albitite outcrops.

Figures 2 and 3 summarize the proposed model from Rubenach (2005a) for metasomatism associated with early albitites in the Snake Creek area. Significant changes in this report are as follows:

1. The most significant early albitization event was during D_{Ab} rather than D_1 or D_2 as in my earlier publications. Structural and microstructural arguments for this are presented in Rubenach (2005), who also determined ages between 1630 and 1660 Ma for the D_{Ab} event. Albitite veins and albitite replacement almost certainly also occurred during D_1 and D_2 by local dissolution and precipitation during active deformation. Another significant albitization event, associated with massive brecciation, occurred during emplacement of the Saxby granites and associated gabbros at around 1527 Ma.
2. A major source of fluids is now believed to be the mantle, possibly distal fluids related to carbonatites (see below).

2.2 Chemical changes associated with metasomatism, Snake Creek

Chemical analyses of schists, albitites, and biotite-rich metasomatic rocks for major and trace element analyses were performed using XRF at the Advanced Analytical Centre, James Cook University, whereas rare earths were analysed either by neutron activation at the Becquerel Laboratory at Lucas Heights, or Kalassay at Kalgoorlie. Element losses and gains were determined from isocon plots (Grant, 1986), with "isocons" lines based on relatively immobile elements (Al, Ti, Zr, Nb, Sc, Ga, and in some cases REE). The average for each component in a particular metasomatic rock was plotted against the same component in the "unmetasomatized equivalent". Components above the isocons were removed during metasomatism, while those below were added, but only those sufficiently distant from the isocon listed in the following summaries.

Figures 4 and 5 illustrate the differences in Na, K and Mg/(Mg+Fe) between unmetasomatized muscovite schists and metapsammites, albitized schists and psammites, and metasomatic biotite-rich schists. The isocons are more informative. Of significance is that albitization of schists involved loss of K, Mn, Fe , Cu, Pb and Zn (Fig. 6). The Eastern Fold Belt is of course noted for its Cu-Au deposits and the Cannington Pb-Zn deposit, although suggestions that albitization was the source of these metals is only speculative. Note also that metasomatic ironstones are common in the district, and Mn-rich minerals occur in some deposits (e.g., Cannington and Maronan). Note that Mg appears constant; this probably results that from some albitites being rich in cordierite, as other albitites almost certainly lost Mg. The change from muscovite-rich to biotite-rich schists involved gain of Mg, Na, Pb, Ni and Ca, and loss of K, Mn, Sr and the light REE's La, Nd, Ce and Eu (Fig. 7). Minor gains in Fe may have occurred, but otherwise it appears that the metasomatic fluids may have introduced Mg along with Na. The loss of light rare earths from the biotite schists but not from the albitites is perplexing.

Figure 8 is an isocon for single samples of unmetasomatized and albitized Corella beds. However, they are from different locations and the carbonate content of unmetasomatized Corella is variable, so conclusions regarding component movement are tentative.

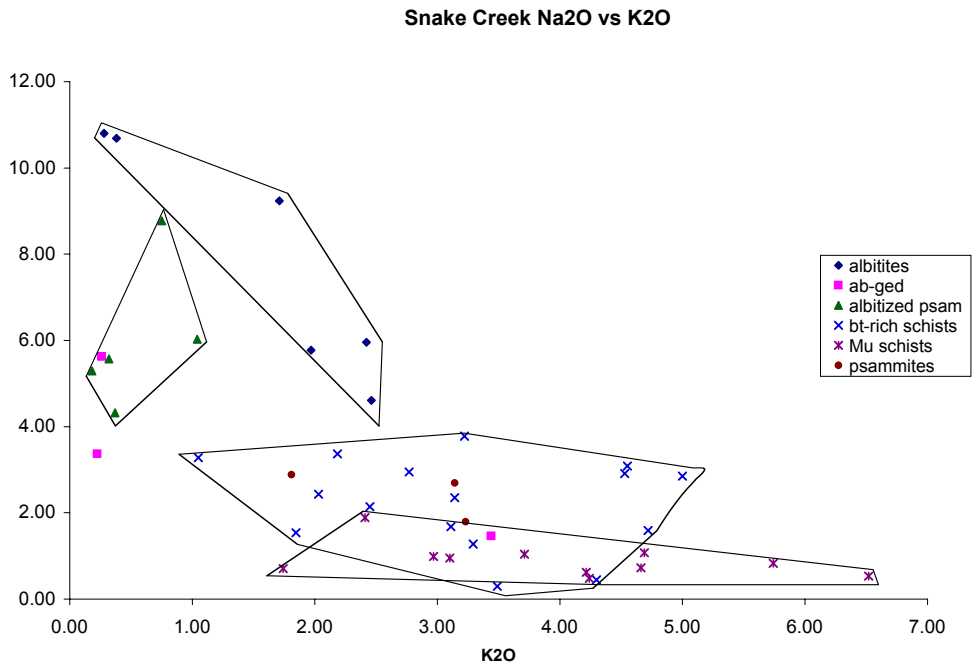

Fig. 4. Plot of weight percent Na_2O against K_2O for Snake Creek rocks. The albitites are mainly derived from schists. The less common gedrite-bearing albitites, one of which has a high content of gedrite and garnet and lower content of albite. Note the clear separation between schists and psammites and their albitized equivalents. The biotite-rich metasomatic schists overlap with muscovite schists on this plot.

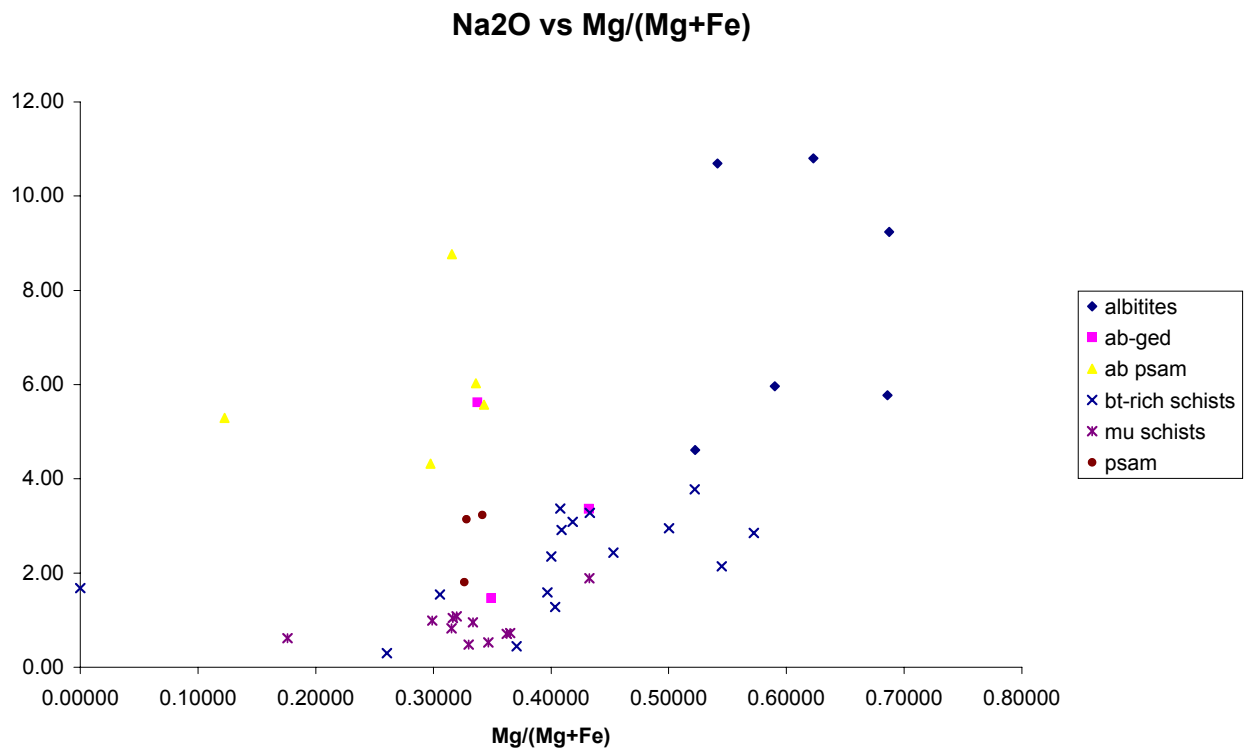

Fig. 5. Plot of weight percent Na_2O versus atomic Mg/(Mg+Fe). Note the clear separation between muscovite schists and albitized schists with the albitites (with the exception of the gedrite varieties) having significantly higher Mg/(Mg+Fe). However, psammites and albititized psammites have similar Mg/(Mg+Fe). Note that the biotite-rich schists lie between the unmetasomatized muscovite schists and the albititized schists.

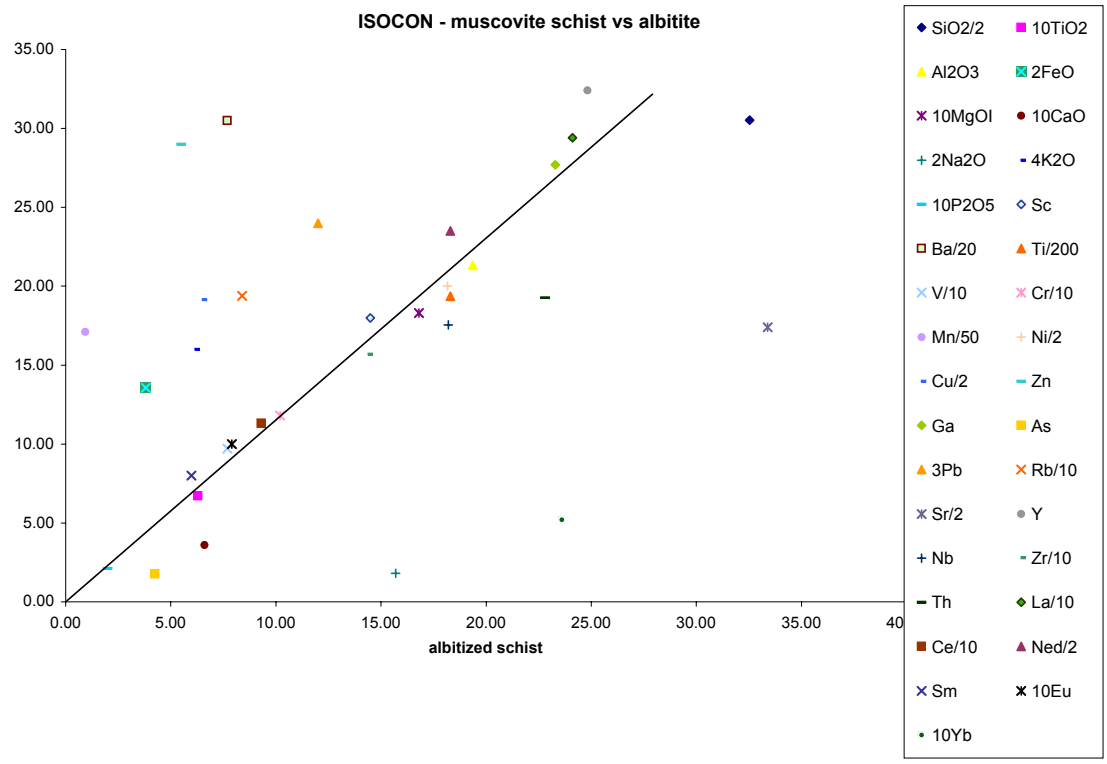

Fig. 6. Isocon plot for average of pelitic schists versus average of albitized schists. The isocon is based on P, Al, Ti, Zr, Y, Nb, Ga and Sc. Clear losses are K, Mn, Fe, Zn, Ba, Pb, Rb, and Cu, while gains are Na, Si, Th, Sr, Yb, As and Ca.

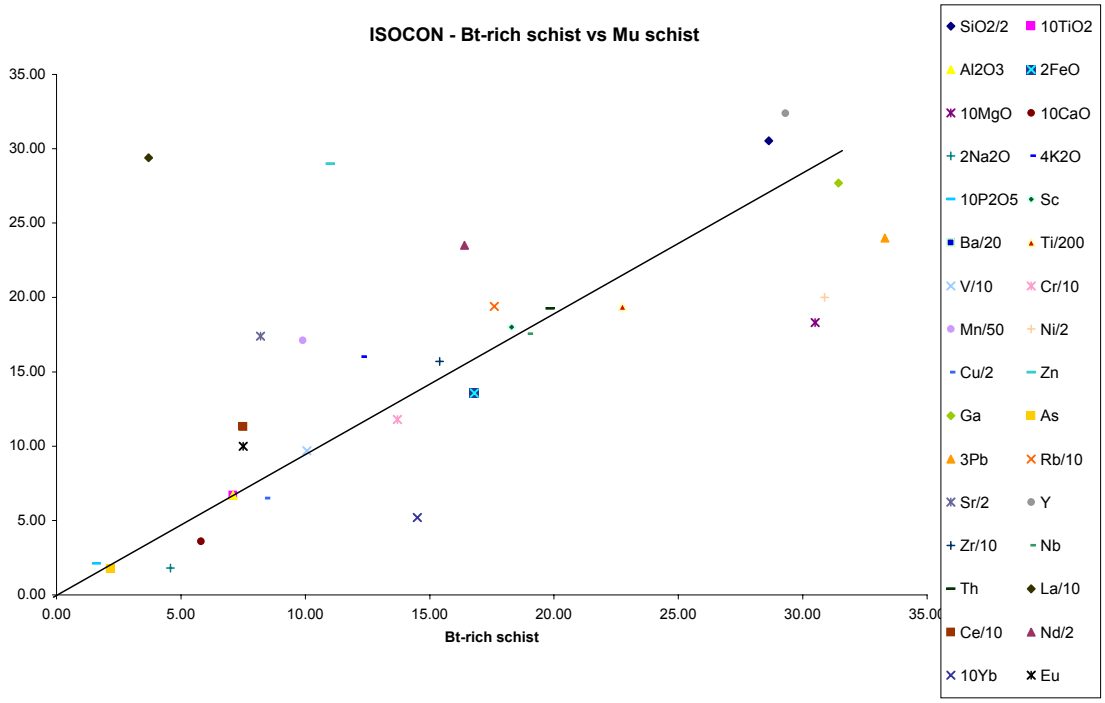

Fig. 7. Isocon plot for average of pelitic schists versus average of biotite-rich schists. The isocon is based on P, Al, Ti, Nb, Sc, Ga and Sc. There was a loss of Mn, K, Sr, Nd, La, Ce, Eu and Zn, and a gain of Mg, Na, Ni, Cu, Pb and Yb.

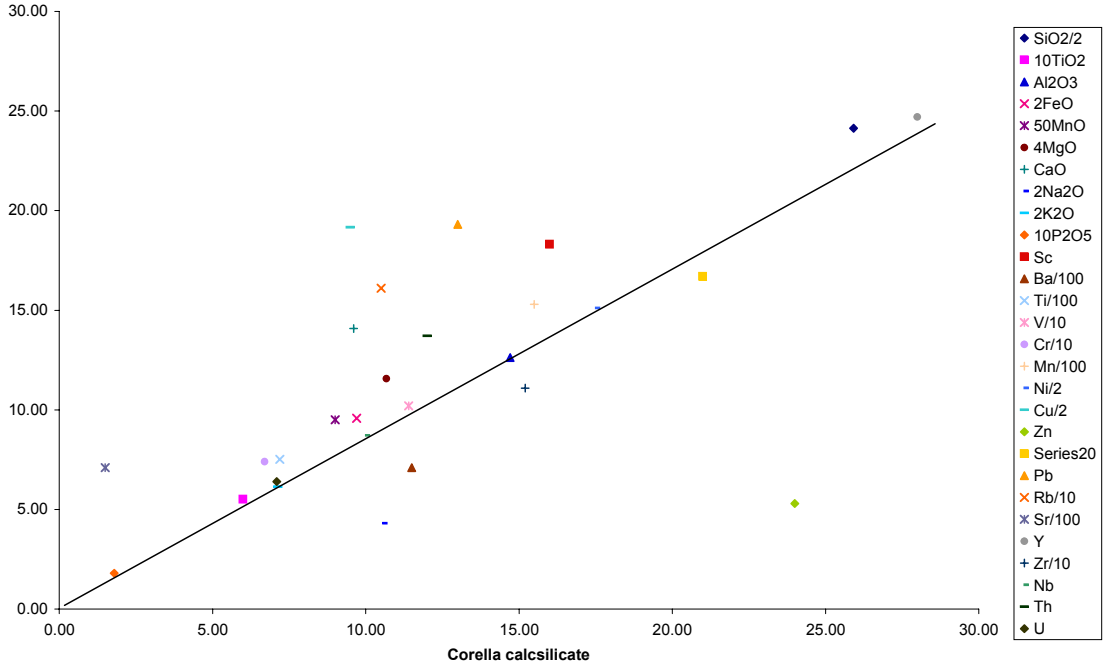

Fig. 8. Isocon for metasomatized (albitikzed) calcsilicate from the Corella beds versus a typical unmetasomatized example. As only one of each is plotted conclusions drawn from this Fig. are less reliable. The isocon is based on Al, Zr, Y, P and Nb (but not Ti). There appears to be a loss of Sr, Cu, Pb, Sc, Rb and Ca, and a gain of Na, Ba and Zn. A 13% mass loss is indicated by the slope of the plot, and would have been achieved mainly by loss of CO_2.

2.3 Chemical changes with albitization at the Osborne Mine

The country rocks at the Osborne Mine are dominantly migmatitic gneisses, ranging from metapsammites (which dominate) to metapelites in composition.Amphibolites and pegmatites are also abundant. The Cu-Au mineralization is spatially associated with ironstones (magnetite) and "silica flooding". Varying proportions of albite occur throughout the gneisses, but a lenticular body up to 250 metres thick consisting of more extreme albitites hosts the various ore lenses.

Typical albitites at Osborne show granular, even polygonal, microstructures. Additional components include quartz, biotite, magnetite, tremolite, cummingtonite, gedrite, sillimanite, garnet and cordierite, generally with accessory ilmenite. An unusual variant consists of albite, andradite, hedenbergite and titanite, commonly with retrograde epidote. The "immobile" trace elements, especially the relatively low Ti values, suggests the latter were derived from metasedimentary rocks rather than being albitized amphibolites, but this is not certain given that the isocons suggest mobility of these elements.

The isocons in Figs. 9 and 10 are not at all well defined. Possible explanations for this include variability in the migmatitic gneisses (including variable granite component), that the "extreme albitites" around the ore lenses were derived from a different package of metasedimentary rocks than the surrounding migmatitic gneisses, and that many of the albitites could be vein infill rather than replacement (this is suggested from the apparent mass gains, Figs. 9, 10). The fact that the albitites formed early and were deformed and recrystallized in the peak of metamorphism (D_2) suggests that such veining would be difficult to identify in mine exposures or drillcore. The isocon shown in Fig. 10 was expected to be more reliable, as the gneiss and albitite are in contact, but this one is just as poor as the averages in Fig. 9. However, the isocons do suggest a loss of K, Fe and Mg, and a gain of Na. It is interesting that both Fe and Mg occur as metasomatic phases in the overall albitite lens, namely Fe in magnetite and Mg in the veins of cummingtonite and anthophyllite. The isocons also suggest a loss of Cu during albitization, but it is not known whether albitization supplied any of the Cu in the mineralization.

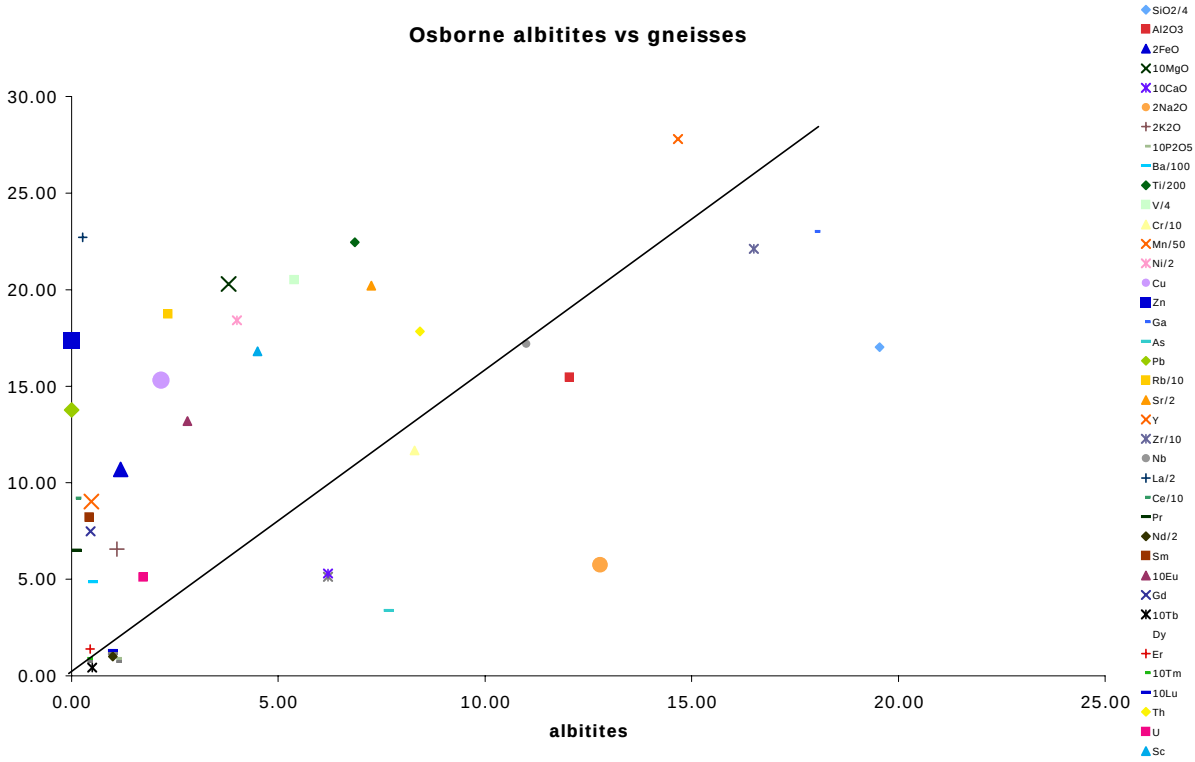

Fig. 9. Isocon plot of average pelitic/psammitic albitites versus average migmatic gneisses, Osborne Mine. The isocon is poor, and is based on Y, Nb, Zr, Ga and P (not Ti, Al). It suggests a gain of Na, Si, As and Ca, and a loss of K, Fe, Mg, Mn, Rb, Pr, Gd, Sm, Ce, Eu, Pb, Zn, Cu, Sc, V, Ni and La. It also suggests a mass gain of up to 50%, which would imply that many of the albitites analysed were vein infill rather than replacement of gneisses. However, it must be emphasized that the analytical data shows considerable variation, so any conclusions are quite tentative.

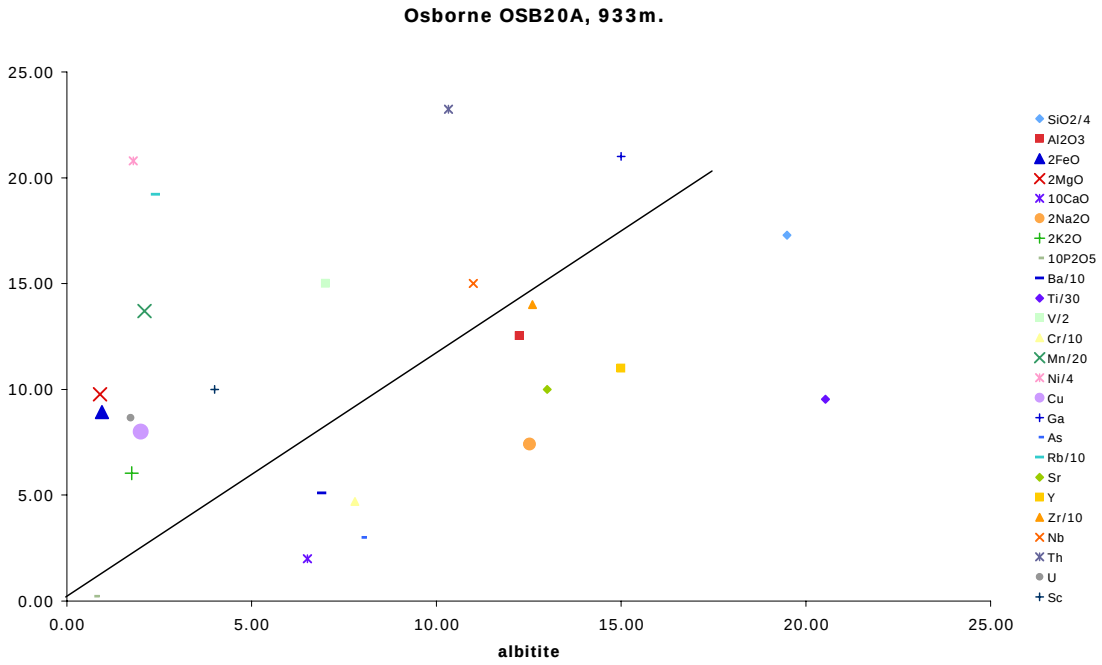

Fig. 10. This isocon is based on an albitite and partly albitized gneiss in contact with each other in drillhole OSB 20A, collected at 933 metres. Relicts of aligned biotite in the albitite suggests it has replaced a gneiss similar to that analysed.. However, the isocon, based on Al, Zr, Nb, and Ga, is still quite poor. It suggests gain of Na, Si, Ca, P, Ti, Y, As and Cr, and loss of K, Fe, Mg, Mn, Rb, Ni, Th, U, V, and Cu, with a mass gain (probably veins) of around 17%.

3. OXYGEN ISOTOPES AND FLUID SOURCES DURING METASOMATISM, EASTERN FOLD BELT

The early albitization largely involved, among others, addition of Na and Cl and removal of K and Fe. H^+ was also involved as this was essential in partitioning of Cl into biotite in most of the biotite-rich schists (Rubenach, 2005a). In Rubenach (2005a) I argue that the H^+ was a biproduct of albitization of muscovite.

Whole rock oxygen isotope analyses for non-metasomatic schists, metasomatic biotite-rich schists and albitites from Snake Creek were done at Monash University and the University of Cape Town. The results are plotted on Fig. 1, and 8 and 10‰ contours drawn as different lithologies from the same location differed by no more than 2‰. Unmetamorphosed pelitic rocks should have $\delta^{18}O$ values of around 14-16‰, so that the results show significant fluid infiltration and isotope resetting. At any given locality, there was no significant difference between non-metasomatic schists and metasomatized rocks, showing that the oxygen isotope fronts extended considerably further than the albitite and biotite fronts, as illustrated in Fig. 3. Note that the contours in Fig. 1 are relatively smooth, although one sample from the centre of the Snake Creek Anticline of a typical andalusite-muscovite-biotite schist gave a value of 14.9‰ that differs significantly from nearby samples with 7.7-8‰. Note that the contours are not parallel to the stratigraphy or isograds, but clearly relate to local albitites, suggesting that the same fluids that produced the albitites, biotite-rich schists and Cl enrichment also caused the isotope resetting. There is also a spatial association with cordierite schists, also believed to have resulted from metasomatism (Rubenach, 2005a). It is also interesting to note that the isotope contours also relate to relatively abundant porphyroblasts, as the SW part of the anticline, with oxygen values of greater than 10‰, are poor in porphyroblasts such as garnet, cordierite, andalusite or sillimanite that has replaced andalusite in comparison with stratigraphic equivalents. Discussion as to possible reasons for this is outside the scope of this report.

Two possible sources of fluids are as follows

1. Fluids derived from the evaporite-rich Corella beds, initially at temperatures less than 100°C migrated up-temperature to around 560°C, the temperature proposed for much of the Llewellyn Creek Formation during the D_{Ab} event (1530-60 Ma).
2. Magmatic fluids. Although the spatial relationships between the breccias in the Corella beds, albitization and granites of the Williams Batholith suggest that the latter could be the source, this would only explain the later albitization and not the albitization and isotope resetting in the Soldiers Cap Group. However, mafic intrusives are associated with both groups of albitites, and it is suggested that mantle-derived fluids, associated with but not exsolving from the mafic rocks, were the principal source of metasomatic fluids. As metasomatic albitites (so-called fennites) are commonly associated with carbonatites, perhaps the albitic fluids at Snake Creek were related to distal albitites (ie not exposed at the current surface).

French (1997) records $\delta^{18}O$ values of 7.6-8.2‰ for albitites from the Osborne Mine. These values are comparable to those from the Snake Creek Anticline, and a magmatic source is again suggested.

Acknowledgments

Analyses for major and trace elements were carried out using XRF at the Advanced Analytical Centre, JCU, and staff of the centre are acknowledged for their quality

control. Dr Ian Cartwright, Monash University, and Dr Chris Harris, University of Cape Town, performed the oxygen isotope analyses.

4. REFERENCES

French, T., 1997. Genesis of albitites and anthophyllite-bearing lithologies of the Osborne Cu-Au deposit, Cloncurry district, Mount Isa Inlier, NW Queensland.Unpublished BSc Hons thesis, James Cook University, Townsville. 98 pp

Grant, J.A., 1986. The isocon diagram – a simple solution to the Gresens' equation for metasomatic alteration. Economic Geol. 81, 1976-82

Oliver, N.H.S., Wall, V.J., & Cartwright, I., 1992. Internal control of fluid compositions in amphibolite-facies scapolitic calc-silicate rocks, Mary Kathleen, Australia. Contribs. Mineralogy and petrology 111, 94-110.

Oliver, N.H.S. Butera, K., Cleverley, J. S., Marshall, L., Rubenach, M. J., Collins, W. J., Fu, B., Mustard, R., & Baker T. 2005. From source to sink: evolution of fluid systems in the Eastern Succession of the Mt Isa Block. I2+3 Final Report, pmdCRC.

Rubenach, M.J., 2005a. Relative timing of albitization and chlorine enrichment in biotite in Proterozoic schists, Snake Creek Anticline, Mount Isa Inlier, Australia. Canadian Mineralogist 43, 349-366.

Rubenach, M. 2005b. Tectonothermal Evolution of the Eastern Fold Belt, Mt Isa Inlier. I2+3 Final Report, pmdCRC.

Rubenach, M.J. and Foster, D.R.W., 1996. Interrelationships between multiple metamorphic episodes, high strain zones, granites and metasomatism, Mount Isa Inlier. In: Buick, I.S. and Cartwright, I., (eds.), Evolution of metamorphic belts. Geological Society of Australia, Abstracts 42: pp. 40-41.

Rubenach, M.J. and Barker, A.J., 1998. Metamorphic and metasomatic evolution of the Snake Creek Anticline, Eastern Succession, Mount Isa Inlier. Australian Journal of Earth Sciences, 45: 363-372.

Rubenach, M.J. and Lewthwaite, K.J., 2002. Metasomatic albitites and related biotite-rich schists from a low-pressure polymetamorphic terrane, Snake Creek Anticline, Mount Isa Inlier, north-eastern Australia: microstructures and P-T-d paths. Journal of Metamorphic Geology, 20: 191-202.

Rubenach, M.J., Adshead, N.D., Oliver, N.H.S., Tullemans, F., Esser, D. and Stein H., 2001. The Osborne Cu-Au deposit: geochronology, and genesis of mineralization in relation to host albitites and ironstones. In Williams, P.J. (ed.) 2001: a hydrothermal odyssey, new developments in metalliferous hydrothermal systems research, extended conference abstracts. EGRU contribution 59: 172-173.

Williams, P.J., 1994. Iron mobility during synmetamorphic alteration in the Selwyn Range area, NW Queensland: implications for the origin of ironstone-hosted Au-Cu deposits. Mineralium Deposita 29, 250-260.

Geochemistry of magmatic fluids from intrusions of the Williams-Naraku Batholith, Cloncurry District, Northwest Queensland: preliminary results from laser ablation ICP-MS analysis.

Roger Mustard[1], Geordie Mark[2], Thomas Ulrich[3], David Gillen[1] and Damien Foster[1].

1. predictive mineral discovery Cooperative Research Centre, Economic Geology Research Unit, School of Earth Sciences, James Cook University, Townsville, Q4811, Australia
2. predictive mineral discovery Cooperative Research Centre, School of Geosciences, Monash University, Clayton Campus, Melbourne, Victoria, 3168
3. Earth and Marine Science Department, Australian National University, Canberra ACT 0200, Australia

ABSTRACT

Fluid inclusions from twenty-three samples, ranging in composition from diorite to granite, from three granitoid suites (Lightning Creek, Mount Angelay, Saxby Granite) of the (1550-1500 Ma) Williams-Naraku Batholith were characterized using a combination of microthermometric and laser ablation ICP-MS (LA-ICP-MS) analysis. Numerous types of primary fluid inclusions are present in monzogranitic samples, and they include: liquid-vapor-halite multisolid ($LVHSn_{1to6}$), halite-liquid (HL), , liquid-vapor-halite (LVH), aqueous CO_2 and mixed LVH-CO_2 inclusions Primary fluid inclusions were analysed by LA-ICP-MS for B, Na, Mg, Si, Cl, K, Ca, Ti, V, Cr, Mn, Fe, Ni, Co, Z, Cu, As, Rb, Sr, Mo, Ag, Cs, Ba, Au, Pb, Bi, and U. Visible chalcopyrite crystals were observed in some of the brine inclusions from Lightning Creek and confirmed by LA-ICP-MS analysis. Significant Cu concentrations occur in liquid-vapor-halite multisolid brines and liquid-vapor-halite inclusions, whereas low-salinity aqueous carbonic inclusions contain only minor Cu (<20 ppm). The presence of Cu elevated concentrations (~4033 ppm) in brines from the Mt Angelay granite suggests that granites within the Williams-Naruku batholith may commonly contain 100 to 1000 ppm levels of copper naturally in their fluid, and as a result indicate that magmatic degassing of saline brine may be capable of providing sufficient copper to supply the copper budget of a Cu-Au deposit. Simple calculations suggest that a 10x10x2 km body of intrusion may have been capable of expelling $1.4x10^7$ tonnes of Cu. No gold was detected in any of the Cu-rich fluid inclusions analysed (except three analysis show apparent detectable Au: GC6a_2a; 9 ppm, LCD14_14; 8 ppm, LCD14_22; 24 ppm). No silicate melt inclusions were recognized in the range of granite samples studied. The absence of melt inclusions may reflect the high temperature of crystallization of the melts and their mid-crustal emplacement depth (~10 km), leading to their re-adsorption during prolonged crystallization.

Keywords. Fluid inclusions, Eastern Succession, Mt Isa, Iron oxide copper gold deposit

1. Introduction

The Williams and Naraku Batholiths of the Cloncurry District comprise older foliated granites that intruded around 1550 Ma (Maramungee, Cowie and Blackeye Granites) and younger, variably deformed intrusive complexes between ca 1540 and ca 1490 Ma (Mount Angelay, Squirrel Hills, Saxby, Wimberu, Mount Dore, Yellow Waterhole, Mount Cobalt Granites). The younger granites were subdivided on geochemical grounds into the Cloncurry and Eureka Supersuites (Pollard et al., 1998). The Williams and Naraku Batholiths, particularly the younger phases (<1540 Ma), are a commonly invoked sources of fluids to regional alteration and hydrothermal Cu-Au mineralization in the Eastern Fold Belt (Wyborn, et al. 1992; Perkins and Wyborn, 1998; Rotherham et al., 1998; Wyborn, 1998; Pollard, 2000; Baker et al., 2001; Mark et al., 2004). A magmatic origin is supported by a range of textural, geochronological, geochemical and isotopic data including:

- A close temporal association between some granitoids, regional Na-Ca alteration and Cu-Au mineralisation (1550-1490 Ma) (Oliver et al., 2004).
- 1540 to 1478 Myrs 40Ar/39Ar dating of alteration and Cu-Au mineralization (Perkins and Whyborn, 1998).
- A close temporal association (<5 km) between granitoids and Cu-Au mineralization (Whyborn, 1998; Budd et al., 2001).
- The moderate temperature (350-500ºC), high salinity (35-60 wt. % NaCl equiv.) nature of ore fluids based on fluid inclusion studies.
- Stable isotope (C, O, H, S) studies indicating fluids were consistent with a dominant magmatic component (Rotherham et al., 1998; Baker, 1998)
- Granite compositions are commonly associated with and considered prospective sources for Cu-Au mineralization elsewhere Blevin and Chappell, 1995).

There have been numerous studies of granites in the Cloncurry region investigating their potential relationship to Cu-Au mineralization and Na-Ca alteration (Mark and Dejong, 1996; Mark, 1998; Mark, 1999; Mitchell, 1993; Nunn, 1995; Tolman, 1998, Perring et al., 2000).

The aims of this study were to:

1) Locate melt inclusions and/or primary fluid inclusions in granite if present in samples from the Williams-Naruku batholith.
2) Document the range and abundance of inclusion types within the samples.
3) Analyse suitable inclusions using laser-ablation ICP-MS at ANU (Canberra) for a range of elements including metals (Cu and Au).
4) Determine if low level gold was capable of being detected in any, but in particular the copper-bearing fluid inclusions.

2. General Geology and Sample Locations.

All three granite suites (Lightning Creek, Mount Angelay, Saxby Granite) belong to the (1550-1500 Ma) Williams-Naraku Batholith located within the Eastern Succession of the Mount Isa Inlier (Fig. 1). The Lightning Creek Sill Complex is the southernmost area, situated 126 km SSE of Cloncurry (475,721mE; 7,587,975mN), at the southern end of the areally extensive Squirrel Hills granite pluton. The Saxby Granite is located 60km SSE of Cloncurry (477,000mE; 7,657,000mN). The Mount Angelay Igneous Complex is located 52km SSE of Cloncurry (466,000mE; 7,662,000mN).

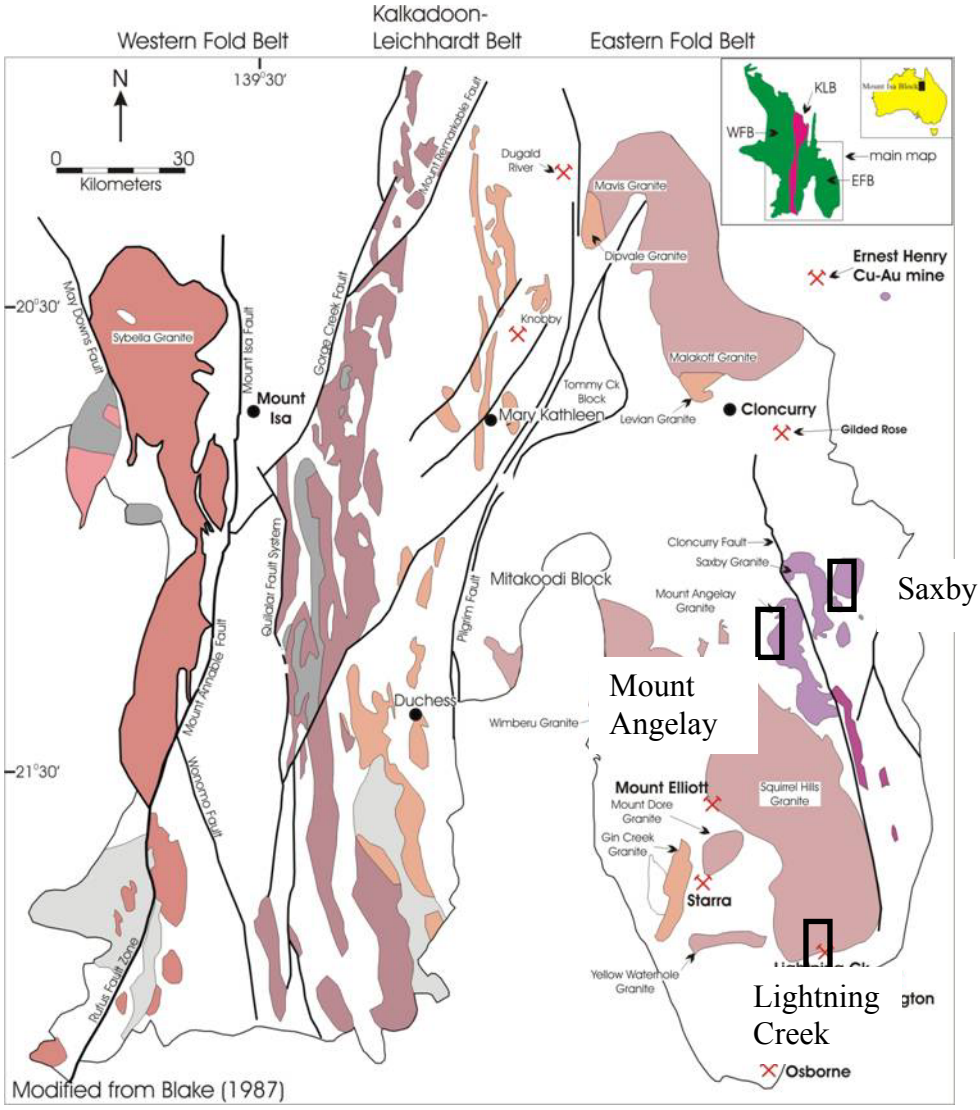

Fig. 1. Granites of the Mt Isa Inlier with the location of the Lightning Creek, Mount Angelay, Saxby Granites highlighted.

2.1 Lightning Creek prospect

The Lightning Creek granites are located at the southern end of the Squirrel Hills granite, and represent a sodic member of the Eureka Supersuite defined by Pollard et al., (1998). The Lightning Creek suite displays a range of compositions evolving from early voluminous quartz monzodiorite and monzogranite to later flat-lying quartz-plagioclase aplitic sills (Fig. 2). The horizontal quartz-plagioclase sills are associated with magnetite veins that display a range of textures indicative of formation at the magmatic-hydrothermal transition. The amount of magnetite present is sufficient to generate a prominent magnetic anomaly and has been estimated to be in excess of 1000 to 2000 Mt (Williams and Pollard 2001; Perring et al., 2000).

Previous studies of high temperature quartz veins have revealed co-existing hypersaline brine (33-55 wt % NaCl equivalent) and CO_2 inclusions. Proton microprobe (PIXE)

analyses of hypersaline brines highlighted high concentrations of Fe (~10 wt %) and Cu (~1 wt %) (Perring et al., 2000, 2001; Williams and Pollard 2001).

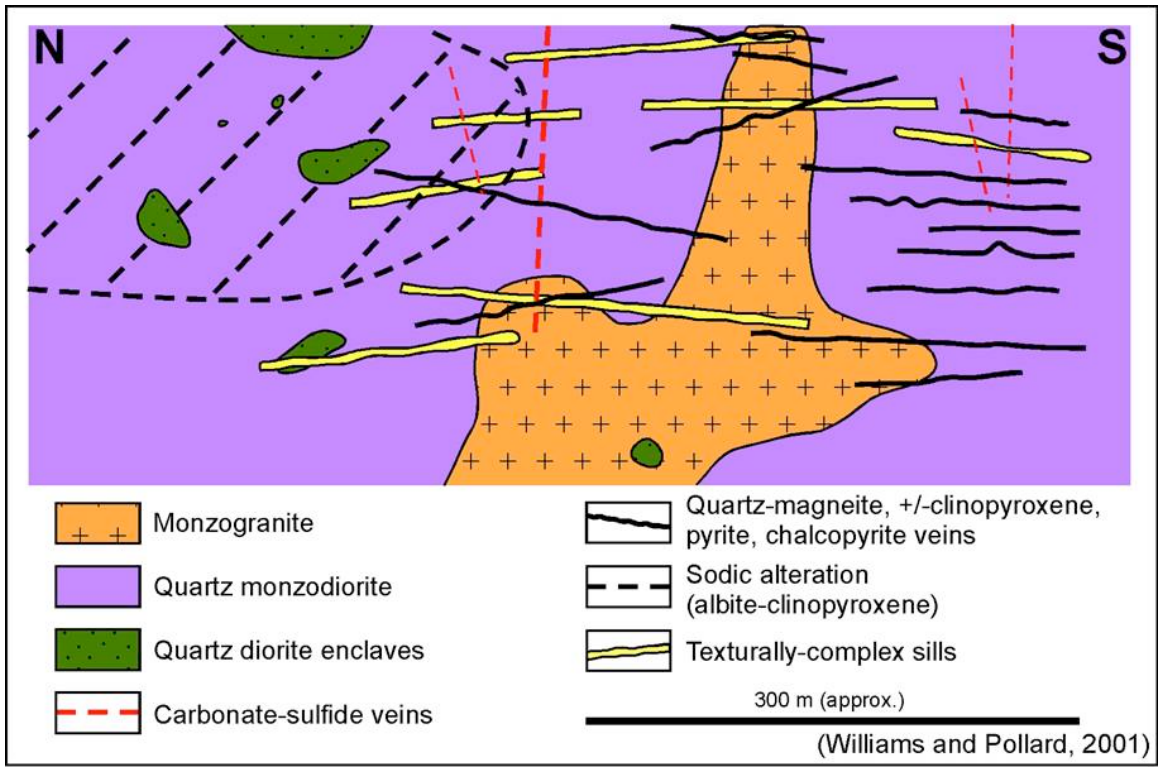

Fig. 2. Interpreted cross-section of Lightning Creek prospect (from Williams and Pollard, 2001)

2.2 Mount Angelay Igneous Complex.

The Mount Angelay igneous complex (~210 km^2) forms a large NNW elongate composite pluton, and consists of ca 1550 Ma Na-rich trondhjemite and a suite of younger, post 1540 Ma K-rich intrusions. They represent a K-rich member of the Eureka Supersuite defined by Pollard et al. 1998, and range between 51 and 77 wt. % SiO_2. Samples studied were selected from a rock suite collected by Tolman (1998) from his honours map area, which is located within the northern part of the complex. The granites range in composition from less evolved quartz diorite and quartz monzodiorite to more evolved quartz syenite and syenogranite (Fig. 3). Late stage N-S to NNE trending aplite and pegmatite dyke swarms intrude the earlier granitoid phases. The dykes were subsequently overprinted by a Na-Ca breccia complex that were studied in detail by Tolman (1998)

The only previous reported fluid inclusion study on the Mt Angelay complex was by Tolman (1998) who identified four inclusion types: liquid-vapor (LV), liquid-vapor-halite (LVH), liquid-vapor-halite ($LVHSn_{1to6}$) multisolid brines and possible vapor or liquid CO_2 inclusions.

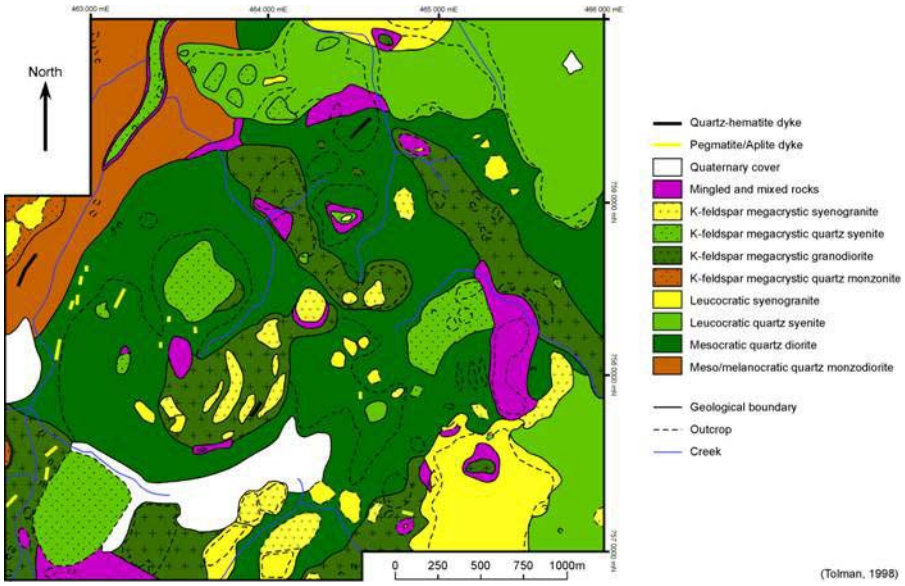

Fig. 3. Geology of the central Mount Angelay igneous complex. Modified from Tolman (1998).

2.3 Whiley Igneous Complex

The Whiley Igneous Complex (>23 km^2) forms an N-S elongate ovoid shaped composite pluton located on the eastern side of the Cloncurry fault. It represents the southern most mass of the Saxby Granite and detailed mapping by Mitchell (1993) revealed a complex association of mafic and felsic magmas consisting of early less evolved hornblende-biotite granite, intruded by biotite-hornblende granite and dolerite, and late-stage more evolved leucocratic granite. They represent a member of the Cloncurry Supersuite defined by Pollard et al. (1996), and range between 57 and 74 wt. % SiO_2.

There has been no previously reported fluid inclusion studies of the Whiley Igneous Complex.

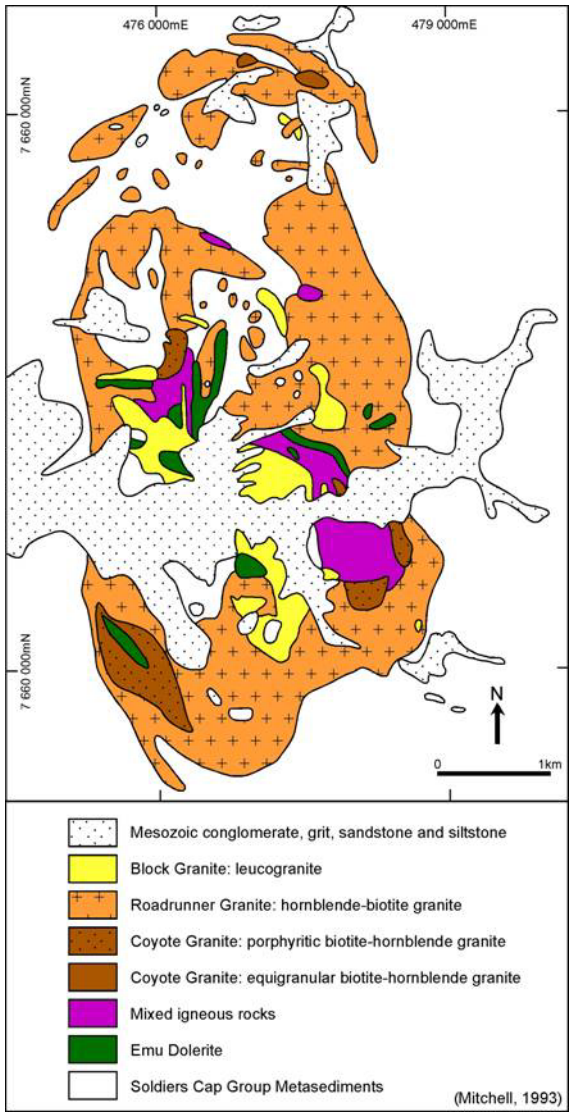

Fig. 4. Geology of the Whiley Igneous Complex (modified from Mitchell, 1993).

3. Method

Suitable granite suites belonging to the Williams-Naraku batholith studied previously at JCU, which display a range of compositions (typically from diorite to granite), and have published wholerock analysis available, were selected. The granite suites include:

1) Lightning Creek (Nunn, 1995; Perring, 2000)
2) Mount Angelay (Tolman, 1998)
3) Saxby Granite (Mitchell, 1993)

23 doubly polished 300 micron-thick thin sections were prepared for inspection, including Lightning Creek (14 samples), Mount Angelay Granite (6 samples) and Saxby Granite (3 samples; Table 1; Appendix 1). Thin sections were studied for the presence of silicate melt and primary fluid inclusions.

Fluid inclusions were analyzed with an ArF Excimer laser (Lambda Physik LPX120i) combined with an Agilent 7500s ICP-MS located at the Research School of Earth Sciences

at the Australian National University (Canberra). The laser spot sizes ranged from 30 to 42 microns according to the size of the fluid inclusion and ablation was carried out till the entire inclusion was sampled and the laser drilled in the underlying host. All fluid inclusions were hosted in quartz, which showed very low trace element content. Elements analysed include: B, Na, Mg, Si, Cl, K, Ca, Ti, V, Cr, Mn, Fe, Ni, Co, Z, Cu, As, Rb, Sr, Mo, Ag, Cs, Ba, Au, Pb, Bi, and U. To quantify the data we used sodium as an internal standard, which was analyzed using conventional micro-thermometric techniques on a Linkam MDS 600 heating-freezing stage linked to a Olympus BX52 microscope at James Cook University (Townsville).

The integrated intensities (counts/second) of the inclusion signals from the laser ablation analyses were background corrected. Further, instrument drift was linearly corrected by applying the bracketing method of an external standard (NIST 612). The concentrations, detection limits and sensitivities were then calculated accordingly to Longerich et al., (1996).

Sample Number	Location	Granite	Composition	Source
LCF01	Lightening Creek	Squirrel Hills	Alkali granite	A. Nunn (1995)
LCF02	Lightening Creek	Squirrel Hills	Tonalite	A. Nunn (1995)
LCF04	Lightening Creek	Squirrel Hills	Monzogranite	C.S. Perring (2000)
LCF09	Lightening Creek	Squirrel Hills	Quartz diorite	A. Nunn (1995)
LCF10	Lightening Creek	Squirrel Hills	Tonalite	A. Nunn (1995)
LCF12	Lightening Creek	Squirrel Hills	Quartz monzodiorite	C.S. Perring (2000)
LCF06A	Lightening Creek	Squirrel Hills	Quartz diorite	A. Nunn (1995)
LCD 14.01	Lightening Creek	Squirrel Hills	Quartz diorite	A. Nunn (1995)
LCD 16.02	Lightening Creek	Squirrel Hills	Tonalite	A. Nunn (1995)
LCD 14_238.15	Lightening Creek	Squirrel Hills	Spherulitic iron-rich sill	C.S. Perring (2000)
LCD 14_214.5	Lightening Creek	Squirrel Hills	Spherulitic iron-rich sill	C.S. Perring (2000)
LCD 14_238.3	Lightening Creek	Squirrel Hills	Spherulitic quartz-feldspar sill	C.S. Perring (2000)
LCD 16_136.5	Lightening Creek	Squirrel Hills	Aplitic Na-Fe quartz-feldspar sill	C.S. Perring (2000)
LCD 31_148.35	Lightening Creek	Squirrel Hills	Aplitic quartz-feldspar sill	C.S. Perring (2000)
GC 01	North	Mount Angelay	Quartz Syenite	J.L. Tolman (1998)
GC 03	North	Mount Angelay	Syenogranite	J.L. Tolman (1998)
GC 05	North	Mount Angelay	Albite-quartz-magnetite rock	J.L. Tolman (1998)
GC 06	North	Mount Angelay	Pegmatite	J.L. Tolman (1998)

GC 06b	North	Mount Angelay	Pegmatite	J.L. Tolman (1998)
GC 07	North	Mount Angelay	Aplite	J.L. Tolman (1998)
26.16	Roadrunner Granite	Saxby Granite	Granite	L.C. Mitchell (1993)
26.18	Wallaby Granite	Saxby Granite	Granite	L.C. Mitchell (1993)
26.19	Block Granite	Saxby Granite	Granite	L.C. Mitchell (1993)

Table 1. Samples from the Williams-Naraku batholith (Lightning Creek, Mount Angelay and Saxby Granite) inspected for the presence of silicate melt and fluid inclusions.

4. Results

4.1 Fluid Inclusion Types and Abundance

The thin sections revealed an absence of recognizable melt inclusions, and a moderate amount of primary fluid inclusions in quartz in specific samples. Fluid inclusion types recognized and their abundance are summarized in Table 2.

Sample No.	MI	H>L±V	LHV_{nS}	LVH	LV	$LVH\text{-}CO_2$	CO_2
LCF01	---	---	5 (P)	2 (S)	1 (S)	---	3 (PS-S)
LCF02	---	4 (P)	4 (P)*	3 (S)	2 (S)	---	3 (PS)
LCF04	---	---	4 (P)	1 (P-S)	2 (S)	---	4 (PS-S)
LCF09	---	---	4 (P)	5 (P)	5 (PS)	5 (P)	5 (P)
LCF10	??	---	5 (P)	2 (S)	4 (S)	---	4 (S)
LCF12	---	---	2 (P-PS)	4 (S)	5 (PS)	---	4 (PS)
LCF06A	---	---	5 (P)	4 (P-PS)	5 (P-PS)	---	5 (P)
LCD 14.01	---	---	5 (P)	3 (PS-S)	5 (P-PS)	---	4 (S)
LCD 16.02	---	5 (PS)	2 (P-PS)*	2 (PS-S)	3 (PS-S)	---	4 (PS-S)
LCD 14_238.15	---	---	2 (P-PS)*#	4 (PS-S)	5 (S)	---	3 (PS-S)
LCD 14_214.5	---	5 (PS)	1 (P-PS)*	2 (PS-S)	5 (S)	---	5 (PS-S)
LCD 14_238.3	---	---	1 (P-PS)	3 (P-PS)	3 (S)	---	5 (PS-S)
LCD 16_136.5	---	---	1 (P-PS)*	2 (P-PS)	3 (PS-S)	---	3 (PS-S)
LCD 31_148.35	---	---	2 (P-PS)	2 (P-PS)	2 (PS-S)	---	4 (PS-S)
GC 01	---	---	2 (P-PS)	3 (P-S)	5 (PS-S)	---	2 (PS)
GC 03	---	---	---	1 (PS-S)	3 (PS-S)	---	4 (PS-S)
GC 05	---					---	
GC 06	---	---	2 (P)*	3 (P-S)	5 (PS-S)	---	4 (PS-S)
GC 06b	---	---	3 (P)*	4 (P-S)	4 (PS-S)	---	5 (S)
GC 07	---					---	
26.16	---	---	---	3 (PS-S)	3 (PS-S)	---	1 (PS)
26.18	---	---	3 (P-PS)	3 (PS-S)	4 (S)	---	5 (S)
26.19	---	---	5 (P-PS)	3 (S)	4 (S)	5 (PS)	1 (S-P)

Note: 1 = abundant, 2 = moderate to abundant, 3 = moderate, 4 = minor, 5 = rare.
P = primary, PS = pseudosecondary, S = secondary.
* = presence of opaque minerals in fluid inclusion, # = presence of chalcopyrite crystal.

Table 2. Distribution and abundance of fluid inclusions within phases of the Williams-Naraku batholith.

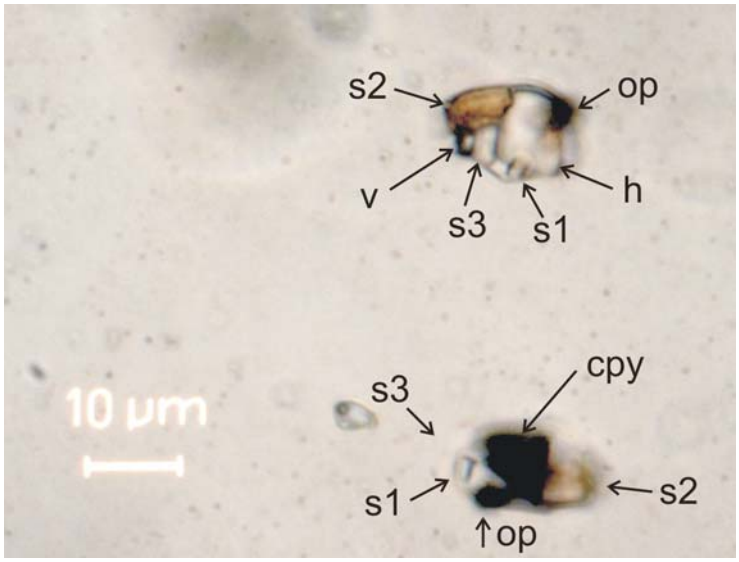

Fig. 5. Photomicrograph of multi-solid brine fluid inclusions containing a opaque phase. The lower inclusion contains a chalcopyrite crystal. (x100 magnification).

4.2 Microthemometry

Microthermometric analysis was completed on a small set of inclusions from Mount Angelay (GC6A) and Lightning Creek (LCD14) (Appendix 2). Heating the $LVHSn_{1to6}$ inclusions from sample GC6A induced halite dissolution between 400 and 500ºC, with several halite crystals remaining at temperatures in excess of 500ºC. Assuming an average homogenization temperature of 500ºC a brine salinity of 60 wt% NaCl equiv. was calculated using the equation of Sterner et al., (1988). The microthermometric data for Lightning Creek $LVHSn_{1to6}$ inclusions indicated a composition of 25% wt % NaCl and 20 wt% $CaCl_2$ using the ternary H_2O-NaCl-$CaCl_2$ plot of Shepard et al., (1985), and compares closely with the calculated salinity (33-50 wt % NaCl equiv.) for similar multiphase inclusions determined by Perring et al. (2000).

4.3 Laser Ablation

The geochemistry of 29 fluid inclusions, 16 from Mount Angelay and the rest from Lightning Creek were analysed by LA-ICP-MS. (see Table 3 summary data). The fluid inclusions from Mount Angelay represented primary multi-solid brine inclusions hosted in quartz from aplite and pegmatite (sample GC06A, Appendix 1), whereas those from Lightning Creek comprise 11 primary multi-solid brine inclusions and 2 pseudo-secondary to secondary CO_2-bearing inclusions hosted in quartz from a spherulitic, iron-rich, quartz feldspar sill (sample LCD12_238.15, Appendix 1).

The $LVHSn_{1to6}$ inclusions from the Mount Angelay igneous complex fall into two groups, those that contain opaques and those that are free of opaques. The opaque-bearing inclusions contain 2083 ppm Cr, 1242 ppm Ni, 11ppm Co, 983 ppm Zn, 4033 ppm Cu, 457 ppm As, 31 ppm Mo, 317 ppm Pb, 40 ppm Bi and 13 ppm U, whereas the opaque-free inclusions contain higher Ag (2.2 ppm), U (18 ppm) and lower Cr (239 ppm), Ni (337 ppm), Co (4ppm), Cu (396 ppm), Zn (683 ppm), As (108 ppm), Mo (5 ppm), Pb (162 ppm) and Bi (4 ppm).

The opaque-bearing $LVHSn_{1to6}$ inclusions at Lightning Creek igneous complex contain 269 ppm Cr, 204 ppm Ni, 9 ppm Co, 164 ppm Zn, 6280 ppm Cu, 16 ppm As, 13 ppm Mo, 0.4 ppm Ag, 32 ppm Pb, 1 ppm Bi, and 5 ppm U, whereas the opaque-free inclusions contain comparatively more Co (27 ppm), Pb (38 ppm), Zn (758 ppm); less Cu (72 ppm), As (52 ppm), Mo (BDL), Cr (246 ppm), Ni (216 ppm) and similar Ag (0.4 ppm) and Bi (2 ppm). The aqueous CO_2 inclusions from the same complex typically contain lower B, K, Ca, Ti, Cr (44 ppm), Mn, Fe, Ni, Co, Zn (99 ppm), As, Cu (20 ppm), Rb, Sr, Mo, Cs, Ba, Pb (7 ppm) and higher Ti (172 ppm) than the $LVHSn_{1to6}$ inclusions. Bi in these CO_2 inclusions are present in similar concentrations to the aforementioned $LVHSn_{1to6}$ varieties.

In general however comparison of ($LVHSn_{1to6}$) inclusions from the two igneous complexes shows that those from Mount Angelay contain higher Cr, Ni, As, Pb, Bi, U, Mo, similar Zn and Co to those from Lightning Creek. Opaque-bearing ($LVHSn_{1to6}$) inclusions from Lightning Creek and Mount Angelay returning 6280 ppm and 4033 ppm respectively, whereas the opaque-free varieties contain appreciably less (Mount Angelay: 396 ppm and Lightning Creek: 72 ppm).

Location	Mount Angelay			Mount Angelay			Lightning Creek			Lightning Creek			Lightning Creek		
Salinity	60 wt% equiv			60 wt% equiv			40.5 wt% equiv			40.5 wt% equiv			5 wt% equiv		
Description	multi-solid brine with opaque			lvh+1 solid			multi-solid brine with opaque			brine, with hematite			CO_2		
Analyses	n=9			n=7			n=8			n=3			n=2		
Element	**Average**	**Max**	**Min**	**Average**	**Max**	**Min**	**Average**	**Max**	**Min**	**Average**	**Max**	**Min**	**Average**	**Max**	**Min**
B11	2952	6294	451	536	1402	102	451	807	131	634	1307	268	349	349	349
Na23	160442	225090	32618	141343	192540	6234	92508	114683	45056	103098	128953	88826	19700	19700	19700
Mg24	111	202	14	325	923	30	60	126	12	29	52	17	BDL	BDL	BDL
K39	63488	172741	19755	59831	121520	25180	53548	108572	16339	32309	41350	21328	6503	12145	861
Ca43	104509	302065	12639	102560	383235	16413	33713	109905	8629	47198	65112	21916	2132	2132	2132
Ti47	4983	18803	19	372	1058	108	1511	3850	133	BDL	BDL	BDL	172	172	172
V51	BDL	BDL	BDL	11	29	1	BDL	BDL	BDL	BDL	BDL	BDL	BDL	BDL	BDL
Cr52	2083	4390	68	239	588	56	269	712	78	246	493	86	44	44	44
Mn55	4225	7257	1405	6071	24567	379	2060	5833	683	6471	10815	2853	156	156	156
Fe57	50011	79557	1036	28295	46089	1006	38910	47428	16532	33874	44576	19902	1438	1438	1438
Ni58	1242	3326	228	337	728	165	204	238	89	216	335	155	BDL	BDL	BDL
Co59	11	17	6	4	7	1	9	21	4	27	56	11	BDL	BDL	BDL
Zn64	1083	4352	174	709	2192	212	164	588	46	685	995	496	99	99	99
Cu65	4033	8071	20	396	1684	11	6280	8020	2636	72	179	13	20	20	20
Zn66	983	4354	184	683	2381	199	167	623	47	758	1164	531	80	80	80
As75	457	1073	34	108	268	22	16	36	8	52	75	28	BDL	BDL	BDL
Rb85	8178	51653	463	1476	3082	612	386	1120	141	785	1131	431	9	9	9
Sr88	1687	4568	72	1763	4976	436	308	1033	27	1126	1462	661	14	26	3
Mo98	31	51	11	5	7	2	13	24	5	BDL	BDL	BDL	BDL	BDL	BDL
Ag109	BDL	BDL	BDL	2.2	4	1	0.4	0.4	BDL	0.4	BDL	BDL	BDL	BDL	BDL
Cs133	1394	4619	106	173	439	26	24	53	7	89	104	59	5	7	3
Ba137	2093	6356	142	3018	5591	659	844	1865	167	2905	4715	1473	19	19	19
Au197	BDL	BDL	BDL	BDL	2	BDL	BDL	BDL	BDL	BDL	BDL	BDL	BDL	BDL	BDL
Pb208	317	644	20	162	473	57	32	118	7	38	43	30	7	7	7
Bi209	40	78	10	4	12	2	1	1	BDL	2	3	BDL	2	2	2
U238	13	21	5	18	31	4	5	8	BDL	BDL	BDL	BDL	BDL	BDL	BDL

All concentrations in ppm

Table 3. Summary of the range and average element concentrations for different fluid inclusions types from Mt Angelay and Lightning Creek.

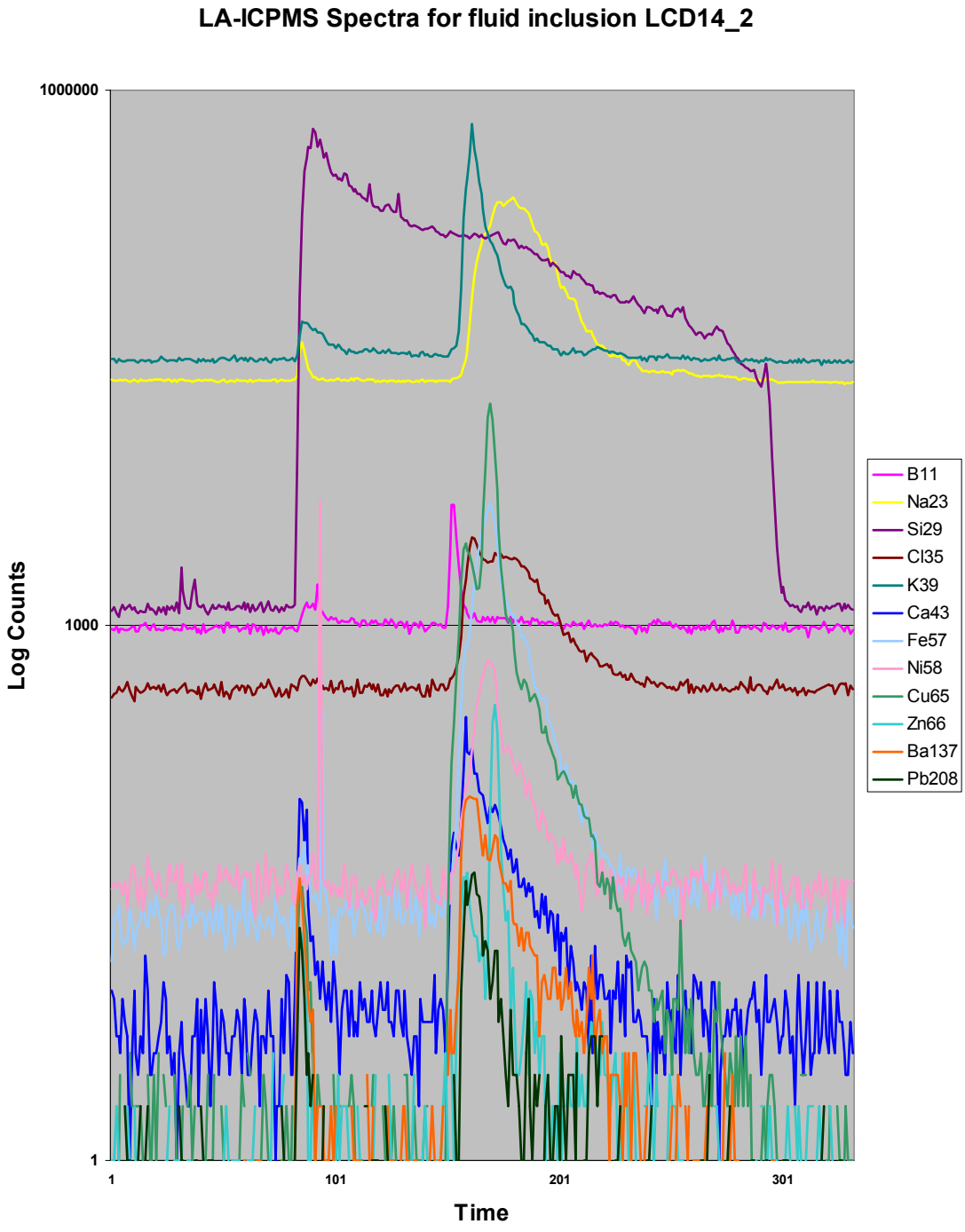

Fig. 6. LA-ICP-MS spectra of LVHSn_{1to6} fluid inclusion from Lightning Creek containing Cu (7491 ppm) Fe (43266 ppm), B (332 ppm), Cr (183 ppm), Ni (224 ppm), Pb (20 ppm) and Zn (132 ppm).

5. DISCUSSION

Fluid inclusion studies of iron-oxide copper gold deposits and sodic-calcic alteration within the Mount Isa Inlier commonly record the presence of both multisolid brines and low-salinity aqueous carbonic inclusions (Oliver, 1995; Adshead et al., 1998; Pollard, 2001; Mustard et al., 2004). Limited studies of fluid inclusions from igneous rocks highlight similar fluids were exsolved from granite-aplite sills at Lightning Creek and S-type pegmatite dykes at Osborne (Perring et al., 1999; Mustard et al., 2004). This study has identified the presence of abundant primary multisolid brines and low-salinity aqueous carbonic inclusions within all three of the granite suites from the Williams-Naraku batholth.

Unequivocal examples of unmixing (the presence of co-existing multisolid brines and low-salinity aqueous carbonic inclusions on the same trail) were observed in samples from Mount Angelay and Lightning Creek. Furthermore, the presence of minor primary mixed LVH-CO_2 inclusions in limited samples from each suite may potentially represent a precursor H_2O-CO_2-NaCl fluid prior to unmixing.

This report documents the first observation of chalcopyrite within some of the fluid inclusions in the Mount Isa region. This is a significant observation that has implications for the nature of the magmatic-hydrothermal fluids at Lightning Creek and for IOCG deposit models in Mount Isa. It suggests that there is sufficient sulfur in the magmatic fluid to form chalcopyrite. The current understanding of hydrothermal fluids related to IOCG deposits in the Mount Isa Inlier has led many researchers to suggest that a separate sulfur source is necessary and that the mixing of a Cu-rich fluid and a separate S-rich fluid or rock was required to cause copper precipitation (Oliver et al., 2004).

The Ernest Henry deposit has a contained metal content of 1,905,699 t Cu and 2,977,639 oz Au (based on previous production of 78,287 oz Au, 66,699 t Cu and an existing resource of 169Mt @ 1.1% Cu and 0.54g/t Au) (pers. comm. D. A-Izzeddin, 2005). A simple calculation can be made to evaluate the metal potential of a typical Williams-Naraku intrusion. Wholerock analyses of granite samples from the Mt Angelay Igneous complex, returned an average Cu content range from 27 ppm Cu (Mark, 2001; 8 samples), to 28 ppm(Mark, 1999; 24 samples), and 30 ppm (Tolman, 1998; 14 samples). A granite body measuring 10 x 2 x 2 km in volume (200 km^3) contains $5.5x10^{11}$ tonnes of magma (using a density of 2750kg/m^3 for granite). Assuming a Cu concentration of 25 ppm Cu the magma contains $1.4x10^7$ tonnes of Cu., which is an order of magnitude more than what ends up in the deposit. Assuming a concentration of 5000ppm Cu in the fluid, the fluid/rock ratio (the amount of fluid needed and the potential mass of rock encountered) is very small (0.0001 or 0.01%).

Acknowledgements
This work was funded by the pmdCRC and personally by R. Mustard. We thank C. Allen and J.M.G. Shelley for technical support with the LA-ICP-MS.

6. REFERENCES

Adshead ND, Voulgaris P, Muscio VN (1998) Osborne copper-gold deposit. In: Berkman DA, Mackenzie DH (eds) Geology of Australian and Papua New Guinean mineral deposits. The Australian Institute of Mining and Metallurgy, Melbourne, pp 793-799.

Baker T (1998) Alteration, mineralisation, and fluid evolution at the Eloise Cu-Au Depsoit, Cloncurry district, Northwest Queensland, Australia. Economic Geology. 93:1213-1236.

Budd, AR, Wyborn LAI, Bastrakova IV (2001) The metallogenic potential of Australian proterozoic granites. Geoscience Australia Record 2001/12.

Longerich, H.P., Jackson, S.E., and Guenther, D., 1996, Laser ablation inductively coupled plasma mass spectrometric transient signal data acquisition and analyte concentration calculation: Journal of Analytical Atomic Spectrometry, v. 11, p. 899-904.

Mark G and De Jong G (1996) Synchronous garnitoid emplacement and episodic sodic-calcic alteration in the Cloncurry district: Styles, timing and metallogenic significance, in Baker T. Rotherham J., Richmond J., Mark G and Williams PJ. Eds. New developments in metallogenic research: The McArthur, Mt Isa, Cloncurry mineral province, James Cook University of North Queensland Economic Research Unit Contribution 55. p81-84

Mark G (1998) Unpublished PhD thesis, James Cook University, Townsville, Australia, Granites and regional alteration in the Cloncurry district, NW Queensland.

Mark G., (1999). Petrogenesis of the Mesoproterzoic K-rich granitoids, southern Mt Angelay igneous complex, Cloncurry district, northwest Queensland. Australian Journal of Earth Sciences, 46: 933-949.

Mark G, Baker T, Williams P, Mustard R, Ryan C and Mernagh T (2004) The geochemistry of magmatic fluids, Cloncurry district, Australia: relations to IOCG systems. In Barnicoat AC and Korsch RJ (Eds) Predictive Mineral Discovery Cooperative Research Centre. Record 2004/9. 123-126.

Mitchell, L.C., (1993). Geology and Geochemistry of the Wiley Igneous Complex, Eastern Fold Belt, Mt Isa Inlier. Unpublished BSc (Honours) thesis, James Cook University, Townsville, Australia, 128p

Mustard R, Baker T, Williams PJ, Mernagh T, Ryan CG, Van Achterbergh and Adshead N. (2004) The role of unmixing in magnetite ± copper deposition in Fe-oxide Cu-Au systems. In Barnicoat AC and Korsch RJ (Eds) Predictive Mineral Discovery Cooperative Research Centre. Record 2004/9. 155-159.

Nunn AJ (1995) The relationship between texturally complex granitic dykes and Cu-Au mineralization at the Lightning Creek Prospect, Selwyn Region, Northwest Queensland. Unpublished BSc (Honours) thesis, James Cook University, Townsville, Australia, 81p

Oliver NHS (1995) Hydrothermal history of the Mary Kathleen fold Belt, Mount Isa Block, Queensland. Australian Journal of Earth Sciences, 42: 267-279.

Oliver NHS, Cleverly JC, Mark G, Pollard P, Fu B, Marshall L, Rubenach MJ, Williams PJ and Baker T (2004) Modeling the role of Sodic alteration in the genesis of Iron Oxide-Copper-Gold Depsoits, Eastern Mount Isa Block, Australia. Economic Geology 99:1145-1176.

Perkins C and Wyborn LAI (1998) Age of Cu-Au mineralization, Cloncurry district, eastern Mt Isa Inlier, Queensland, as determined by 40Ar/39Ar dating. Australian Journal of Earth Sciences. 45: 233-246.

Perring CS, Pollard PJ, Dong, G., Nunn AJ and Blake KL, (2000). The Lightning Creek sill complex, Cloncurry District, northwest Queensland: a source of fluids for Fe oxide Cu-Au mineralsiation and sodic-calcic alteration, Economic Geology, 95:1067-1089.

Perring CS, Pollard PJ, and Nunn AJ (2001) Petrogenesis of the Squirrel Hills granite and associated magnetite-rich sill and vein complex: Lightning Creek prospect, Cloncurry district, Northwest Queensland. Precambrian Research. 106:213-238.

Pollard PJ, Mark G and Mitchell LC (1996) Graintoids of the Mount Angely and Whiley Igneous Complexes: Links to alteration and Cu-Au-Co mineralization in the Cloncurry district, in Baker T. Rotherham J., Richmond J., Mark G and Williams PJ. Eds. New developments in metallogenic research: The McArthur, Mt Isa, Cloncurry mineral province, James Cook University of North Queensland Economic Research Unit Contribution 55. p104-107.

Pollard PJ, Mark G., and Mitchell LC (1998) Geochemistry of post-1540 Ma granites in the Cloncurry district, northwest Queensland: Economic Geology. 93: 1330-1344.

Pollard PJ (2001) Sodic(-calcic) alteration in Fe-oxide-Cu-Au districts: an origin via unmixing of magmatic H2O-CO2-NaCl ± CaCl2-KCl fluids. Mineralium Depsoita. 36: 93-100.

Shepherd, T. J., Rankin, A. H., and Alderton, D. H. M., A practical guide to fluid inclusion studies, Glasgow, Blackie & Son, United Kingdom, 239 p.

Sterner, S.M., Hall, D.L. and Bodnar, R.J. (1988) Synthetic fluid inclusions V: Solubility relations in the NaCl-KCl-H_2O system under vapor-saturated conditions. Geochim. Cosmochim. Acta 52, 989-1005

Tolman J.L., (1998). Origin and formation of complexly textured albite-, actinolite, apatite-rich rocks within the Central Mount Angelay igneous complex, Cloncurry district, Northwest Queensland. Unpublished BSc (Honours) thesis, James Cook University, Townsville, Australia, 174p

Rotherham JF, Blake KL, Cartwright I. and Williams PJ (1998) Stable isotope evidence for the origin of the Mesoproterozoic Starra Au-Cu deposit, Cloncurry district, northwest Queensland. Economic Geology. 93: 1435-1449.

Williams PJ and Pollard PJ (2001) Australia Proterzoic Iron Oxide-Cu-Au Depsoits: An Overview with New Metallogenic and Exploration Data from the Cloncurry District, Northwest Queensland. Explor. Mining Geology. 10(3): 191-213. Canadian Institute of Mining, Metallurgy and Petroleum.

Wyborn LAI, (1988) The younger ca 1500 Ma granites of the Williams and Naraku Batholiths, Cloncurry district, Eastern Mt Isa Inlier: geochemistry, origin, metallogenic significance and exploration indicators. Australian Journal of Earth Sciences 45:397-412.

Appendix 1 – Scanned thin Sections

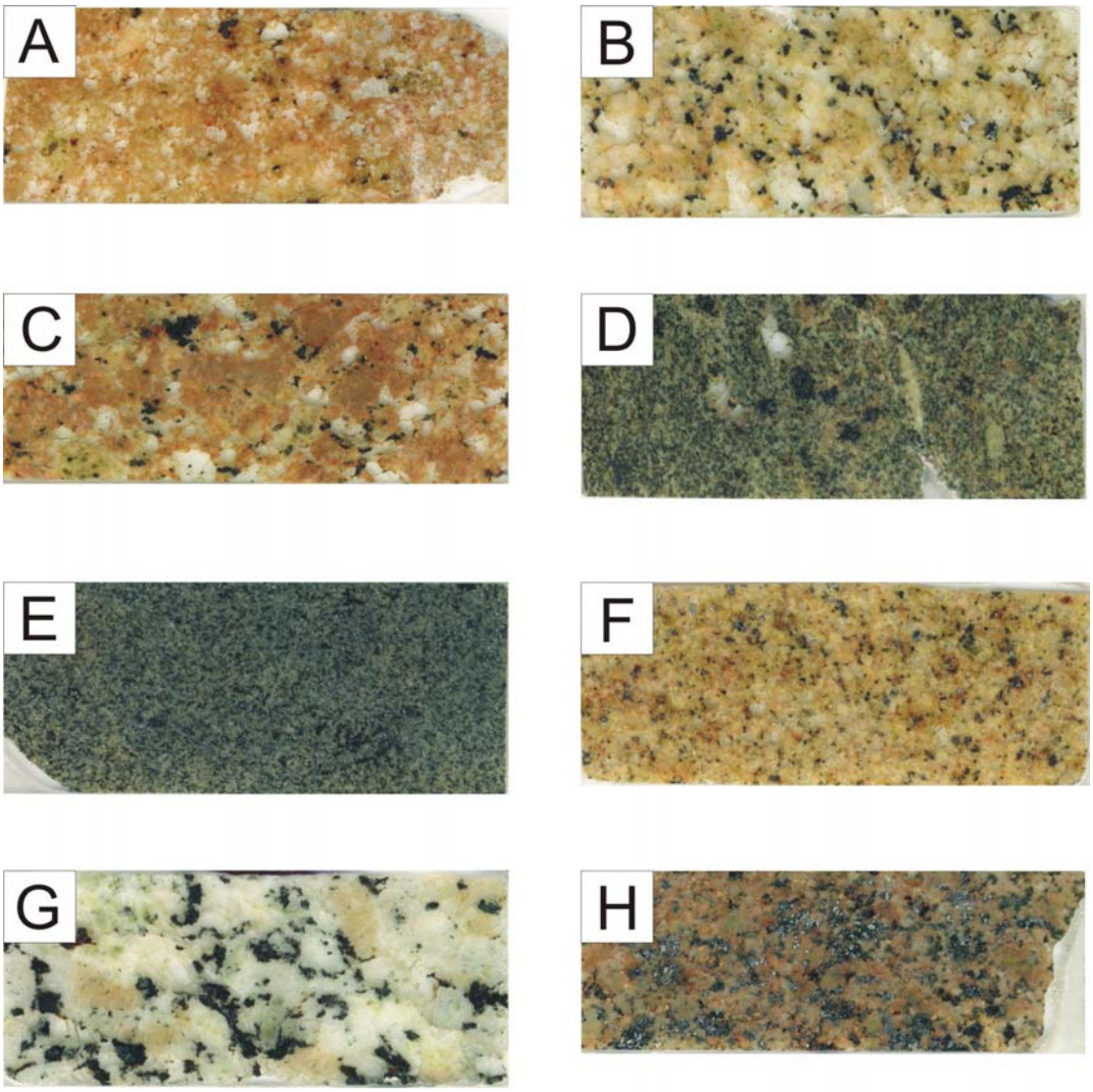

Lightning Creek samples (scans of doubly polished thin sections studied).
A. LCF01. Alkali granite.
B. LCF02. Tonalite.
C. LCF04. Monzogranite.
D. LCF06A. Quartz diorite.
E. LCF09. Quartz diorite.
F. LCF10. Tonalite.
G. LCF12. Monzogranite.
H. LCD14_01. Monzodiorite.

Appendix 1 – Scanned thin Sections cont.

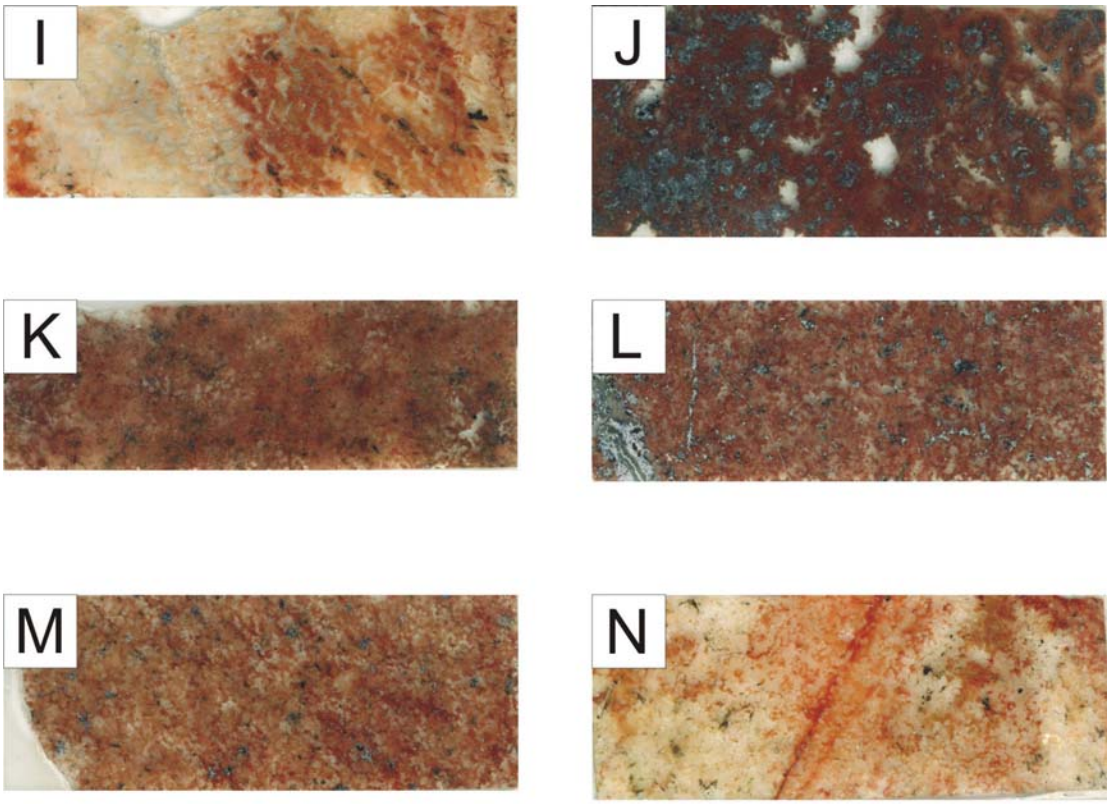

Lightning Creek samples (scans of doubly polished thin sections studied).

I. LCD14_214.5. Aplitic (granophyric) quartz-feldspar sill.
J. LCD14_238.15. Spherulitic iron-rich sill.
K. LCD14_238.3. Spherulitic quartz-feldspar sill.
L. LCD16_136.5. Aplitic (Ca-Fe) quartz-feldspar sill.
M. LCD16_02. Tonalite.
N. LCD31_148.35. Aplitic quartz-feldspar sill.

Appendix 1 – Scanned thin Sections cont.

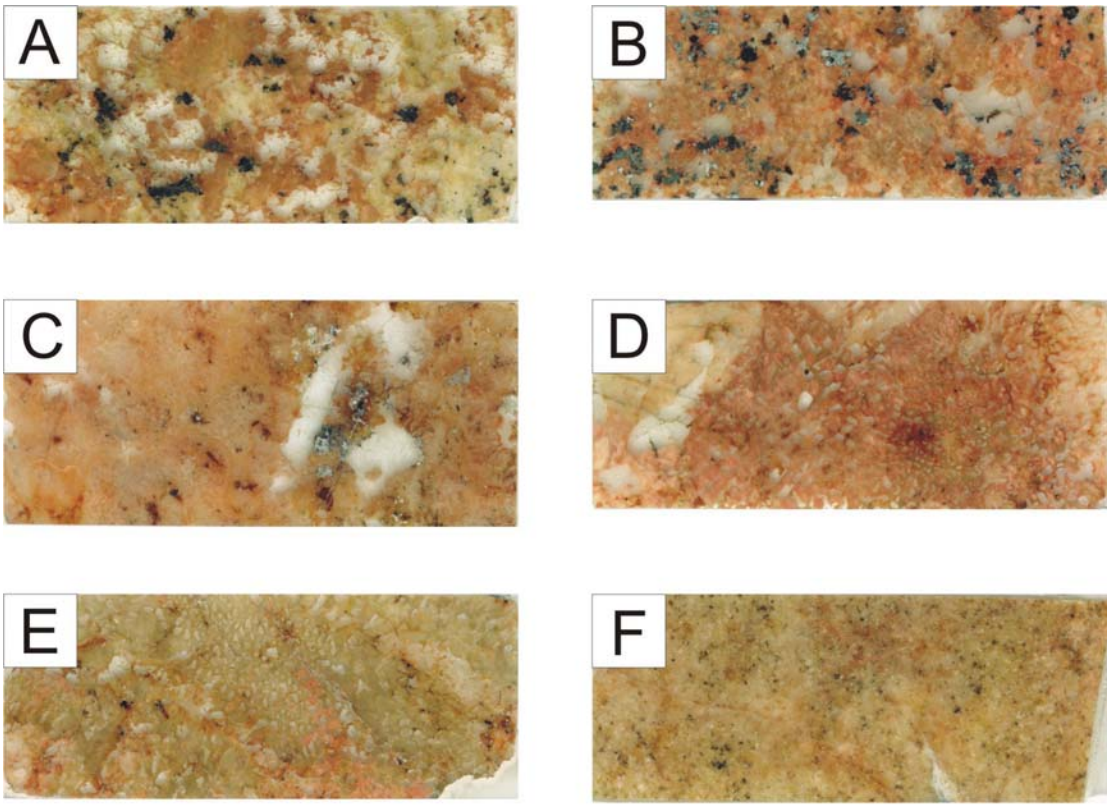

Mount Angely igneous complex samples (scans of doubly polished thin sections studied).

A. GC01. Quartz syenite.
B. GC03. Syenogranite.
C. GC05. Quartz-abite-magnetite rock.
D. GC06A. Pegmatite.
E. GC06B. Pegmatite.
F. GC07. Aplite.

Appendix 1 – Scanned thin Sections cont.

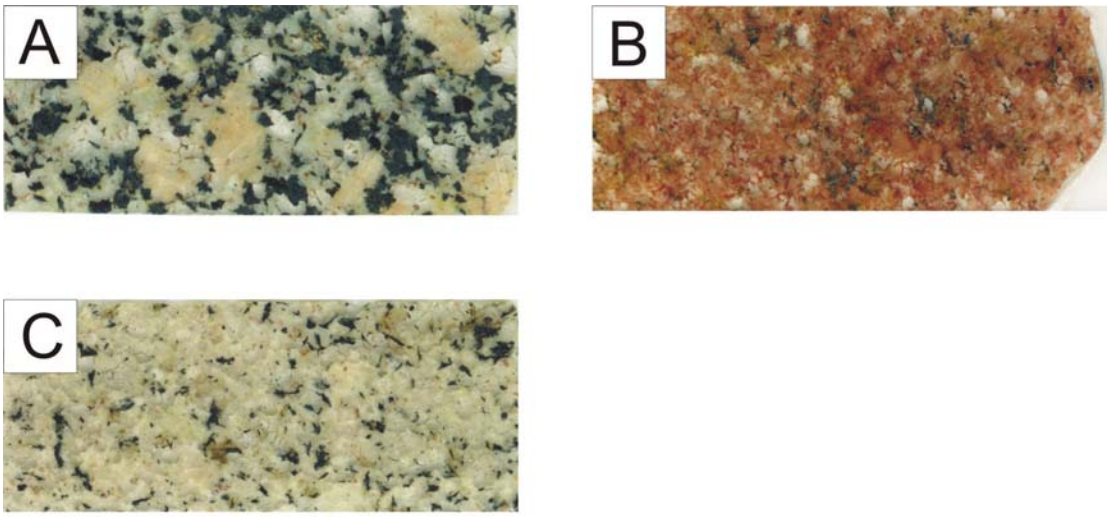

Whiley Igneous complex samples (scans of doubly polished thin sections studied).

A. 26.16. 'Roadrunner' granite.
B. 26.18. 'Wallaby' granite.
C. 26.19. 'Block' granite.

Appendix 2. Microthermometic Analysis.

Inclusion	Chip	Phases	Tfm	Tm ice	Th hh	Th vap	Th hal	Tdecrep	Comments
GC6A	3a	L+3S?					>500		close to decrepitation
GC6A	3b	LS					420		
GC6A	3c	L+V+2S+Op				235	>550		
GC6A	3d	L+S+Op					530		
GC6A	6a	L+V+3S?				150	465		2 small solids unchanged
GC6A	6b	LVS				290	280		
GC6A	6c	L+V+2S?				>400	220		Solid no change up to 400
GC6A	1a	L+V+2S+Op					>>500		Large halite
GC6A	1b							~400	
GC6A	1c	L+2S+2Op						~400	
GC6A	1d	L+3S+2Op						~400	
GC6A	1e						>500		probably Ths 500-600
GC6A	1f						>500		
LCD14	2a	L+V+2S+Op	-55	-28.4	10	140	282		
LCD14	2b	L+V+2S+Op	-50	-30			350/470		
LCD14	2c	L+V+2S+Op							
LCD14	2d	L+V+S+Op	-60	-32	4	139	260		
LCD14	2e	L+V+2S	-58	-37.2		136	305		
LCD14	2f	LVH	-58	-30.7		135	205		
LCD14	2g	L+V+2S	-58	-35	0.7	125		360	

Appendix 3. LA-ICPMS Analysis

Sample No.	Used	Location	Laser	Standard	Description	Comments	B11	Na23	Mg24	K39	Ca43	Ti47	V51	Cr52	Mn55
GC6A_1	Y	Mount Angelay	40um	60 wt% equiv	multi solid brine with opaque		586	149748	197	172741	32599	-160	-12	-542	2872
GC6A_2a	N	Mount Angelay	40um	60 wt% equiv	multi solid brine with opaque		474	61242	3140	34387	274191	11133	70	305	1814
GC6A_2b	Y	Mount Angelay	40um	60 wt% equiv	multi solid brine with opaque		451	165202	176	40262	63511	18803	-3	382	2146
GC6A_3	Y	Mount Angelay	40um	60 wt% equiv	multi solid brine with opaque		-80	32618	32	100078	302065	-34	-3	-167	1405
GC6A_4	N	Mount Angelay	40um	60 wt% equiv	multi solid brine with opaque	Small, Na, Rb only.	1693	216315	-91	50815	-18940	2696	-26	2353	-73
GC6A_7	Y	Mount Angelay	40um	60 wt% equiv	multi solid brine with opaque		-574	121216	-74	129465	111733	-206	-20	-1134	7257
GC6A_8	Y	Mount Angelay	40um	60 wt% equiv	lvh+1 solid	Cu	346	178875	253	77886	28155	-13	-1	140	4651
GC6A_9	Y	Mount Angelay	40um	60 wt% equiv	lvh+1 solid	Cu	1350	71575	842	121520	173922	108	-1	216	24567
GC6A_10	Y	Mount Angelay	40um	60 wt% equiv	lvh+1 solid	Cu	1402	192540	92	33732	16413	340	2	142	2206
GC6A_11	Y	Mount Angelay	40um	60 wt% equiv	lvh+1 solid	Na, Ba, Sr spike removed	162	166270	923	70313	42227	1058	29	588	2819
GC6A_12a	N	Mount Angelay	40um	60 wt% equiv	lvh+1 solid	Cu	111	15774	195	57520	344861	1229	9	64	9123
GC6A_12b	N	Mount Angelay	40um	60 wt% equiv	lvh+1 solid	Cu	1653	124432	-165	97093	95439	1835	-44	7509	29230
GC6A_12c	Y	Mount Angelay	40um	60 wt% equiv	lvh+1 solid	Cu	138	6234	30	53979	383235	-42	-4	-176	379
GC6A_13	Y	Mount Angelay	40um	60 wt% equiv	lvh+1 solid	Cu	250	190777	82	25180	38558	172	1	56	3435
GC6A_14	Y	Mount Angelay	40um	60 wt% equiv	lvh+1 solid, best spectra by far	overall, Ni spike removed, Cu	102	183128	52	36205	35413	180	-1	289	4443
GC6A_15	N	Mount Angelay	40um	60 wt% equiv	lvh+1 solid	spikey, Cu	-142	43467	2234	267177	137344	1244	11	862	10162
GC6A_16	Y	Mount Angelay	40um	60 wt% equiv	multi solid brine with opaque	good Cu	6294	193477	202	19755	-7470	421	-7	2267	5620
GC6A_17	Y	Mount Angelay	40um	60 wt% equiv	multi solid brine with opaque	good Cu	-46	225090	14	22423	-1513	-23	-2	-102	2135
GC6A_18	Y	Mount Angelay	40um	60 wt% equiv	multi solid brine with opaque	good Cu	1306	177531	46	36646	12639	19	2	68	4462
GC6A_19	Y	Mount Angelay	40um	60 wt% equiv	multi solid brine with opaque	Ni, Zn, Pb spikes removed	4057	189739	-62	23728	-12664	687	-16	3309	6006
GC6A_20	Y	Mount Angelay	40um	60 wt% equiv	multi solid brine with opaque	good Cu	5018	189361	-193	26295	-46491	-507	-46	4390	6122
LCD14_1a	N	Lightning Creek	32um	40.5 wt% equiv	brine	good cu	157	20850	338	72276	131814	1669	1	172	10313
LCD14_1b	Y	Lightning Creek	32um	40.5 wt% equiv	brine	good cu	131	45056	12	17290	8629	133	0	80	683
LCD14_2	Y	Lightning Creek	32um	40.5 wt% equiv	brine	good cu	332	100670	40	64706	26267	257	-1	183	1362
LCD14_3	Y	Lightning Creek	32um	40.5 wt% equiv	brine	laser shut down during run	325	112819	53	39710	22959	196	0	78	1484
LCD14_4	Y	Lightning Creek	32um	40.5 wt% equiv	brine	good cu	301	112031	62	49110	15348	277	0	134	1361
LCD14_5	N	Lightning Creek	32um	40.5 wt% equiv	brine		389	125550	-3	46168	23537	27	-1	-45	1130
LCD14_6	N	Lightning Creek	32um	40.5 wt% equiv	brine	good cu	485	48263	-10	98847	130174	670	-3	-177	4218
LCD14_7	Y	Lightning Creek	32um	40.5 wt% equiv	brine	good cu	807	114683	39	16339	34560	3445	-2	712	1664
LCD14_8	Y	Lightning Creek	32um	40.5 wt% equiv	brine	good cu	700	87119	110	107254	25499	3850	-1	262	1984
LCD14_9	Y	Lightning Creek	32um	40.5 wt% equiv	brine	good cu	564	113076	36	25403	26534	2417	-4	432	2109
LCD14_10	Y	Lightning Creek	32um	40.5 wt% equiv	brine, with hematite		328	91514	18	34249	54567	-10	-1	493	10815
LCD14_11	Y	Lightning Creek	40um	40.5 wt% equiv	brine	Ni spikes removed, good cu	1307	88826	52	41350	65112	-4	0	160	5745
LCD14_12	Y	Lightning Creek	40um	40.5 wt% equiv	brine	Ni spikes removed, good cu	268	128953	17	21328	21916	-2	0	86	2853
LCD14_13	N	Lightning Creek	40um	5 wt% equiv	CO2	no good, Au spike removed	2141	19700	867	133071	42735	10083	-16	-1068	145
LCD14_14	N	Lightning Creek	40um	5 wt% equiv	CO2	small	490	19700	1474	47790	45272	2113	22	326	160
LCD14_15	Y	Lightning Creek	40um	5 wt% equiv	CO2		349	19700	-2	861	-575	172	-1	44	-2
LCD14_16	N	Lightning Creek	40um	5 wt% equiv	CO2, trace cu	unclear	-227	19700	-23	4339	10437	-87	-6	-405	1977
LCD14_17a	N	Lightning Creek	40um	5 wt% equiv	brine or CO2	very small	-110	19700	-18	-1916	-4163	-58	-4	-324	1156
LCD14_17b	Y	Lightning Creek	40um	5 wt% equiv	brine or CO2	very small	-53	19700	-8	12145	2132	-28	-2	-155	156
LCD14_18	N	Lightning Creek	40um	40.5 wt% equiv	brine		-1809	23767	-255	62574	195394	-835	-59	-4019	6337
LCD14_19	Y	Lightning Creek	40um	40.5 wt% equiv	brine		-608	54611	126	108572	109905	-310	-22	-1604	5833
LCD14_20	N	Lightning Creek	40um	40.5 wt% equiv	brine	Cu and Mn only	-4501	24608	-693	109050	-184105	-2154	-200	-10443	21452
LCD14_21	N	Lightning Creek	40um	40.5 wt% equiv	brine		1557	39352	7751	36521	144361	-102	151	-481	836
LCD14_22	N	Lightning Creek	40um	40.5 wt% equiv	brine		5236	52237	1469	203383	44427	20315	18	-909	60
LCD14_23	N	Lightning Creek	40um	40.5 wt% equiv	brine	cont? Pb spike remv	4669	60730	1896	185656	39432	-264	24	-1243	96
LCD14_24	N	Lightning Creek	40um	40.5 wt% equiv	brine		302	145753	1003	3868	14492	39390	10	-375	93

Appendix 3. LA-ICPMS Analysis cont.

Sample No.	Used	Location	Laser	Standard	Description	Comments	Fe57	Ni58	Co59	Zn64	Cu65	Zn66	As75	Rb85	Sr88
GC6A_1	Y	Mount Angelay	40um	60 wt% equiv	multi solid brine with opaque		-1966	-95	17	4352	-47	4354	-118	51653	2102
GC6A_2a	N	Mount Angelay	40um	60 wt% equiv	multi solid brine with opaque		10904	5046	8	423	716	494	179	151	22666
GC6A_2b	Y	Mount Angelay	40um	60 wt% equiv	multi solid brine with opaque		43950	228	-2	381	-9	395	182	463	954
GC6A_3	Y	Mount Angelay	40um	60 wt% equiv	multi solid brine with opaque		-549	-24	-3	1235	20	1174	34	1664	4568
GC6A_4	N	Mount Angelay	40um	60 wt% equiv	multi solid brine with opaque	Small, Na, Rb only.	-3323	-191	-24	100	594	-77	-220	2815	-13
GC6A_7	Y	Mount Angelay	40um	60 wt% equiv	multi solid brine with opaque		3458	-144	-19	1134	432	1058	-168	901	2307
GC6A_8	Y	Mount Angelay	40um	60 wt% equiv	lvh+1 solid	Cu	21924	171	-1	274	75	371	22	1445	1481
GC6A_9	Y	Mount Angelay	40um	60 wt% equiv	lvh+1 solid	Cu	22716	468	-1	2192	1684	2381	268	3082	2594
GC6A_10	Y	Mount Angelay	40um	60 wt% equiv	lvh+1 solid	Cu	46089	728	7	212	11	199	223	1900	534
GC6A_11	Y	Mount Angelay	40um	60 wt% equiv	lvh+1 solid	Na, Ba, Sr spike removed	38201	246	-3	898	257	378	56	1143	1772
GC6A_12a	N	Mount Angelay	40um	60 wt% equiv	lvh+1 solid	Cu	10752	815	-1	3000	98	3617	203	1306	4401
GC6A_12b	N	Mount Angelay	40um	60 wt% equiv	lvh+1 solid	Cu	18555	-356	-47	3338	-158	3425	-391	706	2275
GC6A_12c	Y	Mount Angelay	40um	60 wt% equiv	lvh+1 solid	Cu	1006	-29	-4	241	56	271	68	1493	4976
GC6A_13	Y	Mount Angelay	40um	60 wt% equiv	lvh+1 solid	Cu	28715	165	1	520	185	519	61	658	546
GC6A_14	Y	Mount Angelay	40um	60 wt% equiv	lvh+1 solid, best spectra by far	overall, Ni spike removed, Cu	39416	247	-2	623	499	660	54	612	436
GC6A_15	N	Mount Angelay	40um	60 wt% equiv	lvh+1 solid	spikey, Cu	15151	202	-5	2166	608	3082	253	2728	4081
GC6A_16	Y	Mount Angelay	40um	60 wt% equiv	multi solid brine with opaque	good Cu	70719	1030	-8	711	6859	530	1073	3684	-4
GC6A_17	Y	Mount Angelay	40um	60 wt% equiv	multi solid brine with opaque	good Cu	1036	-11	11	233	931	228	438	3315	122
GC6A_18	Y	Mount Angelay	40um	60 wt% equiv	multi solid brine with opaque	good Cu	79557	383	6	174	4218	184	261	2724	72
GC6A_19	Y	Mount Angelay	40um	60 wt% equiv	multi solid brine with opaque	Ni, Zn, Pb spikes removed	76400	3326	-17	956	7701	402	707	4365	-6
GC6A_20	Y	Mount Angelay	40um	60 wt% equiv	multi solid brine with opaque	good Cu	74959	-342	-51	573	8071	518	501	4832	-23
LCD14_1a	N	Lightning Creek	32um	40.5 wt% equiv	brine	good cu	75676	291	119	1030	32629	845	132	1311	938
LCD14_1b	Y	Lightning Creek	32um	40.5 wt% equiv	brine	good cu	16532	89	4	46	2636	47	11	141	73
LCD14_2	Y	Lightning Creek	32um	40.5 wt% equiv	brine	good cu	43266	224	5	134	7491	132	9	343	148
LCD14_3	Y	Lightning Creek	32um	40.5 wt% equiv	brine	laser shut down during run	40957	214	6	98	8020	103	8	259	108
LCD14_4	Y	Lightning Creek	32um	40.5 wt% equiv	brine	good cu	44150	237	4	126	5173	127	16	249	27
LCD14_5	N	Lightning Creek	32um	40.5 wt% equiv	brine		6867	35	-1	77	-3	88	10	656	494
LCD14_6	N	Lightning Creek	32um	40.5 wt% equiv	brine	good cu	1873	-20	-3	652	1381	545	-25	2104	1437
LCD14_7	Y	Lightning Creek	32um	40.5 wt% equiv	brine	good cu	42121	235	11	113	6427	110	-22	244	286
LCD14_8	Y	Lightning Creek	32um	40.5 wt% equiv	brine	good cu	37915	190	21	72	6703	69	36	448	500
LCD14_9	Y	Lightning Creek	32um	40.5 wt% equiv	brine	good cu	47428	238	16	137	7510	125	-29	287	286
LCD14_10	Y	Lightning Creek	32um	40.5 wt% equiv	brine, with hematite		44576	335	56	995	25	1164	28	793	1253
LCD14_11	Y	Lightning Creek	40um	40.5 wt% equiv	brine	Ni spikes removed, good cu	37145	158	15	565	179	577	75	1131	1462
LCD14_12	Y	Lightning Creek	40um	40.5 wt% equiv	brine	Ni spikes removed, good cu	19902	155	11	496	13	531	-2	431	661
LCD14_13	N	Lightning Creek	40um	5 wt% equiv	CO2	no good, Au spike removed	6858	4480	24	3255	1408	3195	823	660	600
LCD14_14	N	Lightning Creek	40um	5 wt% equiv	CO2	small	4247	151	19	5719	745	5746	191	263	1765
LCD14_15	Y	Lightning Creek	40um	5 wt% equiv	CO2		-104	-5	-1	-2	-3	-2	-5	9	3
LCD14_16	N	Lightning Creek	40um	5 wt% equiv	CO2, trace cu	unclear	32159	138	9	109	41	109	-65	-22	123
LCD14_17a	N	Lightning Creek	40um	5 wt% equiv	brine or CO2	very small	13873	74	6	89	26	75	-32	26	65
LCD14_17b	Y	Lightning Creek	40um	5 wt% equiv	brine or CO2	very small	1438	-17	-2	99	20	80	-15	9	26
LCD14_18	N	Lightning Creek	40um	40.5 wt% equiv	brine		-8648	-436	-74	3412	29771	3150	-470	3760	2936
LCD14_19	Y	Lightning Creek	40um	40.5 wt% equiv	brine		-3249	-161	-26	588	-89	623	-185	1120	1033
LCD14_20	N	Lightning Creek	40um	40.5 wt% equiv	brine	Cu and Mn only	-22366	-1172	982	5264	80077	4740	-1387	4948	1874
LCD14_21	N	Lightning Creek	40um	40.5 wt% equiv	brine		25271	258	46	510	1137	713	513	242	20188
LCD14_22	N	Lightning Creek	40um	40.5 wt% equiv	brine		7484	590	35	658	959	506	991	1277	433
LCD14_23	N	Lightning Creek	40um	40.5 wt% equiv	brine	cont? Pb spike remv	6480	-125	26	2548	15154	1658	981	1241	553
LCD14_24	N	Lightning Creek	40um	40.5 wt% equiv	brine		4106	2766	24	382	542	303	237	-17	751

Appendix 3. LA-ICPMS Analysis cont.

Sample No.	Used	Location	Laser	Standard	Description	Comments	Mo98	Ag109	Cs133	Ba137	Au197	Pb208	Bi209	U238
GC6A_1	Y	Mount Angelay	40um	60 wt% equiv	multi solid brine with opaque		-16	-8	4619	-44	-23	131	19	-9
GC6A_2a	N	Mount Angelay	40um	60 wt% equiv	multi solid brine with opaque		21	-2	-5	40809	9	781	4	172
GC6A_2b	Y	Mount Angelay	40um	60 wt% equiv	multi solid brine with opaque		-5	-2	106	1418	-6	71	-2	-3
GC6A_3	Y	Mount Angelay	40um	60 wt% equiv	multi solid brine with opaque		-6	-2	234	6356	-5	20	-2	-4
GC6A_4	N	Mount Angelay	40um	60 wt% equiv	multi solid brine with opaque	Small, Na, Rb only.	-35	-20	-44	-105	-41	-39	-18	-21
GC6A_7	Y	Mount Angelay	40um	60 wt% equiv	multi solid brine with opaque		-17	-15	-37	3806	-27	235	-13	-15
GC6A_8	Y	Mount Angelay	40um	60 wt% equiv	lvh+1 solid	Cu	-1	1	139	3536	2	123	3	-1
GC6A_9	Y	Mount Angelay	40um	60 wt% equiv	lvh+1 solid	Cu	-2	3	261	5591	-2	473	12	21
GC6A_10	Y	Mount Angelay	40um	60 wt% equiv	lvh+1 solid	Cu	2	-1	234	4197	-1	110	2	4
GC6A_11	Y	Mount Angelay	40um	60 wt% equiv	lvh+1 solid	Na, Ba, Sr spike removed	7	4	26	4024	-6	160	2	31
GC6A_12a	N	Mount Angelay	40um	60 wt% equiv	lvh+1 solid	Cu	14	2	359	4399	-2	125	-1	8
GC6A_12b	N	Mount Angelay	40um	60 wt% equiv	lvh+1 solid	Cu	-51	-47	-89	8320	-65	516	-25	-33
GC6A_12c	Y	Mount Angelay	40um	60 wt% equiv	lvh+1 solid	Cu	-4	-4	439	2160	-5	57	-2	-3
GC6A_13	Y	Mount Angelay	40um	60 wt% equiv	lvh+1 solid	Cu	-1	1	68	960	-1	111	2	16
GC6A_14	Y	Mount Angelay	40um	60 wt% equiv	lvh+1 solid, best spectra by far	overall, Ni spike removed, Cu	-2	2	44	659	-2	104	2	-1
GC6A_15	N	Mount Angelay	40um	60 wt% equiv	lvh+1 solid	spikey, Cu	58	21	180	10137	-6	848	7	106
GC6A_16	Y	Mount Angelay	40um	60 wt% equiv	multi solid brine with opaque	good Cu	-9	-6	2393	142	-12	644	78	13
GC6A_17	Y	Mount Angelay	40um	60 wt% equiv	multi solid brine with opaque	good Cu	-2	-2	603	620	-2	302	12	-1
GC6A_18	Y	Mount Angelay	40um	60 wt% equiv	multi solid brine with opaque	good Cu	11	-1	382	216	-1	271	10	5
GC6A_19	Y	Mount Angelay	40um	60 wt% equiv	multi solid brine with opaque	Ni, Zn, Pb spikes removed	51	25	1016	-81	-24	622	64	21
GC6A_20	Y	Mount Angelay	40um	60 wt% equiv	multi solid brine with opaque	good Cu	-54	-32	1798	-188	-63	560	60	-25
LCD14_1a	N	Lightning Creek	32um	40.5 wt% equiv	brine	good cu	81	3	142	2620	-1	79	8	40
LCD14_1b	Y	Lightning Creek	32um	40.5 wt% equiv	brine	good cu	5	0	11	227	0	7	0	0
LCD14_2	Y	Lightning Creek	32um	40.5 wt% equiv	brine	good cu	12	-1	24	361	-1	20	1	3
LCD14_3	Y	Lightning Creek	32um	40.5 wt% equiv	brine	laser shut down during run	13	0	16	324	0	12	0	7
LCD14_4	Y	Lightning Creek	32um	40.5 wt% equiv	brine	good cu	14	0	7	167	0	22	1	7
LCD14_5	N	Lightning Creek	32um	40.5 wt% equiv	brine		-1	-1	44	1419	-1	42	-1	1
LCD14_6	N	Lightning Creek	32um	40.5 wt% equiv	brine	good cu	-4	-2	149	4991	-3	101	-2	-2
LCD14_7	Y	Lightning Creek	32um	40.5 wt% equiv	brine	good cu	8	-2	19	1100	-3	19	-2	7
LCD14_8	Y	Lightning Creek	32um	40.5 wt% equiv	brine	good cu	24	-1	42	1585	-1	31	1	8
LCD14_9	Y	Lightning Creek	32um	40.5 wt% equiv	brine	good cu	16	-2	17	1125	-4	27	-2	5
LCD14_10	Y	Lightning Creek	32um	40.5 wt% equiv	brine, with hematite		-2	-1	103	2528	-1	40	3	-1
LCD14_11	Y	Lightning Creek	40um	40.5 wt% equiv	brine	Ni spikes removed, good cu	-1	0	104	4715	0	30	3	0
LCD14_12	Y	Lightning Creek	40um	40.5 wt% equiv	brine	Ni spikes removed, good cu	0	0	59	1473	0	43	0	0
LCD14_13	N	Lightning Creek	40um	5 wt% equiv	CO2	no good, Au spike removed	-14	39	-29	1997	-19	194	-10	30
LCD14_14	N	Lightning Creek	40um	5 wt% equiv	CO2	small	-4	-2	-9	10072	8	323	4	21
LCD14_15	Y	Lightning Creek	40um	5 wt% equiv	CO2		-1	0	3	-3	-1	-1	0	0
LCD14_16	N	Lightning Creek	40um	5 wt% equiv	CO2, trace cu	unclear	-12	-5	-13	111	-7	-12	-4	-6
LCD14_17a	N	Lightning Creek	40um	5 wt% equiv	brine or CO2	very small	-5	-4	-9	85	-5	-6	-2	-3
LCD14_17b	Y	Lightning Creek	40um	5 wt% equiv	brine or CO2	very small	-3	-2	7	19	-3	7	2	-2
LCD14_18	N	Lightning Creek	40um	40.5 wt% equiv	brine		-78	-54	475	2007	-74	162	-34	-65
LCD14_19	Y	Lightning Creek	40um	40.5 wt% equiv	brine		-32	-17	53	1865	-33	118	-16	-23
LCD14_20	N	Lightning Creek	40um	40.5 wt% equiv	brine	Cu and Mn only	-261	-124	-298	-774	-247	-311	-84	-115
LCD14_21	N	Lightning Creek	40um	40.5 wt% equiv	brine		18	-6	-13	45100	-10	773	-6	23
LCD14_22	N	Lightning Creek	40um	40.5 wt% equiv	brine		-19	83	41	2258	24	225	-11	-14
LCD14_23	N	Lightning Creek	40um	40.5 wt% equiv	brine	cont? Pb spike remv	28	-20	-45	2061	-23	227	-13	-19
LCD14_24	N	Lightning Creek	40um	40.5 wt% equiv	brine		31	67	-15	1291	-8	398	-4	12

From source to sink: evolution of fluid systems in the Eastern Succession of the Mount Isa Block

N.H.S. Oliver, K. Butera, J. S. Cleverley, L.J. Marshall, M. J. Rubenach, W. J. Collins, B. Fu, R. Mustard, & T. Baker.

Predictive Mineral Discovery Cooperative Research Centre @ Economic Geology Research Unit, JCU School of Earth Sciences, Townsville, Qld, Australia 4811.

ABSTRACT

Protracted metal and sulphur contributions to the Eastern Succession iron-oxide-Cu-Au province occurred primarily as a consequence of long-lived fluid and melt fluxes from the base of the crust, stimulated by back-arc emplacement of voluminous mafic magmas. The concentration of iron, copper and gold into the presently observed mineral deposits mostly involved remobilisation and reworking of early initial enrichments (pre- to syn-Isan Orogeny) by later fluids (syn- to post-Isan and syn-Williams/Naraku Batholith). Osborne (eastern domain) and Eloise-type ores formed or were strongly remobilized at c. 1600 Ma by reduced, mafic-derived fluids, whereas oxidised brines released by the Williams/Naraku granitoids overprinted magnetite ± sulphides at Osborne (western domain) and Starra to produce hematite-chalcopyrite associations. Direct, potentially carbonatite-related mantle fluid may have periodically pulsed through the system, manifest now as pyrrhotite-stable carbonate veins and pods. Ernest Henry remains the best candidate for a true syn-Williams orebody, with reduced mantle- or mafic-derived HCOS fluid mixing with saline, oxidised brine derived from the Williams/Naraku Batholith. Exploration for Ernest Henry and Starra style deposits should focus on recognition of oxidised corridors in relation to structurally-defined targets, but recognition of truly large deposits (Ernest Henry and larger) may require recognition in the 3D model of both oxidised and reduced corridors.

Keywords: Cloncurry, iron-oxide-Cu-Au, alteration, mineralization, intrusion

1. INTRODUCTION

Ore genesis models developed in recent years for iron-oxide-Cu-Au deposits of the Cloncurry District have focussed attention mostly on the role of volatile phase separation from the Williams-Naraku Batholiths as the most likely source of metals. This paradigm has not particularly helped explorers because of the apparent distal relationship between the intrusions and known ore deposits, even though an appreciation of the development of upwards fluid flow and brecciation relative to some ore deposits has recently been gained (see below). Our recent work (Butera et al., 2005) has identified a more protracted history of contribution of metals and sulphur, and a spatial distribution implicating, in particular, faults and mafic rocks (see also Mustard et al., 2005; McLellan & Oliver, 2005). We develop these themes here, including also an appraisal of the tectonic evolution that contributed to the protracted metals contribution, and we also attempt to develop a more holistic model that incorporates previous work on the Williams-Naraku as well as the recent data.

1.1 Williams-Naraku Batholith issues

One of the obvious features of the Eastern Succession is the huge volume of metasomatic rocks, even more so than in the west. Decades of research have failed to explain the volume of fluid, with circular arguments about the roles of metamorphism, evaporites and the Williams Batholith, which have not resolved the following issues:

- The lack of Williams-age intrusions in the Mary Kathleen Fold Belt, despite comparable styles, if not extent, of albite alteration to the Cloncurry District, supposedly mostly related to the Williams-Naraku batholiths (Williams, 1998; Oliver et al., 2004)
- The convergence of stable isotopic signature of alteration systems of all ages (from 1740 to 1500 Ma) upon mantle-like values, with outliers clearly related to admixture with Corella marine carbonates, or Soldiers Cap black shales (Oliver et al., 1993; Oliver et al., 1994; deJong &Williams, 1995; Oliver, 1995; Rotherham et al., 1998; Mark et al., 2000; Baker et al., 2001; Marshall, 2003; Oliver et al., 2004). The convergence cannot be related only to the influence of Williams-age magmatic fluids because it includes pre-1530 Ma veins (Fig. 1).
- The apparent metallogenic similarity of IOCG deposits apparently formed at different times, i.e. Osborne at 1600-1590 Ma and Ernest Henry and Mt Elliott at 1530 Ma, with only the latter being coeval with Williams-Naraku Batholiths (Williams, 1998; Rubenach et al., 2001; Mark et al., 2005a)
- The high salinity and variable Br/Cl ratios of fluid inclusion populations throughout the protracted hydrothermal history, implying that the Williams-Naraku system was not the only contributor to the unusual salinities, and that recycling of evaporite (Corella Fm) salt may have occurred several times (Fig. 2)

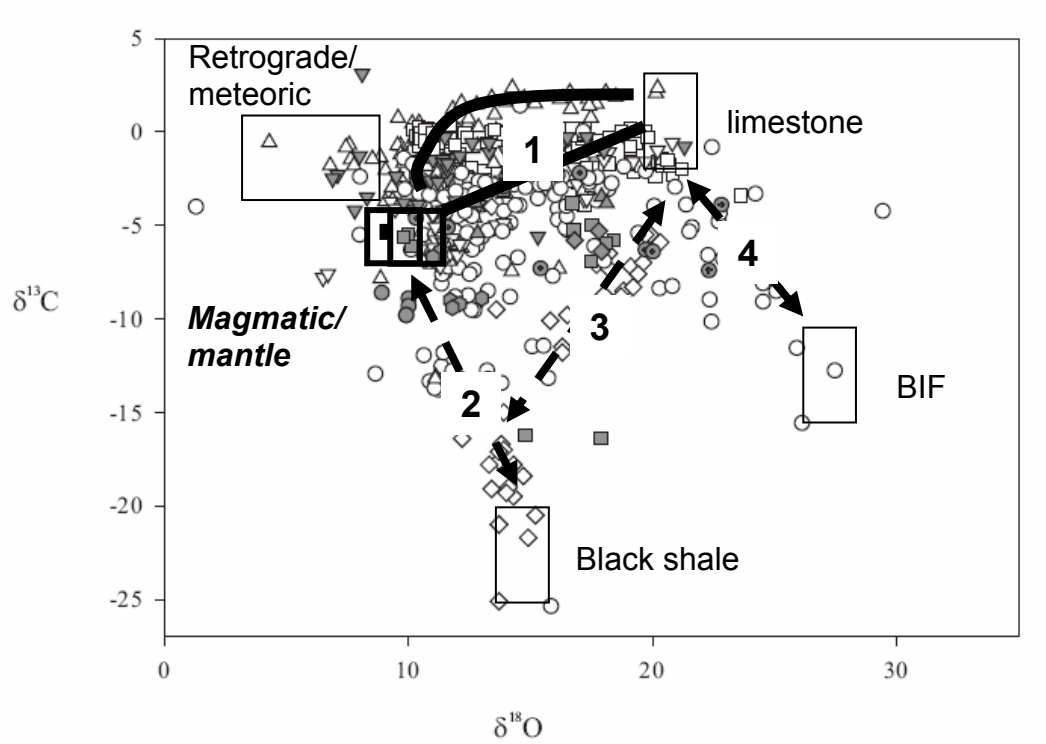

Fig. 1: C and O isotope data for calcite and dolomite from IOCG deposits, veins and alteration systems in the Eastern Succession, from (Oliver et al., 1993; Marshall, 2003) and Marshall et al. (submitted). The red box shows the inferred magmatic or mantle derived signal, the adjacent purple box to the left is the calculated fluid composition for fluid with modest CO_2 content at 450 to 500°C. This box has values intermediate to mafic or mantle fluids, and felsic-derived magmatic-hydrothermal fluids. The other boxes are the end-member isotope reservoirs (as carbonates) as indicated, trends 1and 2 represent admixture of Corella marine carbonates and Soldiers Cap black shales (respectively) with the mantle-like fluid, trend 3 is observed only at Dugald River(Zn-Pb-Mn) prospect and reflects an absence of the mantle signal and admixture of carbonate and black shale signals, and trend 4 is found only at Starra and Osborne in carbonates associated with the earliest iron oxides, which we therefore infer are true BIFs rather than metasomatic products. Data between trends 1 and 3 reflect likely passage of mantle or magmatic fluids through Corella carbonates before interacting with Soldiers Cap schists (Marshall, 2003).

Fig. 2 (overleaf): Fluid inclusion PIXE data from IOCG deposits and regional alteration systems of the Cloncurry District, from Mustard et al. (2004) and Fu et al. (2004). Note that Ernest Henry and Mt Angelay granitoids have similar values, but they plot off the main magmatic/mantle trend (grey areas), in the field in which halite dissolution may have contributed. Lightning Creek, Osborne and Starra cluster mostly in the magmatic field, whereas regional albitization fluids show compositions suggesting bittern brines.

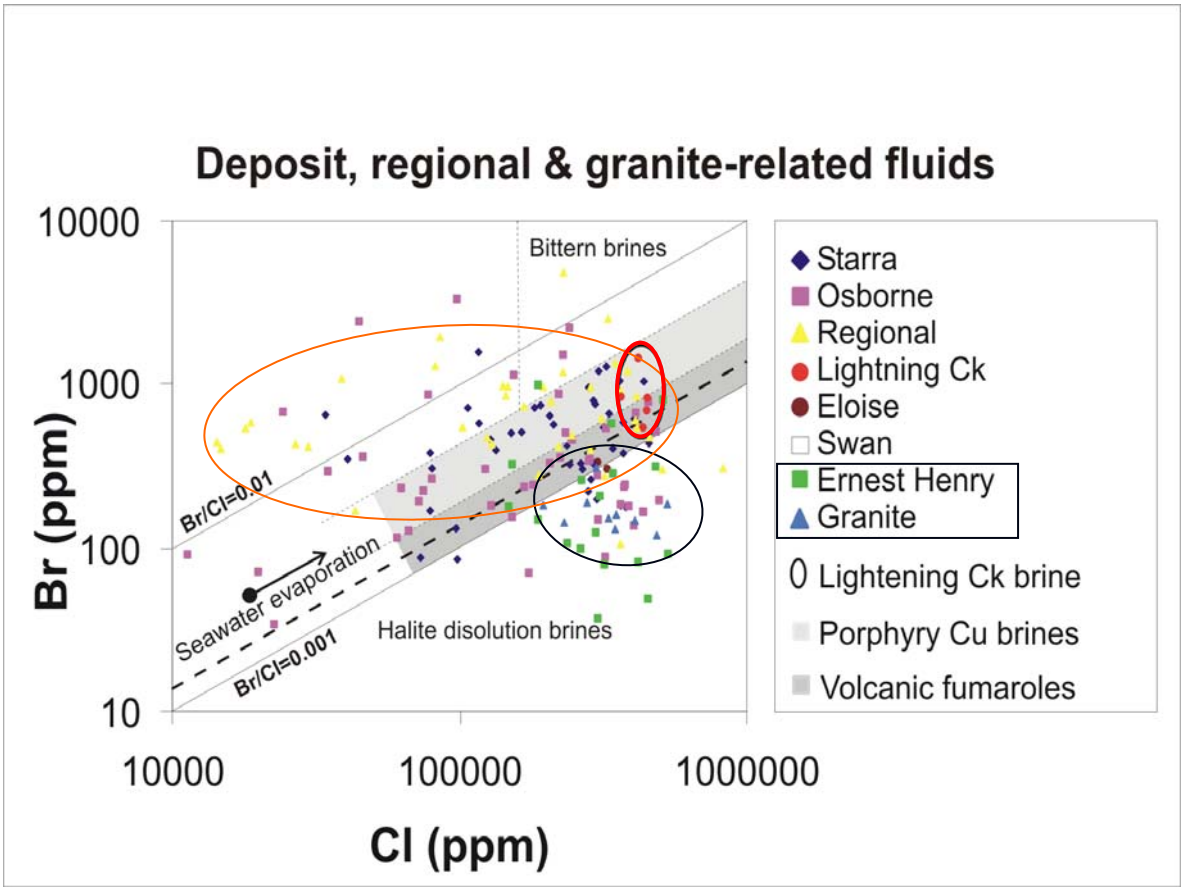

Another feature noted by Williams (1998) for many of the deposits is a strong mafic minor element association for many of the ores and alteration systems, including enriched Ni, Co, V and Mn. Mingling and mixing of mafic magmas with the Williams-Naraku suite prior to or synchronous with fluid exsolution may explain the contribution of some of these elements to the IOCGs, but the same enrichments are apparent at deposits which have a pre-Williams age (i.e. Osborne).

2. OREBODY PARAGENESIS

Despite a proliferation of Ar-Ar ages in the range 1540 to 1490 Ma for Eastern Succession IOCGs and abundant evidence for late sulphides and related alteration, U-Pb and Re-Os ages of many of these deposits point to inherited components. The original understanding of the age of peak metamorphism at the time of these studies was focussed around the 1550 Ma age inferred from the Western Succession and Mary Kathleen orebody, such that the Williams Batholith was regarded as immediately post-peak metamorphic and evolving metamorphic-magmatic fluid systems were seen as viable. More recent recognition of earlier metamorphism, peaking at 1600-1590 Ma with D_2 deformation, and earlier events at 1640 Ma (Rubenach, 2005), requires a reinterpretation of earlier workers' paragenetic stages.

The protracted history of mineralisation and remobilisation is well displayed by Mary Kathleen, which has a clear history of initial U-REE enrichment at km-scales associated with emplacement of the c. 1740 Ma Wonga-Burstall granites (providing a notable prospector's target at 1:100 000 scales), and yet the orebody in its present guise was

assembled at 1550 to 1500 Ma (Page, 1983a; Maas et al., 1988; Oliver et al., 1999). The timing of these events implies initial enrichment followed by repeated recycling and remobilization, leaving behind the ultimate question as to whether the 1550-1500 Ma event involved regional scouring of disseminated U-REE, or remobilization of an already formed orebody or protore. Similar issues are now quite pertinent to the IOCG deposits. Silica alteration forming the envelope to Osborne is locally marked by a banded, gneissic foliation, and this foliation is folded by folds which are correlated with regional D_2 – i.e. this silica alteration is pre-D_2 in timing. The earliest iron oxides in this deposit are clearly pre-D_2 (Fig. 3c), being overprinted by coarse magnetite and chalcopyrite that was apparently introduced (or remobilized) during and after D_2. Similar observations can be made at Eloise, where at least one of the orebodies contains abundant folded and foliated sulphides (Fig. 3b) and *durchbewegung* texture (Fig. 3a). Baker (1998) originally inferred a progression from metamorphism to ore genesis at Eloise, with significant alteration and mineralization occurring during the metamorphic stage. By this reasoning, with the recent geochronology, these stages would be separated now by 70 m.y. or more.

Fig. 3: evidence for pre- to syn-D2 sulphides at Osborne and Eloise.

a) Classic *durchbewegung* texture developed in pyrrhotite-rich ore at Eloise Cu-Au deposit: note the transposed fold remnants in the silicified alteration zone (bottom), texturally younger sulphides remobilized into boudin necks (pale pyrrhotite), and the shredded appearance of most of the pyrrhotite (darker) at the top. If the regional deformation peak accompanied peak metamorphism at c. 1600 Ma, these sulphides must be pre- to syn-1600 Ma, younger than the Ar-Ar ages (c. 1520 Ma)

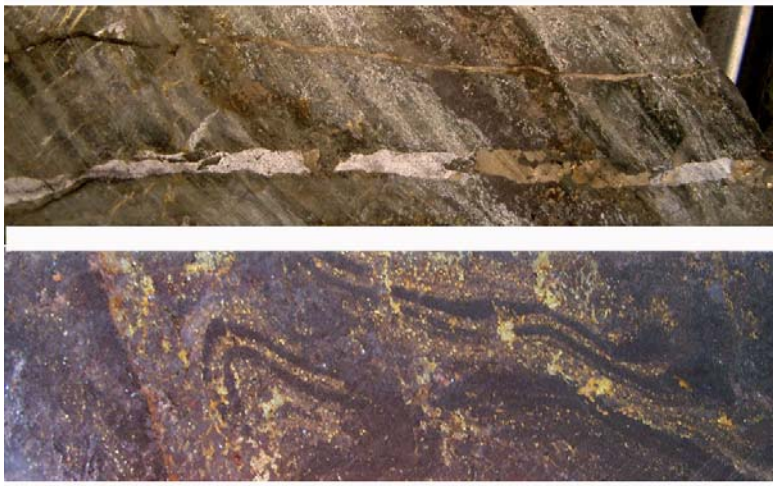

Fig. 3b: Foliated pyrrhotite-calcite-amphibole ore at Eloise – again the presence of deformed ore suggests syn- to pre-1600 Ma timing. This is cut by a later vein that demonstrates diffusional control of infill i.e. later diffusional remobilization

Fig. 3c: Osborne ore with folded magnetite and disseminated chalcopyrite, overprinted by patchy sulphides and zones of sulpide depletion; the latter appear to be syn-D2 (axial planar) structures.

Despite the bulk of the ore at Starra being dominated by coarse chalcopyrite and hematite which transgresses foliations, we have observed rocks in the open cuts containing magnetite and chalcopyrite in which the chalcopyrite forms irregularly spaced bands that look like bedding, and all are folded by D_2 folds (i.e. similar to Fig. 3c). Some or even all of the later paragenesis of hematite-chalcopyrite may have overprinted or remobilized earlier magnetite that already contained chalcopyrite. The

original premise of Davidson & Large (1994) concluding that some ironstones and possibly some sulphides pre-date peak metamorphism is also supported by our stable isotope data which support a clear, non-magmatic origin for early magnetite at both Osborne and Starra (Figs. 1, 3).

Although old ages persist in some of the recent geochronological data for Ernest Henry (Mark et al., unpubl. data; Butera et al., 2005), Ernest Henry does not show any apparent physical or paragenetic inheritance within the orebody. The ore is defined by a fairly sharp-edged breccia in which magnetite-chalcopyrite-pyrite-calcite ore is clearly related to the brecciation, and titanite and molybdenite within ore have precise 1527 Ma ages (Mark et al., 2005a), similar to the nearby 1530 Ma Mt. Margaret Granite. The orebody is also notable for significant enrichment in fluorine (in biotite and fluorite), and F is also enriched in breccias emanating directly off the Mt Angelay intrusion (Rubenach, unpubl. data; Cleverley & Oliver, 2005a), and in the skarn-like Mt Elliott deposit (Wang &Williams, 2001). In addition, the Ernest Henry breccia has very similar internal characteristics (clast spacing, roundness, roughness and particle size distribution) to the unmineralised but magnetite-enriched breccias near the Mt Angelay Granite (Fig. 4), and may share a common physical origin (comminution, chemical corrosion and abrasion in a fluidised breccia pipe or chamber).

Fig. 4: Top – typical Ernest Henry ore breccia with hematite-K-feldspar altered clasts in a magnetite-chalcopyrite-pyrite-Kfeldspar-calcite±barite-titanite matrix. Bottom – typical breccia from a breccia pipe emanating from the Mt Angelay Granite and crosscutting Soldiers Cap Group schists, from the western edge of the Snake Ck anticline, with albite-actinolite-magnetite±Kfeldspar-chlorite clasts set in a albite-magnetite-hematite-actinolite matrix. Scale is similar in both photographs.

3. TECTONIC SETTING – ARCS, MANTLE AND THE CARBONATITE CONNECTION

On the basis of the major early phase of mapping by the GSQ and BMR in the Mt Isa Block, Wilson (1978) proposed, on the basis of the overall asymmetry of the sedimentary-volcanic packages, that the eastern edge of the Mt Isa Inlier was close to a plate boundary. Part of the evidence included an appreciation of the Soldiers Cap Group as relatively deep water, high energy turbidites in comparison to possible time equivalents in the centre and west of the Inlier. Subsequently, a continent-scale model for intra-cratonic rifting and limited thickening was developed (Etheridge et al., 1987), supported by concepts of bimodal igneous geochemistry, lack of andesites and blueschists, and recognition of apparent temporal similarity between packages of rocks in the Western and Eastern Successions. Both these models have some validity in our recent reinterpretation, because the mafic magma chemistry, and indeed the asymmetry of the metal endowments, can be interpreted in the context of a back-arc continental environment (Butera et al., 2005). Modern continental back-arcs are characterised by high heat flow and bimodal igneous activity and any possible blueschists typically lie closer to the trench, such as the relationship between the Basin-and-Range and the Franciscan blueschists in western USA. The global distribution of IOCGs is also certainly not restricted to rifted continental interiors, with several examples lying in arcs or back-arcs in the Cainozoic tectonic context, particularly in the Andes (Williams et al., 2005). Hypotheses of plate boundaries sitting within 200km of the eastern boundary of the exposed Mt Isa Block are well worth reconsidering.

Another feature of arc-related hydrothermal systems worldwide is the capacity of dewatering subducted oceanic slabs to act over a protracted period, to liberate fluids and incompatible elements directly by devolatilization, and to trigger mantle metasomatism, upper mantle partial melting and lower crustal melting, all of which subsequently can lead to further volatile release via emplacement of crustal magmas. The Eastern Succession is marked by c. 250 m.y. of metasomatic activity, not just by two major phases related to metamorphic devolatilization and granite emplacement. In modern convergent systems, porphyry copper deposits and island-arc related epithermal systems are a product of this type of process in fore-arcs, and such deposits are not apparently found at Mt Isa. However, back-arc extension systems can produce both Cyprus-style (magnetite-chalcopyrite-dominant) and Kuroko-type (Cu-Pb-Zn) VHMS deposits, IOCGs, and a range of sediment-hosted deposits, right from the initial volcanism and rift-related sedimentation, through to basin reactivation and local shortening triggered by subduction of oceanic plateaus or continent scale shift in plate vectors. This particular environment, in which early basin metal contributions may be rapidly overprinted by the effects of convergent metamorphism, may be the specific reason for the distinction between BHT Ag-Pb-Zn and the “SEDEX” shale-hosted orebodies in northern Australia, the latter having formed in the distal flanks of the rifting system whereas BHTs may have formed and been reworked in a more arc-proximal setting.

3.1. Is there a carbonatite component in the Eastern Succession?

Carbonatites and kimberlites are a product of long-lived mantle contributions to progressively cratonized continental crust, and their localisation late in the overall tectonic evolution of the Kimberleys (Argyle) and in Archean remnants in eastern South Africa (Phalaborwa), reflects very low % partial melts of metasomatized mantle containing abundant CO_2. Various authors have speculated on the carbonatite connection with IOCGs (e.g. Groves & Vielreicher, 2001), and our current work is aimed at testing this connection. Specifically, the calcite pods of the Mary Kathleen Fold Belt and correlatives in the Cloncurry District, share mineralogical character with the volatile-dominant top part of Phalaborwa carbonatites (Fig. 5). Several other mid-crustal carbonate-rich alteration and vein systems worldwide show definitive mantle signatures (Wickham et al., 1994).

Fig. 5 (a, left): Calcite-magnetite±apatite-pyrrhotite veins from Phalaborwa carbonatite, South Africa, cutting actinolite-biotite-apatite altered host gneisses. Ernest Henry is dominated by magnetite-calcite-sulphide ore with apatite as an accessory, and shows pronounced potassic alteration (biotite, K-feldspar), similar to this association from Phalaborwa. The main distinction is the obvious syenite association at Phalaborwa, and downward transition from veins like this one into igneous-texture apatite-magnetite-calcite intrusive dykes. (b, right) Calcite-actinolite-apatite-titanite-biotite veins from Knobby quarry, MKFB, Eastern Succession, Mt Isa Block, cutting albite-altered calc-silicate rock. The Knobby Quarry rocks have distinctive mantle-like C and O isotope rations (Fig. 1), and may not have been derived from local mafic or felsic rocks, rather from deeper seated sources.

4. HISTORY OF FLUID SYSTEMS AND SOURCES PERTINENT TO METALLOGENESIS

4.1 1750 to 1730 Ma

Prior to Soldiers Cap deposition, the end of the rifting and sag cycle that produced the Corella Fm and equivalents culminated in extensional deformation and the development of upper-crustal hydrothermal systems in which granite-gabbro bodies triggered circulation of basinal and magmatic-hydrothermal fluids (Oliver, 1995). U-REE and probably gold (Tick Hill) were added in subhorizontal shear zones and skarns, despite preponderance of younger geochronological results at both Mary Kathleen and Tick Hill. Widespread dolerites and gabbros were emplaced into the Corellas and probably reflect the first major injection of Cu into the Eastern Succession. However, we cannot determine whether Cu was concentrated to ore grades at this time, even though Au and U-REE possibly reached ore grades. Constraints on the oxidation state and sulphur and metal content of fluids

responsible for the U-REE and gold enrichments are scant; however, widespread scapolitization of dolerites at this time, and some granites, points to the circulation of salty, CO_2-bearing basinal brines probably derived by evaporate dissolution (Oliver et al., 1994).

4.2 1690 to 1620 Ma

4.2.1 Early extension

The 1690 to 1650 Ma part of this time period involved extension, widespread mafic volcanism, intrusion, and sedimentation in the Eastern Succession, and inferred contribution of significant copper via exsolution of a CO_2-H_2O-S fluid late during fractional crystallisation (Butera et al., 2005). In the Mt Isa area, Rubenach et al. (unpubl. report) have recently identified a major extensional hydrothermal system associated with the emplacement of the Sybella Batholith at c. 1660 Ma. Similar to the earlier Wonga-Mary Kathleen system, the Sybella was emplaced into an extensional shear zone, causing widespread circulation of basinal fluids. This system may have been responsible for localisation of syn-sedimentary and diagenetic Pb-Zn and possibly Cu enrichments in the c. 1650 Ma Mt Isa Group. A major mantle or mafic connection to the bulk metal budget at this time is implied from our recent work (Butera et al., 2005).

4.2.2 Onset of orogeny

Later in this time period, shortening and a phase of metamorphism commenced at c. 1640 Ma (Rubenach et al., this report), probably shutting down the prior extension-related events, but also developing the first of a long history of sodic alteration systems in Soldiers Cap Group rocks (e.g. Snake Creek, Osborne). This pre-peak Isan metamorphic activity may have involved circulation of evaporate-derived fluids from overthrust Corella Fm, into the Soldiers Cap Group, driven by deformation and/or topography into the core of the newly developing orogenic belt. The impact of this system on Cu-Au distribution is uncertain, but was probably similar, although more localised, than the effects of the main phase of the Isan Orogeny. It may have leached a large volume of copper previously disseminated or concentrated around Osborne.

4.3 Isan Orogeny 1610 – 1580 Ma

The main phase of the Isan Orogeny liberated metamorphic CO_2 from the Corella Fm and equivalents, and H_2O from the Soldiers Cap Group, as well as significant quantities of salt probably from scapolite breakdown. However, stable isotope data from carbonate veins hosted in Soldiers Cap Group require a mixed CO_2-source, from both Corella Fm carbonates (by dissolution or devolatilisation), but also from a magmatic or mantle source (Fig. 1). As felsic magmas were absent at this time except for pegmatites at Osborne (see below), mafic rocks or the mantle are clearly implicated in the metamorphic fluid budget.

Mafic dykes emplaced into the core of the Snake Creek Anticline at this time share characteristics with earlier mafic rocks emplaced during rifting, implying that although the depth of mafic magma generation had shifted, it was still active (Butera et al., 2005). In situ or proximal partial melting of near-granulite facies metasediments produced localised pegmatites at Osborne, probably triggered by fluid fluxing. The abundance of pyrrhotite preserved in the eastern domain at Osborne suggest that metamorphic or other fluids at this time were relatively reduced, as reflected in the local presence of methane and nitrogen in the fluid inclusions there (Fu et al., 2003). Osborne methane-bearing brines contain elevated Cu concentrations, and this may reflect the capacity of reduced S-poor fluids to

carry Cu as species other than sulphate, i.e. various Cu chlorides (Mustard et al., 2003). CO_2-rich fluids at Osborne display elevated arsenic contents and relatively low chloride – if As acted as a proxy for Au, this may indicate that Au in these systems is carried in an HCOS vapour. This vapour may have exsolved from mafic rocks or come directly from the mantle, although it may have been derived by unmixing (Mustard et al., 2003) of a complex metamorphic fluid.

Elsewhere, metamorphic fluids leached sulphides from mafic rocks (Butera et al., 2005), and earlier sulphide accumulations (e.g. Fig. 3c). If we accept that 1600 to 1590 Ma Re-Os and U-Pb ages at Osborne represent the major time for metal accumulation, then a cycle of leaching by and reprecipitation from metamorphic fluids may explain this deposit (and potentially other enrichments elsewhere such as pre-ore shear zones at Ernest Henry). Alternately, if Osborne was formed earlier, during or soon after sedimentation and volcanism (e.g. similar in timing to metal introduction at Cannington), then the metamorphic fluids both imparted the radiogenic isotope signal and redistributed sulphides (both chemically and mechanically) into favourable D_2 structures. In any case, mantle and/or mafic derived fluids most likely provided the bulk of the metal and sulphur for this deposit, and similar ore types (e.g. Eloise, ?early magnetite-chalcopyrite at Starra). The key characteristic of fluids at this time (metamorphic-magmatic-mantle) was their reduced nature, unlike at least some fluids exsolved off the later Williams Batholith.

4.4 Williams thermal event, 1550 – 1500 Ma

4.4.1 The oxidised brines

Examination of alteration systems in close proximity to the Williams-Naraku Batholith gives the best idea of how these intrusions may have contributed to the IOCG deposits. Mark (1998) first documented the complexity of alteration around the top of intrusions at Mt Angelay, speculating on the exsolution of hypersaline, CO_2-bearing brines as a cause of albite alteration that affected the granite carapace and surrounds. Perring et al. (2000) and Pollard (2001) documented the co-occurrence of sodic alteration and voluminous magnetite at Lightning Creek, inferring an origin for this alteration by unmixing of complex brines upon release from the crystallizing granite-gabbro sill complex. Oliver et al. (2004) built on this work to propose that granite-derived fluids moving through metasedimentary rocks attained elevated Fe- and K-contents by wallrock interaction, prior to their involvement in Ernest Henry-type IOCG genesis. Fluid inclusions at Lightning Creek are distinctive for their highly elevated Fe, Ba and Cu contents (Fig. 6), implying at least one of the fluids present was sulphur-deficient (Perring et al., 2000). The apparent absence of sulphur in these granite-proximal systems, but the presence of sulphur with distinctive mantle- or magmatic $\delta^{34}S$ values in the deposits, requires derivation of deposit sulphur from sources other than the c. 1530 Williams Batholith.

Fluid inclusion data reveal some connections between granites and aspects of the orebodies, although the interpretation is complex, and in some cases, misleading.

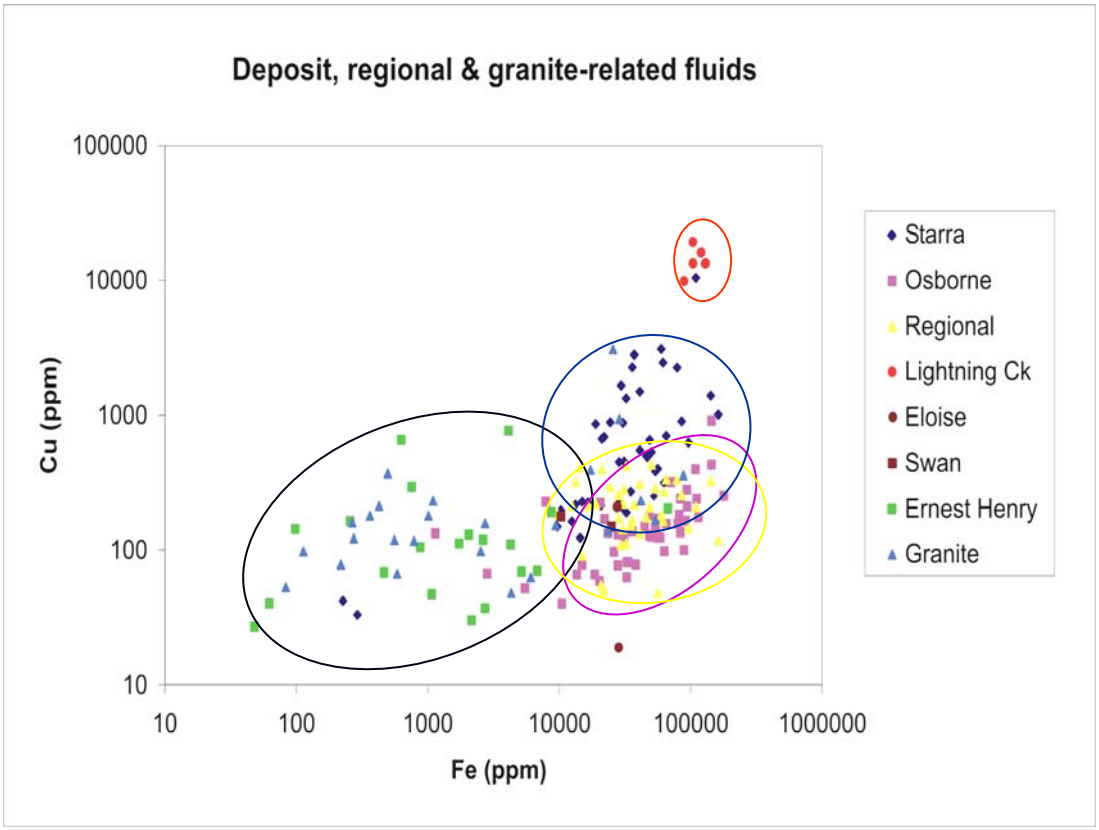

Fig. 6: PIXE fluid inclusion data from Eastern Succession deposits, prospects, Mt Angelay Granite, and regional alteration. From Perring et al. (2001), Williams et al. (2001), Mustard et al. (2004) and Fu et al. (2004).

Figure 6, for example, shows an apparent clear connection between Ernest Henry and fluid inclusions from the top of the Mt Angelay pluton (Mustard et al., 2004), separate from the other (inferred older) deposits. However, Fe and Cu of course are the constituents of chalcopyrite, so the data can also be inferred to be a consequence of depletion of ore fluids in these components as they are precipitated from the original fluids. Lightning Creek, with the highest Fe and Cu contents in fluid inclusions, has no chalcopyrite (although a huge volume of magnetite); and Ernest Henry, with modest Fe and Cu in the fluid, is the biggest orebody. The trend is confused, however, by regional fluids associated with albitization. Overall, the fluid inclusion data probably reflect a close association between granitoids and the inferred oxidised, S-poor fluids at Ernest Henry and Lightning Creek, with the latter in particular lacking sulphur and/or at too high temperatures for ore formation. The data from the other deposits and the regional alteration probably reflect other processes and fluids, as inferred from the inherited age components in those orebodies.

In the Snake Creek area, breccia pipes emanating from contact aureoles of 1530 Ma granitoids are dominated by magnetite, hematite, and albite (Cleverley & Oliver, 2005a). Sulphides are found only in these pipes either within relict gabbro bodies (that themselves were probably emplaced syn-granite) or in distal locations where wallrocks or other fluids may have provided the sulphur. The implication of all of these lines of evidence is that the Williams Batholith released large volumes of oxidised, sulphur-poor fluids that locally carried copper and iron, and released some of this fluid via violent brecciation processes. This fluid may have oxidised earlier reduced iron oxide ± sulphide assemblages at Osborne and Starra, for example in the reaction of oxidised copper chloride brine with previous pyrrhotite – pyrite ± magnetite rocks to produce hematite and chalcopyrite. Without adding

significant copper, such oxidised fluids may simply have remobilized earlier IOCGs and produced hematite-ore associations that reworked or possibly concentrated earlier copper produced during or before peak-metamorphism.

4.4.2 Reduced, mantle-derived fluids

Another important fluid source at this time was probably derived by mantle degassing (the "carbonatite connection"), as inferred from the association of calcite-actinolite-clinopyroxene-apatite with minor titanite-pyrrhotite-chalcopyrite at Knobby Quarry (MKFB) and similar high temperature calcite pods in the Eastern Succession (Fig. 5). These fluids contained reduced sulphur, abundant CO_2, and Ca- and Na-chlorides (Fu et al., 2003). Although the surrounding albitic alteration was previously inferred to be related to salt dissolution or a felsic magmatic component in this fluid (e.g. Oliver et al., 1993), Peacock et al. (1994) has postulated that partial melting of seafloor-altered oceanic crust can carry alkalis into the crust during subduction. Given that there are no Williams-age felsic intrusions in the MKFB, then speculation of a mantle source to these fluids is warranted. Trace element geochemistry of apatite and carbonates will be used to determine the extent to which such fluids were directly mantle-derived.

4.4.3 Ernest Henry fluid mixing and sources

Unlike Osborne or Cannington, the Ernest Henry orebody shows few physical attributes that can clearly be related to pre-Williams-Naraku hydrothermal events: it appears to be a genuine 1530 Ma orebody (Mark et al., 2005a). Furthermore, despite the growing evidence for inheritance and protracted copper addition to the crust over 250 m.y., Ernest Henry still contains about a third of all of the currently mineable or mined Cu ore yet discovered in the Eastern Succession, implying that this event was potentially the most important of all, at least in a targeting sense.

Although inherited source components are present at 1650 to 1600 Ma (Re-Os wholerock and Pb-Pb chalcopyrite, cf. Butera et al., this report), we remain uncertain as to the extent to which local (≤ 1km scales) pre-1530 Ma concentrations of Cu-Au ore, sulphides, or ironstones provided mass for the present orebody. The distinctive K-feldspar-hematite alteration of the host volcanic rocks associated with ore deposition (Mark et al., 2005a) was probably caused by reaction of initially granite-derived fluids, modified by albitization, with the host metavolcanic rock, as suggested by geochemical models (Oliver et al., 2004; Cleverley & Oliver, 2005b). Barian K-feldspar associated with this ore-related alteration (Mark et al. 2005a) again reflects likely absence of sulphur in one of the fluids, whereas the presence of barite late in the ore paragenesis is a classic hallmark of fluid mixing. Using HCh, fluid mixing models for Ernest Henry work best with mixing an oxidised S-poor brine containing Cu as chlorides with a reduced HCOS fluid carrying Au (Figs 7, 8).

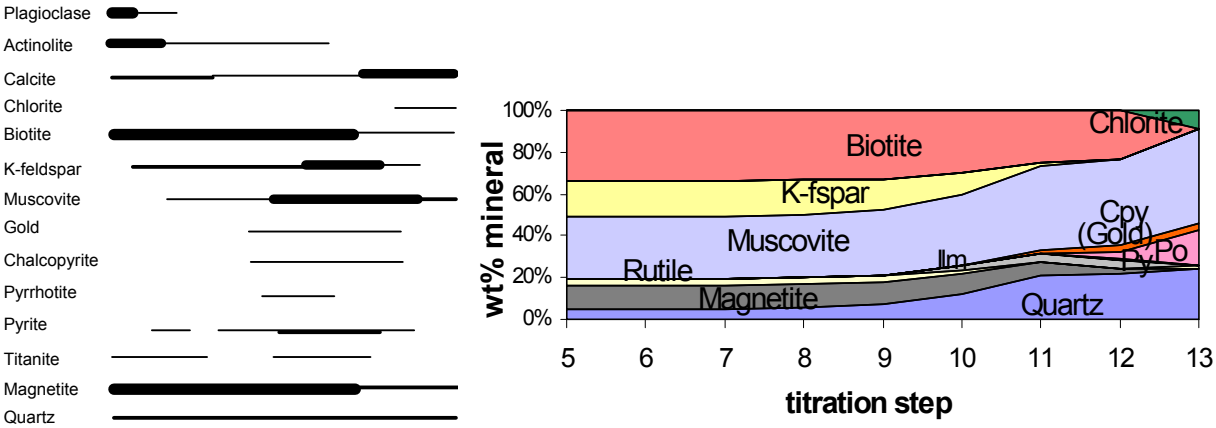

Fig. 7: a (left) Simplified paragenesis from the Ernest Henry orebody, modified from Mark et al. (2000, 2005). b) (right) Predicted paragenesis generated from HCh geochemical modelling software, with increasing proportions of a reduced HCOS fluid (containing gold, on the right) mixed with an oxidized S-poor Na-Ca-Fe-Cu-Cl brine (left), in the presence of K-feldspar altered wallrocks. We have not successfully replicated the high calcite content of the Ernest Henry ores, which we infer to represent infill related largely to pressure drops and increases in CO_2 fugacity possibly upon phase separation. Y-axis is the weight proportions of product minerals (in the 1D mixing space).

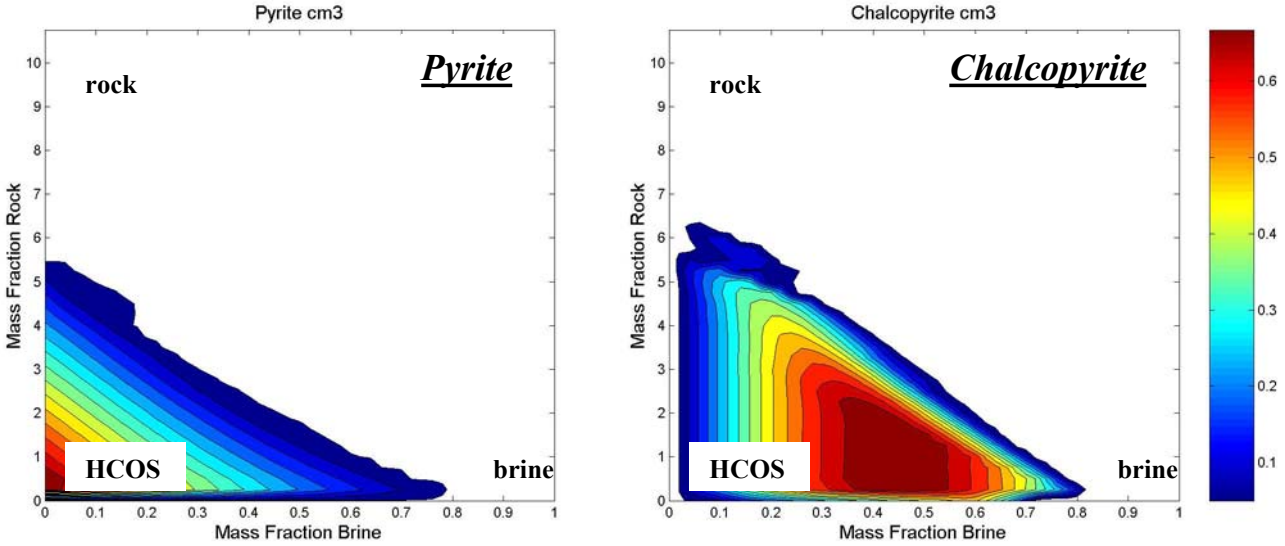

Fig. 8: Assemblage diagrams produced using HCh and Matlab, using an algorithm that mixed proportions of brine (right), HCOS fluid (left), and K-feldspar-altered host rock (Y axis). Pyrite and chalcopyrite are both produced in fluid-dominant conditions (bottom part of diagram). a) Pyrite volume produced in 10kg mixture of the two fluids, the proportion of rock (relative to 10kg total) in that mixture is shown on the Y-axis. b) Chalcopyrite. The results predict chalcopyrite occurs in the middle of the mixing zone whereas pyrite is found more where the HCOS fluid is dominant. This is interesting in the context of the orebody which is zoned towards more pyritic margins. More turbulent flow (and more efficient mixing) would be expected towards the centre of a pipe, so this zonation may reflect the physical mixing process. The results are also consistent with the sulphides precipitating mostly as infill (fluid dominated conditions).

We now regard the key ore-forming fluid ingredients at Ernest Henry (Fig. 9) as:

- Oxidised Fe- and K-rich fluid derived by brine release from the Williams Batholith during violent brecciation events, modified by subsequent wallrock reaction along the transport and deposition sites, and potentially carrying copper

derived from magma mingling with mafic bodies at 1530 Ma (Butera et al., this report)

- Reduced HCOS fluid derived either directly from the mantle, by leaching of pre-existing mafic rocks by mantle-derived fluids, or by release of fluids from crystallising Williams-age gabbros. This fluid may have contained the gold.
- A possible contribution from surface derived fluids is implied by the Br/Cl fluid inclusion data (Mark et al., 2005); however these fluid inclusion results may have been influenced by precipitation of Cl-bearing silicates in Ernest Henry alteration (e.g. biotite, scapolite).

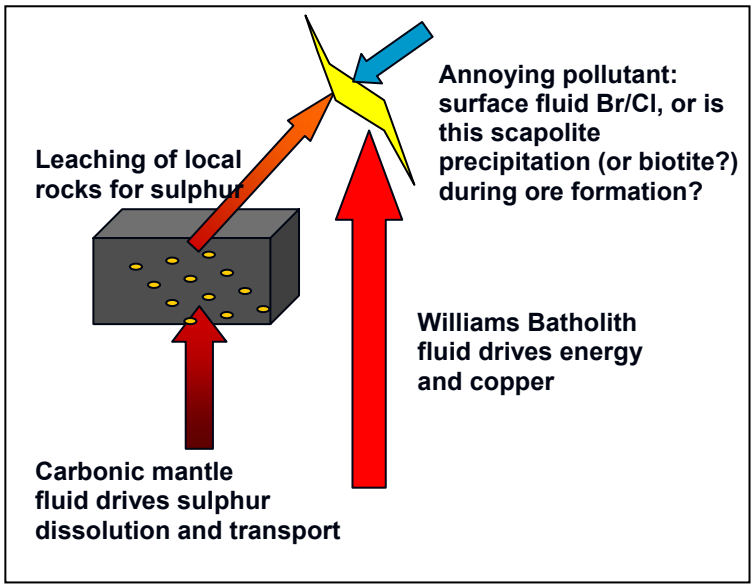

Fig. 9: Cartoon summarizing the key source and sink ingredients of ore components at Ernest Henry.

5. RATIONALISING THE WILLIAMS/NARAKU - MAFIC ROCKS ISSUES, AND EXPLORATION OUTCOMES

5.1 Synopsis

Interaction between mantle-derived fluids, mantle-derived melts, and the lower crust which produced the Williams Batholith (Mark et al., 2005) can explain the diversity of ages and associations in the district, but also the commonalities (Fig. 10). Highly abundant CO_2-rich fluid inclusions in the district are not primarily a consequence of devolatilisation of the Corella Fm carbonates, because the CO_2 is found in inclusions of most ages, and associated carbonates have C- and O-isotope signatures indicative of mantle or magmatic sources. This implies that mantle or magmatic CO_2 was available at almost every stage of the evolution of the belt, a situation most likely to evolve during protracted extension and crystallisation of mafic magmas.

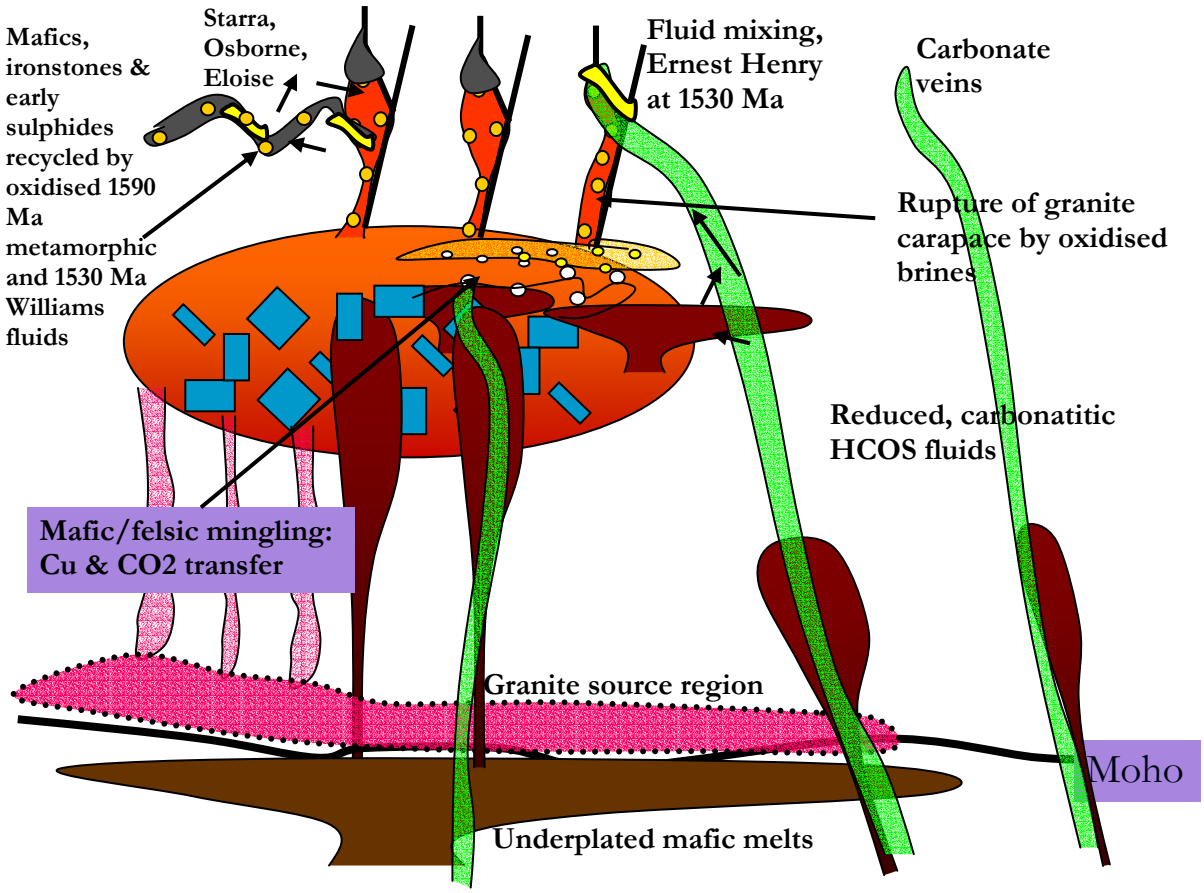

Fig. 10: Cartoon showing the inferred relationships between mantle fluids and melts, granite crystallisation, fluid sources and recycling of early sulphides at the time of emplacement of the Williams Batholith. In some domains, sulphides were overprinted and reworked by Williams age oxidised fluids, leading to dissolution, remobilisation and reprecipitation (e.g. Starra); but in other domains the early reduced signal survived (Osborne eastern domain, Eloise). Release of oxidised brines at the top of the Williams/Naraku batholiths may have been triggered by mafic-felsic mingling and consequent CO_2 contributions; mixing of this fluid with primitive, potentially carbonatitic HCOS fluids can explain fluid mixing attributes of Ernest Henry. In all cases, mantle derived CO2 and sulphur was added to the orebodies, by contamination of granites, release of fluid from mid crustal mafic rocks, recycling of earlier sulphides and carbonates by metamorphic and magmatic fluids, and direct mantle degassing.

The interactions between mantle-derived melts, mantle fluids and generation and emplacement of felsic magmas (Fig. 10) involved:

1. Prior to 1550 Ma, significant concentrations of IOCGs had already occurred, by release of fluids directly off the top of crystallising mafic intrusions, potentially even by exhalation in mixed sedimentary-mafic rock packages, and probably by leaching and reprecipitation during regional metamorphism (Butera et al., this report).

2. At c. 1550 Ma, a phase of extension or possibly volatile fluxes from deep in the mantle lithosphere triggered renewed generation of basaltic melt just below the Moho, and triggered anatexis of lower crustal felsic melts with a distinctive mantle radiogenic isotope signature (Mark, this report).

3. Some felsic intrusions, e.g. Lightning Creek, may have been contaminated with voluminous mafic melts at a relatively early stage of crystallisation, leading to

widespread mingling, mixing, and transfer of metals in the melts. The net result may have been dispersion of metals throughout the mafic/felsic complex, retention of sulphur in the mafic rocks, rapid saturation of iron oxides in the mingled zones, and precipitation of magmatic-hydrothermal magnetite bodies.

4. Other felsic intrusions evolved to a much greater extent by protracted crystallisation (e.g. Mt Angelay, Mt Margaret), such that the remaining felsic liquid was near saturated with large volumes of oxidized, hematite-stable brine. Emplacement of CO_2- and possibly Cu-bearing mafic magmas into these rocks may have triggered release of Cu and CO_2 during quenching of the mafic rocks, which in turn forced exsolution of the brine from the granitoids. Consequently, explosive release of mixed volatiles at the granitoid carapaces produced violent breccia pipes which carried Fe, Mn, K, Na, Ca and possibly Cu to sites above the intrusions, potentially to make orebodies. The same fluid, where it interacted with pre-existing ironstones and/or IOCGs, oxidized these rocks and either redistributed or added copper as sulphide via redox reactions (e.g. Starra, Osborne western domain).

5. Direct release of reduced CO_2- and S-bearing fluids from crystallising mantle melts (or gabbros emplaced at higher levels) produced carbonate-dominated vein systems in rocks away from the Williams Batholith. Because these fluids did not "collide" with crystallising felsic magmas (e.g. MKFB), they did not cross-fertilize with the alkali-laden and potentially Cu-carrying source.

6. Where the primitive mantle- or gabbro-derived HCOS fluids met with the brine-laden fluids evolved off highly fractionated Williams Batholith, Ernest Henry may have formed. Alternately, the S was derived from remobilised sources proximal to Ernest Henry. It is possible that orebodies such as Starra formed where oxidised Williams-derived fluids interacted with pre-existing sulphides until a point where the fluid became sufficiently reduced that sulphide saturation was imminent, with final ore precipitation occurring due to pressure changes and phase separation. However, this "single fluid" model does not explain the fluid inclusion complexity at Starra nor the presence of barite (see also Williams et al. 2001).

5.2 Exploration implications

Recognition of Ernest Henry style deposits requires establishing whether corridors of oxidised rocks and recognisable sulphur sources are present at the current exposure levels. If the deposit was formed by reaction of Williams Batholith oxidised fluids with pre-existing mafic-proximal sulphide concentrations, then the prospectivity and geomechanical models developed by Butera et al., (2005), Ford (2005), McLellan & Oliver (2005), and Mustard et al. (2005) provide a strong basis for identifying such oxidised corridors in the regional datasets, relative to the known areas of good prospectivity (e.g. Fig. 11).

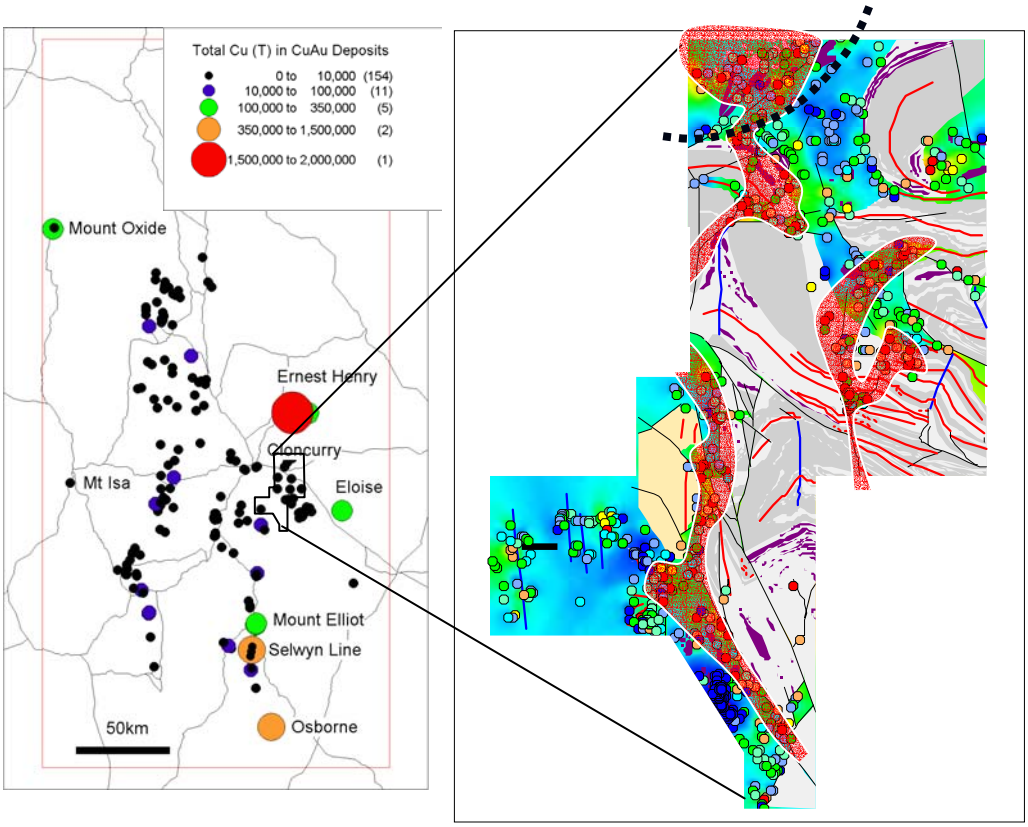

Fig. 11 (after Marshall, 2003 and Mustard et al., 2004): Map of outcrop east of Cloncurry, highlighting areas of oxidised breccias (pink shading) inferred to be related to the c. 1525 Ma Naraku Batholith (dashed line at top shows geophysically interpreted southern edge of main Naraku body). The map also shows the distribution of intact, little altered Corella Fm rocks (blue dots and shading, albitized and in-situ brecciated equivalents (paler blues, greens), which can be separated from oxidized, hematite-K-feldspar altered breccias (red and orange dots) which cut across rock boundaries including penetrating into the Soldiers Cap Group. Greys – Soldiers Cap Gp. with red lines representing fold axes of the D1 and/or D2 stages of the Isan Orogeny; blues and green colours – Corella Fm calc-silicates; purple – felsic and mafic intrusions; black lines - faults. The intersection of the oxidised corridors with key structures, and the more difficult task of identifying reduced domains, is our recommended strategy for defining potential Ernest Henry-style targets.

However, if the sulphur was truly primitive and juvenile (Fig. 10), an understanding of how oxidised brines and reduced mantle-derived fluids could meet to make orebodies by fluid mixing will require close analysis of the 3D model and consideration of how mantle fluid pathways and oxidised Williams corridors could meet. Several clear strategies are apparent to advance this further:

1. define zones of abundant hematite alteration that can be temporally linked with the Williams Batholith;

2. attempt to identify which regional carbonate vein systems contain pyrrhotite±pyrite in preference to magnetite;

3. determine where these two types of chemical indicators intersect with the favoured locations in the prospectivity analysis, and the geomechanical analysis; and

4. Determine to what extent the presence of dense mafic bodies could reflect a source of either sulphur (by leaching) or a juvenile HCOS fluid, by comparing the gravity data with the magnetics and results of petrographic studies that identify the fate of mafic-sourced sulphide.

Acknowledgements

We thank Tom Blenkinsop, Mick Carew, Dave Cooke, Richard Crookes, Damien Foster, Michel Gauthier, Kathryn Lewthwaite, Geordie Mark, John McLellan, Peter Pollard, Rick Valenta, Pat Williams, Dugi Wilson and Bruce Yardley for discussions. Josh Bryant, Perry Collyer, Dan Johnson and Glen Little are thanked for collaboration and access at Ernest Henry, Frank Tullemans and Ian Hodkinson are thanked for their support at Osborne and Eloise respectively, Mustafa Cihan assisted with the recent breccia work as part of an ARC Discovery project, and Ian Cartwright and Garry Davidson provided stable isotope data at various stages. This report is a product of the collaboration between the F1-2 and I2-3 team members of the Predictive Mineral Discovery CRC, but includes concepts and data developed prior to that during the course of ARC- and MIMEX-sponsored research, particularly at Ernest Henry.

6. REFERENCES

Baker, T. (1998). "Alteration, mineralization and fluid evolution at the Eloise Cu-Au deposit." Econ. Geol. **93**: 1213-1236.

Baker, T., Perkins, C., Blake, K. L. and Williams, P. J. (2001). "Radiogenic and stable isotope constraints on the genesis of the Eloise Cu-Au deposit, Cloncurry District, northwest Queensland." Econ. Geol. **96**: 723-742.

Butera, K., Oliver, N., Rubenach, M., Collins, W., and Cleverley, J., 2005. Multiple generations of metal and sulphur contribution from mafic rocks to the IOCG budget of the Mount Isa Eastern Succession. I2+3 Final Report, pmdCRC.

Davidson, G. J. and Large, R. R. (1994). "Gold metallogeny and the copper-gold association of the Australian Proterozoic." Mineralium Deposita **29**: 208-223.

deJong, G. and Williams, P. J. (1995). "Giant metasomatic system formed during exhumation of mid-crustal Proterozoic rocks in the vicinity of the Cloncurry Fault, northwest Queensland." Austr. J. Eth. Sci. **42**: 281-290.

Etheridge, M. A., Rutland, R. W. R. and Wyborn, L. A. I. (1987). "Orogenesis and tectonic processes in the Early to Middle Proterozoic of northern Australia." Am. Geophys. Union, Geodyn. Ser. **17**: 131-147.

Ford, A. 2005. Fractal distribution of mineral deposits for exploration. I2+3 Final Report, pmdCRC.

Fu, B., Williams, P. J., Oliver, N. H. S., Dong, G., Pollard, P. J. and Mark, G. (2003). "Fluid mixing versus unmixing as an ore-forming process in the Cloncurry Fe-oxide-Cu-Au District, NW Queensland, Australia: evidence from fluid inclusions." J. Geochem. Expl. **78-79**: 617-622.

Groves, D. I. and Vielreicher, N. M. (2001). "The Phalabowra (Palabora) carbonatite-hosted magnetite-copper sulfide deposit, South Africa; an end-member of the iron-oxide copper-gold-rare earth element deposit group." Mineralium Deposita **36**: 189-194.

Maas, R., McCulloch, M. T. and Campbell, I. H. (1988). "Sm-Nd isotope systematics in uranium rare-earth element mineralization at Mary Kathleen uranium mine, Queensland." Econ. Geol. **82**: 1805-1826.

Mark, G. (1998). "Albitite formation by selective pervasive sodic alteration of tonalite plutons in the Cloncurry district, NW Queensland." Austr. J. Eth. Sci. **45**: 765-774.

Mark, G., Oliver, N. H. S., Williams, P. J., Valenta, R. K. and Crookes, R. A. (2000). The evolution of the Ernest Henry hydrothermal system. Hydrothermal iron oxide copper-gold and related deposits: a global perspective. T. M. Porter. Adelaide, Australian Mineral Foundation**:** 132-136.

Marshall, L. J. (2003). Brecciation within the Mary Kathleen Group of the Easterrn Succession, Mt Isa Block, Australia: implications of district-scale structural and metasoomatic processes for Fe-oxide-Cu-Au mineralisation. School of Earth Sciences. Townsville, James Cook University**:** 323.

Mark, G., Foster, D., Mustard, R., and Pollard, P. 2005a. Sr-Nd isotopic constraints on the crustal architecture and evolution of the Eastern Succession, Mt Isa Block, Australia. I2+3 Final Report, pmdCRC.

McLellan & Oliver, N.H.S., 2005. Discrete element modelling of stress partitioning and fluid flow in the Eastern Succession of the Mt Isa Block. I2+3 Final Report, pmdCRC.

Mustard, R., Blenkinsop, T., Foster, D., Mark, G., McKeagney, C., Huddleston-Holmes, C., Partington, G., and Higham, M. 2005. Critical ingredients in Cu-Au±iron oxide deposits, NW Queensland:an evaluation of our current understanding using GIS spatial data modelling. I2+3 Final Report, pmdCRC.

Oliver, N. H. S. (1995). "The hydrothermal history of the Mary Kathleen Fold Belt, Mount Isa Block, Queensland, Australia." Aust. J. Earth Sci. **42**: 267-280.

Oliver, N. H. S., Cartwright, I., Wall, V. J. and Golding, S. D. (1993). "The stable isotopic signature of large-scale fracture-hosted metamorphic fluid pathways, Mary Kathleen, Australia." J. Metamorphic Geol. **11**: 705-720.

Oliver, N. H. S., Cleverley, J. S., Mark, G., Pollard, P. J., Fu, B., Marshall, L. J., Rubenach, M. J., Williams, P. J. and Baker, T. (2004). "Modeling the role of sodic alteration in the genesis of iron oxide–copper–gold deposits; eastern Mt. Isa Block, Australia." Econ. Geol. **99**: 1145-1176.

Oliver, N. H. S., Pearson, P. J., Holcombe, R. J. and Ord, A. (1999). "Mary Kathleen metamorphic-hydrothermal uranium-rare-earth deposit: ore genesis and a numerical model of coupled deformation and fluid flow." Austr. J. Eth. Sci. **46**: 467-484.

Oliver, N. H. S., Rawling, T. R., Cartwright, I. and Pearson, P. J. (1994). "High temperature fluid-rock interaction and scapolitization in a large extension-related hydrothermal system, Mary Kathleen, Australia." J. Petrol. **35**: 1455-1491.

Rubenach, M. 2005. Tectonothermal Evolution of the Eastern Fold Belt, Mt Isa Inlier. I2+3 Final Report, pmdCRC.

Page, R. W. (1983a). "Chronology of magmatism, skarn formation and uranium mineralisation, Mary Kathleen, Queensland, Australia." Econ. Geol. **78**: 838-853.

Peacock, S. M., Rushmer, T. and Thompson, A. B. (1994). "Partial melting of subducting oceanic crust." Eth. Plan. Sci. Lett. **121**: 227-243.

Perring, C. S., Pollard, P. J., Dong, G., Nunn, A. J. and Blake, K. L. (2000). "The Lightning Creek sill complex, Cloncurry District, northwest Queensland: a source of fluids for Fe oxide Cu-Au mineralization and sodic-calcic alteration." Econ. Geol. **95**: 1067-1089.

Pollard, P. J. (2001). "Sodic(-calcic) alteration associated with Fe-oxide-Cu-Au deposits: an origin via unmixing of magmatic-derived H2O-CO2-salt fluids." Mineralium Deposita **36**: 93-100.

Rotherham, J. F., Blake, K. L., Cartwright, I. and Williams, P. J. (1998). "Stable isotope evidence for the origin of the Starra Au-Cu deposit, Cloncurry district." Econ. Geol. **93**: 1435-1449.

Wang, S. and Williams, P. J. (2001). "Geochemistry and origin of Proterozoic skarns at the Mount Elliott Cu-Au(-Co-Ni) deposit, Cloncurry District, NW Queensland, Australia." Mineral. Deposita **36**: 109-124.

Wickham, S. M., Janhardan, A. S. and Stern, R. J. (1994). "Regional carbonate alteration by mantle-derived magmatic fluids, Tamil Nadu, Southern India." J. Geol. **102**: 379-398.

Williams, P. J. (1998). "Metalliferous economic geology of the Mt Isa Eastern Succession, Queensland." Austr. J. Eth. Sci. **45**: 329-341.

Williams, P. J., Dong, G., Ryan, C. G., Pollard, P. J., Rotherham, J. F., Mernagh, T. P. and Chapman, L. C. (2001). "Geochemistry of hypersaline fluid inclusions from the Starra (Fe-oxide)-Au-Cu deposit, Cloncurry District, Queensland." Econ. Geol. **96**: 875-884.

Wilson, I. H. (1978). "Volcanism on a Proterozoic continental margin in northwestern Queensland." Precambrian Research : 205-235.

Fault Roughness, Length and Mineral Endowment

Tom Blenkinsop[1] Roger Mustard[1] Frank P. Bierlein[2]
[1]School of Earth Sciences James Cook University, Townsville QLD 4811, Australia
[2]School of Geosciences Monash University, PO Box 28E, Victoria, 3800, Australia

ABSTRACT

Bends on fault surfaces affect fluid flow and can localize mineral deposits. The non-planarity, or roughness, of fault surfaces may therefore affect their mineral endowment. We examine this hypothesis for base metals in the Proterozoic Mount Isa Inlier, NE Australia, a world-class base metal province that contains numerous examples of strongly fault-controlled mineralization. Fractal analysis shows that the roughest faults studied are endowed with orders of magnitude more metal/km^2 than the smoothest faults. Intermediate roughness faults have from none to significant mineral endowments. The rougher faults are also longer. Roughness, but not length per se, is suggested to control mineralization. The relation between roughness and length suggests that as faults grow, they become rougher. Roughness appears to be one important factor that determines mineral endowment of major faults in base metal provinces. Fault roughness can potentially be used as a regional-scale exploration tool.

Keywords: Faults, mineralization, fractals, Mount Isa, base metals

1. INTRODUCTION

The roughness of fault surfaces is a fundamental attribute that affects their mechanical and seismological behavior (e.g., Byerlee, 1967; Sibson, 1986; Scholz, 1990). Fault roughness may be measured by deviations from linearity in fault surface traces, which can be described geometrically (Fig. 1: left and right bends), and kinematically with reference to a slip direction and sense (Fig. 1: restraining and releasing bends; cf. Sibson, 1986). Fault roughness has fractal properties (Scholz and Aviles, 1986; Power et al., 1988).

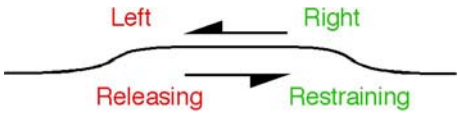

Fig. 1 Bends in fault traces can be described either geometrically or kinematically (after Sibson, 1986).

Faulting, fluid flow and mineralization can be linked from a dynamic point of view (fault pump and fault valve behavior: Sibson et al., 1975; Sibson et al., 1988; Cox, 1999; Sibson, 2001) and by considering the role of permeability in fault zones (e.g. fault-fracture meshes: Sibson, 1996; 2004; Tunks et al., 2004). Bends on faults play a crucial role by creating gradients in mean stress and permeability, and they are sites of preferential mineralization (Holyland and Ojala, 1997). Although releasing bends are most commonly associated with mineral deposits, restraining bends may increase pore fluid pressure or cause greater fluid flow through enhanced permeability (Smith and Wiltschko, 1996).

Discovering these sites of preferential ore deposition, and predictive assessment of the mineral endowment of fault systems, remain fundamental challenges in mineral exploration. We propose and test the hypothesis that fault roughness may be one important factor that can affect the endowment of faults in a base metal province, and we indicate how such an approach might provide a useful aid at the area selection scale in mineral exploration. The fractal nature of fault surfaces suggests that fractal methods to measure fault roughness may be appropriate to test the hypothesis, as implemented here for the Proterozoic Mount Isa Inlier, NE Australia.

2. FAULT ARCHITECTURE AND MINERALIZATION IN THE MOUNT ISA INLIER

The dominant fault architecture of the Mount Isa Inlier was initiated during basin formation from 1.8 to 1.6 Ga (e.g. Giles et al., 2002), although earlier influences from the ~ 1.85 Ga Barramundi orogeny (Etheridge et al., 1987) are possible. Basin formation may have been initially in response to NE-SW or E-W extension, followed by N-S and then NW-SE extension (Oliver et al., 1991; Queensland Department of Mines and Energy, 2000; Betts and Lister, 2002). Subsequently the Isan orogeny (~ 1.6 – 1.5 Ga) caused N-S shortening in places (Bell, 1983) followed by pervasive E-W shortening (Blake and Stewart, 1992; O'Dea et al., 1997), and the rift-associated faults were reactivated (Scott et al., 1998). Veining and fault reactivation may have occurred as recently as 340 Ma (Betts et al. 1997; Mark et al., 2004). The dominant faults in the inlier created by this history are approximately NS, NE-SW and NW-SE (Fig. 2a), and they have had multiphase movement histories.

The Inlier is a world class Proterozoic base metal province. Numerous Cu, Cu-Au, (both associated with Co) and Pb-Zn-Ag deposits (including some of the world's largest) and prospects occur within the Inlier (Fig. 2b). In some cases clear genetic relationships have been demonstrated between individual world-class deposits and major faults (e.g. Cu deposits at Mount Isa: Matthäi et al., 2004; Pb-Zn at Century mine: Ord et al., 2002). However, it is a striking observation that major faults with apparently similar characteristics differ by orders of magnitude in their mineral endowments, for which there has been no satisfactory explanation.

3. METHODS AND DATA

The coastline method (also known as the structured walk, ruler or divider method) is a sensitive measure of fractal roughness (e.g. Aviles et al., 1987). The exponent of a power law relationship between the length of a fault (P) and the ruler length (L) is used to derive D, a measure of the fault roughness:

$$P \sim L^{1-D}$$

D is the coastline dimension of the fault. A straight line has D = 1, and D increases with fault roughness (Aviles et al. 1987).

Assessing fault roughness on the scale of mineral deposit distributions (10^{-1} - 10^{5} km) requires working from fault maps. Thirteen major well-exposed faults or fault segments from throughout the Mount Isa Inlier that dip vertically at surface were selected in order to exclude topographic effects, and to obtain reliable estimates of fault roughness (Fig. 2). Further details of the maps used and the fractal analysis are contained in the Appendix. To test whether topography has an effect on fault roughness, the change in elevation between adjacent pairs of fault nodes was plotted against change in strike for the Mt isa fault (Fig. 3). A topographic effect would be seen in this plot from a concentration of points to opposite quadrants of the graph. No such effect can be seen, clearly demonstrating that topography does not have an effect on roughness.

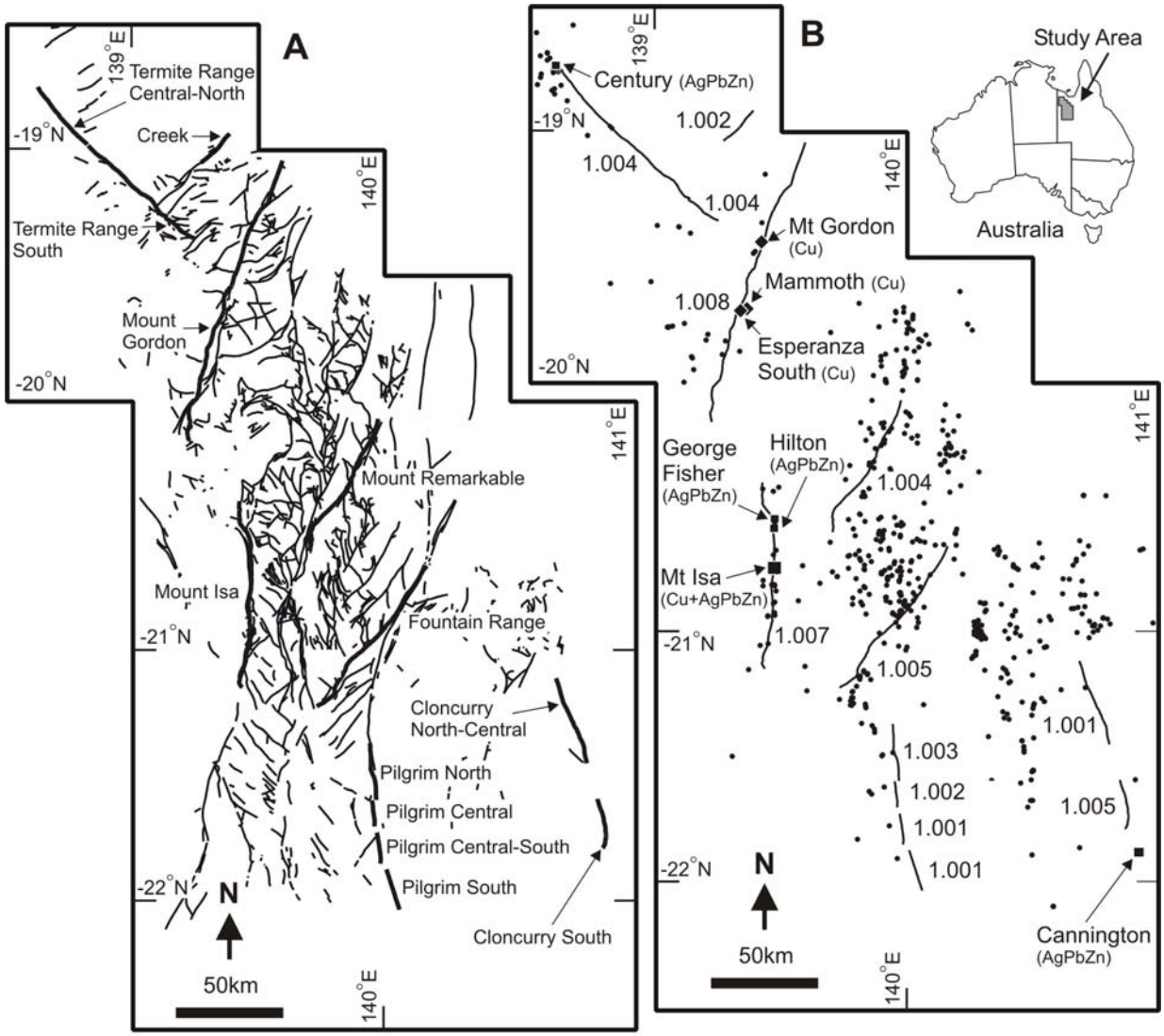

Blenkinsop et al. Fig 2.jpg

Fig. 2. Faults and mineral deposits in the Mount Isa Inlier. a) Studied faults (thick lines) named. Faults from Blake (1987). b) Studied faults and associated major mineral deposits (named) in the Mount Isa inlier. Numbers give fractal dimensions of faults. Other mineral deposits are all deposits that recorded production, or quote a geological resource (Queensland Department of Natural Resources and Energy 2002).

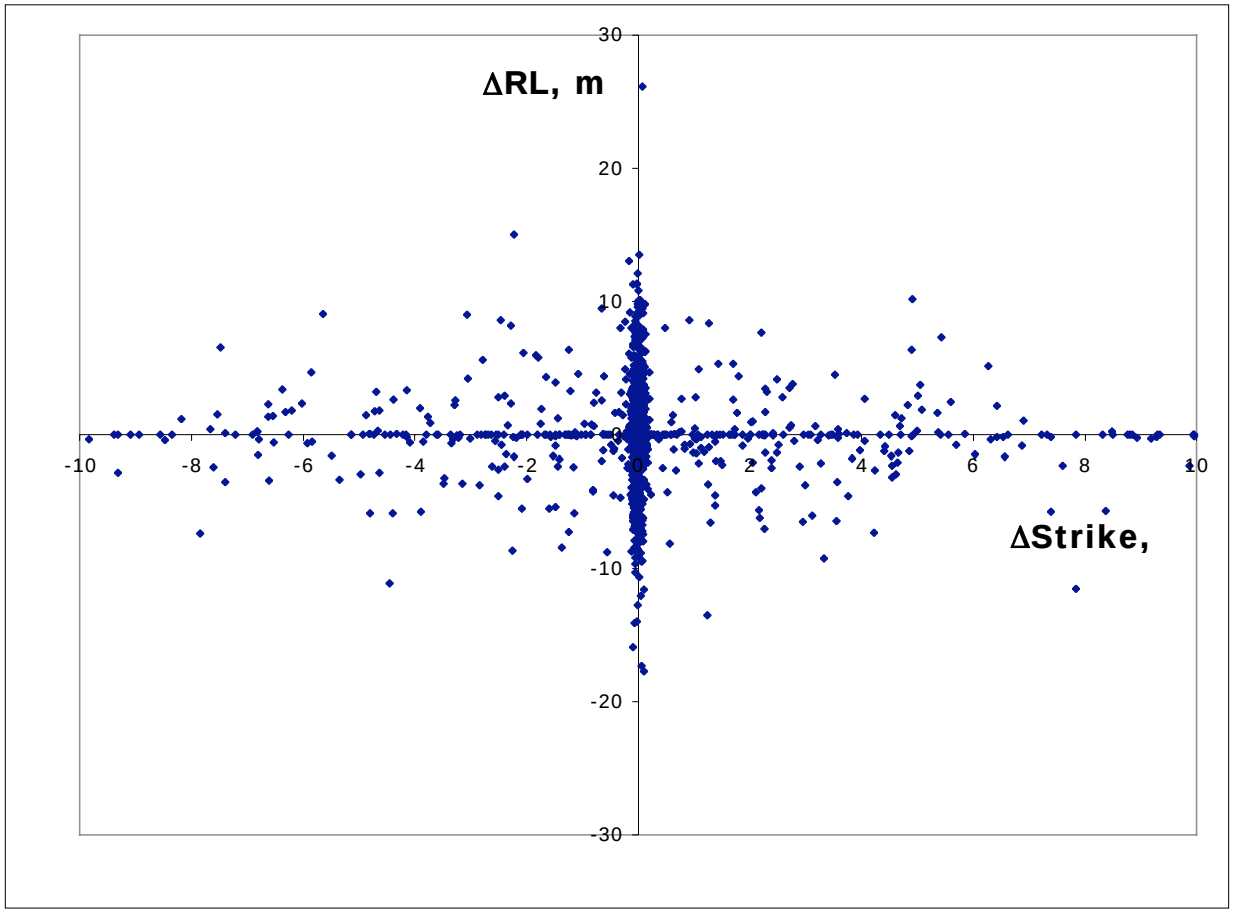

Fig. 3. Change in height (ΔRL, m) ,as a function of change in strike (ΔStrike, º) between adjacent fault segments for the Mt Isa Fault. The even distribution of points between the four quadrants shows that topography has no significant effect on the trace of the fault.

Deposits were considered to be spatially associated with faults if they were situated within 5 km; other buffers down to 1 km were tested but made little difference to the results. Mineral endowment of faults was measured by summing the resources and reserves for Cu, Pb, Zn, Ag and Co (see caption to Fig. 2) divided by the buffer area in order to normalize the results for fault length. The statistical association between all deposits and all faults in the study area was assessed by the Contrast value. The Contrast is the natural log of the ratio between the odds of finding a deposit in the vicinity of a fault to the odds of finding a deposit away from a fault (weights of evidence approach; cf. Bonham-Carter 1994). Contrast values greater than zero indicate greater than chance association between deposits and faults. The confidence in the contrast value was assessed by the confidence statistic, given by the contrast divided by the standard deviation.

4. RESULTS

The contrast value for the relation between all deposits and faults is 1.02, indicating a close spatial association between the deposits and faults. The confidence value of 12.1 is very high (a value of 1.5 is commonly considered to establish confidence: G. Partington pers. comm.).

Table 1 summarizes the roughness measurements and mineral endowments, arranged in order of decreasing roughness as measured by the fractal dimensions.

Table 1. Fault Roughness and Mineral Endowment

Fault	Fractal Dimension	Error	Cu* (t/km^2)	Pb* (t/km^2)	Zn* (t/km^2)	Ag* (kg/km^2)	Co* (t/km^2)
Rough faults							
Mt Gordon	1.008	0.0004	8.99E+02	0.00E+00	0.00E+00	6.91E-01	0.00E+00
Mt Isa	1.007	0.0013	1.13E+04	1.61E+04	1.52E+04	3.26E+04	1.09E+01
Intermediate faults							
Cloncurry South	1.005	0.0011	0.00E+00	0.00E+00	0.00E+00	0.00E+00	0.00E+00
Fountain Range	1.005	0.0005	8.44E+01	0.00E+00	0.00E+00	6.20E+00	0.00E+00
Mt Remarkable	1.004	0.0005	7.88E+00	0.00E+00	0.00E+00	6.39E-01	0.00E+00
Termite North&Central	1.004	0.0005	0.00E+00	0.00E+00	1.45E+04	5.68E+03	0.00E+00
Termite South	1.004	0.0011	0.00E+00	0.00E+00	0.00E+00	0.00E+00	0.00E+00
Pilgrim North	1.003	0.0001	3.33E-02	0.00E+00	0.00E+00	0.00E+00	0.00E+00
Smooth faults							
Pilgrim Central	1.002	0.0008	9.10E-03	0.00E+00	0.00E+00	0.00E+00	0.00E+00
Creek	1.001	0.0002	0.00E+00	0.00E+00	0.00E+00	0.00E+00	0.00E+00
Cloncurry North&Central	1.001	0.0007	6.90E-02	0.00E+00	0.00E+00	0.00E+00	0.00E+00
Pilgrim CentralSouth	1.001	0.0020	8.30E-03	0.00E+00	0.00E+00	0.00E+00	0.00E+00
Pilgrim South	1.001	0.0002	0.00E+00	0.00E+00	0.00E+00	0.00E+00	0.00E+00

* Resources and reserves associated with the faults. See caption for Fig. 2 for data source.

The fractal dimensions of the faults vary over a range that is an order of magnitude larger than the errors. Figure 4 shows the strong contrast in morphology between the roughest and smoothest faults. The faults fall into three categories of roughness: the two roughest faults with D > 1.007, an intermediate group with 1.007 > D > 1.003, and the smoothest faults with D < 1.002. The roughest faults have two to three orders of magnitude more associated Cu than any of the other faults. The intermediate faults have none or some Cu, and the smoothest faults have none or negligible Cu. For Pb and Co, only the roughest faults have any metal endowment. For Zn and Ag, the roughest faults have the most metal, the smoothest faults have none, and some of the intermediate faults have significant resources.

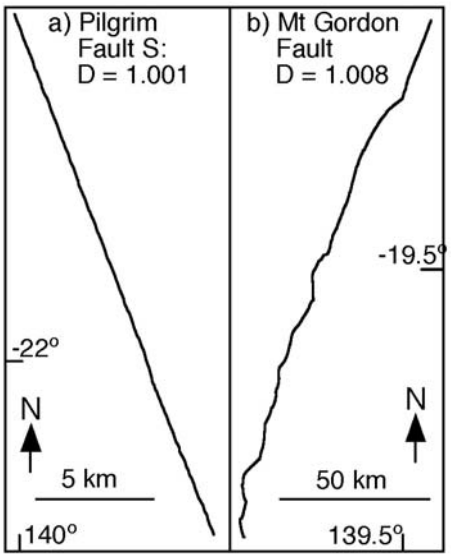

Fig. 4. Contrasts between the smoothest and roughest faults a) the Pilgrim Fault (southern segment) and b) the Mount Gordon Fault. D is the fractal dimension.

The data also suggest a relationship between fault roughness and length (Fig. 5).

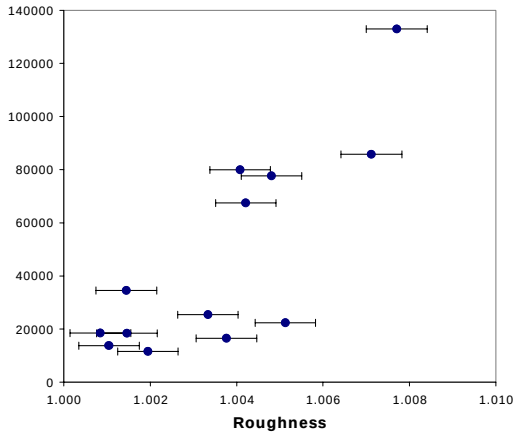

Fig. 5. Fault length (measured from summing the lengths between nodes) against fault roughness. Average errors are indicated on the roughness points.

5. DISCUSSION

The results suggest that metal endowment of faults in the Mount Isa Inlier is related to the categories of fault roughness and length. Several issues need to be considered before these spatial relationships can be interpreted as a causative link.

Roughness of fault surfaces at mm scales is dependent on the section orientation relative to the slip vector (e.g. Power et al., 1988). Additionally, fault roughness may depend on fault history, possibly in complex ways; fault roughness might either increase (due to later deformation or offset on later faults) or decrease with time (as asperities are removed). Moreover, the roughness of a fault may relate to any or all of the pre-, syn- and post-mineralization fault history.

These factors can not be tested explicitly in the Mount Isa example since fault roughness can only be measured at present. However, it is likely that all the major faults examined in this study have had a history extending back to at least pre-Isan orogeny times (Queensland Department of Mines and Energy, 2000). Since the Isan orogeny, the Isan block has behaved as a tectonic entity (Betts et al., 2002). To this extent, the faults in this study can be considered as having a similar history, which involved several periods of movement during the Isan orogeny, with possibly different slip vectors (e.g. Betts and Lister, 2004). This history, together with the 10^2 to 10^4 m scale of the roughness analysis, may reduce any effects of section orientation.

The results of the study are permissive that the geometry of the faults preserve large-scale geometric features that affected mineralization. The detailed geometry of the faults may have changed since mineralization, but heterogeneity can be preserved, as shown for the Boulder-Lefroy fault in the Yilgarn craton recently by Weinberg et al. (2004). Because the faults have been reactivated and deposits may have been displaced from their original position relative to bends, individual deposits may not now relate to specific bends.

A variety of other influences clearly play a role in localizing mineral deposits in the Mount Isa Inlier: these can explain why the intermediate roughness category of faults have such variable

endowments. For example, litho-stratigraphic considerations are important at the Pb-Zn deposits at Century and Mount Isa (Southgate et al., 2000; Ord et al., 2002). Fault intersections may also be important; these commonly occur at fault bends, and this relationship is inferred to be one of the localizing factors at the Mount Isa Pb-Zn-Ag deposit (Betts and Lister 2002). The exceptional Zn endowment of the Termite Range Fault (Fig. 2b) has been related to a fault intersection on the Termite Range Fault in combination with other factors such as carbonaceous content of host rocks (Betts and Lister, 2002; Broadbent et al., 2002). Lithospheric structure may play a role on a large scale (Betts and Lister, 2002).

The role of fault roughness in localizing mineral deposits does not imply any particular genetic mechanism for mineralization beyond stressing the importance of fluid flow. Mineralizing fluids may be focused by fault irregularities in environments ranging from syn-sedimentary to metamorphic, and thus encompassing SEDEX, diagenetic, replacement and convection or fault-driven fluid flow genetic models, all of which have been proposed for base metal deposits of the Mount Isa Inlier (e.g. Large, 1983; McGoldrick and Keays, 1990; Perkins and Bell, 1998; Ord et al., 2002; Davis, 2004; Matthai et al. 2004).

The relation between fault length and roughness is intriguing and requires posing the question of whether it is length or roughness that is controlling endowment. Mineral endowment has been normalized to the area of the fault buffer, a measure proportional to fault length (virtually identical results are obtained if mineral endowment is normalized to length rather than buffer area). No mechanism is known whereby length itself may increase normalized endowment. The most logical interpretation of the results is that as faults grow, they increase in roughness and thereby mineral endowment.

There are several reasons why fault roughness may increase with length. Linkage of faults is the most obvious, but refraction and deformation of faults are also possible. The opposite process of smoothing with growth may also occur due to displacement but appears not to have done so in the Mt Isa faults. One reason for this may be the long-lived history of these faults in which repeated episodes of deformation maintain roughening at great rates than smoothing

The results suggest that fault roughness can be used as a tool in prospectivity studies to complement other approaches. The method may be useful on the regional scale as a discriminator between richly and poorly endowed major faults. The intermediate roughness of the Cloncurry south fault segment is interesting in this respect: although it has no known mineral endowment, Cannington, (the world's largest single Ag mine; Walters et al., 2002), is located along the general strike of the fault to the south under cover (Fig. 2b).

6. CONCLUSIONS

In the Mount Isa Inlier, base metal deposits are strongly associated with major faults, and studies at individual deposits confirm the strong control on mineralization by faults. However, major faults differ by orders of magnitude in their mineral endowment. Fault roughness may have exerted an important, although not exclusive, control on mineral endowment by focusing mineralizing fluids at bends. An exciting implication of this conclusion is that fault roughness

could be used as an exploration tool on a large scale in this and similar terranes where fault geometry can be mapped in detail.

7. REFERENCES

Aviles, C.A., Scholz, CH., and Boatwright, J., 1987, Fractal analysis applied to characteristic segments of the San Andreas Fault: Journal of Geophysical Research, v. 92, p. 331-344.

Bell, T.H., 1983, thrusting and duplex formation at Mount isa, Queensland, Australia: Nature, v. 304, p. 493-497.

Betts, P., and Lister, G.S., 2002, Geodynamically indicated targeting strategy for shale-hosted massive sulphide mineralization in the western Fold Belt, Mount Isa Terrane: Australian Journal of Earth Sciences, v. 49, p. 985-1010.

Betts, P., and Lister, G.S., 2004, Aeromagnetic patterns of half-graben and basin inversion: implications for sediment-hosted massive sulphide Pb-Zn-Ag exploration: Journal of Structural Geology, v.26, p. 1137-1156.

Betts, P.G., Alliéres, L., and Lister, G.S., 1997, Geological overview of the Mount Isa terrane. Structural elements of the Eastern Successions: a field guide illustrating the structural geology of the Eastern Mount Isa terrane, Australia. Technical Publication of the Australian Crustal Resource Centre, v. 63, p. 1– 16.

Blake, D.H., 1987. Geology of the Mount Isa Inlier and environs, Queensland and Northern Territory: Bureau of Mineral Resources Bulletin 225, 83 p.

Blake, D.H. and Stewart, A.J., 1992, Stratigraphic and Tectonic framework, Mount Isa Inlier, *in* Stewart, A.J. and Blake, D.H., eds., Detailed studies of the Mount Isa inlier, Australian Geological Survey Organization Bulletin 243, p. 1-11.

Bonham-Carter, G., 1994, Geographic information systems for geoscientists: modeling with GIS: Oxford, England: Pergamon, 398 p.

Broadbent, G.C., Andrews, S.J. and Kelso, I.J., 2002, A decade of new ideas: Geology and exploration history of the Century Zn-Pb-Ag deposit, Northwestern Queensland, Australia, *in* Goldfarb, R.J., Nielsen, R.L. eds., Integrated Methods for Discovery: Global Exploration in the Twenty-First Century: Society of Economic Geologists Special Publication 9, p. 119-140.

Byerlee, J.D., 1967, Frictional characteristics of granite under high confining pressure: Journal of Geophysical Research, v. 72, p. 3639-3648.

Cox, S.F., 1999, Deformational controls on the dynamics of fluid flow in mesothermal gold systems, *in* McCaffrey, K.J.W., Lonergan, L., Wilkinson, J.J. eds., Fractures, Fluid Flow and Mineralization. Geological Society of London, Special Publication 155, pp. 123–140.

Davis, T., 2004, Mine-scale Structural Controls on the Mount Isa Zn-Pb-Ag and Cu orebodies: Economic Geology, v. 99, p. 543-559.

Etheridge, M.A., Rutland, R.W.R., and Wyborn, L.A., 1987, Orogenesis and tectonic process in the Early to Middle Proterozoic of northern Australia, *in* Kroner, A., ed. Proterozoic Lithosphere Evolution, American Geophysical Union Geodynamic series 1. p. 131-147.

Giles, D., Betts, P., and Lister, G., 2002, Far-field continental backarc setting for the 1.80–1.67 Ga basins of northeastern Australia: Geology, v. 30, p. 823–826.

Holyland, P.W. and Ojala, V.J., 1997, Computer-aided structural targeting in mineral exploration: Two and three-dimensional stress mapping: Australian Journal of Earth Sciences, v. 44, p. 421-432.

Large, D. E., 1983, Sediment-hosted massive sulphide lead–zinc deposits: an empirical model. *In*: Sangster D. F. ed. Sediment-hosted Lead–Zinc Deposits, Mineralogical Association of Canada Short Course Handbook 8, p. 1–30.

Mark, G., Williams, P.J., and Boyce, A.J., 2004, Low-latitude meteoric fluid flow along the Cloncurry Fault, Cloncurry district, NW Queensland, Australia: geodynamic and metallogenic implications: Chemical Geology, v. 207, p. 117-132.

Matthäi, S.K., Heinrich, C.A., and Driesner, T., 2004, Is the Mount Isa copper deposit the product of forced brine convection in the footwall of a major reverse fault? Geology, v. 32, p. 357-360.

McGoldrick P. J., and Keays, R. R., 1990, Mount Isa copper and lead–zinc–silver ores: coincidence or cogenesis? Economic Geology, v. 285, p. 641–650.

O'Dea, M. G., Lister, G.S., MacCready, T., Betts, P.G., Oliver, N.H.S., Pound, K.S. Huang, W., and Valenta, R.K., 1997, Geodynamic evolution of the Proterozoic Mount Isa Terrain, *in* Burg, J.P., and Ford, M., eds., Orogeny through time, Geological Society of London Special Publication, v. 121, p. 99-122.

Oliver, N.H.S., Holcombe, R.J., Hill, E.S., and Pearson, P.J., 1991, Tectono-metamorphic evolution of the Mary Kathleen Fold belt, northwest Queensland: a reflection of mantle plume processes: Australian Journal of Earth Sciences, v. 38, p. 425-455.

Ord, A., Hobbs, B.E., Zhang, Y., Broadbent, G.C., Brown, M., Willets, G., Sorjonen-Ward, P., Walshe, J.L., and Zhao, C., 2002, Geodynamic modeling of the Century deposit, Mount Isa province, Queensland: Australian Journal of Earth Sciences, v. 49, p. 1011-1039.

Perkins, W. G., & Bell T. H., 1998, Stratiform replacement lead–zinc deposits: a comparison between Mount Isa, Hilton and McArthur River: Economic Geology, v. 93, p. 1190–1212.

Power, W.L., Tullis, T.E. and Weeks, J. D., 1988, Roughness and wear during brittle faulting: Journal of Geophysical Research, v. 93, p. 15268-15278.

Queensland Department of Mines and Energy, 2000, Northwest Queensland Mineral Province Report, Queensland Department of Mines and Energy.

Queensland Department of Natural Resources and Mines, 2002, QMIN - Queensland Mineral Resource Database MINOCC 2002 - Microsoft Access Database, Version 3.0, December 2002, Queensland Department of Natural Resources and Mines.

Scholz, C.H., and Aviles, C., 1986, The fractal geometry of faults and faulting, *in* Das, S. Boatright, J., and Scholz, C. eds., Earthquake Source Mechanics, American Geophysical Union Geophysical Monograph 37, Washington D.C. 147-155.

Scholz, C.H., 1990, The mechanics of earthquakes and faulting. Cambridge University Press, 439 p.

Scott, D.L., Bradshaw, B.E., and Tarlowski, C. Z., 1998, The tectonostratigraphic history of the Proterozoic northern Lawn hill platform, Australia: an integrated intracontinental basin analysis: Tectonophysics, v. 300, p. 329-358.

Sibson, R.H., 1986, Earthquakes and lineament infrastructure: Philosophical transactions of the Royal Society of London A, v. 317, p. 63-79.

Sibson, R.H., 1996, Structural permeability of fluid-driven fault-fracture meshes: Journal of Structural Geology, v. 18. p. 1031-1042

Sibson, R.H., 2001, Seismogenic framework for hydrothermal transport and Ore Deposition: Society of Economic Geologists Reviews, v. 14, p. 25-50.

Sibson, R.H., 2004, Controls on maximum fluid overpressure defining conditions for mesozonal mineralization: Journal of Structural Geology, v. 26, p. 1127-1136.

Sibson, R.H., Moore, J. M and Rankin, A.H., 1975, Seismic pumping: A hydrothermal fluid transport mechanism: Journal of the Geological Society of London, v. 131, p. 653-659.

Sibson, R.H., Robert, F., and Poulsen, K.H., 1988, High angle reverse faults, fluid pressure cycling and mesothermal gold-quartz deposits: Geology, v. 16, p. 551-555.

Smith, R.E. and Wiltschko, D.V., 1996, Generation and maintenance of abnormal fluid pressures beneath a ramping thrust sheet: isotropic permeability experiments: Journal of Structural Geology, v. 18, p. 951-970.

Southgate, P.N., Scott, D.L., Sami, T.T., Domagala, J., Jackson, M.J., James, N.P., and Kyser, T.K., 2000, Basin shape and sediment architecture in the Gun supersequence: a strike-slip model for Pb-Zn-Ag ore genesis at Mount Isa: Australian Journal of Earth Sciences, v. 47, p. 509-531.

Tunks, A.J., Selley, D., Rogers, J. R., Brabham, G., 2004, Vein mineralization at the Damang Gold Mine, Ghana: controls on mineralization: Journal of Structural Geology v. 26, p. 1257-1274.

Walters, S., Skrzeczynski, B., Whiting, T., Bunting, F., and Arnold, G., 2002, Discovery and geology of the Cannington Ag-Pb-Zn deposit, Mount Isa eastern succession, Australia: Development and application of an exploration model for Broken Hill-type deposits, *in* Goldfarb, R.J., Nielsen, R.L., eds., Integrated Methods for Discovery: Global Exploration in the Twenty-First Century. Society of Economic Geologists Special Publication 9, p. 119-140.

Weinberg, R. F., Hodkiewicz, P.F., and Groves, D. I., 2004, What controls gold distribution in Archean terranes ? Geology, v. 32, p. 545-548.

The Role of Geophysics in Exploration for Iron Oxide Copper-Gold Deposits

Mark Edmiston[1]
[1] Predictive Mineral Discovery CRC and Economic Geology Research Unit, School of Earth Sciences, James Cook University, Townsville QLD 4810
Email: mark.edmiston@jcu.edu.au

ABSTRACT

A wide range of deposits is encompassed by the term Iron Oxide Copper-Gold, resulting in a wide range of geophysical responses. Thus, deposit detection using regional geophysical data is difficult and often insufficient data resolution is the limiting factor. Studies of several major Australian deposits show that gravity methods have the most consistent results. Magnetic and electrical methods provide varied responses and anomalies are often related to associated features as well as the deposit. Radiometric, seismic and other geophysical data has limited use, mainly in helping to delineate targets for drilling. Experience has shown that no one method is ideal and that successful exploration is the result of persistence and the accurate integration of several methods along with all other geological data.

Keywords: Iron Oxide Copper-Gold deposits, geophysical methods, exploration, Olympic Dam, Prominent Hill, Mount Isa Eastern Succession.

1. INTRODUCTION

The Iron Oxide Copper-Gold (IOCG) deposit class covers a broad range of mineral deposits. When the giant Olympic Dam deposit was discovered in 1975 it was thought to be a new and possibly unique deposit type. It was another decade before academic and industry geologists began to realise that this deposit had similar metallogenic properties to other deposits around the world (Porter, 2000) and that perhaps these deposits all lie on a continuum. This revelation culminated in the paper of Hitzman (Hitzman, 2000) who identified the common characteristics, geology, tectonic setting and mineralogy of IOCG deposits. Several papers have since identified key elements of this deposit class although only Smith (Smith, 2000) has focused specifically on their geophysics. The complex nature and wide spectrum that encompasses IOCG deposits results in a vast array of physical properties, both of the deposit and the surrounding terrain, and varied, sometimes contrasting geophysical signatures.

2. CHARACTERISTICS OF IOCG DEPOSITS

The location of IOCG deposits can be classed into three general tectonic settings; intra-continental orogenic collapse, intra-continental orogenic magmatism and extension along a subduction-related continental margin (Hitzman, 2000). The common links between these environments are high igneous activity, high heat flow and highly oxidised source rocks. Deposits can also be formed over a wide range of depths, from near surface (Olympic Dam) to 10-15 km depth in the Cloncurry district (Pollard, 2000).

The majority of large IOCG deposits have a spatial and temporal association with significant igneous activity (Hitzman, 2000). The igneous rocks associated with these deposits cover a wide range of compositions but are typically related to I-type magnetite-series granitoids (Pollard, 2000). Structural control also appears to influence IOCG deposits with a spatial association existing with major (crustal scale) faults (Hitzman, 2000; Pollard, 2000). Deposits tend to be located on second order high to low angle faults that splay off major (strike-slip?) faults. While there is some structural control, the morphology of deposits is variable and can range from strata-bound sheets to irregular stockwork breccia zones. This limited structural control, vast morphological range and lack of a unique model of formation leads to highly complex and variable deposit geometries and properties.

IOCG deposits are an end member of a continuum of deposits with relatively copper and gold deficient magnetite-apatite deposits forming the other end member (Hitzman, 2000). Compared with other deposit types, IOCGs are characterised by a relative lack of iron sulphide minerals and may contain significant carbonate, Ba, P and/or F. Other elements associated with the deposit class include U, Ag, Mo, Co, As, Zn and Rare Earth Elements. Intense alteration is also associated with IOCG deposits. Magnetite-apatite deposits tend to have a spatial association with sodic or sodic-calcic alteration while IOCG deposits display significant sodic-potassic, potassic or hydrolytic alteration.

3. GEOPHYSICAL SIGNATURES OF DEPOSITS

3.1. Gravity

IOCG deposits are generally associated with significant gravity anomalies. The specific gravity of ore forming minerals is significantly higher than typical upper crustal material densities (Table 1). The anomaly produced by such a density contrast can be on the order of 30 gu. Gravity is also the most reliable geophysical method of IOCG detection as there is no way of "hiding" the anomaly produced by the volume of dense minerals associated

with large economic deposits. Some deposits such as Olympic Dam may be almost undetectable by any other method (Smith, 2000).

Material Type	Density Range (g/cm^3)	Approx. Average Density (g/cm^3)
Sandstone	1.61 – 2.76	2.35
Limestone	1.93 – 2.90	2.55
Granite	2.50 – 2.81	2.64
Gabbro	2.70 – 3.50	3.03
Schist	2.39 – 2.90	2.64
Amphibolite	2.90 – 3.04	2.96
Magnetite	4.90 – 5.20	5.12
Haematite	4.90 – 5.30	5.18
Pyrite	4.90 – 5.20	5.00

Table 1 - Densities of selected geologic materials and ore forming minerals. Data from Telford (1990)

IOCG exploration using gravity becomes difficult when the gravity station spacing becomes much larger than the wavelength of the anomaly produced by a deposit. An isolated near surface ore body (approx diameter of 200 m) will produce an anomaly with wavelengths of less than one kilometre. If gravity station spacings in prospective mineral terrains are greater than 10 km (such as in the Mt Isa Inlier), the deposit's gravity signature will be virtually undetectable in the regional data set. In this situation any correlations that can be established between large scale anomalies or gradients and deposits are of great importance.

3.2. Magnetics

Both induced and remanent magnetisation are important factors in the magnetic signature of IOCG deposits. Magnetic susceptibilities tend to be greatest for rocks with high concentrations of ferromagnetic and/or ferrimagnetic minerals such as magnetite (Clark, 1997). There are many other factors that can affect susceptibility and the actual range of susceptibilities for a given rock can be very large (Table 2). Remanent or permanent magnetisation can be even more complex than induced magnetisation as it is affected by both mineralogy and "magnetic history". Typically, remanence is multi-component and is carried by different subpopulations of magnetic grains producing significant variation in remanent direction and intensity within a rock unit (Clark, 1997). Values of the Koenigsberger ratio, a measure of the relative remanent intensity, are also presented in Table 2 but due to the inherent complexity individual samples can plot well outside this range. Consequently the most important factor for reliable interpretation of magnetic images is a sound understanding of the physical properties that affect the induced and remanent magnetisation of a rock.

The minerals associated with IOCG deposits that contribute significantly to their magnetic response are magnetite, hematite and to a lesser extent maghemite (Smith, 2000). The magnetite of IOCG deposits tends to be fairly coarse grained. Larger grained magnetic minerals are more likely to retain an ancient remanent magnetisation indefinitely (Clark, 1997). In mineralised terrains with a complex history, this ancient magnetisation direction is unlikely to be parallel to the present field so quantitative interpretation may not be valid unless the remanent component is understood. Large discrepancies between magnetic susceptibility models and real world susceptibilities may therefore be used as a rough

indicator of the location of minerals associated with IOCG deposits. In IOCG deposits, hematite is often produced from the partial of total destruction of magnetite during alteration. Coarse-grained haematite can also display significant remanent magnetisation that will also effect quantitative interpretation. Regardless of remanent magnetisation however, significant bodies of magnetite and/or hematite are likely to be associated with large magnetic anomalies.

Material Type	Susceptibility Range (x 10^{-6} SI)	Approx. Average Sus. (x 10^{-6} SI)	Koenigsberger Ratio (REM/IND)
Sandstone	0 – 20 000	400	0.1 – 10
Limestone	0 -3 000	300	0.1 – 10
Granite	0 – 50 000	2 500	0.1 – 10
Gabbro	1 000 – 90 000	70 000	0.1 - 20
Schist	300 – 3 000	1 400	0.1 – 20
Amphibolite	-	700	0.1 – 20
Magnetite	1 200 000-19 200 000	6 000 000	3 – 5 000
Haematite	500 – 35 000	6 500	30 – 30 000
Pyrrhotite	1 000 – 6 000 000	1 500 000	1 – 10 000

Table 2 – Magnetic Susceptibility and Koenigsberger ratio of selected geologic materials and ore forming minerals. Data from Clark (1991, 1997); Telford (1990).

3.3. Radiometrics

Radiometric data can provide direct identification of mineral deposits although it is more commonly used to provide information for geological/structural mapping, as the penetration of gamma rays in typical earth materials is on the order of only 50 to 75 cm (Telford, 1990). Uranium is the only easily detectable radioactive element directly associated with IOCG mineralisation However, any direct correlation between radiometric anomalies and radioactive elements associated with mineral deposits is only possible if the ore body is exposed or very close to the surface, in which case it is likely to have been discovered. Radiometric data applied to mineral exploration can be more useful when used to identify zones of alteration associated with certain types of deposits.

Regional potassic alteration, which is often associated with IOCG (and other) mineralisation, is easily mapped by radiometric data and provides one of the best indicators of potential deposits (Shives et al., 1997). Potassic and sodic-potassic alteration tends to be associated more with economic IOCG mineralisation than the magnetite-apatite deposits, which generally display sodic or sodic calcic alteration. The alteration zones are also very large and easily identifiable from airborne data although narrowing targets from large alteration zones may be difficult.

Potassium anomalies can be produced by normal lithological sequences as well as most hydrothermally altered rocks. To distinguish between the two types of anomalies the potassium thorium ratio (K/Th) can be used as thorium enrichment does not generally accompany potassium during hydrothermal alteration processes (Shives et al., 1997). This important correlation has been shown to hold true in numerous worldwide studies (Galbraith, 1983; Shives et al., 1997) and in ground spectrometry measurements from the Cloncurry district. Figure 1 shows the K/Th ratio for in situ gamma ray measurements of mineralised, altered and unaltered rocks from the Mount Isa Eastern Fold Belt south of

Cloncurry. Altered and mineralised rocks generally display a high K/Th ratio while moderate to high grade ore rocks (K > 15 cps) plot distinctly separate from all other measurements in the area. However, prospectivity analysis (Mustard et al., 2004) has shown a stronger spatial correlation exists between the deposits and U/Th ratio from airborne radiometric measurements. This discrepancy could be due to not all deposits being associated with potassic alteration and the limited sampling range of the in situ measurements. Also, such high K/Th ratios have only been detected within moderate to high grade ore and as such may not be effectively sampled from the air.

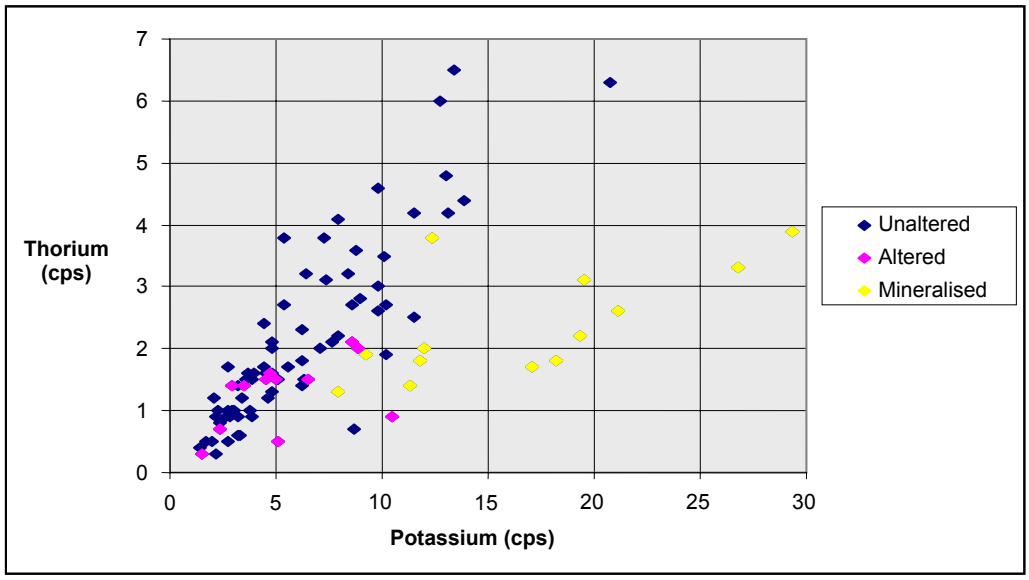

Fig. 1 - Potassium thorium ratios from in situ measurements on rocks from the Cloncurry district

3.4. Electrical Methods

The Earth's electrical resistivity is influenced by many factors. Resistivity of some common geological materials and minerals are presented in Table 3. While rock type is one of the main influences the issue of predicting rock types and geometries from resistivity data is complicated by factors such as weathering, impurities in the rocks, porosity, ground water salinity, etc. Typically in Australian conditions, measured surface resistivity can be on the order of 1 to 10 Ωm due to a deep weathering profile (i.e. high porosity even at depth) and saline ground water (Smith, 2000). However, as highlighted in Table 3 iron and sulphide minerals are still generally an order of magnitude more conductive than typical surface values. Deposits containing significant concentrations of these minerals (i.e. IOCG deposits) should produce distinguishable conductivity anomalies.

Resistivity can be measured directly or indirectly by several methods including resistivity/conductivity profiling or sounding, induced polarisation (IP), spontaneous or self potential (SP), magnetotellurics (MT) and time and frequency domain electromagnetic (TEM and FEM). No one method is ideal for mineral exploration (IOCG or otherwise) but in principal all are capable of detecting large bodies of magnetite, haematite and/or chalcopyrite (Smith, 2000) providing the depth extent is not to large. One method might be advantageous in a particular terrain or under certain conditions. Resistivity and IP are generally very sensitive and able to detect small conductivity changes or small bodies of differing conductivity. IP can also measure chargeability caused by magnetic minerals such as pyrite that conduct electricity through a crystal lattice. This generally produces a higher chargeability than common ore host rocks that conduct electricity through ions in

pore fluid (Smith, 2000). Chargeability can also be used as an estimate of grade as interconnected minerals are more chargeable than disseminated mineral, although measurements are only relative.

Material Type	Average Resistivity Range (Ωm)
Sandstone	$1 – 6.4x10^{8}$
Limestone	$50 – 10^{7}$
Granite	$3x10^{2} – 1x10^{6}$
Gabbro	$10^{3} – 10^{6}$
Schist	$20 – 10^{4}$
Gneiss	$3 - 10^{6}$
Magnetite	$5x10^{-5} – 5.7x10^{3}$
Haematite	$3.5x10^{-3} – 10^{7}$
Chalcopyrite	$1.2x10^{-5} – 0.3$
Pyrite	$2.9x10^{-5} – 1.5$

Table 3 – Resistivity of selected geologic materials and ore forming minerals. Data from (Telford, 1990) and (Reynolds, 1997)

EM has the advantage of being able to be measured from the air, giving large areas of coverage although EM is commonly used in borehole applications as well. In Australia, EM methods tend to have a limited depth penetration due to the highly conductive overburden and complex interpretation procedures are often required to overcome this. Despite the drawbacks, electrical methods are an excellent tool with which to follow up IOCG targets identified by gravity, magnetics, radiometrics and other prospectively methods.

4. REGIONAL DEPOSIT SIGNATURES

Individual deposits are very difficult to detect in regional gravity or aero-magnetic data sets. If magnetic, the deposit will usually be associated with a magnetic high and many deposits under cover have been discovered this way. Various derivatives and frequency filters can also be used to distinguish the deposit anomalies from other magnetic sources. However, a detailed magnetic dataset from a mineralised terrain will often contain hundreds of anomalous magnetic highs. Also, it has been shown that several IOCG deposits from a single district can have rather differing relationships between Cu-Au ore and magnetic sources (Williams and Pollard, 2001). Regional gravity data sets are generally unable to detect the response of an ore body alone due to insufficient station spacing. Regional geophysical data do however make an excellent first pass filter for identifying target areas and large scale features that are often associated with IOCG deposits such as regional highs and steep gradients.

Studies of several IOCG prospective terrains have shown that deposits are hosted in discrete “domains” that are characterised by an “active” magnetic signature (Haynes, 2000). IOCG deposits in the Mount Isa Eastern Succession possess an “active” magnetic appearance especially along the western boundary (Fig. 2). Prospectivity analysis has also shown a very high spatial correlation between magnetic highs and the IOCG deposits in Fig. 2 (Mustard, 2004). Deposits in the Eastern Succession also tend to be located near areas of high and intermediate gravity, i.e. not near gravity lows (Fig. 3).

Both magnetics and gravity can be used to locate igneous rocks and crustal scale faults associated with IOCG deposits. Relatively new wavelet based gradient analysis of

potential field data ("worming") is a valuable tool in identifying such features (Murphy, 2002). The "worming" method works by mapping the point of maximum gradient in potential field data at different levels of upward continuation. This creates a 3D string of points whose shape and associated parameters are a function of physical property contrasts at all levels of the crust (Archibald et al., 1999; Archibald et al., 2000). Hence, the level of upward continuation of a fault associated "worm" provides an indication of its depth extent and its potential to tap deep magmatic fluids that may be important in the formation of IOCG deposits (Barton and Johnson, 2000). To a degree worm analysis removes the ambiguity in potential field data interpretation and provides a rapid and intuitive interpretation of the sub surface.

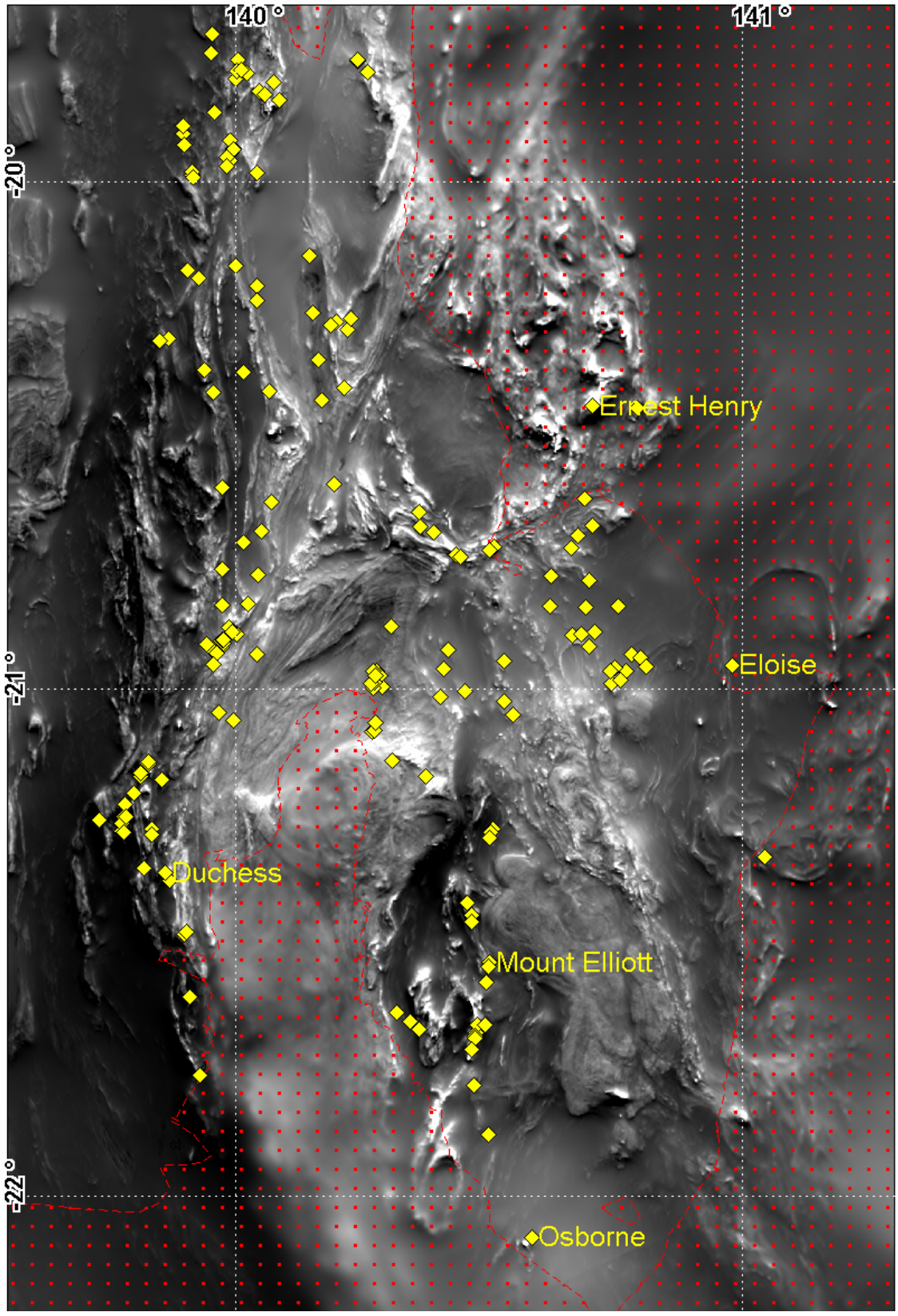

Fig. 2 - Total magnetic intensity image of the Mount Isa Eastern Succession showing IOCG deposits (yellow diamonds) and areas under cover (red dotted area). Data courtesy of Xstrata

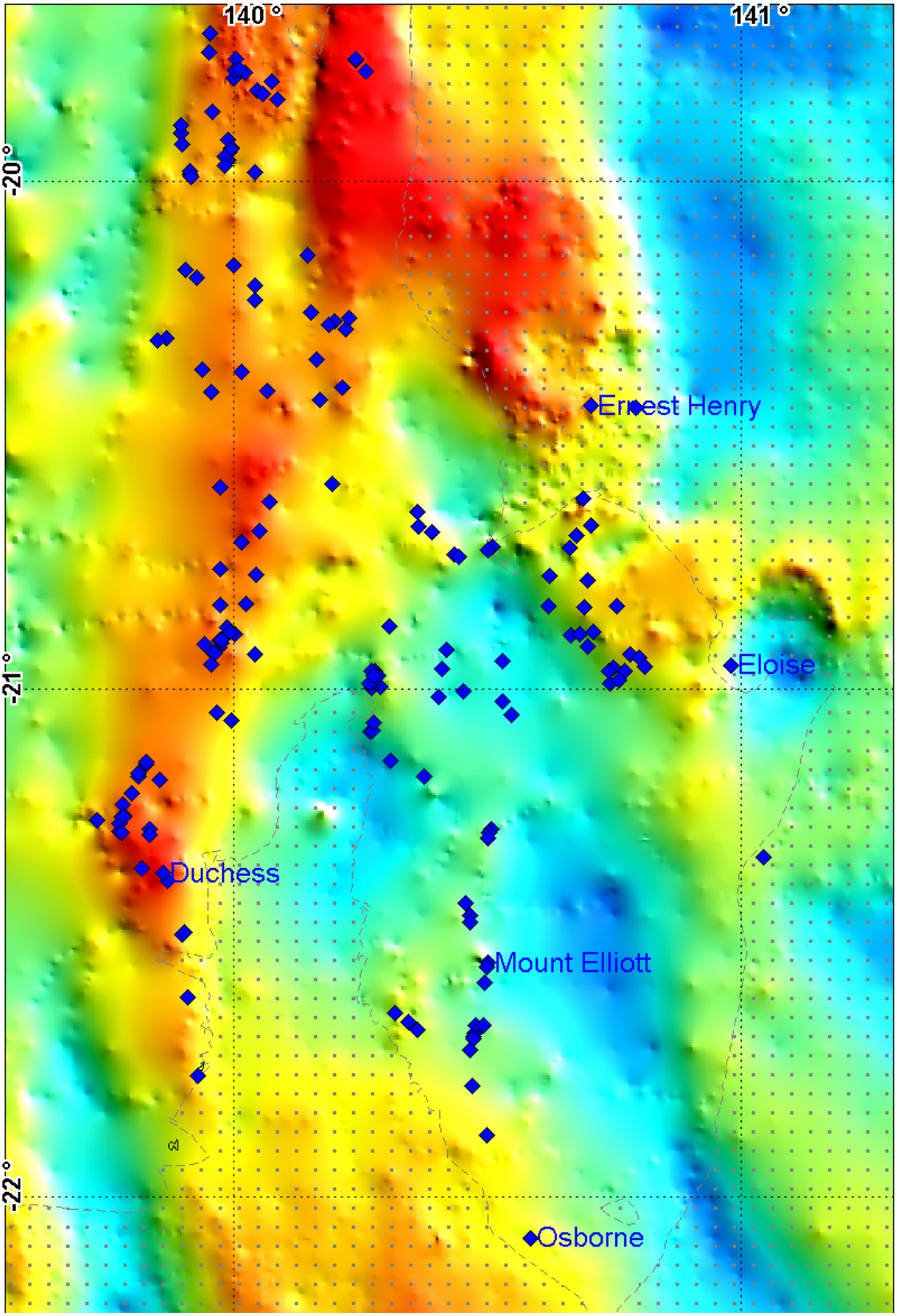

Fig. 3 - Bouguer gravity image of the Mount Isa Eastern Succession showing IOCG deposits (blue diamonds) and areas under cover (grey dotted area). Image is NE sun-shaded and has been coloured with red indicating high gravity and blue indicating low gravity Data from Geoscience Australia's national gravity network.

5. GEOPHYSICS OF AUSTRALIAN IOCG DEPOSITS

Australia, and in particular the Mt Isa Eastern Succession has excellent exploration potential for IOCG deposits. Compared to the rest of the world Australia has a relative wealth of information on the geophysics of IOCG deposits, with publications on six major deposits. These deposits are Olympic Dam and Prominent Hill from South Australia and Ernest Henry, Eloise, Osborne and the Starra Group, from the Mount Isa Eastern Succession. However, there are over 180 IOCG deposits in the Eastern Succession with a historical production or a resource estimate (Figs. 2 and 3) and considering the area of outcropping Precambrian rocks compared with the total area of similar rocks under cover, this is a topic that need further investigation. Summarised in Table 4 is the main geophysical signature of six Australian deposits.

	Geophysical Signature			
Deposit	**Gravity**	**Magnetics**	**Resistivity/IP**	EM
Olympic Dam (Esdale, 1987; Rutter, 1985)	High (~17 gu)	High due to source much deeper than the deposit	Low resistivity and IP anomaly attributed to saline ground water and basement	-
Ernest Henry (Webb and Rowston, 1995)	High	High of 7000 to 10000 nT above background	Near surface IP anomaly possibly due to secondary sulphides	**Small anomaly above SW corner associated with native copper**
Prominent Hill (Hart et al., 2004)	High (~60 gu)	No Response from ore body. Nearby high due to altered volcanics	Low resistivity and moderate chargeability	-
Eloise (Brescianini et al., 1992)	Ridge extending from an amphibolite associated high	1100 nT anomaly on the magnetic ridge of the "Eloise Structure"	No apparent resistivity anomaly but a broad IP feature associated with alteration	**Detectable where depth of mineralisation is typically less than 300 m**
Osborne (Anderson, 1992)	High	High of ~16000 nT with significant remanent	-	**Main anomaly coincident with weakly mineralised ironstone, second smaller anomaly due to higher grade mineralisation**
Starra group (Collins, 1987)	-	**Deposits located on strong NS trending ridge**	-	**Several anomalies due to different sources (Selwyn 251strong response)**

Table 4 - Geophysical response of Australian IOCG deposits

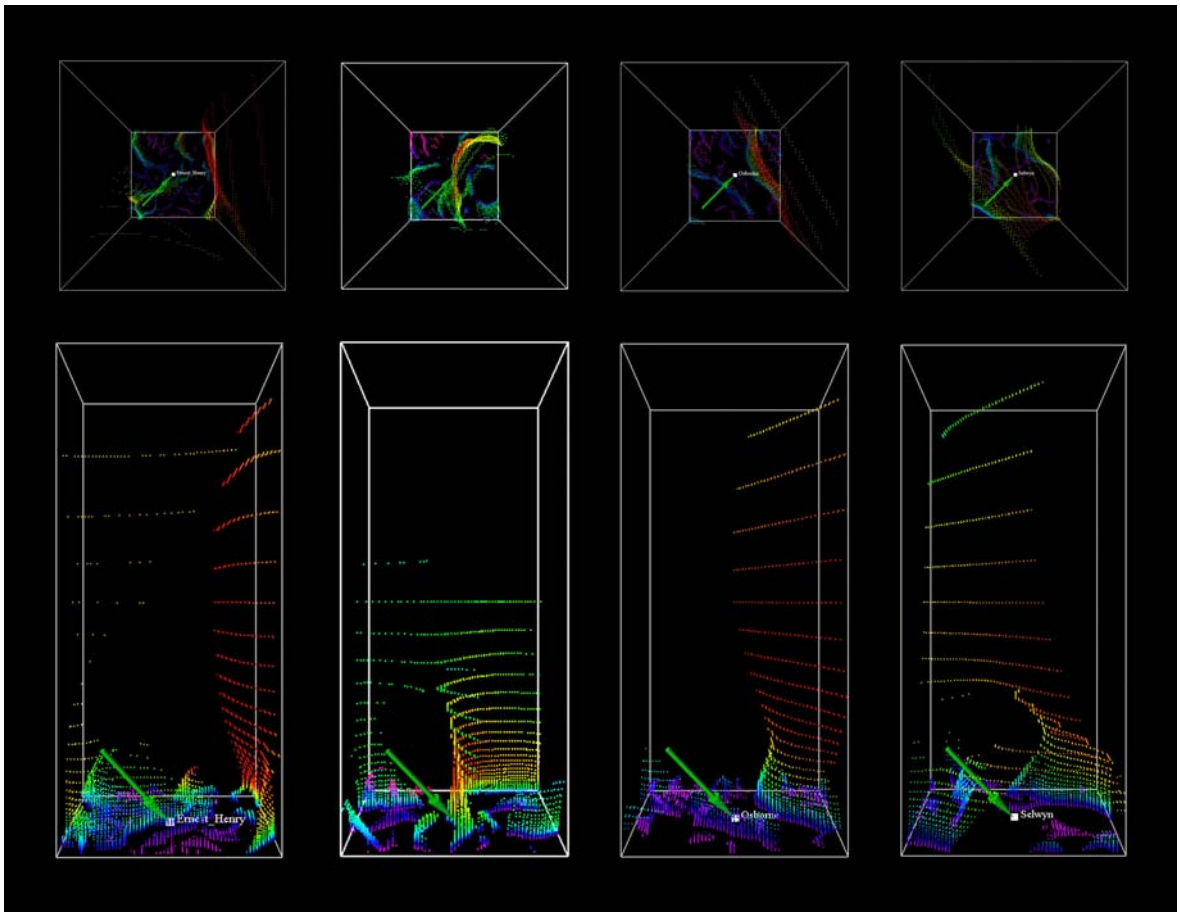

Fig. 4 - Gravity "worms" over IOCG deposits of Ernest Henry, Eloise, Osborne and Starra (Selwyn 257). Shown are top and perspective views of 30x30x70 km prisms centred on the deposits with worms coloured by W_{max} value.

Five of the six deposits listed in Table 4 produce a distinguishable gravity anomaly after detailed gravity studies were conducted over potential target areas. No information has been published on the gravity response of the Starra group but had a similar survey been conducted it is likely to produce a similar response. Density measurements at Ernest Henry and Eloise have shown the massive sulphides bodies to be between 0.6 and 1.0 g/cm^3 denser than the surrounding host rocks. However, the gravity signature of the Eloise deposit is somewhat masked by the much larger volumes of nearby amphibolites. Gravity "worms" over the deposits from the Eastern Succession (Fig. 4) show that their density contrast is insignificant on a crustal scale. Ernest Henry, Osborne and Selwyn 257 are located proximal to a major north to northwest trending gravity "worm" that is still present at 70 km of upward continuation. These "worms" may be expressions of major crustal scale faults associated with IOCG deposits (Hitzman, 2000; Pollard, 2000). There is no evidence of a second order fault linking the deposits to these crustal scale faults in the gravity "worms" data. However, if offsets on the second order faults are relatively small, there may not be a density contrast across the fault, in which case no gravity worm would be expected. The Eloise deposit is also located directly on a moderate to large scale gravity "worm" although this "worm" feature is not directly related to a crustal scale fault.

Magnetics appears to also be a very reliable indicator of IOCG mineralisation although the magnetic sources for each deposit in Table 4 are quite different. High concentrations of magnetite are interpreted to account for a majority of the magnetic anomalies but not

always coincident with the ore body themselves. At Starra, early correlations were recognised between gold bearing zones and magnetic anomalies. However, several thousand susceptibility readings on drill core showed no statistically significant correlation between gold grade and susceptibility and those early correlations were the result of drill locations being biased by the magnetic data (Collins, 1987). The magnetic anomaly at Prominent Hill is produced by altered andesite and no response has been attributed to the hematite body (Hart et al., 2004). The Olympic Dam magnetic anomaly is produced by deeper source rocks that have not yet been intersected by drilling. Ernest Henry's magnetic response in primarily due to magnetite in the foot-wall and hanging-wall shear zones and not the ore mineralisation itself.

The deposits in Table 4 display a wide range of electrical responses and as with magnetics the source is not always directly related to the ore body itself. The exploration strategy used for the Ernest Henry deposit assumed that any economic mineralisation would be a good conductor and responsive to the use of EM (Webb and Rowston, 1995). Initial surface TEM screening of magnetic anomalies revealed a week conductor over the Ernest Henry deposit. Follow up work refined the TEM anomaly and it was modelled as a steeply dipping cylindrical body. Drilling of the body and later downhole EM revealed the anomaly was generated by a relatively thin (~10 m) supergene zone some 20 m above the main ore body. If the supergene enrichment process had not resulted in such a conductive blanket of native copper the deposit may still remain undiscovered (Webb and Rowston, 1995). TEM anomalies at Osborne are also interpreted to be only partially related to the ore body. Testing of drill core suggest that conductivity increases with sulphide content to some extent, but also as a function of magnetite grain size and degree of recrystallisation (Anderson, 1992). On the other hand, mineralisation at Eloise is directly detectable using surface TEM to the north of the Middle Fault where thickness of cover is between 50 and 70 m (Brescianini et al., 1992). Further south where mineralisation is typically deeper than 300 m TEM is not a viable detection technique.

Surface IP and Resistivity, as with EM, generally displays a poor correlation to economic mineralisation. Downhole IP at Ernest Henry shows a good correlation between both the main ore body and the supergene zone and chargeability. The surface IP measurements however occur at shallow depths and are largely sourced from the supergene zone (Webb and Rowston, 1995). Prominent Hill displays strong association of both IP and resistivity to mineralisation but the same association exists for barren hematite bearing rocks (Hart et al., 2004). IP and resistivity anomalies from the other deposits are generated by other factors such as saline ground water in basement rock pores and varying overburden thickness at Olympic Dam and Eloise respectively.

Other techniques have had little or no use in the exploration and discovery of the Australian IOCG deposits in Table 4. Use of radiometrics has only been mentioned at Olympic Dam where down hole measurements show elevated potassium and uranium levels. Seismic reflection surveying has been used with success, also at Olympic Dam, to delineate the top of the ore body after vastly different source depths were modelled from the gravity to the magnetics (Rutter, 1985). However, in general seismic work is too spatially limited to be of use in mineral exploration

6. CONCLUSION

Potential field data is a vital tool in any exploration program for IOCG deposits. High quality data is readily available for most of Australia and many parts of the world and

additional data is relatively cheap and easy to acquire. Deposits themselves may not be magnetic sources but many are associated with magnetic highs. If not for this relation many large under cover deposits such as Olympic Dam may remain undiscovered. Gravity is the most reliable geophysical method of detecting deposits but large station spacing may mask the deposits. Advancements in airborne gravity acquisition and processing will play a vital role in future exploration.

With exploration moving progressively undercover gamma ray spectrometry is becoming a less valuable tool. The use of radiometrics can be extended through down-hole logging applications and by establishing correlations between alteration and magnetic susceptibility at a regional scale in order to constrain magnetic models. Electromagnetic techniques should be considered as a follow up technique over potential targets. While no one method is guaranteed to detect an ore body, the probability of seeing an anomaly from at least one method is high. However, great care needs to be taken to correctly model and understand the source of any EM, IP or resistivity anomaly so as to correctly target drilling.

7. REFERENCES

Queensland Department of Mines and Energy, 2000, Northwest Queensland Mineral Province Report: Brisbane, Queensland Department of Mines and Energy.

Anderson, C. G., Logan, K. J., 1992, The history and current status of geophysical exploration at the Osborne Cu & Au deposit, Mt. Isa: Exploration Geophysics, v. 23, p. 1-8.

Archibald, N., Gow, P., and Boschetti, F., 1999, Multiscale edge analysis of potential field data: Exploration Geophysics, v. 30, p. 38-44.

Archibald, N. J., Holden, D. J., Boschetti, F., Horowitz, F., and Hornby, P., 2000, Interpreting crustal scale features using wavelet-based multi-scale edge analyses of regional gravity datasets: Exploration beyond 2000; conference handbook Preview, v. 84, p. 107.

Barton, M. D., and Johnson, D. A., 2000, Alternative brine sources for Fe-oxide(-Cu-Au) systems; implications for hydrothermal alteration and metals, Hydrothermal iron oxide copper-gold and related deposits; a global perspective: Vol 1, p. 43-60.

Brescianini, R. F., Asten, M. W., and McLean, N., 1992, Geophysical characteristics of the Eloise Cu-Au deposit north-west Queensland: Exploration Geophysics, v. 23, p. 33-42.

Clark, D. A., 1991, Notes on Rock Magnetization Characteristics in Applied Geophysical Studies: Exploration Geophysics, v. 22, p. 547-555.

Clark, D. A., 1997, Magnetic petrophysics and magnetic petrology; aids to geological interpretation of magnetic surveys, AGSO Journal of Australian Geology and Geophysics, Vol. 17(2), p. 83-103.

Collins, S., 1987, The Geophysics of the Starra Gold/Copper Deposits: 5th ASEG Conference, p. 20-22.

Esdale, D. J., Pridmore, D. F., Coggon, J. H., Muir, P. M., Williams, P. K., Fritz, F. P., 1987, Olympic Dam Deposit - Geophysical Case History: Proceedings of the 5th ASEG conference, p. 47-49.

Galbraith, J. H., Saunders, D.F., 1983, Rock classification by characteristics of aerial gamma ray measurments: Journal of Geochemical Exploration, v. 18, p. 49-73.

Hart, J., Freeman, H., and Dentith, M. C., 2004, Geophysics of the Prominent Hill Prospect, South Australia: Preview June 2004: Special Publication - Australian Society of Exploration Geophysicists, Vol. 12, p. 93-100.

Haynes, D. W., 2000, Iron oxide copper(-gold) deposits; their position in the ore deposit spectrum and modes of origin, Hydrothermal iron oxide copper-gold and related deposits; a global perspective, Vol 1, p. 71-90.

Hitzman, M. W., 2000, Iron Oxide-Cu-Au Deposits; What, Where, When, and Why, in: Hydrothermal iron oxide copper-gold and related deposits; A Global Perspective, Volume 1; PGC Publishing, Adelaide, p. 9-25.

Murphy, C. F., 2002, Structural Framework and Target Generation In Proterozoic Mt Isa Region, Queensland, through analysis of Potential Field Multiscale Wavelets ("Worms"): I2+3 Final Report, pmdCRC.

Mustard, R., Blenkinsop, T., McKeagney, C., Huddlestone-Holmes, C., Partington, G., 2004, New perspective on IOCG deposits, Mt Isa Eastern Succession, northwest Queensland: Procedings of SEG 2004: Predictive Mineral Discovery Under Cover, p. 281-284.

Pollard, P. J., 2000, Evidence of a magmatic fluid and metal source for Fe-oxide Cu-Au mineralization, in: Hydrothermal iron oxide copper-gold and related deposits; A Global Perspective, Volume 1; PGC Publishing, Adelaide, p. 27-41.

Porter, T. M., 2000, Hydrothermal iron-oxide copper-gold & related ore deposits, in: Hydrothermal iron oxide copper-gold and related deposits; A Global Perspective, Volume 1; PGC Publishing, Adelaide, p. 3-5.

Reynolds, J. M., 1997, An Introduction to Applied and Environmental Geophysics: Chichester, England, John Wiley and Sons.

Rutter, H., Esdale, D. J., 1985, The Geophysics of the Olympic Dam Discovery: Proceedings of the 4th ASEG conference, p. 273-276.

Shives, R. B. K., Charbonneau, B. W., Ford, K. L., and Asten, M., 1997, The detection of potassic alteration by gamma-ray spectrometry; recognition of alteration related to mineralization, Society of Exploration Geophysicists, Tulsa, OK, p. 2001-2011.

Smith, R. J., 2000, Geophysics of iron oxide copper-gold deposits, in: Hydrothermal iron oxide copper-gold and related deposits; A Global Perspective, Volume 1; PGC Publishing, Adelaide, p. 357-367.

Telford, W. M., Geldart, L. P., Sheriff, R. E., 1990, Applied Geophysics: Second Edition: Cambridge, Cambridge University Press.

Webb, M., and Rowston, P., 1995, The geophysics of the Ernest Henry Cu-Au deposit (N.W.) Qld: Exploration Geophysics, v. 26, p. 143-145.

Williams, P. J., and Pollard, P. J., 2001, Australian Proterozoic iron oxide-Cu-Au deposits; an overview with new metallogenic and exploration data from the Cloncurry District, Northwest Queensland: Exploration and Mining Geology, v. 10, p. 191-213.

Fractal distribution of mineral deposits for exploration

Arianne Ford[1]
[1] predictive mineral discovery Cooperative Research Centre
Economic Geology Research Unit
James Cook University
Townsville, Qld 4811, Australia

ABSTRACT

Copper deposits in the Mount Isa Inlier have a fractal distribution. Through the use of a shifting box counting algorithm the fractal dimensions of the copper deposits are shown to vary over the study area from 0.589 to 1.786. Fault geometry has a high correlation with the clustering of the copper deposits in the Mount Isa Inlier and may have significance when generating exploration strategies.

Keywords: Fractal dimension, mineral deposits, controls on clustering, targeting, exploration

1. INTRODUCTION

The fractal dimension (FD) of the spatial distribution of a set of mineral deposits provides a measure of how clustered they are in a given study area. A low fractal dimension value indicates a high level of clustering, and vice versa. Mineral deposits with a random or space filling distribution have FD's of 2.

Intensive exploration in the Mount Isa Inlier has resulted in the discovery of several major deposits within the last 20 years, but further progress depends on the application of innovative techniques. Fractal geometry has not so far been applied to exploration in the region.

This study was undertaken to determine how the clustering of the mineral deposits might vary over a given study area. By adapting Carlson's (1991) box counting algorithm, a map of how the fractal dimension varies can be generated for the purpose of determining what is controlling the clustering of the mineral deposits and predicting exploration targets.

2. STUDY AREA

The location for this study includes the whole of the Proterozoic Mount Isa Block as defined by the Northwest Queensland Mineral Province Report (Queensland Department of Mines and Energy, 2000). Mineral deposits within this study area have been extracted from the MINOCC database (Queensland Department of Natural Resources and Mines, 2002).

3. METHODS

The fractal geometry of the mineral deposits was analysed using the box counting technique, because it has proven to be applicable to mineral deposits elsewhere in the world. The aim of the box counting method is to calculate the minimum number of boxes with a specified side length required to cover all points in the data set. One box counting method is described by Carlson (1991) for a given set of ore deposit locations:

1. divide the area into a grid of many square cells with side length *r*
2. count the number of cells containing at least one deposit *N(r)*
3. replace the current grid with a scaled version
4. repeat the second and third steps for a range of scaled grid sizes
5. plot r vs N(r) on a log-log graph
6. calculate the absolute value of the slope for the line of best fit to get fractal dimension

Carlson's (1991) box counting method was adapted to evaluate the spatial variation in fractal dimension. A sliding box - side length (maximum side length of study area)/4 - which moves systematically over the study area was created, taking a snapshot of the mineral deposits in the region. Box counting was then performed for each of these regions and the fractal dimensions calculated. The sliding box moved in increments of 50km over the study area to allow a considerable number of regions to be examined.

Though box counting is widely used in fractal analysis, the method for analysing the spatial variability of the fractal dimension used highlighted some issues when calculating the final fractal dimension value. The upper and lower limits for performing linear regression on a large number of graphs could not be estimated manually for all data sets. This issue was addressed by selecting a random sample of graphs and detecting a common range of values over which to perform the regression, the fractal dimension could be calculated using these limits for all data sets to produce accurate results. It was found that by ignoring the largest box size used in the box counting that an accurate fractal dimension value could be calculated eliminating any issues with the largest box size being fixed with respect to the study area.

4. RESULTS

Table 1 shows the results obtained for the global fractal dimension box counting method for a variety of different deposit types in the Mt Isa Inlier study area.

Table 1:
Results of Fractal Dimension Calculations for Mt Isa Inlier with correlation coefficient R and standard error E

Deposit Type	No. of Deposits	Fractal Dimension	R	E
Cu	1869	1.4	0.988	0.032
Au	416	0.7	0.981	0.022
CuAu	416	1.4	0.980	0.063
IoCG	198	1.3	0.989	0.038
U-REE	144	0.9	0.993	0.016

Figure 1 shows how the fractal dimension of copper deposits varies over the Mount Isa Inlier with values ranging from 0.589 to 1.786 indicating that the clustering of the deposits varies greatly over the study area.

In order to determine what could be controlling the clustering of the mineral deposits, various layers from the Northwest Queensland Mineral Province Report (NQMPR) were examined and compared to the fractal dimension values obtained for the copper deposits. By extracting fault intersections and fault bends from the NQMPR fault database to point locations using the MapInfo Spatial Data Modeller (MI-SDM) software and performing subsequent regional box counting fractal analysis of the data in the Mount Isa Inlier study area, a 39.1% correlation was revealed between the clustering of the fault intersections and the clustering of the copper deposits, while a 76.2% correlation was found for a similar analysis of fault bends (between 5º and 45º). These values for the fault bends were chosen to account for any inconsistencies in the MI-SDM software used.

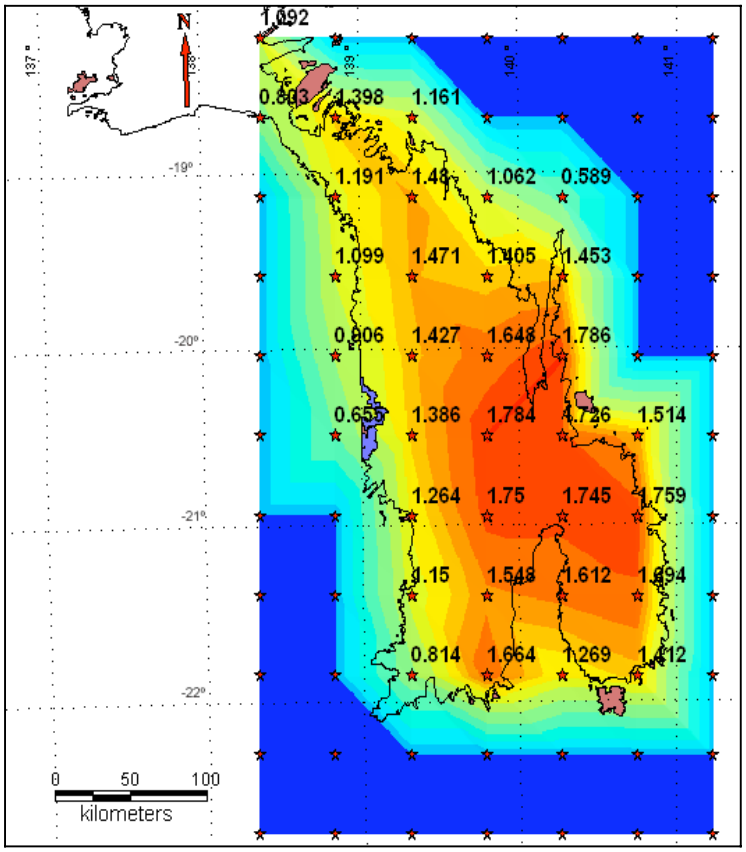

Fig. 1: Variation of Fractal Dimension for Cu Deposits in the Mt Isa Inlier

5. DISCUSSION

By looking at the fractal distributions of the mineral deposits in conjunction with Weights of Evidence and prospectivity analysis, correlations between the deposits and the regional geology can be determined. Examining areas with a similar geology for anomalous fractal dimension values may then allow exploration targets to be generated. Weights of evidence based on fractal analysis is something which warrants further investigation.

The exhibited variation in fractal dimension of the copper deposits shown in Figure 1 could be a result of different exploration histories. Blenkinsop and Sanderson (1999) discuss possible exploration implications based on fractal analysis of mineral deposit distributions. Two different exploration histories are proposed each resulting in different strategies for future exploration.

Regions with comparatively low fractal dimensions may not have been fully explored; therefore exploration around known existing deposits could produce results. However in order to make any comparison, the global fractal dimension of copper deposits in other study areas must be investigated so that a "normal" value can be determined for the given deposit type. This "normal" value is currently being investigated through examination of the spatial distribution of copper deposits for study areas in the Gawler Craton, Yilgarn Craton, Broken Hill Block and Georgetown Province. Archaean lode gold deposits have previously been found to have an approximate fractal dimension of 1 (Blenkinsop and Sanderson, 1999), allowing comparisons to be made when sufficient gold deposit data is available for a given study area.

However, comparatively normal fractal dimension values coupled with a relatively low number of deposits in the area may turn out new discoveries through exploration based on regional geology. If no known deposits exist in parts of the study area and the reason for this can not be simply explained by the regional geology, a search for new deposits within these areas might prove successful. As such, exploring in close proximity to fault bends in seemingly barren areas of regions of the Mount Isa Inlier with normal fractal dimensions for copper deposits may produce results.

By examining more regions in the study area (eg. using a smaller sliding box, decrease in how far sliding box moves at each stage) and determining how clustered the deposits in these regions are, these targeting procedures can be refined to produce smaller exploration target areas.

6. REFERENCES

CARLSON, C. A. 1991. Spatial Distribution of Ore Deposits. *Geology*, **19**, 111-114.

QUEENSLAND DEPARTMENT OF MINES AND ENERGY, TAYLOR WALL AND ASSOCIATES, SRK PRY LTD AND ESRI AUSTRALIA. 2000. North-West Queensland Mineral Province Report. Technical Report, Queensland Department of Mines and Energy.

QUEENSLAND DEPARTMENT OF NATURAL RESOURCES AND MINES. QMIN - Queensland Mineral Resource Database MINOCC 2002 – Microsoft Access Database, Version 3.0, December 2002.

BLENKINSOP, T.G. AND SANDERSON. D. J. Are gold deposits in the crust fractals? A study of gold mines in the zimbabwe craton. *In*: K. MCCAFFEREY AND J. WILKINSON (editors), *Fractures, Fluid Flow and Mineralization*, Geological Society, London, Special Publications, **155**, pp: 141-151, 1999.

Discrete element modelling of stress partitioning and fluid flow in the Eastern Succession of the Mount Isa Block

J.G McLellan[1] & N.H.S. Oliver[1]

[1] Economic Geology Research Unit, James Cook University, Townsville, Queensland, 4817

Abstract

Numerical modelling using the discrete element technique is employed here to examine the response of a fracture system (Eastern Succession) to an applied stress regime. Areas of low minimum principal stress and low mean stress indicate dilation and potential sites of fluid focusing, and areas of high differential stress indicate increased deformation. An initial relatively simple model is followed by more complex ones containing younger granite suites and different fault architecture. The sequence of these models corresponds to pre- and syn- to post- mineralisation for many deposits in the region. Areas that show a combination of 1) low values of mean stress ($_m$), minimum principal stress ($_3$) and fluid pressure required for failure (PF_f), in conjunction with 2) increased differential stress (Δ) predicting shear failure or low values predicting tensile failure, provide the best targeting solution for mineralisation. Many areas with these features correlate well with deposits and prospects in the region. These models also predict areas that at present have no known deposits.

Keywords: Numerical modelling, Discrete elements, stress, fluid flow, Prospectivity, Mt Isa

1.0 GENERAL INTRODUCTION

The ability to numerically simulate and 'map' the effects of deformation can provide important data in understanding the spatial and temporal consequences of such processes. 'Stress Mapping' is a technique that has been used in determining the magnitude and distribution of stress in many mineralised terranes (e.g. Oliver *et al*., 1990, 2001a; Holyland *et al*., 1993; Holyland & Ojala, 1997; Jiang *et al*, 1997; Mair *et al*., 2000; Stephens, 2003). Areas of low minimum principal stress (σ_3) and low mean stress (σ_m) may indicate dilation and potential sites of fluid focusing, and are of great interest in mineralised hydrothermal systems. The ability to predict areas that are more susceptible to failure, and hence focus fluids, can be advantageous in defining sites of increased prospectivity within any region. The close relationship between deformation and fluid flow has been considered as the main process involved in genesis of many hydrothermal ore deposits, and the role of faulting in this process has been explored by many previous authors (e.g. Philips, 1972; Sibson *et al*., 1988; Cox, 1995).

There are two main modelling techniques employed to simulate the response of rocks to deformation and subsequent fluid flow, and these can be broadly categorised as continuous and discontinuous modelling. Continuous modelling treats rock masses as an elasto-plastic continuum and focuses on pervasive fluid flow through this medium (Chapters 3, 4 and 6), whereas discontinuum modelling treats rock masses as elastic fractured discrete systems or blocks and focuses on the fluid flow along boundaries between such blocks. The distinct element program UDEC (Universal Distinct Element Code, Itasca 2000b) is used here to examine the effects of deformation and fluid flow along faults and rock boundaries in the Eastern Succession of the Mt. Isa Block, during several stages of its protracted deformation history. Discrete Element Modelling was considered the technique most suited to this study as economic grade mineralisation and the majority of the deposits in the Eastern Succession have a close spatial relationship with faults. The results are then used for comparisons and integration with prospectivity analysis of the district.

1.1 Background Geology

This section presents a synthesis of the general tectonostratigraphic and intrusive history of the Mt. Isa Block, particularly the Eastern Succession. It will then examine the fault architecture of the area and give a current synthesis of a prospectivity analysis undertaken by Mustard *et al*. (2004) in relation to fault orientations.

1.1.1 Mount Isa Block

The Mount Isa Block of Northwest Queensland is essentially comprised of three major tectonic units; from west to east, The Western Fold Belt (Western Succession), the Kalkadoon-Leichhardt Belt and the Eastern Fold Belt (Eastern Succession)(Fig 1), which are predominantly north-south trending sedimentological and structural domains

(O'Dea *et al*. 1997; Blake & Stewart, 1992). The general geology of the area is characterised by lower to middle Proterozoic meta-sedimentary rocks, rhyolitic and basaltic meta-volcanic rocks, gabbro, dolerite and widespread I-type granites.

Two major stratigraphic cycles have been recognised within the Mt. Isa Block, both of which are proposed to have been deposited in intraplate sedimentary basins (Blake & Stewart, 1992). The first cycle is represented by a spatially restricted basement sequence, comprising the Yaringa Metamorphics, Kurbayia Migmatites, Plumb Mountain Gneiss and Double Crossing Metamorphics, which were deformed and metamorphosed during the Barramundi Orogeny (1870 Ma) (Etheridge *et al.* 1987). The second cycle took place during at least four episodes of intrcratonic rifting, and these rift cycles deposited three cover sequences (Page & Sun, 1998; Blake & Stewart, 1992), prior to the Isan Orogeny (ca. 1600-1500 Ma; Blake & Stewart, 1992).

Cover sequence 1 (1870 – 1840 Ma) is restricted to a narrow strip, mainly represented by the Leichhardt Volcanics and intrusions of I-type Kalkadoon granites, and known as the Kalkadoon-Leichhardt Belt. This belt then acted as a 'high', and Cover sequences 2 and 3, related to separate basin forming events, were consequently formed on the eastern and western sides (Eastern & Western Successions).

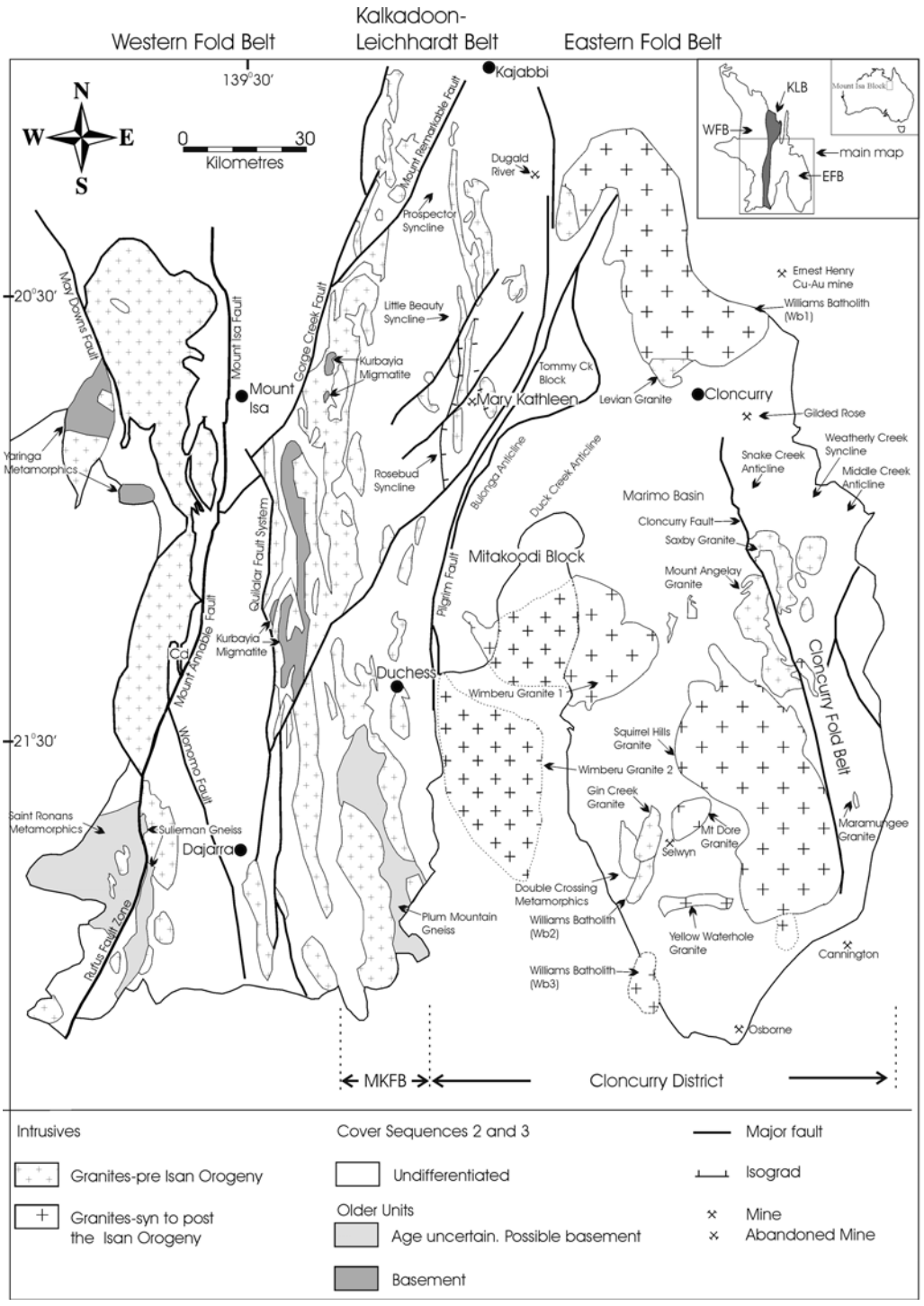

Fig. 1. Location (inset) and general geology of the Western, Kalkadoon-Leichhardt and Eastern Fold Belts showing the further division of the Eastern Fold Belt into the Mary Kathleen Fold Belt (MKFB) and Cloncurry District. The spatial distribution of Cover Sequences 1-3 and intrusive features pre- and syn- to post- Isan Orogeny are shown, as well as some of the major mineral deposits in the Eastern Succession (redrawn from Foster, 2003, adapted from original geology by Blake, 1987). Modifications include interpreted geology from NWQMP report, 2000.

Cover sequence 2 (ca. 1790-1720 Ma), is dominated by bimodal volcanic rocks, clastic and carbonate metasediments, and deposited on both east and west sides of the Pilgrim Fault. The development of Cover Sequence 2 also involved widespread intrusive

igneous activity (e.g. Wonga Batholith, 1750-1740 Ma; Page, 1983) (Fig. 2). Cover sequence 3 (ca. 1680 -1595 Ma), best represented in the Western Fold Belt, unconformably overlies Cover Sequence 2, and consists mainly of metamorphosed volcanoclastic rocks, conglomerates, sandstones, shales and carbonate rocks. During Cover sequence 3 bimodal volcanism accompanied sedimentation (Hill *et al.* 1992), and several large intrusions including the Sybella Batholith (~1670 Ma) were emplaced (Page & Bell, 1986).

1.1.2 Eastern Succession tectonostratigraphy

The Eastern Fold Belt (or Eastern Succession) can be further divided into the Mary Kathleen Fold Belt (MKFB) and the Cloncurry District, which are separated by the Pilgrim fault zone (Fig. 1). The Eastern Succession is host to metamorphosed sediments and mafic volcanic rocks (Soldiers Cap Group), calcareous meta-sedimentary rocks (Corella and Doherty Formations) minor pre-Isan intrusions and widespread post Isan Orogeny intrusive rocks (Williams and Naraku Batholiths). Links with the rest of the Mt. Isa Block and Australian Proterozoic sequences have been tenuous mainly due to structural complexity, but hold great economic interest as a result of the Cloncurry District discoveries of the 1990's (e.g. Osborne, Ernest Henry, Cannington). Page & Sun (1998) demonstrated that the Soldiers Cap Group (ca. 1655 Ma), which was previously dated at 1880-1810 Ma (Beardsmore *et al.* 1988), and 1800-1780 Ma (Blake, 1987), is now younger and considered part of Cover Sequence 3. This has an interesting consequence, as the Soldiers Cap Group, which is host to mineralisation in the Eastern Succession, is now thought to be similar in age to the Mt. Isa and McNamara Groups of the Western Fold Belt, which host giant shale-hosted Pb-Zn-Ag ± Cu deposits.

The lowest stratigraphic units of Cover Sequence 2 to outcrop in the Eastern Succession are the Magna Lynn metabasalt, and clastic sediments and felsic metavolcanic rocks of the Argylla Formation (ca. 1762 ± 3 Ma to 1781 ± 3 Ma). Overlying this formation is the Marraba Volcanics (flood basalts) and the Mitakoodi Quartzite (clastic sediments) of the Malbon Group (ca. 1755 ± 3 Ma) which has a corresponding stratigraphic equivalent (Ballara Quartzite) in the Mary Kathleen Fold Belt. The Mary Kathleen Group comprised of calcsilicate rocks and the marble dominated Corella Formation (ca. 1750 ± 7 Ma) conformably overlies the Mitakoodi and Ballara Quartzites. The Mt. Fort Constantine Volcanics (ca. 1742 ± 6 Ma), which is spatially restricted to the northern Cloncurry district, are temporally associated with several 1750 – 1740 Ma intrusions in the area (e.g. Gin Creek and Levian Granites). The uppermost unit of Cover Sequence 2 is represented by the calcsilicate and marble dominated Doherty Formation (ca. 1725 ± 3 Ma), but as this Formation is also intruded by 1740 Ma granites, it is probably equivalent to the Corella Formation.

The lowest stratigraphic unit of Cover Sequence 3 in the Eastern Succession is represented by the Fullarton River Group, which comprises the Gandry Dam Gneiss (ca. 1676 ± 5 Ma) and the New Hope Arkose, which corresponds to the Kuridala Formation (< 1670 Ma) on the western side of the Cloncurry Fault. The stratigraphy on the west of the Cloncurry fault e.g. Kuridala Formation, Answer Slate (< 1670 Ma), Marimo Slate (ca. 1655 ± 4 Ma) and the Staveley Formation, formerly known as the Mary Kathleen Group (Blake, 1983), now appears laterally continuous with the Soldiers Cap Group. The Llewellyn Creek Formation, which conformably overlies the Fullarton

River Group, is comprised of thick bedded turbidites, and this forms the basal unit of the Soldiers Cap Group. Conformably overlying the Llewellyn Creek Formation are the Mount Norna Quartzite (ca. 1654 ± 4 Ma) mainly composed of metamorphosed sandstones, siltstones and mudstones, and the Toole Creek Volcanics (ca. 1658 ± 8 Ma) comprised of metadolerites, metabasites and minor meta-sediments. Rubenach (pers. comm.) has identified parts of Cover Sequence 3 which are intruded by 1686 ± 8 Ma tonalites, placing further uncertainty on the stratigraphy of the Eastern Succession.

1.1.3 Intrusive history

The earliest intrusive phases in the Eastern Succession, prior to Cover Sequence 3, are coincident with the 'Wonga' extensional event (Holcombe *et al*., 1992; Pearson *et al*., 1992; Davis *et al.*, 2001) and include the Wonga Batholith (ca. 1750 – 1730 Ma), Dipvale Granite (ca. 1746 ± 7 Ma), Levian Granite (ca. 1746 ± 8 Ma) and the Gin Creek Granite (ca. 1741 ± 7 Ma). This intrusive period was accompanied with Na-Ca-K metasomatism, NaCl-rich scapolitization and skarn development (Oliver, 1995), and corresponds to the 'Big' event in the Western Succession (Southgate *et al*., 2000). The Ernest Henry Diorite (1660 ± 13 Ma to 1657 ± 7 Ma) was contemporaneous with the 'Sybella' event and emplacement of the Sybella Granite in the Western Fold Belt, and coincides with the 'Gun' event in the Western Succession (Southgate *et al*., 2000). The 'Williams and Naraku' event comprise multiple K-rich intrusive phases which have been spatially and temporally associated with at least some of the Proterozoic Fe oxide Cu-Au-Co mineralisation in the Cloncurry district (Pollard *et al.* 1998; Williams, 1998), and represent the most voluminous distribution of intrusive rocks in the Eastern Fold Belt. The oldest intrusions related to the Williams and Naraku Batholith, and informally known as the Saxby or Mt. Angelay Igneous Complex, are; the Marramungee Granite (ca. 1545 ± 11 Ma), Mt. Margaret Granite (ca. 1530 ± 8 Ma) and the Mt. Angelay Granite (ca. 1523 ± 4 Ma). A younger suite of the Williams and Naraku Batholith is comprised of the Mount Dore Granite (ca. 1516 ± 10 Ma), Squirrel Hills Granite, Wimberu Granite (ca. 1508 ± 4 Ma), and the Yellow Waterhole Granite (ca. 1493 ± 8 Ma). There are no clear links to major intrusive activity in the Western Fold Belt at this time, however, minor pegmatitic intrusions are coincident e.g. Mica Creek Pegmatites (ca. 1532 ± 7 Ma).

1.1.4 Deformation, Metamorphism and Metallogenesis

A complex and protracted deformational and metamorphic history is evident within the Mt. Isa Block, related to tectonic disturbance and ensialic rifting between 1900 and 1500 Ma. Following the 'Wonga' extensional event (ca. 1750 – 1730 Ma) there are three main deformational events during the Isan Orogeny (D_1, D_2 and D_3) as initially proposed by Bell (1983)(see Table 4.1. Chpt. 4). Several authors have attempted to correlate the deformational events across both the Eastern and Western Fold Belts (Page & Bell, 1986; Etheridge *et al*. 1987; Holcombe *et al.* 1991; O'Dea *et al.* 1997; Adshead-Bell, 1998; Bell & Hickey, 1998; Laing, 1998; Mares, 1998), however, within fold and thrust belts structural history can be complicated and Betts *et al*. (2000) warns of relying on a holistic regional correlation. Although these deformational events are

not well correlated throughout the Mt Isa Block, it remains a useful classification for the Eastern Fold Belt.

Sub-horizontal extensional shearing during the 'Wonga' event is evident by early tectonic features recognised so far only in the Mary Kathleen Fold Belt (Holcombe *et al*., 1991; Pearson *et al*., 1992). Following the 'Wonga' event several faulting and folding events have been recognised throughout the Eastern Fold Belt (O'Dea *et al*., 1997). The (ca. 1600 Ma) Diamantina Orogeny (e.g. Laing, 1998) was originally thought to predate the 1550 – 1500 Ma Isan Orogeny, but abundant recent ages for the Isan Orogeny stretching back to 1590 Ma place the separation of these orogenies in doubt, and here the term Isan Orogeny covers the 1590 – 1500 Ma period.

Within the Eastern Fold Belt, D_1 is thought to have taken place as a result of north-south compression (Page & Sun, 1998; Rubenach & Lewthwaite, 2002; Sayab, 2003a; 2003b) and may have been responsible for the juxtaposition of Cover Sequence 3 against Cover Sequence 2 (Laing, 1998). A major east-west compressional event (D_2)(ca. 1590 – 1550 Ma), resulting in N/S trending tight to isoclinal upright folds and pervasive steep axial plane foliations, is commonly coincident with the peak of metamorphism in the Eastern Fold Belt. Several major shear zones have also been attributed to this D_2 event e.g. The Mount Dore and Eloise shear zones (Laing, 1998). Overprinting of many D_2 structures is attributed to one or more (ca. 1540 -1500 Ma) compressional events (D_3), resulting in NW and NE trending open folds, faults and shear zones, broadly coincident with emplacement of the Williams & Naraku Batholiths and Cu-Au mineralisation.

The peak of metamorphism in the Mt. Isa Block (upper amphibolite facies) was reached during D_2, and this displays a complex low-pressure, high-temperature anticlockwise P-T-t path, (e.g. Rubenach, 1992; Rubenach & Barker, 1998; Rubenach & Lewthwaite, 2002). In particular, the metamorphic peak in the southeast region, is thought to have taken place around 1590 Ma (Perkins & Wyborn, 1998; Giles & Nutman, 2003), although earlier work suggested somewhat younger ages around 1550 Ma (Page, 1983; Page & Bell, 1986). The Western Fold Belt displays a growth of peak metamorphic assemblages that statically overprint S_2 fabrics (O'Dea *et al.*, 1997) which implies there may have been a hiatus between D_2 and D_3. D_3 folding, shear zones and related faults were retrograde relative to D_2 (e.g. Oliver, 1995), but the absolute timing is poorly constrained. Relationships with granites of the Williams Batholith suggest D_3 occurred between 1540 and 1500 Ma.

The Mt. Isa Block shows extraordinary extensive regional sodic-calcic metasomatism, such as in the Mary Kathleen Fold Belt (Oliver, 1995) and the Cloncurry District (Williams, 1998; De Jong & Williams, 1995). Two major metasomatic events are distinguishable a) pre – syn metamorphism (1600 – 1590 Ma) which has been noted around the Osborne deposit (Rubenach *et al*., 2001) and b) post-peak metamorphism (1540-1480 Ma), during granite emplacement e.g. Williams and Naraku Batholiths, in the Cloncurry District (Mark, 2001; Pollard, 2001; Pollard *et al*., 1998; De Jong & Williams, 1995). Metasomatic fluids utilised major structural conduits (e.g. Cloncurry Fault, Pilgrim Fault) for infiltration into the surrounding country rocks, but is also very widespread. Na-Ca alteration commonly predates mineralisation in many of the Fe oxide Cu-Au deposits (Perkins & Wyborn, 1998; Williams, 1998; French, 1997; Adshead, 1995).

The Mt. Isa Block is host to many economic deposits, some world class, such as Mt. Isa Cu, Mt. Isa Pb-Zn-Ag, Cannington Ag-Pb-Zn, Century Zn-Pb and Ernest Henry Cu-Au. Many of the deposits remain controversial in both ore genesis mechanisms and timing of mineralisation. Epigenetic processes are predominantly responsible for the majority of the Cu-Au deposits in the eastern Mt. Isa Block, with most models (e.g. Williams, 1998; Mark *et al*., 2001; Wang & Williams, 2001) favouring a role for igneous-related hypersaline fluids. Fluid inclusion characteristics, stable isotope data and the close temporal relationships of mineralisation to felsic intrusions suggest that granitic fluids were responsible, at least in part, for many Cu-Au iron oxide deposits of the eastern succession (Pollard *et* al., 1998; Williams, 1998; Oliver *et al*., 2001b; Wang & Williams, 2001). Most deposits within the region are characterised by strong structural controls (Bell *et al*., 1988; Laing, 1993; Valenta, 1994; Oliver, 1995) and major faults in the area have been suggested as fluid conduits responsible for mineralisation. Many of the deposits e.g. Osborne, Starra-Selwyn, Mt. Elliot, Monakoff, Eloise and Ernest Henry Cu-Au deposits, share several similar characteristics, all of which define the Cloncurry association of mesothermal ironstone-hosted Cu-Au deposits (Williams, 1998). At least one of these deposits (Osborne), however, may have formed during regional metamorphism prior to emplacement of the Williams Batholith (Rubenach *et al*., 2001). The numerical modelling in the main part of this chapter focuses attention on the structural scenarios pertinent to the latter part of the Isan Orogeny in which fluid flow and mineralisation was hosted mostly in D_3 structures.

1.1.5 Prospectivity

Recent work within the pmd*CRC has evaluated the prospectivity of the Eastern Fold Belt (Mustard *et al*., 2004). One of the primary aims of the analysis was to determine the relationship of faults and fault architecture to mineralised terrains. Prospectivity analysis indicates that the main fault orientations favourable for mineralisation are N/S, S/SE or E/NE trending structures, particularly where jogs or bends are indicated. Fault intersections also appear to be important, in particular intersections of E/NE and S/SE faults with all other fault orientations. The faults developed synchronously with D_3, or represent earlier faults reactivated during D_3.

Partitioning of stress during deformation is important, as this may have a considerable effect on 1) strain rates within rock packages, 2) distribution of failure within and around faults e.g. fault reactivation, and 3) effects on fluid flow within faults and porous media (Oliver *et al*., 1990). The presence of igneous intrusions within the area will have affected how the fault architecture and rock packages responded to an applied stress, particularly when the solidified intrusions acted as competent bodies.

2.0 NUMERICAL MODELS

Prior to any numerical study a conceptual model needs to be derived. This allows the user to define many ‘what if’ scenarios and allows major questions to be addressed. This section describes the methodology used, questions to be addressed and the conceptual models derived to enhance the present work of the Pmd*CRC prospectivity analysis of the Eastern Fold belt.

2.1 Methodology and conceptual models

Examination of geological maps of the Eastern Fold Belt (Fig. 2) provided information required in setting up two conceptual models (Fig. 3, 4). These models were based on two distinct temporal periods 1) Model 1 (1540-1530 Ma), post regional metamorphism and older plutons but pre-Williams Batholiths, and 2) Model 2 (1530-1480 Ma), with additional younger fault architecture and post-tectonic plutons including the Williams-Naraku Batholiths (1530-1480 Ma). These time periods were selected to bracket and overlap with the main mineralisation period for many deposits in the district, coinciding with and following granite emplacement around 1530 Ma.

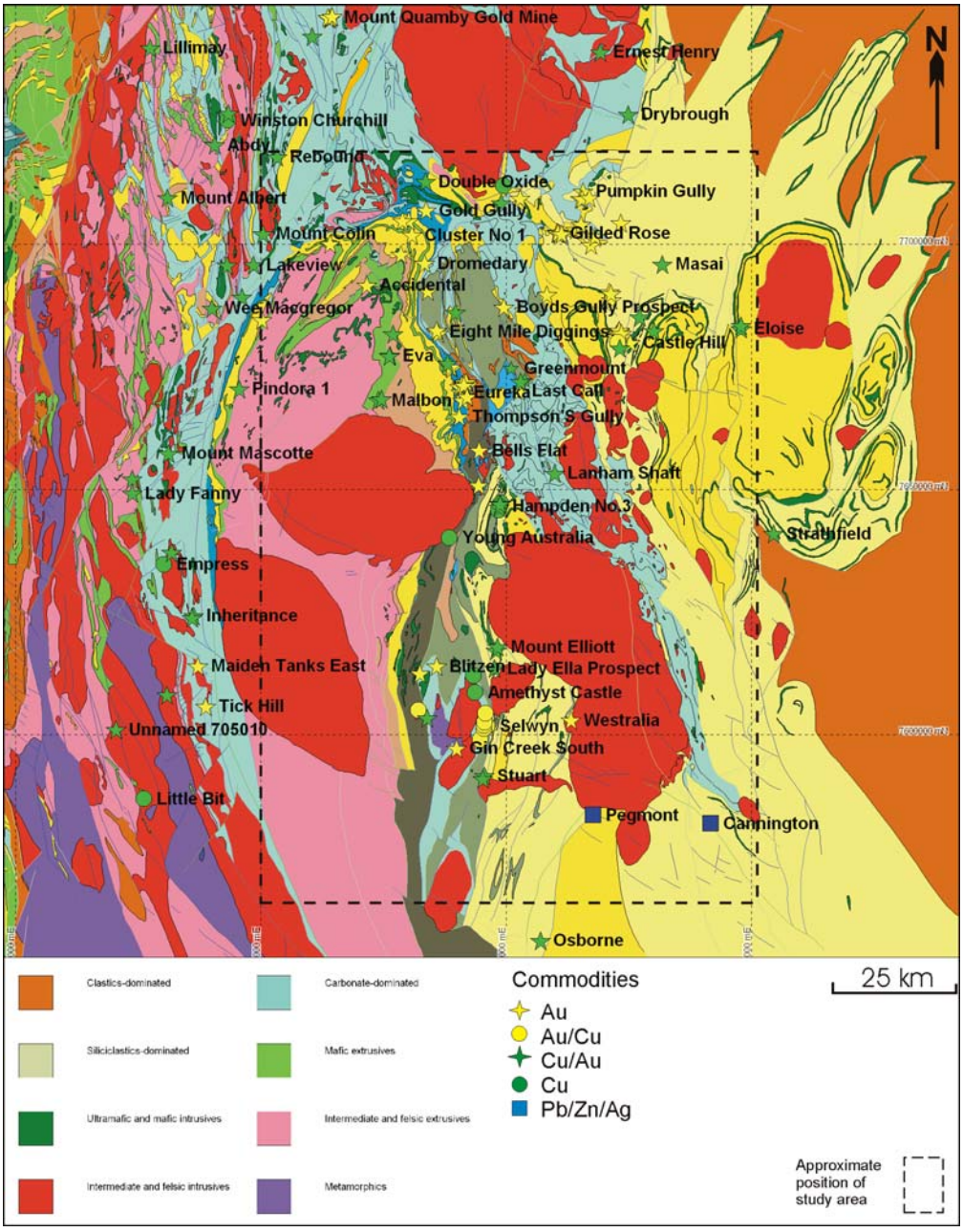

Fig. 2. A detailed geological map of the Eastern Fold Belt highlighting the major deposits and study area undertaken (modified from NWQMP report, 2000).

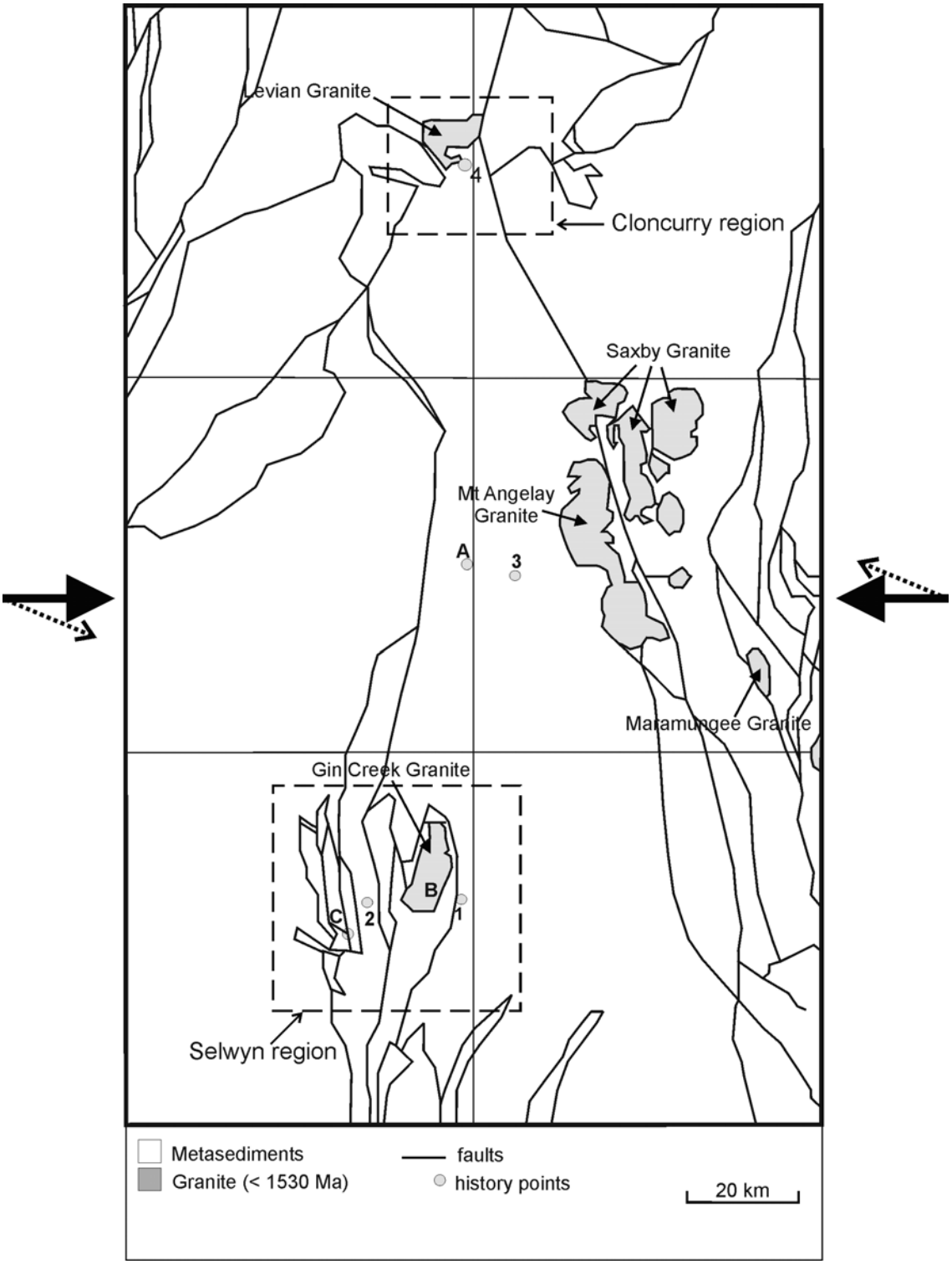

Fig. 3. Conceptual Model 1 showing basic geological features and structures. Boundary conditions are appropriate to an east-west compression (σ_1 = 90°) and a rotation of σ_1 to 112.5°. Note: history point locations and inset locations of the Selwyn and Cloncurry regions are shown.

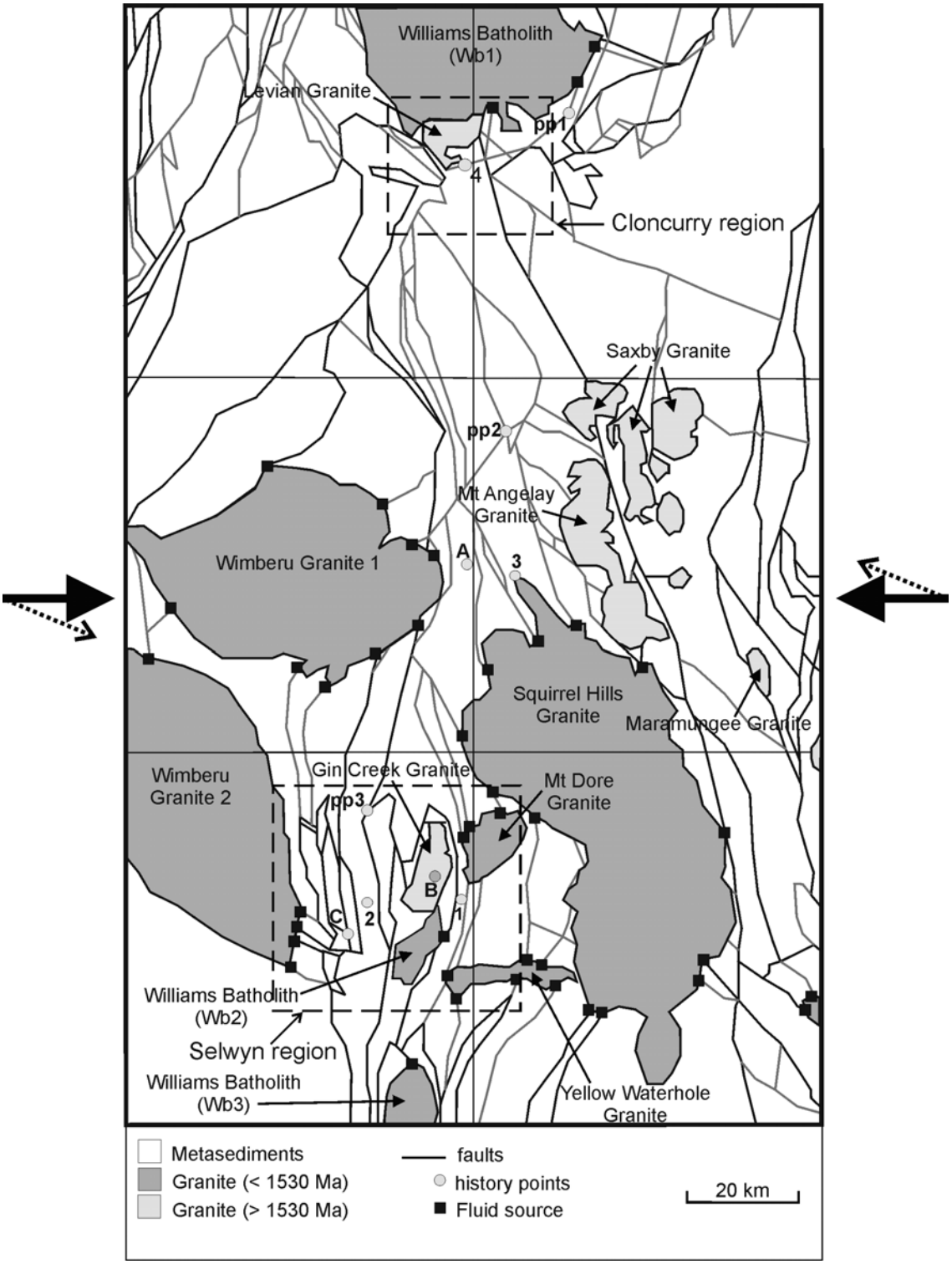

Fig. 4. Conceptual Model 2 showing more complex geological features and structures. Boundary conditions are appropriate to an east-west compression (σ_1 = 90°) and a rotation of σ_1 to 112.5°. Note: history point locations and inset locations of the Selwyn and Cloncurry regions are shown.

Mapping information and a literature review (including the Qld. Dept. of Natural Resources, Mines and Energy (QDNRME) NW Qld. Minerals Province Study) provided the approximate timing of intrusive features and faults. Model 1 was set up to simulate the effect of an applied far field stress on the area. The models consist of early intrusive features such as the Wonga Granite and Gin Creek Granite (~1740 Ma), and examines their spatial and temporal association with major faults. Model 2 consists of younger intrusions and a more detailed fault architecture, which allows examination of the response of the intrusive bodies and younger faults to the imposed stress regime. As these models are based on 2-dimensional data they have limitations and a lower confidence level than a 3-dimensional study, however, a 2-dimensional study can be validated by certain assumptions prior to the modelling process. Several deposits within the area are structurally controlled and have a close association with faults; therefore it is assumed that these faults have acted as the main fluid pathways for mineralising processes. Many fault geometries within the area also display a strike-slip displacement; hence the main modelling interest is based on lateral fluid flow rather than vertical flow or a dip-slip fault environment. Finally, the ability to determine the influence of granites on stress partitioning in 2-dimensions may be useful in understanding their effect on structural controls on a broader scale. This conceptual approach allowed the following questions to be addressed;

1. What influence have intrusions in the Eastern Succession had on the partitioning of stress during deformation?
2. What influence has deformation had on the fault architecture and potential opening and closing of fluid pathways?
3. What faults, or orientation of faults, have a greater influence on failure and fluid flow?
4. What influence has fluid had on the failure of faults?
5. Does discrete numerical modelling predict areas of known mineralisation and any potentially unknown prospective locations?

2.2 Numerical Modelling

Following the conceptual model setup, several conditions must be set. These conditions include the numerical approach, boundary conditions and model parameters. This section introduces the modelling approach and gives an overview of the software used and its capabilities. The ‘hard model’ boundary conditions and input parameters used in this study are also described.

2.2.1 Modelling approach

The localisation of most deposits in the Eastern Succession, on or very close to faults, suggests that discrete element modelling of faults and contacts may be a suitable approach. The discontinuous approach to modelling the interfaces or contacts between discrete bodies must take into account two types of mechanical behaviour; 1) behaviour of the discontinuities, and 2) behaviour of the solid material involved. Blocks of material within these models may be assigned rigidity or a deformable property, and the contacts between blocks may also be given a deformable property.

2.2.2 UDEC (Universal Distinct Element Code) overview

UDEC is a two dimensional numerical program based on the distinct element method for discontinuum modelling (Itasca, 2000b). The code enables a numerical simulation of the response of discontinuous media e.g. jointed or fractured rock mass, subjected to either static or dynamic loading. The models are represented by discrete blocks, and the discontinuities represented as boundary conditions between blocks. UDEC allows large displacements and rotation of blocks and discrete blocks. The discrete blocks are subdivided into a finite difference mesh and each zone or element within the mesh behaves according to a prescribed linear or non-linear stress/strain law. UDEC uses a time-marching scheme to solve equations of motion (Zhang and Sanderson, 2002), and the relative motion of the discontinuities is governed by a linear or non-linear force displacement relationship for movement, in both the normal and shear directions.

UDEC calculates force and displacement according to Newtons law's of motion. As the force depends on displacement, the force/displacement calculation is done over one time instant. The central difference scheme is 'second order accurate' which is an important characteristic that prevents long-term drift in a distinct element model (Zhang & Sanderson, 2002). Fracture deformability or the response of fractures, in the normal direction, is based on the stress-displacement relationship which is assumed to be linear, and is governed by the stiffness properties applied to the fractures. The fractures have a limiting tensile strength and when exceeded, failure occurs. Similarly in shear, the response is controlled by the shear stiffness, and shear stress is limited by a combination of cohesive and frictional strength of the fracture. Dilation of fractures may occur at the onset of slip, and this dilation is governed by a specified dilation angle. Fluid flow is allowed through the fractures and calculated by a fully coupled mechanical-hydraulic analysis. Fracture conductivity is dependent on mechanical deformation and, conversely, fluid pressure affects the mechanical behaviour of the fractures. Fluid flow in joints is modelled as flow between domains, and flow rates can be calculated in two different ways depending on the contact present. In the case of a point-to-edge contact, flow is primarily derived by a pressure gradient ($p_1 - p_2$), however, when an edge-to-edge contact is present flow is calculated by the 'cubic law' (see Chpt. 2 section 2.2.5) for flow in a planar fracture, which accounts for contact edge lengths. UDEC has been proven as a useful numerical tool in simulating geological processes (e.g. Oliver *et al.*, 2001a, 1990; Mair *et al.*, 2000; Holyland & Ojala, 1997), and in particular for fault arrays and fluid flow (e.g. Oliver, 1995; Jiang *et al.*, 1997; Zhang and Sanderson, 2002). The main and obvious disadvantage of UDEC is the inability to model porous media flow through deformable blocks in conjunction with discrete fracture flow. Also, there are geometric restrictions on fault geometries (see 2.4).

2.3 Sensitivity Analysis

Several sensitivity analyses were carried out to examine the effect of geometry, boundary conditions, rock properties and joint properties. This allowed a more comprehensive insight into what parameters were most likely to affect the modelling procedure.

As the geometry was based on map inferences many of the faults at the scale of operation consisted of sharp bends and corners. It was therefore important to examine

the effect of sharp vs. smooth bends and what influence this would have on the modelling results (Fig. 5ab). There is a notable partitioning of stress around the smooth bends compared to the sharp bends (Fig. 6a-d); however, there is no major influence on the stress patterns at the broader modelling scale. It was therefore considered feasible to model the geometry inferred from the available mapping, even if the input fault bends were sharper than actual field patterns.

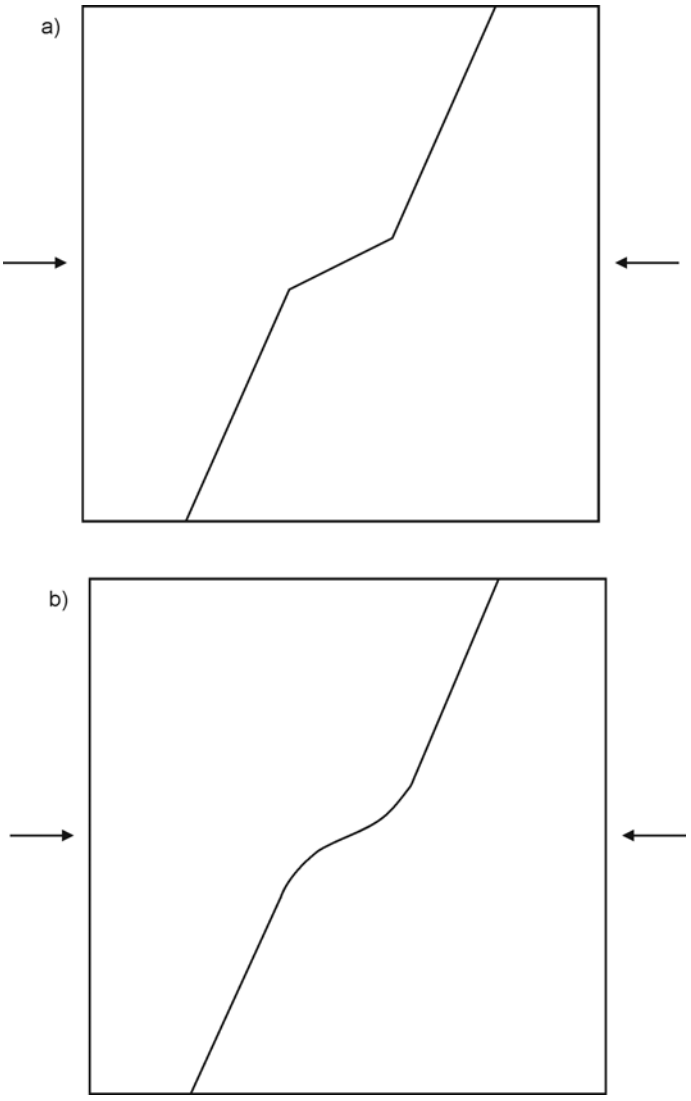

Fig. 5. Conceptual models for sensitivity testing of **a**) sharp versus **b**) smooth geometrical bends. Boundary conditions are appropriate to east-west compression.

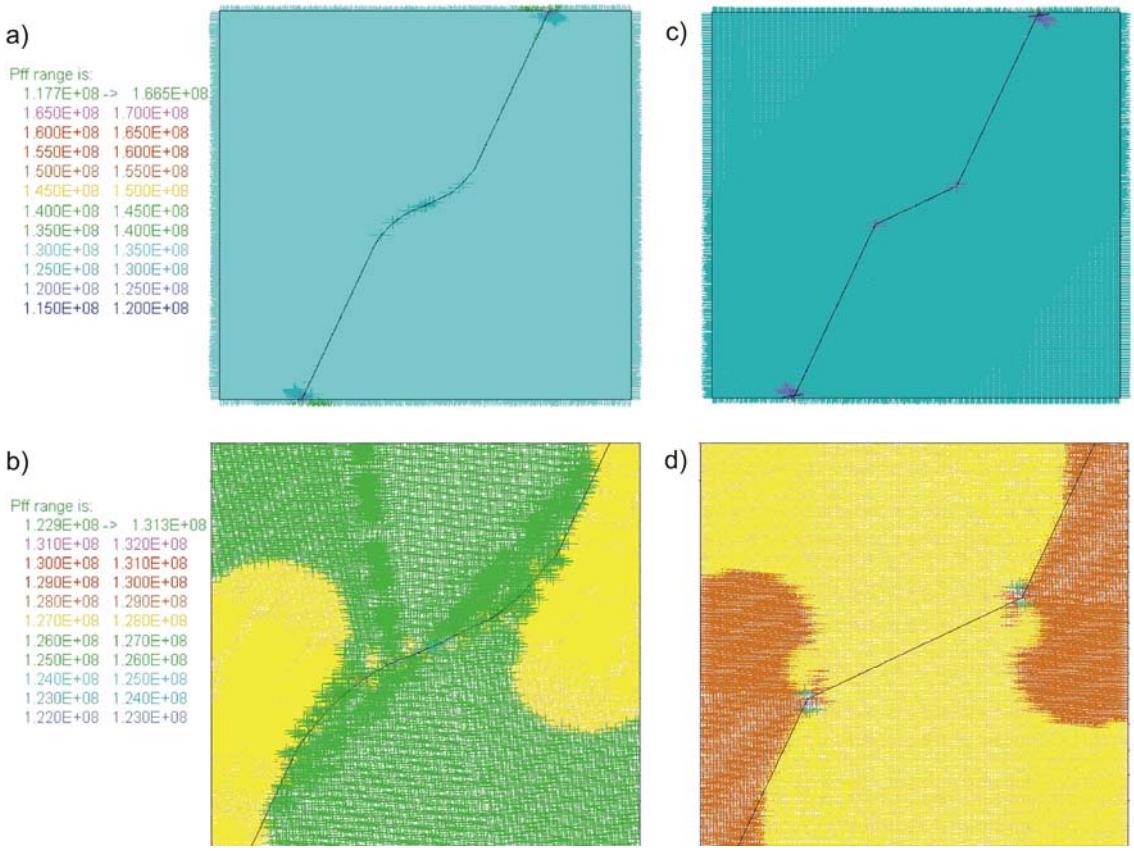

Fig. 6. UDEC results of sensitivity testing of geometrical features a) fluid pressure required for failure (PF_f) for a smooth geometrical bend b) magnified plot of same c) PF_f for a sharp geometrical bend, and d) magnified plot of same. Note: similar overall result in values, with a more gradual spread of values noticeable in the smooth models.

Joint friction angle appears to be one of the most sensitive parameters in relation to the potential failure of faults. Friction angles were modified from 5° to 35° to examine the change in deformation patterns and to compare any differences in areas of failure. A reduction in joint friction angle increased the incidence of fractures reaching their shear stress limit and also lowered fluid pressure required for failure, especially for friction angles less than 10° (Fig. 7a-d). A moderate to high friction angle was used in the main models of this study, similar to faults and geological contacts of previous authors (e.g. Oliver *et al*., 1990; Jiang *et al*., 1997; Stephens, 2003). Cohesion values were also

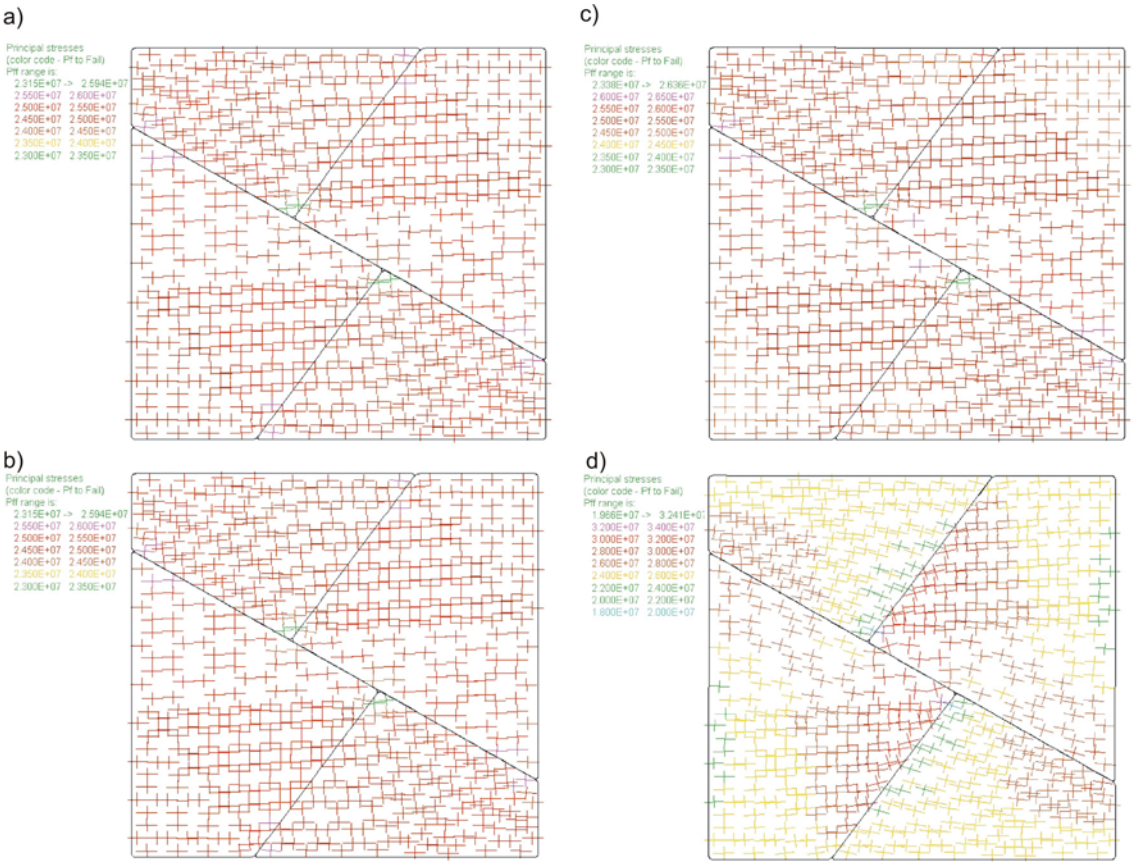

Fig. 7. UDEC results of sensitivity testing of four variations in friction angle values. All values given are for PF_f. Friction angle values for the four models a) 35° b) 20° c) 10° and d) 5°. Note the least variation between models is seen in the higher friction angle values; lower values produce significantly different results.

investigated and fault contacts were given very low cohesion values in accordance with Sibson (1985) and Zhang & Sanderson (2002). Joint normal and shear stiffness also has a major effect on the deformation of fractures. The normal displacement of fractures is controlled by the normal stress and normal stiffness of the fracture according to the relationship of stress displacement and stiffness, such that;

$$\Delta_n = -k_n \Delta_n \tag{7.1}$$

where Δ_n is the effective normal stress increment, k_n the normal stiffness and Δ_n the normal displacement increment. Sensitivity testing showed that lowering the stiffness of the fracture results in more closure during deformation which in turn decreases the aperture of the fracture and hence reduces volumetric fluid flow and increases fluid velocities (Fig. 8a-f). Results from the sensitivity testing were incorporated into the setup of the main Eastern Succession models.

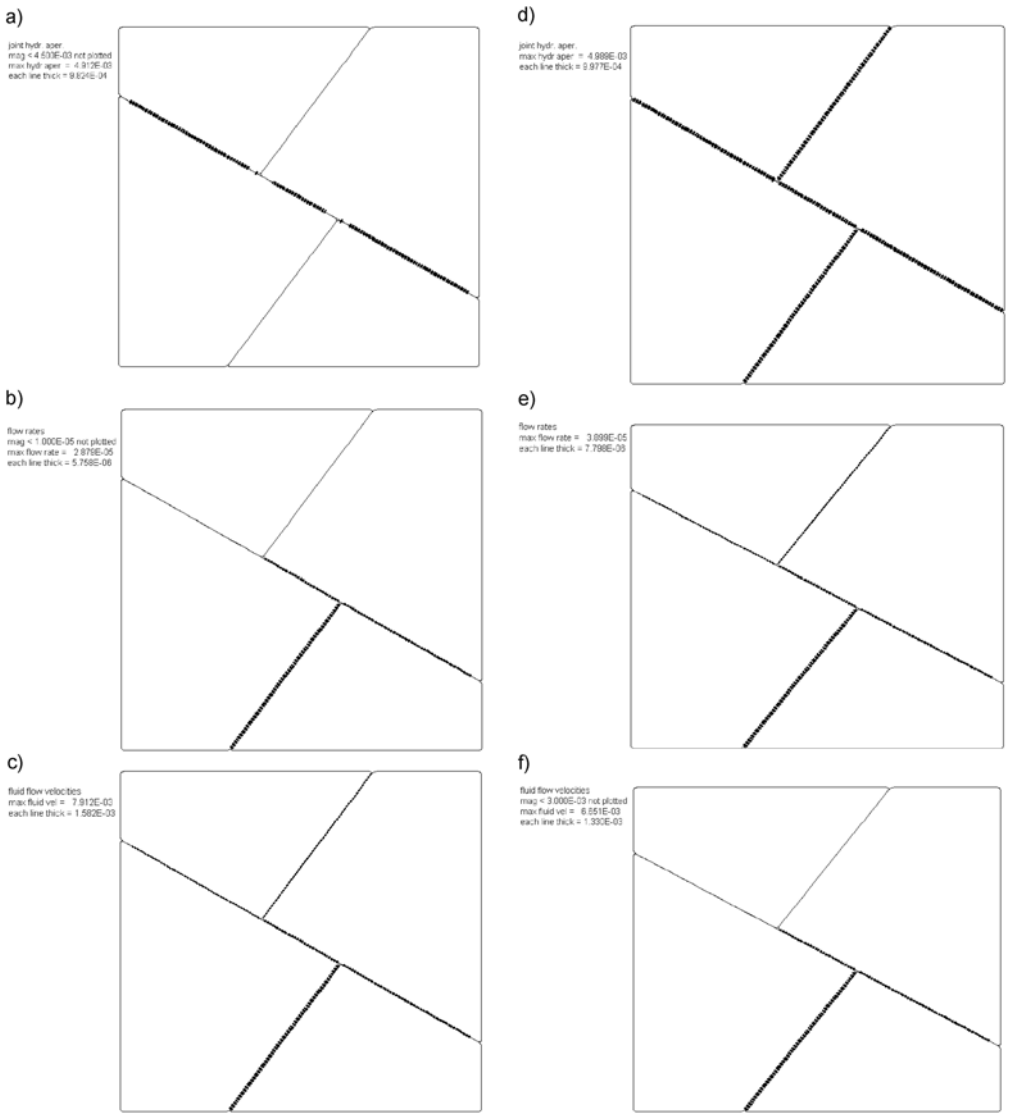

Fig. 8. UDEC results of sensitvity testing of stiffness parameters of fractures. Results display the effects on aperture width, volumetric fluid flow rates and fluid flow velocities. Diagrams a to c represent joints with lower fracture stiffness values and d to f representing higher fracture stiffness values. Lower fracture stiffness result in greater closure of apertures, lower volumetric flow rates and higher flow velocities (a to c). Higher fracture stiffness results in less closure of apertures, higher volumetric flow rates and lower flow velocities (d to f).

2.4 Boundary conditions and model parameters

Models 1 and 2 both cover an area 200km x 124km within the Eastern Succession. The geometry of the models was constructed by drawing fractures from the 1:100 000 maps of the area. Due to limitations of the UDEC program, no fractures can be inserted that are not directly or indirectly connected to the model edges, hence all fractures are joined. A rounding parameter is assigned to each block, which applies to the contact mechanics, to prevent unrealistic locking of the corners during the modelling process. All blocks are divided into smaller zones of a maximum of 1 km edge length. The constitutive model behaviours are elastic-plastic Mohr-Coulomb for the deformable blocks, and Coulomb slip failure for the fault and granite contacts.

In all models a compressive tectonic setting is applied with boundary conditions representing an overall east-west shortening with σ_1 orientated at 90° (some models have a rotation of σ_1 to 112.5°) and the in-situ and boundary stress conditions correspond to around 7 km depth. These stress conditions are set at a ratio of $\sigma_1 / \sigma_2 = 1.2$ and $\sigma_3 / \sigma_2 = 0.8$, which are similar ratios to values used by Mair *et al*. (2000), Zhang & Sanderson (2002) and Stephens (2003). The imposed stresses ($\sigma 1 = 210$ MPa, $\sigma_2 = 175$ MPa, $\sigma_3 = 140$ MPa) are within reasonable ranges of CO_2 fluid inclusion entrapment pressures estimated for the Eastern Succession to be equivalent or greater than 200 MPa (e.g. Adshead, 1995; Rotherham *et al*., 1998; Mark *et al*., 2001) and general depths of ore formation for many deposits found in the district, e.g. Starra – 7.5 km (Rotherham *et al*., 1998) and Lightning Creek – 6.25 km (Perring *et al*., 2000), correspond well to the estimated depth and stress applied to the models (σ_2 – 175 MPa at 7 km).

Models were run to equilibrium by examining the relationship between unbalanced forces and displacements. The unbalanced force indicates when a mechanical equilibrium state (or the onset of joint slip or plastic flow) is reached for a static analysis, and a model is in exact equilibrium if the net nodal force vector at each block centroid or grid point is zero. The maximum nodal force vector is also referred to as the "unbalanced" or "out-of-balance" force (Itasca, 2000b). The maximum unbalanced force will never exactly reach zero for a numerical analysis and the model is considered to be in equilibrium when the maximum unbalanced force is small compared to the representative forces in the problem. If the unbalanced force approaches a constant non-zero value, it is indicative of joint slip or block failure and plastic flow within the model. The unbalanced force for these models was monitored and a settling or constant no-zero value was seen by approximately 1500 steps (Fig. 9). Mohr circle diagrams were constructed to calculate changes in stress and failure criteria as a means of validating the numerical simulations (Fig. 10). History points were placed (see Fig. 3, 4) to monitor changes in physical parameters at particular locations throughout the procedure.

Physical properties chosen for both the rocks and joints materials (Table. 5.1) are similar to those of previous authors (e.g. Oliver *et al*., 1990; Holyland & Ojala, 1997; Jiang *et al*, 1997; Zhang & Sanderson, 2002; Stephens, 2003) and represent metasediments, granite, lithological contacts and faults. Granite intrusions were chosen to be the most competent rock type, and the lithological contacts were assigned a higher stiffness than the faults (Table. 1).

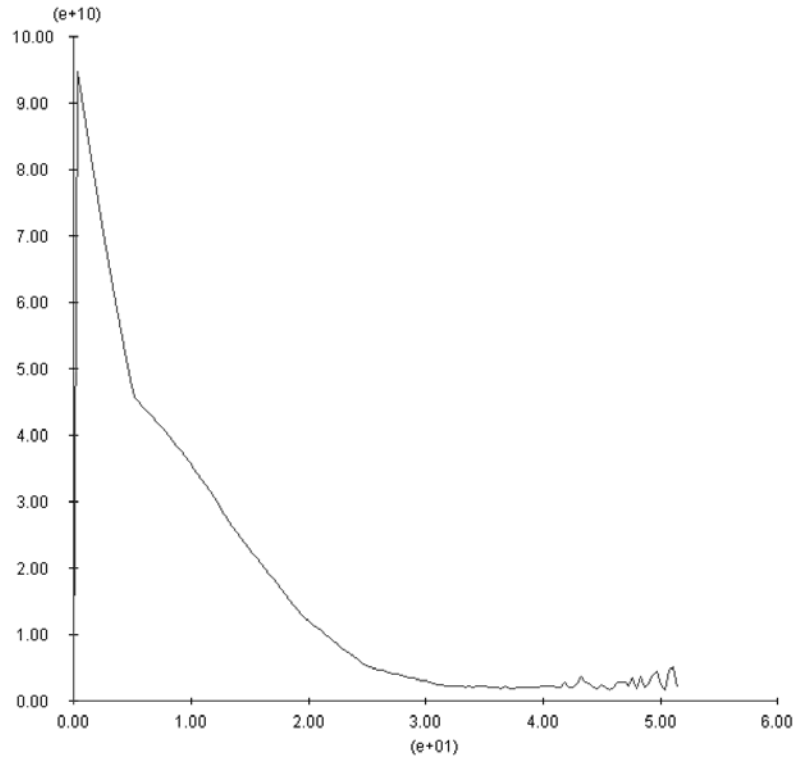

Fig. 9. UDEC plot of unbalanced history at approx 1500 cycles for Model 1.

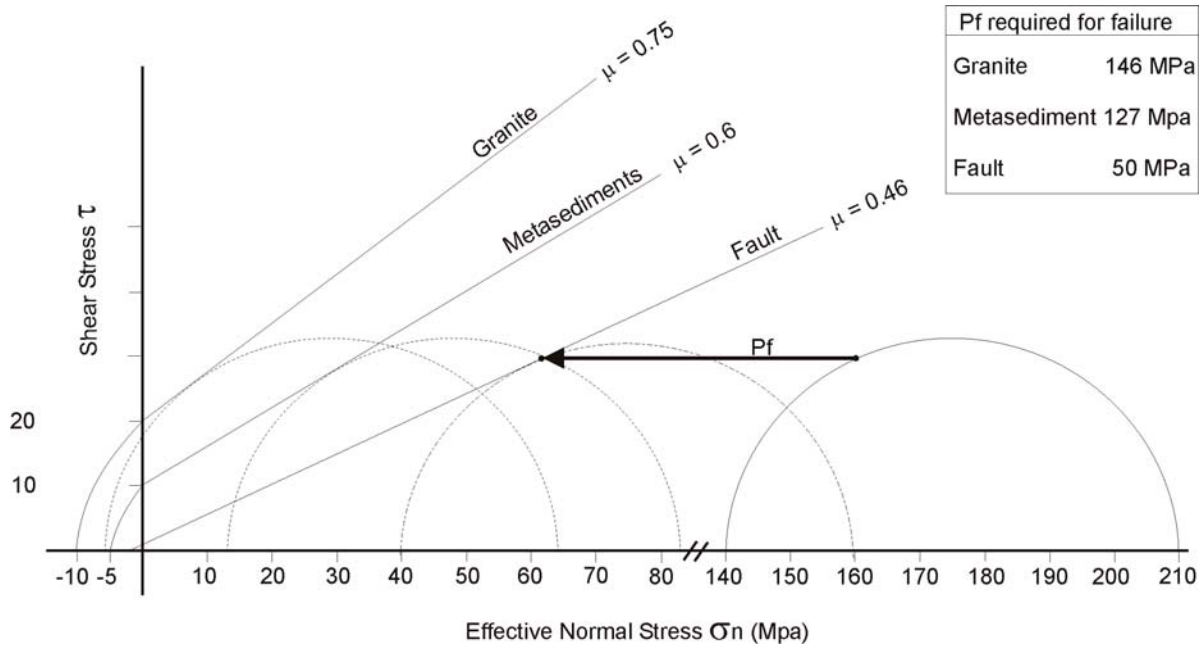

Fig. 10. Mohr diagram with failure envelopes representing granite, metasediments and faults. Fluid pressure required for contact with the failure envelopes was calculated using a fixed differential stress value, as a baseline for comparison with model results.

Table. 1. Physical properties of rocks, contacts and faults

Property	Granite	Metasediments	Lithological contact	Fault
Density (kg/m^3)	2650	2850	-	-
Bulk modulus (Pa)	49e9	25e9	-	-
Shear modulus (Pa)	27e9	25e9	-	-
Cohesion (Pa)	20e6	10e6	10e2	4e2
Tensile strength (Pa)	10e6	5e6	3e6	2e6
Friction angle (°)	37	31	35	30
Dilation angle (°)	5	4	5	5
Normal stiffness (Pa/m)	-	-	5e9	5e6
Shear stiffness (Pa/m)	-	-	1e5	1e3
Permeability factor (Pa/s)	-	-	238	300
Aperture at zero normal stress (m)	-	-	0.03	0.05
Residual hydraulic aperture (m)	-	-	0.01	0.03

3.0 RESULTS MODEL 1

Four different variants of this model were run to examine the effects of rotation of $_1$ and the addition of fluid to the fractures. Certain aspects of the models have greater graphical clarity when examined in detail. The following section examines both the whole (large scale) model and smaller areas - Selwyn and Cloncurry regions (see Fig. 3, 4). Models were initially cycled in non-saturated conditions, which provided a comparison with subsequent saturated models in which high fluid pressures were established in the fractures. The variation of the orientation of $_1$ to the initial stress regime was also compared for both saturated and non-saturated conditions. Many aspects of the models were investigated, however, this contribution will focus on the criteria required for failure, mean stress ($_m$), minimum principal stress ($_3$), and differential stress (Δ) values. On Mohr circle diagrams, failure may occur when effective stress conditions are such that the initial in-situ stress conditions are driven to the failure envelope by the fluid pressure (P_f). The amount of P_f required for this to occur for a given stress state can be termed 'fluid pressure required for failure' and will be referred to from this point on as PF_f (Fig. 10).

3.1 **Model 1a:** no fluid pressure, E-W compression ($_1$ = 090°)

Settling of this "dry" model was observed by ~1500 time steps (Fig. 9). The initial regional model displays values of mean stress ($_m$) generally ranging from ~170 MPa to 210 MPa, with the higher $_m$ values being found around lithological contacts (Fig. 11a). On closer inspection of the Selwyn region, variations in $_m$ (140 to 190 MPa) are observed with highest values on N/S trending faults, and lowest values on S/E to E/W trending faults and particularly intersections of S/E to E/W trending faults with all other orientations (Fig. 11b). Several areas show dilation (positive volumetric strain) which correspond well to low values of $_3$ (Fig. 12a), and within the Selwyn region these areas are to the west of the Gin Creek Granite (Fig. 12b). On the regional scale, Δ within the model varies by around 20 MPa, and several high and low areas are apparent (Fig. 13a). In the Selwyn region higher values of Δ are seen to the west of the Gin Creek granite and are associated with fault intersections (Fig. 13b). Lowest values of PF_f are primarily restricted to fault bends and intersections (Fig. 14a), and this is more apparent at the more detailed scale (Fig. 14b), which displays values of 60 to 100 MPa

on most fault intersections, 20 to 60 MPa less than the surrounding metasediments and granite.

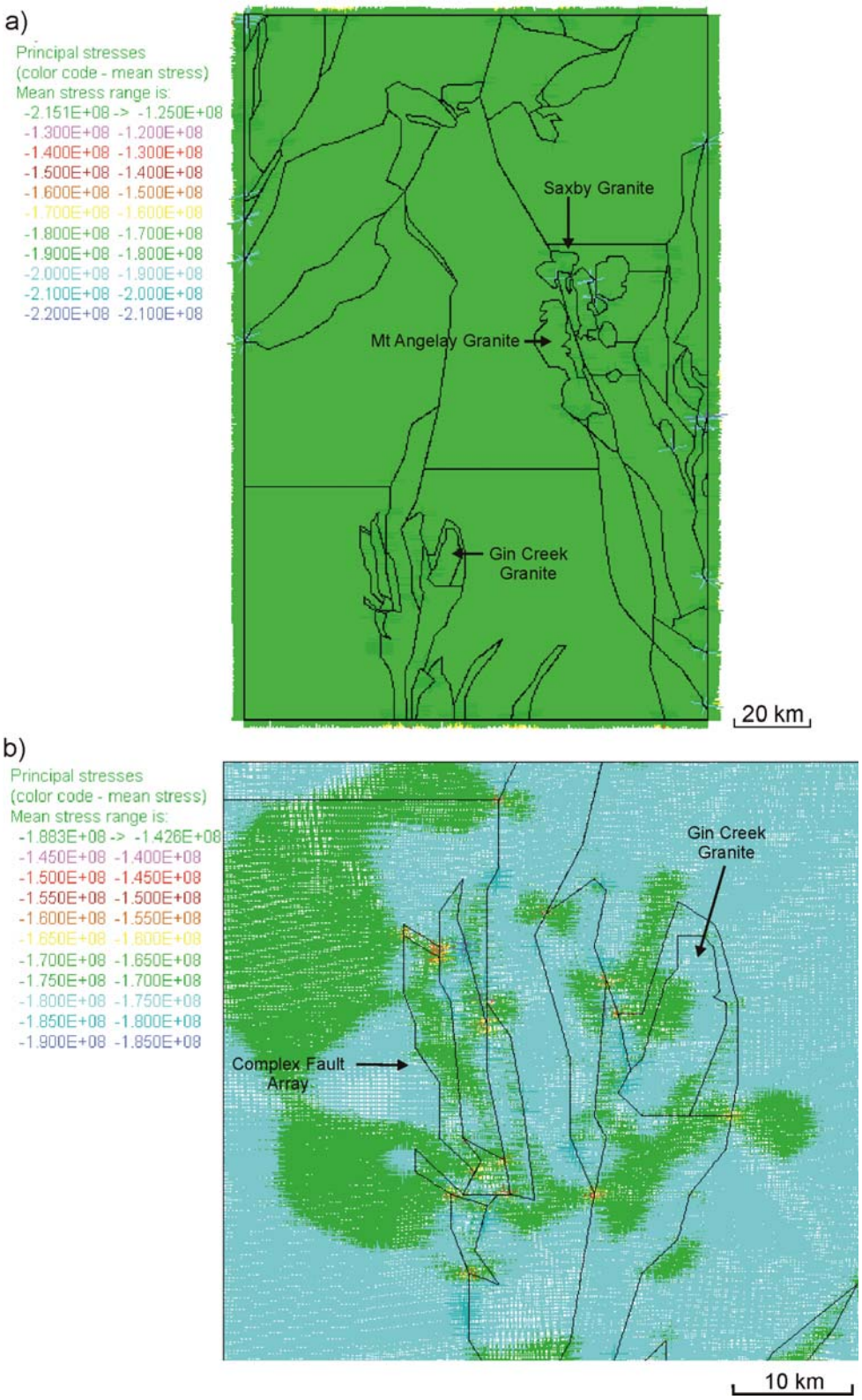

Fig. 11. Plots of mean stress for Model 1a a) regional plot illustrating a homogenous mean stress in the majority of the model, with variations mostly noted on fault bends and granite contacts b) magnified plot of the Selwyn area showing both increased and decreased values on fault contacts.

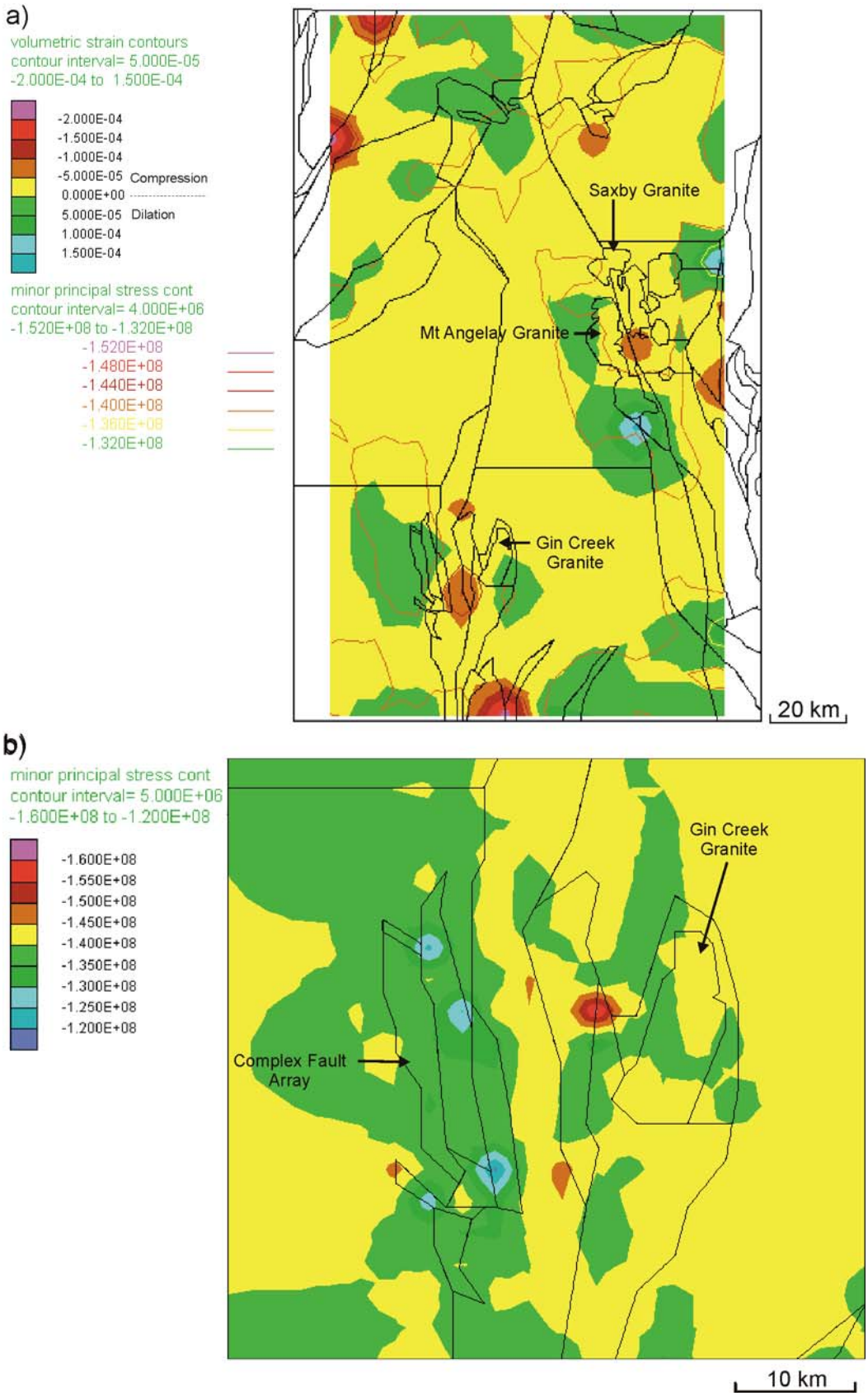

Fig. 12. Plots of volumetric strain (dilation) and minor principal stress for Model 1a a) regional plot displaying several areas of low minimum principal stress values, which correspond to dilation or positive volumetric strain b) magnified plot of the Selwyn area showing low values at specific fault intersections west of the Gin Creek Granite.

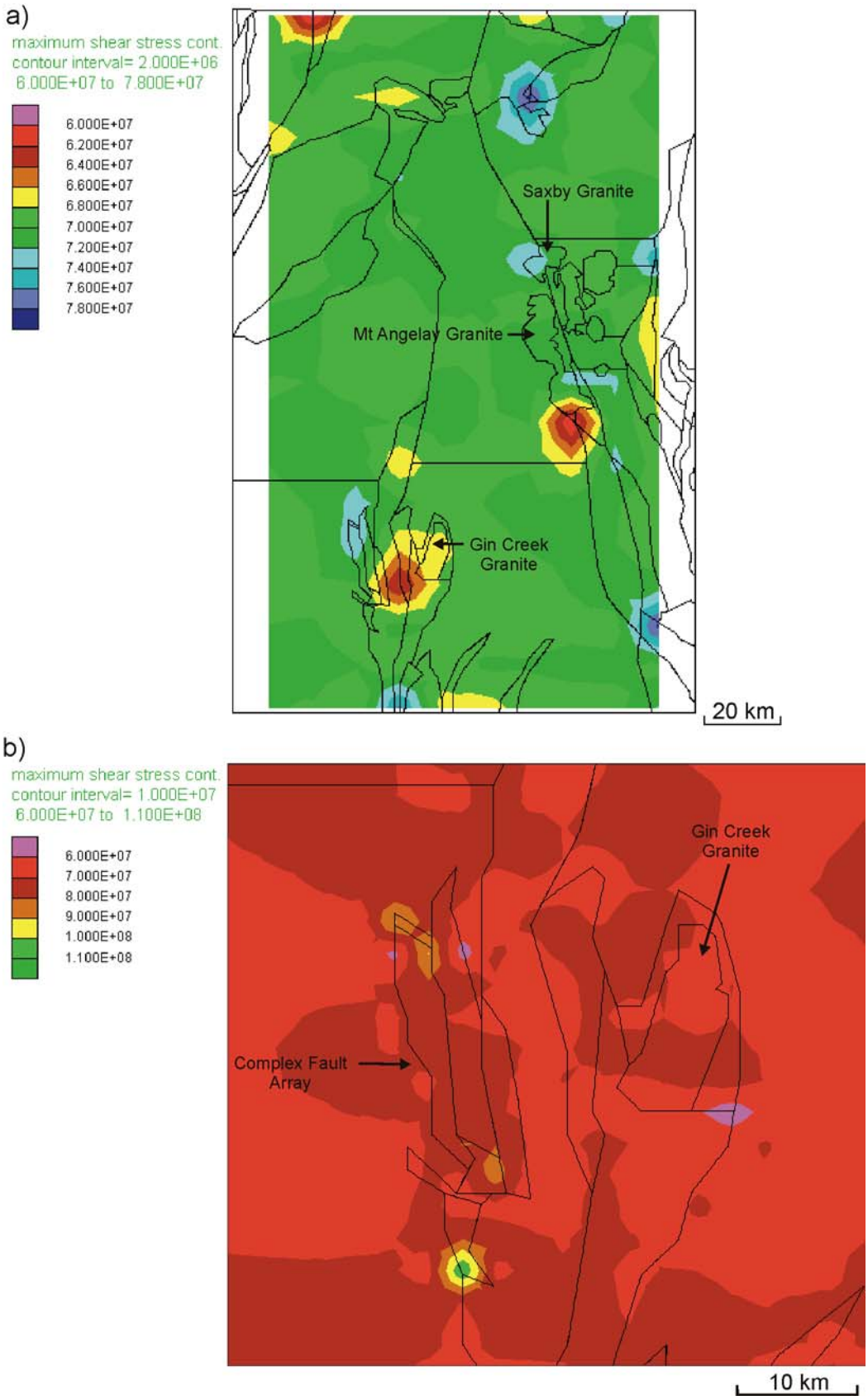

Fig. 13. Plots of differential stress for Model 1a a) regional plot illustrating high values at the northern and southern ends of the Cloncurry fault and lowest values indicated at the base of the Mt Angelay granite and in the Selwyn region b) magnified plot of the Selwyn region.

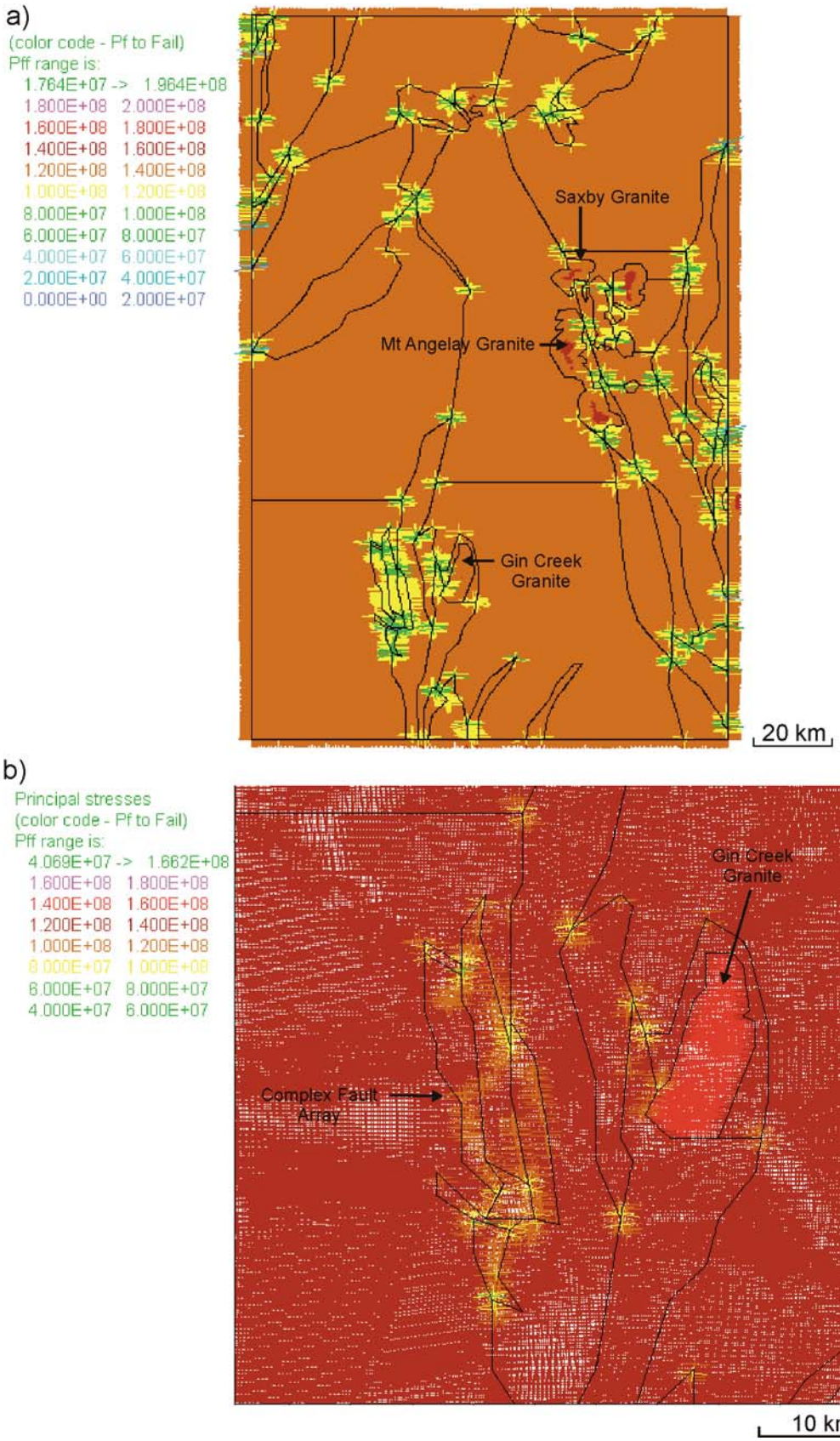

Fig. 14. Plots of fluid pressure required for failure for Model 1a a) regional plot illustrating areas most likely to fail with minimum fluid pressures b) magnified plot of the Selwyn area showing several fault contacts and intersections most likely to fail.

In summary, this model displays preferential failure conditions around fault bends and intersections, particularly faults that are orientated at a low angle to $_1$. Dilation and low $_3$ correspond well with areas that show lower values of $_m$ and increased Δ , which indicate suitable conditions for shear failure.

2.5 **Model 1b**: no fluid pressure, $_1$ orientated ESE-WNW (112.5°)

Rotation of $_1$ has little effect on $_m$, which displays similar values to the previous model, ranging from 170 to 200 MPa. The Selwyn region again displays lowest values on similarly orientated fault intersections (Fig. 15), relative to the previous model. However, values and overall distribution of $_3$ display a considerable variation from the previous model, with a decrease in some areas of up to 30 MPa (Fig. 16a). The distribution of low $_3$ in the Selwyn region highlights dilational areas in the southern end of the complex fault array to the west of the Gin Creek granite (Fig. 16b); again fault intersections appear to play an important role in this distribution. Regional distribution of Δ (Fig. 17a) is broadly similar to the previous model, with a low area at the southern end of the Mt Angelay granite, however, the Selwyn area does display a marked variation in values (Fig. 17b). Overall values of Δ are greater than in the previous model by up to 50 MPa. An overall decrease by up to 30 MPa in PF_f is seen in this model (Fig. 18a) and again fault intersections and bends in the Selwyn region display a higher potential for failure relative to other areas (Fig. 18b).

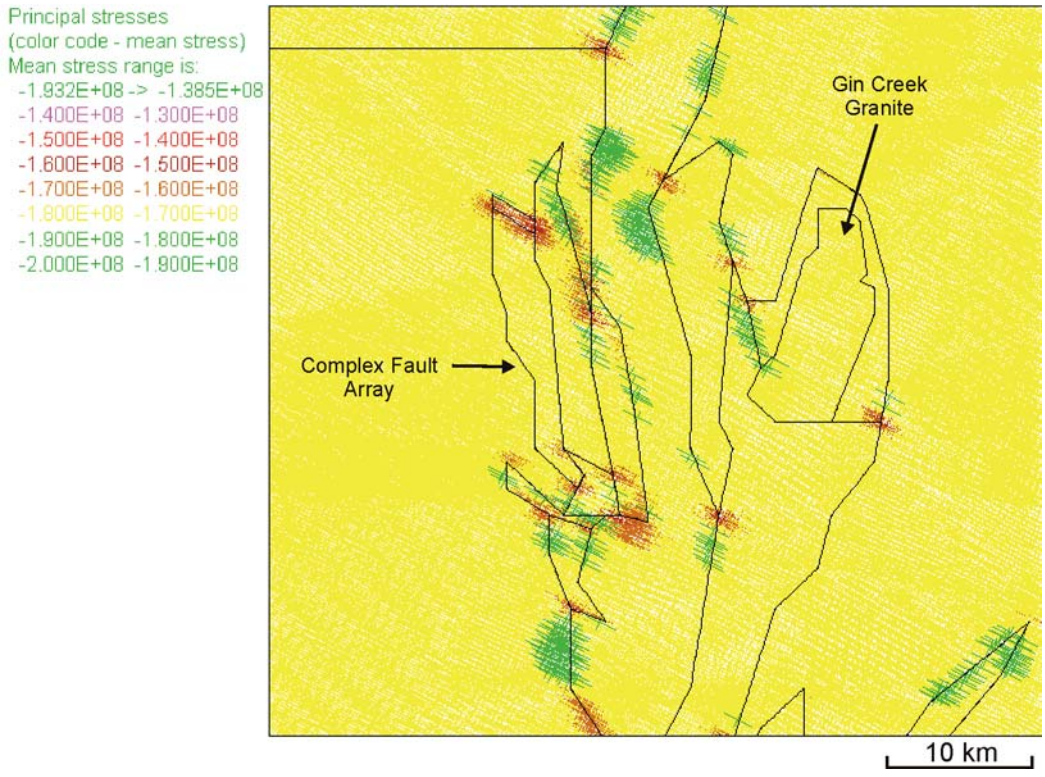

Fig. 15. Plot of mean stress for Model 1b in the Selwyn region, illustrating homogenous values within the granite and metasediments, with large variations mostly noted on fault bends and granite contacts.

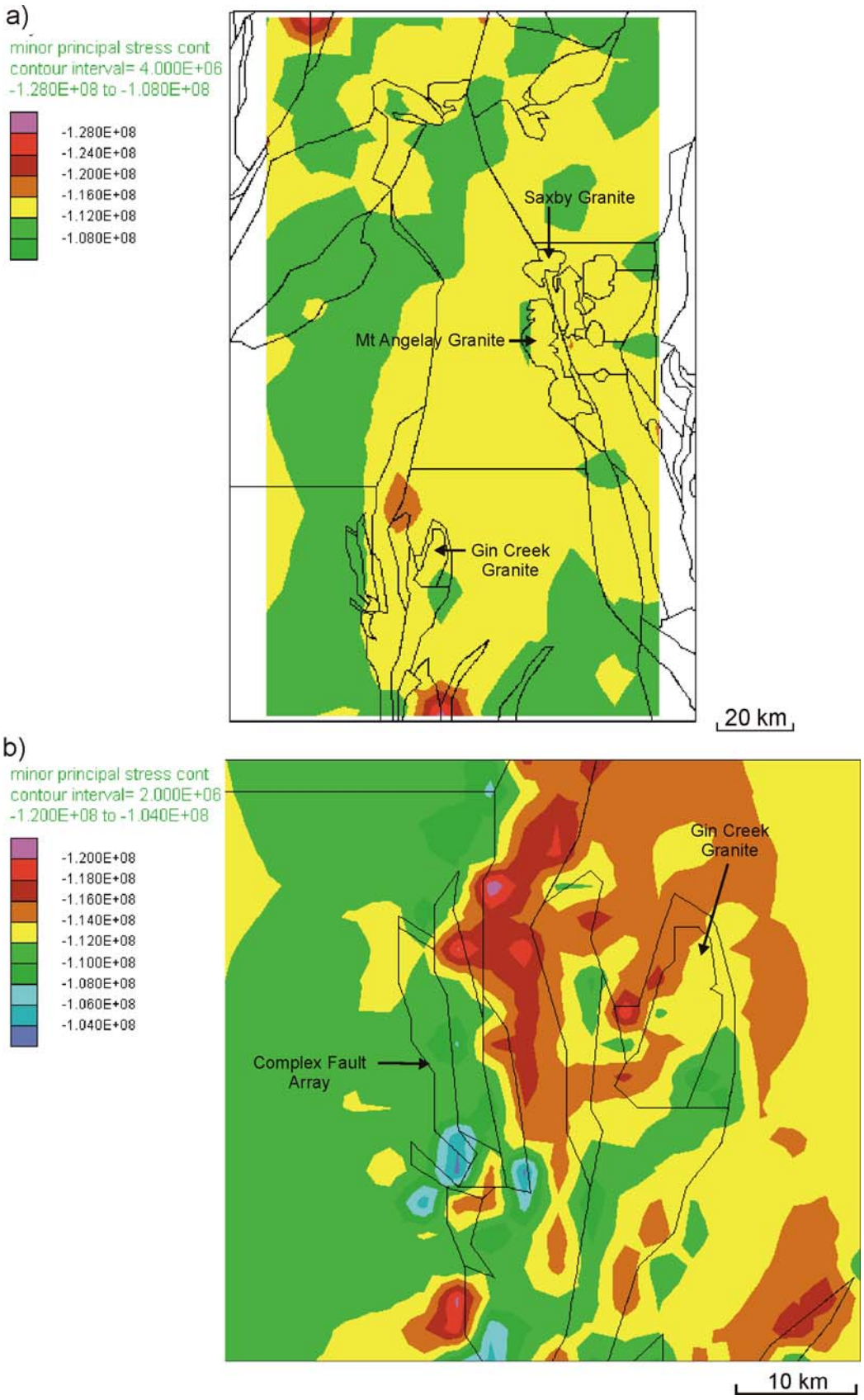

Fig. 16. Plots of minor principal stress for Model 1b a) regional plot illustrating values which are lower than Model 1a b) magnified plot of the Selwyn area showing low values at specific fault intersections.

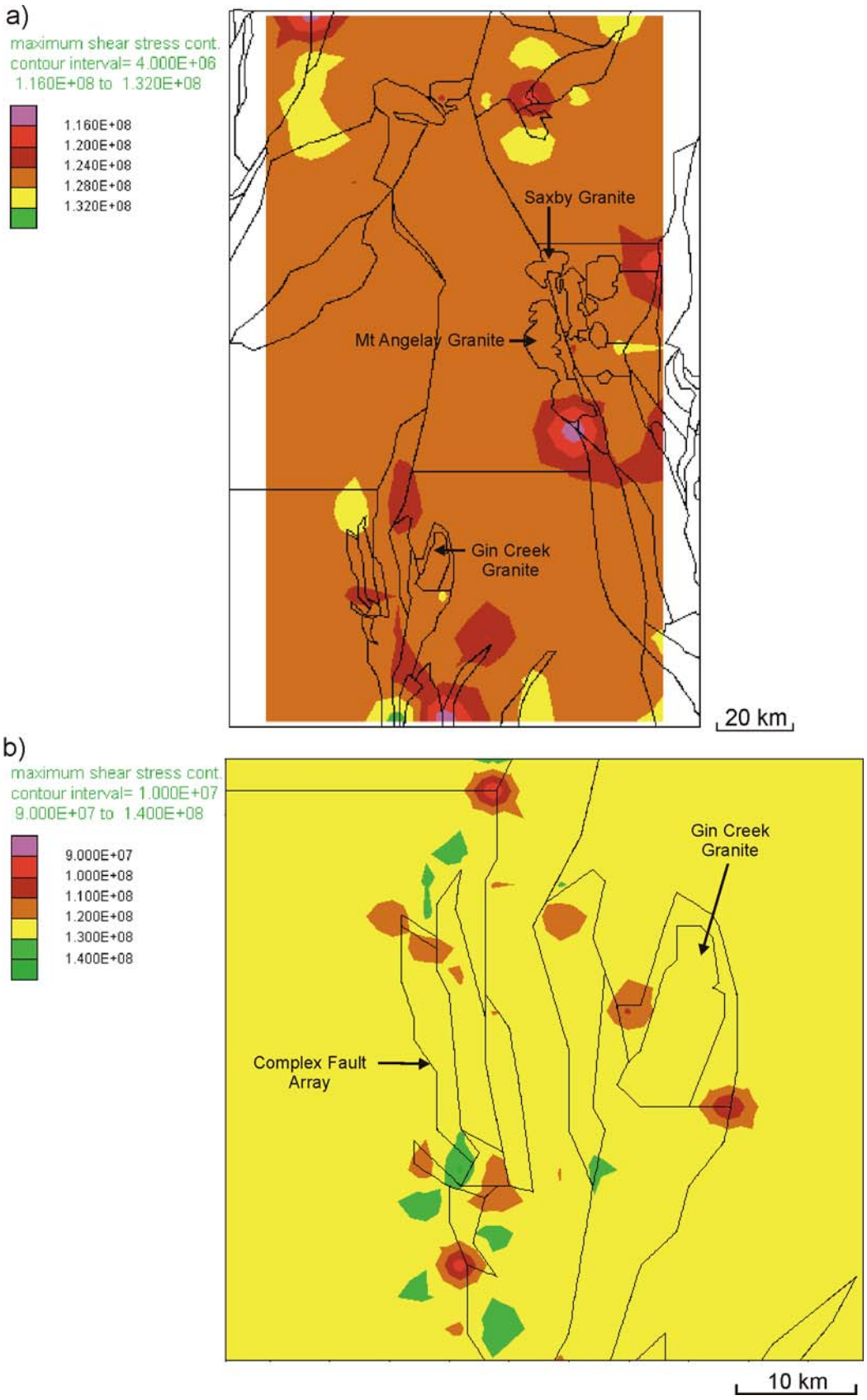

Fig. 17. Plots of differential stress for Model 1b a) regional plot illustrating high values particularly in the Selwyn region b) magnified plot of the Selwyn region.

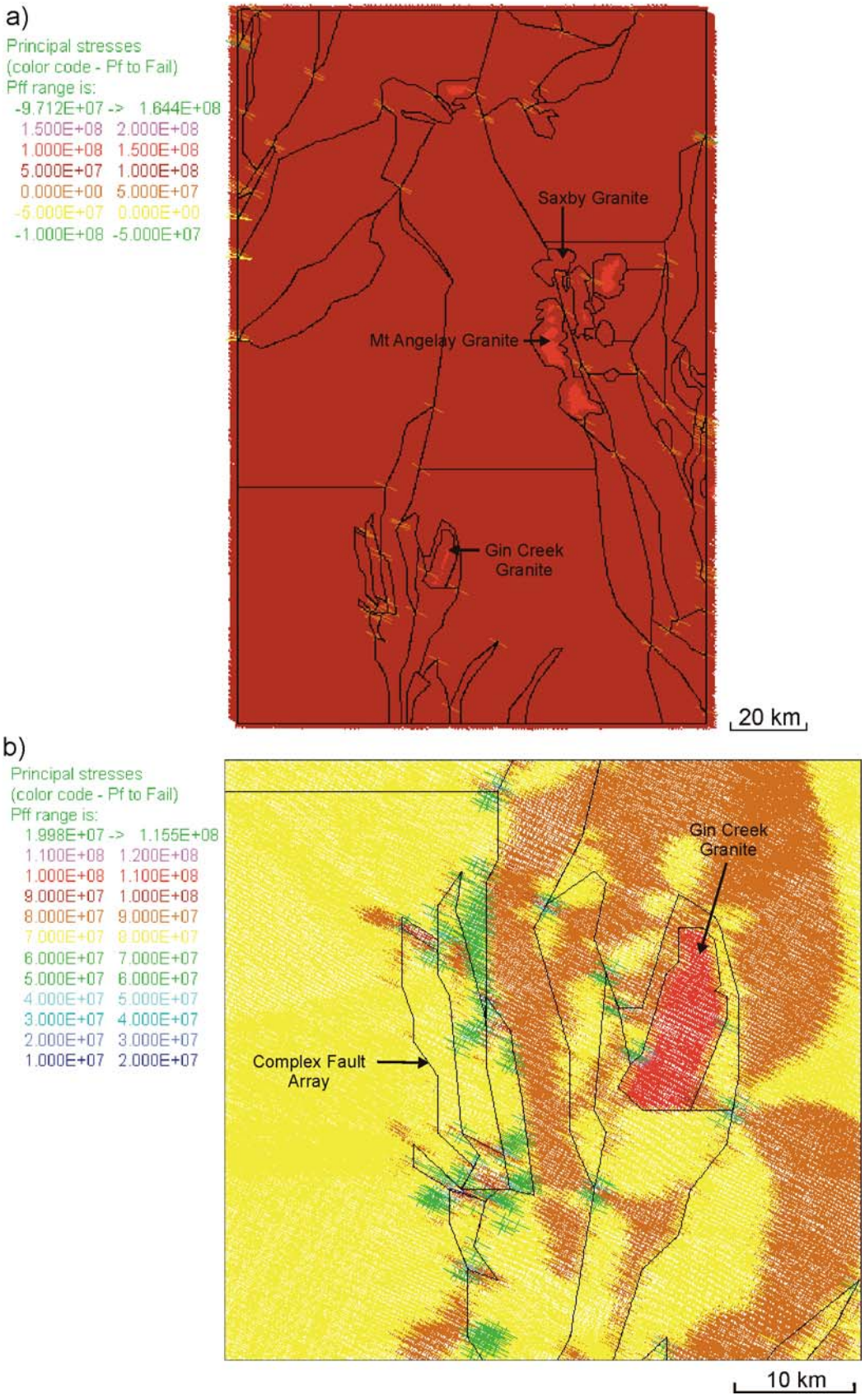

Fig. 18. Plots of fluid pressure required for failure for Model 1b a) regional plot illustrating granites with highest values and overall values have lowered considerably from Model 1a b) magnified plot of the Selwyn area showing several fault contacts and intersections most likely to fail.

In summary, the change in orientation of $_1$ shows little effect on the values or distribution of $_m$. However, a considerable variation in the values and distribution of $_3$ relative to the previous model can be seen. The regional distribution of Δ remains broadly similar to the previous model, however higher values and a greater variation in the range of values is evident. The overall decrease in values of PF_f in this model can be linked or attributed to the increase of Δ in particular areas, which has shifted the Mohr circle towards the failure envelope.

2.6 **Model 1c**: fluid pressure, E-W compression ($_1$ = 90°)

The introduction of fluid into model fractures results in a considerable variation in the distribution and values of $_m$ from the previous models, with most faults and lithological contacts highlighted at a regional scale (Fig. 19a). The Selwyn region displays a clustering of higher $_m$ around faults and granite contacts; with the west side of the Gin Creek granite showing the highest values (Fig. 19b). Regional distribution of $_3$ displays several distinctive areas that have low values, including the Selwyn and Cloncurry regions (Fig. 20a). The Selwyn region displays low values of $_3$ within the corridor separating the Gin Creek granite and the more complex fault array to the west, and low values are also seen around fault bends and intersections to both the east and west of the Gin Creek granite (Fig. 20b). These areas also correspond well to dilation and have increased values of Δ both on a regional scale (Fig. 21a) and at the Selwyn scale (Fig. 21b). The broader model scale displays two regions in the north that show increased dilation and low values of $_3$ and PF_f, otherwise the main areas of interest are in the Cloncurry region, the Mt Angelay granite and areas in the southern half of the model (Fig. 22a). The Selwyn area again displays a distinct corridor with lowest values of PF_f (Fig. 22b).

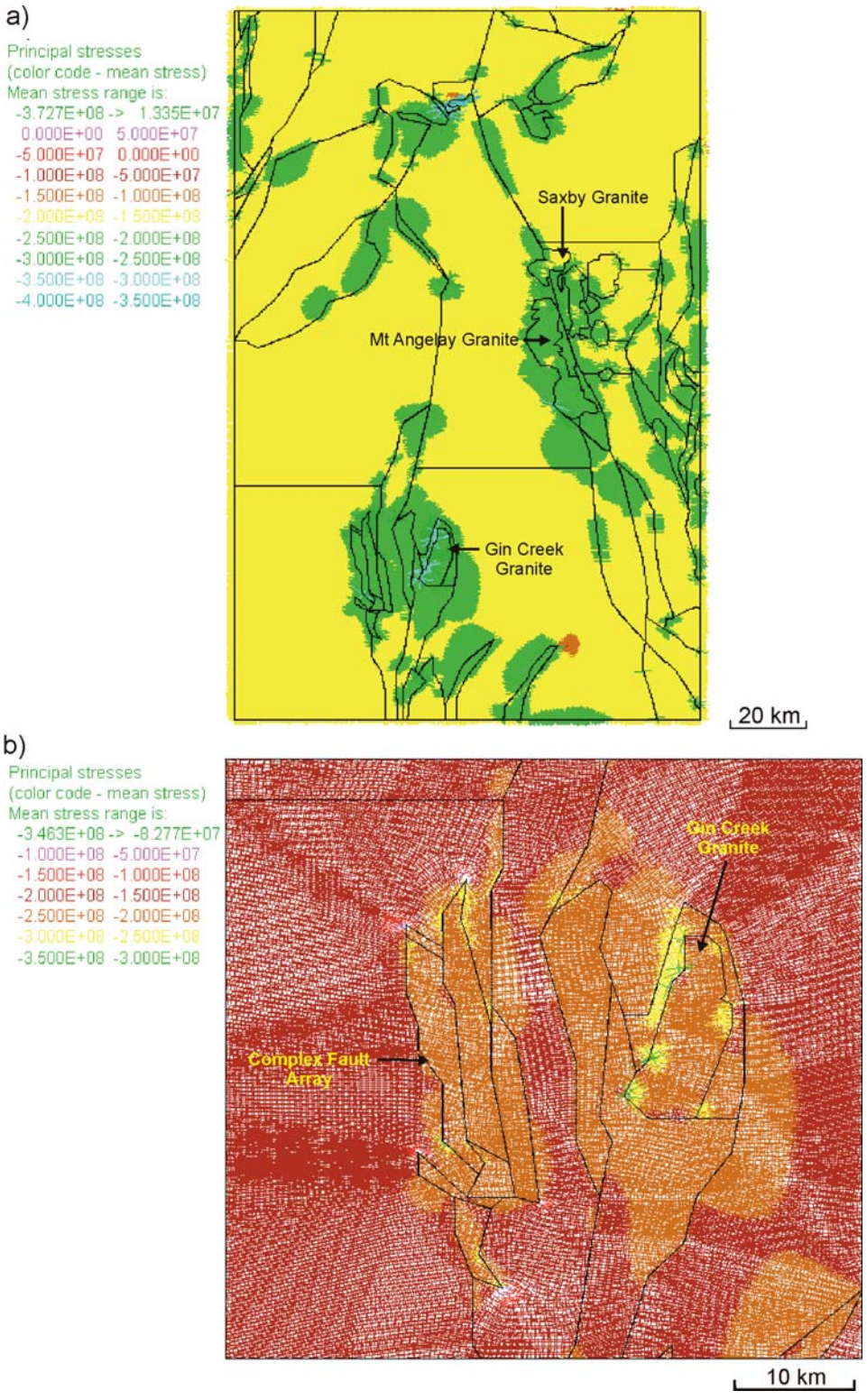

Fig. 19. Plots of mean stress for Model 1c a) regional plot illustrating a considerable increase in mean stress values in comparison to earlier models, with variations mostly noted on fault bends and granite contacts b) magnified plot of the Selwyn area showing partitioning of stress in and around fault contacts.

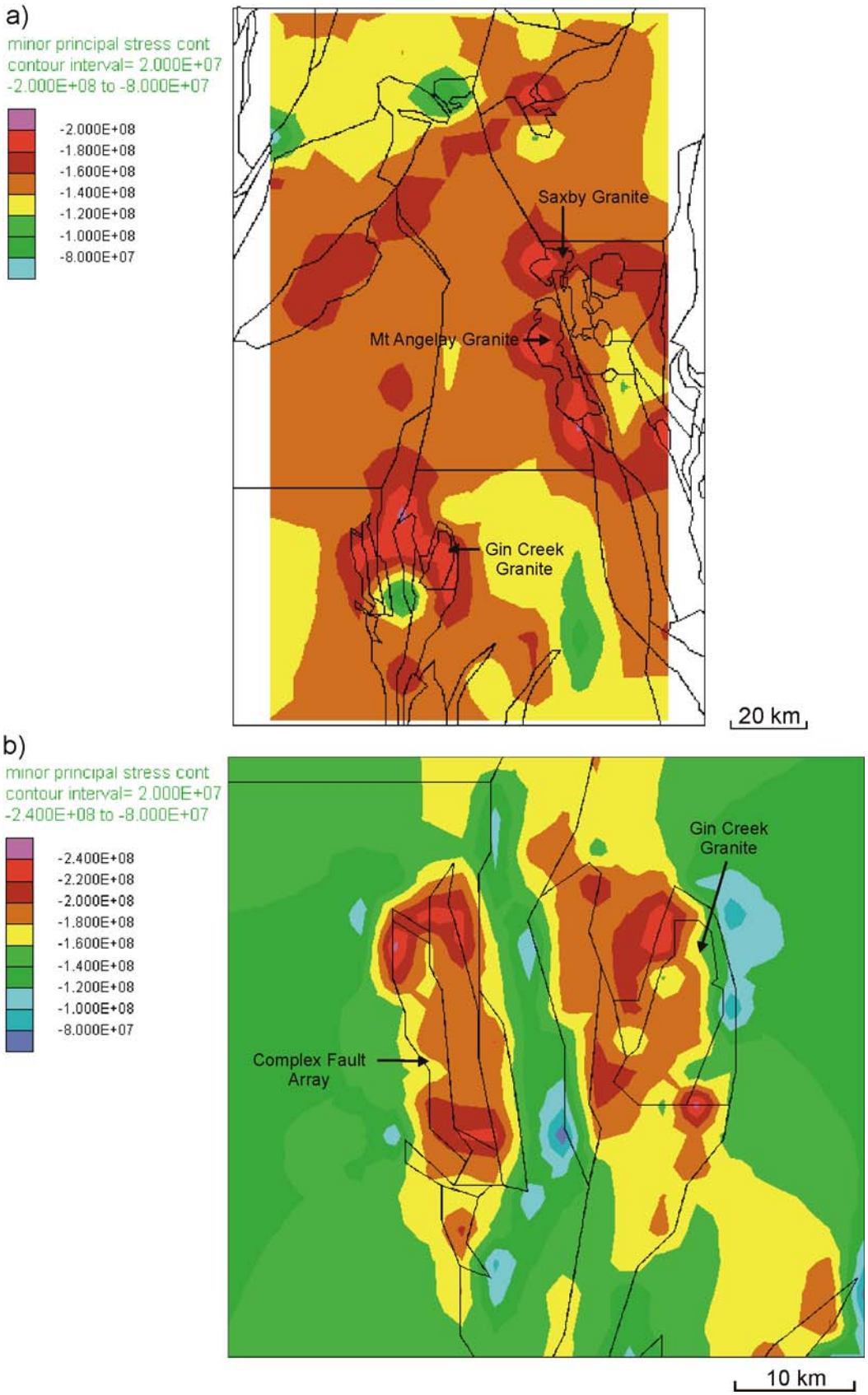

Fig. 20. Plots of minor principal stress for Model 1c a) regional plot illustrating low values in the Cloncurry and Selwyn regions b) magnified plot of the Selwyn area showing low values at specific fault intersections and a north-south trending corridor between fault sets.

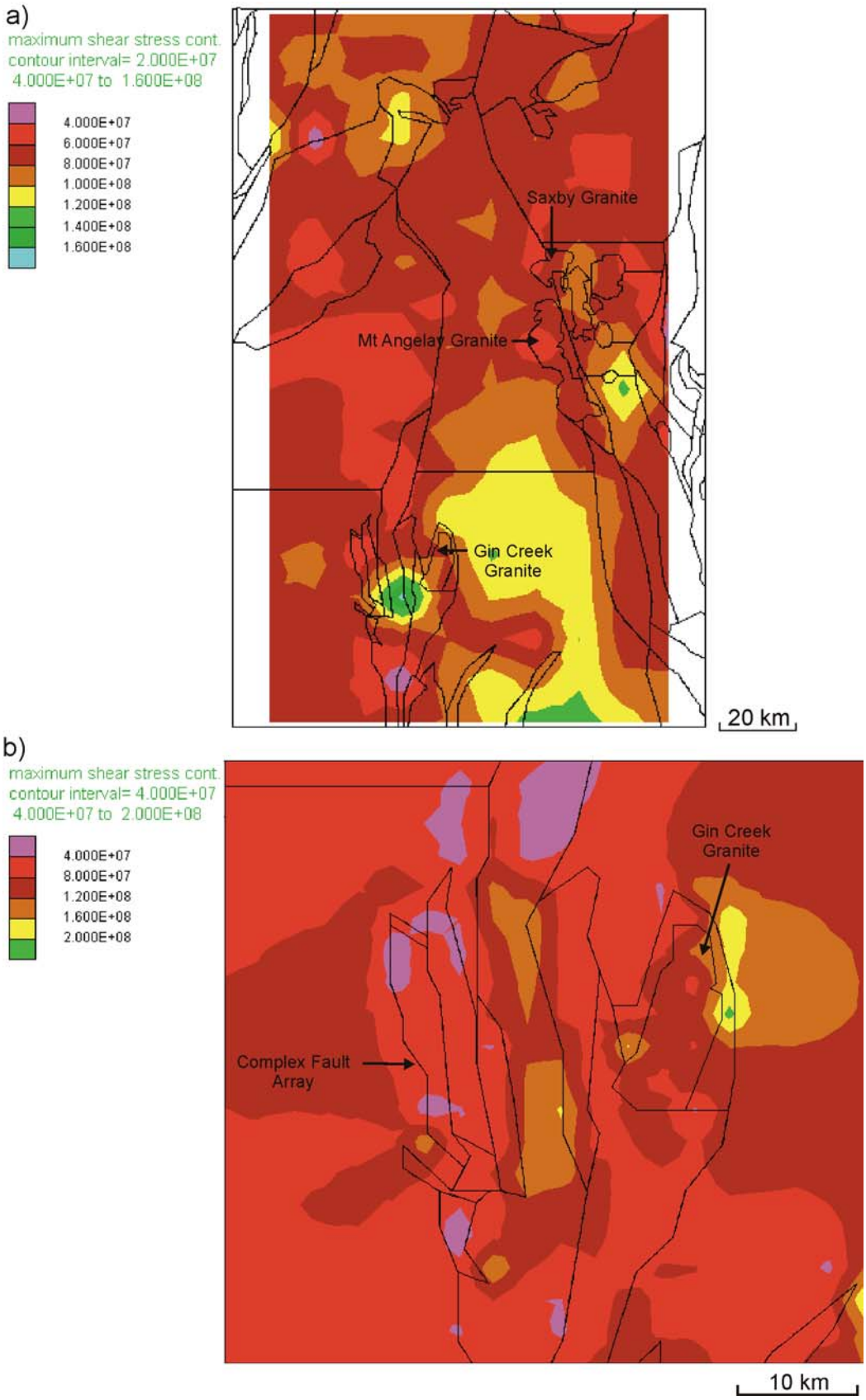

Fig. 21. Plots of differential stress for Model 1c a) regional plot illustrating high values particularly in the Selwyn region b) magnified plot of the Selwyn region displaying a north-south trending corridor.

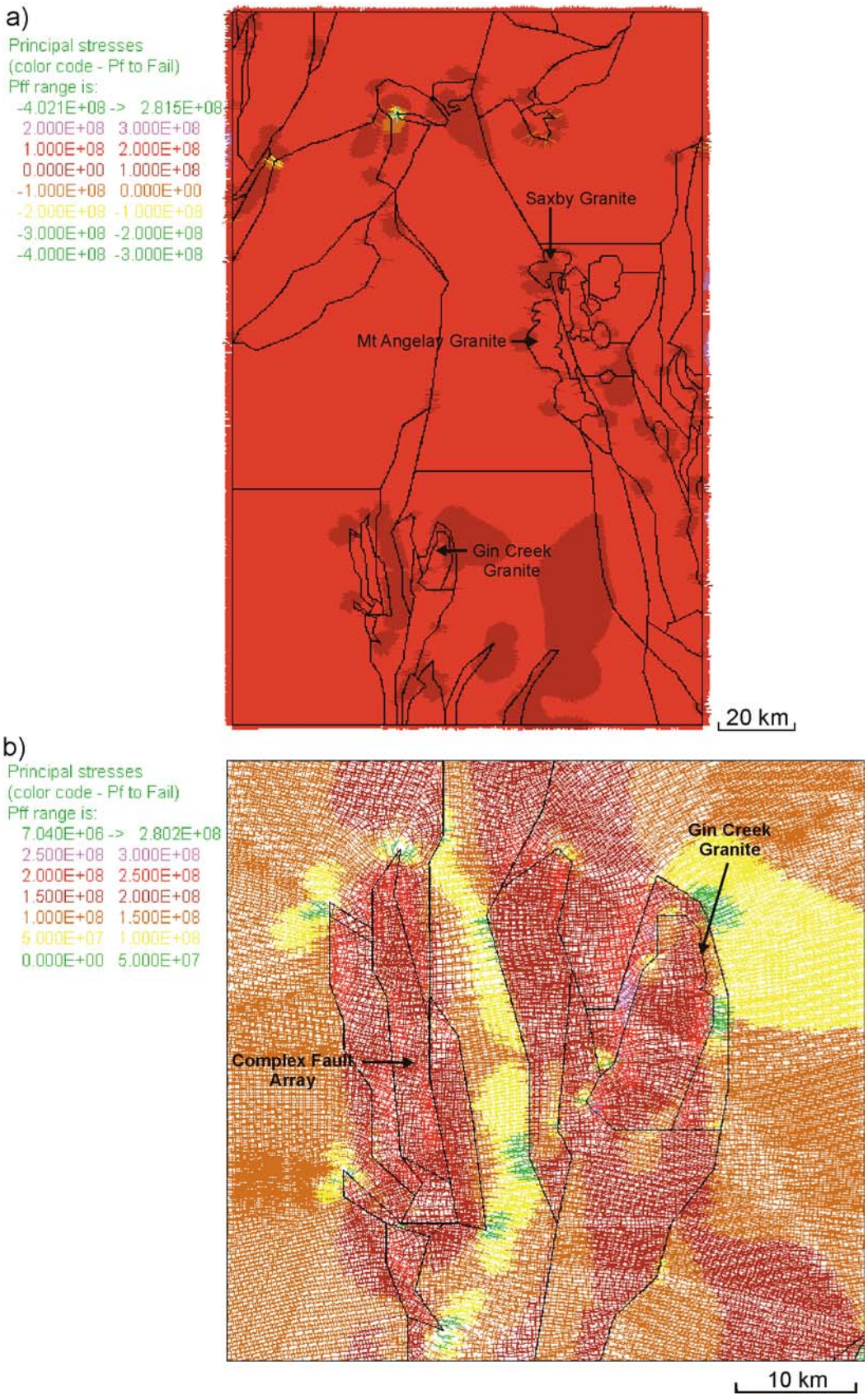

Fig. 22. Plots of fluid pressure required for failure for Model 1c a) regional plot displaying main areas of interest in the Cloncurry and Selwyn regions b) magnified plot of the Selwyn area showing the partitioning within and around fault sets. Note: negative values indicate areas at yield.

In summary, the influence of fluid pressure within the fractures of the model results in a considerable variation in the distribution of $_m$ and $_3$ from the previous models discussed. Low values of $_3$ correspond well to dilation and higher values of Δ , and a distinct corridor separating the Gin Creek granite and the more complex fault array to the west is noticeable. The overall influence of fluid pressure drastically changes the distribution of all parameters, increases the overall range of values and decreases the values of $_3$, $_m$, Δ and PF_f at several specific locations highlighted above.

2.7 **Model 1d**: fluid pressure, $_1$ orientated ESE-WNW (112.5°)

Rotation of $_1$ has an influence on the distribution of $_m$ from the previous models, with highest values found around complex fault arrays and granites. Distinctive low values are apparent on the northern tip of the Mt Angelay granite, Cloncurry area and the southwest of the model (Fig. 23a). The Selwyn region displays highest values of $_m$ on the northern end of the Gin Creek granite and lowest values on the west side of the complex fault array (Fig. 23b). On the regional scale, lowest values of $_3$ can be seen in the Cloncurry and Selwyn regions (Fig. 24a), with a notable decrease in values around fault arrays. In the Selwyn region there is a distinct change in distribution of $_3$, with a noticeable area northwest of the complex fault array with lower values relative to the previous model (Fig. 24b). This area also corresponds to areas of high Δ , as does the Saxby Granite region (Fig. 25a). The Selwyn region also indicates higher values of Δ (up to 80 MPa greater) than the previous model (Fig. 25b). Several areas in the north of the model indicate dilation and require minimum PF_f (Fig. 26a), and the Selwyn region also shows areas of low PF_f, which correspond with both low $_3$ and high Δ (Fig. 26b). Overall, PF_f displays a larger range of values relative to the previous model, with specific areas indicating decreased values.

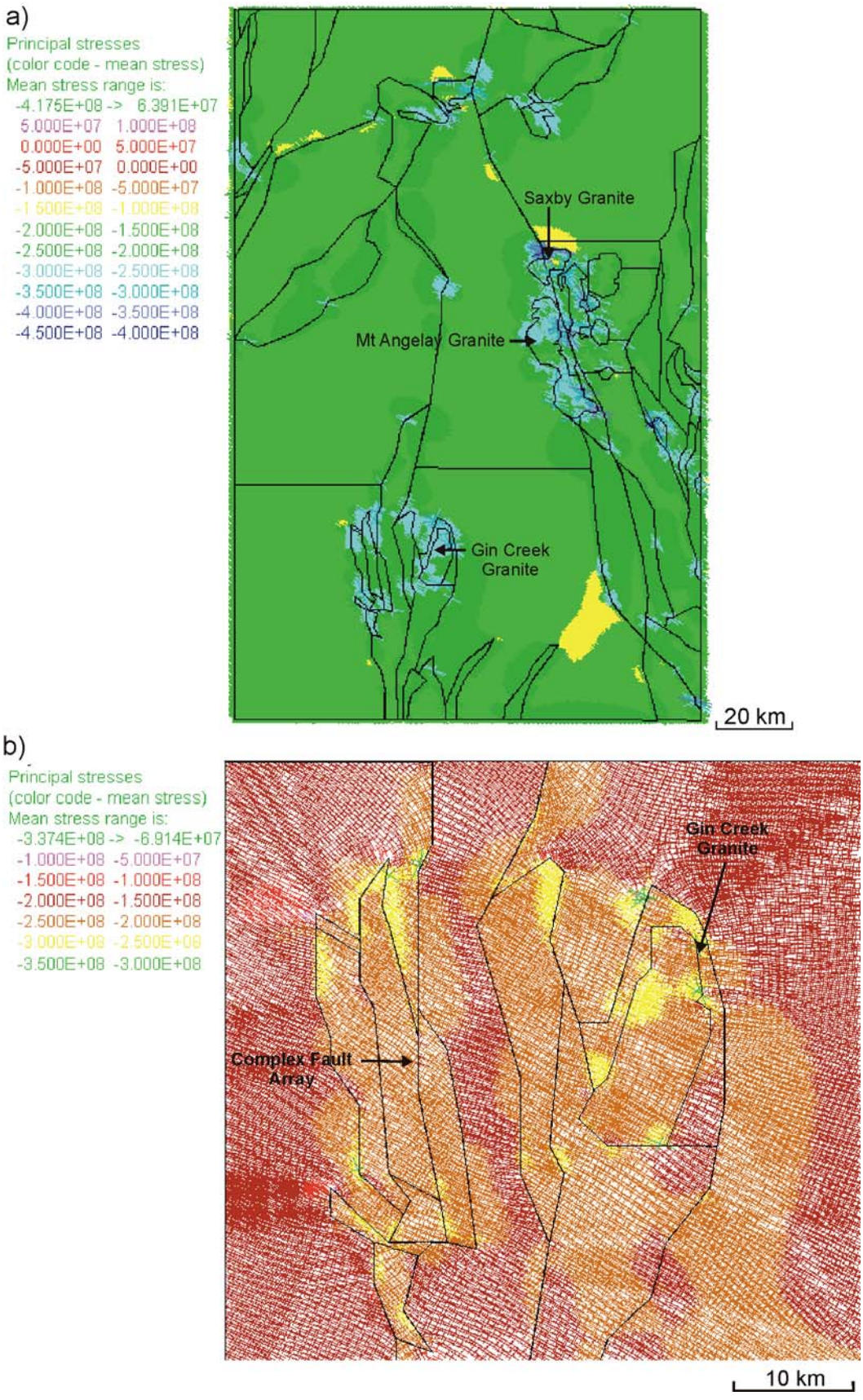

Fig. 23. Plots of mean stress for Model 1d a) regional plot displaying similar mean stress values to the previous model b) magnified plot of the Selwyn area showing partitioning of stress in and around fault contacts. Highest mean stress values are associated with fault bends and around intersections.

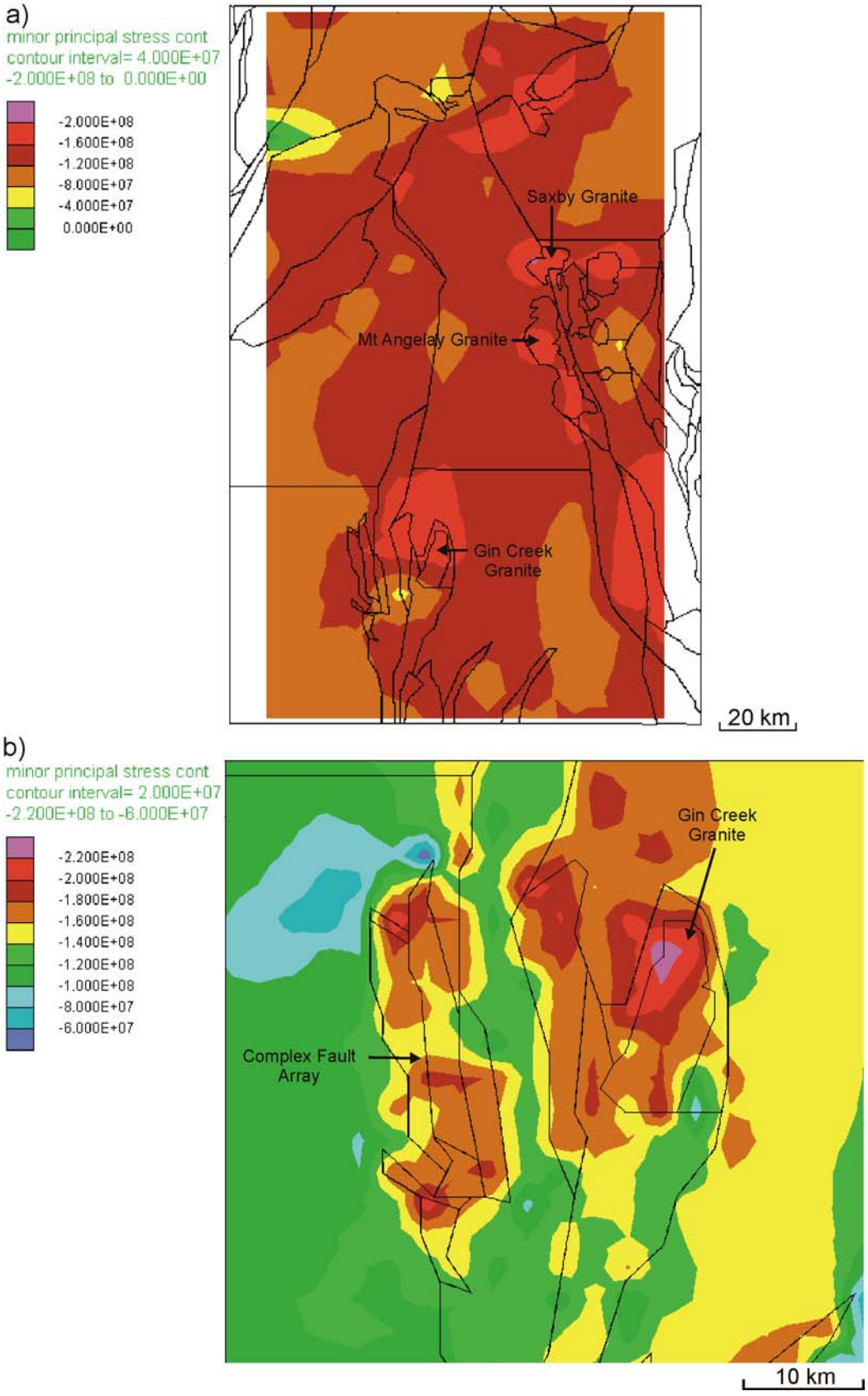

Fig. 24. Plots of minor principal stress for Model 1d a) regional plot illustrating areas of low minimum principal stress in the Cloncurry and Selwyn regions b) magnified plot of the Selwyn area showing low values in an area northwest of the complex fault array.

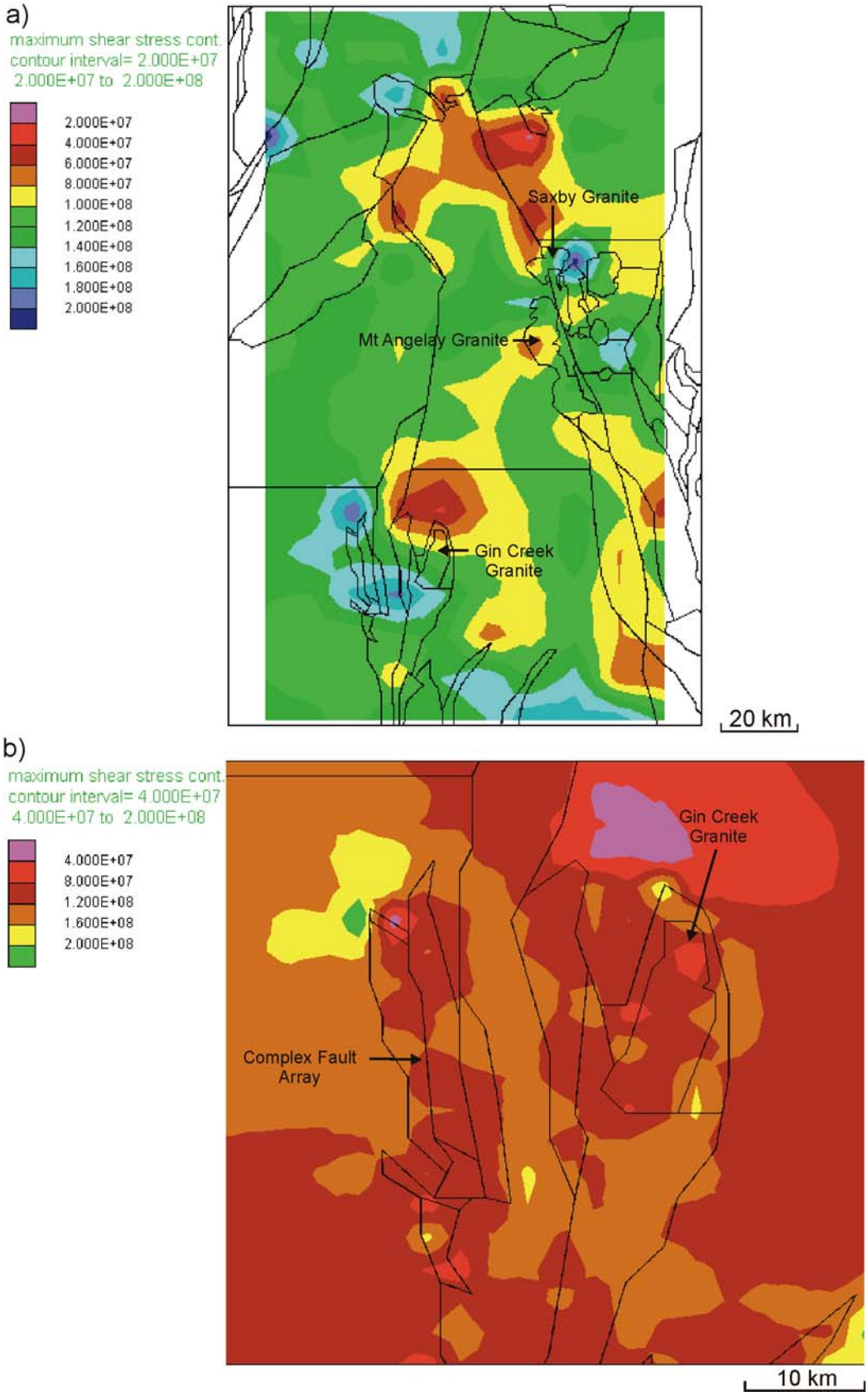

Fig. 25. Plots of differential stress for Model 1d a) regional plot illustrating highest values around the Saxby granite and Selwyn region b) magnified plot of the Selwyn region again displaying a north-south trending corridor and an increase in values corresponding to low minimum principal stress from the previous plot.

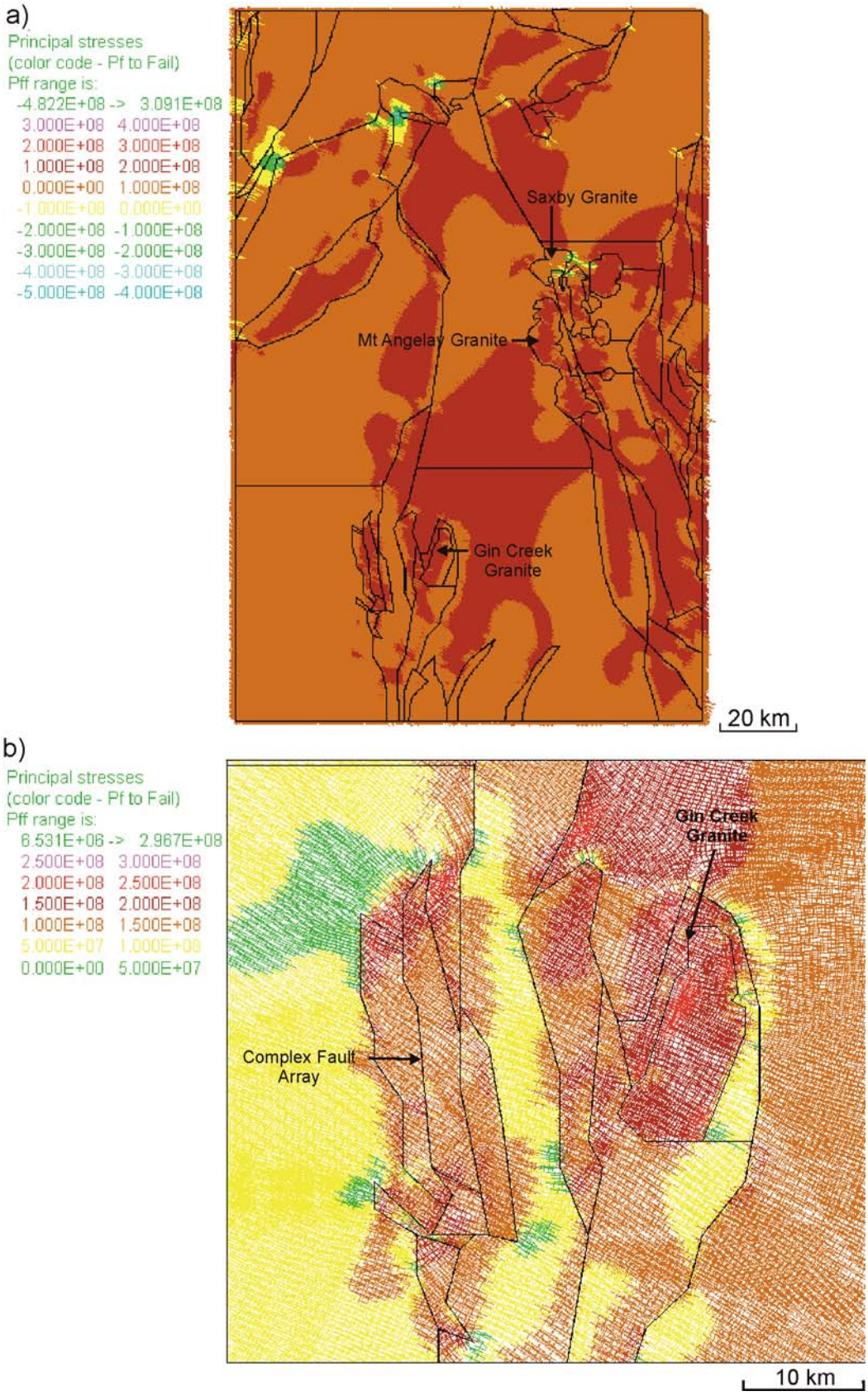

Fig. 26. Plots of fluid pressure required for failure for Model 1d a) regional plot displaying areas of interest in the Saxby granite regions and west of the Cloncurry region b) magnified plot of the Selwyn area displaying areas of low PF_f which correspond with both low $_3$ and high Δ .

In summary, the rotation of $_1$ and addition of fluid has had an influence on the distribution of the $_m$ relative to the previous models. A distinct change in the distribution of $_3$ and Δ is also apparent, with an increase in the range of Δ and PF_f values.

4.0 RESULTS MODEL 2

Four different variants of this model were run to examine the effects of rotation of $_1$ and the addition of fluid to the fractures. All conditions are the same as for Model 1; however, a more complex geometry and younger granite suites have been added, to simulate the effects of potential syn-mineralisation fluid flow and deformation after 1530 Ma.

4.1 **Model 2a:** no fluid pressure, E-W compression ($_1 = 90°$)

The values of $_m$ in the majority of the model correspond reasonably well with the values of Model 1a, and higher values of $_m$ are preferentially located on fault intersections, bends and lithological contacts (Fig. 27a). Areas that show the largest variation in $_m$ from Model 1a are primarily located on the model boundaries, which may suggest a boundary effect. The Selwyn region displays lowest values of $_m$ at fault intersections, particularly with faults of S/E, E/W and E/NE orientations (Fig. 27b). The distribution of $_3$ shows both similarities to and variations from Model 1a, with similar patterns indicated by low values in the S/E and N/W corners of the model (Fig. 28a). However, a distinct low $_3$ area at the northern tip of the Squirrel Hills granite can be attributed to the additional fault geometry and competence contrasts of the granite and metasediments. Within the Selwyn region similarities to Model 1a are evident,

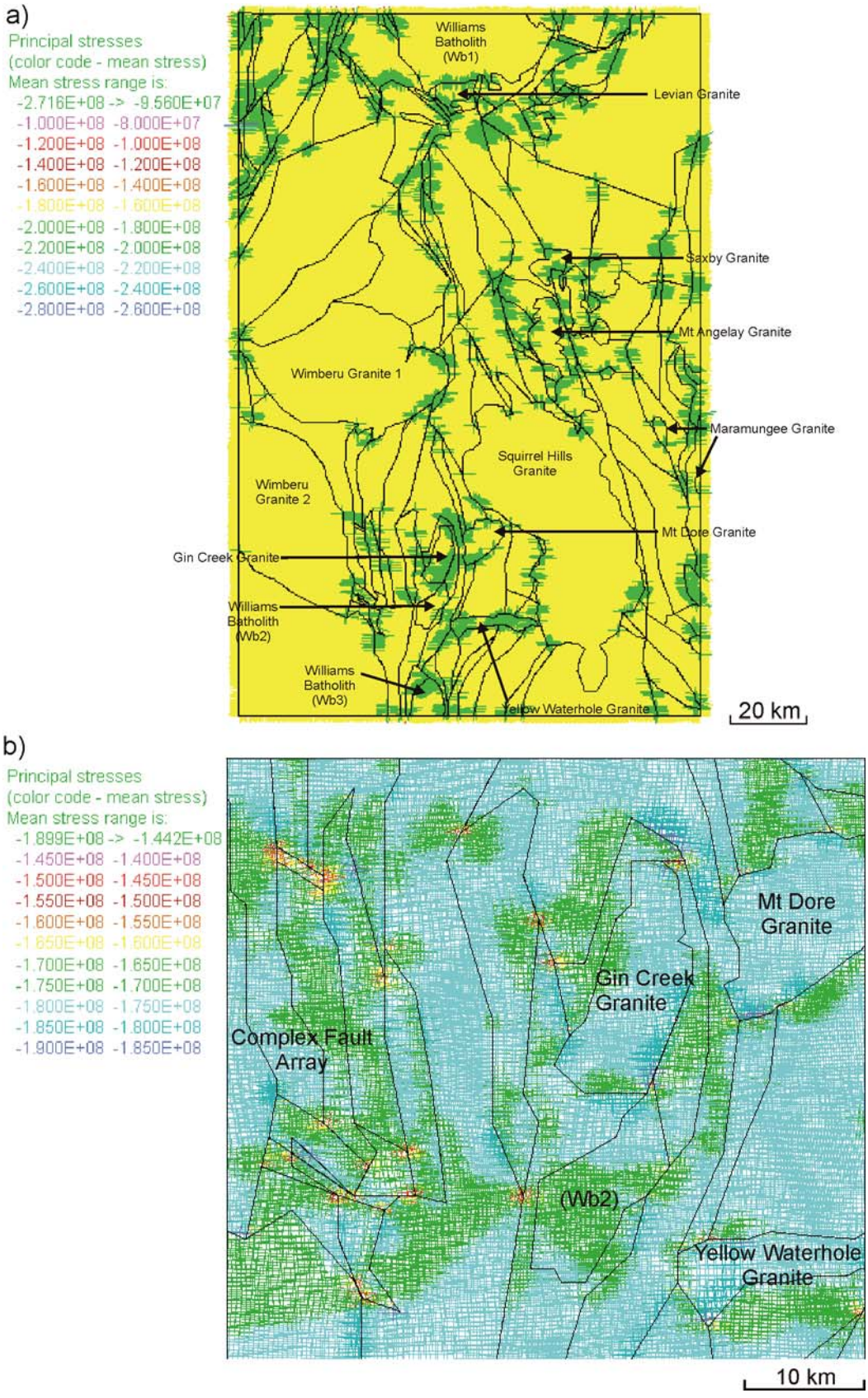

Fig. 27. Plots of mean stress for Model 2a a) regional plot displaying higher mean stress values at many fault intersections and fault bends b) magnified plot of the Selwyn area showing partitioning of stress in and around fault contacts. Lowest mean stress values are associated with fault bends and around intersections.

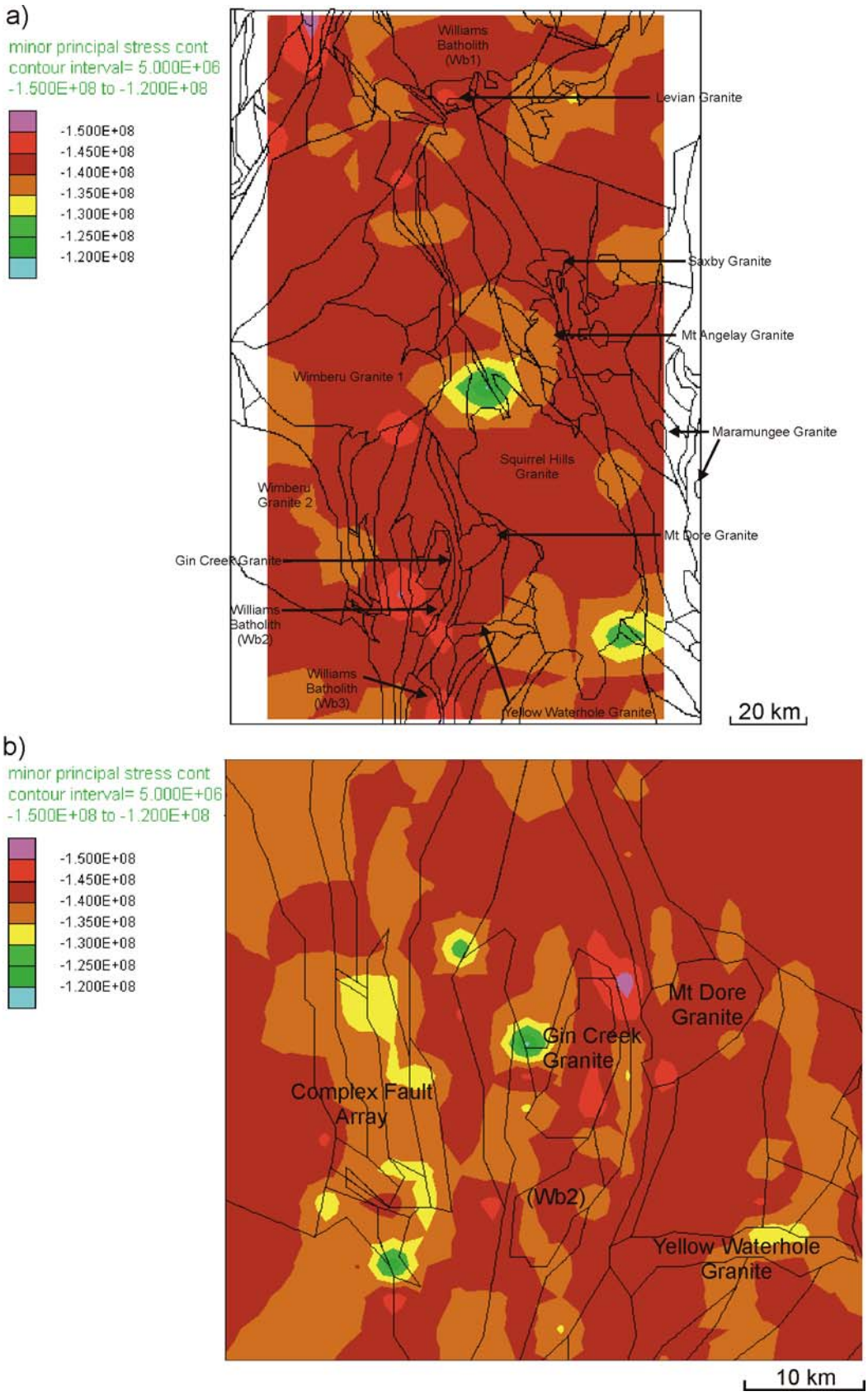

Fig. 28. Plots of minor principal stress for Model 2a a) regional plot indicating lowest values at the north and south of the Squirrel Hills granite and highest values in the Selwyn region b) magnified plot of the Selwyn area showing low values at specific fault intersections and a notable high value between the Mt Dore Granite and the Gin Creek Granite.

indicated by low values of $_3$ associated with fault intersections in the complex fault array to the west of the Gin Creek granite (Fig. 28b). However, the fault array directly on the west side of the Gin Creek granite displays two areas of low $_3$, which are situated at fault intersections. These two areas have values of around 30 to 40 MPa less than in Model 1a. The other obvious difference is the high $_3$ area at the NE corner of the Gin Creek granite and west of the Mt Dore granite. On the regional scale, values of Δ have a greater range (58 to 80 MPa) than in Model 1a, and areas of high Δ are evident at the north and south ends of the Squirrel Hills granite (Fig. 29a), and at the Selwyn scale high values of Δ are mostly related to fault intersections and bends (Fig. 29b). Lowest values of PF_f are found at fault intersections N to N/W of the Squirrel Hills granite and also near the Cloncurry region (Fig. 30a). The Selwyn region shows very similar distribution patterns to Model 1a; however values are around 20 to 30 MPa less (Fig. 30b).

In comparison to Model 1a (equivalent conditions), the addition of younger intrusions and a more complex fault pattern has a significant effect on many aspects of the model. The distribution and values of $_m$ are relatively unchanged in comparison to Model 1a, and patterns at the smaller Selwyn scale are very similar. Variation is noted in the distribution and values of $_3$ however, which can be attributed to the more complex fault patterns and competence contrasts between the metasediments and intrusions. Both values and distribution of Δ are significantly different relative to Model 1a, and are more noticeable at the Selwyn scale. There are similarities in the distribution of PF_f to Model 1a, but this model shows a significant variation in values, which are up to 30 MPa less.

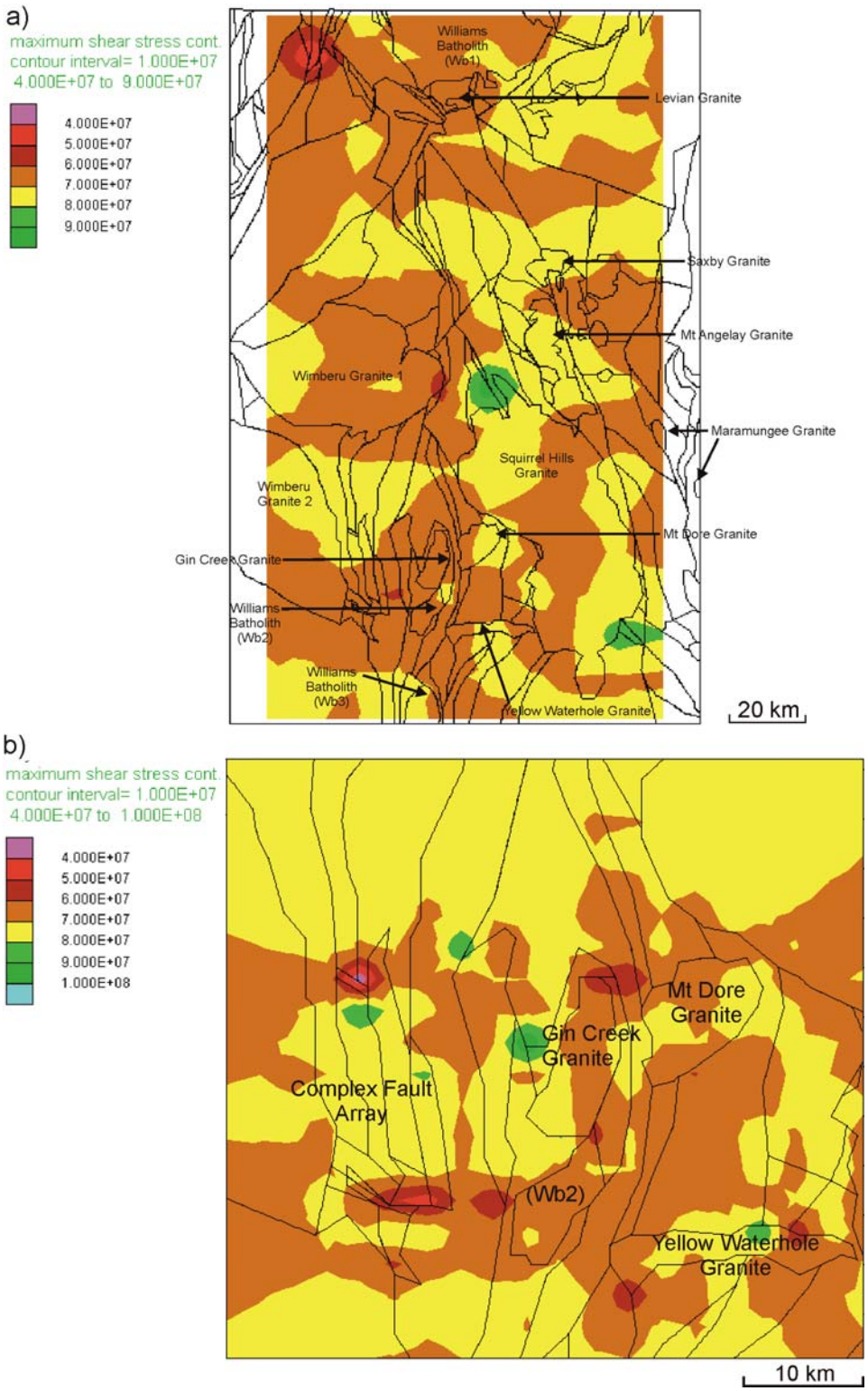

Fig. 29. Plots of differential stress for Model 2a a) regional plot illustrating highest values located at the northern and southern ends of the Squirrel Hills granite b) magnified plot of the Selwyn region displaying several specific areas of both high and low values associated with fault intersections.

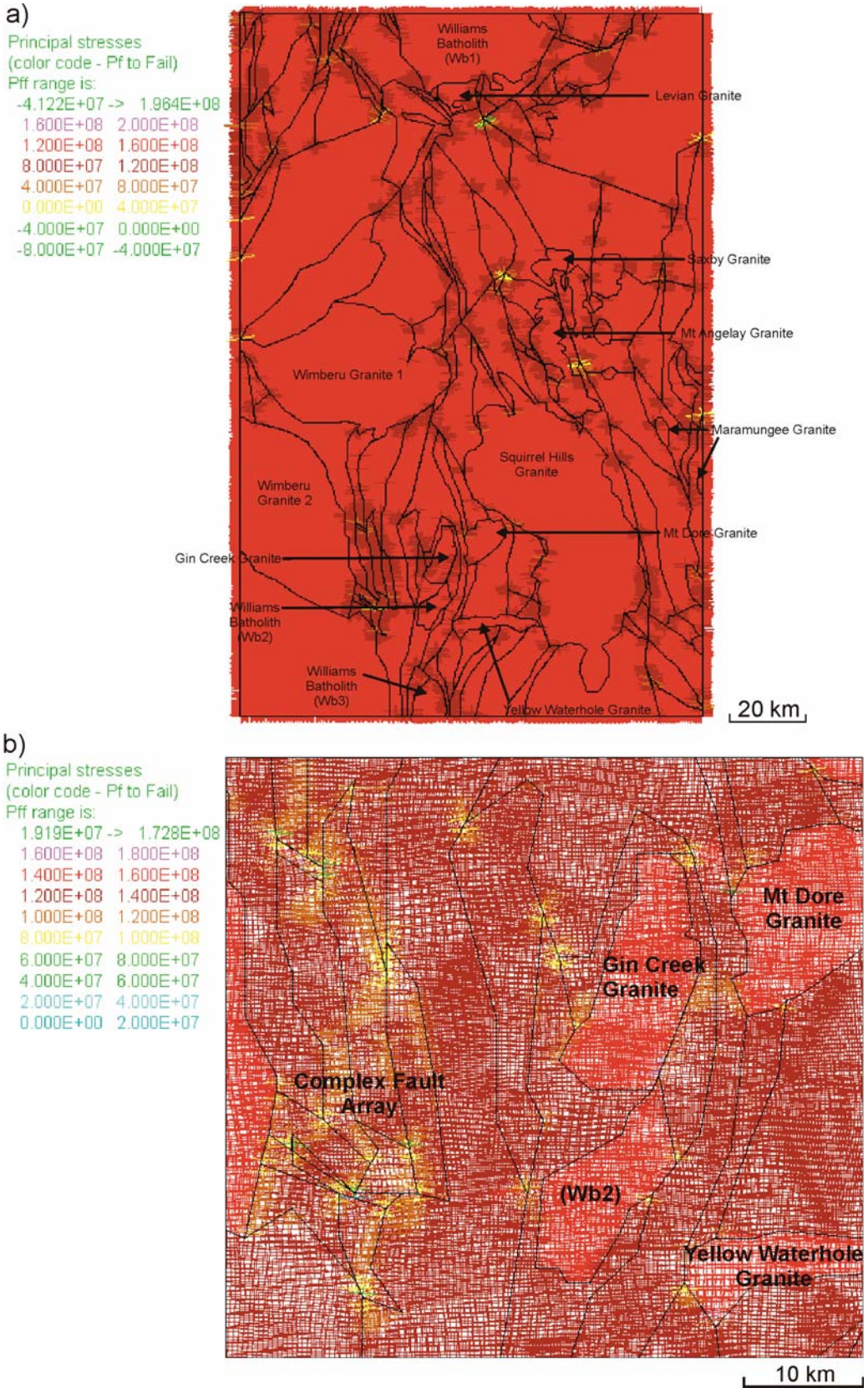

Fig. 30. Plots of fluid pressure required for failure for Model 2a a) regional plot displaying higher potential for failure mostly on fault bends and intersections. Note areas with negative values at yield, which correspond to deposits at Greenmount, Great Australia and on the Cloncurry fault b) magnified plot of the Selwyn area displaying very low values for failure at fault intersections.

4.2 **Model 2b**: no fluid pressure, $_1$ orientated ESE-WNW (112.5°)

The rotation of $_1$ has little effect on the distribution or values of $_m$, in comparison to the previous model and to Model 1b (Fig. 31). On the regional scale, a variation is apparent in magnitude and distribution of $_3$ when compared to the previous model (Fig. 32a), and this is more noticeable (up to 50 MPa less) at the Selwyn scale (Fig. 32b). Higher values of Δ are noticeable in comparison to the previous model, as is the distribution of Δ at both the regional and Selwyn scales. At the regional scale, areas of high Δ are most apparent at the northern and southern ends of the Squirrel Hills granite (Fig. 33a), and in the south are more prevalent in the complex fault array to the west of the Gin Creek granite and the east side of the Williams batholith (WB2) to the south (Fig. 33b). No major change relative to the previous model is noted in the PF_f on a regional scale (Fig. 34a), however an apparent compartmentalised pattern of PF_f emerges at the smaller scale (Fig. 34b), as a result of stress partitioning between intrusive bodies and fault arrays.

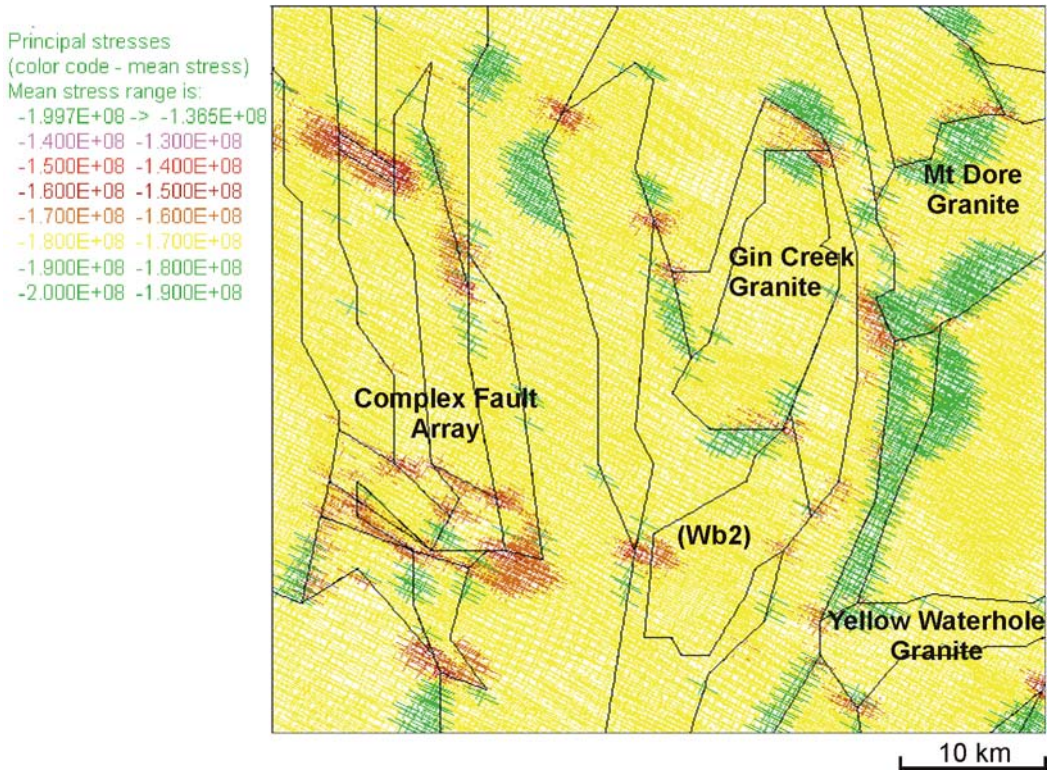

Fig. 31. Plot of mean stress for Model 2b in the Selwyn region, illustrating a modified stress distribution from Model 1b, particularly around the northern and eastern ends of the Gin Creek Granite.

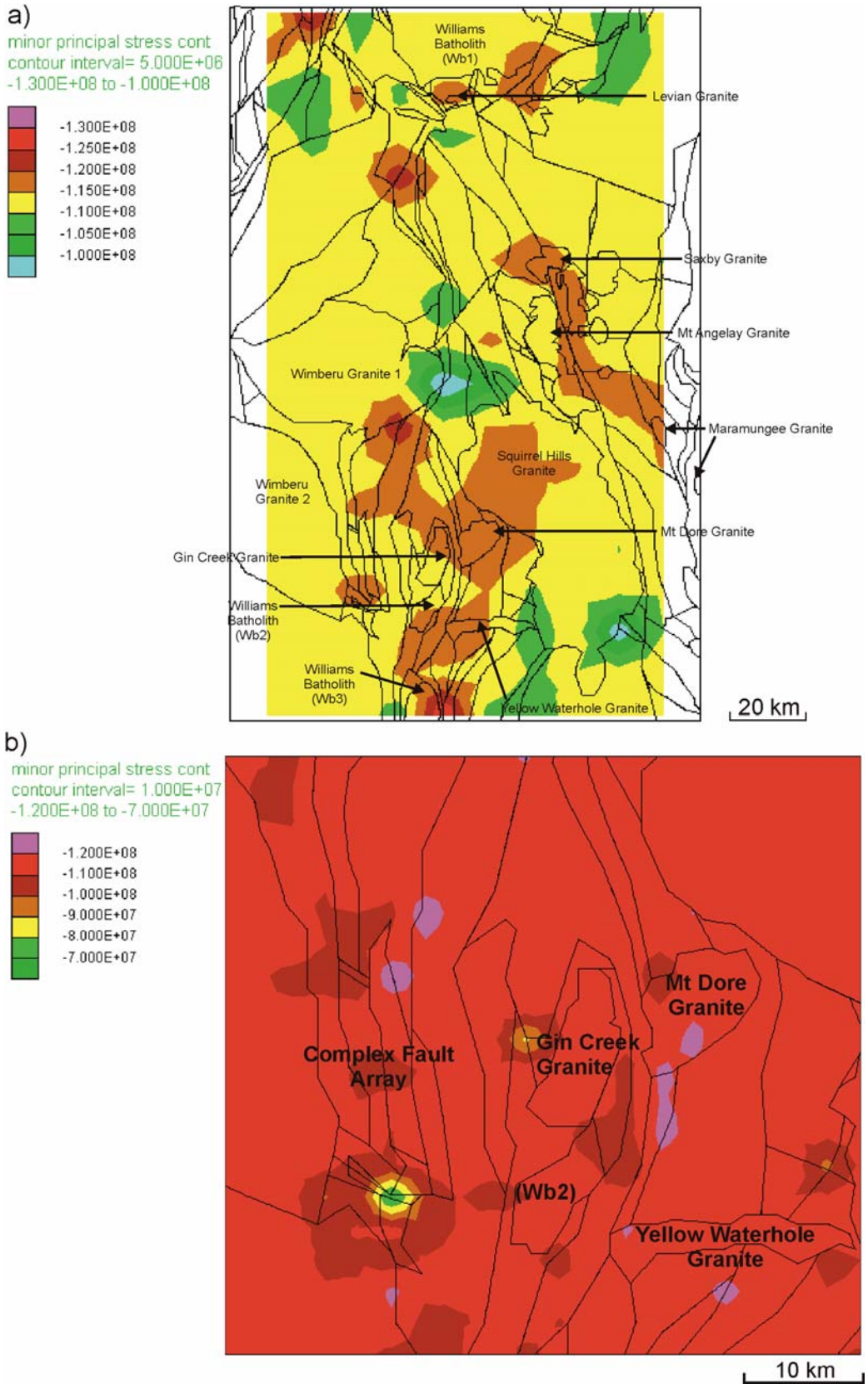

Fig. 32. Plots of minor principal stress for Model 2b a) regional plot indicating lowest values at the northern and southern ends of the Squirrel Hills Granite and the eastern side of the Wimberu granite b) magnified plot of the Selwyn area showing isolated low values to the west and south-west of the Gin Creek Granite. Values are considerably lower than the previous model.

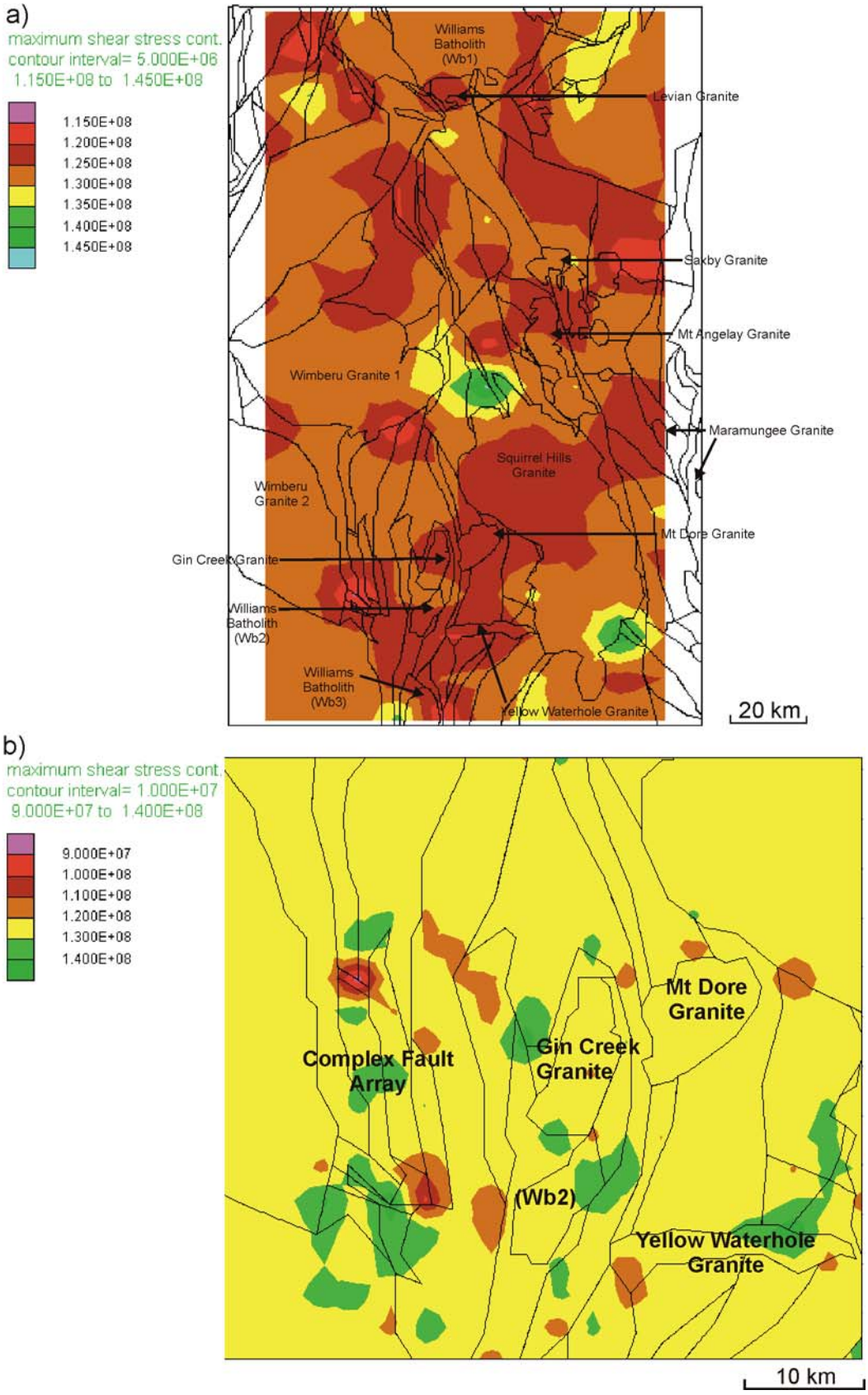

Fig. 33. Plots of increased differential stress for Model 2b in comparison to the previous model a) regional plot illustrating high values particularly in the northern and southern ends of the Squirrel Hills Granite b) magnified plot of the Selwyn region with high values again associated with fault intersections.

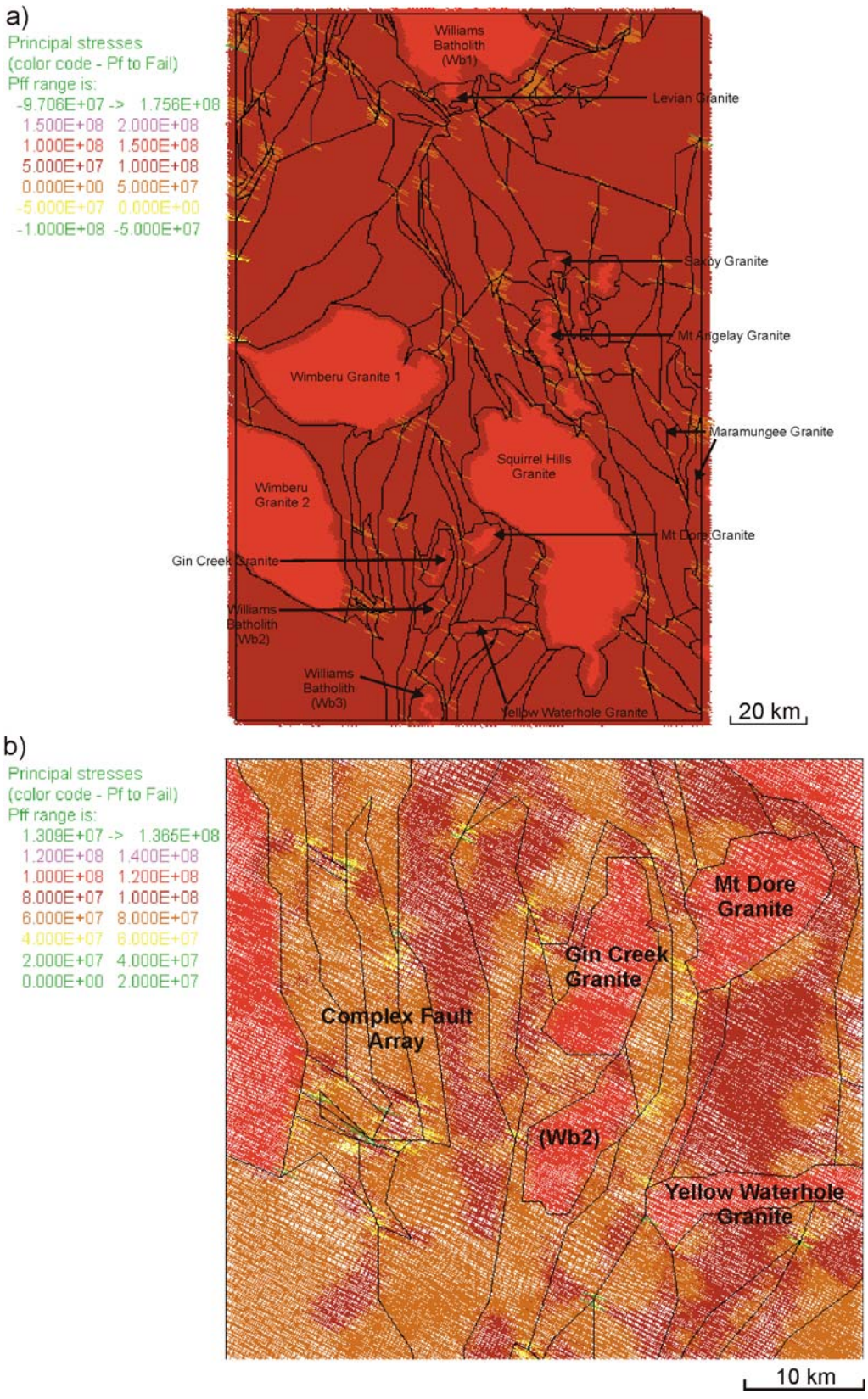

Fig. 34. Plots of fluid pressure required for failure for Model 2b, showing an overall decrease in values from the previous model a) regional plot displaying a distinct variation between granites and metasediments b) magnified plot of the Selwyn area displaying very low values for failure at fault intersections and a compartmentalised pattern emerging. Note: negative values indicate areas at yield.

In summary, no significant variation on the magnitude of $_m$ is noted relative to Model 1b, although there are minor effects on the distribution of $_m$ surrounding some of the new granites and faults. There is a considerable variation in the magnitude and distribution of $_3$ relative to the previous model. The regional distribution of Δ remains broadly similar to the previous model, however values generally increase. Overall a decrease in values of PF_f and significant compartmentalisation of PF_f is seen in this model.

4.3 **Model 2c**: fluid pressure, E-W compression ($_1$ = 90°)

The introduction of fluid into the model fractures results in a considerable variation in the distribution and magnitude of $_m$ relative to Model 2a, with highest values concentrated around granite contacts in the Cloncurry and Selwyn regions, and around the northern parts of the Squirrel Hills granite (Fig. 35a). The Selwyn region also displays a significant change in distribution of the magnitude of $_m$, with a noteable partitioning of stress between fault blocks (Fig. 35b). Two distinct areas of low $_3$ are evident in the regional model, west of the Gin Creek granite and at the southern tip of the Squirrel Hills granite (Fig. 36a) with values around 20 MPa less than in Model 2a. At the Selwyn scale a significantly different distribution of $_3$ is apparent with low values associated with fault bends and intersections (Fig. 36b) which do not correspond to similar areas in Model 2a. On the regional scale, Δ is distinctly different from the previous two models, showing highest values in the Selwyn region and the northern tip of the Mt Dore granite (Fig. 37a). The Selwyn region displays highest values of Δ in the corridor between the Gin creek and Mt Dore granite and on the Squirrel Hills granite contact north of the Mt Dore granite (Fig.
5.37b). Minimum PF_f on the regional scale is more apparent around the Cloncurry region, the Selwyn region and the southern tip of the Squirrel Hills granite (Fig. 38a) and two distinct corridors can be seen near the Gin Creek and Mt Dore granite. This is more obvious at the Selwyn scale, which displays two distinct corridors of low PF_f anastomosing between the more competent granite bodies and compartmentalised by fault arrays (Fig. 38b).

In summary, the influence of fluid pressure within the fractures of the model results in a distinct variation in the distribution of $_m$ and $_3$ relative to Model 2a. Low values of $_3$ correspond well to dilation and these areas correspond to areas of increased values of Δ . Within the Selwyn region two distinct corridors, separating the Mt Dore and Gin Creek granite and the more complex fault array to the west, show high values of Δ and low values of PF_f.

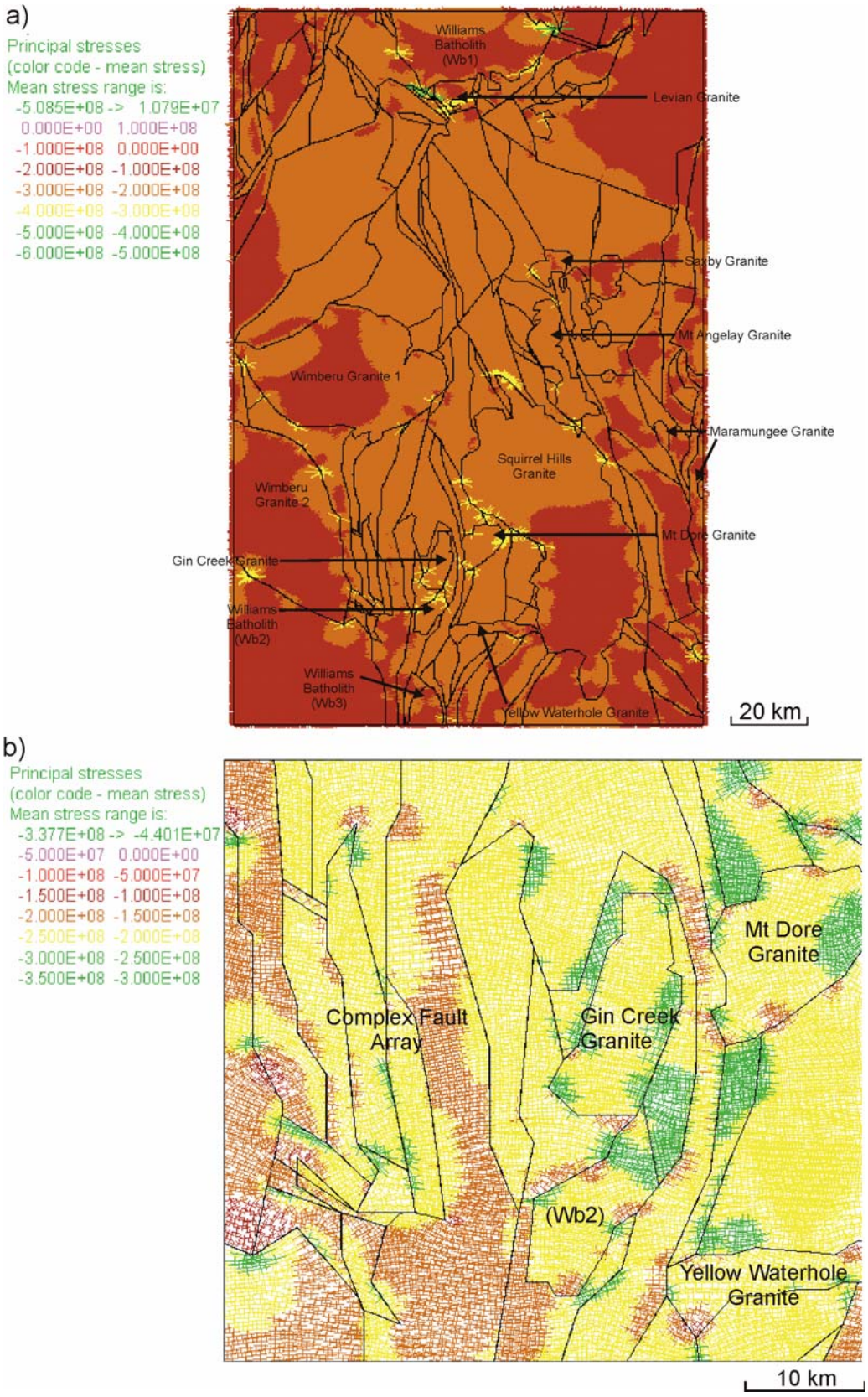

Fig. 35. Plots of mean stress for Model 2c showing a marked increase from previous models a) regional plot displaying high mean stress values at metasediment-granite contacts, isolated fault intersections and bends b) magnified plot of the Selwyn area showing a large variation in values.

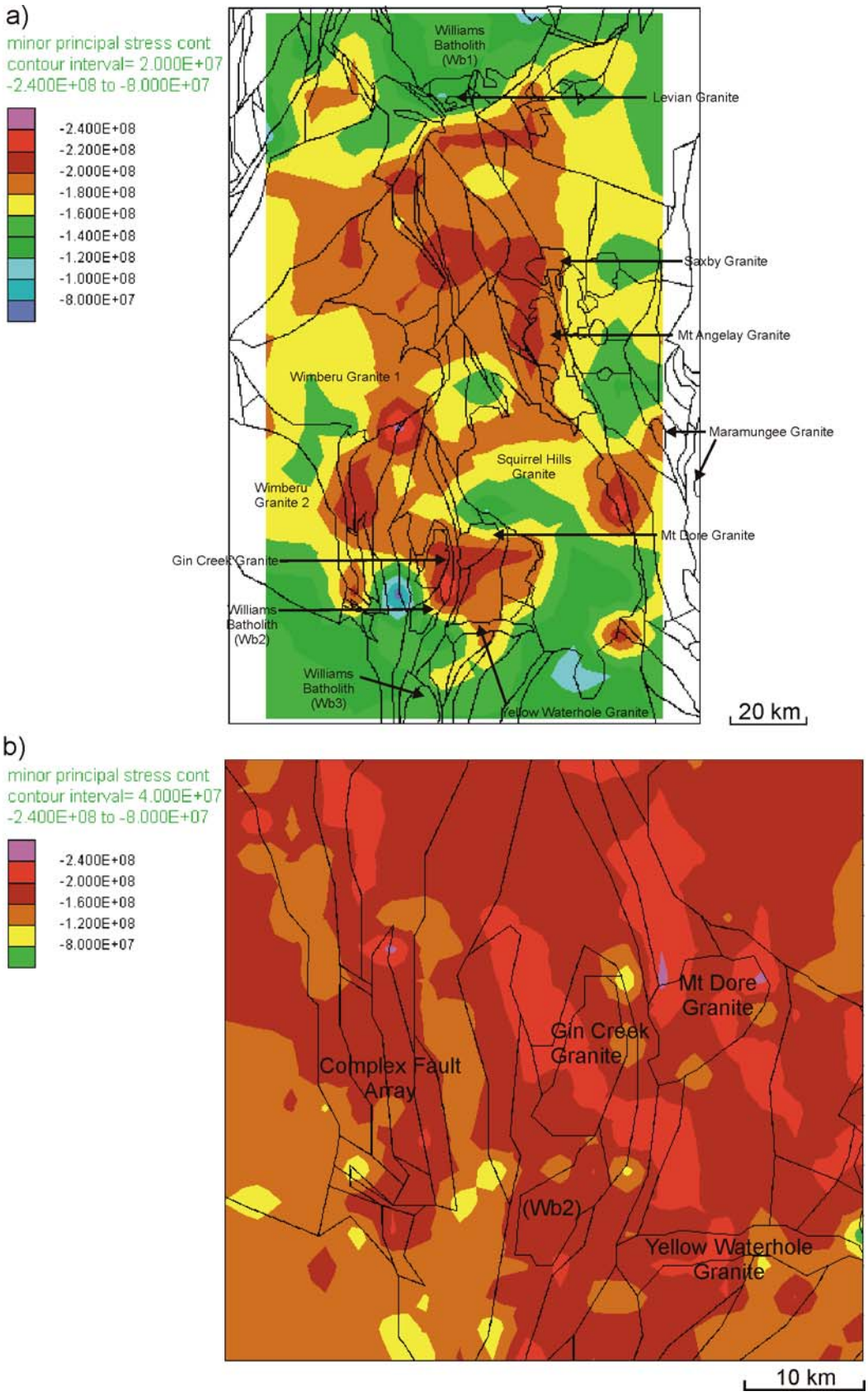

Fig. 36. Plots of minor principal stress for Model 2c a) regional plot indicating lowest values in the Selwyn region and southern end of the Squirrel Hills Granite b) magnified plot of the Selwyn area showing distinct trends in low values particularly between the Mt. Dore and Gin Creek granites and fault bends and intersections.

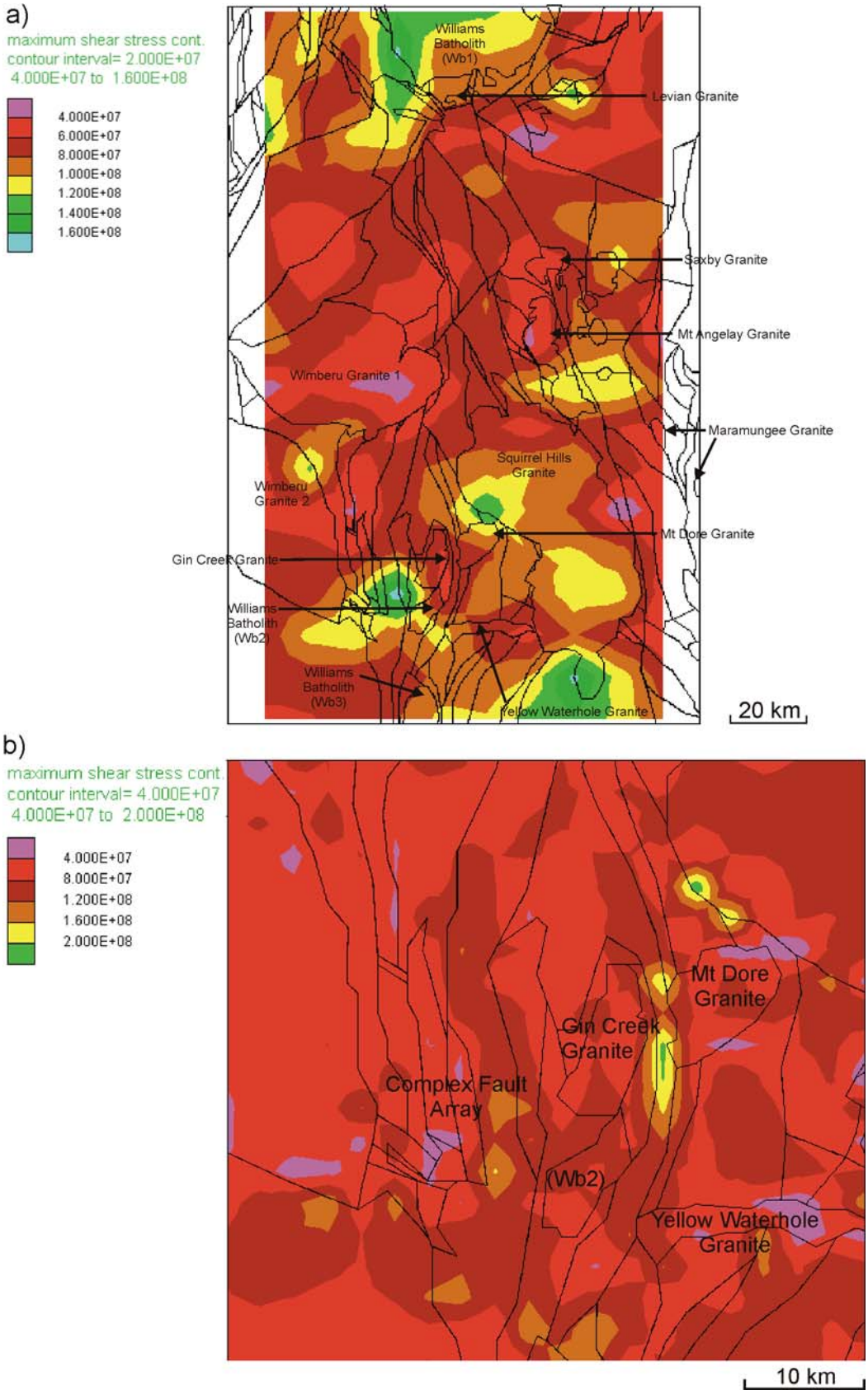

Fig. 37. Plots of increased differential stress for Model 2c in comparison to the previous model a) regional plot illustrating high values particularly in the northern region, Selwyn region and the Squirrel Hills Granite b) magnified plot of the Selwyn region with high values apparent in the Selwyn high strain zone.

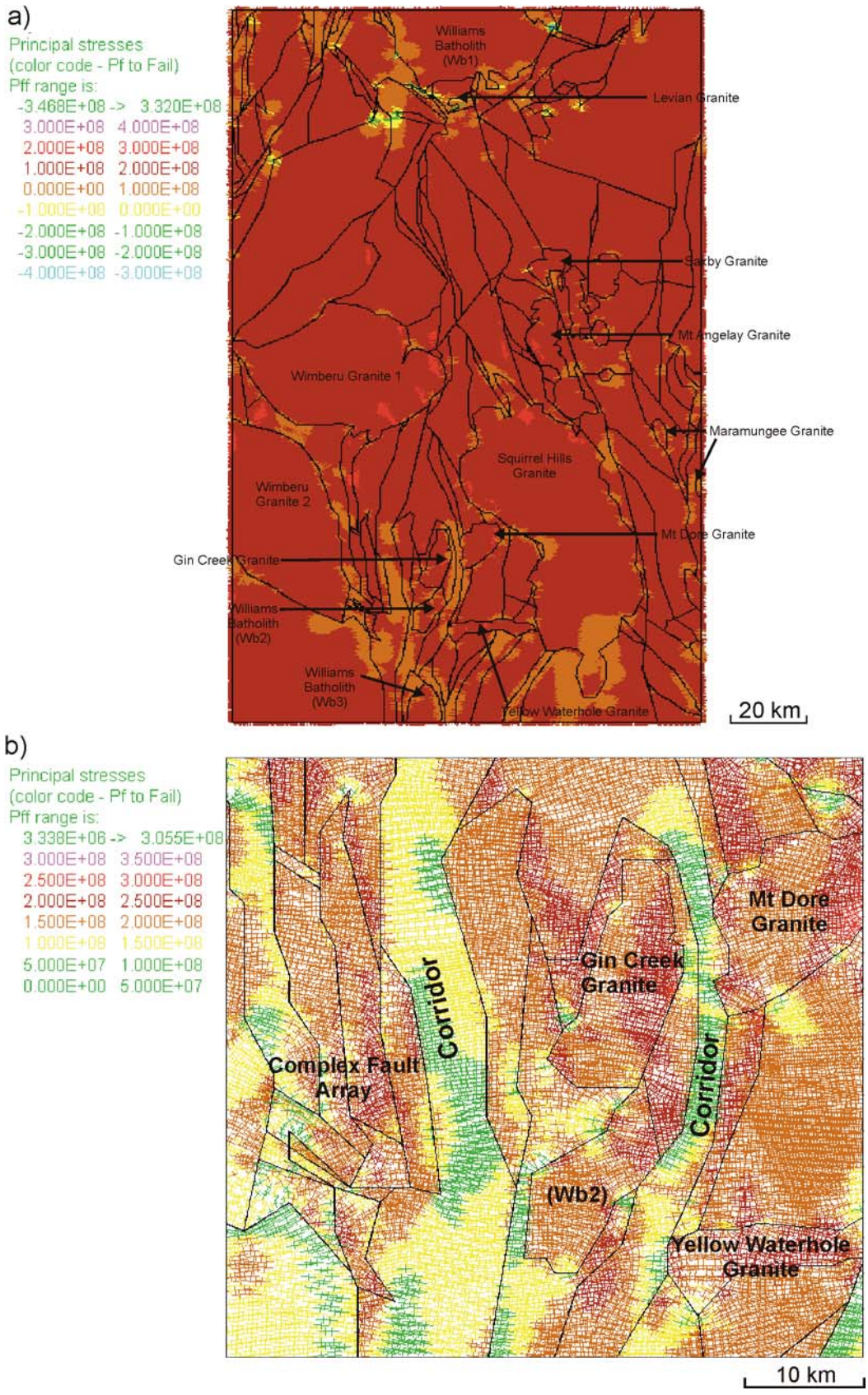

Fig. 38. Plots of fluid pressure required for failure for Model 2c, a) regional plot displaying several areas in the northern region at yield, and strong trends in the Selwyn region anastomosing the granite bodies b) magnified plot of the Selwyn area displaying distinct north-south trends forming 'corridors'. Note: negative values indicate areas at yield.

4.4 **Model 2d**: fluid pressure, $_1$ orientated ESE-WNW (112.5°)

Rotation of $_1$ results in a similar but more intense distribution of high $_m$ around lithological contacts and little variation at fault bends or intersections when compared to the Model 2c (Fig. 39). On a regional scale both the magnitude and distribution of $_3$ show similarities to Model 2c, however areas such as the east side of the Wimberu granite (1) and the southern tip of the Squirrel Hills granite display much lower $_3$ values (Fig. 40a). At the Selwyn scale, similarities to the Model 2c are also apparent, although areas of low $_3$ can be found around the Yellow Waterhole and Mt Dore granite (Fig. 40b). The distribution of Δ has some marked differences to the Model 2c, primarily a very high value at the southeast contact of the Squirrel Hills granite (Fig. 41a); however at the Selwyn scale these differences are less obvious (Fig. 41b). One striking difference is the three areas of high Δ to the northeast of the Gin Creek granite, which indicate values of up to 200 MPa greater than the same area of Model 2c. Both the distribution and magnitude of PF_f on the regional scale have little variation relative to Model 2c (Fig. 42a). At the smaller scale, patterns and values of PF_f are broadly similar to Model 2c, with distinct corridors of PF_f noted between granite bodies and fault arrays (Fig. 42b).

In summary, the rotation of $_1$ intensifies the distribution of high $_m$ which is primarily noted on lithological contacts. Several differences in distribution of $_3$ are also apparent relative to Model 2c. The most marked effect in this model is the change in both distribution and magnitude of Δ , which indicates the potential for more intense deformation in these regions. PF_f is overall relatively unchanged in comparison to the previous model.

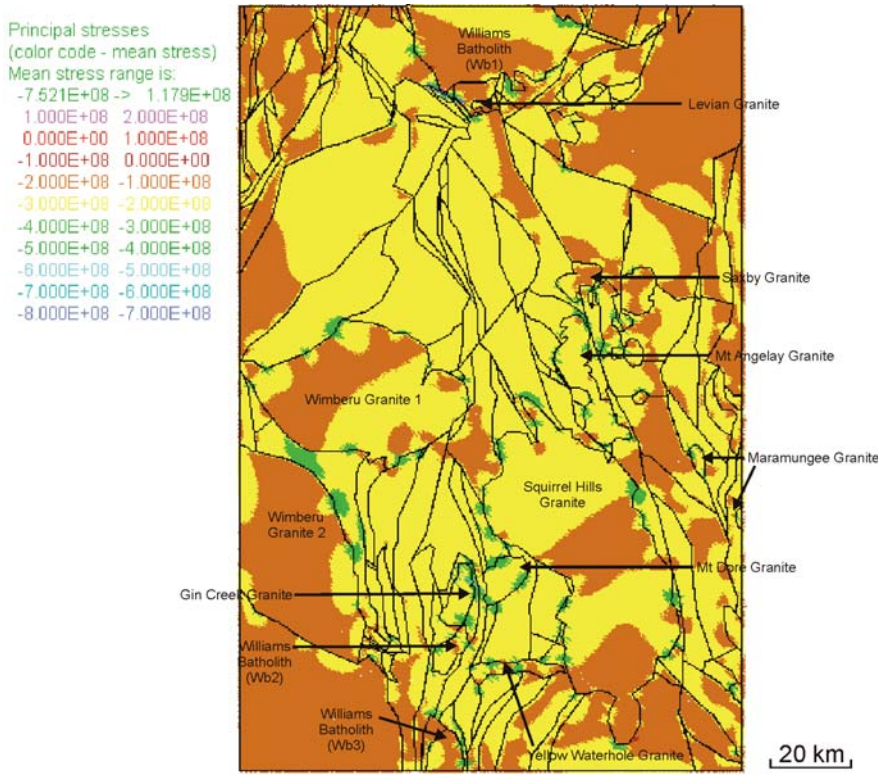

Fig. 39. Regional plot of mean stress for Model 2d displaying high mean stress values at metasediment-granite contacts, isolated fault intersections and bends.

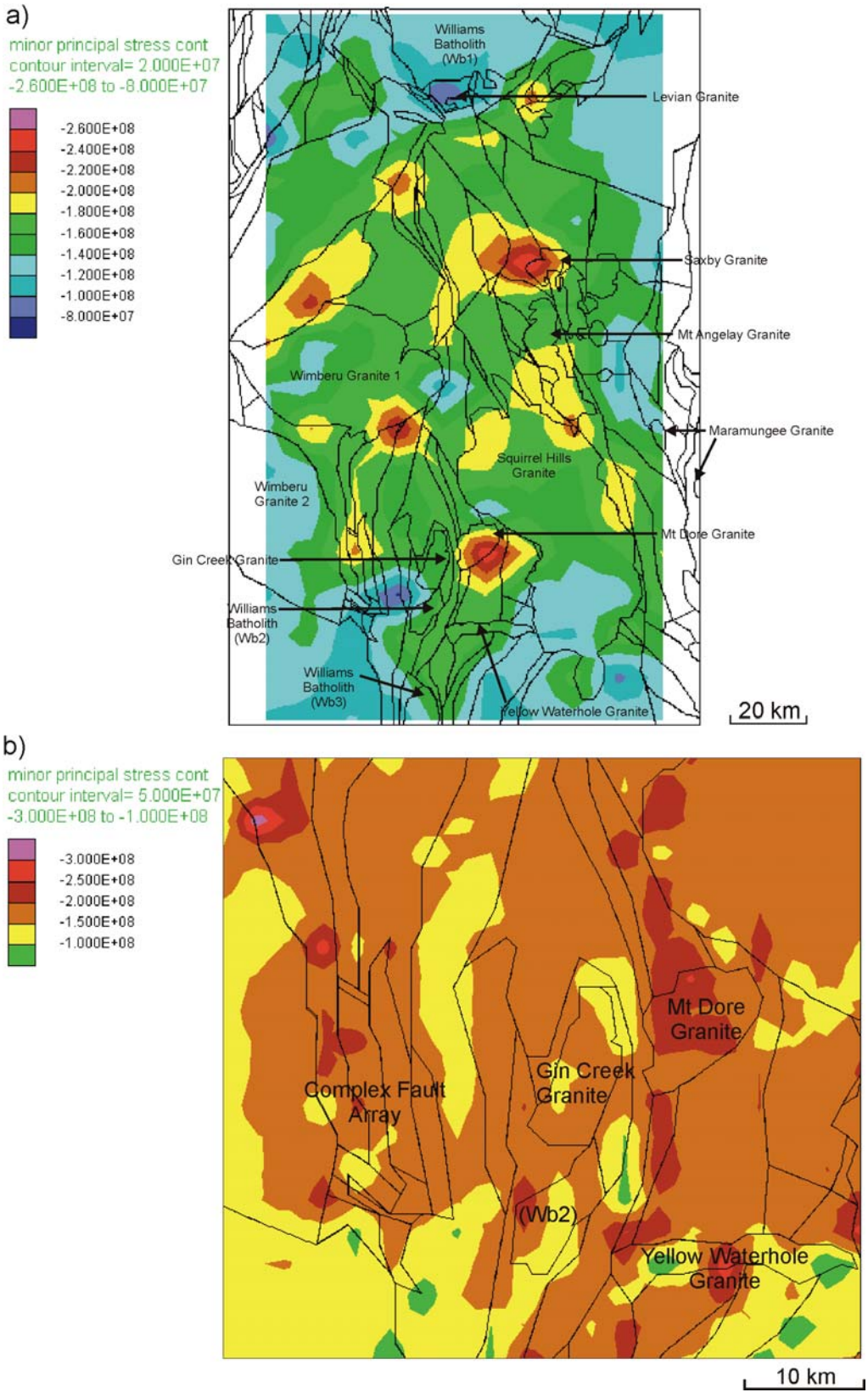

Fig. 40. Plots of minor principal stress for Model 2d a) regional plot indicating isolated areas of increased values north of the Mt. Angelay Granite, northern and southern contacts of the Wimberu Granite and the southeast side of the Mt. Dore Granite. Lowest values correspond to the south end of the Squirrel Hills Granite, the Cloncurry region and around the Selwyn region b) magnified plot of the Selwyn area showing distinct trends in low values particularly between the Mt. Dore and Gin Creek granites.

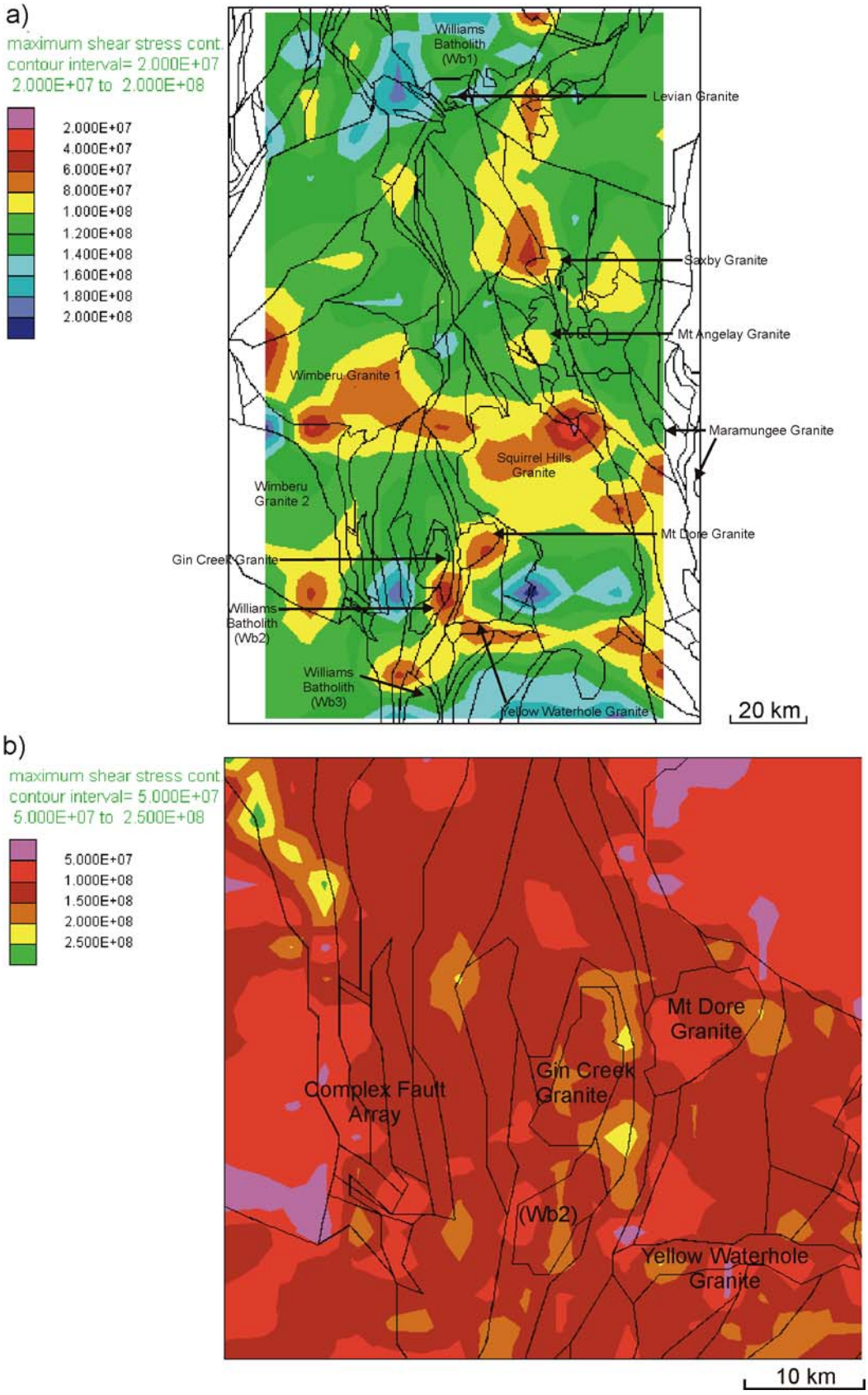

Fig. 41. Plots of increased differential stress for Model 2d in comparison to the previous model a) regional plot illustrating high values particularly in the Selwyn region and on the west side of the Squirrel Hills Granite b) magnified plot of the Selwyn region with very high values apparent east of the Gin Creek Granite and close to the Wimberu Granite (2).

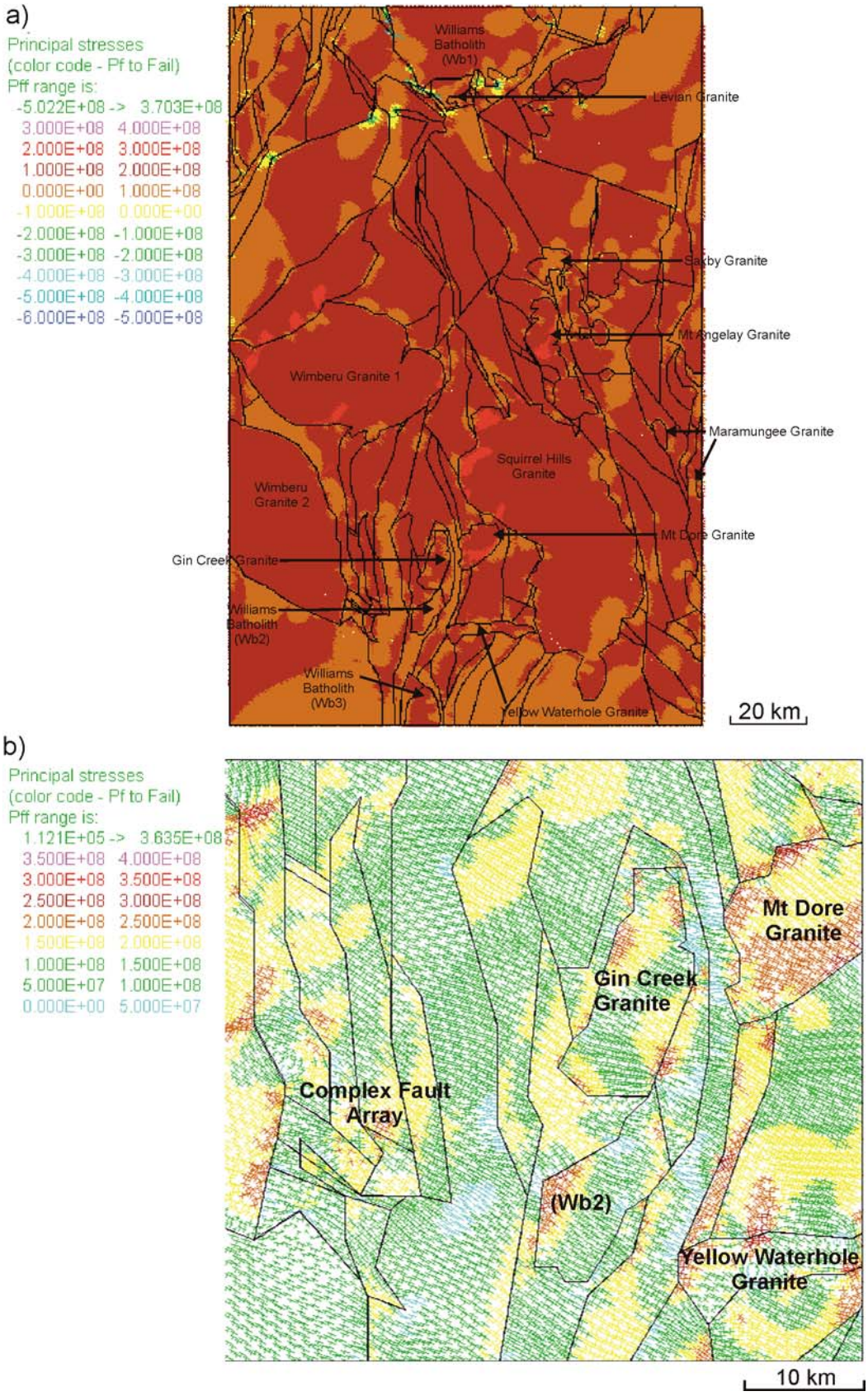

Fig. 42. Plots of fluid pressure required for failure for Model 2d a) regional plot displaying a general decrease in area requiring high PF_f b) magnified plot of the Selwyn area showing lowest values focussed between the Mt. Dore and Gin Creek granites. Note: negative values indicate areas at yield.

5.0 APERTURE AND FLUID FLOW BEHAVIOUR

The effect of stress on the opening and closing of fractures, and its relationship to fluid flow, was explored. Models were set up with the same geometry as Model 2, and given initial fracture properties such as permeability and aperture sizes. Flow was then initiated from source points around younger granite bodies e.g. < 1530 Ma (see Fig. 4) and direction, flow velocities and rates of flow were monitored. Due to limitations of two dimensional modelling, fluid flow directions only represent a component of three dimensional flow, and may have little actual significance. The potential for lateral fluid flow in this area is less likely than upward or vertical fluid migration, even during strike-slip deformation, as described by Sibson (1996); hence these results are used only to estimate potential maximum values of lateral flow within this system. These results have little bearing on the overall prospectivity analysis of the area in comparison to the results stated previously, as areas that show a higher potential for mineralisation are primarily related to the partitioning of stress during deformation. However, these results do provide insight into lateral flow rates from potential fluid point sources.

Faults or contacts at low angles to $_1$ generally display an increase in aperture, with maximum apertures recorded at 0.15m which correspond to maximum flow velocities in the Cloncurry region of up to $3.337e^{-5}$ ms^{-1} and maximum volumetric flow of up to $9.767e^{-7}$ m^3s^{-1} (Fig. 43ab). Volumetric flow rates (volume/time) were examined in the Selwyn and Cloncurry regions at history points pp1 and pp3 (see Fig. 4). Volumetric flow rates in the Cloncurry region display an initial sharp increase, which then becomes stable and attains a steady state flow condition (Fig. 44a), whereas flow rates in the Selwyn region display an initial sharp increase followed by a relatively constant increase throughout time (Fig. 44b). These differences may be linked to the spatial association of these areas with fluid point sources, as the Selwyn area has a greater number of proximal fluid sources relative to the Cloncurry region, therefore higher volumetric rates would be expected. On closer examination, dilatancy of fractures or increase in aperture, and hence volumetric flow, has a close association with decreased values of $_3$ and increased values of Δ and dependant on relative orientation to $_1$ (Fig. 45a). However, this statement is a generalisation, as aperture behaviour and ultimately fluid flow is strongly controlled by local stress fields. As complex patterns of deformation partitioning emerge, it is clear that local patterns and block geometry (i.e. orientation to $_1$) have a strong influence on fracture behaviour, as similarly orientated fractures throughout the model behave differently. Fractures that exhibit dilation and increased aperture width are primarily controlled by a decrease in normal stress adjacent to the fracture walls, and this is commonly related to the fracture orientation to $_1$ and local deformation patterns (Fig. 45b). Further useful work on this aspect of the model could only be achieved in 3D.

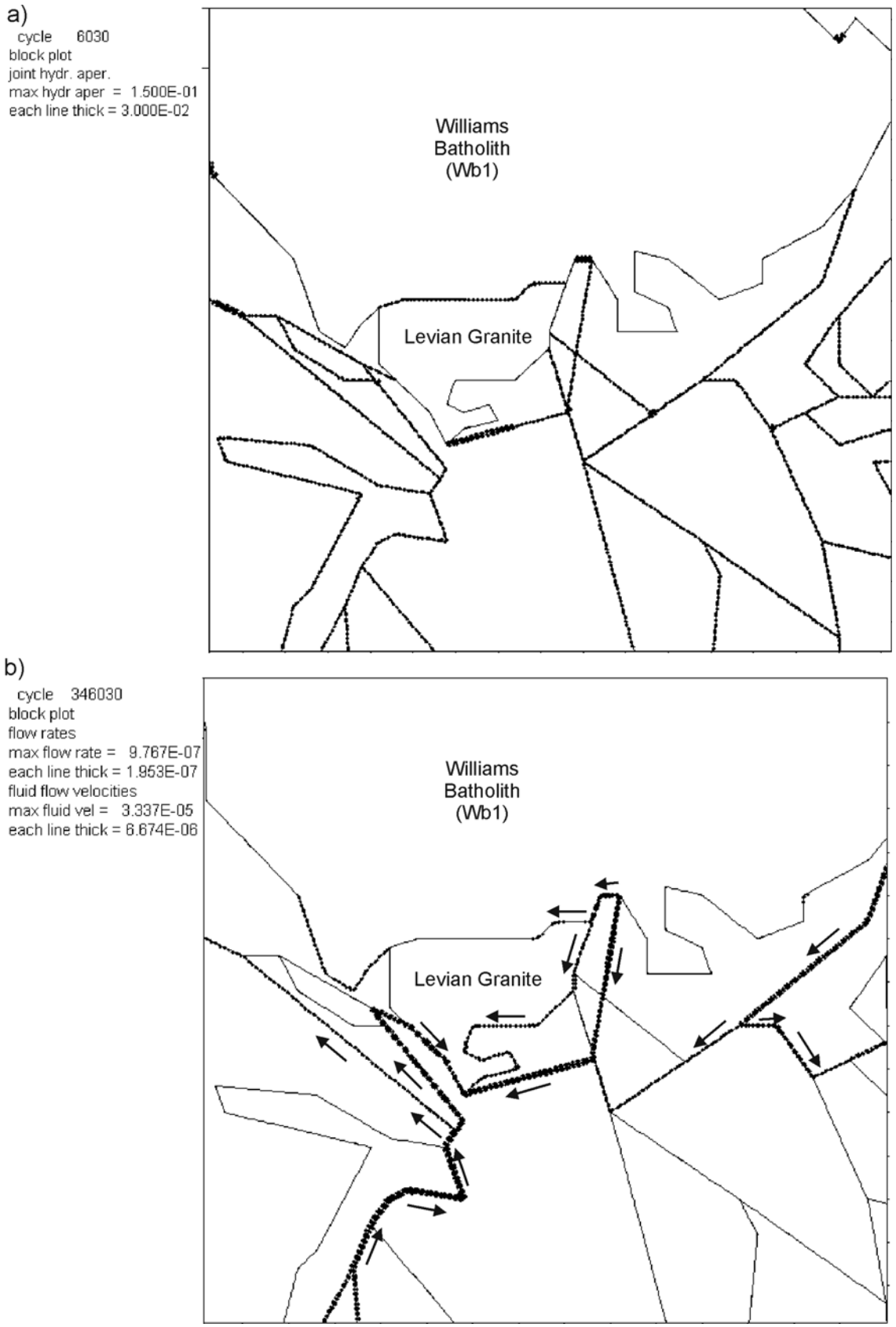

Fig. 43. Plots of joint hydraulic aperture, flow rates and velocities for the Cloncurry region Model 2 a) aperture widths of the fractures, maximum aperture opening generally found on faults at low angles to maximum principal stress b) maximum flow rates of the Cloncurry region (arrows represent flow direction).

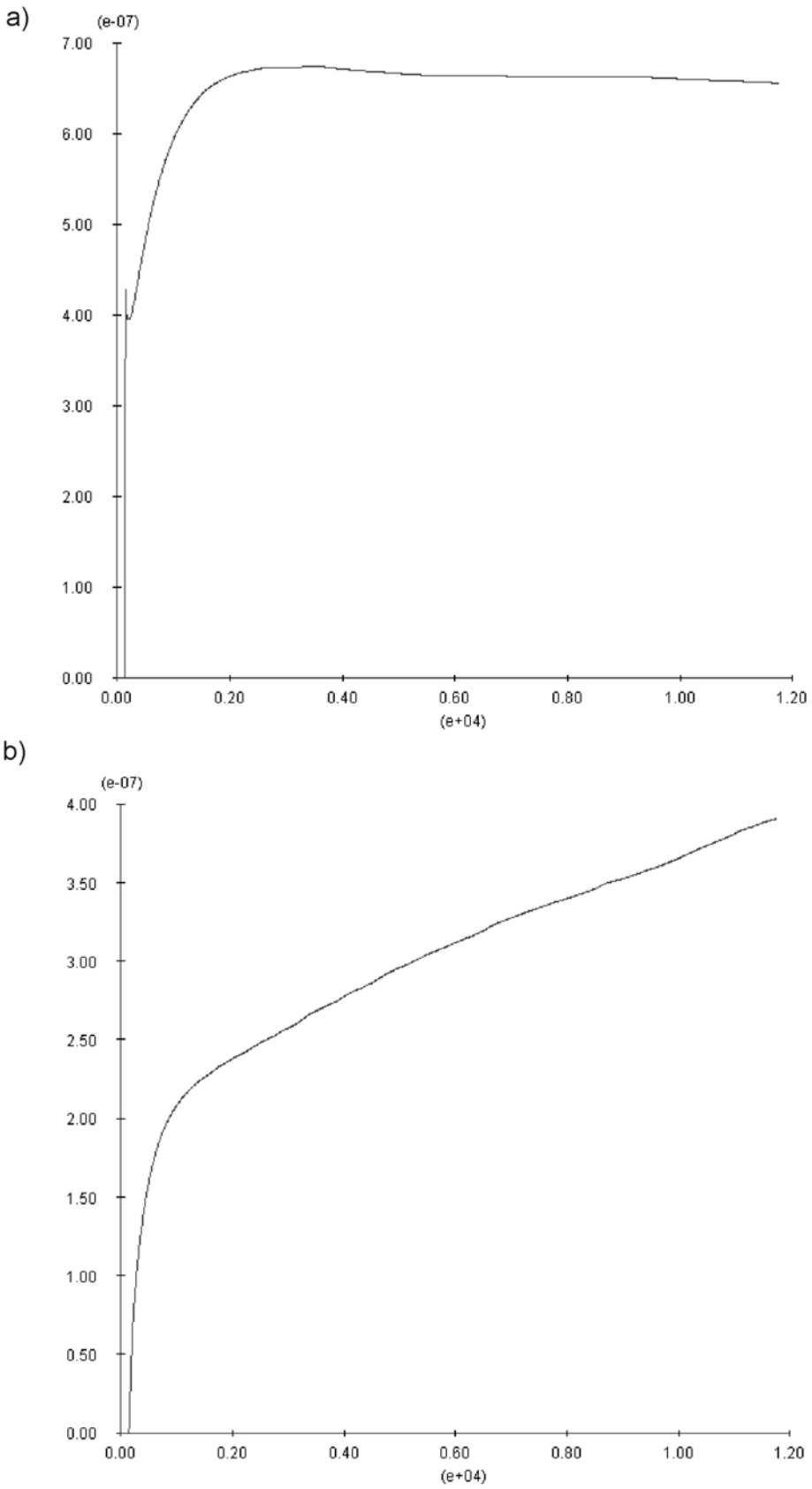

Fig. 44. Volumetric flow rates at history points pp1 (Cloncurry region) and pp3 (Selwyn region) a) history point pp1 displays an initial rapid increase in flow rate which after reaching its peak produces a stable rate b) history point pp3 displays an initial rapid increase in flow rate and continues to increase throughout the model run.

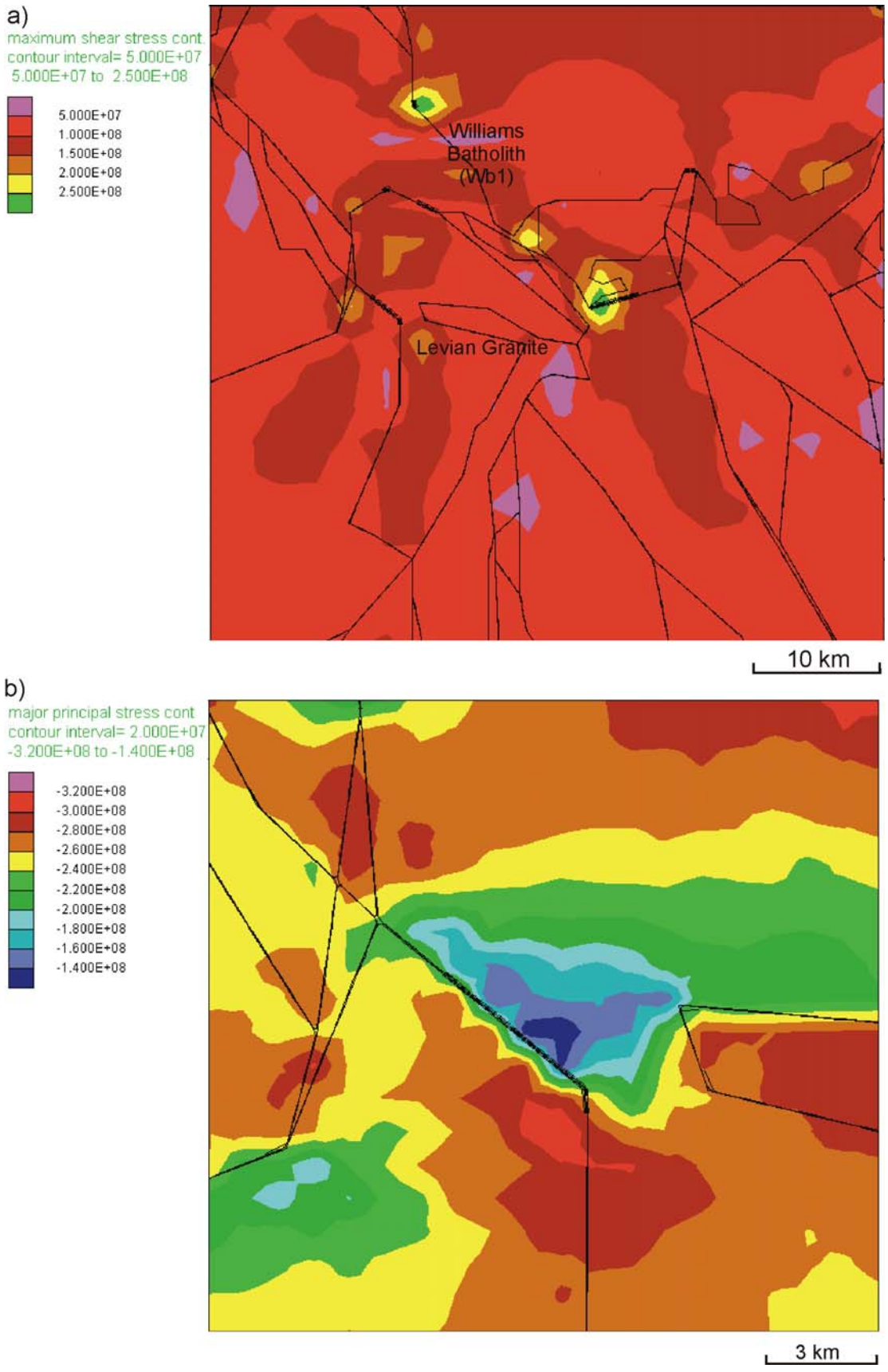

Fig. 45. Plots of aperture widths and mean stress a) Cloncurry region illustrating the relationship between high values of differential stress and increased aperture width b) fracture indicating the relationship between low values of major principal stress and aperture width.

6.0 PROSPECTIVITY AND MINERALISATION

Mustard *et al*. (2004) identified several ingredients in their prospectivity analysis that favoured deposit localisation. In order of importance, these were considered to be a) fault orientations, b) fault intersections, c) fault bends, d) magnetic anomalies and e) proximity to the boundary between Corella Formation and Soldiers Cap contacts. Butera (2004) also notes a strong correlation between deposit distribution and mafic intrusions in a more detailed area of the Eastern Succession, similar in size to the Selwyn region of this study. Unlike the work by Mustard *et al.* (2004), this work focuses on the complex interactions involved in both the mechanical and fluid plumbing systems within the Eastern Succession. No single specific factor has been highlighted as highly prospective, however, the main combinations of ingredients required to increase the potential for mineralisation have been explored.

Comparisons with known areas of mineralisation has been encouraging, in that several areas have been highlighted that contain medium to large deposits (e.g. Selwyn, Greenmount, Pegmont, and Great Australia) and many smaller deposits and prospects. Another interesting observation is the fact that 'barren' areas have also been highlighted (e.g. N/NE trending faults north of the Selwyn region, N/NW trending faults east of the Squirrel Hills granite, and N/E trending fault northwest of the Wimberu granite). Several areas have also been highlighted that at present have no current known deposits.

The ability to predict areas at yield or failure within the region allows a better understanding on the effects of fluid pressure and stress on the architecture of the system, and ultimately potential sites for fluid focussing and mineralisation. The plasticity indicator in UDEC allows the examination of these potential sites. The initialisation of fluid pressure within the fractures has a significant effect on failure within the model, as does changing the orientation of the stress field. The 'dry' models indicate only a few sites at yield (Fig. 46ab), and a significant effect can be seen when fluid pressure is added and then rotation of $_1$ both at the regional scale (Fig. 47ab) and the Selwyn scale (Fig. 48ab). The results from this study indicate that a 'wet' model with a rotation of $_1$ to 112.5° provides the best correlation with known deposits in the region, hence better for predicting mineralisation. The correspondence between the results of the prospectivity analysis by Mustard *et al.* (2004) and these results, show many correlations with many areas considered prospective within this study both regionally (Fig. 49ab) and at the Selwyn scale (Fig. 50ab). Of the many deposits and prospects indicated by Mustard *et al*. (2004), around 80% of them are predicted by this UDEC modelling. Further targets areas have been predicted by this UDEC modelling and these locations may make good exploration targets.

A major consideration relevant to highlighting areas with potential prospectivity appears to be linked to deformation and fluid flow relationships. As this modelling is mainly focussed on fracture systems, areas that provide a combination of low values of $_m$, $_3$ PF_f, increased Δ and high volumetric flow rates provide the best targeting solution for mineralisation.

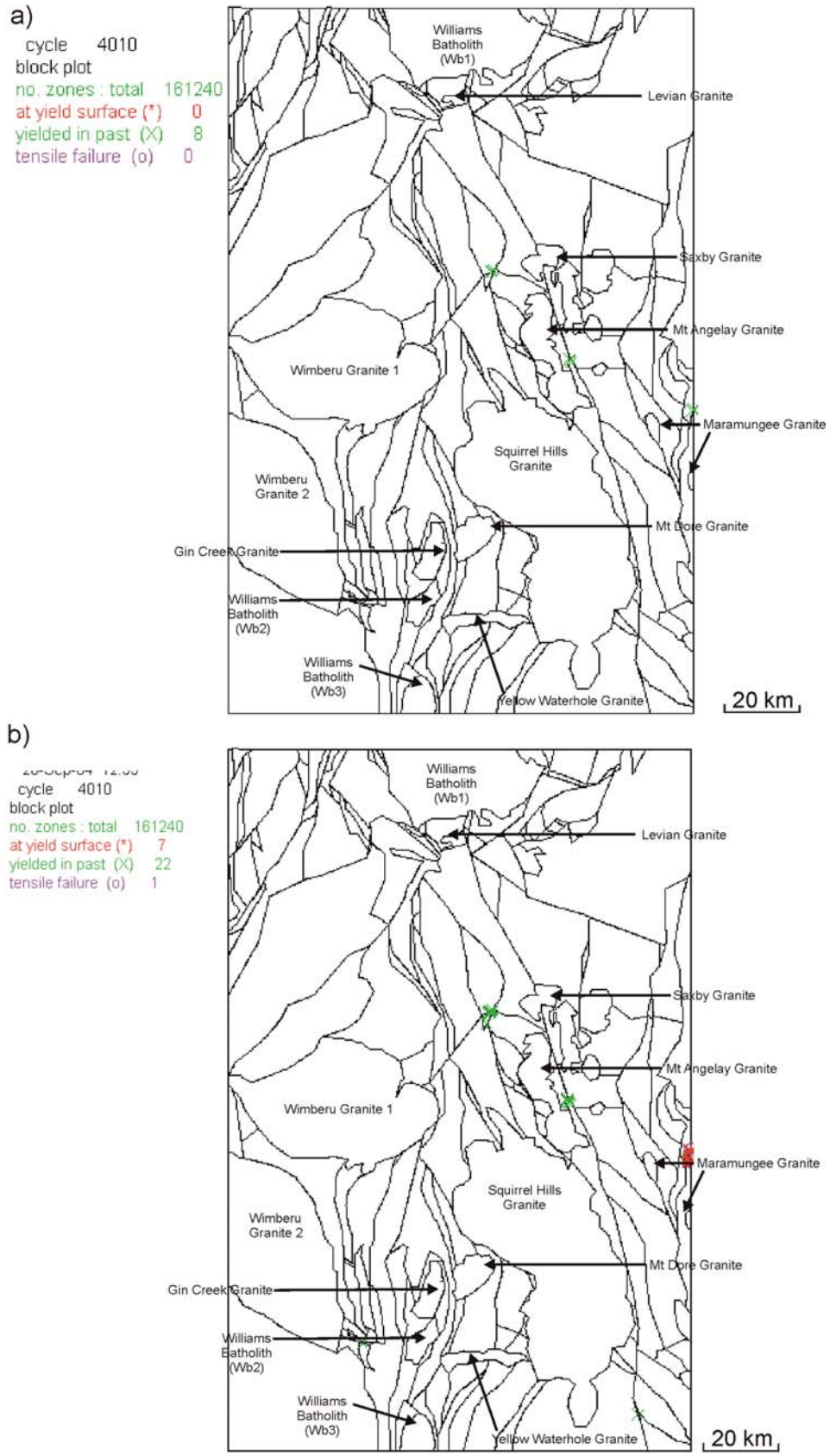

Fig. 46. Plasticity state comparison of Models 2a and 2b a) 'dry' model $\sigma_1 = 90°$ and b) 'dry' model $\sigma_1 = 112.5°$. Rotation of σ_1 has caused greater failure although has limited effect on distribution. Note: red indicates areas at yield, green indicates previously at yield but now not in contact with the failure envelope, and purple indicates areas in yield in tension.

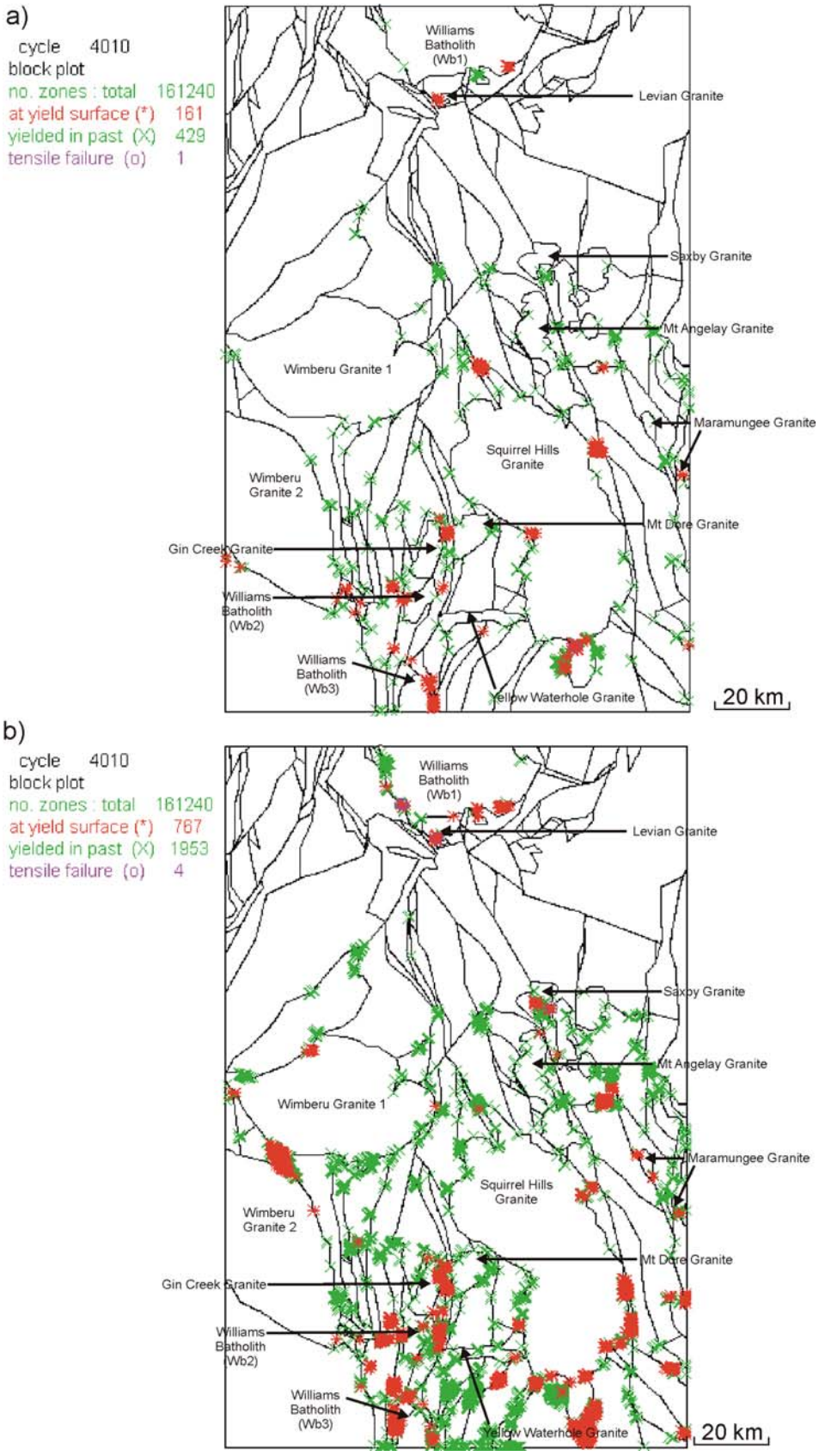

Fig. 47. Plasticity state comparison of Models 2c and 2d a) 'wet' model $\sigma_1 = 90°$ and b) 'wet' model' $\sigma_1 = 112.5°$. Rotation of σ_1 has a strong influence on failure and distribution. Note: red indicates areas at yield, green indicates previously at yield but now not in contact with the failure envelope, and purple indicates areas in yield in tension.

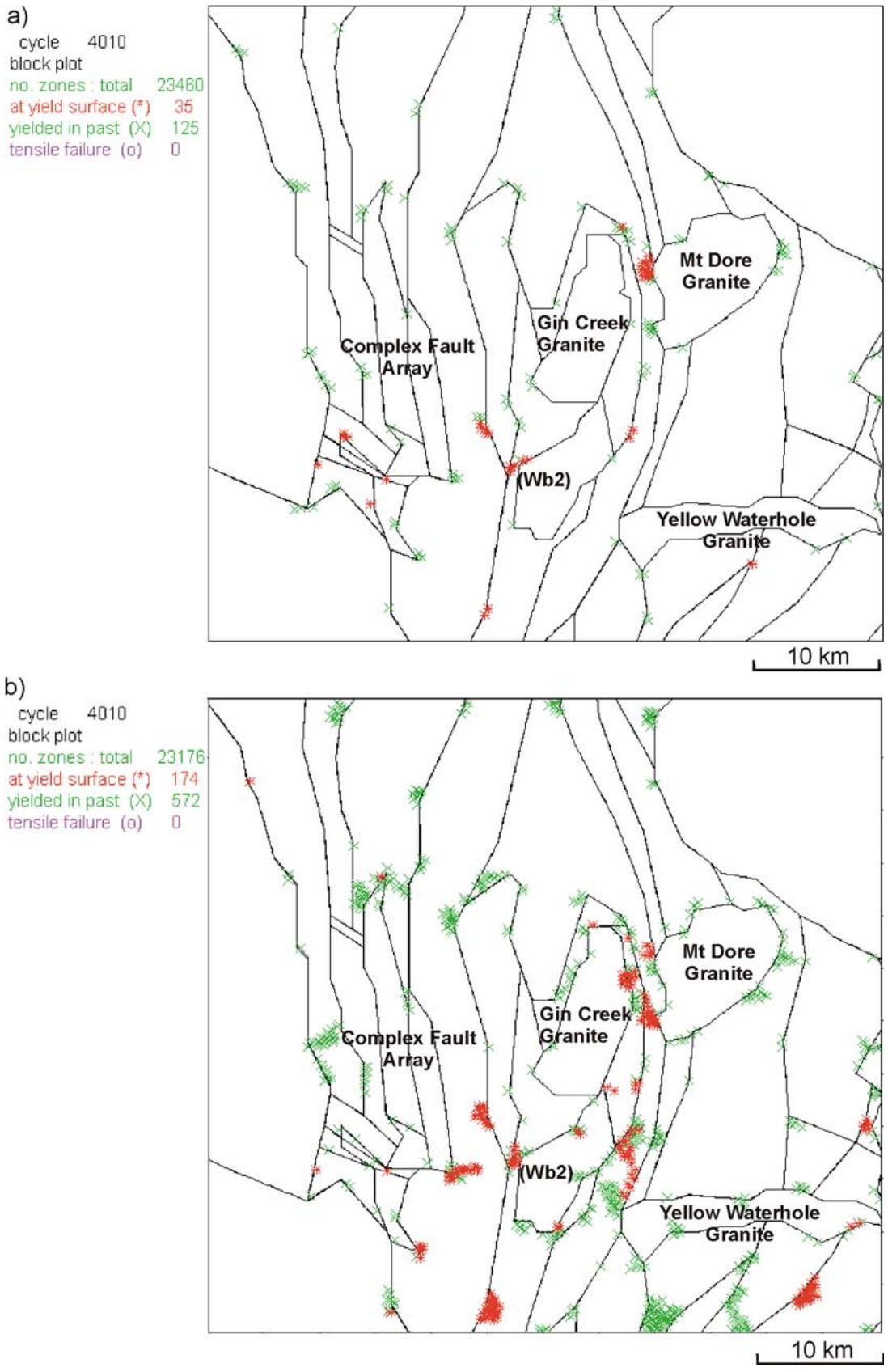

Fig. 48. Plasticity state comparison of Models 2c and 2d a) 'wet' model σ_1 = 90° and b) 'wet' model' σ_1 = 112.5° at the Selwyn scale. Rotation of σ_1 has a strong influence on failure and distribution. Note: red indicates areas at yield, green indicates previously at yield but now not in contact with the failure envelope, and purple indicates areas in yield in tension.

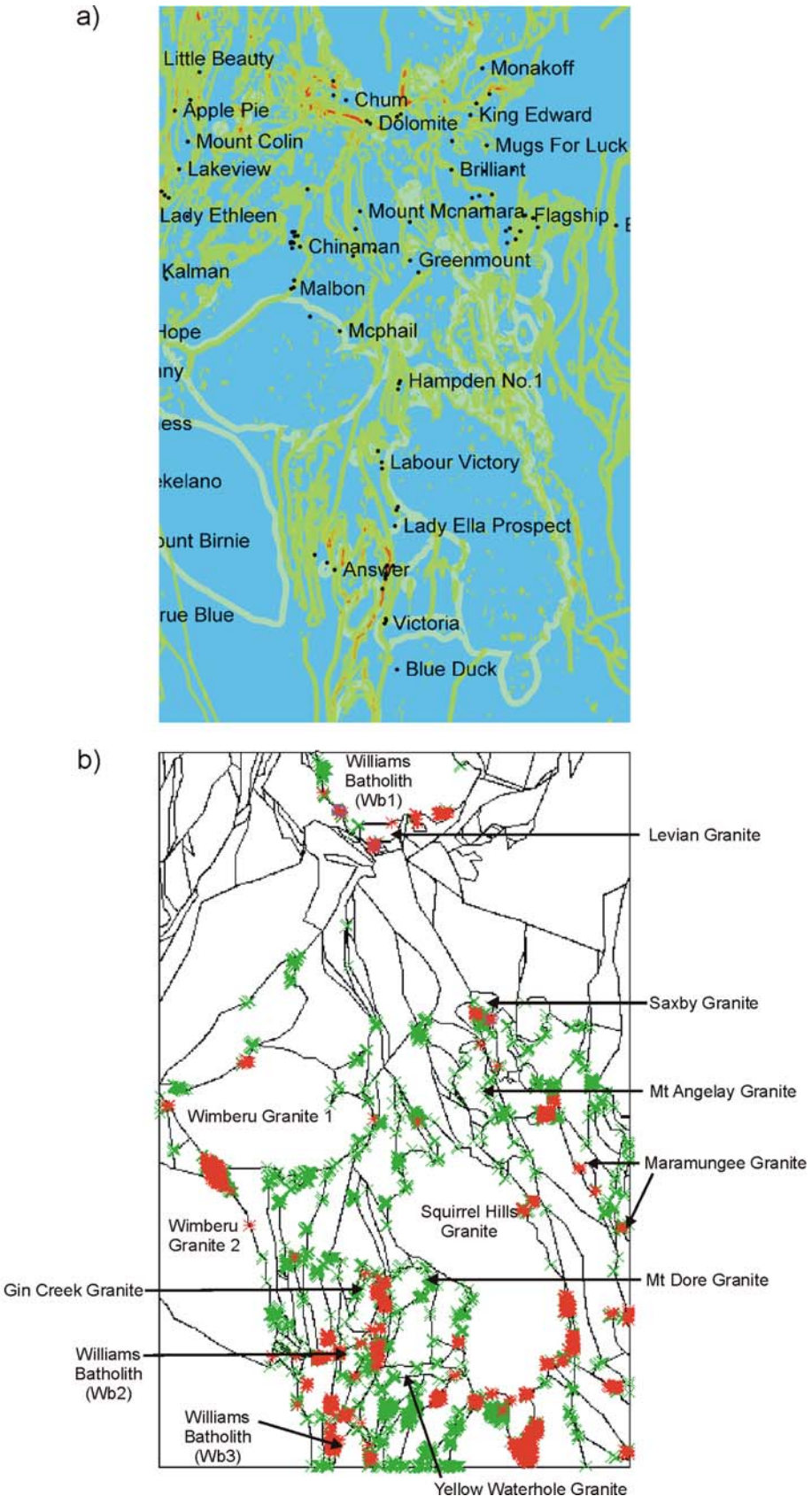

Fig. 49. Comparison of prospectivity analysis by Mustard *et al.* (2004) and plasticity indicators for Model 2d. a) prospectivity analysis, blue colours indicating no prospectivity and yellow to red indicating lower to higher prospectivity, with deposits and prospects indicated b) plasticity indicator for Model 2d (see Fig. 48 for legend).

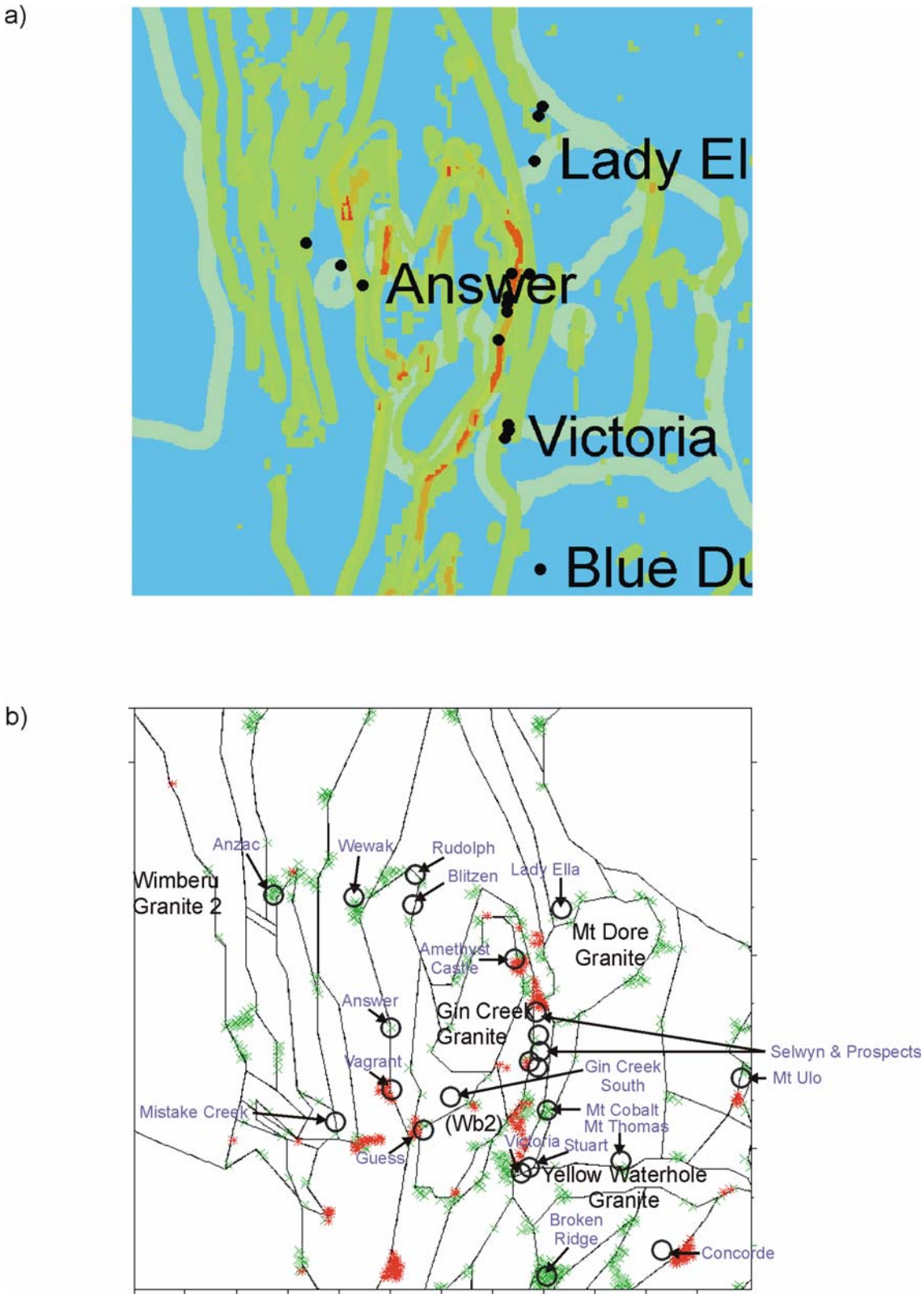

Fig. 50. Comparison of prospectivity analysis a) by Mustard *et al.* (2004), blue colours indicating no prospectivity and yellow to red indicating lower to higher prospectivity respectively b) plasticity indicators for Model 2d of the Selwyn region, indicating areas at yield.(see Fig. 48 for legend). Known deposits and prospects of the Selwyn area are named and marked by circles.

7.0 DISCUSSION AND CONCLUSIONS

Several factors and locations have been highlighted in these models that appear to contain the essential ingredients for a potentially mineralised system. The modelling procedure and analysis have also highlighted the effects of increasing the complexity of the geometry, rotating the orientation of σ_1 and introducing fluid into specific parts of the system. This section will discuss the results of the main models and the relationship between mechanical and fluid processes, leading to a summary which focuses on prospectivity of the Eastern Succession.

Competency contrasts between the granitic intrusions and metasediments in association with a fault or fracture system, results in significant changes in the partitioning of stress around these structures. The initial model (Model 1) has few pre-tectonic intrusions and a basic fault array, which provides a baseline model for examining the response to tectonic processes that correspond to an E/W shortening episode. This model displays preferential failure conditions around many fault bends and intersections, and along faults orientated at a low angle to the maximum principal stress. Although this orientation of faults provides the best conditions for failure, not all faults of this orientation show the same results throughout the entire model. This is due to the more complex interactions of block geometry or fault blocks, which assists in partitioning stress as these blocks move and deform. Many areas of interest can be highlighted, which display lower magnitudes of mean stress, minimum principal stress and fluid pressure required for failure. These parameters indicate a higher potential for failure at specific locations within the model, and hence provide an increased prospectivity interest. The rotation of the maximum principal stress to 112.5° significantly modifies the distribution and variation in magnitudes of both minimum principal stress and differential stress, with lower values of minimum principal stress and mean stress corresponding well with areas showing higher differential stress. These conditions provide a greater likelihood of shear failure and probable dilation, and have a strong potential for focussing fluid flow. Areas that show a decrease in the values of mean stress, minimum principal stress in combination with low differential stress provide conditions most suitable for tensile failure, which is a particularly good environment for mineralisation. Altering the orientation of the maximum principal stress has little consequence on the distribution of magnitude of the mean stress in the Model 1; however it does have a strong influence on redistribution of minimum principal stress values. This can be attributed to the orientation of faults in relation to the maximum principal stress and as stated before, this is variable throughout the models due to complex geometry and block interactions. The introduction of distributed fluid throughout the model fractures results in a considerable variation in the range of values of all parameters investigated, and leads to a significant modification in the pattern of distribution. Overall values of all parameters decrease for many areas, which provide more suitable conditions for failure. In a Mohr space this corresponds to reduced effective stress values and a shift of the Mohr circle towards the failure envelope, with enhanced potential for failure in these rocks. With both fluid introduction and a rotation of the maximum principal stress we see distinct changes in the distribution of many parameters, increases in the range of many values, an increased incidence of failure within the models and a better correspondence with known deposits.

Increasing the complexity of the models by introducing younger intrusions and faults, allows a comparison of stress partitioning on a broad scale with the earlier models.

Model 2 displays similar effects to Model 1 when fluid pressure is introduced into the fractures and a rotation of the minimum principal stress to 112.5° is initiated. As a result of the more complex geometry there is less confidence in a generalised fault orientation within the whole region being more prone to failure, due to the heterogeneous patterns of deformation and stress partitioning. Unlike the work of Mustard (2004) no clear or obvious fault orientations or intersections were highlighted overall, due to the complexity of stress partitioning. Interesting observations were made in smaller areas, such as the Selwyn region, where the localisation of deformation was compartmentalised. Areas of high differential stress correspond well to high strain zones e.g. Selwyn high strain zone, which is situated between the Mt Dore and Gin Creek granites. Due to shear displacement of blocks between the granite bodies and the fault systems, this area has accommodated higher strains.

In conclusion, this work has shown that the partitioning of stress during deformation is a complex process, and that no single attribute can be shown to be a high level indicator for mineralisation. However, these models show that a combination of low mean stress, minimum principal stress and high differential stress are good indicators for deformation and dilation as a result of shear failure in the rocks, and in combination with low fluid pressure required for failure, may act as a prospectivity guide. The results of these models have a good correlation with present known deposits and prospects, and also highlight areas that currently have no known mineralisation. This UDEC analysis has proven to be an effective tool and compares well with at least several prospectivity layers from the work of Mustard *et al*. (2004).

Implications for exploration in the Eastern Succession may be enhanced by the findings of this study. To fully develop this process as an effective exploration tool, areas that show a strong potential for mineralisation should be re-examined and modelled at a local scale, incorporating a more detailed geometry including lithological contacts and small-scale structures. To fully constrain the stress distribution in the Eastern Succession, a three-dimensional model would be preferable, as low angled faults and vertical fluid flow on steep fault intersections would have an effect on the partitioning of stress. However, this would require detailed information on all structures involved and considerable computational time to process the model. In cases where low angle faults are present, cross sectional modelling could be utilised to provide an understanding in the third dimension. However, these two-dimensional models provide a basis for further modelling studies, and highlight the basic conditions required to ascertain why certain areas may be more prospective than others.